DEPOSITIONAL FRAMEWORK OF THE GWNA GROUP MÉLANGES OF ANGLESEY AND NORTH-WEST WALES, UK

by

ROSEMARY DARTNALL

A thesis submitted to the
University of Birmingham
for the degree of
DOCTOR OF PHILOSOPHY

School of Geography, Earth and Environmental Sciences
College of Life and Environmental Sciences
University of Birmingham
October 2018

ABSTRACT

The Gwna Group contains chaotic, disrupted mélange of unknown genetic history. Publications that speculate on Gwna Group formation often cast the mélange in a pivotal role: the regional co-location of blueschist and greenschist with the Gwna Group has inspired hypotheses of tectonic mélange formation during accretionary orogen subduction, yet no specific published studies of the Gwna Group exist.

Detailed field study of the Gwna Group has distinguished primary features from those overprinted by later events, over four defined outcrop belts within which combined stratigraphic relationships are determined.

The Gwna Group is emphatically redefined as a sedimentary, gravity flow deposit;

- Four basal unconformities demonstrate sedimentary superposition.
- Pre-Sturtian molar tooth microspar is described in abiotic Neoproterozoic dolo-limestone clasts within the Gwna Group – the first account in Britain.
- A regionally ubiquitous, internally conformable coherent sedimentary system of three main lithofacies is interbedded within repeated megacycles.
- The sediments record early Palaeozoic passive margin evolution.

New U-Pb zircon investigations and meta-analysis of published ages show the Gwna Group began to accumulate near the Gondwanan margin during early Cambrian rifting and crucially demonstrate no genetic relationship with the Penmynydd Zone as Gwna Group deposition followed exhumation of the blueschists at 560 - 550 Ma.

ACKNOWLEDGEMENTS

I would like to thank my supervisors Ian Fairchild (University of Birmingham), Paul Smith (University of Oxford), David Schofield (British Geological Survey) and James Wheeley (University of Birmingham) for the generosity with which they have shared seemingly limitless knowledge and experience. I have received sound advice, encouragement, endless patience and understanding. My research project was carried out alongside the British Geological Survey's Anglesey remapping project and I thank Graham Leslie (BGS) for additional help and great enthusiasm during fieldwork. Thanks are due to the many staff and colleagues at the University of Birmingham, and beyond, who have been ready to help with open-hearted support.

Financial support was gratefully received in grants from the Gill Harwood Memorial Fund, for fieldwork, and from NIGL/NERC that enabled the U-Pb zircon geochronology project. Huge thanks are due to Daniel Condon, Nick Roberts and Adrian Wood and others at NIGL, for guiding me through all aspects of U-Pb zircon analysis. The School of Geography, Earth and Environmental Sciences at the University of Birmingham funded my research project and I am thankful for this and for being offered the opportunity to take on various employment contracts in the years spent at the University of Birmingham. I am particularly grateful for the opportunity to work as Assistant Curator at the Lapworth Museum of Geology and to teach foundation level Earth Science to Birmingham International Academy students, from Rwanda and Ivory Coast, who came to the University of Birmingham to study Geology undergraduate degrees.

TABLE OF CONTENTS

DEPOSITIONAL FRAMEWORK OF THE GWNA GROUP MÉLANGES OF ANGLESEY AND NORTH-WEST WALES, UK

TABLE OF CONTENTS (Continued) Page

TABLE OF CONTENTS (Continued) Page

TABLE OF CONTENTS (Continued) Page

LIST OF FIGURES

LIST OF FIGURES (Continued) Page

LIST OF FIGURES (Continued) Page

LIST OF FIGURES (Continued) Page

LIST OF FIGURES (Continued) Page

LIST OF FIGURES (Continued) Page

LIST OF TABLES

Chapter 1

THE GWNA GROUP MÉLANGES OF ANGLESEY AND NORTH-WEST WALES

1.1 Introduction

The Gwna Group crops out in Anglesey and the Lleyn Peninsula, north-west Wales in an area bound to the south-east by mylonitic rocks of the Lleyn Shear Zone (Fig. 1.1). The shear zone is a lineament considered to be the continuation of the Menai Strait Fault System (MSFS) that comprises several parallel branching faults, all of which are orientated north-east to south-west (Gibbons, 1987). This orientation is evident in map view: the lithotectonic slices of the Monian Supergroup and associated rocks (Fig. 1.1). Such as, the blueschist and greenschist units, the Coedana Complex of Neoproterozoic gneisses intruded by Coedana Granite, all of which combine to form the regional geology, that, pre-Ordovician, is distinct from outcrop south of the MSFS in mainland Wales (Matley, 1928). The lithotectonic units within the tessellated regional geology are mostly fault-bounded and have collectively proven resistant to deconstruction through a protracted study history. There is disagreement in the literature about the history of Monian geology.

The Gwna Group consists of several lithofacies but is most known for the mélange component, the presence of which has contributed to a wide variety

---

Figure 1.1 → Map featuring the pre-Ordovician geology of the Monian Supergroup and associated lithostratigraphic units in Anglesey and the Lleyn Peninsula of north-west Wales. Outcrop belts 1 – 4 are related to the methodology of this study (see section 1.7). Map after Greenly, 1920 - British Geological Survey (BGS) Anglesey Special Sheet, BGS - Anglesey map, in press and BGS map Sheet 133. Menai Strait Fault System and Lleyn fault linework after Gibbons (1987). Anglesey major fault and fold linework after BGS Anglesey map, in press.

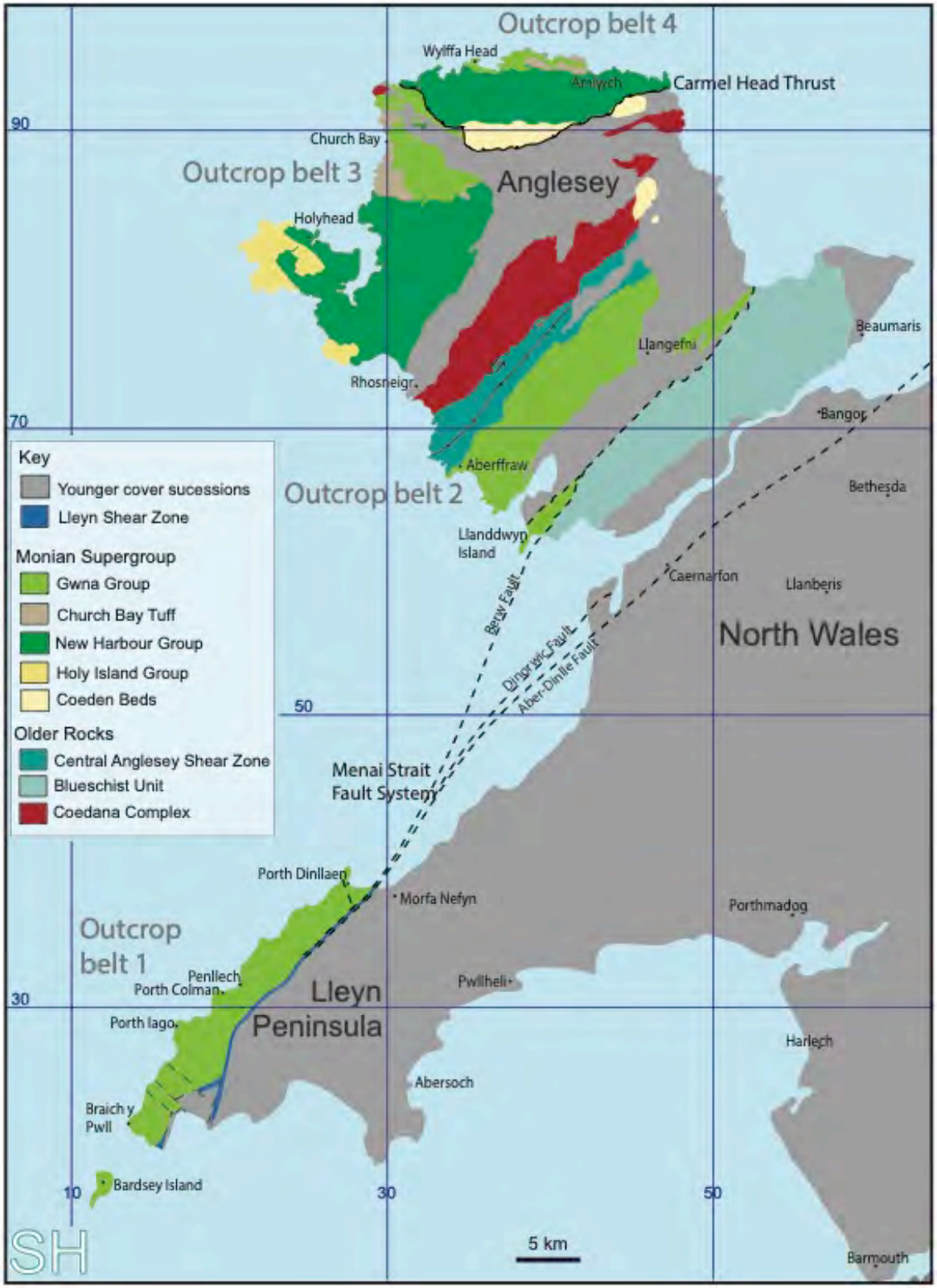
Outcrop belt 4
Wylffa Head
Carmel Head Thrust
Church Bay
Outcrop belt 3
Anglesey
Holyhead
Llangefni
Beaumaris
Rhosneigr
Bangor
Aberffraw
Outcrop belt 2
Bethesda
Llanddwyn Island
Caernarfon
Llanberis
Berw Fault
Dinorwic Fault
Aber-Dinlle Fault
North Wales
Menai Strait Fault System
Porth Dinllaen
Morfa Nefyn
Porthmadog
Outcrop belt 1
Penllech
Porth Colman
Pwllheli
Lleyn Peninsula
Porth Iago
Harlech
Abersoch
Braich y Pwll
Bardsey Island
Barmouth
5 km
SH
90
70
50
30
10
30
50
Key
Younger cover sucessions
Lleyn Shear Zone
Monian Supergroup
Gwna Group
Church Bay Tuff
New Harbour Group
Holy Island Group
Coeden Beds
Older Rocks
Central Anglesey Shear Zone
Blueschist Unit
Coedana Complex

of genetic interpretations of Anglesey and Lleyn geological history, yet no detailed studies of the Gwna Group have been published. The Gwna Group mélange is chaotic: decimetre-scale clasts are mixed with others, commonly metres, or tens of metres in diameter, all entrained within a swirling mud- to siltstone matrix that is injected into every clast cavity. The mélange itself does have a chaotic appearance that is likely to pertain to genetic history, however, Caledonian deformation has resulted in highly disrupted geology in the region.

This study is motivated by;

- A lack of detailed understanding of the Gwna Group
- The need to identify pattern, if it exists, among the apparently chaotic deposit
- Clarification of genetic and overprinted characterisitcs

The aims are to clarify the mode of emplacement and the tectonic setting in which the Gwna Group formed, combined with U-Pb zircon geochronology of relevant components to provide robust constrains on Gwna Group age.

1.2 Summary of regional study history

The geological history of the ~ 7.5 km thick Monian Supergroup of Anglesey and the Lleyn Peninsula of north-west Wales (Fig.1.1) is complex and contentious (Greenly, 1919; Shackleton, 1969, 1975). The island of Anglesey consists of a series of elongate lithostratigraphic units, interpreted by some as tectonic slices (Gibbons, 1987) aligned north-east to south-west. This orientation is parallel to

the MSFS, a complex set of converging fault lines where contacts are rarely observable and many inter-block relationships have not been established (Barber and Max, 1979; Gibbons, 1987; Gibbons and Horák, 1990).

Extensive study in the late 19th and early 20th centuries described the nature of many of the field relationships that crop out in the area and most authors considered the Monian rocks to be of Precambrian age (Blake, 1888; Greenly, 1896, 1919; Matley, 1899, 1900, 1901, 1913). Shackleton revisited fundamental aspects of this early research and revised significant interpretations, for example, reversing the younging direction of the Monian Supergroup (Shackleton, 1951, 1954a, 1954b, 1975). Subsequent research, which was particularly intense in the 1970s – 1990s following the dawn of plate tectonic theory in the 1960s, began to synthesise the Monian Supergroup into a broader geological context, at first looking for correlation with Precambrian outcrop on the Irish Sea margins (Baker, 1969; Dewey, 1969; Thorpe, 1972; Max, 1975; Tietzsch-Tyler,1996) and more recently assessing the potential for a peri-Gondwanan association (Gibbons and Horák, 1990; Horák and Evans, 2010; McIlroy and Horák, 2006; Waldron *et al*., 2011). A younger Cambrian age began to be discussed as field relationships became clearer (Barber and Max, 1979) however, clarity about age has not been fully achieved although some age constraints have been established (Moorbath and Shackleton, 1966; Bates, 1972; Dallmeyer and Gibbons, 1987; Tucker and Pharaoh, 1991; Collins and Buchan, 2004; Strachan *et al*., 2007; Asanuma *et al*., 2015; Asanuma *et al*., 2017) which together set up a broad late Neoproterozoic to early Palaeozoic framework.

In Anglesey Baker (1969) recognised the convergence of differing metamorphic regimes arranged around a tectonic junction and Wood (1974) saw that the pre-Mesozoic geology of north Wales and Anglesey was unique among the British terranes in featuring a combination of the phenomena indicative of a palaeo-

subduction zone. In Ireland, several Precambrian outcrops identified on the east coast at Howth, Bray Head, Wicklow and Wexford were suggested as having Monian association (Baker, 1969) and at Rosslare, near Wexford, further west along the trajectory of the Lleyn Shear Zone, the Cahore Group is considered to have affinity with all three formations of the South Stack Group (Baker, 1969; Tietzsch-Tyler, 1989). Barber and Max (1979) re-evaluated the regional geological history using a tectono-stratigraphic model which took account of the fundamentally segmented nature of the geology, ordering the units based on structural, metamorphic and stratigraphic boundaries and hypothesised the presence of a subduction zone and accretionary complex. However, all subduction related models were soon dismissed as oversimplification (Gibbons, 1983a), but the Anglesey fault-bounded block configuration was considered to be evidence for the presence of suspect terranes (Gibbons, 1987), a model further was developed using differing metamorphic P-T conditions throughout the supergroup to identify four composite terranes in Anglesey and Lleyn, said to record terrane dispersal and oblique accretion with the terranes finally docking along the MSFS at ~550-540 Ma (Gibbons and Horák, 1990).

Kawai *et al*., (2007) returned to the subduction zone theme, producing a Pacific-type accretionary orogen model relating a long-lived Neoproterozoic - Caradocian south-east directed subduction front with the volcanics of the Sarn, Coedana, Malvern Hills, Charnian and Uriconian Groups. In this hypothesis the Monian Supergroup was formed as an accretionary prism landward of the subduction suture and the blueschist facies unit of the Anglesey (of Greenly's (1919) Aethwy Zone) was exhumed from a depth of ~ 35 km via the subduction channel situated at the MSFS and the Lleyn Shear Zone (Kawai *et al*., 2006). A subsequent series of publications were published supporting the Pacific-style orogenic model in the following years that studied various aspects of the

regional geology (Maruyama *et al*., 2010; Kusky *et al*., 2013; Saito *et al*., 2015; Asanuma *et al*., 2015; Asanuma *et al*., 2017).

The Gwna Group, in its original concept, contained rocks altered by metamorphism to greenschist and blueschist facies, and fractured tectonic breccia and/or olistostrome deposits (sedimentary mélanges) of sandstone, basalt, carbonate, jasper and quartzite clasts on all scales often supported by a foliated matrix. The Gwna mélange was recognised by Edward Greenly (1919) as a regional scale fault breccia. He was the originator of the geological term mélange and described the rocks as an autoclastic fault breccia. Greenly mapped the geology of Anglesey over many years culminating in the 1919 publication of the Geological Survey of Britain memoir - The Geology of Anglesey. Charles Matley's work of the same period focused on the Monian Supergroup and early Palaeozoic outcrop of the Lleyn Peninsula (Matley, 1901, 1913, 1928). The geological map of Anglesey produced from Greenly's work at that time (Greenly, 1920) is currently under review but has served as the base document for editions of the geology maps for a century. Shackleton (1954a) reviewed Greenly's work: he reversed the stratigraphic order of the Monian Supergroup based on sedimentary way-up criteria such as normal grading and the facing direction of basalt pillows (Max, 1975, Shackleton, 1954a, 1954b). Greenly's memoir continues to serve as an underpinning baseline reference for the many geologists

---

Figure 1.2 → Summary logs of the Gwna Group within the Monian Supergroup and associated Anglesey lithotectonic units, showing the hypothesis for two depositional episodes of the same succession: the same sediment supply and the same process sedimentology. An older Gwna A, exposed in outcrop belts 1 and 2 (Lleyn and south-west Anglesey - see Figure 1.1), followed by a younger Gwna B, exposed in outcrop belts 3 and 4 (north-west and north Anglesey – see Figure 1.1).

Central - south-west Anglesey and Lleyn
Gwna A
Outcrop belts 1 and 2

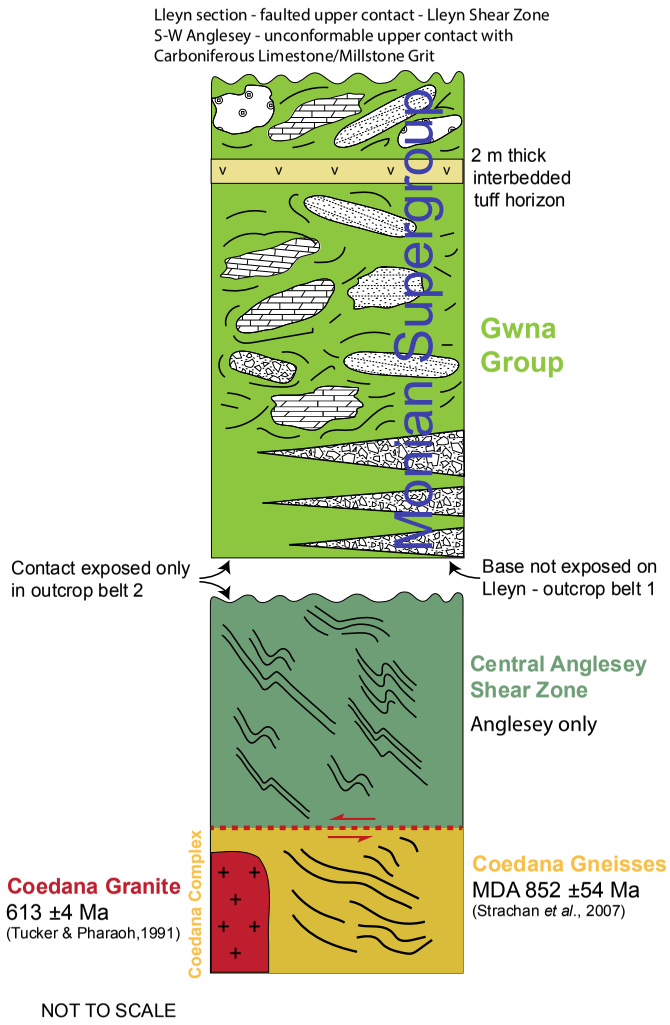

North-west and north Anglesey
Gwna B
Outcrop belts 3 and 4

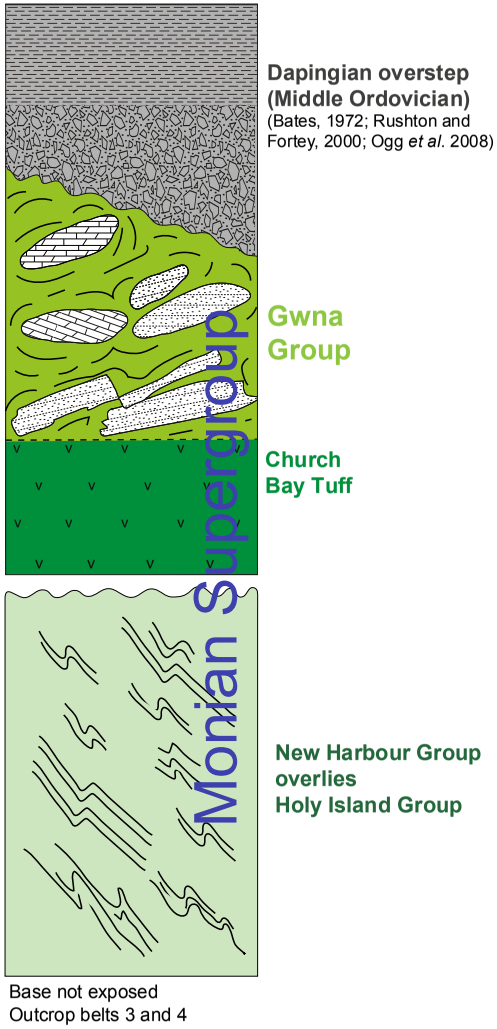

who continue to study the challenging geological questions raised by the complex geology of Anglesey, the Monian Supergroup and associated stratigraphic units.

1.3 Geological setting

The pre-Ordovician geology of Anglesey and the north-west of the Lleyn Peninsula differs from that of mainland north Wales, divided by the MSFS and the Lleyn Shear Zone (Fig. 1.1). The Monian Supergroup (Fig. 1.2 and Table 1.1), a sedimentary sequence of varied metamorphic grade and deformation history, crops out in many localities on Anglesey but only on the north-west tip of Wales on the Lleyn Peninsula, including Bardsey Island (Fig. 1.2). On Anglesey, Gwna Group deposits, the youngest of the Monian groups (Figs. 1.1 and 1.2), are overlain by unconformable Dapingian (Middle Ordovician) sediments at Porth Wen on the north coast. The Berw Fault, that bisects Anglesey in a north-east to south-west direction, is the northern strand of the fault system (Barber and Max 1979). The MSFS, a tectonic suture that divides the differing geological histories of Anglesey and the Lower Palaeozoic Welsh Basin and comprises three main high-angled faults (Gibbons, 1987). These are the Berw (Anglesey), Dinorwic (Menai Strait) and Aber-Dinlle (north Wales) (Fig. 1.1) each orientated north-east to south-west, broadly parallel to the Menai Strait, and which then converge on land, expressed on the surface in the Lleyn Shear Zone (Barber and Max, 1979, Gibbons 1987).

Table 1.1 → The lithostratigraphy of the Monian Supergroup, redrawn after Phillips (2010), which is based on Tietzsch-Tyler and Phillips (1989) and Phillips (1991a).

Group	Formation	Thickness	Type section	Boundaries
Gwna Group		3000 m	Llanbadrig (SH 375 946)	Top - not exposed Base - gradational (Gibbons and Ball, 1991)
New Harbour Group	Skerries Formation	200 - 300 m	The Skerries (SH 260 940)	Top - gradational into the Gwna mélange (Greenly, 1919) (SH 300 915; SH 315 907) Base - gradational
	Lynas and Bodelwyn formations	North-western Anglesey 1000 - 2000 m		Top - gradational into the Gwna mélange (Gibbons and Ball, 1991) Base - not exposed, possibily tectonic
		South-western Anglesey 2000 - 3000 m	Port-y-Post (SH 2436 7600) to Bwa Du (SH 2600 7625)	Top - faulted contact with Skerries Formation (SH 2890 8580) Base - tectonised sedimentary contact with the Holy Island Group (SH 2700 7464; SH 2420 8035; SH 2362 8370)
Holy Island Group	Rhoscolyn Formation	300 m	Rhoscolyn between (SH 2647 7495) and Porth-y-Corwgi (SH 2700 7470)	Top - tectonised sedimentary contact with the New Harbour Group Base - conformable upon the Holyhead Formation (SH 2647 7495)
	Holyhead Formation	500 m	Bwa Du (SH 2600 7640) to Porth Saint (SH 2595 7590)	Top - corresponds to the top of the Holyhead Quartzite (SH 2647 7495) Base - conformable upon the South Stack Formation (SH 2048 8230; SH 2580 7544)
	South Stack Formation	400 m	Penrhyn Mawr (SH 2110 8062)	Top - conformable with the overlying Holyhead Formation Base - not exposed

1.4 The Gwna Group mélange

The Gwna mélange, part of the Gwna Group, was named by Greenly (1919) after the Gwna river in the south-west of Anglesey, the locality where he considered all Gwna Group constituent lithologies crop out together. Greenly coined the descriptive geological term mélange whilst studying the highly colourful mixture of rocks to be found at the western tip of Llanddwyn Island. He interpreted the unit as having formed by tectonic means and called it an autoclastic mélange. Greenly (1919) assigned the Gwna Group to the base of the Bedded Succession within the Mona Complex – the stratigraphic framework he erected for Precambrian Anglesey geology. The stratigraphy was later reversed by Shackleton, making the Gwna Group the youngest unit of the Bedded Succession, or as it is known today, the Monian Supergroup. Shackleton considered the mélange to have formed as a sedimentary gravity slide deposit (Shackleton, 1951, 1954a, 1954b; Max, 1975).

Greenly (1919) described the mélange as highly disrupted, saying it was a many coloured mélange. He noted that clasts of all scales were contained within a muddy matrix and used words such as wreckage, and indescribable. Schuster (1980) in his unpublished thesis, examined three areas (Cemaes Bay on the north Anglesey coast, a short section of the Anglesey south-west coast near Aberffraw Beach and Bardsey Island in Lleyn – Fig. 1.1) of the mélange in detail and his impression can be summarised as follows: Although comprising a wide variety of clasts and matrix types which on first impression appear highly chaotic, the Gwna Group records a macro-scale stratigraphy. In areas the lithic blocks consist of segmented deep marine sequences, broken formations, commonly rafts twenty to thirty metres wide composed of layered successions several metres thick of pillow basalt, jasper, carbonate, quartz arenite and mudstone where

clasts outrank matrix volumetrically.

In other places the mélange is dominated by individual blocks of shelf and shoreface deposits such as sandstone or carbonate supported within a pervasively foliated matrix and a ghost stratigraphy is present (Schuster, 1979, 1980). Shackleton (1975) interpreted the Gwna Group as recording a progressive deepening of the basin to the south-east with sediment supplied from the north-west.

Although mélange deposits are often associated with subduction complexes they have also been recognised in other settings such as fore-arc basins, passive margins and major fault zones (Raymond, 1984; Festa *et al*., 2010; Zagorevski *et al*., 2012; Festa *et al*., 2016). An inferred association with subduction/accretion has inspired many structurally based studies of the Monian rocks such as Barber and Max (1979). In contrast, Schuster's (1980) work bore a sedimentological focus. Detailed study of the selected field areas led Schuster to the firm conclusion that the Gwna mélange is genetically sedimentary, a gravity slide deposit, potentially formed in a subduction zone. Alluding to the polarised discussion in geological circles where one faction insisted that Greenly's intention for the term mélange and therefore its correct usage should be limited to tectonic breccias, Schuster noted that the interpretation of a sedimentary debris flow deposit is entirely consistent with an active margin setting (Schuster 1979, 1980).

The age of the Gwna Group

The emplacement age of the Gwna Group and the wider Monian Supergroup has not been established unequivocally. Greenly (1919) concluded that the Mona Complex, including sedimentary and crystalline components, was Precambrian

but later authors have allowed the possibility of Cambrian age for the sedimentary rocks (Greenly, 1919; Barber and Max, 1979). Certain key dates have been established which constrain the deposition of the Gwna Group, at least in the north of Anglesey, to between late Cambrian and Middle Ordovician age (Bates, 1972; Collins and Buchan, 2004). This study includes zircon U-Pb geochronology aimed at constraining the age of the Gwna Group, which is presented, in Chapter 3, with a reassessment of recently published studies (Collins and Buchan, 2004; Asanuma *et al*., 2015, Asanuma *et al*., 2017). Existing geochronological constraints for all Anglesey geology is presented in detail in Chapter 3.

Figure 1.2 illustrates the stratigraphy above and below the Gwna Group throughout the region. It is divided into two sections, respectively entitled Gwna A and Gwna B — a hypothesis developed during fieldwork for this study. The field evidence shows that the Gwna Group consists of a restricted group of lithofacies that are ubiquitous in all exposure. These lithofacies comprise the Gwna Group and they remain constant in terms of composition, and in terms of depositional process throughout the region (see Chapter 2). In the so-called Gwna mélange component, there is consistent matrix composition and consistent clast composition throughout all deposits. However, there is one group of additional lithologies; pillow basalt, hyaloclastite, jasper and cherty mudstones, that are present only in restricted sections of the Lleyn Peninsula and south-west Anglesey. The presence of these additional lithologies has led to the hypothesis that although the Gwna Group consists of a single deposit it may have formed in two sequential episodes. This will be discussed in detail in Chapter 2, which addresses the sedimentology and the geochronology study in Chapter 3.

1.5 Provenance: Peri-Gondwanan terranes and the North American Appalachian Front

After the development of the plate tectonic paradigm in the 1960s, it was recognised that the geographical association of the Gwna Group mélange with a blueschist unit, greenschist metasediments and volcanics of the Central Anglesey Shear Zone (CASZ) (Gibbons and Horák, 1990) and the gneisses of the Coedana Complex (Fig. 1.1) potentially placed constraints on the tectonic setting of the island. Subsequent interpretations identified the co-location of high-grade metamorphic rocks and mélange as evidence for the development of an ancient subducting plate margin (Wood, 1974; Barber and Max, 1979; Gibbons, 1987). Consideration of the stacked, fault block configuration of Anglesey geology and its fundamentally different nature compared to that south of the MSFS, led to a suspect terrane accretion model, on the north coast of mainland Wales (Gibbons and Horák, 1990). The subduction-accretion hypothesis was developed further by Kawai *et al.* (2007), who viewed the Gwna mélange as subduction trench deposits incorporated into an accretionary orogen complex comprising the whole Monian Supergroup. Prior geochronology studies constrained the timing of sediment deposition, intrusions and subsequent deformation within the region (Dallmeyer and Gibbons, 1987; Tucker and Pharaoh, 1991; Collins and Buchan, 2004; Strachan *et al.,* 2007), and recent publications (Asanuma *et al.*, 2015; Asanuma *et al.*, 2017) used selected data to support the Pacific-style accretionary orogen model (Kawai *et al.*, 2007).

In common with southern Britain and southern Ireland, Anglesey was recognised, until recently, as Avalonian, one of the late Neoproterozoic to early Palaeozoic peri-Gondwanan terranes (Fig. 1.3A) (Gibbons, 1990; McIlroy and Horák, 2006) associated with present day Laurentia both in Appalachian Atlantic

Canada and North America and in Britain and Ireland (Fig. 1.4B), collectively the Appalachian – Caledonides (Waldron *et al.,* 2014). During the late Neoproterozoic break-up of the supercontinent Rodinia (Li, *et al.,* 2008), tripartite rifting between Gondwana, Laurentia and Baltica (Fig. 1.3A) was associated with Iapetus Ocean formation between 615 and 550 Ma. The peri-Gondwanan terranes, five elongate landmasses: Avalonia, Ganderia, Meguma, Carolinia and Suwanee (Fig. 1.3A), separated individually from the northern margin of Gondwana in the early Palaeozoic, during incipient Rheic Ocean rifting (Murphy *et al.,* 2010; Pollock *et al.,* 2012). Episodic translation onto Laurentia was accomplished by the closure of the Iapetan tract (Fig. 1.3B), which began in the Ordovician and completed in the Middle Silurian. Subsequent closure of the Rheic Ocean was Carboniferous, associated with the formation of the supercontinent Pangaea. The onset of Mesozoic rifting divided and distributed parts of the composite orogen on either side of the proto-Atlantic Ocean (Fig. 1.4B), suggesting that Anglesey and the Monian Supergroup developed on the northern fringe of Gondwana (Fig. 1.3A) (McKerrow and Soper, 1989; Gibbons, 1990; Gibbons *et al*., 1993; Murphy *et al*., 2010; Pollock *et al.,* 2012; van Staal *et al*., 2012; Waldron *et al.,* 2014; Pothier *et al*., 2015; Schofield *et al*., 2016).

Figure 1.3 → The supercontinent Gondwana, the continents of Laurentia and Baltica and the peri-Gondwanan terranes of Avalonia (a), Ganderia (g), Carolinia (c), Meguma and Suwanee. **A.** Middle Cambrian southern hemisphere palaeogeographic reconstruction showing how the peri-Gondwanan terranes: Avalonia (a), Ganderia (g), Carolinia (c) and Meguma are co-located with respect to Laurentia, Baltica and the Iapetus and Rheic Oceans (modified after Pollock *et al.,* 2012). Iapetan subduction at the Laurentian margin and rifting beneath the Rheic Ocean between Avalonia and Ganderia - Carolinia were ongoing at this time. **B.** Simplified lithotectonic map of the present-day North American Appalachian Orogen showing the accreted configuration of the Laurentian margin and peri-Gondwanan terranes; Avalonia, Ganderia, Carolinia and Meguma (Hibbard *et al*., 2006). The area summarised covers the east coast of the North American continent from, left to right, South Carolina, USA to New Foundland, Canada.

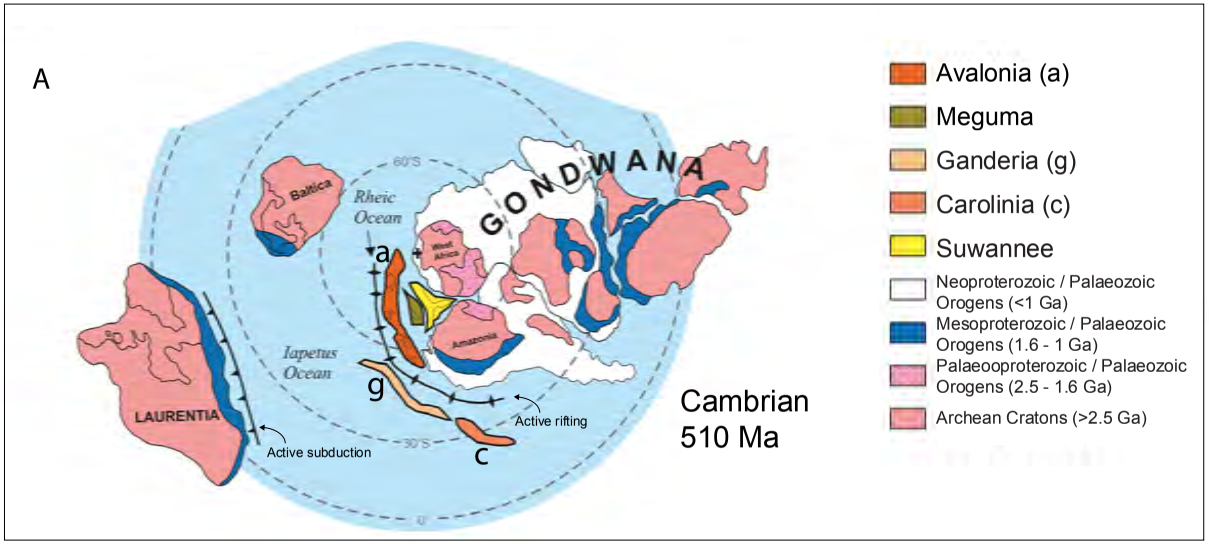
A
GONDWANA
Baltica
Rheic Ocean
a
Iapetus Ocean
g
LAURENTIA
Active subduction
Active rifting
c
Cambrian
510 Ma
Avalonia (a)
Meguma
Ganderia (g)
Carolinia (c)
Suwannee
Neoproterozoic / Palaeozoic Orogens (<1 Ga)
Mesoproterozoic / Palaeozoic Orogens (1.6 - 1 Ga)
Palaeooproterozoic / Palaeozoic Orogens (2.5 - 1.6 Ga)
Archean Cratons (>2.5 Ga)

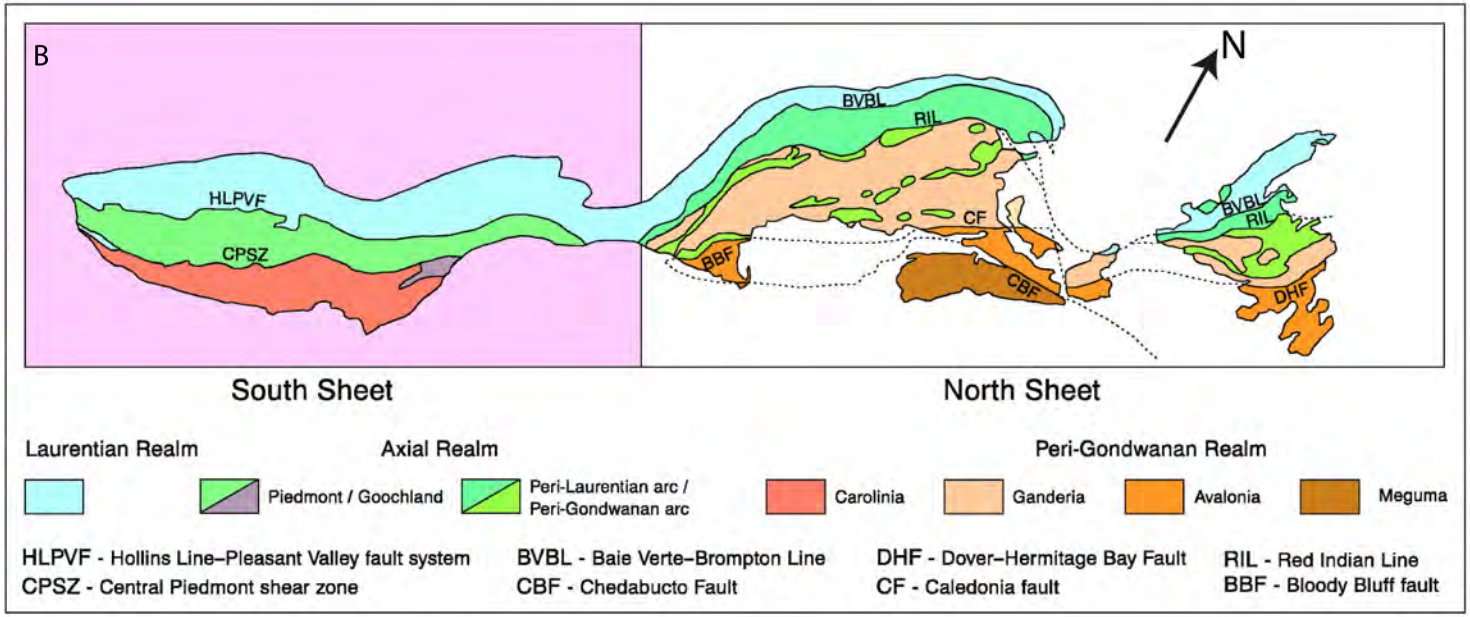
B
N
HLPVF
CPSZ
BVBL
RIL
CF
BBF
CBF
DHF
South Sheet
North Sheet
Laurentian Realm
Axial Realm
Peri-Gondwanan Realm
Piedmont / Goochland
Peri-Laurentian arc / Peri-Gondwanan arc
Carolinia
Ganderia
Avalonia
Meguma
HLPVF - Hollins Line–Pleasant Valley fault system
CPSZ - Central Piedmont shear zone
BVBL - Baie Verte–Brompton Line
CBF - Chedabucto Fault
DHF - Dover–Hermitage Bay Fault
CF - Caledonia fault
RIL - Red Indian Line
BBF - Bloody Bluff fault

Studies of palaeomagnetism, faunal province, geochronology, isotope geochemistry, seismic exploration, lithotectonic and stratigraphical comparison have lead many workers to consider the Monian Supergroup to be Ganderian (Figs. 1.3A and B) (Rast *et al.,* 1976; Gibbons, 1990; Gibbons and Horák, 1996; Nance and Thompson, 1996; van Staal, 1998; Nance *et al.,* 2004; Li *et al.,* 2008; Waldron *et al.,* 2009; Pollock *et al.,* 2012).

Anglesey and the peri-Gondwanan terranes

The striking difference in the pre-Ordovician geology north and south of the MSFS has given rise to a variety of tectonic models (Fig. 1.4A), many of which have been referenced above. Not all look to the present day west for provenance but discussion of a circum-Atlantic correlation with the North American Appalachian front has continued for more than 40 years (it was first postulated by Rast *et al.,* 1976) and there is a wide range of research combined in an ongoing synthesis of the terrane history on the North American side of the Atlantic (Figs. 1.3 and 1.4). Recent U-Pb zircon provenance geochronology has proved peri-Gondwanan provenance affiliation between the Welsh Basin and Meguma Terrane in Nova Scotia and north-west Africa (Waldron *et al*., 2011; Pothier *et al*., 2015) and also linked Newfoundland Gander Terrane with the English Midland Platform (Schofield *et al*., 2016).

Deep seismic surveys of Anglesey and the Irish Sea have interpreted the cratonic basement beneath the Ganderian cover to be Avalonian (Klemperer *et al*., 1990). A typical Ganderian sequence of predominantly continent sourced arenites of Lower Cambrian to Tremadoc age extends in Canada – USA from East Newfoundland to the Miramichi Highlands, New Brunswick and south-west into Maine, New England (van Staal *et al.,* 1996) — interpreted as passive margin

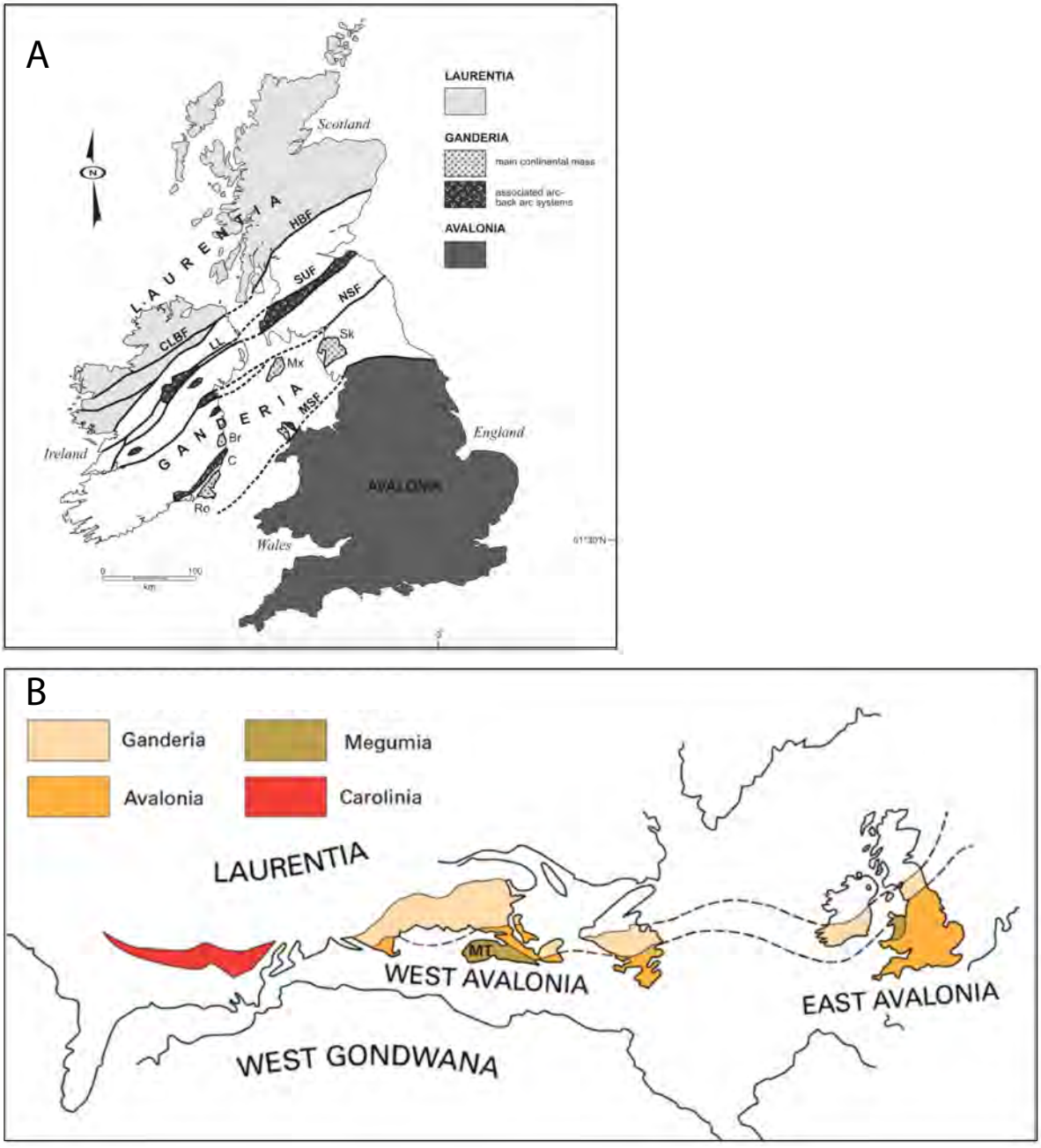

Figure 1.4. Maps of the peri-Gondwanan terranes in the British Isles and Ireland and present-day circum-Atlantic configuration. **A.** The position of Ganderia, the Gander Terrane, in Britain and Ireland, accreted onto the north of the (East) Avalonian margin at the Menai Straight Fault System and in contact, to the north, with Laurentia. Here the Gander Terrane encompasses Anglesey, north-west Lleyn in Britain, and Rosslare, in Ireland (Pollock *et al.,* 2012). **B.** A terrane reconstruction map of the North American Appalachian and British Caledonide orogens with the north Atlantic Ocean removed (Schofield *et al*., 2016, after Waldron *et al.,* 2011 and 2014).

sedimentary cover, deposited seaward of a volcanically active Gondwanan back arc margin (van Staal *et al*., 1998; Pollock *et al*., 2012) and the quartz arenites may correlate with the arenaceous sequence recorded by the Holy Island Group and/or the quartz arenite clasts that dominate the Gwna mélange in Anglesey and north-west Wales.

Establishing the provenance of the 860 – 800 Ma megaclast (Horák and Evans, 2010), the largest known clast in the Gwna mélange, that crops out at Trwyn y Parc on the north Anglesey coast, using strontium isotope correlations with Neoproterozoic ocean composition curves (Halverson, 2007) will likely involve a correlation with peri-Gondwanan terranes. Horák and Evans (2010) suggested the Ashburn Formation of the Greenhead Group of New Brunswick as a possible source on the grounds of similar age. If confirmed this may have implications for the peri-Gondwanan dispersal age and the timing of Gwna mélange emplacement as the Greenhead Group was subject to greenschist metamorphism at ~560 Ma and, since the megaclast exhibits low level alteration, mélange emplacement would have to be complete before the end of the Precambrian (Horák and Evans, 2010). Such an age would conform with the underthrust geotectonic accretionary emplacement model of Kawai *et al*., (2007) but would be problematic in terms of the existing age constraints which frame current Gwna Group understanding.

The enigmatic pre-Ordovician geology of Anglesey and north-west Lleyn has potential for a historical relationship with the Iapetus Ocean that existed ~620 and 450 Ma (Fig. 1.3A and Fig. 1.4B) (McKerrow and Cocks, 1986; Cawood *et al.,* 2001). Rifting, subduction, continental collision, and orogeny are the tectonic processes involved in the cycle of continental break-up and accretion. Continental fragments can be formed by the repetition of these cycles and the isolated presence of the Monian Supergroup on the north-west margin of Wales

and south-east Ireland gives rise to an Appalachian terrane accretion model via the translation of a peri-Gondwanan craton.

1.6 What is a mélange?

Mélanges are stratigraphic units of mappable scale characterised by a chaotic mixture of clasts or broken formations within a muddy matrix. Clast provenance may be autochthonous and/or allocthonous. Mélanges are associated with active margins, formed by the dynamic processes that dominate such settings, for example, subduction, accretion, orogeny, translation, underplating and exhumation. Mélanges have been recognised on all continents, with the exception of Antarctica (Raymond and Terranova, 1984).

In use for almost a hundred years, the application of the term mélange has survived controversy but, as workers have continued to grapple with the real subject matter, disagreement has abated. Historically, many have argued for mélange exclusively for tectonic emplacement, an accretionary wedge in a subduction zone, a tectonic mélange (for example, regarding the Gwna mélange; Greenly, 1919, Barber and Max, 1979, Kawai, 2007). Others prefer a sedimentary application, an olistostrome deposited by gravity slide or mass flow, mobilised by a catastrophic event such as continental shelf collapse or in a subduction zone where lithified and semi-lithified clasts are stretched into boudins, ripped up and deformed during rapid transport in a liquefied matrix. Exponents of a sedimentary mode for Gwna mélange emplacement include Shackleton (1951, 1954, 1975), Wood (1974) and Schuster (1979, 1980). Wood (1974) noted that Matley (1899) had referred to the mélange as a crush breccia and that Greenly had later used the term autoclastic mélange which he used to support the

removal of kinetic origin and the use of mélange to describe the style of rock (Wood, 1974). Hsü (1968) disagreed, stating that Greenly used mélange merely as a helpful abbreviation for autoclastic (tectonic) mélange. It is widely accepted that the emplacement mechanism may not be discernible in many mélanges as, by definition, there is likely to have been a combination and/or sequence of sedimentary and tectonic events in the history of any mélange (Hsü, 1968; Schuster, 1979, 1980).

However, recent publications show that reliable evidence for the petro-genetic history of mélanges are observable in outcrop (Raymond, 1984; Orange, 1990; Kopf, 2002; Dela Pierre *et al*., 2007; Camerlenghi and Pini, 2009; Wakabayashi, 2011; Barber 2013). While allowing that many authors may not accept this interpretation Schuster (1980) argues for a descriptive and not a genetic usage for mélange and relies on the following definition from Silver and Beutner (1980) who argue that Greenly's term is simply a tool for highlighting a lithological unit where the accepted rules of stratigraphy and superposition may not apply. Indeed, it may be timely to note that the word "mélange" is simply the French for "mixed". Definitions for a mélange include:

- "*Mélange is a general term describing a mappable (at 1:25,000 or smaller scale), internally fragmented and mixed rock body containing a variety of blocks, often in a matrix. The term refers to rock mixtures formed by tectonic movement, sedimentary sliding, or any combination of such processes, with no mixing process excluded.*" (Silver and Beutner, 1980, p. 32).
- "*A mélange is a body of rock mappable at 1:24000 or smaller and characterised both by the lack of internal continuity of contacts or strata and by the inclusion of fragments and blocks of all sizes, both*

exotic and native, embedded in a fragmented matrix of finer grained material." (Raymond, 1984, p.7). In this much cited publication Raymond moves the debate firmly from semantics back to geology by remarking that while contentious, most workers agree that acceptable mélange definitions must be based on observable features rather than assumptions about genetic history.

Hsü (1968) recognised that mélanges are not rare but are frequently found in orogenic belts such as the Franciscan Mélange, the Indo-Burman and Apennine *argille scagliose* and *wild flysch*, the exotic blocks zone of the Himalaya and the coloured rocks of north-east Iran. Warning of the dangers of applying a standard geological toolset including the laws of sedimentary superposition, stratal continuity and faunal assemblage, each reliant on assumptions not applicable to mélanges.

Hsü (1968) listed rules for the field assessment of mélanges;

"Rule 1. The making of a geologic map of a mélange terrane cannot be based upon a presumption of stratal continuity" (Hsü, 1968, p. 1067). The application of standard contact mapping techniques where the presence of a mélange has not been recognised leads to inaccurate interpretations.

"Rule 2. The stratigraphy of a mélange sequence cannot be established on a presumption of normal superposition" Hsü (1968, p. 1067) cautions that if rule 1 is ignored, rule 2 is likely to be broken as a direct consequence quoting Greenly's (1919) dismissal of some of Blake's (1888) earlier study of the Gwna mélange.

"*Rule 3. The assignment of a time-range of deposition to all the rocks in a mélange on the basis of the oldest and youngest fossils found in such a mélange is wrong*" (Hsü, 1968, p. 1067). Hsü warned us of using a single line of evidence

and invokes Greenly's description of the Gwna mélange. Greenly (1919) refers here to Ordovician fault slices in the Gwna mélange: he was not misled by the presence of Ordovician graptolites. Ordovician material, he explains, had become entrained within the Gwna mélange during post-Arenig thrusting and how he did not see this as recording an Ordovician age for the mélange, but merely a superimposed event further mixing already chaotic rocks. Post-depositional mixing should be classified as a polykinematic mélange (Hsü, 1968).

"*At Porth Padrig . . . an extraordinary mélange of black shale, grit, limestone, quartzite, Gwna Green-schist, and schistose tuff, beyond which . . . rocks of the (Precambrian) Mona Complex rise en masse. The shale and some of the limestone are certainly Ordovician; the quartzite, greenschist, and tuff are as certainly part of the Mona Complex, to which a portion of the limestone and some of the grits also seem to belong . . . . The Ordovician rocks here have been caught in a thrust and slipped infold . . . . Had that floor been homogeneous, a succession of regular thrusts would have resulted. But it happened, at this place, to be composed of the already autoclastic mélange of the Gwna Group (of the Mona Complex), with lenticular quartzites and limestones in a matrix of ashy greenschist and schistose tuff. These, under new strain, broke up once more along their ancient thrust planes, once more isolating their harder masses, which were driven bodily into the Ordovician sediments above. But those sediments themselves, by a singular coincidence, contained, not only conglomerates full of epiclastic fragments derived from the Mona Complex, but masses of limestone . . . . These lent themselves readily to the production of new limestone phacoids, which were carded in-and-in with the old lenticular Gwna limestones, these being driven up among them from below, both sets gliding over one another along strips of old Gwna Greenschist and of Ordovician shale, superimposing mélange upon mélange, and producing a well-nigh inextricable confusion*." (Greenly, 1919,

p.551).

"*Rule 4. The contact between a rock-stratigraphic unit and a subjacent or superjacent mélange may be a depositional contact or a dislocation contact*" (Hsü, 1968, p. 1070). Clast scale within a mélange is likely to cover several orders of magnitude. Tectonic blocks with kilometre dimensions may contain an extensive stratigraphic boundary, the interpretation of which could be misleading. If both lithologies are present elsewhere as clasts within the mélange the block must be seen as a clast and not mistaken for a superpositional contact (Hsü, 1968).

Olistostromes or sedimentary mélanges

Olistostromes are the product of gravitational sedimentary processes: debris flow deposits formed by the disruption and downslope mobilisation of lithified, semi-lithified and unlithified sediments caused by slope instability, shelf collapse and continental margin wasting. Fragmentation, disarticulation and mixing of sedimentary and other successions, liquefaction of matrix, gravity sliding and brittle, plastic and synsedimentary deformation are commonly associated with olistostromes. Silver and Beutner (1980) suggested the following important areas in the study of sedimentary mélanges:

- The nature of the upper and lower contacts – gradational or sharp sedimentary contacts can only be sedimentary.
- Tectonic mélanges, by definition, are bound by faulted contacts.
- The presence, or lack of a ghost stratigraphy
- The environments of initial deposition for the constituent lithologies
- Soft sediment deformation or injection
- Clast armour

- Evidence for transport direction
- Recognition of tectonic overprint

Camerlenghi and Pini (2009) recognised olistostromes by these criteria:

- An impressively chaotic deposit: on all scales – from outcrop to map scale
- Diverse clast size distribution: sub-millimetre to 100s of metres diameter
- Isometric clasts are dominant over triaxial blocks (the latter are restricted to the basal detachment where transport deformation is greatest)
- Matrix is argillaceous and contains grain sized clasts: the matrix is a microbreccia
- Matrix lacks banding
- Individual clasts and matrix exhibit varied metamorphic grade or diagenesis
- Olistostromes are polymict

While olistostromes can form in association with passive margins they are mainly found in accretionary orogenic settings where preservation potential is greater (Camerlenghi and Pini, 2009).

Tectonic mélanges

Tectonic mélanges are created at the interface of a subducting oceanic plate and an overriding continental plate where sediments, lithified or semi-lithified

are translated from the upper surface of the down-going oceanic plate onto the overriding plate. The sediments are absorbed into the imbricate zone of the foreland basin. As sediments are repeatedly scraped and thrust into the imbricate zone, fragmentation and mixing occurs accompanied by rounding, stretching and alignment of the clasts within the tectonic fabric. Accretionary prisms are generally unstable critical wedges constantly on the verge of failure (Gutscher *et al*., 1998) where relationships of superposition are unlikely to be preserved. Wedge geometry is a function of the strength of the basal detachment and the competence of the lithic materials of which it is formed (Gutscher *et al*., 1998), closely related to plate collision speed and trench geometry (Royden, 1993; Royden and Husson, 2006). Low basal friction results in almost all sediments removed from the down-going plate being accreted subaerially in a series of imbricate thrusts at the foot of the wedge whereas high friction levels cause underplating (Gutscher *et al*., 1998).

Hsü (1968) is firmly of the view that mélanges are tectonically created. In discussion of the various genetic possibilities ("mélanges versus olistostromes") he compares two styles of gravity sliding; firstly those that are tectonically induced, which would take place at a detachment surface beneath an overburden, mixing rocks and fragments in a manner analogous to boulders reworked and deposited in glaciation, and secondly a sub-marine slide of partially lithified sediments flowing without constraining overburden. He asserts that there should be clearly defined differences in the resulting deformation styles observed in outcrop.

Mediterranean tectonic mélanges are monomict. The shared deformation history of the mélange entity is demonstrated by uniformity of shear direction, clast morphology and orientation, metamorphic continuity and the presence of pseudo bedding and matrix banding. Diagnostic micro- and meso-features able

to indicate a tectonic mélange or olistostrome are probably only observable in detailed field study (Camerlenghi and Pini, 2009).

Diapirism — diapiric mélanges

There is a growing body of literature linking subduction zone mantle wedge convection, mud volcanoes and diapirism with the development of mélanges within accretionary prisms based on the study of currently active margins. Mud diapirs or mud volcanoes form where subsurface water, gas and mud are mobilised forming structures up to tens of kilometres in diameter and a few hundred meters thick (Kopf, 2002). Westbrook and Smith (1983) found during investigation of the Barbados Ridge that overpressured pore fluids within sediments on the downgoing plate were forced to migrate seaward by the proximal weight of the accretionary prism, exploiting sub-horizontal permeable boundaries. Mud volcanoes formed at the surface where distance from the overburden allowed the upward migration of pore fluids, causing disaggregation, mixing with sediments (and biogenic gases) and finally vertical expulsion (Kopf, 2002; Westbrook and Smith, 1983). Diapirism due to elevated pore pressure is common in Indonesia in the Banda forearc which is in collision with the Australian plate. Here mud volcano fields are found landward of the leading subduction thrust (Silver *et al*., 1986), where overpressured impermeable shales are subject to thrusting (Masson *et al*., 1991). These cylindrical features disrupt basin sediments but once incorporated into the accretionary prism they become elongate in plan form and the deformed sediments become indistinguishable from otherwise folded wedge material (Silver *et al*., 1986). In a comparative study of two mélanges in the Neogene Hoh accretionary complex, Washington, the identification of a diapiric and a tectonic mélange was made using field

criteria (Orange, 1990). The diapiric Duck Creek mélange showed evidence of radial control on the spatial distribution of variably rounded clast forms, clast deformation and matrix fabric as well as opposing vergence directions on opposite margins. In contrast, the tectonic Hogsback mélange contained mostly phacoidal clasts with rare angular bodies aligned coherently within the uniform well-developed mélange fabric and consistent vergence (Orange, 1990).

The field relationships and deformation structures within three discrete but interrelated Tertiary units that form a composite mélange in the Italian Piedmont Basin are interpreted individually as formed by tectonic, sedimentary and diapiric processes (Dela Pierre *et al*., 2007). The tectonic mélange is identified by stratigraphic repetition, block-in-matrix texture and consistent shear direction within the matrix fabric, the latter consistent with the orientation of the mélange body as a whole. The sedimentary mélange which overlies the tectonic unit, is marked by the random orientation and distribution of clasts of varied angularity within a muddy matrix. A lack of heterogeneous fabric in the sedimentary mélange clearly contrasts with the pervasive deformation of the tectonic mélange. The 10 m wide diapiric mélange pierces both the sedimentary and tectonic mélanges and is characterised by radial deformation: arcuate axial traces of asymmetrical folds, clustered angular clasts and indicators of opposing shear directions at opposite boundaries of the diapir. In addition, evidence for methane-rich diapir fluids is found nearby in several mélange clasts of authigenic carbonate (Dela Pierre *et al*., 2007).

In a thorough review of the abundant mélange deposits of all genetic types in the Mediterranean region Camerlenghi and Pini (2009) show that the three mélange types are intimately related by describing a series of composite mélange sequences where tectonic, olistostrome and diapiric sections are both identifiable and interrelated. They assert in conclusion that mud diapirs, mud

volcanoes, submarine slides and tectonic mélanges are all associated with the formation of olistostromes within the evolution of both passive and active margins prior to the onset of collisional orogeny.

Potential genetic mechanisms for the Gwna mélange

Greenly (1919) characterised the Gwna Group mélange as an autoclastic fault breccia: a regional scale, tectonically derived, cataclastic rock unit and coined the term mélange for this deposit. Later work revised this assessment, suggesting the mélange was sedimentary (Shackleton, 1954b). From the 1970s, at the advent of plate tectonic theory, alternative regional interpretations arose of an ensialic collision zone, subduction and subsequent accretionary orogen: all gave pivotal significance to the proximity of the Gwna mélange with the Anglesey greenschist and blueschist units, along with the juxtaposition of contrasting bedrock geology to the south of the complex MSFS, thought to be a tectonic suture (Wood, 1974; Barber and Max, 1979; Gibbons, 1987; Kawai *et al*., 2007; Kusky *et al*., 2013). In contrast, several authors, who find a lack of evidence for subduction, have supported a transpression driven, oblique accretionary model derived from geochemical, geophysical and structural field evidence (Kohnstamm and Mann, 1981; Nutt and Smith, 1981; Gibbons, 1983a; Phillips, 1991b; Horák *et al*., 1996).

Comparing the Gwna Group with published mélange characteristics (Hsü, 1968; Abbate *et al.*, 1970; Hsü, 1974; Hibbard, 1979; Silver and Beutner, 1980; Cowan, 1985; Cloos and Shreve, 1988; Raymond, 1984; Raymond and Terranova, 1984; Shreve and Cloos, 1986; Silver *et al.*, 1986; Orange, 1990; Cousineau and St-Julien, 1992; Robertson, 2000; Kopf, 2002; Şengör, 2003; Huang *et al.*, 2008; Camerlenghi and Pini, 2009; Cavazza and Barone, 2010; Festa *et al.*, 2010; Dilek

et al., 2012; Barber, 2013) allows testing of the genetic hypotheses for the Gwna Group mélange (Table 1.2). The table was designed for systematic comparison. Worldwide mélange characteristics, on all scales, were extracted from the publications and built into a framework used to interrogate the Gwna mélange asking a single question: is a classification of the broad genetic mode signposted in the regional outcrop? Table 1.2 lists diagnostic properties of the Gwna mélange with the aim of measuring the results against existing research to determine whether any potential mélange formation processes could be ruled out. This method was also used to distinguish between primary mélange features, which could elucidate the genetic history, and overprinted features – by definition, superimposed by later events and unrelated to primary nature. Highlighted characters are found in the Gwna mélange and these are discussed throughout Chapter 2.

Table 1.2 confirms the Gwna Group is not a diapir, neither as a whole nor the mélange sections within the group. The two diapiric characters present are also diagnostic of olistostromes. Diapiric mélanges are mud volcanoes fundamentally characterised by cylindrical 3D form and radial internal attributes — dictated by the violent release of subsurface pore fluid pressure that disrupts overlying strata. These effects are distributed around a central fulcrum, creating a radial internal stratigraphy. The overall body morphology of the Gwna Group cannot be determined with certainty from the existing disrupted outcrop. Although nothing indicates a cylindrical deposit an asymmetrical body form is likely, pinching out to the north. Diapiric mélange formation is eliminated.

The characteristics of tectonic mélanges include faulted lower and upper contacts as well as tabular body morphology (Table 1.2). These combine into a defining set of requirements for a mélange formed by tectonic slicing in subduction-driven accretion, yet none are primary properties of the Gwna

mélange. There are upper faulted contacts of the Gwna Group, potentially related to the Taconic or Caledonian orogenies, some of which are associated with displacement on the Menai Straight Fault System (Matley, 1928; Nutt and Smith, 1981; Gibbons, 1987). The faulting has removed some of the primary relationships and as such, is not relevant to the group's genetic history. Chapter 2 contains descriptions of Gwna Group basal and upper unconformable sedimentary contacts.

Metamorphic continuity is also essential for a tectonic mélange – the formation processes affect clasts and matrix contemporaneously. This is not the case in the Gwna mélange: metamorphosed clasts are commonly surrounded by matrix that is unaltered. For example, psammite and metacarbonate clasts are commonly co-located with unmetamorphosed clasts in a mud matrix that is not recrystallised. The mélange genetic test scheme demonstrates that the Gwna mélange is definitively not a tectonic mélange: it was not formed by subduction.

The Gwna Group and mélange formed through sedimentary processes.

Table 1.2 → Mélange genetic testing scheme compiled with extracted data from publications about a variety of mélanges worldwide – citations list on page 29. **A.** Mélange genetic testing scheme. Properties used to distinguish between three possible mélange emplacement modes. **B.** Comparison of the summary stratigraphic and general properties of the Gwna Group with the testing scheme indicates a sedimentary mode of emplacement. Tectonic and diapiric modes are shown to be impossible. **C.** A comparison of meso-scale internal properties within the Gwna mélange component of the Gwna Group with the testing scheme strongly indicates a sedimentary origin. Although there are some properties that could indicate a sectonic or diapiric genesis, the Gwna mélange properties that are diagnostic in diapiric mélanges are those also found in olistostromes. All Gwna mélange properties found in tectonic mélanges are also indicative of olistostromes, or, alternatively, are overprinted, non-primary features which cannot pertain to the genetic history. Table 1.2B/C is an abbreviated version of table 2.2, which summarises the data described in the context of the evidence described in Chapter 2.

A

	Properties	Olistostrome (sedimentary mélange)			Tectonic mélange		Diapiric mélange	
Stratigraphic properties	Nature of lower contact	Gradational	Sharp sedimentary		Faulted		Cross-cutting	
	Nature of upper contact	Gradational	Sharp sedimentary		Faulted		Cross-cutting	
	Metamorphic continuity	Clasts and matrix same metamorphic grade	Clasts of varied metamorphic grade	Inconsistent metamorphic grade throughout mélange	Consistent metamorphic grade in clasts and matrix	Mineral banding continuity between clasts and matrix		
	Mélange body morphology	Chaotic	Pinched out		Tabular	Uniform thickness	Cylindrincal	
Internal properties	Clast supported	Yes	No	Bimodal				
	Clast spatial distribution	Inverse graded	Not graded		Not graded		Radial control on grading	
	Clast morphology	Isometric			Triaxial (flattened)			
	Clast angularity	Rounded	Angular		Rounded		Rounded (radial control)	Angular (radial)
	Clast basinal derivation	Native	Exotic		Exotic			
	Clast types present	Single lithofacies per clast	Broken formation within clasts	Ghost stratigraphy present	Monomict			
	Clast types present	Highly variable - contains exotics	Polymict		Monomict		Polymict*	
	Clast auto brecciation	Boudinage	In-situ shearing	Synsedimentary slumping	Boudinage	In-situ shearing	Radially controlled deformation	
	Clast alignment	Random	Lithologically controlled	Transport controlled	Uniform	Lithologically controlled		
	Transport direction	Cleavage	Clast tails	Debris flow run out	Unidirectional		Radially controlled	
	Matrix supported	Yes	No	Bimodal	Yes	No	Bimodal	Clasts in clusters
	Matrix injection	Around clasts	Intraclastic	Between boudins	Around clasts	Intraclastic		
	Matrix composition	Argillaceous	Polymict	Microbreccia	Banded?	Monomictic		
	Mud matrix basinal derivation	Native			Exotic			
	Synsedimentary fault-controlled stratigraphic repetition	Not present			Present		Not present	
	Metamorphic continuity	Consistent metamorphic grade in clasts and matrix	Clasts of varied metamorphic grade		Consistent metamorphic grade in clasts and matrix	Mineral banding continuity between clasts and matrix		

	Properties	Olistostrome (sedimentary mélange)			Tectonic mélange		Diapiric mélange	
B Gwna Group	Nature of lower contact	**Gradational**	**Sharp sedimentary**		Faulted		Cross-cutting	
	Nature of upper contact	Gradational	**Sharp sedimentary**		**Faulted**		Cross-cutting	
	Metamorphic continuity	Clasts and matrix same metamorphic grade	**Clasts of varied metamorphic grade**	**Inconsistent meta-grade throughout mélange**	Consistent metamorphic grade in clasts and matrix	Mineral banding continuity between clasts and matrix		
	Mélange body morphology	Chaotic	Pinched out		Tabular	Uniform thickness	Cylindrincal	
C Gwna mélange	Clast supported	Yes	No	**Bimodal**				
	Clast spatial distribution	**Inverse graded**	**Not graded***		**Not graded***		Radial control on grading	
	Clast morphology	Isometric			Triaxial (flattened)			
	Clast angularity	**Rounded***	Angular		**Rounded***		Rounded (radial control)	Angular (radial)
	Clast basinal derivation	**Native**	**Exotic***		**Exotic***			
	Clast types present	**Single lithofacies per clast**	Broken formation within clasts	Ghost stratigraphy present	Monomict			
	Clast types present	Highly variable - contains exotics	**Polymict***		Monomict		**Polymict***	
	Clast auto brecciation	**Boudinage***	**In-situ shearing***	**Synsedimentary slumping**	**Boudinage***	**In-situ shearing***	Radially controlled deformation	
	Transport direction	Cleavage	Clast tails	Debris flow run out	Unidirectional		Radially controlled	
	Matrix supported	Yes	No	**Bimodal***	Yes	No	**Bimodal***	Clasts in clusters
	Matrix composition	**Argillaceous**	Polymict	**Microbreccia**	Banded?	Monomictic		
	Mud matrix basinal derivation	**Native**			Exotic			
	Metamorphic continuity	Consistent metamorphic grade in clasts and matrix	**Clasts of varied metamorphic grade**		Consistent metamorphic grade in clasts and matrix	Mineral banding continuity between clasts and matrix		

Commonly present
Commonly present* - property shared by different mélange types
Present, but not common
Not present
Present but overprinted: not a primary feature

1.7 Summary of outstanding questions

There is broad consensus in the literature that the Monian Supergroup formed in an accretionary setting, probably related to the development of the Iapetus Ocean but the mode of emplacement of the Gwna Group is far from agreed. Uncertainty exists regarding the age of deposition and there has been no consideration of the number of events the Gwna Group deposits represent: was there one event or a series of events triggered in a developing scenario? The lower Monian Supergroup Holy Island Group is proximal and the New Harbour Group is turbiditic (Phillips, 1991a, 1991b) and contains evidence for periodic unstable slope environments in the coarser lithofacies (Schuster, 1980) which may be consistent with the early stages of collision leading towards a catastrophic palaeoslope collapse.

Questions to be addressed and the intentions of this study include:

- Examining the field evidence to establish understanding of the Gwna Group, both as a whole and any constituent parts. Is the Gwna Group chaotic and indescribable? Or is there order — a pattern that can be understood?
- What are the relationships between any constituent parts of the Gwna Group?
- Open-minded comparison of the field evidence with described successions in the literature to develop a realistic emplacement model.
- Use published material to fit any emplacement model within a framework of known tectonic events.

The Gwna Group is in a highly disrupted state and any attempt to describe it needs a considered approach. Four outcrop belts have been chosen as representative of the stratigraphic bounds within which the Gwna Group was deposited. Wherever possible, the outcrop belts (Fig. 1.1) contain a lower contact with Gwna Group deposits up to an upper contact. This is not possible in all belts, for example, Lleyn (outcrop belt 1) has no exposed lower contact and the upper part of the Gwna Group is faulted into the Lleyn Shear Zone. It is included in this study however, as the exposure is widespread. Outcrop belt 2, south-west Anglesey, has exposure of a folded basal contact but very limited upper contacts. Outcrop belt 3, north-west Anglesey has excellent basal contact exposure but limited outcrop of the upper relationship. Outcrop belt 4, north Anglesey contains good outcrop of both lower and upper relationships. By combining all four outcrop belts, a coherent, albeit disrupted, Gwna Group succession can be examined, and relationships extrapolated, if the results allow. There is further Gwna Group outcrop on Anglesey, but these exposures are in minor faulted sections, where the primary stratigraphical relationships are not displayed. Such sections have been excluded from the reporting of this study as they do not contribute to the depositional framework of the Gwna Group.

The aim of this study is to create a full depositional framework that encompasses:

- classification of the depositional environment and sedimentary process of the Gwna mélange and the Gwna Group from primary sedimentary characteristics exhibited in outcrop.

- clarify the lithostratigraphic hierarcy of the Gwna Group.

- constrain the depositional age of the Gwna Group.

- constrain the provenance of the Gwna Group.

- develop a depositional framework that combines evidence from this study with the existing literature.

Chapter 2

THE PROCESS SEDIMENTOLOGY OF THE GWNA GROUP

First appearances suggest the Gwna Group is a chaotic deposit (Fig. 2.1), devoid of pattern and lacking even basic sedimentary features such as discernible bedding planes and way-up criteria. In consequence, many accessible Gwna mélange localities attest to Edward Greenly's description; *"…quartzite, limestone, diabase and jasper, ripped away from the beds between which they originally lay,..torn and rubbed into phacoids or ellipsoids, have been driven in among the wreckage of the alternating grits and phyllites; producing a many-coloured mélange that is really indescribable, and must be seen in the field to be envisaged*." (Greenly, 1919, Vol. 1, p. 306).

Fundamental to this study is the view that fieldwork should provide a clear conclusion to the open questions about the genetic history of the Gwna Group and the Gwna mélange component: by which process was it created and under which tectonic setting did those processes operate? It has been shown (section 1.7) that the Gwna Group is sedimentary, but what evidence exists for the process sedimentology involved in the fragmentation and transport of the clasts and their subsequent emplacement into the mélange?

The aims are, first, to examine the Gwna Group and the subordinate Gwna mélange within the group, to establish whether systematic pattern can be determined, whether identifiable lithofacies exist and, whether any such pattern

---

Figure 2.1 → Structureless Gwna Group mélange. **A.** A view to the north-east: from Llanbadrig Point (SH 374 947) to the distant overstep at Ogof Gynfor (SH 378 948) shows polymict debris flow outcrop typical of lithofacies C in outcrop belt 4. **B.** Porth Twyn-Mawr (SH 363 658), facing north-west: well-preserved outcrop of a clast-supported megaconglomerate debris flow horizon in outcrop belt 2. One metre rule for scale.


A


B

relates to recognised surface processes. Current understanding is that a sedimentary mélange may be created in a variety of tectonic settings. Therefore, this chapter investigates whether there is pattern within the Gwna Group mélanges that can reveal the specific mode and environment of deposition.

The second aim of this chapter is to consider whether or not the Gwna Group was formed in a single event: given that the Gwna mélange is likely to be an olistostrome, was it formed following a catastrophic collapse on a regional scale or in a sequence of related events within either a discrete period, or over extended time? Thirdly, there is a need to differentiate between primary and subsequently overlaid characters as there is confusion in the literature. There are primary features, of course related to genetic history, and others that pertain to subsequent geological events: both are important in developing a full understanding of the regional geological history, but only the former can offer evidence for the framework within which the sedimentary Gwna Group was deposited.

Authors who have studied the Gwna Group and considered it to be a sedimentary deposit, at least in part, include:

- Matley (1928) recognised thinly bedded mudstones in association with undifferentiated autoclastic mélange in Lleyn and called them Aber Geirich Phyllites.
- Shackleton (1954a) noted the sedimentary nature of the Gwna Group generally and highlighted specific localities where sections of outcrop are decipherable. He estimated the total thickness of the Gwna Group to be 3 km (Shackleton, 1969; Shackleton, 1975).
- Schuster (1979; 1980) studied three localities: Cemaes Bay, north Anglesey, a small section of the coast south of Aberffraw and Bardsey

Island, Lleyn. He concluded the Gwna Group was a < 10 km thick olistostrome formed at an unstable continental margin in a putative late Precambrian subduction zone.

- Gibbons and Ball (1991) found an absence of coherent internal stratigraphy in the Gwna Group mélange.

The Gwna Group today, is highly disrupted. Recognisable stratigraphic sections are fragmentary, and this imposes a limit on what can be achieved in terms of conventional sedimentological analysis. It is, for example, difficult to log in a meaningful way and there is a complete lack of distinctive horizons that might allow correlation between the outcrop belts. Despite the inherent difficulties, this chapter is focussed on what can be understood of the genetic history through new observations made in the following text, including:

- Detailed descriptions of three basal unconformities
- Identification of three major lithofacies
- Demonstration of important sedimentary features
- Illustrations of lithofacies associations

The above are consistently present within the Gwna Group on Anglesey and the Lleyn Peninsula.

Table 2.1 → Estimated thickness of the Gwna Group in the four outcrop belts on Anglesey and Lleyn. The stratigraphy is highly disrupted, and this cannot therefore be considered robust.

Gwna Group Thickness estimate	Notes	Gross dip estimate	Folding?	Faulted repetition?	Estimate of thickness
Outcrop belt 1 Lleyn Peninsula Southern section - south of Porth Oer	The southern Lleyn outcrop is folded and networked with faults on varied scales, some of which related to the Lleyn Shear Zone, to the east.	40 - 90º NE 40 - 90º SW	Yes, fold axes orientated between N to S and SSW to NNE	Probably	1800 m
Northern section - north of Porth Oer	The northern Lleyn section dips NW to N between 60 and 90º. Large sections are subvertical. Small sections are overturned, but young to NW	~ 010/65 - 80º NW	Yes	Possibly	1500 m
Outcrop belt 2 South-west Angelsey	Mostly subvertical with tight folds	~ 85º SE/NW	Yes, fold axes orientated SW to NE	Locally	2000 m
Outcrop belt 3 North-west Anglesey	Beds in the lowest section dip ~ 40-45ºNNE, from Porth Trefadog to Church Bay dip is 15-22º NE	~ 18º NE	Yes, but the main coastal section is contained within one limb	Locally - minor	650 m
Outcrop belt 4 North Anglesey	Turbidites are subvertical - young to north. Debris flows are variably orientated with sometimes less dip angle - consistently northwards younging	~ 85º N	Locally	Yes - the eastern section only - from Cemaes to Bull Bay	850 - 1000 m

There is further discussion of an additional group of ocean floor lithologies: gabbro, basalt, pillow basalt and interstitial jasper and carbonate, which occur in combination within the sedimentary architecture, albeit in restricted areas.

Estimating thickness, as can be seen from the variation in the historical estimates above, is not a simple matter due to the deformed and fragmented condition of the outcrop. An estimate is made here (Table 2.1) but it cannot be considered fully robust: there is overprinted stratigraphic repetition within outcrop belts and it is impossible to say whether or not there is repetition of the stratigraphy between some outcrop belts. It is safe to say that outcrop belts 3 and 4 do not repeat what is seen in 1 and 2, as will become clear, but there may be duplication between 1 and 2, which are situated in part within the complex MSFS (Fig. 2.2).

2.1 The physical evidence

The siliciclastic Gwna Group consists of a restricted group of lithofacies that crop out intermittently on Anglesey and occupies much of the north-western coast and tip of the Lleyn Peninsula. For this study, the area is subdivided into four outcrop belts (Fig. 2.2) of stratigraphic continuity. Although the basal and upper contacts are not consistently seen, the four outcrop belts combined, between lower and upper bounding surfaces, provide an opportunity to clarify both the internal sedimentology of the Gwna Group including the sedimentary

---

Figure 2.2 → Geological map of the Monian Supergroup and associated Precambrian to lower Palaeozoic rocks in Anglesey and north-west Wales (map after Greenly 1920, Gibbons, 1987 and British Geological Survey Anglesey map currently in production). The four outcrop belts of Gwna Group and related stratigraphic units that form the basis of this study are noted, as are major fault lines. The insert tabulates the framework of basal and upper contacts that crop out, providing a framework in the region.

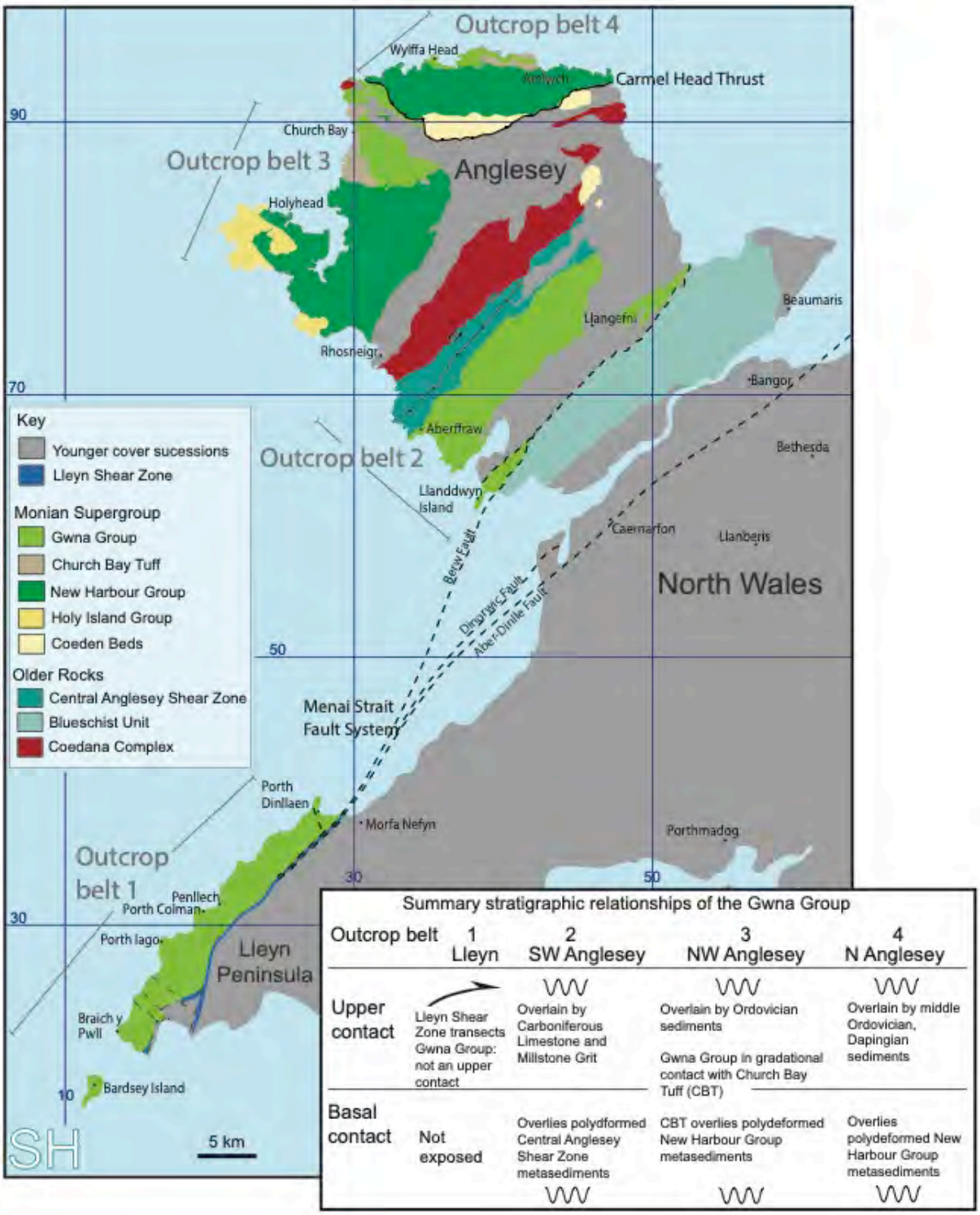

Summary stratigraphic relationships of the Gwna Group

Outcrop belt	1 Lleyn	2 SW Anglesey	3 NW Anglesey	4 N Anglesey
Upper contact	Lleyn Shear Zone transects Gwna Group: not an upper contact	Overlain by Carboniferous Limestone and Millstone Grit	Overlain by Ordovician sediments Gwna Group in gradational contact with Church Bay Tuff (CBT)	Overlain by middle Ordovician, Dapingian sediments
Basal contact	Not exposed	Overlies polydformed Central Anglesey Shear Zone metasediments	CBT overlies polydeformed New Harbour Group metasediments	Overlies polydeformed New Harbour Group metasediments

mélange within, but also its stratigraphic position in the context of the Monian Supergroup. Additional small fault-bound sections of the Gwna Group that occur beyond the four identified outcrop belts in the region are out of stratigraphic context and are therefore not included in this analysis as they provide limited insight, being dislocated from the associated underlying and overlying geology. Between the four sections there are many shared features and others that are geographically limited. However, when considered collectively, the four outcrop belts provide a coherent view of the whole Gwna Group sedimentary system (Fig. 2.2).

Successful research into polymict mélanges in the field is recognised to be dependent on continuous outcrop: mapping practices considered standard for laterally extensive stratigraphic units can lead to misguided assumptions and incorrect interpretations if applied to mélanges (Hsü, 1968). For example, working around ground cover is manageable for laterally and stratigraphically extensive rock units, but is not advisable where mélanges are concerned. All field work in this study is concentrated on coastal outcrop.

The Gwna Group is mostly anchimetamorphic, with very low grade metamorphic rocks exhibiting secondary alteration to the point at which diagenesis becomes metamorphism (Árkai *et al*., 2007). There is a locally developed schistosity throughout the Gwna Group which provides evidence for post-depositional deformation: for example, siliciclastic schists of the Gwna Group juxtaposed to the south with plutonic rocks and gneisses of the Sarn Complex, comprise the early Cambrian Lleyn Shear Zone (Gibbons, 1983b) – a greenschist facies band that locally achieves higher metamorphic grade (glaucophane greenschist facies and mylonitic texture (Gibbons, 1983b)) transects the Gwna Group on the Lleyn Peninsula marking the contact between the Gwna Group and younger Ordovician sediments. In the wider region

deformation has, however, rarely changed the appearance of clasts within the mélange matrix – throughout individual clasts remain distinct from the matrix in respect of texture, colour, competence, relief and sometimes orientation. This is also true of the matrix: whether it is mud-, silt- or sand-grade there appears to be no recrystallisation that alters the grainsize. The few exceptions, where competent clasts are smeared into the matrix, are noted in the text below.

Despite the deformation, many primary features are retained, and this chapter considers the sedimentary protoliths and key features in an attempt to reveal the depositional framework by isolating the primary from the overprinted characteristics and therefore sedimentary terminology is used throughout to maintain clarity and enable comparison between localities and outcrop belts.

The field study results are presented in this chapter by describing each of the main lithofacies found throughout the Gwna Group. Subsequently, the facies associations are discussed by outcrop belt, first considering outcrop belts 3 and 4, both of which are located in the northern half of Anglesey, beyond the direct influence of the MSFS. The two outcrop belts associated with the MSFS are considered next: outcrop belt 2, which is the most deformed and fragmented section studied and finally outcrop belt 1. This running order may seem curious, particularly when considering that it runs broadly backwards through geological time from the youngest sediments to the oldest, but the presentation structure is so ordered to establish first a clearer illustration of the least disrupted sediments which can then be built upon by consideration of the more deformed rocks exposed to the south.

Lithofacies analysis

The Gwna Group unconformably overlies polydeformed metasedimentary rocks of the CASZ and the New Harbour Group in outcrop belts 2, 3 and 4. The base of outcrop belt 1 is not exposed. Outcrop belts 2, 3 and 4 are unconformably overlain by middle Ordovician marine sediments and outcrop belt 1 is transected by the Lleyn Shear Zone, the subaerial trace of the MSFS, which marks a sheared contact between the Gwna Group sediments and Sarn Complex volcanic rocks, both overlain unconformably by middle Ordovician sediments (Gibbons, 1983b).

The Gwna mélange represents a subordinate volume of the Gwna Group. This study separates the Gwna Group into three main lithofacies, which include the mélange and show the internal characteristics of each facies as well as the relationships between them, as they occur consistently throughout the four outcrop belts.

The sedimentary lithofacies that comprise the Gwna Group are listed below in descending order of prevalence.

Lithofacies A

Laminated to finely bedded mudstone to heterolithic mud-siltstone

Thick sedimentary sequences dominated by laminated or finely bedded mudstone to heterolithic mudstone - siltstone are ubiquitous in all outcrop belts of the Gwna Group (Fig. 2.3A - F). The sediments are distinctively green, parallel-bedded between 2 and 8 cm thick, with sharp tops and some evidence of normal grading within a restricted grain size distribution. Mildly erosive contacts exist in

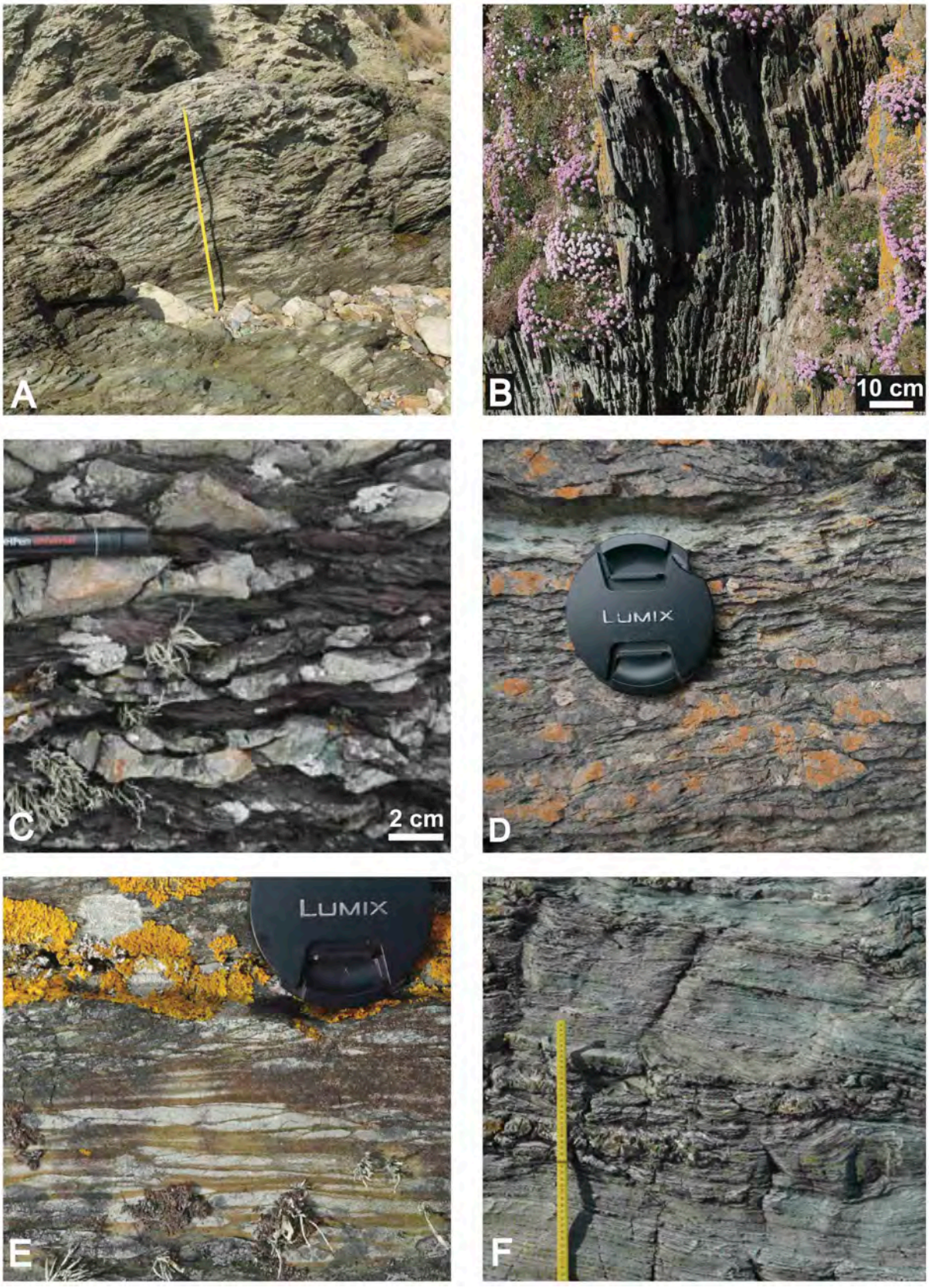
A
B
10 cm
C
2 cm
D
LUMIX
E
LUMIX
F

Figure 2.3 ←Lithofacies A - laminated mud to finely bedded heterolithic sediments interpreted as turbidites. **A.** Buff-green weathered, laminated heterolithic turbidites, at Wylfa Head (SH356 943), outcrop belt 1. One metre rule for scale. **B.** Vertically orientated green weathered laminated silt-mud turbidites, at Pen y Parc (SH368 650), outcrop belt 2. **C.** Red weathered laminated mudstone interbedded with thin silt channels. Braich y Pwll (SH135 255), outcrop belt 1. **D.** Buff-green weathered side-by-side minor silt channels with interbedded laminated mudstone, west of Aberffraw (SH345 676), outcrop belt 2. 6 cm lens cap for scale. **E.** Laminated heterolithic turbidites, south of Porth Cadwaladr (SH361 659), outcrop belt 2. 6 cm lens cap for scale. **F.** Laminated mudstone turbidites, with intermittent, disrupted silt channels, near Borth Wen (SH268 410), outcrop belt 1. Visible length of rule is 45 cm.

Figure 2.4 → Discrete scoured channels in lithofacies A. **A.** Flat topped, pink arenite channel 2.2 m long x < 75 cm thick (partially seen) with a graded mud/sandstone base cut into finely bedded turbidites with numerous smaller channels beneath – composed of arenite and siltstone with a mud matrix. This section is folded and youngs to the north-west - top left of the image. Porth Twyn-Mawr (SH363 658), outcrop belt 2. Hammer length 28 cm. **B.** Sand – siltstone channels composed of pink arenite and siltstone with green mud matrix scoured into laminated to finely bedded turbidites. Younging direction to the north-west. Penllech Beach (SH196 343), outcrop belt 1. **C.** "Winged" carbonate channel, or starved gutter cast with pink arenite channel alongside in a laminated mudstone – heterolithic succession. Penllech Beach (SH196 343), outcrop belt 1. **D.** Siltstone and minor carbonate channels (left) in laminated mud-heterolithic strata. Penllech Beach (SH208 356), outcrop belt 1. **E.** Buff-weathered mud-silt laminated beds with 80 long x 40 cm thick siltstone channel with mud matrix, overlain by thinly bedded siltstone. Penllech Beach (SH204 344), outcrop belt 1. **F.** Stacked thin pink weathered arenite bodies of a composite channel. Twyn Maen Mawr (SH138 252), outcrop belt 1.

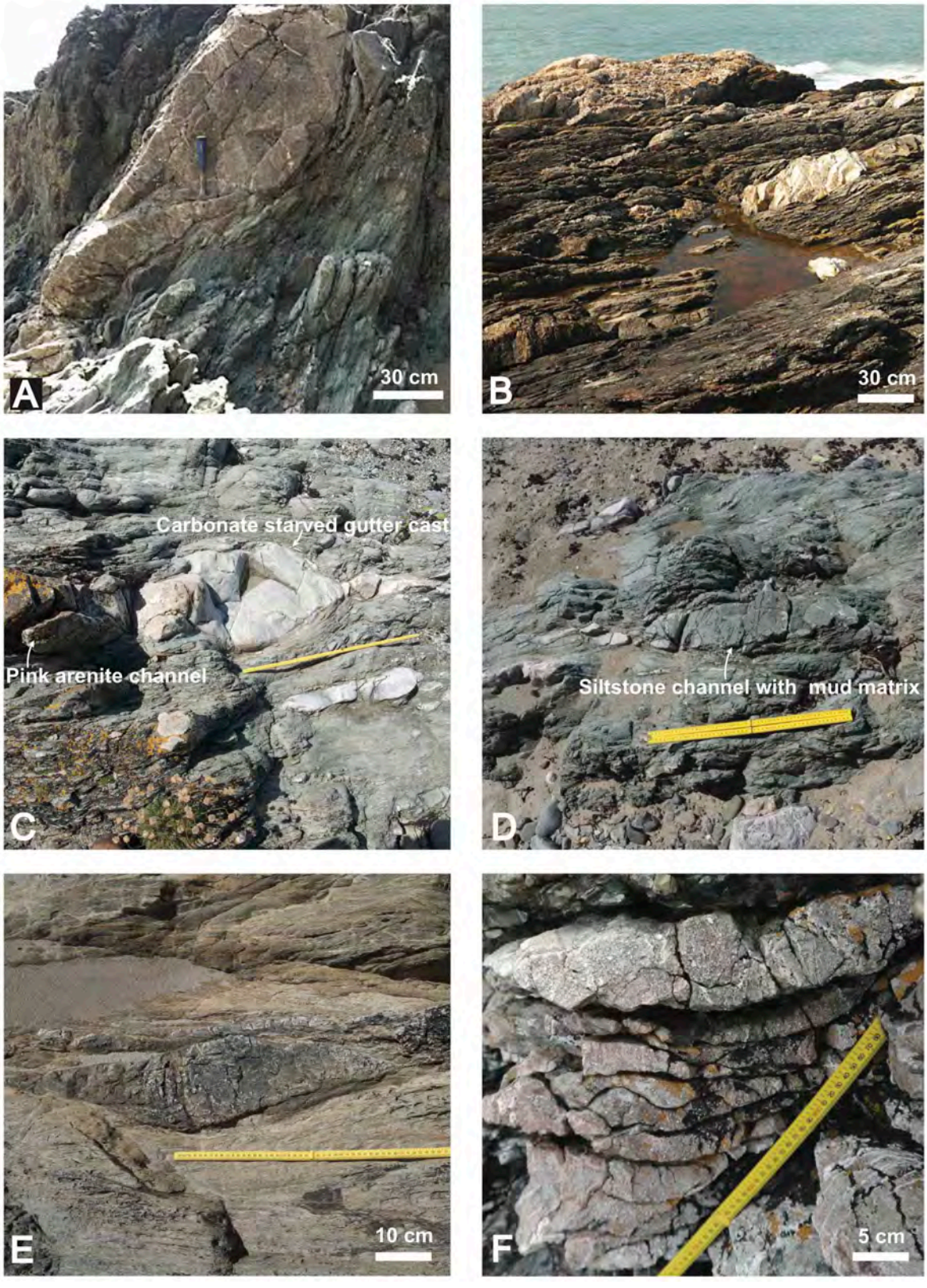
A
30 cm
B
30 cm
Carbonate starved gutter cast
Pink arenite channel
C
Siltstone channel with mud matrix
D
E
10 cm
F
5 cm

cases where silt forms the base of a bed or channel (Fig. 2.3C) and with fining upwards, returning to mud over a centimetre or two. Alternatively, prominent silt beds of one to two centimetres thickness are interbedded with weathered-out mud laminae in sequences several metres thick (Fig. 2.3F). These repeated silt layers have poor lateral continuity (Fig. 2.3C, D and E) – they take the form of a side-by-side series of lensoid, or thin channels, each 20 to 30 cm wide. There are some grey-white weathered, fine sand to silt beds that are extensive: 8 – 15 cm thick, mildly erosive bases, flat tops and some fining upwards can be observed.

White - green silt channels which consist of quartz grains in a green mud matrix, 5 – 15 cm wide and 2 – 5 cm thick are commonplace (Fig. 2.4D) and so too are conspicuously pink erosive, quartz arenite sand channels, of medium to coarse grains (Fig. 2.4A, B, C and E). The latter are larger: commonly 20 – 60 cm wide and 8 – 30 cm thick but they can be as small as 8 cm wide by 2 cm thick and extend to 4.5 m width and 1.3 m depth and may consist of stacked, thin channels – each of which is topped by up to a centimetre of green mud: 8 to 15 of these can make-up a composite sand channel (Fig. 2.4F). Rare larger channels are composed of very coarse-grained sand containing up to medium pebble grains within a green-grey mud matrix. Alternatively, and less frequently, the channels have an aspect ratio of 1:1 or 1.2:1, where channel depth is more-or-less equal to width and the two-dimensional cross-section takes the form of a winged channel (Fig. 2.4B and C). These isolated sand bodies are almost always devoid of internal sedimentary structure, apart from limited normal grading and very rarely, ghost cross-stratification. Pink- or white-weathered, abiotic carbonate channels of similar physical form and size (Fig. 2.4C) supplement the sand channels in certain sections and they too lack convincing internal structure. It is interesting to note that sand and carbonate channel forms can be positioned a

few metres along strike from each other but there is no mixing of these two lithologies in any channel.

In outcrop belt 2, there are two sizeable sand-rich zones, each about 12 m thick (Fig. 2.5D), which take the form of repeated, normally graded medium- to fine-grained quartz greywacke in beds between 20 – 60 cm thick, some of which are laterally extensive but most pinch out over 3 – 4 metres, overlain by mud laminae typically 3 – 5 cm thick. Alternatively the sandstone is interbedded with < 60 cm thick debris flows (Fig. 2.5F). Similarly, stratigraphy of a more coarse-grained character is also found in outcrop belt 1 (Fig. 2.5A, B, C and E). In outcrop belt 3, there is a succession of laterally extensive, sand-rich beds exposed on the north-west Anglesey coast, each up to 1 m thick, with erosive bases and flat tops, interbedded with finer grained, silt and mud laminae.

All the silt and sand of this lithofacies, with the exception of the clean, pink arenitic channels, is mixed with a green-grey mud matrix – it is the same mud that comprises the laminated sections. There is subtle variation in the mud content, both within and between outcrop belts, in that the weathered colour varies between green, to green-grey or buff-yellow-green and rarely, red-brown.

Figure 2.5 → Subordinate sand-rich horizons within lithofacies A. **A.** Folded, metre scale, graded sand beds overlying mud-silt finely bedded turbidites, south coast of Braich y Pwll (SH137 244), outcrop belt 1. One metre rule for scale. Facing north. **B.** Decimetre-scale sand-rich beds overlying mud-silt turbidites, Braich y Pwll (SH137 244), outcrop belt 1. Facing east. **C.** Fining upwards succession. Graded siltstone beds < 8 cm thick pass upwards to thinly bedded siltstone, each graded to mudstone between layers. Braich y Pwll (SH136 236), outcrop belt 1. Hammer length 28 cm. **D.** Open folding in metre scale sand-rich graded beds, overlying mud-dominated finely bedded turbidites. North of Porth Cadwaladr (SH359 667), outcrop belt 2. **E.** Narrow sand-rich horizon south of Borth Wen (SH262 403), outcrop belt 1 that consists of near laterally continuous silt – fine sandstone channels 20 - 40 cm thick. **F.** Sand-rich beds, marked A, with interbedded < 1 m thick polymictic conglomerate horizons. Some conglomerate clasts are outlined with orange. North of Porth Cadwaladr (SH359 667), outcrop belt 1. One metre rule for scale.

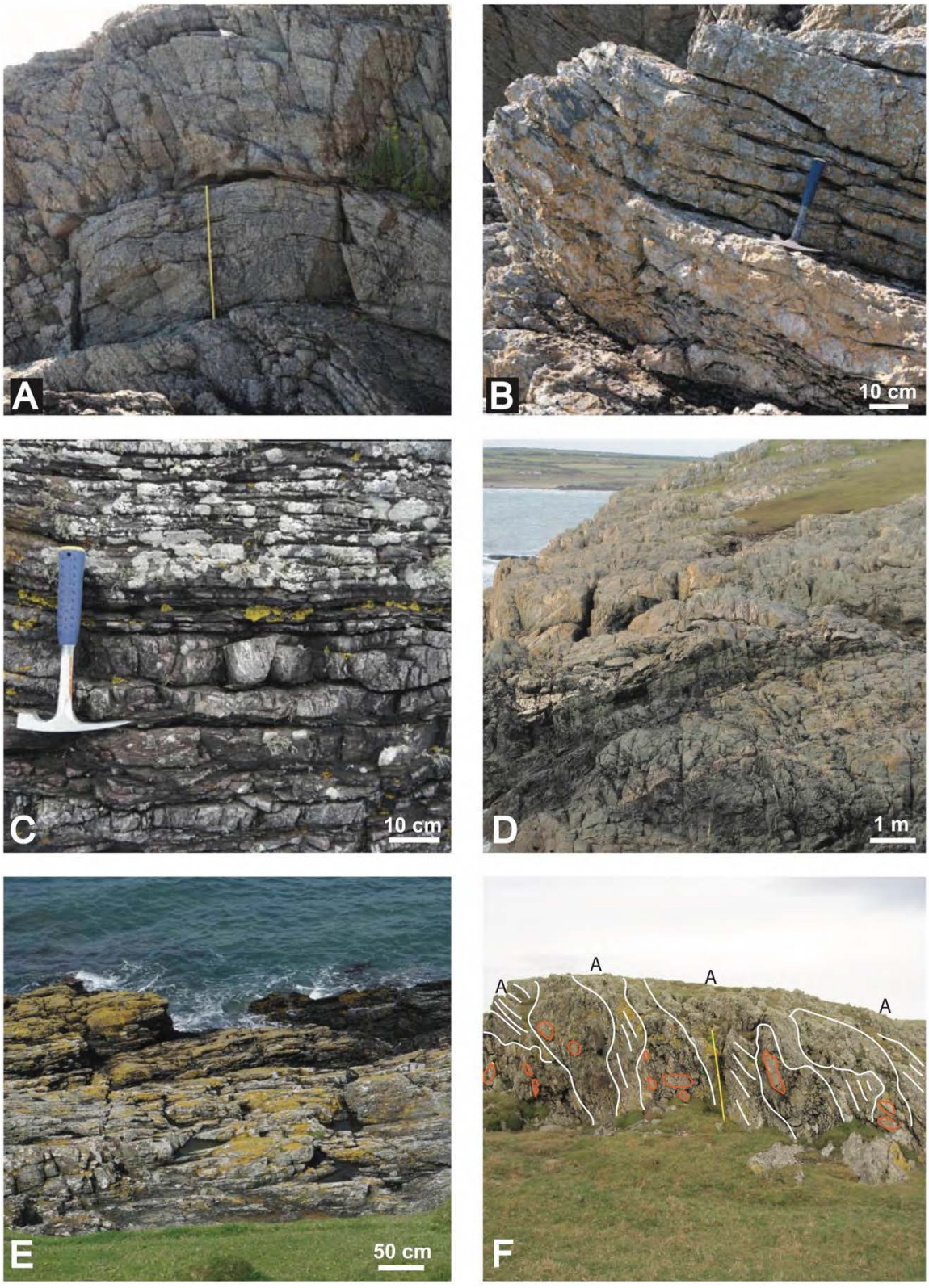
A
B
10 cm
C
10 cm
D
1 m
E
50 cm
F
A
A
A
A

Lithofacies A – Interpretation

The repeated siliciclastic sequences of finely bedded, fine-grained sediments are interpreted as continent-derived sediment supply into a deep marine depositional environment: a marine sedimentary basin. The muted variation in the mud supply indicates temporal and geographical fluctuations in the delivery of mud and volcaniclastic grains into the system. Although in many areas there is little grading due to the limited grain size variation, the sediments do not possess any hallmarks of continuous pelagic or hemi-pelagic accumulations, such as a lack of internal fabric in dominantly clay-grade sediment. Conversely, the sharp parallel bedding and subtle grading evident throughout indicates that a series of individual events are recorded by this lithofacies.

Potential processes involved are turbidity or contourite currents. Contourites, which have many forms, often result in irregular, positive relief structures with little internal fabric and polished tops, delivered by dominantly shore-parallel currents thought to be driven by local atmospheric turbulence, storm events combined with the wider control of the Coriolis Effect. They are composed of sorted silts rather than repeated graded units (Stow and Lovell, 1979; Stow, 2009; Hernández-Molina *et al*., 2017). The thoroughly uniform nature of the Gwna Group mud-heterolithic strata rules out the possibility of contourite current as a depositional mechanism, while pointing more certainly towards deposition by gravity flows. Turbidity currents, or density flows are efficient mechanisms for cycles of fluidised downslope delivery of substantial amounts of terrestrial detritus from the continental shelf to sedimentary basins in the deep marine realm (Bouma, 2000; Mutti *et al*., 2009).

Turbidites, although varied in thickness, grain-size distribution and internal structure, always fine upwards. Size sorting is a defining turbidite characteristic

borne of the physics of sediment suspension sustained within a hyperpycnal stream forging a path through a body of deep water (Haughton *et al*., 2009). Through flow partitioning the coarsest sediment in a turbidity event bed falls from suspension first, therefore most proximally and as the flow slows, as it runs out into deeper water, ever finer sediment is deposited until there is none left.

Turbidite systems form fan-shaped sediment stacks of complex architecture on continental shelves, continental slopes and into the deep marine realm of basin plains (Stow and Mayall, 2000; Haughton *et al*., 2009; Mutti *et al*., 2009). Canyons in the shelf or deltas feed the system with terrestrial detritus through a system of channels which sort and distribute sediment carried by density currents to more distal sites (Haughton *et al*., 2009; Mosher *et al*., 2017). The channels are overwhelmed periodically which creates levee deposits in a similar way to that of a terrestrial river's overbank sediment drapes. Graded sand lobes form downslope and layered fine grained to mud deposits build up in the lower fan to basin plain region (Bouma, 2000).

Progressive deposition of a continuously fine grained turbidite sequence such as that seen in the Gwna Group would require numerous slope instability events of nearly equal measure, repeatedly sampling the same sediment source, suggesting a sustained sediment supply and tectonic setting.

The white-green sandstone channels are interpreted as a component of the background depositional system as they share the same mud matrix of the turbidites and are considered representative of the limited quantities of sand present in the basin – insufficient at most levels to form laterally extensive sand bodies. The discrete channels of pink arenite and carbonate within the turbidites are found in close proximity to each other but they are never mixed. They are interpreted as exotic to the basinal turbidite system: point-sourced, reworked,

continental lithologies delivered into the ocean basin, circulated in concentrated flows via bottom currents, independent of the turbidite system and deposited as a series of ribbon-shaped channels. The Sirius Passet Lagerstätte of North Greenland consists of anoxic mudstones deposited from suspension that includes density flow deposits containing sponge spicules and annelid worms in more distal locations than their natural habitat (Botting *et al*., 2015). The density flow deposits were identified by sedimentary features not normally found in pelagic fall-out successions, such as erosive bases, grading and cross stratification. The disarticulated fossil beds are interpreted as point-sourced from an upslope location, redeposited distally by an erosive density current (Faggetter *et al*., 2016).

The overall fine-grained nature of the Gwna turbidites and the general impression of sand-starvation throughout suggests two possible turbidite sequence sites: either a series of overbank flows in a mid-fan setting where the main distribution channels are intermittently inundated or, within the lower fan of a turbidite system (Bouma, 2000; Mutti *et al*., 2009).

The finer grained and sand-poor facies of the Northern Apennine turbidites have been classified as having mid to lower fan association (Mutti and Ricci Lucchi, 1973). The general uniformity of the turbidites indicates a low-fan environment, although the thicker sand-rich horizons are likely to represent time-restricted proximal deposition (Shanmugam *et al*., 1988; Bouma, 2000; Stow and Mayall, 2000).

Lithofacies A is a fine-grained turbidite sequence with point-sourced channels.

Lithofacies B

Minor matrix-supported conglomerate

Numerous minor conglomeratic strata can be identified interbedded within the fine-grained turbidite facies (lithofacies A). Close compositional similarity with the host beds and tectonic overprinting conspire to conceal the lithological contrast, but with practice these relatively small-scale horizons are identifiable (Fig. 2.6A, D and F).

Matrix supported conglomerates, 20 cm to 3 metres thick, contain unsorted rounded clasts of white-green greywacke, pink arenite and pink- or white-weathered abiotic carbonate in a green mudstone or mud-silt matrix (Fig. 2.6A, B, C, E and F). There is no discernible grading within the matrix (Fig. 2.6C). The clast population is rounded to well-rounded, of low to moderate sphericity,

---

Figure 2.6 → Monomictic matrix-supported conglomerates. **A.** Conglomeratic horizon cutting into underlying thin siltstone-mudstone beds, clasts that maintain stratification can be seen incorporated into the base of the upper bed, interpreted as a fluidised flow. Porth Felen (SH145 248), outcrop belt 2. 60 mm diameter lens cap for scale. **B.** Well-mixed fluidised conglomeratic horizon at the base with overlying plastically deformed beds of lithofacies A. Braich y Pwll (SH137 244), outcrop belt 1. One metre rule for scale. **C.** Plastic and brittle deformation in a fluidised conglomeratic layer. Clasts are folded and boundinaged, sometimes to the point of fracture, but the matrix is always efficiently distributed in the space between clasts and fragmented clasts and therefore this plastic deformation is interpreted as a primary sedimentary feature, despite this section being part of a much later deformation event. Trwyn Maen Melyn (SH138 252), outcrop belt 1. 50 cm of rule visible. **D.** Stratified sand-rich section transported as a coherent block on top of a > 1.8 m thick well-mixed conglomerate horizon, near Borth Wen (SH268 409), outcrop belt 1. **E.** Intense plastic and brittle deformation in a matrix supported conglomerate. Clasts of clean pink arenite are folded and stretched beyond the point of failure within a mud-silt matrix that fills all available interclast space. The long clast axes are aligned within the flow of the matrix fabric. Porth Iago (SH167 316), outcrop belt 1. **F.** Interbedded lithofacies A and B young to the north-west, to the left in the image at a point in the sedimentary cycle where lithofacies B is equal to or in greater abundance than A. There is poorly developed inverse grading in the lower (righthand) conglomerate layer with larger clasts protruding from the matrix at the top of the bed (some are outlined in orange) which are overlain by an inferior section of mud-silt laminations with a few small arenite channels. The upper surface of the laminated beds is disrupted by an incoming conglomerate. Porth Cadwaladr (SH363 661), outcrop belt 2.

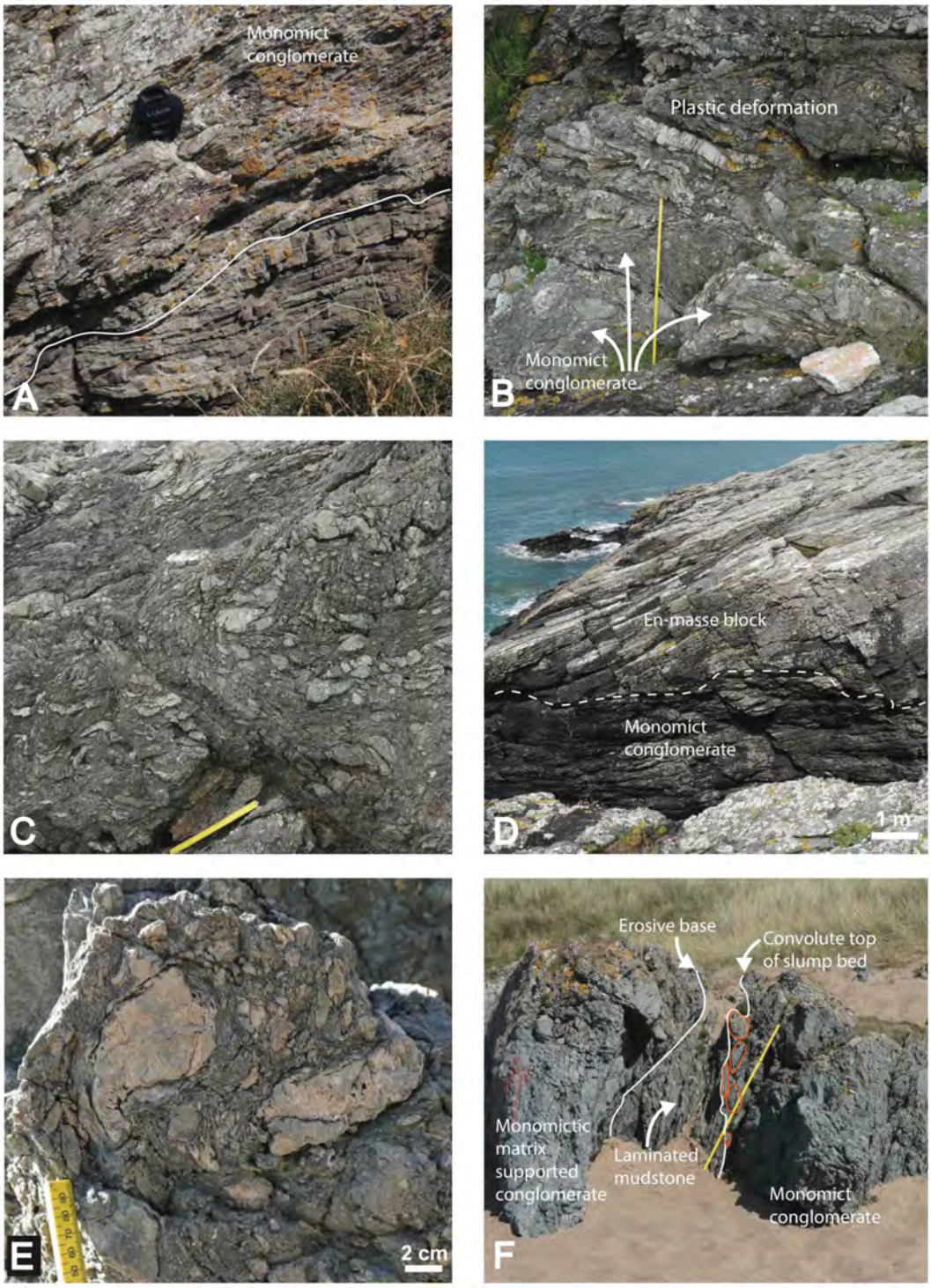
Monomict conglomerate
A
Plastic deformation
Monomict conglomerate
B
C
En-masse block
Monomict conglomerate
1 m
D
2 cm
E
Erosive base
Convolute top of slump bed
Monomictic matrix supported conglomerate
Laminated mudstone
Monomict conglomerate
F

measuring between 5 and 40 cm maximum diameter (Fig. 2.6A, B, C and D). The long clast axis is often aligned concordant with bedding and plastic deformation of both clasts and matrix is commonplace throughout:

- A scaly fabric in the matrix, intense where clasts and matrix are in contact (Fig. 2.6A and C)
- Boudinaged clasts with matrix injected into deformed areas (Fig. 2.6 C and E)
- Folded clasts and matrix injected into deformed areas (Fig. 2.6C and E)
- Fractured clasts in a jigsaw-fit formation with matrix injected between them (Fig. 2.6E)

Conglomerate bases are erosional, scoured into the underlying turbidite strata (Fig. 2.6A and F) conversely bed tops provide an uneven surface with clasts protruding a few millimetres or centimetres above the relatively flat matrix surface (Fig. 2.6F). Minor matrix-supported conglomerates are interbedded at varied intervals within continued deposition of the fine-grained turbidite system (Fig. 2.6A, B and F).

Lithofacies B – Interpretation

The minor conglomeratic horizons are exclusively monomict – they are composed entirely of material derived from the fine-grained turbidite system. The rounded clasts of white-green silt- and sandstone, pink arenite, pink- and white-weathered carbonate are dislocated channels and the matrix is a homogeneous mixture of a portion of the turbidite strata. Their formation within the turbidite system is considered to have occurred by repeated down-slope gravitational slump events of semi-lithified turbidites, related to intermittent slope instability, caused by sediment loading, storm events or minor earthquakes

(Bailey *et al*., 1989; Haughton, 2009). The matrix entirely lacks primary stratification and is closely wrapped around the clasts, suggesting sufficient transport distance to allow amalgamation of the turbidite beds into a homogeneous mud-silt matrix. The lack of mixing between clasts and matrix and the relative coherence of the clasts implies a differential degree of lithification at the time of formation: the clasts were more lithified than the matrix. There is abundant evidence of primary plastic deformation within the fabric of this lithofacies, related to the downslope transport of intrabasinal sediments within a series of discrete translational slides occurring intermittently throughout the development of the fine grained turbidite system (Stow and Mayall, 2000; Mutti *et al*., 2009). Lithofacies B is a series of matrix-supported, monomict translational slump beds deposited in a deep marine environment composed of material demonstrably native to the basin.

Despite the transference of the many slump beds from a proximal basin location to a distal deep marine fan setting there is no evidence for any grain size difference between the host turbidites and the translated material. They have travelled far enough in a fluidised flow to allow mixing of the turbidites into a homogenous matrix and also to plastically deform the channels. In other words, the fine-grained character of the turbidite system was maintained over considerable distance within the sedimentary basin (Bouma, 2000; Haughton, 2000).

Lithofacies B is a series of interbedded matrix-supported, monomict translational slump beds consisting of material native to the sedimentary basin - semi-lithified turbidites with subordinate channels delivered downslope following dislocation during minor slope instability events. Slump beds are an inherent feature of many turbidite systems, to a greater or lesser degree.

Lithofacies C

Polymict megaconglomerate

Dramatic, eye-catching outcrops of polymict megaconglomerate are well-known in the region, particularly where located in open beach settings subject to tidal processes that over time, have winnowed away much of the matrix (Figs. 2.1 A and B, 2.7A, C, D and E). This leaves disorderly monuments: stacked clasts of different lithology and size with little remaining matrix due to the work of modern tidal processes (Fig. 2.7A and E). This is Edward Greenly's (1919) Gwna mélange, a term that he coined for the rocks he determined to be a regional scale autoclastic breccia, a fault breccia.

All four outcrop belts contain chaotic megaconglomerate deposits of mud-silt to coarse sand grade matrix, supporting a mix of sub-rounded to rounded clasts (a minority are sub-angular) of quartz arenite, shallow-marine lime-dolostone, deep- marine lime-dolostone, greywacke, mudstone, jasper, chert, basalt, psammite and granite (Fig. 2.7A - F). The diverse range of clast lithologies is

---

Figure 2.7 → Lithofacies C: Polymict megaconglomerate. **A.** and **B.** Photograph and sketch to clarify interpretation. West of Cemaes Bay (SH365 938), outcrop belt 4, facing north. 1 – 3 m diameter clasts of carbonate and quartz arenite sit atop a well-preserved debris flow and demonstrate inverse grading and the often clast-supported mode of this lithofacies. The upper layer is supported by a zone of high shear developed during transport over the dislocation plane where matrix and clasts are efficiently mixed and plastically deformed. Beneath this is a low shear zone created by cutting down into the underlying layer, which feeds material into the high shear zone during transport. **C.** 3 m diameter carbonate clast in a carbonate-dominated conglomerate horizon near Borth Wen (SH271 411), outcrop belt 2. **D.** Polymictic megaconglomerate section at Porth Cadwaladr (SH361 665), outcrop belt 2. Facing south-east. **E.** Clast-supported conglomerate south of Carmel Head on the north-west coast of Anglesey SH292 918), north of outcrop belt 3. **F.** Sub-vertically orientated minor polymictic conglomerate horizon north of Porth Cadwaladr (SH359 667), outcrop belt 2. 60 mm diameter lens cap for scale.

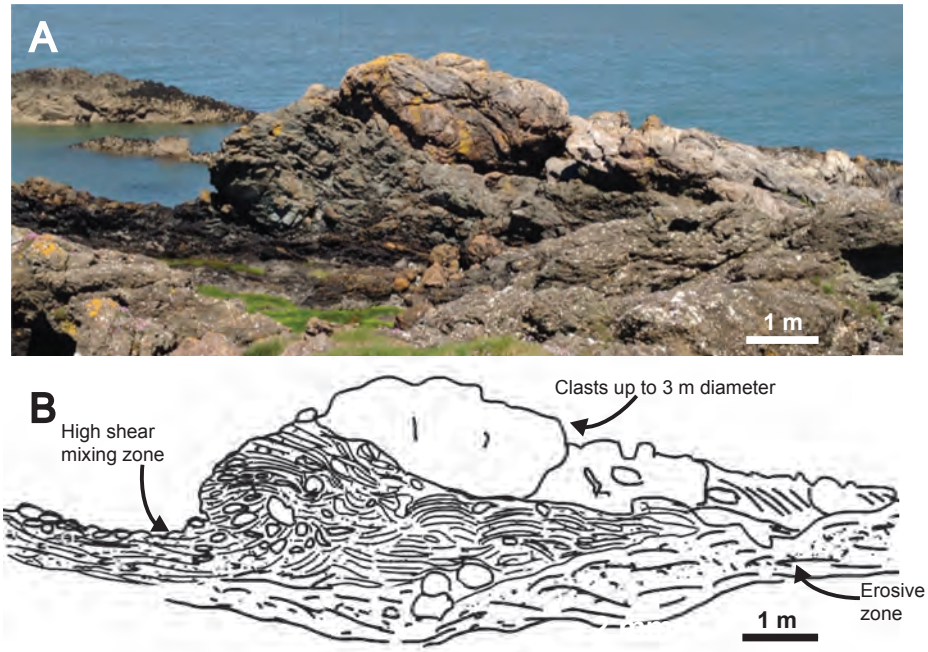
A
1 m
B
High shear
mixing zone
Clasts up to 3 m diameter
Erosive
zone
1 m
C
1 m
D
1 m
E
F

dominated numerically and volumetrically in all outcrop belts by first, quartz arenite and second, shallow- marine carbonate (Fig. 2.7A, C and E). Consistently the largest clasts of the megaconglomerate are composed of quartz arenite – "broken beds", lens- and sphere-shaped clasts of medium to thickly bedded or massive arenite and rounded lenses and blocks of shallow-marine carbonate (see also Chapter 4). Elongate, lensoid clasts outnumber all other shapes in the megaconglomerate facies – clasts of high sphericity are common below 3 cm diameter but are atypical of the larger clasts. Broken beds: rare stacks of arenite strata (no carbonates or other lithologies are seen in this form) that have been snapped from position and incorporated into the conglomerate that remain in close proximity to each other despite inclusion in a debris flow and thus having

---

Figure 2.8 → Conglomerate matrix fabrics and microscopic textures. **A.** Green silt-coarse sand grain size polymictic conglomerate matrix injected into a fractured arenite clast. Trwyn Maen Melyn (SH138 253), outcrop belt 1. Facing north. **B.** Polymict brecciated matrix injected into an angular clast margin. Subangular to angular clasts are outlined with orange. This lack of roundedness is unusual in the Gwna Group and is interpreted here as the result of cataclasis in the final stage of transport, as the debris flow lost momentum and came to a halt. Trwyn Maen Melyn (SH138 253), outcrop belt 1. Facing east. **C.** Microconglomeratic matrix injected into each and every space available between pink arenite clasts. The matrix, that is the mud quotient of it, has a glassy, siliceous texture and there is a lack of schistosity. The matrix texture is interpreted as a primary sedimentary kinematic feature reflective of shear and subsequent mixing during transport. Porth Cadwaladr (SH363 661), outcrop belt 2. Facing north-east. 60 mm lens cap for scale. **D.** Plane-polarised light photomicrograph demonstrates the microconglomeratic nature of the matrix – mud is dominant but there are numerous > 100 μm well-rounded quartz grains. There is a lack of schistosity in the matrix fabric, visible at macroscopic scale. North of Pen y Parc (SH366 655), outcrop belt 2. **E.** Polymictic breccia – the erosive base at the back end of a debris flow. Some clasts are outlined with orange – the angular clasts are interpreted as extrabasinal fragments not subjected to lengthy transport - there has been insufficient distance travelled to round them. Rounded clasts can also be seen – these are interpreted as reworked point-sourced channels native to the basin. Church Bay (SH300 895), outcrop belt 3. **F.** Asymmetric clast boudinage - the clast sits within a conglomeratic - mud matrix and, despite the presence of numerous mm – 2 cm scale clasts, schistosity (parallel to white lines) in the upper half of the image is developed during later deformation: the schistosity is not a primary sedimentary fabric but was overprinted by later deformation. Beneath the large cast, in the bottom right of the image the matrix has a scaly fabric or scaly cleavage. North Lleyn coast (SH222 376), outcrop belt 1.

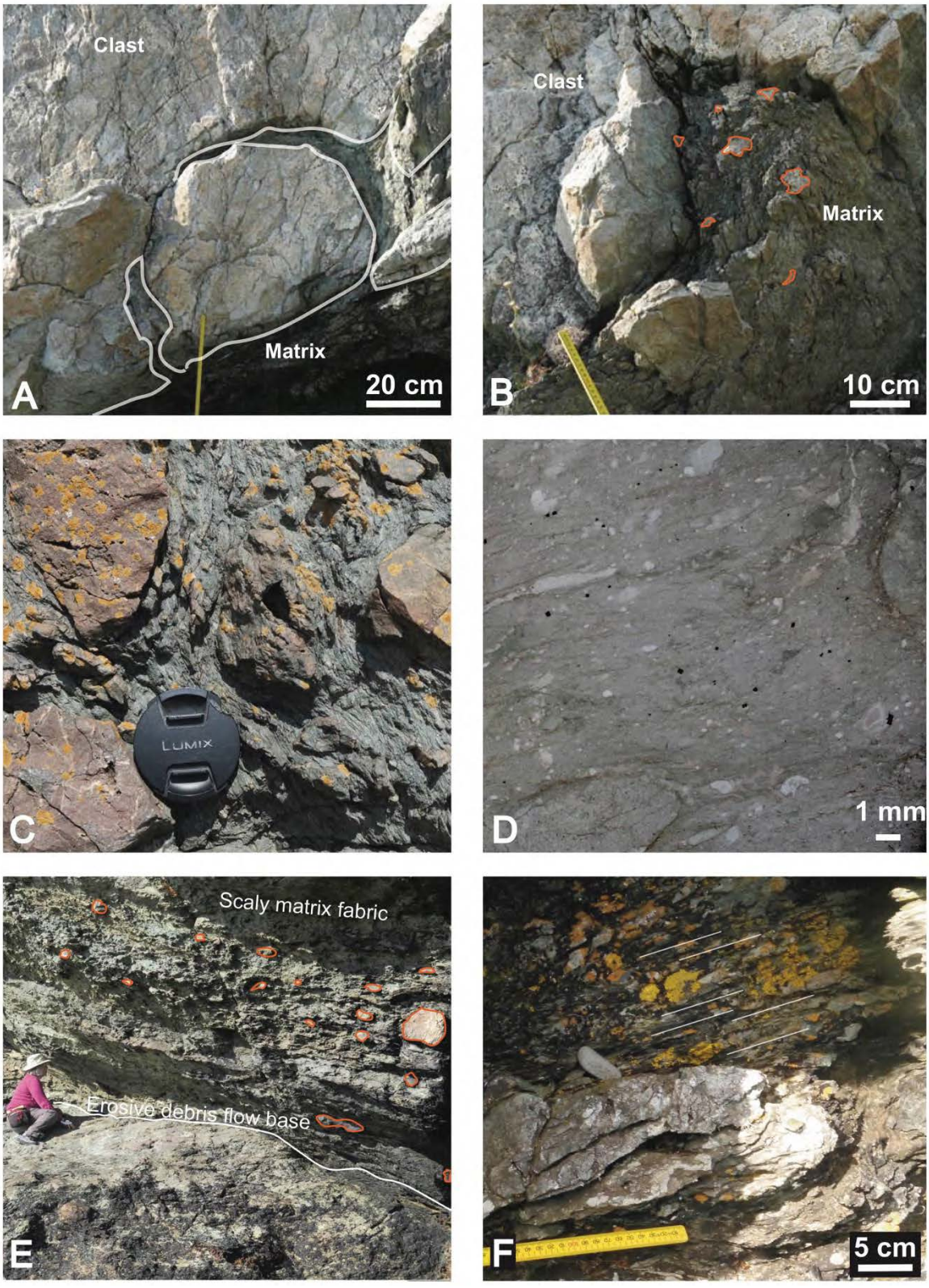
Clast
Matrix
20 cm
A
Clast
Matrix
10 cm
B
LUMIX
C
1 mm
D
Scaly matrix fabric
Erosive debris flow base
E
5 cm
F

experienced some transport. Broken beds may remain contiguous, or contain rotated blocks, alternatively they may be arranged in a jigsaw-fit configuration that clearly shows how they were positioned within the parent stratigraphy. They are significantly less rounded than other clast morphologies within lithofacies C and are interpreted as recording incipient brecciation.

Individual polymict megaconglomerates vary in size, with rare smaller exceptions, from ~ 8 m to as large as a few hundred metres thick. A degree of inverse grading is often, but not exclusively, present with the largest clasts borne at, or towards, the top of the conglomerate bed (Fig. 2.1A and B). Bed forms are erosive at the base, cutting down into the underlying strata and the tops consistently exhibit clasts protruding to varying degrees through a relatively flat matrix surface (Fig. 2.1A and B). Megaconglomerates crop out in stacked piles, rather than single layers. There is positive correlation between overall bed thickness and:

- Matrix grain size
- The larger the megaconglomerate bed (Fig. 2.8A, B and E), the coarser the matrix. The thinnest conglomerates contain a mud to coarse sand matrix (Fig. 2.8D) but the matrix of the thickest conglomerates consist
- of a mud, with coarse sand to granule microconglomerate or occasionally, a microbreccia (Fig. 2.8B).
- Clast maximum dimension measurement, i.e. thicker megaconglomerates contain the largest clasts.

Clast size variation is diverse: overall, 2 mm to 650 m maximum diameter. However, the majority of clasts (Fig. 2.9A-F) are:

- 2 cm to 65 m maximum diameter (Fig. 2.9A-F)

- Composed of a single lithology
- Low sphericity: elongate, lensoid or disc-shaped - the smallest clasts can be highly spherical (Fig. 2.9A – F)
- Sub-rounded or rounded (Fig. 2.9B, D, D, E and F)

Most sedimentary clasts of greater than 1 m maximum dimension, have been broken from the parent unit more-or-less along bedding planes and the longest two axes are usually bedding parallel, therefore clasts contain a limited amount of sedimentary information individually.

Matrix composition is always siliceous: commonly a green-grey mud that varies to coarse sand grain size. At the finest grade, matrix can appear as a glassy, siliceous ooze (Fig. 2.8C and D). In the thickest megaconglomerate beds the matrix takes the form of a coarse-grained polymict microconglomerate (Fig. 2.8B and D) or less commonly, a microbreccia containing myriad angular to sub-angular clasts. Consistently the matrix exhibits a swirling fabric (Fig. 2.8B and C), closely adhering to each clast perimeter (Fig. 2.8A, C, C and F): this can give the visual impression of ongoing movement of the clasts within the matrix. This fabric, in places where smaller clasts dominate, can be described as a scaly

---

Figure 2.9 → Clast shapes and sizes in lithofacies C. **A.** Overturned, boudinaged arenite starved gutter cast originally deposited in lithofacies A, now a megaconglomerate clast surrounded by numerous 1-3 cm diameter clasts in a grey-green muddy matrix. This is a common clast shape within lithofacies C. Llanbadrig (SH377 947), outcrop belt 4. Facing east. **B.** Spheroidal arenite clasts, or cobs within lithofacies C at Llanbadrig Point (SH374 946), outcrop belt 4. Facing east. **C.** 8 m diameter quartz arenite clasts of high sphericity – probably two parts of what was previously a single lens-shaped clast. Wylfa Head (SH353 943), outcrop belt 4. Facing north. **D.** Metre scale quartz arenite clasts of moderate sphericity with lens-shaped carbonate clasts in a polymictic megaconglomerate, Wylfa Head (SH353 944), outcrop belt 4. Facing north-east. **E.** Vertically orientated megaconglomerate lithofacies composed mainly of pink arenite, well-rounded, lens-shaped clasts, sized 1 – 70 cm diameter in a green mudstone matrix exhibiting schistosity. Pen-y-Parc (SH 368 653), outcrop belt 2. Facing south-east. **F.** Elongate, lens-shaped clasts of quartz arenite and carbonate up to 60 m diameter sit in a polymictic megaconglomerate. West of Cemaes Bay (SH367 938), outcrop belt 4. Facing north-west.

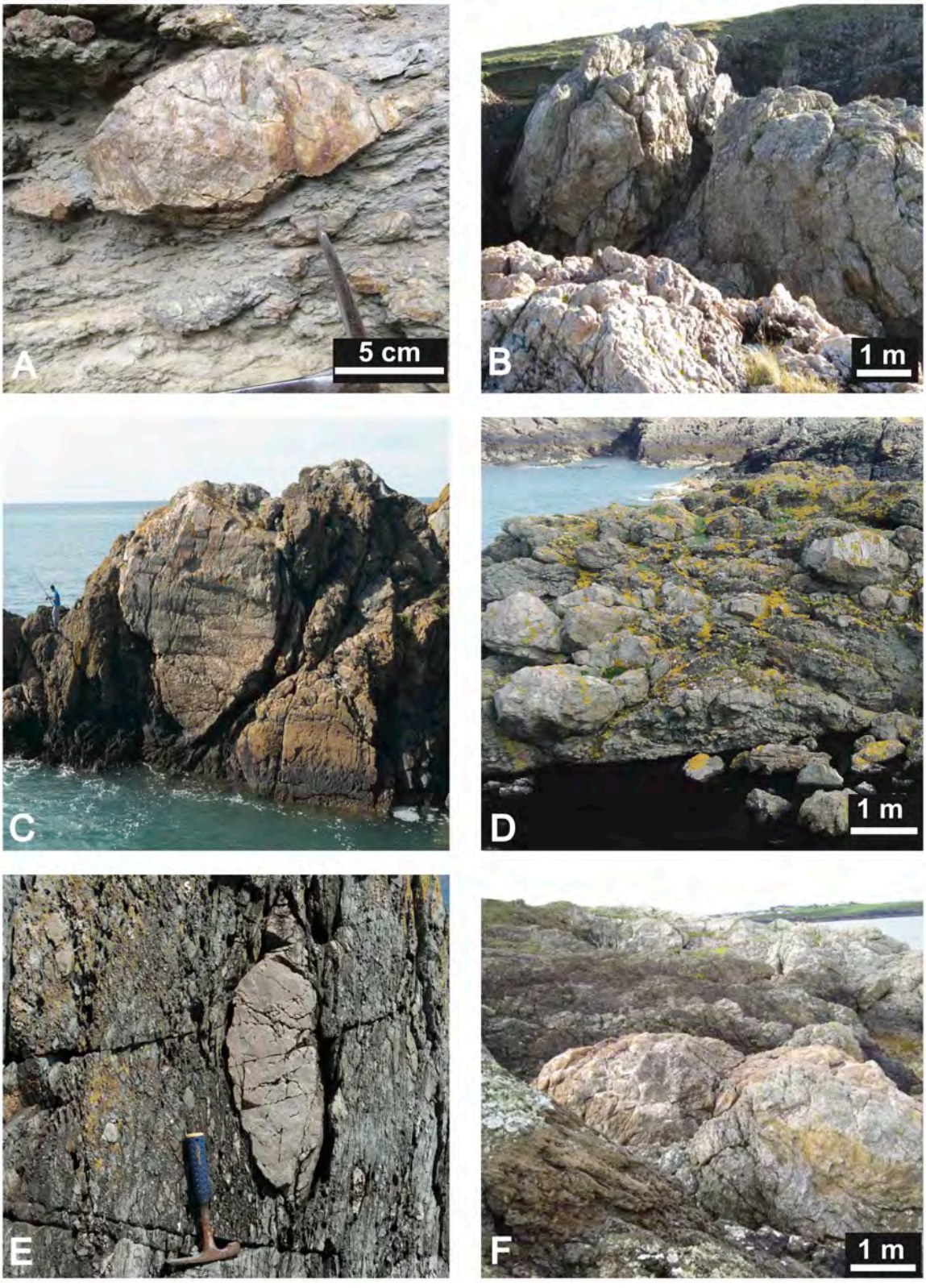
A
5 cm
B
1 m
C
D
1 m
E
F
1 m

“cleavage” (Fig. 2.8E and F) or in others, as a weakly-developed schistosity (Fig. 2.8F). In a very few places, no internal matrix fabric can be determined (Fig. 2.8).

Exposed cross sections of intact megaconglomerate reveal a broadly matrix-supported lithology with minor clast-supported zones but, localities with preferentially weathered matrix reveal in 3-D bimodal character with clusters of clasts and syntaxial contact between them a standard feature (Fig. 2.7A and B).

Lithofacies C – Interpretation

The polymict megaconglomerate lithofacies is comprised of clasts, broken beds and matrix of both intrabasinal and exotic, extrabasinal lithologies implying partial but substantial change in the environment and sediment source on a temporary basis. The conditions applicable to lithofacies A and B endured, but there was a contemporaneous supplementary supply of detrital material supplying and controlling these repeated horizons.

There are reworked upper slope semi-lithified components – the same materials supplied for the matrix-supported, monomict slump beds, indeed the matrix is predominantly formed of mixed mud-heterolithic turbidites with the addition of coarser grained quartz, lithic fragments, chert and other lithologies attributed to comminution of the clasts entrained in the conglomerate. In addition, well-cemented clasts of many different lithologies are included, most notably large (> 1 m maximum diameter) bedded white-pink and white-orange weathered arenite and carbonate clasts which dominate these megaconglomerates. These are the same lithologies as the material point-sourced for the many channels in the fine grained turbidite system and it is suggested that these rock types would have been exposed at the time in a proximal position regularly providing small amounts of winnowed material into

the basin, progressively creating instability in the source rock so that massive blocks and broken beds could fracture and be shed into the sediment supply intermittently within the sedimentary cycle. Megaconglomerate clasts greater than 5 mm diameter, many of which are well-cemented and competent, are sub-rounded to rounded which implies a considerable time within the erosive zone prior to being incorporated into a debris flow and this fits with a coastal margin supply source and an outer fan resting place. The diversity of less significant clast types within the megaconglomerate includes those incorporated during transport, which in itself must have been a highly erosive process, in addition to those obtained at the primary source.

The brittle fracture or collapse under wasting conditions of clasts of all sizes plucked from their host beds, plus the crushing and grinding together of all components during mass transport is the source for the microconglomeratic matrix. Microbreccia matrix is less common and represents comminution in clast supported zones as the flow came to a halt, leaving little transport time for rounding.

Lithofacies C is a sedimentary mass transport deposit - a series of polymict, bimodal, megaconglomeratic debris flows dominated by continental margin derived exotic, extrabasinal lithologies but also containing native sediments from further upslope, deposited in a marine basin within a coherent sedimentary cycle.

Analogues for the Gwna Group

The Gwna Group is an internally conformable turbidite system interbedded with autochthonous slump beds and debris flows that contain a mixture of basin-derived and allochthonous detritus. The sedimentary system is defined as coarsening upwards, through repeated megacycles (see Chapter 5).

Sedimentary successions that share some properties with the Gwna Group are briefly discussed below.

- Modern turbidites of the Amazon Fan are dominated by mud, deposited in a stacked channel levee system in a deep-sea fan that grade from silt laminae to mud with only restricted quantities of sand present (Piper and Deptuck, 1997).
- Late Miocene turbidites of the Tabernas Basin of south-east Spain consist of sandstone sheet turbidites, sand-starved marls, ponded turbidites, infilled ribbon-like incisions, drape-healed fault-controlled topography and highly sinuous sand channels topped by a single regional scale debris flow that probably records a seismically induced slope failure (Haughton, 2000).
- The latest Ordovician to early Silurian Nant Brianne turbidite system of Central Wales is sand-rich, with axial conglomeratic deposits formed from varied sediment supplies during the tectonic evolution of the marine basin (Schofield *et al*., 2008).
- The Proterozoic Blackstone Group of the Boston, Massachusetts region is an example of a stratigraphically concordant marine succession that is dominated by downslope translational slump beds that consist of quartz arenite and carbonate clasts, repeatedly interbedded with subordinate shale – siltstone horizons (Bailey *et al*., 1989).
- The Ordovician (late Arenig) Lady Port Formation, Manx Group, Isle of Man of laminated silt- to mudstone turbidites contains numerous slump beds composed of native basin material interbedded with debris flows that contain additional clast types suggesting a supplemented sediment supply temporarily sourced from a greater distance. Both the slump beds and the debris flows were delivered downslope following a series of slope

instability events (Woodcock and Morris, 1999).

- The late Precambrian Westboro Formation of Boston, Massachusetts, USA, is a conformable 1,100 m thick sedimentary and basic volcaniclastic metamorphic succession that consists of laminated to thinly bedded silt- and sandstone turbidites with intrabasinal slump horizons, repeatedly interbedded with 20—30 m thick olistostromes containing lenticular quartz arenite clasts in a mudstone matrix, overlain by coherent quartz arenite beds (Bailey *et al*., 1989).

The Tabernas Basin and Nant Brianne turbidite systems were deposited during ongoing seafloor deformation driven by tectonic shortening, which in the case of Nant Brianne, exerted a topographical control on sediment supply (Haughton, 2000; Schofield *et al*., 2008).

The Blackstone Group, Westboro Formation and the Lady Port Formation, although now geographically dispersed, were formed in Avalonia, on the Gondwanan margin, during tectonic extension (Bailey *et al*., 1989; Woodcock and Morris, 1999). The Amazon Fan occupies a passive margin setting (Piper and Deptuck, 1997).

Figure 2.10 → Stratigraphic relationships of outcrop belt 3. **A.** Geological map (simplified after BGS Anglesey Map currently in production). The location of map B is indicated. **B.** Basal unconformity map illustrating gradual transgressive overstep of the underlying subaerial relict surface which passes upwards to lithofacies A. **C.** Summary log of outcrop belt 3 shows the ~650 m thick (this section) Gwna Group is unconformity bounded. The underlying New Harbour Group is overstepped in a three-part succession beginning with transgression, deposition of the volcanic and volcaniclastic turbidites and, in turn, a gradational contact with polymict debris flows of lithofacies C.

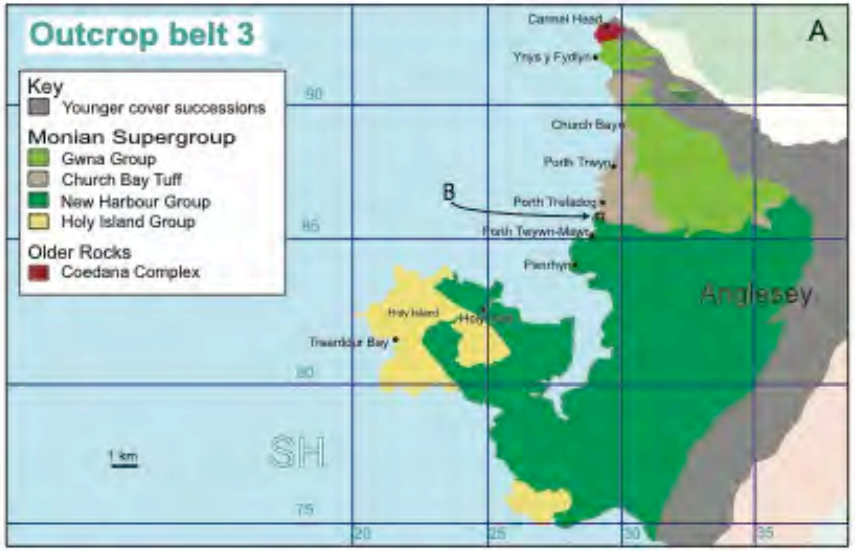
Outcrop belt 3
A
Key
Younger cover successions
Monian Supergroup
Gwna Group
Church Bay Tuff
New Harbour Group
Holy Island Group
Older Rocks
Coedana Complex
Carmel Head
Ynys y Fydlyn
Church Bay
Porth Trwyn
Porth Trefadog
Porth Twywn-Mawr
Pierhyrn
Anglesey
Holy Island
Holyhead
Trearddur Bay
B
90
85
80
75
20
25
30
35
1 km
SH

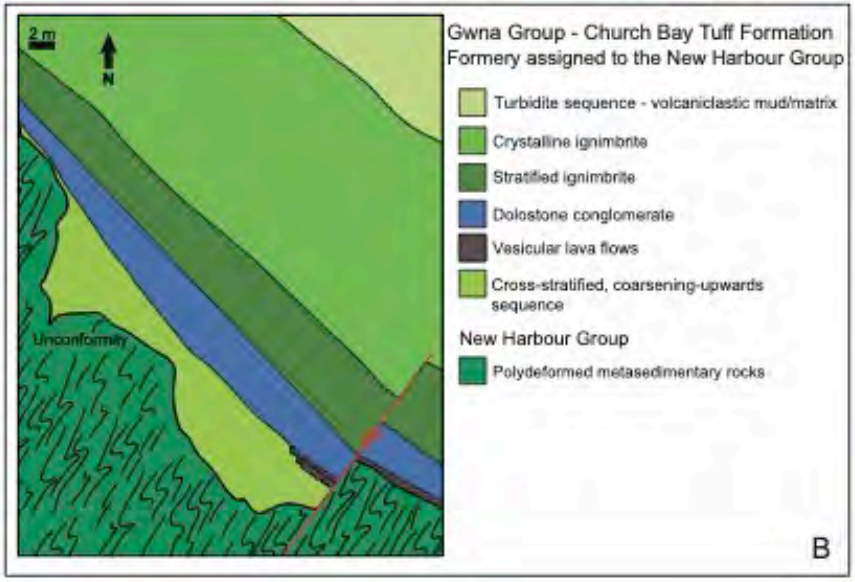
2 m
N
Unconformity
Gwna Group - Church Bay Tuff Formation
Formery assigned to the New Harbour Group
Turbidite sequence - volcaniclastic mud/matrix
Crystalline ignimbrite
Stratified ignimbrite
Dolostone conglomerate
Vesicular lava flows
Cross-stratified, coarsening-upwards sequence
New Harbour Group
Polydeformed metasedimentary rocks
B

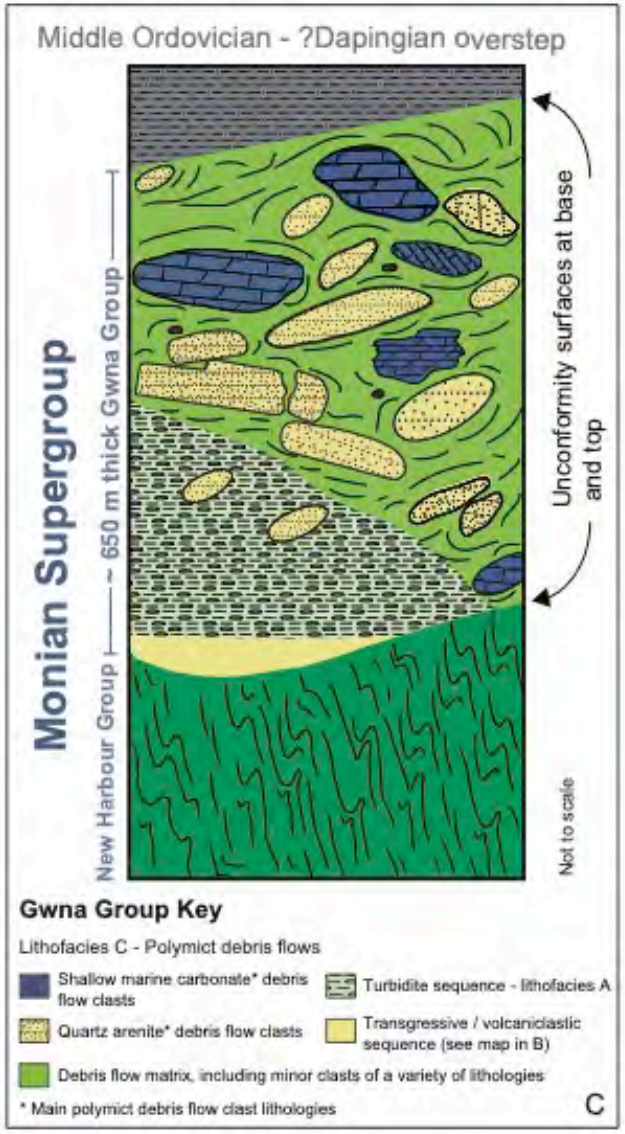
Middle Ordovician - ?Dapingian overstep
Monian Supergroup
New Harbour Group
~ 650 m thick Gwna Group
Unconformity surfaces at base and top
Not to scale
Gwna Group Key
Lithofacies C - Polymict debris flows
Shallow marine carbonate* debris flow clasts
Turbidite sequence - lithofacies A
Quartz arenite* debris flow clasts
Transgressive / volcaniclastic sequence (see map in B)
Debris flow matrix, including minor clasts of a variety of lithologies
* Main polymict debris flow clast lithologies
C

2.2 Facies associations: Sections beyond the direct influence of the Menai Straight Fault System

North-west Anglesey – Outcrop belt 3

The Gwna Group unconformably overlies polydeformed schist and volcaniclastic psammites (Phillips, 1991a) of the New Harbour Group, exposed south of Porth Trefadog (SH289 858) (Fig. 2.10A and B). The pelites display a complex combination of cleavages and metamorphic foliation recording three generations of recrystallisation and deformation (Fig. 2.11A). The Gwna Group sediments conversely show far less alteration and deformation indicating the presence of a significant tectonic break (Fig. 2.11A) (See Chapter 3). The most recent tectonic episode recorded in the New Harbour Group is named the Monian Orogeny by Waldron *et al.*, (2018).

The conspicuously buff-yellow-brown penetrative weathering of the New Harbour Group metasediments at, and several metres below, the topographically sculpted basal surface (Fig. 2.10B and C) is distinct from the strongly green colour of the New Harbour Group elsewhere. The presence of a palaeosol, evidenced by pseudomorphs after ankerite, or ferroan dolomite (pers. comms. P. R. Wilby, A. G. Leslie and D. I. Schofield, September 2015) indicates subaerial exposure for

---

Figure 2.11 → The basal unconformity of the Church Bay Tuff Formation/Gwna Group, south of Porth Trefadog (SH288 857), outcrop belt 3, north-west Anglesey. Images face to north-north-east. **A.** Cross-stratified siliciclastic conglomerate unconformably downstepping onto the surface of the polydeformed New Harbour Group. **B.** Vesicular lava in baked contact with the underlying conglomerates. One metre rule for scale. **C.** Flat-topped lava flow – interpreted as subaerial emplacement, overlain by dolostone conglomerate. **D.** The direct contact of lava over the New Harbour Group is interpreted as evidence for a gradual overstep of topographical relief in the unconformity surface. **E.** Laminated ignimbrite. **F.** Crystalline ignimbrite with laminated patches.

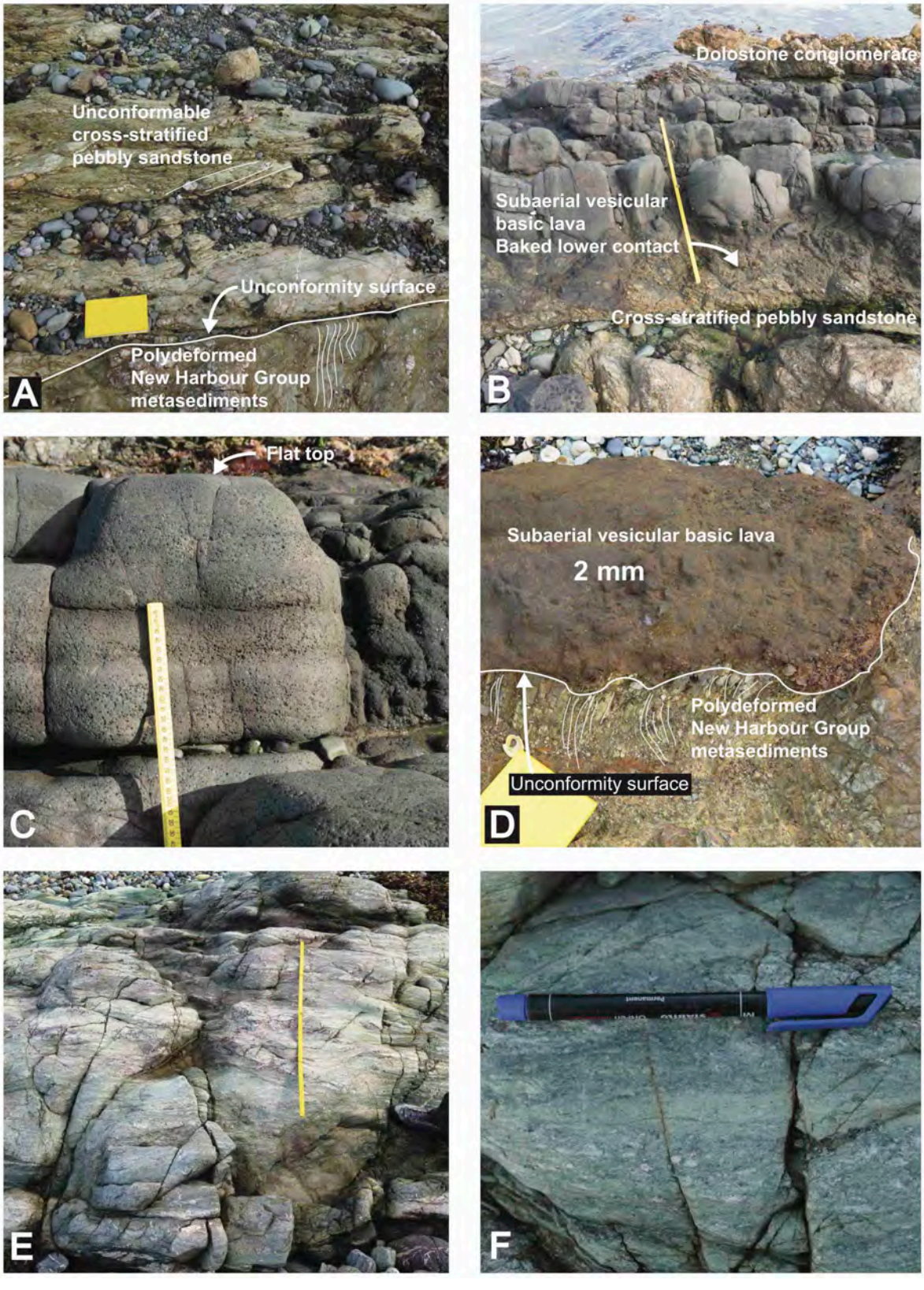
Unconformable
cross-stratified
pebbly sandstone
Unconformity surface
Polydeformed
New Harbour Group
metasediments
A
Dolostone conglomerate
Subaerial vesicular
basic lava
Baked lower contact
Cross-stratified pebbly sandstone
B
Flat top
C
Subaerial vesicular basic lava
2 mm
Polydeformed
New Harbour Group
metasediments
Unconformity surface
D
E
F

sufficient time to allow soil formation. Therefore, the unconformity represents a relic terrestrial profile that is a significant stratigraphic boundary.

The once-exposed palaeosurface is partially infilled by cross stratified arenite conglomerates in downlapping formation (Fig. 2.11A) and topped by a < 1.2 m thick stack of basic vesicular lavas (Fig. 2.11B and C), which, along strike is in direct contact with a section of the unconformity closest to the current cliff edge (Fig. 2.10B and C, Fig. 2.11D), and later faulted (Fig. 2.10B) to create a complex boundary zone. The convolute base of the lava infills the uneven top of the conglomerate (Fig. 2.11B); its top is conspicuously flat, leading to a subaerial interpretation. The position of the faulted block and the overlying contact of the lavas with both New Harbour Group and Gwna Group sediments confirms relic surface relief of at least 10 m (Fig. 2.10B and C). A clast-supported dolostone conglomerate, with a silt-mudstone matrix up to 2.5 m thick is infilled and overlain by ~ 10 m thick, green-red weathered fine-grained felsic ignimbrite, exhibiting a degree of parallel to anastomosing laminar fabric (Fig. 2.11E). Moving upwards through the succession there are blocky crystalline ignimbrites

---

Figure 2.12 → Church Bay Tuff Formation and the gradational contact with the Gwna Group, lithofacies C, at Church Bay, outcrop belt 3. **A.** Sand-rich turbidites with volcaniclastic matrix, south of Church Bay (SH299 888). Facing north-east**. B.** Discrete sand channels in laminated volcaniclastic mudstone at Church Bay (SH301 894). 60 mm lens-cap for scale. Facing east. **C.** An orange weathered, spheroidal arenite clast within disrupted laminated volcaniclastic mudstone marks the gradational contact with the Gwna Group mélange at Church Bay (SH301 894). 60 mm lens-cap for scale. Facing north-east. **D.** Minor breccia of quartz arenite clasts in volcaniclastic mud matrix, Church Bay (SH301 894). 60 mm lens-cap for scale. Facing east. **E.** Undisrupted turbidites at the base of a debris flow containing tabular quartz arenite beds, or broken beds, Church Bay (SH300 895). 1 m rule for scale. Facing north-east. **F.** Broken beds of quartz arenite overly a carpet of conglomeratic megaconglomerate matrix. The broken beds are separated by < 1 m thick layers of fine grained turbidites and minor arenite channels. Church Bay (SH300 895). Facing north.

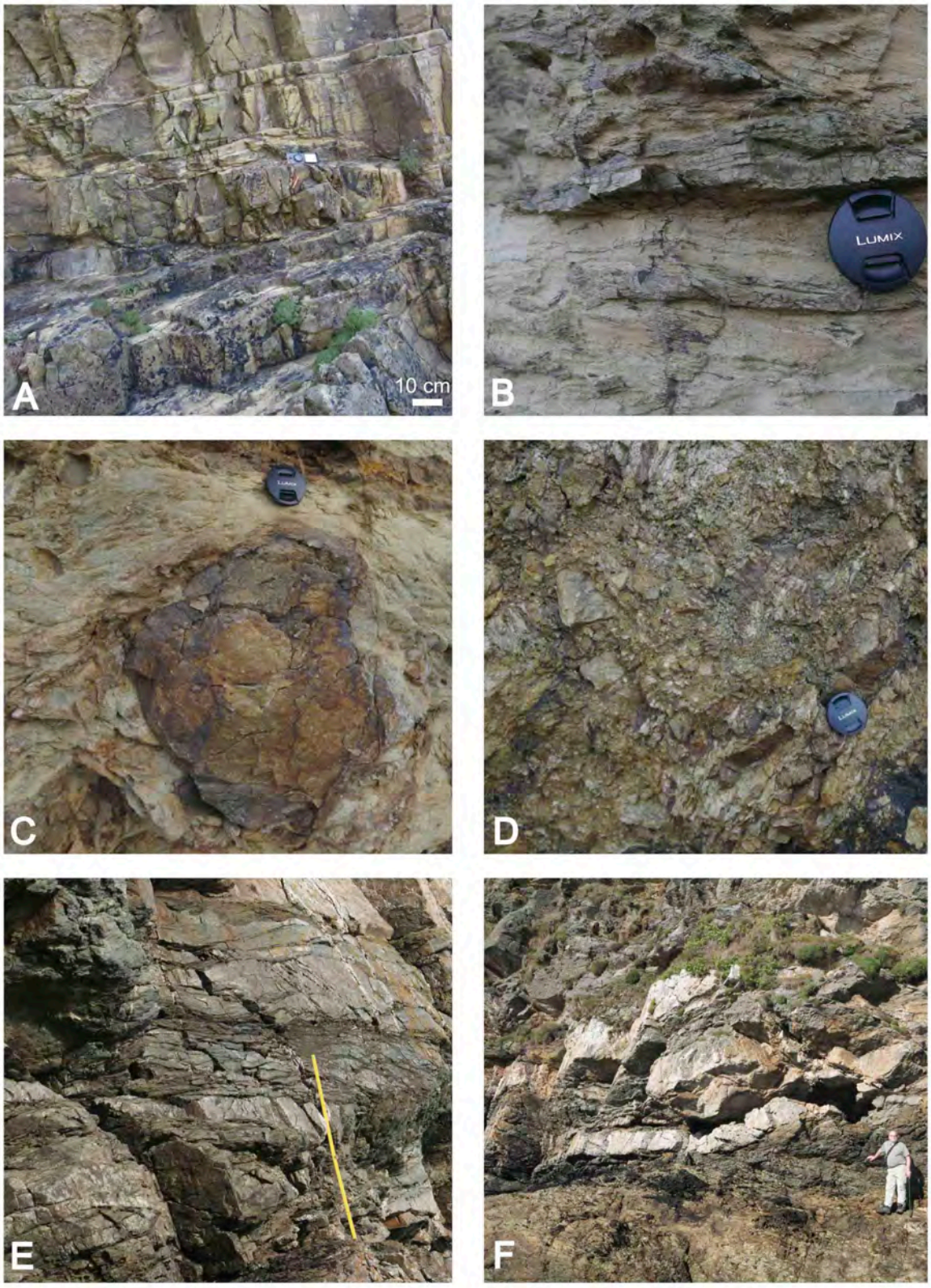
A
10 cm
B
LUMIX
C
D
E
F

(Fig. 2.11F) totalling up to 30 m thickness, within which there are patches of fine grained, laminated volcanic mud (Fig. 2.11F).

The ignimbrite gives way to finely laminated silt-mudstone beds, weathered green or buff-yellow, which, further up the sequence contains coarse-medium grain size greywacke beds up to one metre thick (Fig. 2.12A). This succession continues for several hundred metres thickness until halfway along Church Bay (NGR SH300 896) where a normal fault/fault breccia is seen in the cliff (Fig. 2.12D) and isolated, rounded – sub-rounded, arenite clasts (Fig. 2.12C) sit, within the bedded strata, their longest axes orientated with bedding (Fig. 2.12B). At the north end of the bay, broken beds – large tabular rafts of grey-white weathered arenite (Fig. 2.12F), in beds 50-100 cm thick are stacked and interbedded within the background sediments (Fig. 2.12E). Following this gradational transition, polymict megaconglomerates containing large clasts of arenite and carbonate dominate the coastal exposure of the sequence upwards, towards Carmel Head, where middle Ordovician sediments unconformably overly the Gwna Group. A combination of folding, topography and south-directed overthrusting reveals a repetition of the upper section just south of Carmel Head.

It should be noted that the glimpse of the megaconglomerate facies on offer at Church Bay represents the upslope margin of the debris flows: outcrop inland, distal in basin terms, is extremely limited due to ground cover. Therefore, it is not possible to fully describe the clast content, but, there is sufficient exposure of arenite clasts at the coast, and carbonate clasts immediately up-section and exposed inland at Llanfaethlu (SH214 874) to confirm uniformity with the polymict megaconglomerate regional style. The map view (Greenly, 1920), (Fig. 2.10A) illustrates the field relationships and outcrop pattern, which confirm a progressive overstep of the sub-aerial lower contact, with sediment supplied broadly from the west or north-west (Fig. 2.10C). This palaeodirection is

determined from the orientation of the basal cross-stratified beds that onlap the unconformity surface, the section younging direction (NNE at the base and NE through most of the section), the current gross orientation of the lowest megaconglomerate bed, the map view outcrop pattern and the fact that the basal unconformity is overstepped progressively in three stages. It is demonstrated above that there must have been substantial relief on the unconformity surface and the easterly half of the contact is not contiguous with the basal subaerial or turbidite facies, but is instead directly overlain by Gwna Group megaconglomerates, that have prograded further into the marine basin than the turbidite system (Fig. 2.10C). Alternatively, the turbidites may have been removed and reworked during megaconglomerate transport and deposition.

Outcrop belt 3 records a prograding sequence of sediments and volcanic rocks that began in a terrestrial environment followed by steady transgression to a submarine marine setting through a ~ 650 m thick coarsening upwards succession (Table 2.1) of proximal to relatively distal turbidites of lithofacies A, followed by megaconglomerates of lithofacies C. There is a lack of lithofacies B in this outcrop belt, as the translational slump beds consist of reworked basin-derived material of a more distal fan environment. The coastal exposure of this contact is a cross section through the most proximal debris flow facies (Fig. 2.12F): the unusual tabular broken formation style of clasts here is interpreted as relatively less travelled, less fragmented and less rounded therefore than the vast majority of clasts within the polymict megaconglomerate (Fig. 2.9A-F).

North Anglesey – Outcrop belt 4

The polydeformed volcaniclastic pelite and psammite metasediments of the

New Harbour Group in this succession, crop out along the north Anglesey coast from Cemlyn Bay to Wylfa Head (Fig. 2.14) and are unconformably overlain by megaconglomerate Gwna Group facies (Fig. 2.13D). The New Harbour Group is less deformed here than in outcrop belt 3 but can still be termed polydeformed (Fig. 2.13A). The boundary with the Gwna Group is an important delineation that is marked by stratigraphic angularity, and metamorphic and deformational discontinuity (Fig. 2.13A), as is the equivalent surface in outcrop belt 3, although here there is direct no evidence here for a subaerial environment.

Although continuously exposed, the along strike outcrop provides at most 1 km stratigraphic thickness (Table 2.1). However, there is the opportunity to view lateral changes in sedimentology where primary features are preserved. The younging direction is consistently to the north which is overprinted by a north-west to south-east fabric (Fig. 2.15). The basal unconformity, exposed intact o

---

Figure 2.13 → Outcrop belt 4 – the north Anglesey coast. **A.** Outcrop of the basal unconformity: Gwna Group polymictic conglomerate overlies polydeformed pelitic metasediments of the New Harbour Group. Clasts are outlined in orange. Younging direction to the north, or left of the image. Porth Wylfa (SH408 945). One metre rule for scale. Facing north-east. **B.** Subhorizontal thin silt-mudstone turbidite system beds, interbedded with slump bed 1 – a non-fluidised translational slump, probably a listric dislocation of semi-lithified sediments followed by a short downslope slide. Slump bed 2 is a fluidised flow of intrabasinal material – lithofacies B. Wylfa Head (SH353 943). Facing north-west. 1 m rule for scale. One metre rule for scale. **C.** Cross-section through disrupted successions of steeply north-dipping beds of interbedded lithofacies A and B displayed in the cliffs on the west coast of Wylfa Head. The conglomerate is not accessible, so cannot be described fully, clasts are ~30 – 40 cm diameter and smaller clasts are also visible – lithofacies B. Wylfa Head (SH354 946). Facing south-east. **D.** Inverse grading in a polymict debris flow ~ 60 m above the Porth Wylfa unconformable base (SH408 945). Conglomeratic matrix in the foreground. Facing north-east. **E.** The upper contact of the Gwna Group unconformably overstepped by Dapingian sediments at Ogof Gynfor (SH378 948). Several larger clasts are outlined with orange. Facing north-east. **F.** An alternative view of the Dapingian overstep – from between Ogof Gynfor and Porth Llanlleiana: Subvertical and steeply north-dipping Gwna Group polymictic conglomerates occupy the lower right foreground of the image and several large clasts are outlined in orange. Gently north-east dipping, parallel stratified Dapingian sediments occupy the distant cliff in the centre left. Image taken east of Ogof Gynfor, facing north-east towards Porth Llanlleiana (View to SH383 951.)

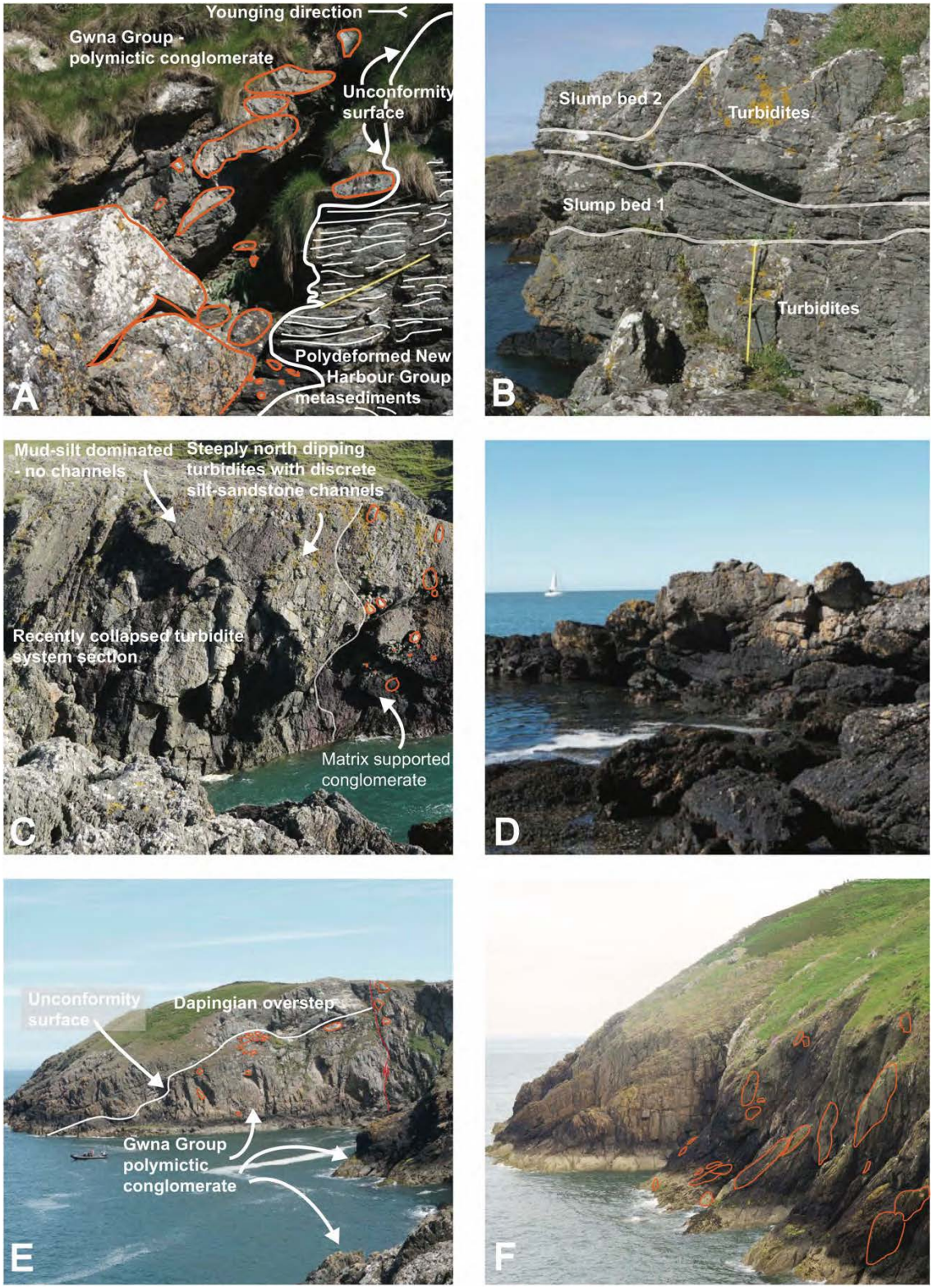
Younging direction
Gwna Group -
polymictic conglomerate
Unconformity
surface
Polydeformed New
Harbour Group
metasediments
A
Slump bed 2
Turbidites
Slump bed 1
Turbidites
B
Mud-silt dominated
- no channels
Steeply north dipping
turbidites with discrete
silt-sandstone channels
Recently collapsed turbidite
system section
Matrix supported
conglomerate
C
D
Unconformity
surface
Dapingian overstep
Gwna Group
polymictic
conglomerate
E
F

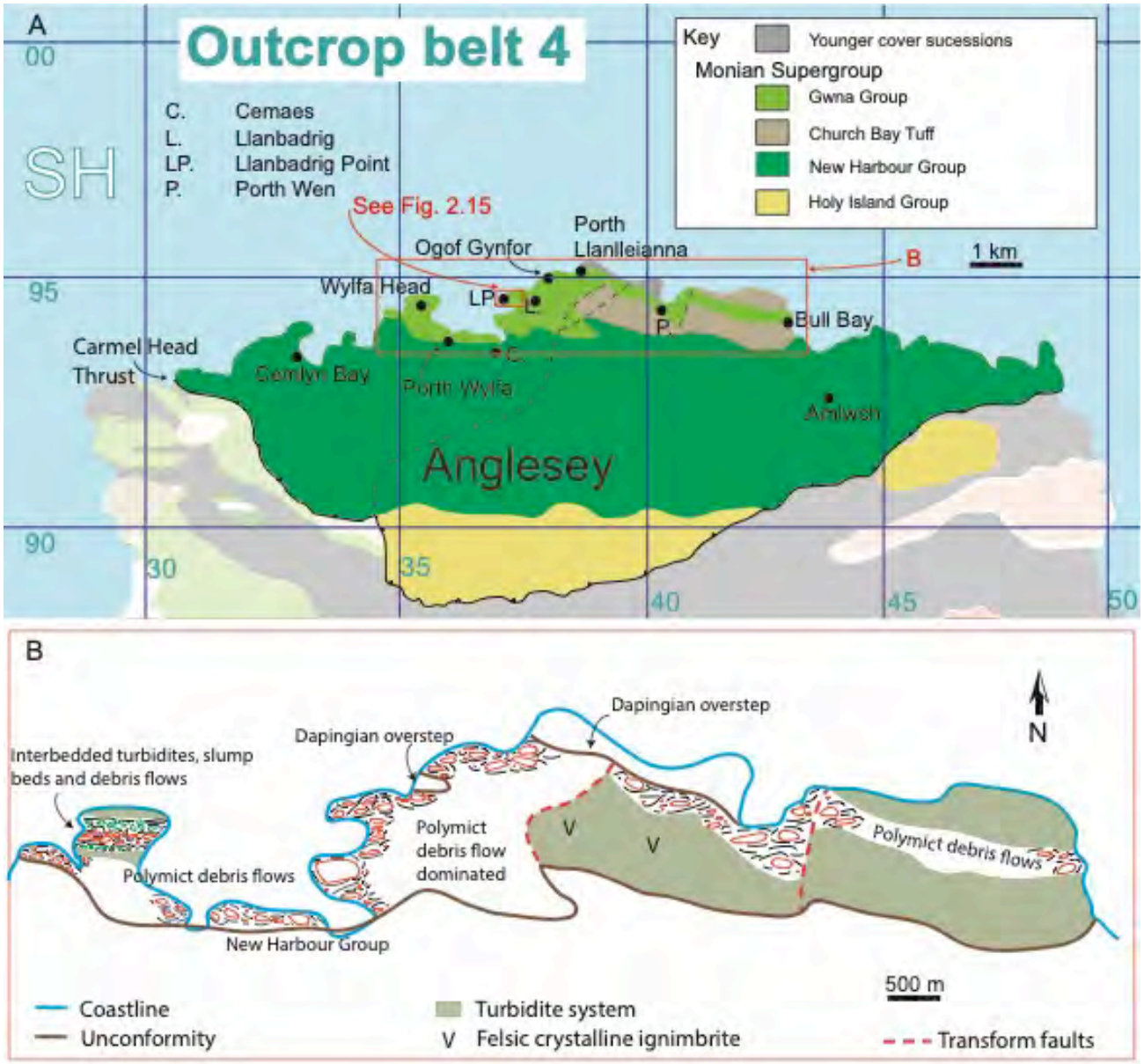
A
Outcrop belt 4
00
SH
95
90
30
35
40
45
50
C. Cemaes
L. Llanbadrig
LP. Llanbadrig Point
P. Porth Wen
See Fig. 2.15
Key
Younger cover sucessions
Monian Supergroup
Gwna Group
Church Bay Tuff
New Harbour Group
Holy Island Group
Porth Llanlleianna
Ogof Gynfor
B
1 km
Wylfa Head
LP
L
P
Bull Bay
C
Carmel Head Thrust
Cemlyn Bay
Porth Wylfa
Amlwch
Anglesey
B
N
Dapingian overstep
Dapingian overstep
Interbedded turbidites, slump beds and debris flows
Polymict debris flows
Polymict debris flow dominated
V
V
Polymict debris flows
New Harbour Group
500 m
Coastline
Unconformity
Turbidite system
V Felsic crystalline ignimbrite
Transform faults

Figure 2.14 ← Geological map and sketch map of outcrop belt 4. **A.** Geological map, redrawn after BGS Anglesey map, currently in production. The outcrop is bounded to the south by the Carmel Head Thrust and to the north by the sea: it is a hanging wall slice, containing a sequence of Monian Supergroup lithologies delivered in situ by south-directed thrusting. This tectonic shortening is not related to the formation of the Gwna Group but is a part of its subsequent history. **B.** Field sketch map showing the distribution of lithofacies A- C along strike in outcrop belt 4.

Wylfa Head (SH353 943) and at Porth Wylfa (SH361 938 and SH363 937), is directly overlain by polymict conglomerate (Fig. 2.13A), including clasts up to 12 m maximum diameter and up sequence, at Wylfa Head, laminated to finely bedded turbidite system layers (Fig. 2.13B and C) are exposed in a series of cross sections which show interbedded turbidites with clean pink arenite, rare carbonate and abundant white-green wacke channels as well as monomict translational slide deposits (Fig. 2.13C and D). Despite the limited outcrop thickness available, the three main Gwna Group lithofacies are clearly exposed in the section (Fig. 2.9C and F, 2.13A-F, 2.15).

The entire content of outcrop belt 4, a translational slice of Monian Supergroup constituents: the Coeden Beds of the Holy Island Group, New Harbour and Gwna Groups, was delivered *in situ* by broadly south-directed tectonic thrusting (Fig. 2.14) (pers. comms. A. G. Leslie) and later sliced into north-east to south-west

---

Figure 2.15 → Sketch map of Llanbadrig Point (SH373 947) showing the distribution along ~ east-west strike of numerous polymictic debris flows, dominated by quartz arenite and shallow marine carbonate clasts within a matrix of grey-green mud to silt grain size. At Llanbadrig Point there is a conspicuous stack of substantial quartz arenite channels with very little matrix squeezed between them – which is unusual and interpreted as en masse block transported within a debris flow. Although the clasts are irregularly shaped, the long axes are rotated into alignment with the matrix fabric – interpreted as non-primary but as a later artefact related to deformation. The matrix, as is common in the debris flows, contains many cm scale clasts of varied lithology tightly packed around, between and sometimes within the clasts where cavities are present. The section youngs to the north. (see Fig. 2.14 for location within outcrop belt 4 map).

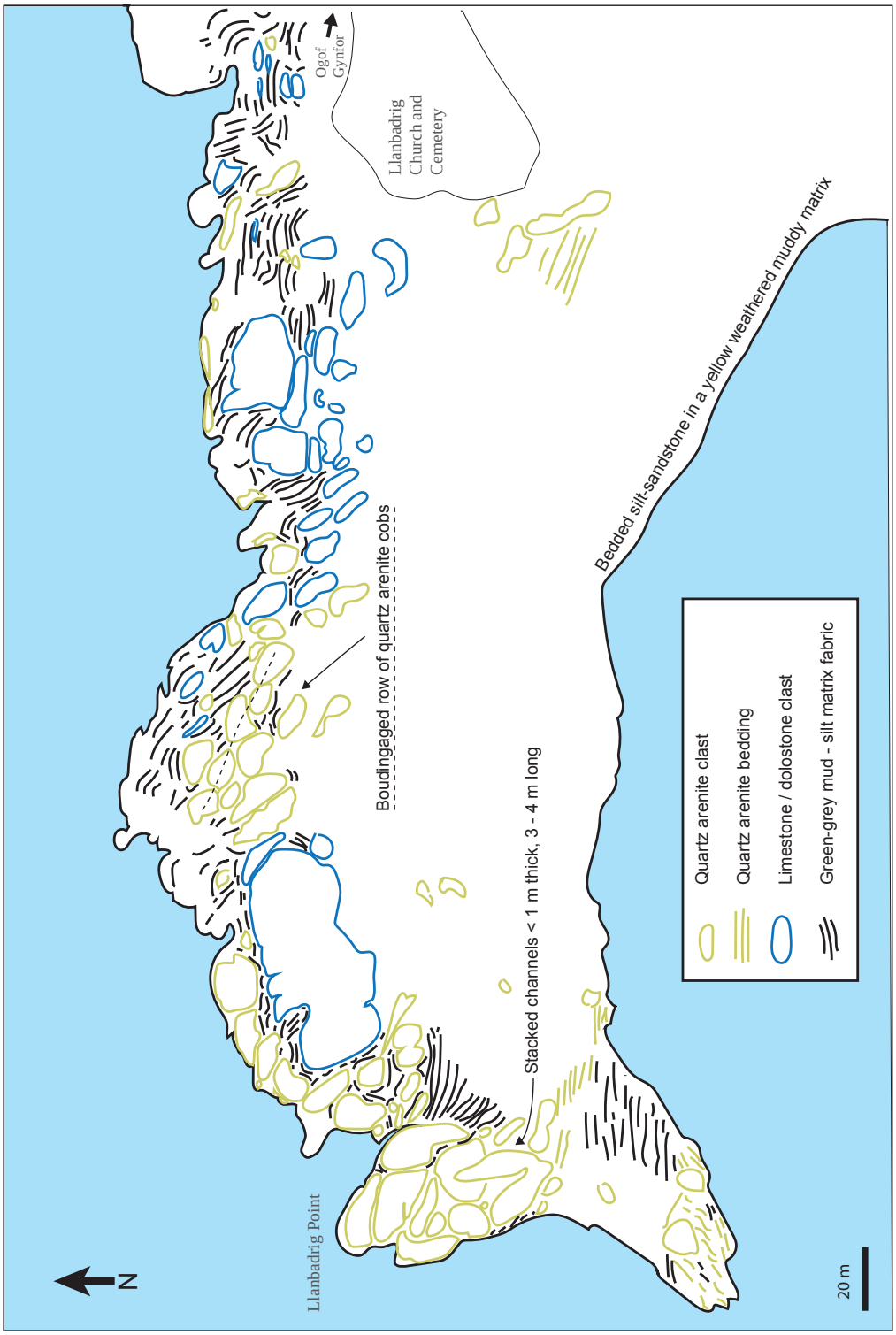
Ogof Gynfor
Llanbadrig Church and Cemetery
Boudingaged row of quartz arenite cobs
Stacked channels < 1 m thick, 3 - 4 m long
Bedded silt-sandstone in a yellow weathered muddy matrix
Llanbadrig Point
N
Quartz arenite clast
Quartz arenite bedding
Limestone / dolostone clast
Green-grey mud - silt matrix fabric
20 m

trending blocks that juxtapose filets of Gwna Group overlying the New Harbour Group with polymict megaconglomerate (facies C) or the turbidite system (facies A), the latter presently classified as Church Bay Tuff (Greenly, 1919). The faulting discussed above was not part of this study: as with all linework other than sedimentary boundaries, the information is taken from published maps and the new BGS geological map of Anglesey, currently in production.

There is informative exposure of polymict megaconglomerates along the coast from Wylfa Head to Porth yr Ogof (SH35 93 to SH37 94) (Fig. 2.9B-D and F, 2.13C-F and 2.15), but particularly between Porth Wylfa and the west side of Cemaes Bay (NGR SH36 93), where the section is free from the intense faulting that cross-cuts the continued exposure, east of Cemaes Bay (Fig. 2.7A and B, 2.13D). In the west, inverse grading of clasts and the clast-supported aspect of the megaconglomerate can be seen (Fig. 2.7A, B and 2.13D). Farther east, at Trwyn y Parc (SH372 943) the largest exposed Gwna Group clast sits within a polymict megaconglomerate surrounded and injected by mud to silt green-grey matrix (see Chapter 4), but in this region many arenite and carbonate clasts extend to between 20 to 60 m diameter (Fig. 2.15). Abundant smaller clasts (mostly 5 mm – 30 cm diameter) of yellow sandstone, jasper, black sandstone, chert, granite and diorite populate the megaconglomerate. The tip of Llanbadrig Point (SH374 946) is composed of a stack of thick arenite channel forms (Fig. 2.15), each < 80 cm thick, pinching out laterally over 4 – 8 m. There are beds 4 – 8 cm thick beneath the cliff edge: these broken beds seem to have been transported within the megaconglomerate *en mass* – the combined block is surrounded by grey mud-silt matrix on the landward sides but there is no matrix to be seen outboard. Farther along strike there is a linear trace of 5 – 9 m diameter, spherical, white-orange weathered arenite “cobs” siting within a thick smear of matrix wrapped around numerous smaller clasts (Fig. 2.15). Moving

farther east, at Llanbadrig (SH377 947) the megaconglomerate is dominated by large shallow-marine dolo-limestone clasts (Fig. 2.15). The alternation of arenite and carbonate dominance within the larger clast content along the roughly east-west trending basal unconformity suggests spatially controlled sampling of sediment from a continental margin source.

At Ogof Gynfor (SH378 947), east of Llanbadrig, the Gwna Group is unconformably overlain with angular discordance by parallel-bedded Ordovician sediments (Fig. 2.13E). The contact is repeated by faulting, and glimpses of this are seen from the coastal path to the east of Ogof Gynfor (Fig.2.13F) revealing a striking sedimentary overstep, later subject to south-directed thrusting, exposed at Porth Llanlleiana (SH387 952).

2.3 Facies associations: Sections associated with the Menai Straight Fault System

South-west Anglesey – Outcrop belt 2

The simply deformed Gwna Group here overlies polydeformed metasediments of the CASZ (Gibbons and Horák, 1990) (Fig. 2.16A). The contact bears the same stratigraphic relationship as those discussed above at outcrop belts 3 and 4: stratigraphic angularity, and metamorphic and structural discontinuity. The unconformity is exposed on the coast in three places (Fig. 2.16B and C):

- South of Porth Cwyfan and north of Aberffraw at SH337 675
- Later faulting repeats the exposure in parallel several metres south
- At Porth Nobla, south of Rhosneigr, at SH327 714

Gwna Group sediments young to the south from the duplexed basal unconformity near Porth Cwyfan. An anticline with an axial trace orientated north-east to south-west folds the CASZ metasediments (Fig. 2.16) and with it, the contact between the CASZ and the Gwna Group (Fig. 2.17B). Hence an exposed slice covering an area < 500 m^2, later faulted and locally intruded, juxtaposes the Coedana Granite with a repetition, in the northern fold limb, of the CASZ/Gwna Group contact and overlying Ordovician rocks in well-established sedimentary sequence on the foreshore at Porth Nobla (Fig. 2.16B), in which a polymict debris flow ~ 12 m thick infills the CASZ palaeosurface (Fig. 2.17B), and is itself overlain by Gwna Group turbidites and translational slump beds, younging to the north-west. One of the many north-south orientated Palaeozoic dolerite dykes (Greenly, 1920) orthogonally cuts through the CASZ/Gwna Group

---

Figure 2.16 → Geological and basal relationship maps for outcrop belt 2. **A.** Geological map of outcrop belt 2 (after Greenly 1920, BGS Anglesey map, in production). The position of inset maps B and C are indicated. NB the geological map A does not show the Gwna Group outcrop at B due to scale. **B.** A sketch map of the unconformable contact between CASZ psammitic metasediments and Gwna Group polymictic debris flows. The Gwna Group here consists of a minor slice cropping out on the beach at Porth Nobla that is easily recognisable with clasts of sandstone, pink arenite and carbonate as well as a large granite clast, rare in the mélange - perhaps derived from the nearby Coedana Granite. The debris flows are matrix supported and intensely deformed in a <20 m thick band ~ 30 m above the unconformity. Debris flows and siltstone-mudstone thinly bedded turbidites give way to Ordovician sediments south of Rhosneigr. **C.** A sketch map of the unconformable contact between the polydeformed pelitic metasediments of the CASZ and debris flows of the Gwna Group. The contact crops out twice, more or less parallel, around the narrow inlet south of Porth Cwyfan. There is complex faulting and thrusting and the repetition is interpreted as a duplex. Conspicuous clasts of quartz arenite, carbonate, yellow sandstone and jasper sit in a green matrix – the debris flows here are matrix supported. Fine grained matrix on both outcrops of the unconformity are strongly sheared and those on the lower exposure are submylonitic. The upper outcrop of the unconformity contains smeared clasts, similar to those in the deformed band at Porth Nobla. **D.** Field sketch map of outcrop belt 2 showing the sedimentary relationships between the Gwna Group lithofacies A, B and C. *The orientation of the repeated isoclinal fold axes is approximate due to nature of the outcrop.

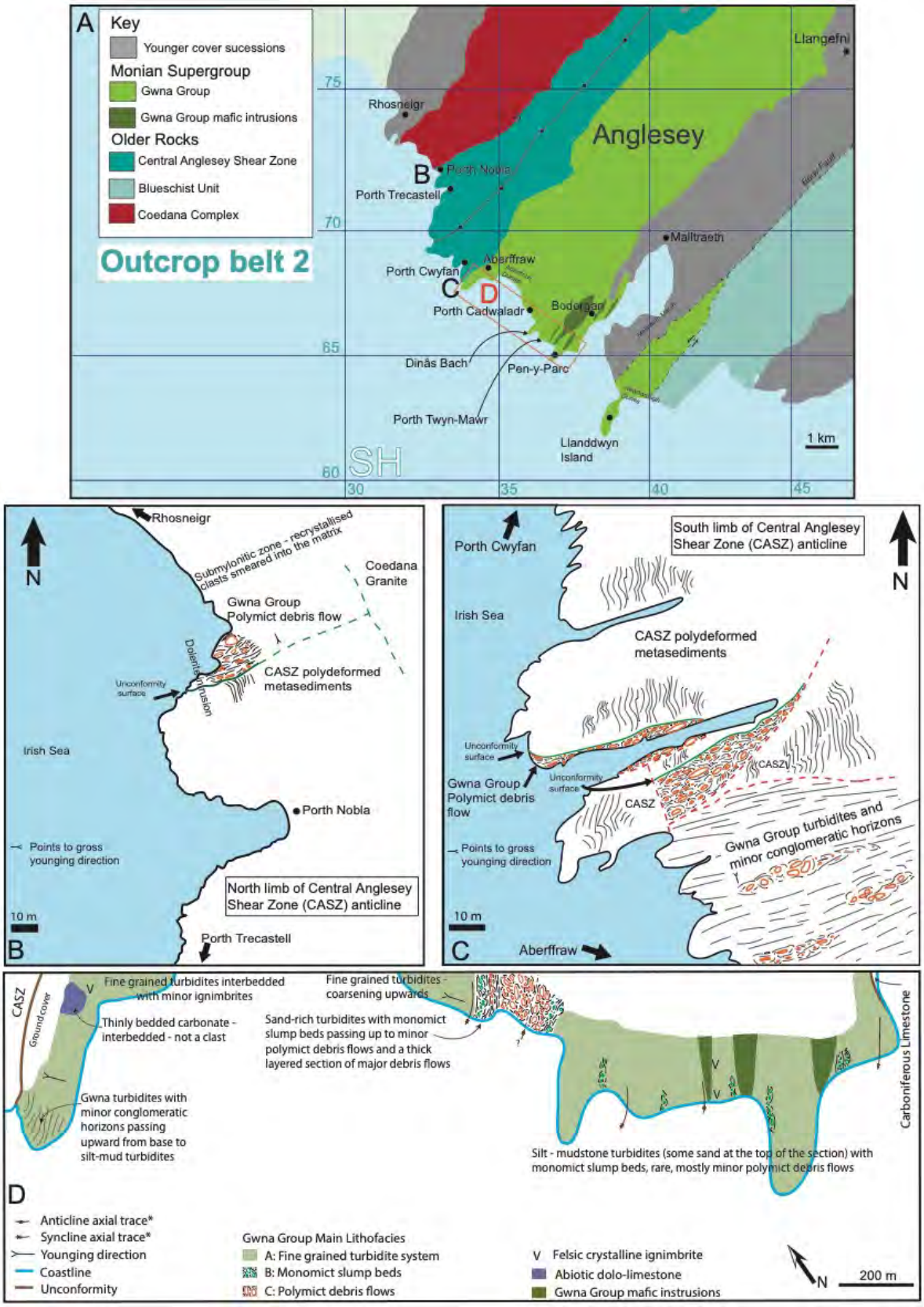
A
Key
Younger cover sucessions
Monian Supergroup
Gwna Group
Gwna Group mafic intrusions
Older Rocks
Central Anglesey Shear Zone
Blueschist Unit
Coedana Complex
Outcrop belt 2
Llangefni
Rhosneigr
Anglesey
B
Porth Nobla
Porth Trecastell
Malltraeth
Aberffraw
Porth Cwyfan
C
D
Porth Cadwaladr
Bodorgan
Dinas Bach
Pen-y-Parc
Porth Twyn-Mawr
Llanddwyn Island
1 km
SH
75
70
65
60
30
35
40
45
N
Rhosneigr
Submylonitic zone - recrystallised clasts smeared into the matrix
Coedana Granite
Gwna Group Polymict debris flow
Dolerite intrusion
Unconformity surface
CASZ polydeformed metasediments
Irish Sea
Porth Nobla
Points to gross younging direction
North limb of Central Anglesey Shear Zone (CASZ) anticline
10 m
B
Porth Trecastell
Porth Cwyfan
South limb of Central Anglesey Shear Zone (CASZ) anticline
Irish Sea
CASZ polydeformed metasediments
Unconformity surface
CASZ
Gwna Group Polymict debris flow
Gwna Group turbidites and minor conglomeratic horizons
Points to gross younging direction
10 m
C
Aberffraw
CASZ
Groundcover
Fine grained turbidites interbedded with minor ignimbrites
V
Thinly bedded carbonate - interbedded - not a clast
Gwna turbidites with minor conglomeratic horizons passing upward from base to silt-mud turbidites
Fine grained turbidites - coarsening upwards
Sand-rich turbidites with monomict slump beds passing up to minor polymict debris flows and a thick layered section of major debris flows
Silt - mudstone turbidites (some sand at the top of the section) with monomict slump beds, rare, mostly minor polymict debris flows
Carboniferous Limestone
D
Anticline axial trace*
Syncline axial trace*
Younging direction
Coastline
Unconformity
Gwna Group Main Lithofacies
A: Fine grained turbidite system
B: Monomict slump beds
C: Polymict debris flows
V Felsic crystalline ignimbrite
Abiotic dolo-limestone
Gwna Group mafic instrusions
N
200 m

contact (Fig. 2.16B). Deformation has subsequently altered the turbidite and slump beds from about 50 m above the unconformity, so that the normally well-defined channels and clasts are recrystallised and smeared into the glassy green muddy host beds. The basal debris flow is not altered to this extent suggesting the folding had less impact than later events. Clasts of carbonate, arenite, red chert and yellow sandstone upward of a few cm diameter are mixed in a swirling green matrix with others of 80 cm to 2 m diameter, including a conspicuous orange weathered granite clast > 1 m diameter.

The southern limb, and main exposure of this section, is complex in deformation terms – the unconformity is exposed twice (over a few metres) as a result of later, intense faulting (Fig. 2.16C) and there is more evidence of folding on north-east to south-west trending axes throughout the section. The boundary, as in outcrop belts 3, 4 and Porth Nobla, above, exhibits stratigraphic angularity, metamorphic and deformation discontinuity. Figure 2.16C shows the deformed and altered state of the CASZ polydeformed semipelite and comparison with heterolithic laminated sediments from the overlying Gwna Group (Fig. 2.17D) enforce the tectonic and metamorphic break represented by the unconformity. Although there is less deformation above the unconformity than below it, a single bedding-parallel cleavage is present in the Gwna Group — the deformation is Waldron *et al*.'s (2018) Floian Monian Orogeny, exhumation of which is isotopically dated using K-Ar in phengite in New Harbour Group schists (Asanuma *et al*., 2017). Minor relief in the CASZ surface is infilled by a 3 m thick polymict matrix supported conglomerate (Fig. 2.17A) with clasts of arenite, carbonate, chert and yellow sandstone, from a few cm to 80 cm maximum diameter, the mud-silt matrix is green and is thoroughly injected between the clasts and into the irregularities of the lower contact. In the repeated section of the contact (Fig. 2.16C) many clasts are smeared into the matrix, as at Porth

Nobla. Above the basal conglomerate, a sequence of sub-vertical, fine grained laminated and finely bedded turbidites are faulted into position against polydeformed CASZ pelites. At around 60 m up the section, the laminated turbidite mud has a dusty, buff weathered colour, and is interbedded with crystalline felsic ignimbrite (NGR SH343 677). A substantial carbonate unit sits alongside the tuff beds, and this is overlain by green laminated turbidites (Fig. 2.17D), containing green-white siltstone channels up to 10 cm wide and 2 – 3 cm thick. The 750 m wide bay at Aberffraw is covered by thick sand dunes and continuity of the underlying bedrock cannot be verified, although Gwna Group

---

Figure 2.17 Sedimentary relationships in outcrop belt 2. **A.** Image facing south-west shows the small inlet (SH337 675) where the main Gwna Group outcrop begins, south of Porth Cwyfan and south-west of Aberffraw. CASZ metapelites are in faulted contact with a minor slice of Gwna Group polymictic debris flow. The unconformity is repeated by the faulting – a few metres to the right and left of this view (see also Fig. 2.16C). **B**. The unconformable contact between psammites of the CASZ and a Gwna Group polymict debris flow on the margin of the north limb of the CSZ anticline at Porth Nobla (SH328 714) (see also Fig. 2.16A). Clasts within a green mud-silt matrix sit on the contact and are distributed throughout the 5 - 6 m thick layer. The matrix records the deformation in well-developed schistosity. Facing west. 8 cm long compass-clinometer for scale. **C.** Plane-polarised light photomicrograph of polydeformed CSZ semipelite, from ~50 m below the unconformity, south of Porth Cwyfan (SH338 679). **D.** Plane-polarised light photomicrograph of deformed Gwna Group laminated mud-heterolithic distal turbidites, south-west of Aberffraw (SH344 676). Grading from silt to mud is repeatedly seen in <2.5 mm thick laminations and there is subtle grading within several silt layers - seen to the left of the grading symbols. The mud layers are stylolitised, the silt layers are laterally shortened: the effects of non-genetic, later deformation. **E.** Northwards younging (to the left) coherent Gwna Group section in the south limb of a syncline. The base of polymictic debris flow 1 contains all clasts within the matrix – there are no clast protrusions, the top of the bed has relief, infilled by mud-heterolithic turbidite system beds, with minor sand channels (2). Debris flow 3 has cut down into 2. 4 may be a combined clast within 3, or may record in situ deposition that infills the relief at the top of 3 – this could not be determined with any certainty. The sand channel is among the largest in this section and is unusual in containing up to granule sized grains. It is poorly graded. Laminated mud layers <30 cm thick sit on top of the sand channel –the retained laminar fabric of these layers implies that this bed was deposited in situ, infilling the relief of the debris flow. Polymict debris flow 5 is the youngest deposit in this succession. This section shows the dominance of polymictic debris flows over “background” sedimentation during lowstand conditions, when the debris flow lithofacies was formed. Image taken facing north-east, at Porth Twyn-Mawr (SH363 658). One metre rule for scale.

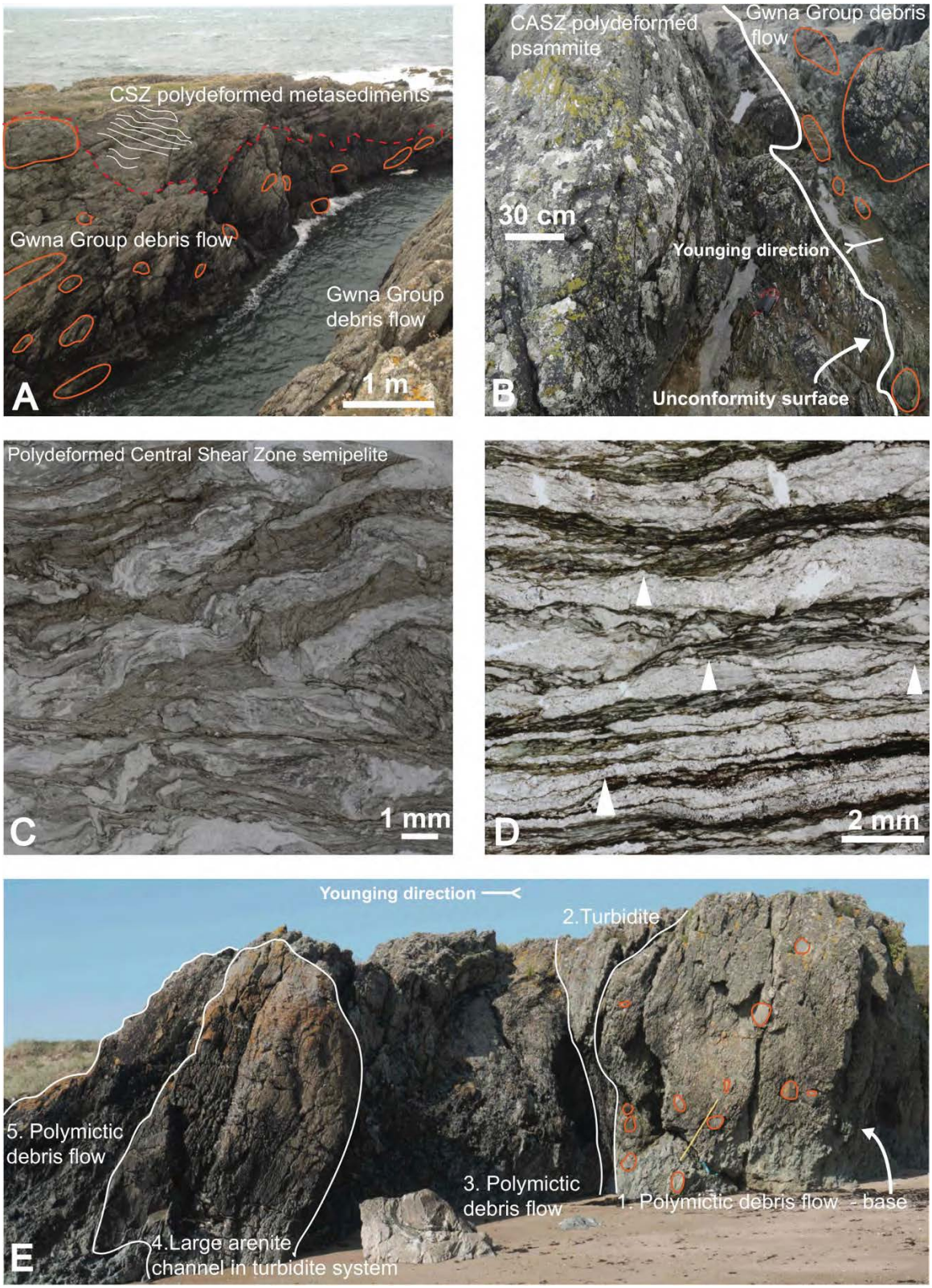
CSZ polydeformed metasediments
Gwna Group debris flow
Gwna Group debris flow
1 m
A
CASZ polydeformed psammite
Gwna Group debris flow
30 cm
Younging direction
Unconformity surface
B
Polydeformed Central Shear Zone semipelite
1 mm
C
2 mm
D
Younging direction
2.Turbidite
5. Polymictic debris flow
3. Polymictic debris flow
1. Polymictic debris flow - base
4.Large arenite channel in turbidite system
E

deposition is thought to be continuous.

South of the beach, sub-vertical, fine grained turbidites continue: mud and siltstone strata, muddy sand channels and some pink arenite, starved gutter casts/channels are intermittently accompanied by discrete monomict slump beds, < 50 cm thick (Fig. 2.7F). Moving upwards the dominance of mudstone-siltstone in the turbidite system gives way to a 12 m thick, sand-rich horizon just north of Porth Cadwaladr (SH358 666 and SH359 667) which, towards the top, incorporates several 40 - 60 cm thick polymict conglomerate debris flows interleaved between medium grain-sized, sand dominated event beds (Fig. 2.5F). The sandstone beds are synformal with an open fold hinge in the finer grade sediments below, at the coast (Fig. 2.5D).

Debris flows of polymict megaconglomerate totalling about 500 m thickness crop out at Porth Cadwaladr. Broken beds and stacked clasts of arenite, carbonate, red chert and granite a few centimetres to 20 m diameter are mixed within a swirling silty green matrix. The southern end of the bay is composed of fine-grained turbidites, an absence of debris flows and a further exposure of sand-rich beds at Dinâs Bach (SH361 658) followed by a section of interbedded turbidites and polymict debris flows (Fig. 2.17E) at Porth Twyn-Mawr that young to the north – the southern limb of a synformal fold, probably a repetition of the Porth Cadwaladr stratigraphy. Continued fine-grained turbidite beds occur, interbedded with numerous matrix-supported translational slump beds and which revert to sand-rich event beds towards Pen-y-Parc (SH368 649), where a series of lens shaped mafic intrusions are exposed at the surface (Fig. 2.16A). The mafic lenses are younger than the Gwna Group and older than the Palaeozoic ~ north-south orientated basic dykes that intrude them in the region.

The Gwna Group is unconformably overlain just north of the Malltreath Estuary

by Carboniferous Millstone Grit. Parallel to the estuary on the southern side lies the Berw Fault, a major linear structure that cross cuts Anglesey from north-east to south-west (Fig. 2.2). The Berw Fault is the northern expression of the MSFS (Fig. 2.2), the immediate southern side of which is buried under beach sand and dunes, and the only coastal outcrop is farther south, where stacks of pillow lavas and minor interstitial sand-siltstone and jasper consistently dip 20 – 25° south-east. Here the short tidal causeway leads to Llanddwyn Island, an isthmus dominated by colourful geology comprising basalt, pillow basalts, hyaloclastite, deep marine carbonate, bedded red chert, green sandstone, jasper and nodular chert, gabbro sills and dolerite dykes. Substantial pillow lava stacks and several thoroughly decomposed mafic blocks crop out in Newborough Dunes (SH39 64 and SH40 65). The island itself is faulted, and there is evidence throughout for alteration, probably by hydrothermal fluids or brines associated with fault movement and ocean floor metamorphism. Dolostones show signs of dedolomitization. Gwna Group lithofacies A, B and C are completely absent in this section. Greenly (1919) included this deep marine sequence within the Gwna Group but there are no means available to this study that enable confirmation of this association although, within the wider Gwna Group there is potentially related outcrop on the Lleyn Peninsula, at the very north of outcrop belt 1.

Lleyn Peninsula – Outcrop belt 1

The Gwna Group occupies the area north and west of the Lleyn Shear Zone (Figs. 2.2 and 2.18) on the Lleyn Peninsula – a thin band of mylonitic metamorphic rocks forming the south-westerly trajectory of the MSFS (Fig. 2.2),

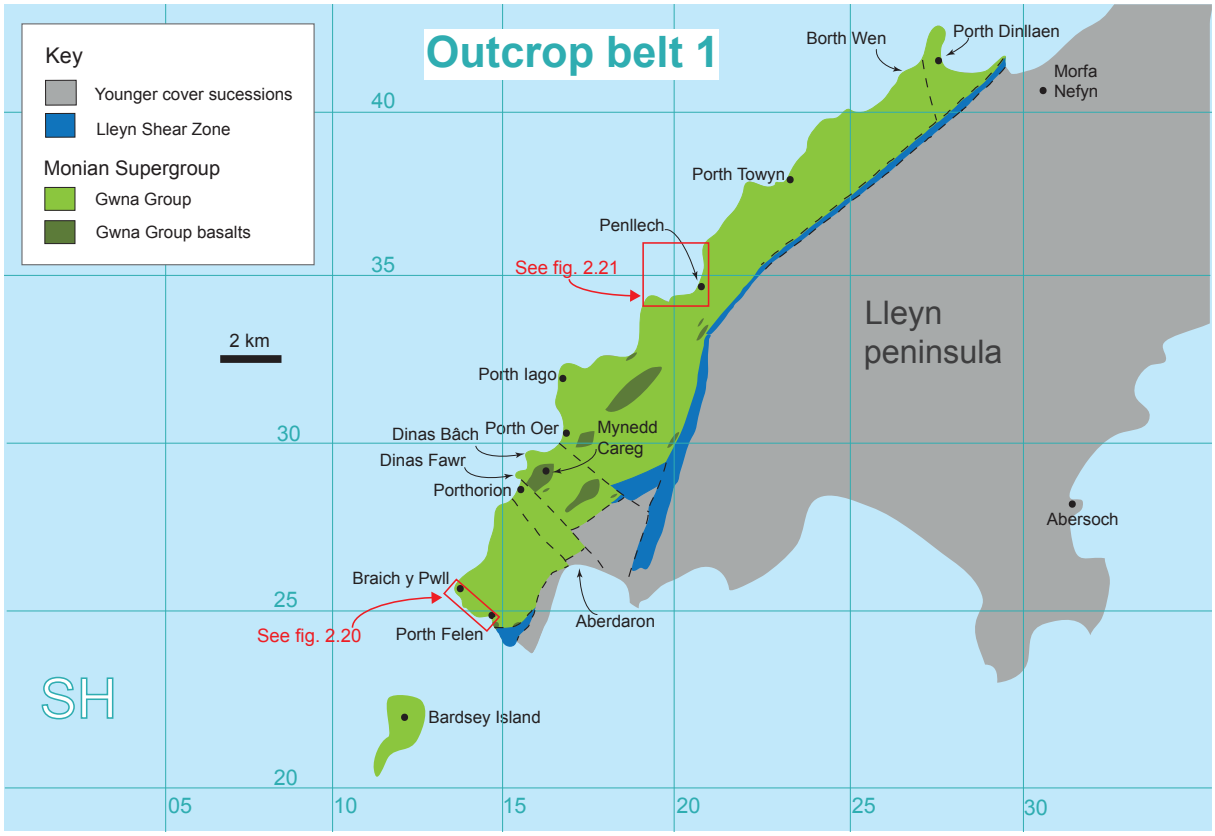

Figure 2.18 Geological map of outcrop belt 1, Lleyn Peninsula, simplified after BGS map Sheet 133.

Figure 2.19 → Laminated to finely bedded mud-dominated – heterolithic sections in outcrop belt 1, Lleyn Peninsula. **A.** Red chert-mudstone with subordinate buff chert thin beds grade upwards into sandstones with a grey volcaniclastic matrix, formerly known as the Gwyddel Formation. Porth Felen (SH144 250). One metre rule for scale. Facing west. **B.** Cherty silt-mudstone thin beds patchily weathered green and red. Hammer is 28 cm long. Braich y Pwll (SH135 255). **C.** Green-red weathered laminated mud with cm-scale siltstone lenses shows a scaly fabric. Braich y Pwll (SH135 256). Hinge on rule is at 50 cm. **D.** Deformed carbonate channel in laminated red chert-mudstone. Braich y Pwll (SH135 258). Facing east. **E.** Thin, red weathered chert-silt to buff weathered mud-topped event <8 cm thick event beds grade into laminated cherty mudstone (section youngs to the left). Porth Oer (SH166 298). Facing south-east. **F.** <10 cm long silt channels in laminated red-weathered cherty mudstone. Braich y Pwll (SH135 256). Hammer is 28 cm long.

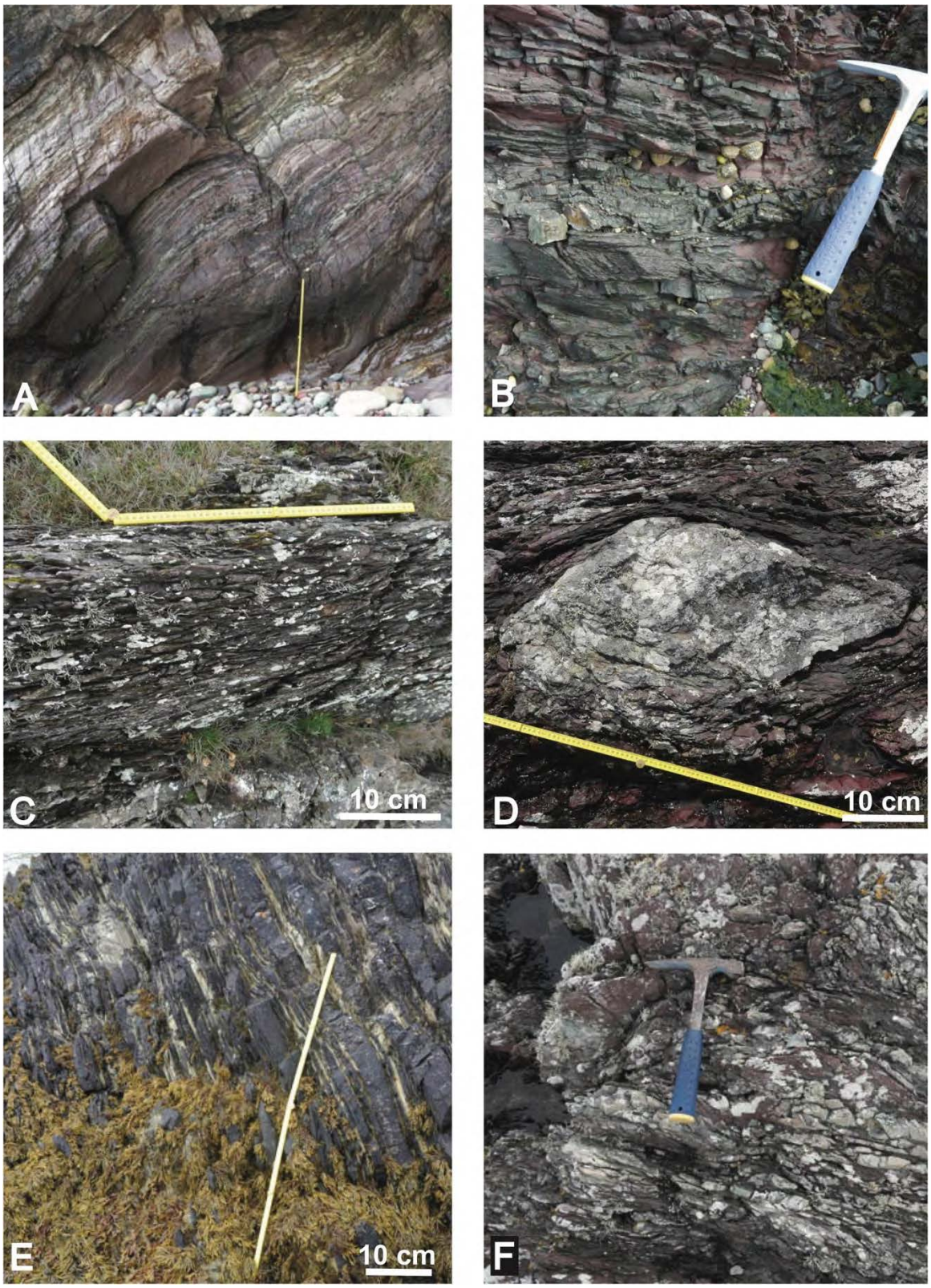
A
B
C
10 cm
D
10 cm
E
10 cm
F

and in contact with younger Ordovician cover to the south-east. The faulted relationship is continuous: no bounding sedimentological surfaces of the Gwna Group are exposed. Unsurprisingly, given that the entire outcrop belt is contained within twin strands of a major fault system, there is deformation throughout including folding along the southern coast that correlates with that in outcrop belt 2 assigned to the Monian Orogeny (Waldron *et al*., 2018).

Interbedded successions of lithofacies A, B and C form the majority of the stratigraphy albeit, in the southern half of the section, juxtaposed with a set of ocean floor lithologies, occurring either as mafic lens-shaped intrusions or in broken stratigraphic fragments, dissected by thrust faulting into “fault blocks” of tens of metres diameter. Fault blocks are defined as substantial stratigraphic fragments that do not appear to be clasts of the debris flow lithofacies because they are not contained within a matrix (Fig. 2.20E) but instead occur with faulted boundaries placing them in association with any element of the Gwna Group - they are not physically restricted to the debris flow facies. The blocks are not surrounded by matrix and are not associated with individual debris flows. They do not hold within their fabric any form of matrix: there is no matrix injection, which is a common feature throughout the Gwna Group. The basal relationship of the fault blocks cannot be determined as they do not crop out. There is no evidence therefore that would allow the fault blocks to be interpreted as debris flow clasts.

Some authors refer to ocean plate stratigraphy (OPS) as a series of ocean floor intrusive and extrusive rocks, such as gabbro, basalt, pillow basalt, overlain by deep marine lithologies, for example, mudstone, nodular chert and deep marine carbonate, that collectively record the history of new crust formation during rifting, the subsequent deposition of sediments, through to exhumation during

subduction as part of the Wilson cycle (Wakita and Metcalfe, 2005; Kawai *et al.*, 2007; Maruyama *et al.*, 2010). Internally coherent sections within such Gwna Group fault blocks include:

- Basalt, pillow basalt, interstitial jasper, carbonate and dark mudstone
- Basalt pillows, interstitial and overlying carbonate
- Basalt pillow peperite – pillows intruded into lime mud or cherty mudstone
- Basalt pillows with interstitial jasper or siltstone or carbonate
- Red chert-mudstone interbedded with dolostone
- Red chert-mudstone overlaid by yellow sandstone

Figure 2.20 → The relationship of Gwna Group lithofacies A, B and C and the Gwyddel beds on the south-west tip of the Lleyn peninsula, around the coast of Uwchmynydd (See Fig. 2.18 for area). **A.** Sketch map of Uwchmynydd with localities for annotated image sections B – E. The Gwyddel Formation megaclasts are shown from the current BGS geological map (Gibbons and McCarroll, 1993). This interpretation of the Gwyddel blocks as exotic megaclasts, is not accepted here based on the evidence within their mapped extent for lithofacies recognised in this study as major Gwna Group constituents. The Gwyddel blocks are considered representative of the sand-rich element of the turbidite facies (see also Figs. 2.5A and B). Some larger clasts are outlined with orange. Pink weathered arenite thin channels in stacks (composite channels) are marked blue. **B.** Image facing strike of a series of turbidites with channels interbedded with debris flows exposed on the headland of Trwyn Maen Melyn (SH138 253). Large clasts of arenite and carbonate are outlined with orange. The largest clast is ~ 5 m diameter. Image taken facing south-east. **C.** → → Section though turbidites with channels and debris flows at Trwyn Maen Melyn (SH138 251), facing north. PDF = polymictic debris flow. T + c = mud dominated turbidites with discrete channels of pink/white weathered arenite, carbonate or green-white channels of siltstone in a mudstone matrix. ST = Silt – sand dominated turbidites. MSB = monomictic slump bed. Some clasts are outlined with orange. The beds are the right way up – younging to the north-east (top right of the image). **D.** Cross-section of monomict, matrix-supported slump beds interbedded with turbidites. The beds are the right way up: each successive bed has infilled the surface relief. East of Trwyn Maen Melyn (SH139 251). Image taken facing north-east. 50 cm rule for scale**. E.** Fragmented block of pillow basalts in normal sedimentary continuity with a draped Gwna Group matrix supported debris flow. There is no matrix surrounding the pillow basalts, nor is any matrix injected into the fault block – the debris flow overlies the basalt and has more-or-less infilled the surface relief. Several basalt pillows are outlined with green. Porth Felen (SH144 247). Facing north-west.

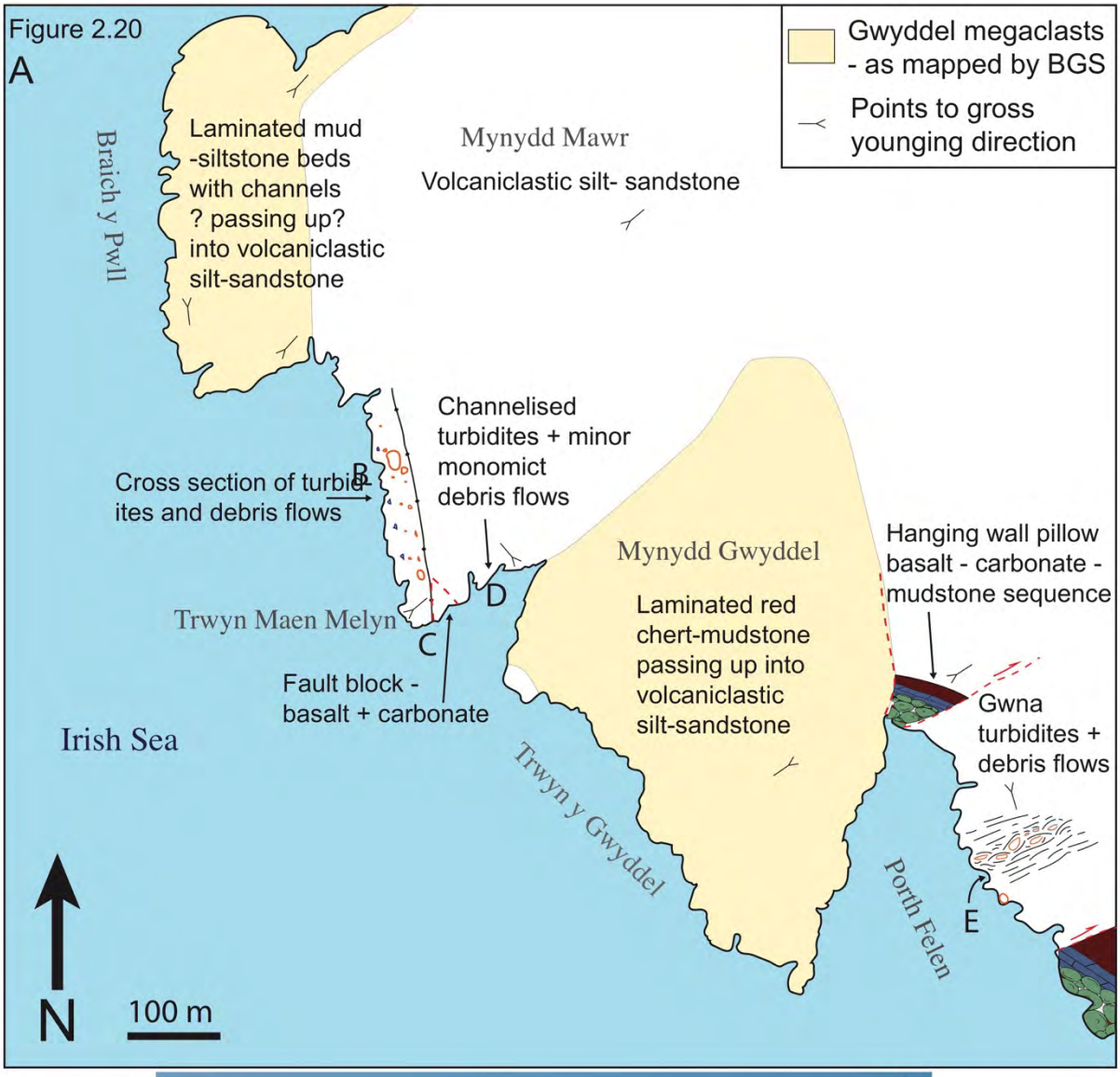
Figure 2.20
A
Gwyddel megaclasts - as mapped by BGS
Points to gross younging direction
Braich y Pwll
Laminated mud -siltstone beds with channels ? passing up? into volcaniclastic silt-sandstone
Mynydd Mawr
Volcaniclastic silt- sandstone
Channelised turbidites + minor monomict debris flows
Cross section of turbidites and debris flows
B
D
C
Trwyn Maen Melyn
Fault block - basalt + carbonate
Mynydd Gwyddel
Laminated red chert-mudstone passing up into volcaniclastic silt-sandstone
Hanging wall pillow basalt - carbonate - mudstone sequence
Gwna turbidites + debris flows
Irish Sea
Trwyn y Gwyddel
Porth Felen
E
N
100 m


B

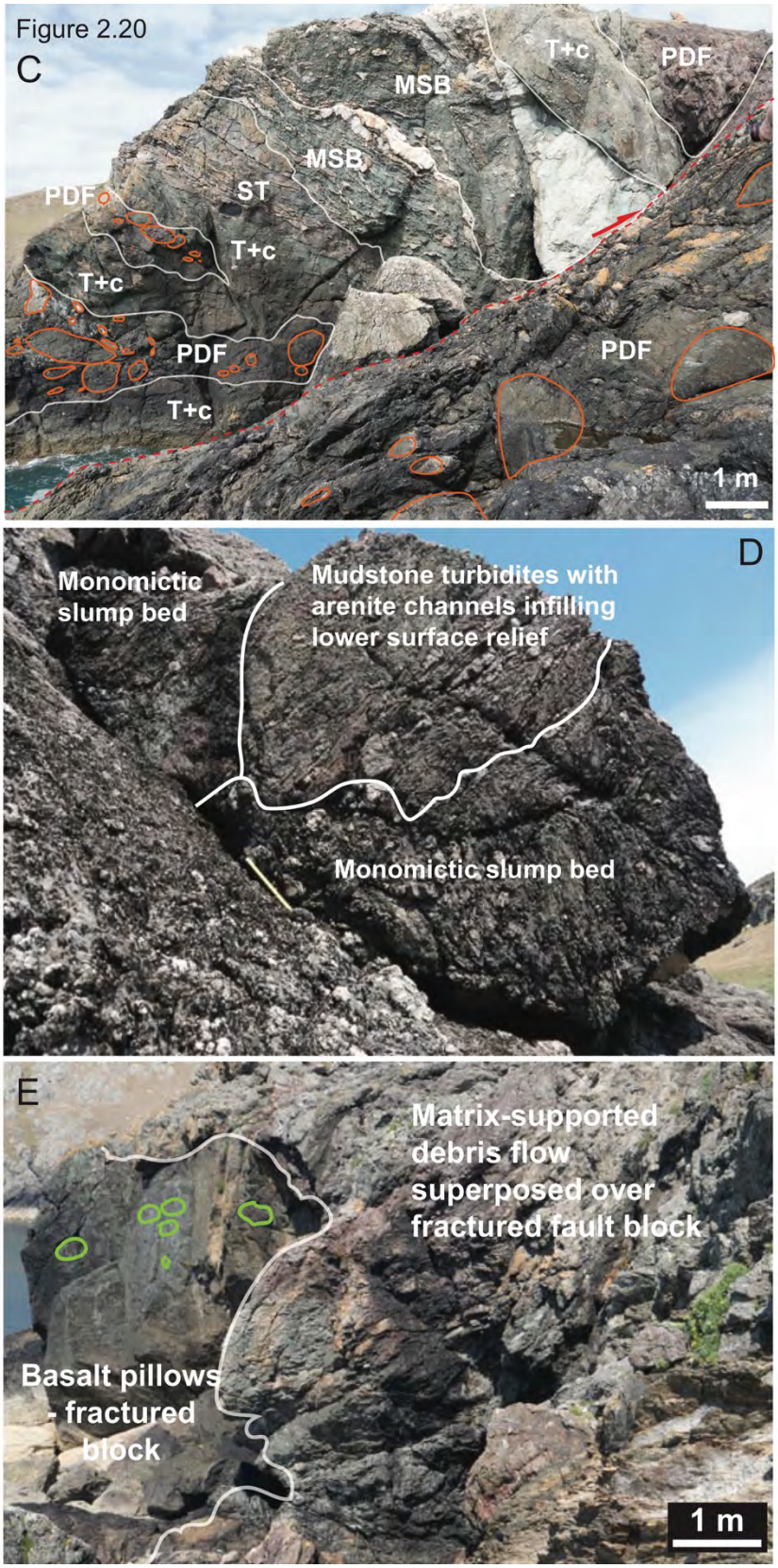
Figure 2.20
C
T+c
PDF
MSB
MSB
PDF
ST
T+c
T+c
PDF
PDF
T+c
1 m
D
Monomictic slump bed
Mudstone turbidites with arenite channels infilling lower surface relief
Monomictic slump bed
E
Matrix-supported debris flow superposed over fractured fault block
Basalt pillows - fractured block
1 m

Many of the fault blocks, particularly the pillow lavas and associated carbonates, show signs of metasomatic alteration, effects not generally shared by lithofacies A, B and C.

Successions of laminated red and buff weathered mudstone that pass upwards to decimetre scale bedded volcaniclastic cherty mud-siltstone (Fig. 2.19A), previously the Gwyddel Felsitic Formation (Matley, 1928), form the topographical highs of the southernmost Lleyn section, as do the sand-rich turbidite sections in outcrop belt 2. The Gwyddel beds account for much of the surface exposure of the Gwna Group south of Porth Oer and through time have been variously interpreted as a section of the Skerries Formation and New Harbour Group (Matley, 1928) and were later mapped as Gwna megaclasts (Gibbons and McCarroll, 1993).

The main Gwna Group facies, relating to a fine-grained turbidite system with translational slumps and polymict debris flows, dominate this outcrop belt as pervasively as it does on Anglesey but there are some subtle variations. South of Porth Oer the fine grained turbidites can exhibit a deep red weathered colour (Fig. 2.19B-F) – either throughout or in irregular patches, interspersed with more characteristic green-weathered strata, implying haematite concentrations. Similar fine beds or laminated beds form the base of several Gwyddel successions, particularly at Porth Felen (SH144 249) (Fig. 2.19A) and Porth Oer (SH164 298) (Fig.2.19E). Folded turbidites pass upwards into sand-rich volcaniclastic beds (Fig. 2.5A and B) at Braich y Pwll (SH137 255) which suggests that the Gwyddel beds may form part of the regional turbidite system. Shackleton (1954a) noted that at Mynydd Anelog (SH152 272) the Gwna mélange is conformably overlain by Gwyddel beds but Gibbons and McCarroll (1993) suggested they could be mapped as Gwna mélange clasts which they considered to be contained within a matrix. This study was unable to verify the

latter statement but instead agrees with Shackleton's observation of sedimentary conformity.

The field relationships between Gwna Group facies A, B, and C, the fault blocks and the so-called Gwyddel beds is illustrated along the south Lleyn coast between Braich y Pwll and Porth Felen (Fig. 2.20A-E). In the northern Lleyn (above Porth Oer) lithofacies A and B dominate the geology. There are no seafloor fault blocks but instead several notable outcrops of polymict debris flows (Fig. 2.21A-F). At Penllech Beach (SH19 34 to SH 20 35), a 2 km wide bay, there are, exposed at intervals, coherent sections of interbedded turbidites and the largest examples of monomict slump beds, mixed with polymict debris flows, containing clasts from a few millimetres to 5 m diameter (Fig. 2.21B, C and E), set within a mud to silt green matrix.

Just south of Borth Wen (SH 271 411) an extensive fine grained turbidite sequence with white-green sandstone filled channels (Fig. 2.22C) overlies highly deformed felsic tuff beds approximately 5 m thick (Fig. 2.22A) and coarsens

---

Figure 2.21 Penllech Beach – sketch map, log and three images demonstrate the relationship between Gwna lithofacies A, B and C. See figure 2.18 for location of map area. **A.** Sketch map of Penllech Beach with locations for figures B – F, showing the lateral variation in outcrop of Gwna Group lithofacies. **B.** Log through sand-rich turbidite system with interbedded intrabasinal monomict slump beds at the south-west corner of Penllech Beach. The log starts at SH19798 34162 and ends at SH19782 34166. **C.** At the centre of the beach (SH205 347) subvertical siltstone – medium grain size sandstone beds of the turbidite system (ST) are repeatedly interrupted by polymict debris flows (PDF). One metre rule for scale. Facing north-east. **D.** North-west (left) younging, steeply dipping heterolithic turbidites with laterally extensive, thin sand beds and channels (T+c) alternate with polymict debris flows and monomict slump beds (MSB). (SH205 347) Facing north-east. **E.** Image of interbedded lithofacies A, B and C in a well-preserved stack in the centre of Penllech Beach (SH208 349). Typical lithofacies C characteristics: inverse grading, clast-supported and matrix-supported areas are evident in the polymict debris flow. In contrast, the overlying slump bed is matrix-supported, contains clasts on a cm-scale and the matrix exhibits a scaly fabric. Facing north. One metre rule for scale. **F.** Beyond the northern tip of Penllech Beach (SH208 358) a north-west (left) younging cross-section of interbedded monomict slump beds and thinly bedded turbidites crops out. Facing north-east.

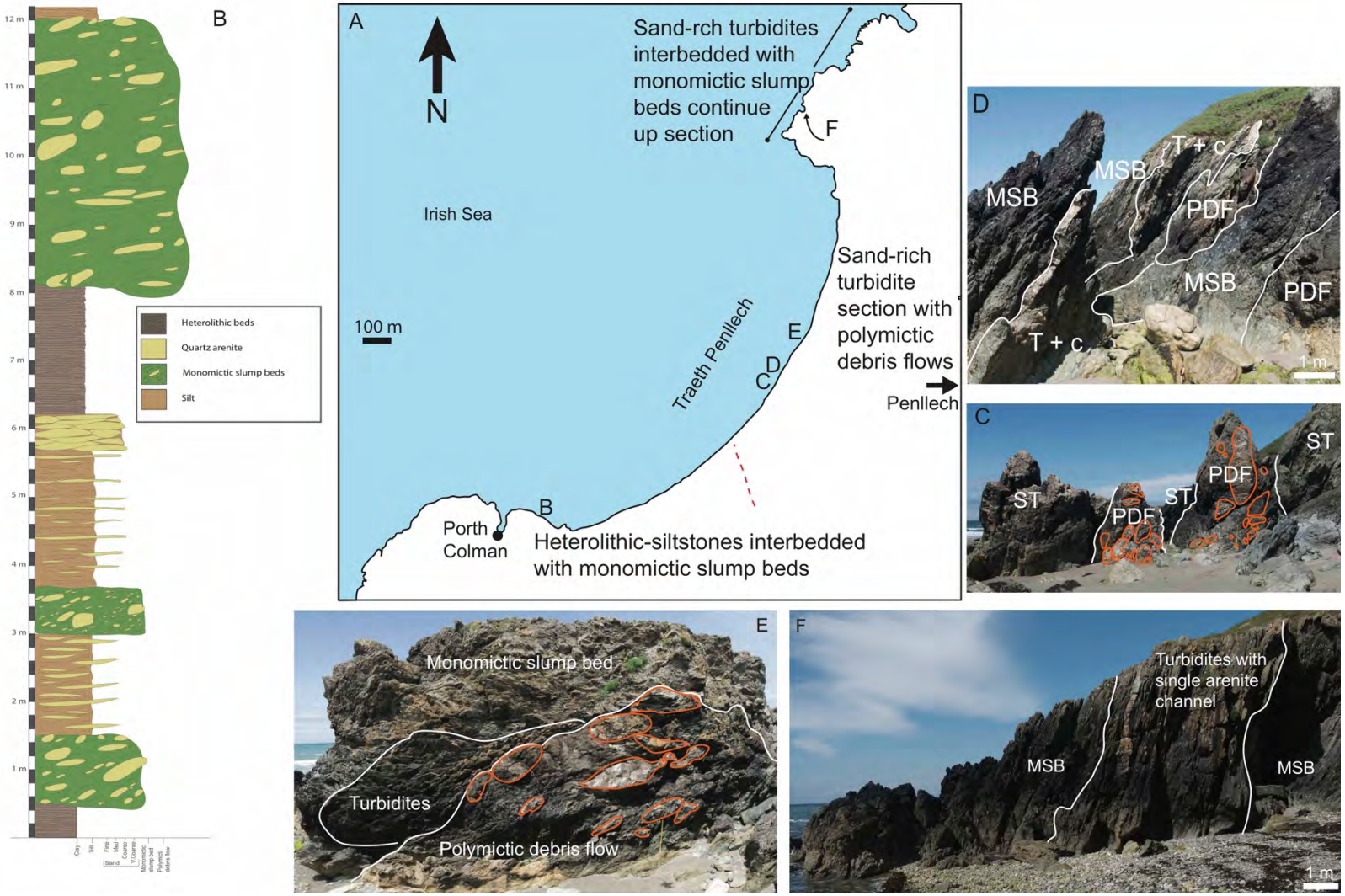
B
12 m
11 m
10 m
9 m
8 m
7 m
6 m
5 m
4 m
3 m
2 m
1 m
Heterolithic beds
Quartz arenite
Monomictic slump beds
Silt
A
N
Sand-rch turbidites interbedded with monomictic slump beds continue up section
F
Irish Sea
100 m
Traeth Penllech
E
D
C
Sand-rich turbidite section with polymictic debris flows
Penllech
B
Porth Colman
Heterolithic-siltstones interbedded with monomictic slump beds
D
MSB
T + c
MSB
PDF
MSB
PDF
T + c
1 m
C
ST
PDF
ST
ST
PDF
E
Monomictic slump bed
Turbidites
Polymictic debris flow
F
Turbidites with single arenite channel
MSB
MSB
1 m

upwards to a thin sand-rich section of decimetre beds topped by a well-preserved polymict debris flow (Fig. 2.22B and C), beneath a faulted mass of sand-rich beds and debris flow clasts in igneous contact with a mafic intrusion (Fig. 2.22E). A thermal contrast at the time of intrusion is recorded by the baked margin above which the rocks pass upwards into amygdaloidal basalt and basalt pillows, with interstitial jasper and siltstone (Fig. 2.22F) and rare fine sandstone beds. The basalt pillow unit makes up the whole of Penrhyn Nefyn point and the western end of Porth Dinllaen beach, where the Gwna Group sedimentary exposure comes to an end. Mylonitic schists of the Lleyn Shear Zone crop out at the east side of Porth Dinllaen.

Figure 2.22 → Monomict matrix-supported conglomerates and associated facies, in the Borth Wen to Penrhyn Nefyn area, outcrop belt 1. **A.** Laminated mudstone overlying siltstone beds, west of Borth Wen SH265 406). Facing south-east. **B.** Turbidite system overlaid by an erosive polymict bimodal debris flow west of Borth Wen (SH271 411). Some clasts are outlined with orange. The succession youngs to the west – view to the west. One metre rule for scale. **C.** Subvertical turbidite succession with discrete sandstone channels and a 50 cm thick sandstone horizon – lithofacies A overlies a monomict slump bed of lithofacies B. Some clasts are outlined with orange. The younging direction is to the left. South-west of Borth Wen (SH268 409). Facing north-west. **D.** A polymict bimodal debris flow of lithofacies C forming a small isthmus south-west of Borth Wen (SH259 399). Some clasts are outlined with orange. The development of schistosity in the matrix and the alignment of clasts within this later imposed fabric can be seen – it is indicated with white lines. Image taken facing west. **E.** The baked margin of a dolostone debris flow clast <10 m diameter (right) intruded by dolerite (left) - orientated east-west, on the beach at Borth Wen (SH274 411). Facing south-east. **F.** Pillow basalts on the west coast of Penrhyn Nefyn (SH274 416). The pillows are commonly small – up to 40 cm diameter, but in the image up to 25 cm. They overlie amygdaloidal basalt and have been deposited with interstitial silty hyaloclastite and some jasper. Facing north.

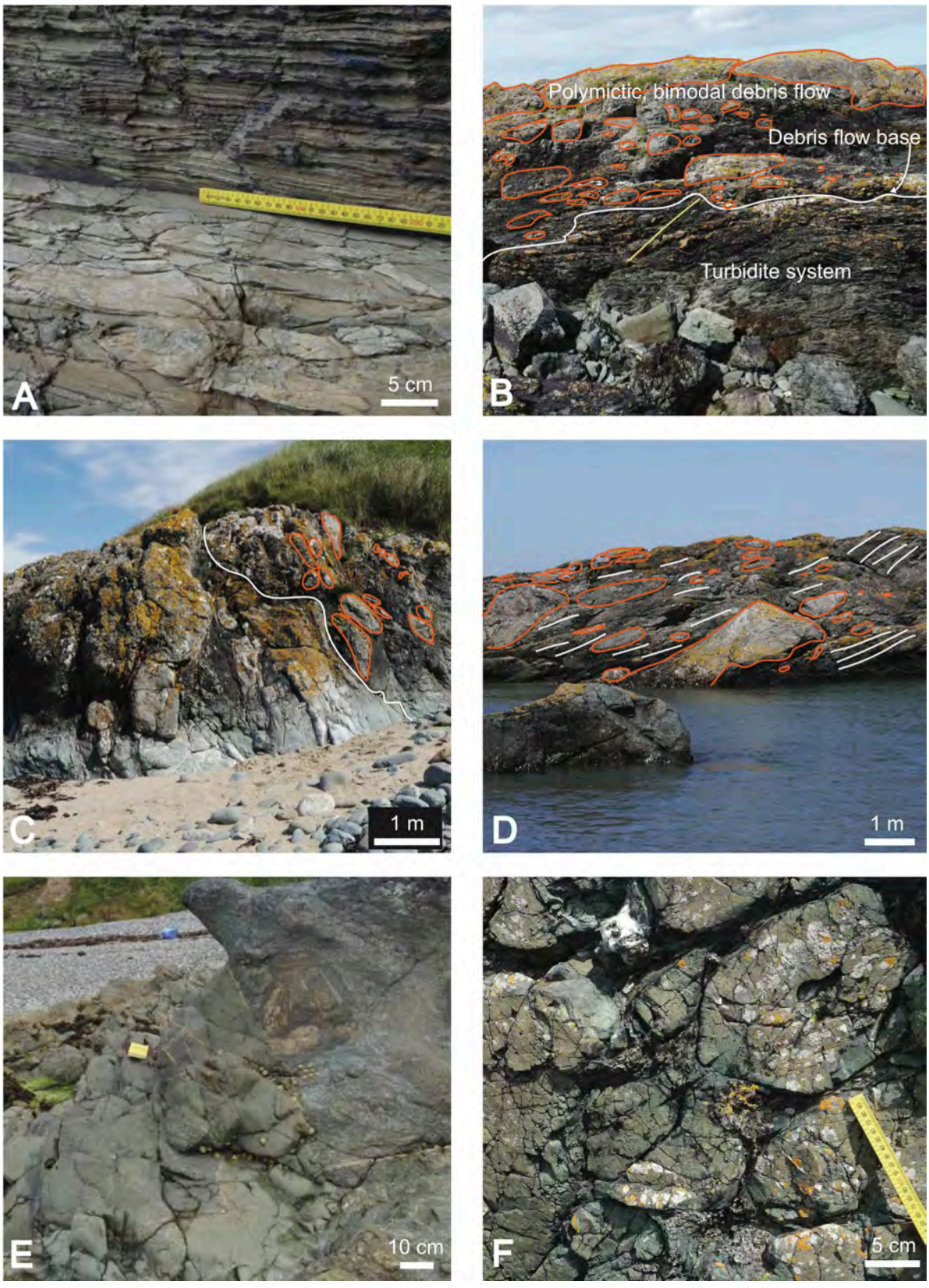
A
5 cm
B
Polymictic, bimodal debris flow
Debris flow base
Turbidite system
C
1 m
D
1 m
E
10 cm
F
5 cm

2.4 Sedimentary overview

The Gwna Group consists of a coarsening-upwards turbidite system punctuated with subordinate point-sourced sand-starved channels, interbedded with numerous intrabasinal monomict slump beds, passing upwards to a series of extrabasinal polymict debris flows that occur in association with the coarse-grained quotient of the turbidite system (Fig. 2.23). The sequence repeats again and again, following a return to fine-grained turbidite deposition. The system has delivered terrigenous continent-derived sediment into a marine environment in a cyclical manner, which began before the tectonic events that provide a significant discontinuity at the base of the Gwna Group in outcrop belt 3, north-west Anglesey. The style of sediment supply and sediment composition, with the exception of the felsic volcanics of outcrop belt 3, remain constant throughout all outcrop belts over the tectonic divide (Fig. 2.23). The Gwna Group lithofacies

---

Figure 2.23 → Summary logs of the four outcrop belts of the Gwna Group illustrating primary sedimentary cycles that repeat throughout the now disrupted stratigraphy of the Gwna Group. The logs record accurately the number of megacycles recorded by outcrop belt, but are not drawn to vertical scale – total thickness estimates are indicated. Coarsening upwards successions occur within all four outcrop belts, interpreted as evidence for relative base level change on a cyclical basis. The association with a set of ocean floor fault blocks and lens-shaped mafic intrusions in outcrop belts 1 and 2, their absence in outcrop belts 3 and 4, and the tectonic break following the Monian Orogeny (Waldron *et al.,* 2018) at the base of the Gwna Group in outcrop belt 3, collectively underpin the assertion of gross younging from the south-west to the north/north-west of the region. It is not possible at this time to be clear about correlative relationships between all outcrop belts. Based on K-Ar dating of the Monian Orogeny Asanuma *et al.* (2017) outcrop belts 3 and 4 (Gwna B) appear to be younger than 1 and 2 (Gwna A). Whether or not the cycles represented in outcrops belt 3 and 4 are contemporaneous cannot be clarified. Neither can it be said that the cycles recorded in outcrop belts 1 and 2 are successive and/or equivalent. However, at least four sedimentary cycles are identifiable and there may be as many as seven. This shows that continuous sediment supply of the main lithologies and sedimentary process was sustained in the region during the following events: the deposition of the Gwna Group in outcrop belts 1 and 2 (Gwna A), their subsequent deformation in the Monian Orogeny, followed by further deposition of belts 3 and 4 (Gwna B).

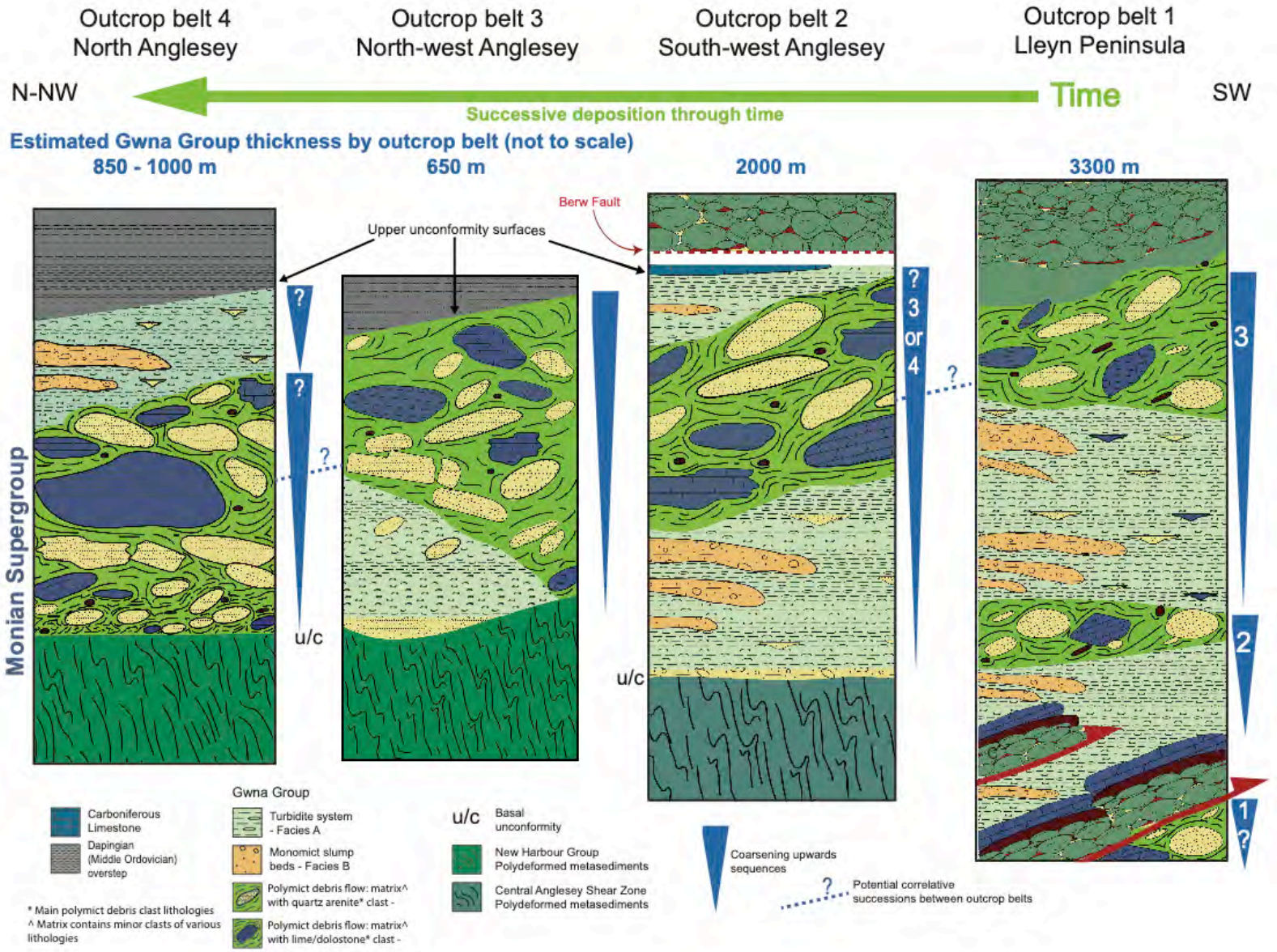
Outcrop belt 4
North Anglesey
Outcrop belt 3
North-west Anglesey
Outcrop belt 2
South-west Anglesey
Outcrop belt 1
Lleyn Peninsula
N-NW
Time
SW
Successive deposition through time
Estimated Gwna Group thickness by outcrop belt (not to scale)
850 - 1000 m
650 m
2000 m
3300 m
Berw Fault
Upper unconformity surfaces
Monian Supergroup
u/c
? 3 or 4 ?
3
2
1 ?
Gwna Group
Carboniferous Limestone
Dapingian (Middle Ordovician) overstep
Turbidite system - Facies A
Monomict slump beds - Facies B
Polymict debris flow: matrix^ with quartz arenite* clast -
Polymict debris flow: matrix^ with lime/dolostone* clast -
u/c Basal unconformity
New Harbour Group Polydeformed metasediments
Central Anglesey Shear Zone Polydeformed metasediments
Coarsening upwards sequences
? Potential correlative successions between outcrop belts
* Main polymict debris clast lithologies
^ Matrix contains minor clasts of various lithologies

A, B and C are interpreted collectively as a series of sedimentary megacycles deposited in a continent-ocean transition zone. The group is bounded above and below by unconformities with conspicuous basal contact surfaces each characterised by stratigraphic angularity and tectonic discontinuity. The style of sedimentation is ubiquitous across all four outcrop belt sections defined in this study, as well as in all other minor outcrops of the Gwna Group on Anglesey and the Lleyn Peninsula.

The coarsening upwards cycle is responsible for the deposition of sediment grainsizes of many orders of magnitude from a continental margin into an oceanic basin through an evolving sedimentary system. That system managed mud-heterolithic grade sediment to polymict debris flows containing clasts up to tens of metres diameter (the largest is ~ 650 m maximum diameter) traveling downslope under gravitational control: the repeated delivery of three identifiable sedimentary lithofacies, sourced from a continental margin or from further upslope within the basin in a series of hundreds of slope instability events. It is a coarsening upwards cycle that repeats several times through the Gwna Group succession (Fig. 2.23).

Mechanisms for creating slope instability on continental margins include lowering of sea level, high rates of sedimentation and gas hydrate disassociation (Mutti *et al*., 2009; Festa *et al*., 2016) and tectonic events, such as earthquakes (Haughton 2000; Bailey *et al*., 1989) or eruptions but many of these occur sporadically, rather than recurring in a systematic manner. The only credible cycle for this is one that can provide sequence boundaries. Potential drivers for base level fluctuation, which must be the mechanism controlling such varied slope instability within the megacycle, include glacio-eustacy combined with either (1) tectonic uplift – either in a collision zone (Festa *et al*. 2016), or (2) thermal uplift – the formation of a crustal bulge in tectonic rifting, or (3) multiple

extensional faults associated with crustal thinning in a rift or continental drift setting.

Base level change is intimately linked to eustatic fluctuation which on a first order basis increased steadily from the Ediacaran to the Upper Ordovician. Lower order sea level fluctuations of < 70 m occurred frequently over restricted time frames of a few million years within that cycle (Snedden and Liu, 2010) and third and fourth order repetitions would have produced rhythmic sea level change on even shorter timescales. Sequence stratigraphic principles are employed to understand the systematic changes in sediment supply and accommodation space created by sea level change. When sea level is low, or at lowstand, sediment supply, which is intimately linked to erosion rates, increases but accommodation space is reduced, coarser sediments are deposited more distally. Alternatively, when sea level is high, or at highstand, accommodation space increases but erosion rates are lower and sedimentation takes place more proximally under the maximum flooding surface. The transition between lowstand and highstand is called a transgressive systems tract and the reverse is a falling systems tract. The response to sea level change in the sedimentary system that deposited the Gwna Group is interpreted as working in this way: Lowstand conditions reveal more of the continental shelf where sediment that has bypassed the turbidite system is stored (Mutti, 2009). A reduction in the hydrostatic pressure confining the shelf and upper slope leads to slope instability increasing the likelihood of debris flows. Conversely, during highstand, sea level is high and fine-grained material is deposited repeatedly via density currents (Bouma, 2000; Stow, 2000).

Each megacycle is controlled by and intimately linked with slope instability and base level change: the transgressive Gwna Group was deposited onto a polydeformed unconformity surface with deformational and erosional relief —

the latter generated under lowstand conditions. The development of a transgressive systems tract to highstand is recorded throughout the turbidite system with slope instability evidenced by the downslope reworking of semi-lithified basin material in the repeated slump bed/turbidite successions. Subordinate sand-rich turbidite horizons in the south (outcrop belts 1 and 2) were laid down on the finely bedded mud-silt turbidites as sea level fell. Thick sandy turbidites in the prograding volcaniclastic succession in outcrop belt 3 provide a cross-section through the most proximal sediments, including the rear portion of the debris flow fan. Last but not least, the megacycle terminates with the dominance of polymict debris flows during which there is virtually no trace of what must have been an ongoing gravity driven system. The debris flow facies, the product of a temporary return to a eustatic low, is followed by further fluctuation in the base level as deep marine conditions returned, represented by fine-grained turbidite deposition.

The megacycle described above (Fig. 2.23) incorporates all the sedimentary evidence from outcrop belts 2, 3 and 4, as well as that from the northern portion of outcrop belt 1. The southern half of the Lleyn Peninsula (outcrop belt 1) does show variation, with fine-grained and sand-rich turbidites, containing channels and numerous slump beds with polymict debris flows as well as seafloor fault blocks. The fault blocks are not considered to be analogous with the debris flow facies as they lack evidence for fluidised transport, but there must be another mechanism for the apparently contemporaneous inclusion of these substantial broken beds with the deposition of the turbidite, slump bed and debris flow facies.

The basalt and seafloor sediment fault blocks could be derived from diametrically opposed tectonic settings: a convergent margin subduction trench where dismembered lower plate material periodically slides downslope into the

accumulating turbidite system. Alternatively, in a divergent setting, horsts and rift shoulders would readily supply disaggregated sections for gravitational delivery into the sedimentary basin. A third possibility is that the seafloor blocks represent the basin floor, fragments of which were episodically delivered upwards into the sedimentary succession by thrust faulting. In this last setting, the co-location of lens-shaped mafic intrusions in outcrop belt 1 and the upper part of 2, as well as the basalt pillows of Penrhyn Nefyn (belt 1) and Llanddwyn Island (belt 2) would be explained as the product of progressive crustal thinning. Further discussion on this subject is included in the summary in Chapter 5.

Correlation between the variously deformed outcrop belts is no simple matter: first, the monotonous nature of the fine-grained turbidite system does not provide any distinctive marker beds traceable through the region. Second, structural discontinuity exists between the underlying metasediments but also within the Gwna Group itself as outcrop belts 1 and 2, respectively south and north of the Berw Fault, display folding from an event that also deformed the CASZ and New Harbour Group in belts 2 and 3. This deformation is absent from the two northern Gwna Group sections, suggesting a temporal framework for the basin architecture, with the oldest Gwna Group facies of belts 1 and 2 in the south-west, deposited before those in the north-west and north, belts 3 and 4.

The regionally stable nature of the turbidite – slump bed— debris flow system recorded in the Gwna Group requires constant sediment availability over time, composition and accommodation space: the current extent of spatial distribution must be attributable to the original geography but in part, also to later transcurrent and thrust faulting, particularly with regard to Lleyn (outcrop belt 1) and the Anglesey north coast (outcrop belt 4), that respectively transcurrently extend and shorten the Gwna Group.

A brief reconsideration of the mélange testing scheme

Chapter 1 (Table 1.2) confirmed that the Gwna mélange formed by sedimentary processes. In gross terms, the bounding surfaces, internal metamorphic continuity and probable body form clearly indicate a sedimentary origin, while excluding the possibility of tectonic and diapiric emplacement. In the light of this chapter's evidence, Table 2.2 compares the mélange testing scheme individually with properties of two Gwna Group lithofacies: the monomict translational slump beds and the polymict debris flows.

Field evidence demonstrates that although today the Gwna Group is highly disrupted, a coherent depositional system comprised of cycles containing three interbedded lithofacies created by numerous slope instability events of varying orders of magnitude was deposited. The Gwna Group is internally conformable and as such, records sustained conditions over several megacycles which could only be deposited by sedimentary processes. There is a complete absence of evidence to support an accretionary orogen setting for the Gwna Group.

Table 2.2 Mélange testing scheme. The upper section summarises the internal properties of lithofacies B, the translational slump beds indicating the vast majority of properties confirm sedimentary accumulation. There are no diapiric properties and those that might suggest tectonic emplacement include a lack of grading and the monomict nature of the slump beds. They are monomict because they consist exclusively of reworked material from the turbidite system. All other tectonic properties are shared with sedimentary mélanges. The lower section summarises the internal properties of lithofacies C, the polymict debris flows and the conclusion is clear – most properties confirm sedimentary character. Both diapiric properties present in the debris flows – polymict clast composition and bimodal clast support are also sedimentary properties. Tectonic mélange properties are absent, with the exception of a lack of clast grading, which is party true of the debris flows – there is either inverse or no grading in individual flows. All other primary tectonic properties are shared with sedimentary mélanges. Therefore, tectonic and diapiric genetic mechanisms are excluded by the field evidence for the entire Gwna Group.

	Properties	Olistostrome (sedimentary mélange)			Tectonic mélange		Diapiric mélange	
Lithofacies B - Monomict translational slump beds	Clast supported	Yes	**No**	Bimodal				
	Clast spatial distribution	Inverse graded			**Not graded**		Radial control on grading	
	Clast mophology	Isometric			Triaxial (flattened)			
	Clast angularity	**Rounded***	Angular		**Rounded***		Rounded (radial control)	Angular (radial)
	Clast basinal derivation	**Native**	Exotic		Exotic			
	Clast types present	**Single lithofacies per clast**	Broken formation within clasts	Ghost stratigraphy present	Monomict			
	Clast types present	Highly variable - contains exotics	Polymict		**Monomict**		Polymict	
	Clast auto brecciation	**Boudinage***	**In-situ shearing***	**Synsedimentary slumping**	**Boudinage***	**In-situ shearing***	Radially controlled deformation	
	Clast alignment	Random	Lithologically controlled	**Transport controlled**	Common	Lithologically controlled		
	Transport direction	**Cleavage**	**Clast tails**	Debris flow run out	Unidirectional		Radially controlled	
	Matrix supported	**Yes***	No	Bimodal	**Yes***	No	Bimodal	Clasts in clusters
	Matrix injection	**Around clasts***	**Intraclastic***	**Between boudins**	**Around clasts***	**Intraclastic***		
	Matrix composition	**Argillaceous**	Polymict	Microbreccia	Banded?	Monomictic		
	Mud matrix basinal derivation	**Native**			Exotic			
	Synsedimentary fault-controlled stratigraphic repetition	**Not present**			Present		Radial stratigraphy	
	Metamorphic continuity	**Consistent metamorphic grade in clasts and matrix***	Clasts of varied metamorphic grade		**Consistent metamorphic grade in clasts and matrix***	Mineral banding continuity between clasts and matrix		
Lithofacies C - Polymict debris flows	Clast supported	Yes	No	**Bimodal**				
	Clast spatial distribution	**Inverse graded**			**Not graded**		Radial control on grading	
	Clast morphology	Isometric			Triaxial (flattened)			
	Clast angularity	**Rounded***	Angular		**Rounded***		Rounded (radial control)	Angular (radial)
	Clast basinal derivation	**Native**	**Exotic***		**Exotic***			
	Clast types present	**Single lithofacies per clast**	Broken formation within clasts	Ghost stratigraphy present	Monomict			
	Clast types present	Highly variable - contains exotics	**Polymict***		Monomict		**Polymict***	
	Clast auto brecciation	**Boudinage***	**In-situ shearing***	Synsedimentary slumping	**Boudinage***	**In-situ shearing***	Radially controlled deformation	
	Clast alignment	Random	Lithologically controlled	**Transport controlled**	Common	Lithologically controlled		
	Transport direction	Cleavage	Clast tails	Debris flow run out	Unidirectional		Radially controlled	
	Matrix supported	Yes	No	**Bimodal***	Yes	No	**Bimodal***	Clasts in clusters
	Matrix injection	**Around clasts***	**Intraclastic***	**Between boudins**	**Around clasts***	**Intraclastic***		
	Matrix composition	**Argillaceous**	Polymict	**Microbreccia**	Banded?	Monomictic		
	Mud matrix basinal derivation	**Native**			Exotic			
	Synsedimentary fault-controlled stratigraphic repetition	Not present			Present		Radial stratigraphy	
	Metamorphic continuity	Consistent metamorphic grade in clasts and matrix	**Clasts of varied metamorphic grade**		Consistent metamorphic grade in clasts and matrix	Mineral banding continuity between clasts and matrix		

Commonly present
Commonly present* - property shared by different mélange types
Present, but not common
Not present
Present but overprinted: not a primary feature

Sedimentary summary

- The “chaos” of the Gwna Group is a misnomer in terms of genetic history. It is the product of the challenging appearance of some debris flows combined with later deformation.

- The Gwna Group records throughout Anglesey and Lleyn a sedimentary succession with internal variability that is demonstrably systematic and cyclical, through time and space in a continent—ocean transition zone.

- Although two distinct periods of Gwna Group deposition appear to be recorded in Gwna A and Gwna B, both sedimentary successions are similar in sedimentary character: clast shape and composition, matrix composition and the process sedimentology are constant throughout all outcrop.

- There is no evidence for subduction within the Gwna Group sedimentary megacycles.

- The presence of seafloor successions in fault blocks and lens-shaped basic intrusions within restricted areas of the Gwna Group is not explained within the confines of the internally conformable sedimentary system evidenced in the rocks and detailed above but, is probably related to the overall tectonic setting either during Gwna Group deposition or, subsequent to it.

- The lens-shaped basic intrusions do not provide evidence for subduction in the region.

- The seafloor fault blocks underlie Gwna A, in outcrop belt 1 only.

- The only possible evidence for subduction may be related to the aforementioned seafloor fault blocks.

It is important to note that the division of the Gwna Group into two sequential successions, Gwna A and Gwna B, is predicated on a single K-Ar age of 474 ± 9 Ma from Asanuma *et al*. (2017) from phengites in the New Harbour Group where all other analyses, from a total of nine, provided ages between 578 ± 11 Ma and 530 ± 10 Ma. This age is interpreted as dating exhumation, subsequent to the Monian Orogeny of Waldron *et al*. (2018) (See further discussion in Chapters 3 and 5.)

Chapter 3

THE AGE OF THE GWNA GROUP MÉLANGES AND ASSOCIATED LITHOSTRATIGRAPHIC UNITS

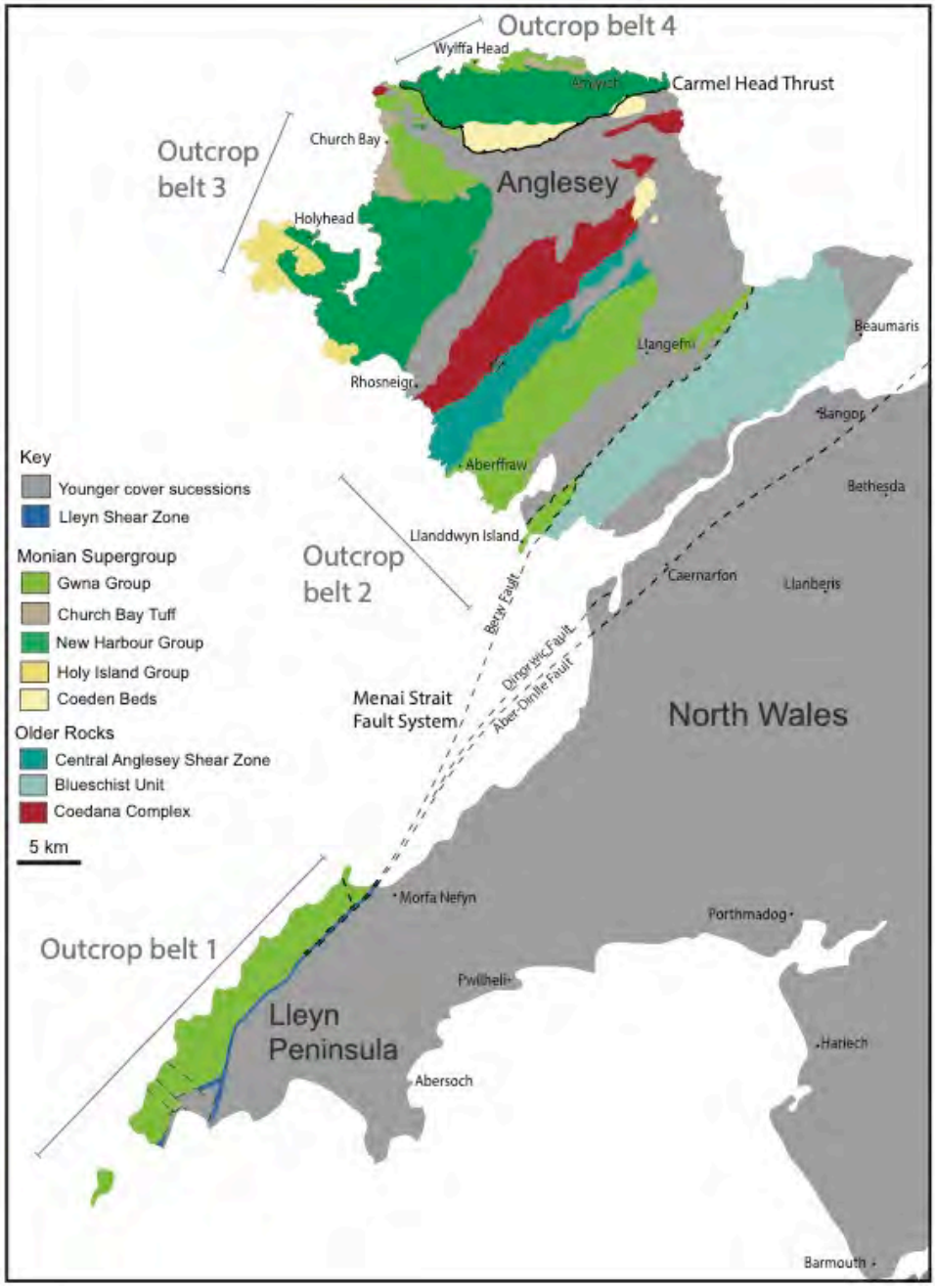

Figure 3.1 ← Geological map of the Anglesey. Lleyn and west Wales region highlighting pre-Ordovician bedrock of the Monian Supergroup, underlying and related successions indicating the four outcrop belts defined for this study. Map after Greenly, 1920 - British Geological Survey (BGS) Anglesey Special Sheet, BGS - Anglesey map, in press and BGS map Sheet 133. MSFS and Lleyn fault linework after Gibbons (1987). Anglesey major fault and fold linework after BGS Anglesey map, in press.

The pre-Ordovician geology of Anglesey and the Lleyn Peninsula of north-west Wales contains an olistostrome bearing turbidite succession - the Gwna Group of the Monian Supergroup (Fig. 3.1) of elusive origin and age. The age of the Gwna Group has never been established convincingly and for good reason: the existing age constraints are inconclusive, even contradictory, for a single regional deposit, further compounded by the lack of palaeontological data, and herein lies the main motivation for this study.

The clear sedimentary character of the Gwna Group demonstrated in Chapter 2 provides important new primary data but additionally, creates the opportunity to constrain the depositional age and to examine geochemically the question of provenance, in both cases using U-Pb zircon geochronology. The interbedded nature of the three Gwna Group lithofacies allows for zircon geochronology studies, such as;

- Primary zircon crystallisation ages for the interbedded ignimbrites in outcrop belts 2 and 3. Such ages would provide a tight age constraint on the sedimentary layers within which the volcanic rocks were deposited.

- Detrital zircon analysis will provide a zircon age population spectrum for the turbidite facies that may indicate sedimentary provenance and inform the peri-Gondwanan terrane hypothesis (Chapter 1).

- Detrital zircon analysis should provide an age population spectrum of zircons within the metasedimentary rocks that underlie the Gwna Group, which may clarify provenance.

- The detrital zircon analyses may, if the results allow, provide helpful maximum depositional age constraints (MDA).

There are viable and non-viable components of the olistostrome-bearing Gwna Group in respect of zircon geochronology. These can be characterised as follows;

- *Fine-grained turbidite sequence with point-sourced channels*. Siliciclastic rocks generally are suitable for detrital zircon studies but these rocks are too fine grained to contain a large number of inherited zircons. Primary zircons within ignimbrite horizons could provide a depositional date.

- *Interbedded matrix-supported, monomict translational slump beds.* As the slump beds consist of reworked intrabasinal turbidites they are not ideal (above) for detrital zircon studies or direct depositional age determination.

- *Polymict megaconglomerate debris flows.* Clasts within this facies cannot provide depositional dating as they are exotic to the Gwna Group system. Clast age analysis might inform sediment provenance and southern hemisphere Neoproterozoic – Palaeozoic crustal evolution investigations. The matrix is reworked: it contains both intrabasinal and allochthonous detritus which renders it useful for provenance but unsuitable for direct depositional ages.

3.1 Provenance of the Monian Supergroup

Section 1.6, Chapter 1 contains a review of the peri-Gondwanan terrane hypothesis for the Monian Supergroup.

Early crustal evolution reconstructions were based on regional facies distributions, such as thick deep marine Ganderian siliciclastic successions of early Cambrian age (van Staal *et al.,* 1996), and faunal province affinities, but modern isotopic investigations have enabled fine-tuning (Waldron *et al*., 2018). A substantial body of work has been published in recent years supported by extensive provenance geochronology that establishes greater clarity of affinities across the Atlantic Ocean with the British Midlands and Welsh Basin (Waldron *et al*., 2011; Pothier *et al*., 2015; Schofield *et al*., 2016). In Maritime Canada Laurentia and peri-Laurentian terranes dominate the north-west region above the Ordovician Iapetus suture, the Red Indian Line (Williams *et al*., 1988). Peri-Gondwanan terranes occupy the area south-east of this delineation (Hibbard *et al*., 2007). The picture is mirrored in Britain: Laurentia underlies Scotland north of the Solway Line, the suture that represents final closure of the Iapetus Ocean, and to the south lies the Avalon Platform (Rast *et al*., 1976), called Eastern Avalonia to clarify distinction from Canadian West Avalonia. In Canada Avalonia is associated with peri-Gondwanan terranes Ganderia and Meguma. Each terranes has characteristic zircon age spectra representative of their individual geological histories, that enable correlation (Waldron *et al*., 2018):

- Avalonia — Distinctively large peaks between 650 - 540 Ma, derived from Gondwanan assemblage linked orogens.
- Meguma —650 and 540 Ma Avalonia peak, plus a minor peak of ages ~ 2.2 Ga recording the Eburnean Orogen with a notable absence of dates between the peaks.

- Ganderia — 650 and 540 Ma Avalonia peak plus a broad spectrum of Neo- Mesoproterozoic ages between 1.2 and 2 Ga.
- Peri-Laurentian spectra lack Neoproterozoic ages in an asymmetric profile that pivots around 1 – 1.2 Ga zircon ages between 950 Ma and 1.6 Ga.

Recent work has exploited these characteristics and demonstrated terrane linkage between Meguma in Nova Scotia, north-west Africa and the Welsh Basin - the Harlech Dome of Mid Wales situated south of Anglesey and the Monian Supergroup (Waldron *et al*., 2011; Pothier *et al*., 2015) and linked Ganderia with the English Midland Platform, previously considered to be a central point of East Avalonia, using U-Pb in detrital zircon (Schofield *et al*., 2016). This increases the likelihood of correlation between Newfoundland Ganderia and the Monian Supergroup, first suggested in 1976 (Rast *et al.*, 1976; Kennedy, 1979).

Iapetus Ocean, despite extensive coverage (Fig. 1.3A) was short-lived. Waldron *et al*., (2014) suggested 35 million years between rifting and the onset of subduction and subsequent diachronous closure during regional tectonic shortening: late Ordovician in the west, Silurian in the east (McKerrow and Soper, 1989). There is, therefore, regional scope for late Precambrian to early Palaeozoic rifting and accretion, when the Gwna Group was deposited.

Understanding the genetic history of the Gwna Group is critical for interpreting the stratigraphic development of Anglesey since the deposits typically unconformably overlie metamorphic rocks with a complex deformation history, and are in turn overlain by more weakly deformed deep-marine sediments. Clearly, understanding the age of the Gwna Group will place critical constraints on the depositional environment and hence our understanding of the tectonic development of the island.

A geochronological investigation into the Gwna Group was undertaken with two aims: (1) to constrain the timing of Gwna Group sedimentation via the analyses of zircon in interbedded felsic tuffs and ignimbrites, and (2) to understand the provenance of the psammitic rocks in the underlying Monian Supergroup and CASZ units on Anglesey via the analysis and synthesis of inherited zircon ages. This study involved the acquisition of new radio-isotopic data combined with a critical evaluation of published data to develop a robust temporal model for the evolution of the region.

The wider context for this study is the need to distinguish primary characteristics from those superimposed by later tectonic events recorded within the Gwna Group. Macroscopic features observed in outcrop and others revealed at microscopic levels will allow the tectonic-palaeogeographic setting of the Gwna Group to be determined within the history of Anglesey and the Monian Supergroup.

Questions addressed in this chapter are:

- Can felsic volcanic horizons interbedded with the Gwna Group turbidite facies provide a crystallisation date and therefore an age for the contiguous sediments?
- What is the maximum depositional age of the Gwna Group?
- Is there depositional age variation between the Gwna Group outcrop belts?
- What is the provenance of the Gwna Group and the underlying metasediments?

3.2 Geological context

Field evidence records the presence of a debris flow and slump bed bearing

fine grained turbidite succession deposited in a series of sedimentary megacycles on Anglesey and north-west Wales: the Lleyn Peninsula (Figs. 3.1 and 3.2). The Gwna Group sediments, in two combined Gwna outcrop regions, Gwna A and Gwna B – each composed of two outcrop belts, 1 and 2 in A, and 3 and 4 in B (Fig. 3.2), respectively, has different associations and characteristics. It is, in some part, compositionally distinct, although there are many common features shared by all Gwna Group exposures.

Figure 3.2 illustrates and compares the stratigraphy of the two Gwna Group successions identified: Gwna A and Gwna B. Gwna A in south-west Anglesey (outcrop belt 2), unconformably overlies a substantial metasedimentary greenschist unit, the CASZ of Gibbons and Horák (1990). The CASZ is in faulted contact with the Coedana Complex, a lithotectonic unit consisting of Neoproterozoic gneisses, of maximum depositional age 852 ± 54* Ma and metamorphic age 666 ± 14* Ma (U-Pb zircon ID-TIMS, *adjusted here to 2σ) (Strachan, *et al*., 2007) intruded by the Coedana Granite at 613 ±4 Ma (ID-TIMS, U-Pb zircon) (Moorbath and Shackleton, 1966; Tucker and Pharaoh, 1991). Primary sedimentary features are preserved: the Gwna A succession is seen to consist of distal turbidites punctuated by volumetrically varied slump

---

Figure 3.2 → The stratigraphy of the Gwna mélange deposits and associated rocks of Anglesey and Lleyn, north-west Wales with dating targets identified. Gwna A is hypothesised for outcrop belts 1 and 2: Lleyn and south-west Anglesey, and Gwna B for outcrop belts 3 and 4: north-west and west Anglesey. Gwna A is associated with Precambrian blueschist and greenschist of the CASZ and the Lleyn Shear Zone. Gwna B is associated with older, polydeformed Monian Supergroup metasediments.

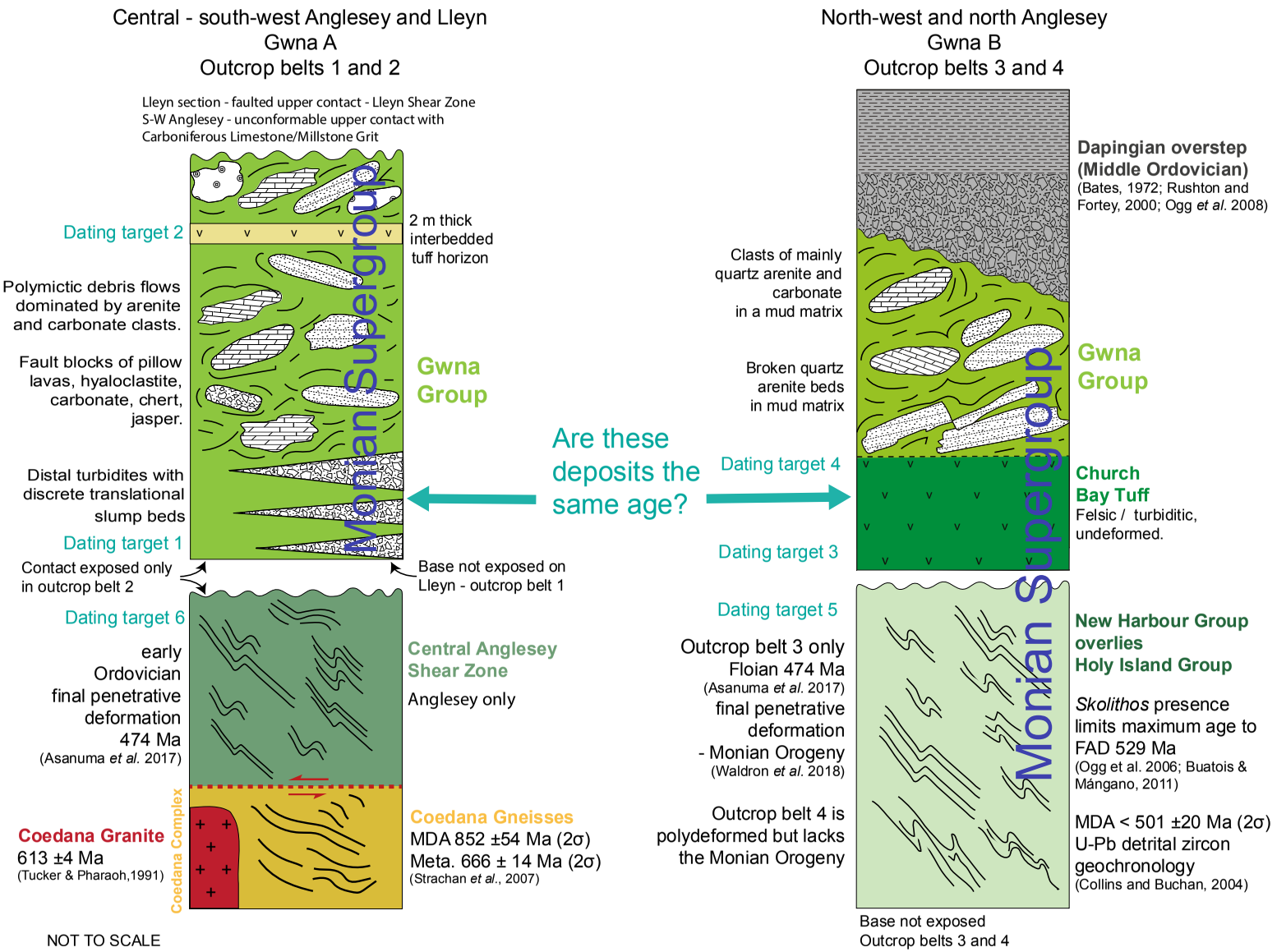
Central - south-west Anglesey and Lleyn
Gwna A
Outcrop belts 1 and 2
Lleyn section - faulted upper contact - Lleyn Shear Zone
S-W Anglesey - unconformable upper contact with
Carboniferous Limestone/Millstone Grit
Dating target 2
2 m thick interbedded tuff horizon
Polymictic debris flows dominated by arenite and carbonate clasts.
Fault blocks of pillow lavas, hyaloclastite, carbonate, chert, jasper.
Gwna Group
Monian Supergroup
Distal turbidites with discrete translational slump beds
Dating target 1
Contact exposed only in outcrop belt 2
Base not exposed on Lleyn - outcrop belt 1
Dating target 6
early Ordovician final penetrative deformation 474 Ma
(Asanuma et al. 2017)
Central Anglesey Shear Zone
Anglesey only
Coedana Granite
613 ±4 Ma
(Tucker & Pharaoh,1991)
Coedana Complex
Coedana Gneisses
MDA 852 ±54 Ma (2σ)
Meta. 666 ± 14 Ma (2σ)
(Strachan et al., 2007)
NOT TO SCALE
Are these deposits the same age?
North-west and north Anglesey
Gwna B
Outcrop belts 3 and 4
Dapingian overstep (Middle Ordovician)
(Bates, 1972; Rushton and Fortey, 2000; Ogg et al. 2008)
Clasts of mainly quartz arenite and carbonate in a mud matrix
Broken quartz arenite beds in mud matrix
Gwna Group
Monian Supergroup
Dating target 4
Church Bay Tuff
Felsic / turbiditic, undeformed.
Dating target 3
Dating target 5
Outcrop belt 3 only
Floian 474 Ma
(Asanuma et al. 2017)
final penetrative deformation
- Monian Orogeny
(Waldron et al. 2018)
Outcrop belt 4 is polydeformed but lacks the Monian Orogeny
New Harbour Group overlies Holy Island Group
Skolithos presence limits maximum age to FAD 529 Ma
(Ogg et al. 2006; Buatois & Mángano, 2011)
MDA < 501 ±20 Ma (2σ)
U-Pb detrital zircon geochronology
(Collins and Buchan, 2004)
Base not exposed
Outcrop belts 3 and 4

beds and polymict debris flows that contain clasts of quartz arenite, limestone and dolostone, yellow sandstone, jasper, chert and granite lenticular or spheroidal bodies and rare epiclastic or tuffaceous horizons. Fault blocks of ferroan dolostone, bedded chert, volcanogenic lithologies, hyaloclastite and pillow lavas are also present in restricted sections of the Lleyn Peninsula, and on Llanddwyn Island. The basal contact of Gwna A on the Lleyn Peninsula (outcrop belt 1) is unseen (Fig. 3.4) and is presumed to be offshore under the Irish Sea. The upper contact is faulted. The mylonitic Lleyn Shear Zone divides the Gwna Group to the north and west from lower Ordovician, Floian rocks of the Nant Ffrancon Subgroup (Gibbons and McCarroll, 1993) that crop out to the south and east. Although the repeated sedimentary cycles of Gwna Group lithofacies are present in all outcrop belts (see Chapter 2), additional lithologies crop out in outcrop belts 1 and 2, that are restricted to Gwna A area; substantial pillow lava sections, internally coherent fault blocks of basalt, carbonate, jasper, chert crop out.

Gwna B is located in outcrop belts 3 and 4 (Fig. 3.1). The polydeformed Holy Island and New Harbour Groups of the lower Monian Supergroup are unconformably overlain by the relatively undeformed Church Bay Tuff Formation in outcrop belt 3 and in parts of outcrop belt 4. Felsic ignimbrites and volcaniclastic turbidites of the Church Bay Tuff Formation pass gradationally into a megaconglomerate debris flow consisting of broken beds of quartz arenite and rounded lens-shaped carbonate clasts. The age of the basal Holy Island Group has been inferred to be < 501 ±20 Ma (published age 501 ± 10 Ma, 1σ, adjusted to equate to 2σ, used for this study) based upon the youngest U-Pb Secondary Ion Mass Spectrometry (SIMS) date obtained from a suite of detrital zircons (Collins and Buchan, 2004). The accuracy of this age is dependent upon the SIMS analyses reflecting closed system U-Pb and not being affected by Pb-loss. The top

of Gwna B is overlain unconformably, in outcrop belt 4, by transgressive Dapingian conglomeratic deposits of the Torllwyn Formation, or locally, mudstones of *Nemagraptus gracilis* Graptolite Biozone age (Bates, 1972; Rushton and Fortey, 2000; Ogg *et al.*, 2008) which constrains the age of the Monian Supergroup and the mélange in this area to late Cambrian–early Ordovician. Based on these constraints, the estimated age of the Church Bay Tuff is 474 - 470 Ma.

The disagreement in the literature about the age of the Gwna Group (Greenly, 1919a; Shackleton, 1954b; Shackleton, 1954a) is understandable since in different outcrop belts a credible case can be made for either a late Precambrian (outcrop belt 2) or Cambro-Ordovician (outcrop belts 3 and 4) age, due to the varied lack of basal or upper contact outcrop. What is currently not known is whether a common age, restricted to late Cambrian/early Ordovician, can be applied to these sections or whether the Gwna Group records a more protracted history of mélange formation. The presence of a gradational contact in the north-west Anglesey area (outcrop belt 3) with the Church Bay Tuff provides the opportunity to date the volcanogenic deposit and further constrain the emplacement age of the Gwna Group (Gwna B) in the north Anglesey sequence. Dating the bedded tuff or epiclastic unit within the southern sequence (Gwna A) will test the hypothesis of a much earlier, potentially subduction-related mélange in the southern sequence.

U-Pb zircon analyses presented herein have been aimed at obtaining robust age constraints for the stratigraphic horizons within the mélange deposit. In the Gwna B section the Church Bay Tuff Formation was targeted. This unit is ca. 400 m thick and unconformably partially oversteps the lower Monian Supergroup (Holy Island and New Harbour Groups) (Fig. 3.2). Two samples at the top and bottom of the unit were targets for dating. In the Gwna A section an identified

felsic tuff from the upper Gwna Group (Fig. 3.2) and a suitable horizon in the lower part of the unit (outcrop belt 2) were targets. It was later decided to sample for detrital zircon analysis from within the underlying New Harbour Group and CASZ metasediments of the three Anglesey outcrop belts (2, 3 and 4). Combined, these data should permit integration of the stratigraphy of the two Gwna sections. The absolute timing of Gwna Group sedimentation, determined by the dating of the volcanic deposits, will allow temporal location of the mélange formation into the tectonic model developed for the region, therefore improving the understanding of the geological history of Anglesey and the Monian Supergroup within the wider context of the peri-Gondwanan terranes: Avalonia, Gander, Laurentia and Meguma – all currently divided by the North Atlantic Ocean, considered to have been dispersed from the margins of the Gondwana Supercontinent during the opening and closure of the Neoproterozoic to Silurian Iapetus Ocean (van Staal *et al.*, 1998; Murphy *et al.*, 2010; J. W. F. Waldron *et al.*, 2014; Pothier *et al.*, 2015; Schofield *et al.*, 2016).

3.3 Summary of pre-existing age constraints by outcrop belt

Outcrop belt 1 – Lleyn Peninsula

Although the basal Gwna Group contact is not seen and assumed to be situated offshore of north-west Wales, the upper contact is defined by the Lleyn Shear Zone (Penmynydd Zone of Metamorphism (Matley, 1901; Greenly, 1919a)) and overlain unconformably by Floian (lower Ordovician) rocks of the Wig Bach Formation, Nant Ffrancon Subgroup (Gibbons and McCarroll, 1993) (Fig. 3.4). Asanuma *et al.*, (2015), in research published after the current study had begun, have interpreted selected zircon U-Pb dates as evidence for a late

Neoproterozoic subduction zone incorporating the Gwna Group as part of an accretionary prism formed by imbricate thrusting at the head of a tectonic collision, translating deep marine sediments and volcanic rocks from the downgoing plate onto the upper plate (Avalonia, the present Welsh mainland basement). Asanuma *et al*., (2015) used single youngest U-Pb dates to infer maximum depositional ages for the Gwna Group in outcrop belt 1 (Table 3.1), and extrapolated from this data a hypothesis for two stages of deposition for lithologically varied mélange sections.

Locality	Published maximum depositional age
Porth Felen – LLY173	564 ±14 Ma
Porthorion – LLZ277	539 ±19 Ma
Mynydd Careg	678 ±4 Ma
Porth Oer	550 ±11 Ma
Porth Iago	601 ±6 Ma

Table 3.1 Examples of published Gwna Group maximum depositional ages for outcrop belt 1 (Asanuma *et al.,* 2015).

Outcrop belt 2 – South-west Anglesey

The Gwna Group unconformably overlies greenschist-facies siliciclastic metasediments of the CASZ that have been subjected to three generations of deformation. The base of the CASZ is marked by a left-lateral contact with the Coedana Complex. Hornfelsed metasediments of sand-rich character and Coedana Gneiss, intruded by the Coedana Granite, dated at 613 ±4 Ma; (U-Pb

zircon, ID-TIMS) (Tucker and Pharaoh, 1991), are in faulted contact with the CASZ. As the relationship between the Coedana Complex and the CASZ is faulted, the intrusion age cannot provide a minimum depositional age for the Gwna Group. However, the inclusion of rare granite clasts in the Gwna Group, particularly those close to the Coedana/CASZ contact at Porth Nobla, suggest detrital input from the igneous block into the Gwna Group debris flows and, if these are proven to be of Coedana Granite origin, would provide a maximum Ediacaran age for Gwna Group deposition in outcrop belt 2.

The basal Gwna Group relationship is unconformable. CASZ polydeformed amphibolite facies of thinly layered psammites and pelites are overlain with angular unconformity by simply deformed polymictic debris flows of the Gwna Group. The Gwna Group is sub-vertical, younging both to the south-east and north-west. The CASZ succession near Aberffraw is the southern limb of an anticline with an axial trace orientated south-west to north-east (Fig. 3.3). The northern limb contains the disconformable contact of the basement rocks with a minor slice of Gwna Group sediments in outcrop at Porth Nobla, just south of the sinistral strike-slip boundary with the Coedana Complex block. On southern limb the Gwna Group sequence crops out continuously from Aberffraw (Fig. 3.3) to the south-east, extending as far south as Llanddwyn Island in a series of sub-vertical siliciclastic sediments: heterolithic beds, interleaved with minor slump beds and major debris flows. Towards Pen y Parc (Fig. 3.3) subordinate felsic ash beds are present. The Gwna Group is unconformably overlain by Carboniferous

---

Figure 3.3 → Anglesey U-Pb dating sample locations for this study, with Gwna Group and associated lithologies, divided by outcrop belt. Map after Greenly, 1920 - British Geological Survey (BGS) Anglesey Special Sheet, BGS - Anglesey map, in press and BGS map Sheet 133. Anglesey major fault and fold linework after BGS Anglesey map, in press.


U-Pb dating samples
Sample sites that did not yield enough zircons have no sample number
Key
Younger cover sucessions
Monian Supergroup
Gwna Group
Church Bay Tuff
New Harbour Group
Holy Island Group
Coeden Beds
Older Rocks
Central Anglesey Shear Zone
Blueschist Unit
Coedana Complex
Outcrop belt 4
Outcrop belt 3
Outcrop belt 2
Ogof Gynfor
Porth Llanlleiana
Wylfa Head
Cemlyn Bay
Bull Bay
Carmel Head Thrust
CB14.1
CB14.2
CB14.5
Church Bay
Anglesey
Holyhead
Baron Hill
Beaumaris
VY473
Llangefni
Rhosneigr
Porth Nobla
Bangor
Porth Cwyfan
Aberffraw
Malltraeth
A15.1
A14.16
Bodorgan
Pen y Parc
Bethesda
Wales
Llanddwyn Island

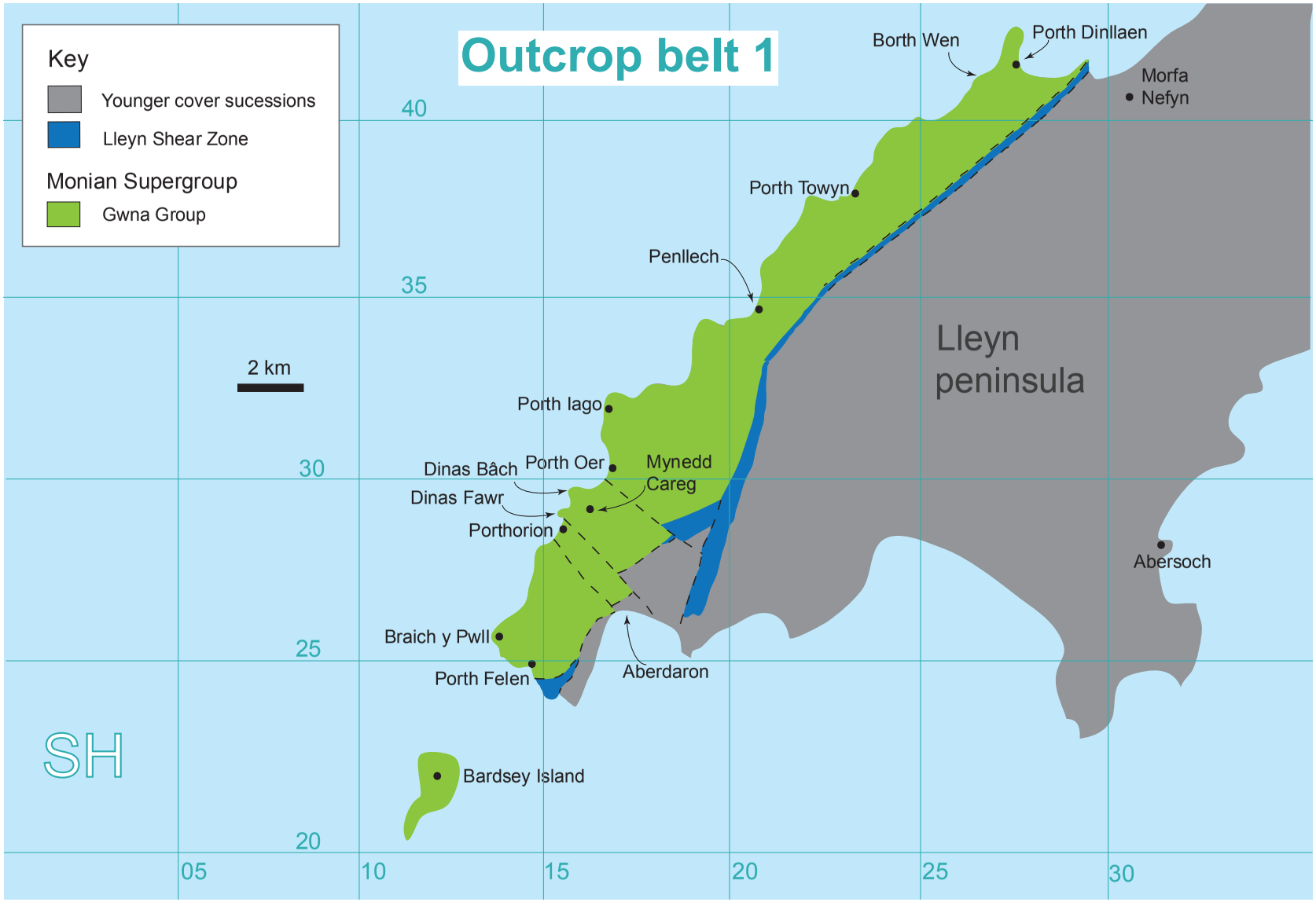
Outcrop belt 1
Key
Younger cover sucessions
Lleyn Shear Zone
Monian Supergroup
Gwna Group
2 km
Borth Wen
Porth Dinllaen
Morfa
Nefyn
Porth Towyn
Penllech
Lleyn
peninsula
Porth Iago
Dinas Bâch
Porth Oer
Mynedd
Careg
Dinas Fawr
Porthorion
Abersoch
Braich y Pwll
Porth Felen
Aberdaron
Bardsey Island
SH
40
35
30
25
20
05
10
15
20
25
30

Figure 3.4 ← Geological map of outcrop belt 1, Lleyn Peninsula, showing the Gwna Group and Lleyn Shear Zone with locality place names for geochronology sampling in Asanuma *et al.* (2015). Map after BGS map Sheet 133. MSFS and Lleyn fault linework after Gibbons (1987).

Limestone and Millstone Grit, a contact that runs along the north side of the Malltreath estuary (Fig. 3.3). The steep Berw Fault lines the southern margin of the estuary and cross cuts Anglesey in a south-west to north-east orientation. Stratigraphic contact cannot be established in the geographic area between the estuary and Llanddwyn Island, which is a basalt, pillow basalt and hyaloclastite domain, with gabbroic intrusions, bedded red chert and nodular limestone, and was attributed by Greenly (1919) to the Gwna Group.

The youngest single zircon from Asanuma *et al* (2015), aged 878 ± 43 Ma, obtained from the upper Gwna Group at Bodorgan (Fig.3.3), is offered by the authors as a maximum age constraint on Gwna Group deposition. Further published dates in the same study of outcrop belt 2 Gwna Group samples include:

- Aberffraw 571 ±20 Ma
- Llanddwyn Island 550 ±24 Ma (Asanuma *et al*., 2015)

Outcrop belt 3 – North-west Anglesey

Depositional basal age constraints are provided by the presence of penetrative Skolithos (Greenly, 1919) that penetrate metasandstones (Phillips, 1991b) of the South Stack and Holyhead formations of the Holy Island Group giving a maximum depositional age of 529 Ma (see Chapter 2) for the oldest Monian Supergroup unit. Additionally, a detrital zircon geochronological study of the South Stack and Holyhead formations gave maximum depositional dates of 522 ± 12 Ma and 501 ± 20 Ma respectively (Collins and Buchan, 2004). These ages used the single

youngest > 90% concordant $^{206}Pb/^{238}U$ grain sampled, originally at 1σ, but are here adjusted to 2σ. Collins and Buchan (2004) note that the stratal thickness of the entire Holy Island Group (> 1km), indicates that the maximum age of the Holyhead Formation, 501 ± 20 Ma, should be considered more robust as it is unlikely that formation of the entire Holy Island Group occurred over an extended time period of > 30 million years. There is further discussion later in this chapter (section 3.5 – Holy Island Group) of this significant element of the Collins and Buchan (2004) interpretation. However, these lines of evidence confirm the Holy Island Group is indisputably of Cambrian age, specifically between the latest Terreneuvian (529 Ma) and upper Jiangshanian (491 Ma) (Ogg *et al*., 2016).

Polydeformed metapelites and volcaniclastic sandstones (Phillips, 1991b) of the 2 – 3 km thick (Tietzsch-Tyler, 1989; Phillips, 1991a; Howells, 2007) New Harbour Group overlie the Holy Island Group. The upper contact of the New Harbour Group with the Church Bay Tuff Formation, south of Porth Trefadog (Fig. 3.3) assigned at times to either the New Harbour Group or the Gwna Group, is of major importance as it demonstrates stratigraphic angularity and a tectonic break providing a lower age constraint for the Gwna Group in this outcrop belt, and above in belt 4. The New Harbour Group was exhumed following the most recent metamorphic event at 474 ± 9 Ma according to phengite K-Ar analysis (Asanuma *et al*., 2017). The Gwna Group is in gradational contact with the upper Church Bay Tuff Formation, seen to the north of Church Bay and is in faulted upper contact towards the north-western tip of Anglesey with lower Ordovician rocks entrained within the hanging wall of the Carmel Head Thrust System (Fig. 3.3). The lower and upper contacts are repeated twice in outcrop in the north-west corner of Anglesey in thrusted and folded hanging-wall slices (Fig. 3.3). However, Asanuma *et al*., (2017) published a maximum depositional age of 596

±10 Ma for the Church Bay Tuff Formation, based on U-Pb of detrital zircons.

Outcrop belt 4 – North Anglesey

The main north Anglesey section of Gwna Group outcrop is exposed in the region between Wylfa Head and the west side of Bull Bay, contained within a hanging wall slice called the Carmel Head Thrust (Fig. 3.3). Overall, the contact is orientated east-west and the Gwna Group unconformably overlies the New Harbour Group directly in the west but locally, in the east, some faulted sections overlie Church Bay Tuff (Fig. 3.3). As is the case in outcrop belts 2 and 3, the Gwna Group overlies the New Harbour Group in angular unconformity. The New Harbour Group consists of polydeformed (two recognisable phases) metasedimentary pelites and psammites. In the west of the section, unlike belts 2 and 3, the basal Gwna Group dominantly consists of a series of polymictic bimodal debris flows, containing clasts between 2 mm and 650 m diameter. Zones of laminated mud to finely bedded heterolithic turbidites with conspicuous arenite sand channels are present, particularly at Wylfa Head, where there is continued stratigraphy on display, but shallow-marine carbonate clasts and broken beds or rounded clasts of quartz arenite populate the muddy matrix up to the Dapingian (~471 Ma) overstep (Bates, 1972; Rushton and Fortey, 2000; Ogg *et al*., 2008) at Ogof Gynor. Controlled by topography and polyphase deformation, the upper contact is repeated in outcrop, most notably at Porth Llanlleiana where it is seen to be a sedimentary angular unconformity, later overthrust. The biostratigraphy of the Middle Ordovician overstep provides the only upper age constraint on the Gwna Group: emplacement of the Gwna Group must predate 468 Ma therefore, but must also postdate the latest deformation, the Monian Orogeny (Waldron *et al*., 2018) at 474 ± 9 Ma (K-Ar

phengite analysis) (Asanuma *et al*., 2017) in the New Harbour Group in outcrop belt 3.

3.4 Methodology

Sample selection rationale

In the pursuit of a direct depositional date for the Gwna Group, volcanogenic strata interbedded with minor conglomeratic slump beds in outcrop belts 2 and 3 were closely examined. Sample selection in a mélange requires particular care when the intention is to date the formation of the deposit, rather than a constituent clast or a fault block, particularly given that Gwna Group clasts vary in size over many orders of magnitude. It was imperative to establish that potential sample sites consisted of material interbedded with the debris flows: clasts were not sampled for this study because they are always older than the mélange. Instead, near-basal volcanic deposits were targeted and comparative sampling prioritised coarse grained crystalline ignimbrite horizons but also included stratified volcanogenic sections, despite the inclusion of potentially reworked material, in the latter. The aim was to date the primary zircons formed in the volcanic eruption, and by so doing, date the formation of the intercalated sediments.

Detrital samples were collected from the metasedimentary sections of the CASZ and New Harbour Groups, beneath the basal unconformity surfaces of the Gwna Group in outcrop belts 2, 3 and 4. These units are dominantly pelitic but contain some heterolithic and a few sand-rich protolith beds. Here the coarsest psammite layers were the target and it was hoped that these samples would yield appropriate populations of inherited zircons able to indicate peri-

Gondwanan provenance. In addition, a small sample of mudstone was taken from the thin mudstone layer deposited directly on the basal Gwna Group angular unconformity near Aberffraw (Fig. 3.3) for detrital zircon analysis. If successful, the inherited grain populations would provide information on sediment source for the various units sampled.

All sample sites are on Anglesey (Fig. 3.3); outcrop belt 1 is not directly included in this U-Pb study because this section lacks both: a) felsic volcanic units clearly interbedded with the siliciclastic background sedimentary succession of the Gwna Group and, b) outcrop of the basal contact and the underlying rocks.

3.5 Principles of zircon U-Pb geochronology

Zircon is a common silicate accessory mineral ($ZrSiO_4$) in many igneous, metamorphic and sedimentary rocks. The voids within the tetragonal crystal lattice readily allow for the interstitial inclusion and retention of radiogenic trace amounts of uranium, thorium, hafnium and REE within the crystal, yet Pb is almost entirely excluded from the structure at the time of formation. This is one of the key criteria for a mineral radio-isotope chronometer: incorporation of a parent isotope (e.g. ^{238}U, ^{235}U) that have long half-lives, and that the daughter isotopes (^{206}Pb and ^{207}Pb, respectively) are effectively excluded at crystallisation such that the measure parent/daughter (ie. $^{238}U/^{206}Pb$) can be combined with knowledge of the half-life, or decay constant, to calculate a radio-isotopic mineral date. Zircon isotope half-lives are:

- ^{238}U 4.5 billion years
- ^{235}U 700 million years (Davis *et al.*, 2003)

Zircon U-Pb systematics are relatively resistant to many geological processes due to their high closure temperature; > 900°C (Cherniak and Watson, 2003) however radiation damage can result in Pb-loss. Fluid-mediated reactions under crustal conditions can result in dissolution and re-precipitation of zircon resulting in concentric, euhedral, external overgrowth (Cherniak and Watson, 2003). This can happen repeatedly as each zircon encounters a series of crustal events, often separated by many millions or billions of years, culminating in a physically and isotopically complex zircon morphology typically comprised of a core, outlined by multiple rimmed overgrowths (Fig. 3.5). The U-Pb systematics of these discrete growth zones are preserved owing to sluggish diffusion capacity within the

Figure 3.5 Zircon morphology is variable because individual grains are affected in differing ways during repeated generations of tectonic, metamorphic, magmatic and surface processes through geological time. Scale bars = 100 μm. Example zircon images (Corfu *et al*., 2003) show **A.** An acicular zircon core surrounded by a series of zoned overgrowths. **B.** and **C.** Multiple zoned overgrowths surround a fragmentary core. **D.** A fractured, prismatic crystal. **E.** Zoned overgrowth rims.

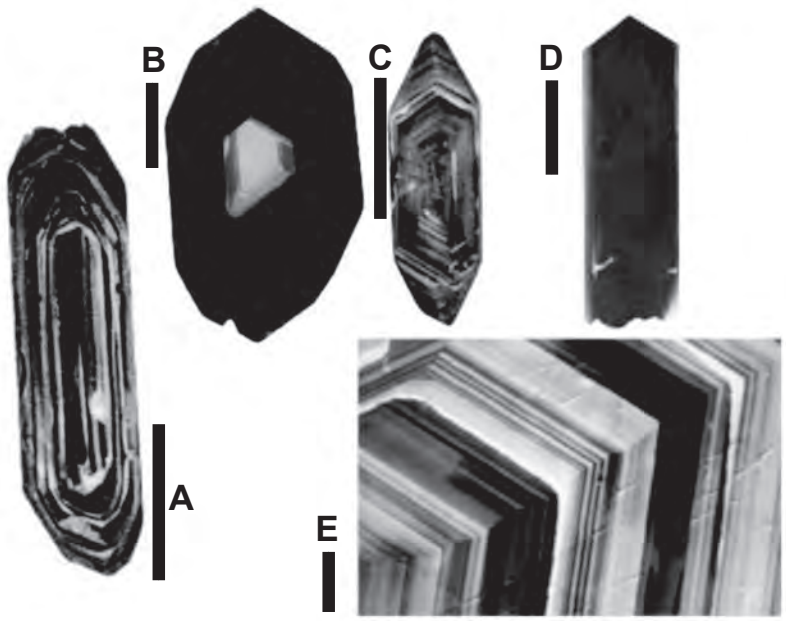

crystal lattice (Cherniak and Watson, 2003). Ideally the different radioactive clocks work autonomously, in a closed system, each commencing at the time the zone crystallised, thereby potentially recording the dates of the episodic events that forged each of them. Combined, these characteristics dictate zircon's value as a reliable chronometer in certain geological circumstances (Finch and Hanchar, 2003; Hoskin and Schaltegger, 2003; Parrish and Noble, 2003).

The zircon population within a given host rock is likely to consist of both authigenic and allogenic crystals. Authigenic zircon is crystallised in most leucocratic lavas between intermediate and Si-saturated and felsic ignimbrites from zirconium-enriched parent material. Conversely, acid lavas undersaturated with zirconium may adsorb inherited zircon xenocrysts and in such circumstances, no primary grains are crystallised (Hoskin and Schaltegger, 2003). Allogenic zircons are inherited in lavas, ignimbrites, and meta-igneous rocks, intermixed with authigenic grains, and are often present in significant quantities in sand-grade, silicate sedimentary and metasedimentary rocks. Zircons contained within detrital sedimentary rocks are contributed through time via the weathering of pre-existing rocks (Hoskin and Schaltegger, 2003) and are preserved throughout surface processes because of their physical robustness. Effectively, zircons are recycled through Earth history in a continuum consisting of inclusion in sedimentary and igneous rocks, alteration during episodic metamorphism, exhumation and weathering.

Sedimentary and metasedimentary rocks containing significant volumes of zircon therefore possess an inherent potential to record the thermal history and crustal evolution of their sediment (or protolith) source units, up to the time of burial. Zircon-bearing igneous, and meta-igneous rocks contain similar inherited populations, but with the addition of authigenic, or primary zircon which could reveal the absolute date of zircon crystallisation within the parent magma,

through radiometric dating. The interpretation of zircon U-Pb geochronology relies on the understanding of these distinct genetic processes by analysing the isotopic concentrations and ratios of U and Pb of each grain, or zone within each grain, and can provide:

- Characteristic age distributions record the provenance of a given sedimentary or metamorphic rock and can be correlated to source areas where suitable data exist. Individual source terranes have a zircon age distribution signature: a proxy for the tectonic and metamorphic events that comprise the geological history of the craton. This data informs crustal evolution studies.
- Age. In the case of plutonic and extrusive rocks and most crystalline pyroclastic rocks, establishing the age of the primary zircons within, provides a zircon crystallisation age for the rock. Older, inherited zircons will likely be present but are excluded from age calculation, and are often avoided prior to analysis on morphological grounds, for example by only analysing acicular grains. This is particularly useful where pyroclastics or extrusive lavas are interdigitated with sedimentary rocks.
- Maximum depositional age constraint of sedimentary or metasedimentary rocks. Individual grains contained within any sediment rock or protolith, must pre-date the formation of the rock. Age constraints of this type are of limited use – the youngest zircon present within a given detrital deposit may be many millions or hundreds of millions of years older than the host sediment. Most geochronology specialists consider minimum age interpretations with caution as they are often misleading.

Zircon geochronology

To establish meaningful geochronological data from rock units it is necessary to mechanically grind samples and progressively purify the material through a series of density-controlled sorting processes, aiming to isolate the densest minerals: specifically, the zircons (zircon density is 4.68 g/cm^3).

Zircon hosts several predictable systems used to interpret crustal evolution and for dating studies; U-Pb, Th-Pb, Lu-Hf, Sm-Nd and ^{18}O:^{16}O (Hanchar and Watson, 2003; Roberts and Spencer, 2015). In this study we are focussed on the U-Pb system to provide constraints on the timing of sedimentation and sediment provenance. Measurement of the parent/daughter isotope ratios within the U-Pb system: $^{206}Pb/^{238}U$ and $^{207}Pb/^{235}U$ allows the crystallisation date to be calculated by comparing these twin values in a concordia plot (Fig. 3.6 Wetherill concordia diagram), derived from the U-Pb radioactive decay system over extended time periods (Davis *et al.*, 2003). Analysis is achieved using mass spectrometry to assess the elemental and isotopic composition of an electron microbeam drilled, nanoscopic sample, or series of samples, from the core and/or overgrowth zones, of single zircon grains within a representative selection from the whole rock zircon population. Ideally the twin U-Pb ratios ($^{206}Pb/^{238}U$ and $^{207}Pb/^{235}U$) will produce an agreed age, which is a remarkable, naturally inbuilt test of the isotopic analysis exploiting the differing decay rates and half-lives of the uranium isotopes.

However, there is sometimes discordance between the two sets of data determined from a single analysis, attributable to open-system behaviour during which lead is lost by diffusion or inheritance following metamiction or fracture of the zircon crystal. Although this does not normally occur to a significant extent, zircon is able to lose lead at relatively low temperatures (Cherniak and Watson,

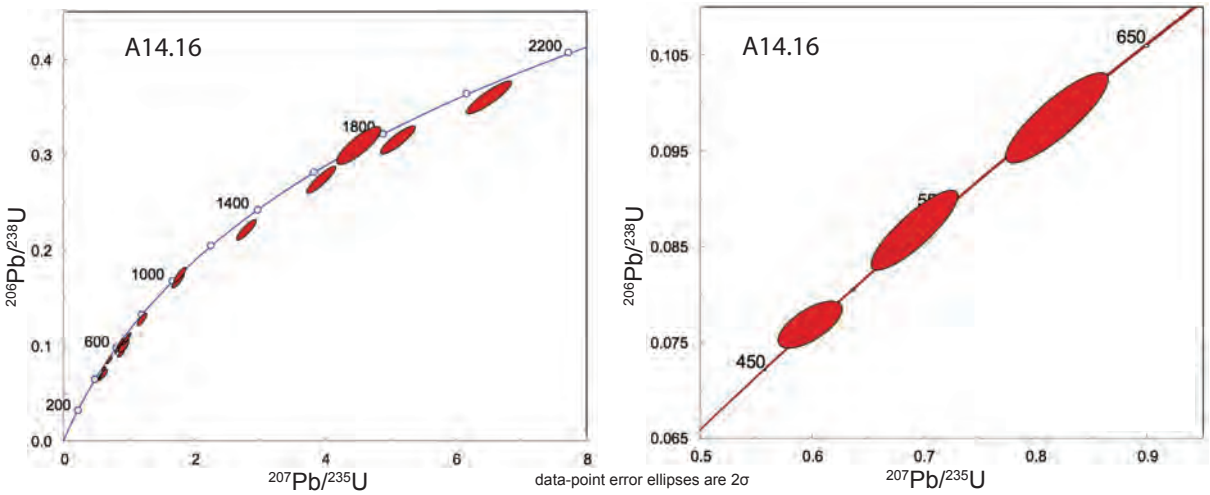

Figure 3.6 Example Wetherill concordia diagrams (Wetherill, 1956). Wetherill concordia diagrams are commonly used to demonstrate U-Pb results graphically, (**A**) all data-points measured for Gwna Group sample A14.16 and (**B**) the three youngest >90% concordant grains from A14.16. The Wetherill concordia curve is a precise joint geochronometer – it records 100% concordance between ^{206}Pb-^{238}U and ^{207}Pb-^{235}U ratios and the less frequently used Tera-Wasserburg diagram (Tera and Wasserburg, 1972) plots concordance between measured ^{207}Pb-^{206}Pb and ^{238}U-^{206}Pb. The position in relation to the concordia curve of data ellipses demonstrates the extent to which any analysis is concordant: normally discordant ages (those positioned in the segment beneath the concordia curve) can, if linear, indicate the age of the event that caused lead loss. This date is indicated by the upper intercept of a line connecting the normally discordant datapoints with the Concordia line. Lead loss, an indicator of open system behaviour, can produce misleading younger dates as reduced concentrations of Pb move the analysed data-points along the concordia line towards zero.

2003; Parrish and Noble, 2003). Decoupling of U and Pb, often during surface exposure and due to varied diffusion rates, requires that the $^{207}Pb/^{206}Pb$ system dates are employed as a more reliable measure for older ages (Condon and Bowring, 2011). This is most often the case in rocks aged > 800 – 1200 Ma: current standards for geochronological studies require combinations of $^{206}Pb/^{238}U$ and $^{207}Pb/^{206}Pb$ ages. Workers use different parameters for this, for example Strachan and Asanuma (Strachan *et al.*, 2007; Asanuma *et al.*, 2015; Asanuma *et al.*, 2017) use $^{206}Pb/^{238}U$ dates for ages up to 1000 Ma and $^{207}Pb/^{206}Pb$ for older data-points, others (Waldron *et al.*, 2018) set the switch

point at 800 Ma. This study makes the change at > 1000 Ma for two reasons: to comply with the published geochronology of the Monian Supergroup and, because there is an absence of dates at this point in time meaning the data is unlikely to be skewed.

Zircon crystals possess an external coating of high-U which, if breached, allows substantial lead loss (Krogh, 1982; Davis *et al.*, 2003) and Krogh consequently invented a method of zircon crystal air-abrasion to be undertaken prior to mass spectrometry, and in so doing, analytical accuracy was increased (Krogh, 1982; Davis *et al.*, 2003; Parrish and Noble, 2003). Zircons can be similarly 'repaired' using chemical abrasion, etching, leaching and annealing techniques, in the latter grains are heated to 900°C for ~ 60 hours, and subsequent partial dissolution. The object of this pre-treatment is to remove altered zircon domains for improved accuracy and precision in mass spectrometry (Mattinson, 2005).

Results suitable for interpretation within a broader geological framework must be derived from the most concordant zircon analyses. Discordant results are less accurate, imprecise and may even lead to incorrect conclusions (Spencer *et al.*, 2016).

Sample contamination is an ever-present problem under constant review in geochronology laboratories. Processing samples through a series of machines employed to crush, mill, grind, sieve and sort rock material requires exacting protocols for deep-cleaning of all equipment several times per day. Gold-standard approaches to methodology and interpretation of the data finally obtained must be applied if the resulting models are to stand the test of time. Contamination is a known enemy which it is impossible to eliminate.

Mass spectrometry

There are two methods of elemental analysis used in geochronology: microbeam laser ablation and isotopic dilution. The analyses undertaken in this study at NIGL used:

- Laser-ablation inductively coupled plasma mass spectrometry (LA-ICP-MS)
- Isotope-dilution thermal ionisation mass spectrometry (ID-TIMS)

LA-ICP-MS uses a microbeam to ablate the mounted zircon and inject the resulting aerosols into a plasma tube for analysis. ID-TIMS involves the addition of tracer isotopes before dissolving individual zircon crystals, followed by separation for analysis of U and Pb (Condon and Bowring, 2011). Individual microbeam analyses are completed with a washout flow and sample measurement is regularly interspersed by ablation of standard zircon materials such as Plešovice, 91500 and GJ-1. Frequent measurements of these standards provide an ongoing record of instrument "drift" (elemental fractionation effects) in a given session and facilitate calibration of the mass spectrometric results against recognised and accepted values. The isotopic data presented in this study comes from LA-ICP-MS analysis.

3.6 Results

Data presentation and age interpretation

Dating projects should use several lines of evidence to support interpretation of the ages determined. Biostratigraphy combined with geochronology can

provide fine-tuned dating but, with the single exception of *Skolithos* (penetrative vertical burrows, in the Holy Island Group) the Monian Supergroup is abiotic. This project combines field evidence with geochronology, to include and exclude arguments – both new and old, about the Gwna Group and related lithostratigraphic units.

Maximum caution must be applied to the interpretation of geochronological studies if misleading models are to be avoided. This is an ongoing challenge within the geoscience field, borne of the relative ease with which microbeam studies can now be made due to the increased number of isotope laboratories worldwide. Thus, many workers are pushing for improved protocols designed to increase the robustness of results and interpretation (Fedo *et al.*, 2003; Gehrels, 2012; Vermeesch, 2012). For example, Vermeesch (2012) argued for the replacement of standard probability density plots with kernel density estimations (KDE), and Gehrels (2012) recommended multiple ablations of single zircon grains to reduce misinterpreted ages from open-system behaviour in metamict zircon grains – by analysing all available areas of the zircon, zones of lead loss can be identified, reducing the number of inaccurate ages.

In this study, analyses that are 90% concordant, or greater (Table 3.2), are used. All other data points are ignored. Concordance is calculated by considering the variance in ages obtained from the three parent/daughter decay systems measured:

- ^{206}Pb-^{238}U age / ^{207}Pb-^{235}U age
- ^{206}Pb-^{238}U age / ^{207}Pb-^{206}Pb age

Both positive and negative concordance is permitted, so that if the variance between the radiometric dates calculated for a given ablation is outside of the range -10% to 10%, the analysis is excluded from the admissible data. This has

led to data-points considered acceptable in other studies being excluded from the results discussed here.

Obtaining a robust depositional age for the Gwna Group, by dating interbedded tuffs and crystalline ignimbrites was the main aim of the work, but this was not achieved since no primary zircon of an age that accords with the pre-existing constraints listed above (section 3.2) were present in the samples. The expectation was that a zircon crystallisation date in the Gwna Group interbedded ignimbrite would provide a late Cambrian to early Ordovician age, as these two constraints pre-exist this study, namely metasediments beneath the basal Gwna Group unconformity, in the Holy Island Group are of early to mid Cambrian age (Collins and Buchan, 2004; Buatois and Mangano, 2011) and the overstep is of middle Ordovician age. It is therefore concluded that the ignimbrite was undersaturated with zirconium and zircons did not crystallise. This is further supported by a paucity in the number of inherited zircons. All analyses undertaken, therefore, have instead been combined into a wider detrital zircon study, focussed on understanding the provenance of the Gwna Group and related Monian Supergroup sedimentary and metasedimentary units. A side issue is the consideration of maximum depositional ages. However, using detrital studies for this purpose is controversial albeit a widespread practice. Using the single youngest zircon grain to establish a maximum depositional age is fraught with problems, not least the risk of contamination. Geochronology current best practice suggests at least three zircons from the youngest age analysed to underpin an acceptable maximum depositional age, which rules out single grains as representative. Accordingly, in this study, the three youngest concordant (> 90%) ages from the youngest age population is averaged to obtain a maximum depositional age (Gehrels, 2012; Spencer *et al.*, 2016).

Provenance

Concordant analytical results from this study are summarised in Table 3.2. Appendix 1 contains the complete primary dataset and an extended version of table 3.2 can be found in appendix 2). For discussion and interpretation these new analyses have been combined with results that meet current best practice for concordance and maximum depositional age from these publications:

- Collins and Buchan (2004), which gave a maximum depositional age of 501 ± 20 Ma for the Holyhead and South Stack formations of the Holy Island Group
- Asanuma *et al.* (2015), a U-Pb geochronological study of the Gwna Group, Lleyn
- Asanuma *et al.* (2017), a geochronological study, including U-Pb ages for the Monian Supergroup and related units on Anglesey

Figures 3.7, 3.8 and 3.9 contain combined KDE plots (Vermeesch, 2018) and histograms that show the zircon age populations of the concordant grains within the Holy Island, New Harbour and Gwna Groups and the CASZ from this study and the three published works.

Table 3.2 → Summary table of > 90% concordantlaser-beam U-Pb analysis ages (full version in appendix 2 and primary data (all analyses) are listed in appendix 1). Samples are located with a National Grid Reference with a brief lithological description. The sample locations are shown graphically in figure 3.3. All Gwna Group samples are from background sediments – the turbidite sequence or interbedded ignimbrites, that is to say no debris flow or slump bed clast or fault block material is included as this would not reveal depositional information. Two discordance calculations are shown for each data point, comparing the ^{206}Pb-^{238}U and ^{207}Pb-^{206}Pb ages – the maximum discordance allowance is 10%. The three pairs of columns on the right list the ages determined from elemental and isotopic ratio analysis, with 2σ absolute age uncertainties. The green highlighted ages are those used for plots in this study: ^{206}Pb-^{238}U ages are used for dates < 1,000 Ma and ^{207}Pb-^{206}Pb ages are used for > 1,001 Ma.

Samples	Discordance %		Ages					
Analyses	6-38/7-6	6-38/7-35	$^{207}Pb/^{206}Pb$	2s abs	$^{207}Pb/^{235}U$	2s abs	$^{206}Pb/^{238}U$	2s abs
Sample A14:16. Outcrop belt 2. Aberffraw. NGR SH3380 6754. Mudstone layer, directly overlying the basal Gwna Group unconformity								
A14.16_04	9.8	1.7	489	23	449	16	441	17
A14.16rd5_02	-2.9	-0.5	465	32	476	15	478	12
A14.16_10	-3.3	-0.6	520	26	533	19	537	20
A14.16.RD4a_4	0.7	0.1	610	26	607	21	606	23
A14.16_12	-7.3	-1.6	595	22	629	20	639	23
A14.16_01	6.6	1.6	705	24	668	21	658	23
A14.16.RD4a_1	7.3	1.8	727	23	686	22	674	24
A14.16.RD4a_2	5.5	1.5	827	28	794	26	782	29
A14.16_07	-3.6	-1.1	1007	21	1031	27	1043	36
A14.16.RD4a_3	3.6	1.1	1047	24	1021	29	1010	36
A14.16rd5_01	9.5	3.8	1433	21	1349	33	1297	47
A14.16_09	6.8	3.0	1682	19	1616	37	1567	57
A14.16rd5_04	-2.3	-1.0	1708	31	1728	49	1746	78
A14.16.RD4a_8	6.6	3.1	1899	18	1832	35	1775	58
A14.16_11	5.3	2.7	2098	17	2042	37	1988	65
Sample A15:1. Outcrop belt 2. Aberffraw. NGR SH3417 6764. Ignimbrite interbedded with laminated tuff								
A15.1_08	-2.5	-0.6	590	25	601	20	604	22
A15.1_10	0.5	0.1	607	24	605	20	604	22
A15.1_21	-0.3	-0.1	606	24	608	20	608	21
A15.1_14	0.5	0.1	611	24	609	21	608	23
A15.1_11	1.9	0.4	621	23	612	20	609	22
A15.1_01	4.9	1.1	641	22	616	20	610	22
A15.1_12	-0.3	-0.1	614	31	615	23	616	24
A15.1_03	4.5	1.0	658	23	635	21	629	23
A15.1_19	1.8	0.4	657	25	648	21	645	23
A15.1_17	0.4	0.1	650	26	648	21	647	24
A15.1_09	2.8	0.6	667	25	653	21	649	23
A15.1_16	4.0	0.9	680	26	659	22	653	23
A15.1.rd5_04	-3.4	-0.8	668	20	685	18	690	20
A15.1.rd5_03	2.2	0.5	755	18	742	17	738	19
A15.1rd6_01	1.2	0.3	748	15	741	17	739	20
A15.1.rd5_05	-1.7	-0.5	742	18	751	18	754	22
A15.1.rd5_02	-2.4	-1.0	1427	18	1447	28	1461	42
A15.1_20	-0.8	-0.4	1497	20	1504	35	1510	53
A15.1_07	2.4	1.1	1736	19	1712	36	1693	59
A15.1_15	2.3	1.1	1982	18	1959	39	1937	68
A15.1.rd5_06	-0.8	-0.4	1926	17	1934	35	1942	60
A15.1_23	0.8	0.4	2719	17	2709	51	2698	112
Sample CB14:1. Outcrop belt 3. Porth Trefadog. NGR SH2899 8587. Laminated ash tuff								
CB14.1.rd1_21	6.0	0.7	316	20	299	7	297	7
CB14.1.rd4_01	9.2	1.1	340	26	312	9	309	7
CB14.1.rd4_06b	0.3	0.0	318	23	317	8	317	7
CB14.1.rd4_06a	5.7	0.7	337	22	320	9	318	8
CB14.1.rd1_20a	6.9	0.9	346	22	325	9	323	8
CB14.1.rd1_04	-1.3	-0.2	323	22	327	8	328	7
CB14.1.rd1_19	4.1	0.5	379	24	366	10	364	8
CB14.1.rd4_09	-0.2	-0.1	411	22	412	10	412	9
CB14.1.rd1_01	4.4	0.7	458	20	441	10	438	10
CB14.1.rd1_15	9.9	1.7	487	27	446	12	439	11
CB14.1.rd1_11	-5.8	-0.9	426	24	446	11	450	10
CB14.1.rd5_04	3.1	0.5	470	28	457	15	455	15
CB14.1.rd1_06a	-3.5	-0.6	474	27	487	14	490	12
CB14.1.rd4_10	-8.5	-1.6	516	18	551	12	559	12
CB14.15rd5_06	7.4	1.6	643	27	606	16	596	14
CB14.15rd5_04	-0.1	0.0	597	21	597	13	597	13
CB14.1.rd1_03	-0.6	-0.2	596	17	599	12	600	13
CB14.1.rd4_05	4.8	1.0	630	20	606	14	600	14
CB14.1.rd1_14	2.1	0.4	635	19	624	14	621	14
CB14.1.rd5_02	-2.5	-0.6	609	22	620	16	624	18
CB14.1.rd1_10	2.4	0.5	640	18	628	13	625	14

Samples	Discordance %		Ages					
Analyses	6-38/7-6	6-38/7-35	$^{207}Pb/^{206}Pb$	2s abs	$^{207}Pb/^{235}U$	2s abs	$^{206}Pb/^{238}U$	2s abs
Sample CB14:1. Outcrop belt 3. Porth Trefadog. NGR SH2899 8587. Laminated ash tuff								
CB14.1.rd1_22a	1.1	0.2	740	18	733	15	731	17
CB14.1.rd5_05	5.9	1.8	1001	19	959	21	941	25
CB14.1.rd4_07b	0.8	0.2	959	21	953	20	951	23
CB14.1.rd4_07a	-0.2	-0.1	956	16	957	17	958	20
CB14.1.rd4_04	1.1	0.3	1049	18	1041	20	1038	23
CB14.1.rd4_02a	3.1	1.1	1156	18	1132	21	1120	26
CB14.1.rd1_07	-2.6	-0.9	1161	19	1180	23	1191	29
CB14.1.rd4_02b	0.4	0.1	1169	18	1165	21	1164	27
CB14.1.rd1_09	0.7	0.2	1175	23	1169	26	1166	31
CB14.1.rd1_27a	7.9	3.3	1503	15	1431	26	1384	37
CB14.1.rd4_03	1.6	0.7	1515	16	1501	24	1491	34
CB14.1.rd1_12	-3.5	-1.5	1606	16	1637	24	1662	35
CB14.1.rd5_01	1.0	0.4	1622	15	1612	27	1605	42
CB14.1.rd1_18	-2.9	-1.3	1668	15	1694	23	1716	33
CB14.1.rd1_26a	1.0	0.4	1685	13	1675	22	1668	34
CB14.1.rd1_05	-2.9	-1.3	1732	14	1759	22	1783	35
CB14.1.rd4_08a	0.6	0.3	2048	13	2041	23	2036	37
CB14.1.rd1_23	5.6	3.1	2617	12	2552	25	2472	46
CB14.1.rd1_13	-2.2	-1.3	2712	14	2737	30	2772	61
CB14.1.rd1_17	-1.1	-0.7	2758	13	2771	27	2789	54
Sample CB14:2. Outcrop belt 3. Porth Trefadog. NGR SH2902 8587. Ignimbrite								
CB14.2.RD1_14	1.6	0.3	593	17	586	12	584	12
CB14.2.rd4_08b	8.3	1.8	641	24	598	15	587	13
CB14.2.rd4_02b	8.5	1.9	646	24	602	15	590	14
CB14.2.RD1_12	5.9	1.3	633	16	603	12	596	12
CB14.2.RD1_23	4.0	0.8	622	14	602	10	597	11
CB14.2.rd4_14a	2.5	0.5	618	18	605	13	602	13
CB14.2.RD1_11	6.9	1.5	647	18	611	12	602	11
CB14.2.rd4_05b	4.7	1.0	634	22	610	15	604	15
CB14.2.RD1_22	3.8	0.8	633	19	614	12	609	12
CB14.2.rd4_02a	-3.6	-0.8	591	20	607	14	612	15
CB14.2.rd4_08a	0.7	0.1	617	19	613	13	612	14
CB14.2.RD1_02	1.2	0.2	620	19	614	14	613	14
CB14.2.RD1_05	6.2	1.4	654	16	621	11	613	11
CB14.2.rd4_10b	3.0	0.6	632	22	617	14	613	13
CB14.2.rd4_10a	-0.7	-0.2	609	22	612	15	613	15
CB14.2.RD1_10	4.5	1.0	643	21	620	14	614	14
CB14.2.rd4_01	-5.1	-1.1	588	19	611	13	618	14
CB14.2.rd4_12	2.1	0.4	634	20	623	15	621	16
CB14.2.rd4_05a	-1.3	-0.3	614	18	620	13	622	14
CB14.2.rd4_06	2.4	0.5	639	26	627	19	623	19
CB14.2.RD1_06	2.0	0.4	640	16	630	12	627	13
CB14.2.rd4_09	-6.1	-1.3	596	23	624	16	632	16
CB14.2.RD1_21a	7.8	1.8	702	17	659	12	647	12
CB14.2.RD1_18	6.0	1.4	702	20	669	14	660	14
CB14.2.RD1_08a	9.1	2.2	728	13	677	10	661	10
CB14.2.rd4_03a	-1.8	-0.4	690	17	699	15	702	17
CB14.2.rd4_13	2.9	0.7	727	17	711	14	706	15
CB14.2.RD1_16	9.6	2.5	782	15	725	12	707	12
CB14.2.RD1_08b	1.4	0.3	726	15	718	12	716	13
CB14.2.RD1_09	1.2	0.3	733	13	726	11	725	11
CB14.2.RD1_20	2.6	0.6	746	18	731	14	726	14
CB14.2.rd4_03b	0.0	0.0	738	17	737	14	738	15
CB14.2.RD1_21b	0.5	0.1	742	18	739	15	738	17
CB14.2.rd4_04	-1.3	-0.4	766	19	773	17	776	19
CB14.2.RD1_24	1.3	0.5	1432	12	1421	18	1414	25
CB14.2.rd4_11	4.0	1.7	1507	15	1471	22	1446	31

Samples	Discordance %		Ages					
Analyses	6-38/7-6	6-38/7-35	$^{207}Pb/^{206}Pb$	2s abs	$^{207}Pb/^{235}U$	2s abs	$^{206}Pb/^{238}U$	2s abs
Sample CB14:2. Outcrop belt 3. Porth Trefadog. NGR SH2902 8587. Ignimbrite								
CB14.2.RD1_01	-4.5	-2.0	1593	12	1633	18	1664	27
CB14.2.RD1_04	-1.2	-0.6	1598	12	1609	18	1618	26
CB14.2.RD1_13	5.6	2.4	1605	13	1553	18	1516	26
Sample CB14:5. Outcrop belt 3. Port Trefadog. NGR SH2903 8589. Coarse crystalline ignimbrite								
CB14.5.RD1_15	1.7	0.3	594	18	585	12	583	12
CB14.5.RD1_22	7.3	1.6	645	18	608	13	598	14
CB14.5.RD1_18	6.2	1.4	642	21	610	14	602	14
CB14.5.RD1_02	7.5	1.7	658	21	619	14	609	13
CB14.5.RD1_04	-0.9	-0.2	608	22	612	14	613	13
CB14.5.RD1_14	7.1	1.6	660	18	623	13	613	13
CB14.5.RD1_03	4.5	1.0	664	25	641	15	634	13
CB14.5.RD1_09	-3.3	-0.8	660	18	677	13	682	13
CB14.5.RD1_19	-0.4	-0.1	1086	18	1088	18	1090	21
CB14.5.RD1_05	-1.8	-0.7	1222	15	1236	18	1244	24
CB14.5.RD1_16	2.7	1.0	1255	18	1233	21	1222	26
CB14.5.RD1_08	-0.1	-0.1	1439	15	1439	20	1440	27
CB14.5.RD1_17a	-5.0	-2.1	1476	14	1519	20	1550	29
CB14.5.RD1_17b	-1.0	-0.4	1513	14	1521	21	1528	30
CB14.5.RD1_21b	1.1	0.5	1571	15	1561	22	1554	30
CB14.5.RD1_21a	0.8	0.3	1572	16	1564	21	1559	28
CB14.5.RD1_20	0.4	0.2	1612	14	1608	22	1606	33
Sample NHG15:12. Outcrop belt 3. Penrhyn. NGR SH2845 8491. Volcaniclastic psammite								
NHG15.12rd6_81	9.5	1.9	581	17	536	14	526	15
NHG15.12rd6_31	3.1	0.6	548	20	534	12	531	11
NHG15.12rd6_63	8.4	1.7	580	18	540	11	531	10
NHG15.12rd3_21	2.1	0.4	544	20	534	15	532	15
NHG15.12rd3_05	4.4	0.8	559	21	538	14	534	14
NHG15.12rd6_23	2.9	0.5	550	21	537	13	534	12
NHG15.12rd6_76	3.4	0.6	554	17	539	14	535	16
NHG15.12rd6_84b	8.0	1.6	582	14	544	12	535	14
NHG15.12rd6_28	3.0	0.6	552	19	538	11	535	10
NHG15.12rd6_25	0.7	0.1	541	19	537	11	537	11
NHG15.12rd6_64a	2.6	0.5	551	16	540	10	537	9
NHG15.12rd6_77a	1.4	0.2	545	15	539	12	538	13
NHG15.12rd6_45	5.7	1.1	571	18	544	12	538	12
NHG15.12rd6_84a	6.8	1.4	578	16	546	14	538	15
NHG15.12rd6_64b	2.8	0.5	554	18	541	11	538	10
NHG15.12rd6_92a	4.2	0.8	565	18	546	14	542	15
NHG15.12rd6_03	7.4	1.5	586	24	551	13	543	11
NHG15.12rd6_47	-1.7	-0.4	537	18	544	12	546	12
NHG15.12rd6_77b	6.4	1.3	584	17	553	13	546	13
NHG15.12rd6_75	4.7	0.9	580	15	558	12	553	13
NHG15.12rd6_26	-4.3	-0.8	532	22	550	13	555	12
NHG15.12rd6_42	8.0	1.7	604	20	565	13	556	13
NHG15.12rd6_100	-2.6	-0.5	543	17	553	13	556	14
NHG15.12rd6_32a	8.2	1.7	607	29	567	16	557	14
NHG15.12rd6_29	-2.7	-0.5	543	19	554	12	557	12
NHG15.12rd3_12	4.7	0.9	586	24	563	16	558	16
NHG15.12rd6_57	3.0	0.6	582	15	567	11	564	11
NHG15.12rd6_24a	8.3	1.8	616	22	574	13	564	13
NHG15.12rd3_03	4.2	0.8	590	22	570	16	565	16
NHG15.12rd6_82b	8.3	1.8	619	19	577	15	567	16
NHG15.12rd6_62	4.8	1.0	599	20	576	12	570	12
NHG15.12rd6_82a	-1.7	-0.4	562	16	569	13	571	15
NHG15.12rd6_101	0.7	0.1	581	17	577	14	577	15
NHG15.12rd6_24b	3.6	0.7	604	19	586	13	582	12
NHG15.12rd6_71	4.3	0.9	611	16	590	13	585	14

Samples	Discordance %		Ages					
Analyses	6-38/7-6	6-38/7-35	$^{207}Pb/^{206}Pb$	2s abs	$^{207}Pb/^{235}U$	2s abs	$^{206}Pb/^{238}U$	2s abs
Sample NHG15:12. Outcrop belt 3. Penrhyn. NGR SH2845 8491. Volcaniclastic psammite								
NHG15.12rd6_79	8.0	1.7	639	16	599	13	588	15
NHG15.12rd6_58	1.3	0.2	599	18	592	11	591	11
NHG15.12rd6_49b	8.7	1.9	651	16	606	10	595	10
NHG15.12rd6_78a	6.0	1.3	633	16	603	13	595	15
NHG15.12rd6_19	9.4	2.1	658	21	609	15	596	14
NHG15.12rd3_07	-1.0	-0.2	594	20	599	15	600	16
NHG15.12rd6_33a	7.8	1.7	652	28	611	18	601	18
NHG15.12rd3_13	3.9	0.8	626	18	606	15	601	16
NHG15.12rd6_78b	5.6	1.2	638	18	609	15	602	16
NHG15.12rd6_89	6.3	1.4	643	19	611	14	602	14
NHG15.12rd6_72	2.8	0.6	620	12	606	12	603	14
NHG15.12rd6_60	2.6	0.5	620	17	607	12	604	12
NHG15.12rd6_59	5.5	1.2	640	20	612	12	604	11
NHG15.12rd6_93	4.0	0.9	632	15	611	13	606	14
NHG15.12rd6_09	4.4	0.9	635	22	613	15	607	15
NHG15.12rd3_19	2.6	0.5	624	22	611	17	608	18
NHG15.12rd6_85	3.3	0.7	633	17	617	14	612	15
NHG15.12rd6_33b	6.3	1.4	655	24	622	14	613	13
NHG15.12rd3_20	6.3	1.4	657	19	624	16	615	17
NHG15.12rd6_50a	4.1	0.9	643	26	622	16	617	14
NHG15.12rd6_11	2.2	0.5	631	30	620	18	617	16
NHG15.12rd6_40	2.4	0.5	633	24	620	14	617	12
NHG15.12rd6_15	4.9	1.1	649	19	624	13	617	12
NHG15.12rd6_39	3.5	0.7	641	19	623	13	619	13
NHG15.12rd6_83	0.1	0.0	619	16	619	14	619	16
NHG15.12rd6_02	6.5	1.5	662	21	628	14	619	14
NHG15.12rd6_99	-2.5	-0.6	605	15	616	14	620	16
NHG15.12rd3_14	2.8	0.6	640	21	626	17	622	18
NHG15.12rd6_10	-0.9	-0.2	617	18	621	13	622	13
NHG15.12rd6_41	8.1	1.9	678	19	635	14	623	13
NHG15.12rd6_55	3.2	0.7	645	16	628	12	624	13
NHG15.12rd6_50b	3.1	0.6	645	20	630	14	626	14
NHG15.12rd6_66	2.7	0.6	644	17	630	11	626	11
NHG15.12rd6_01	-2.1	-0.5	614	27	624	19	627	19
NHG15.12rd6_51	5.4	1.2	663	19	635	13	628	13
NHG15.12rd3_06	-1.7	-0.4	618	22	626	17	629	18
NHG15.12rd6_08	4.2	0.9	663	22	641	16	635	16
NHG15.12rd6_21a	6.0	1.4	676	22	644	16	635	16
NHG15.12rd6_53	-4.7	-1.0	608	17	630	12	637	12
NHG15.12rd6_49a	-5.2	-1.1	606	17	630	12	637	12
NHG15.12rd6_20	3.5	0.8	666	27	647	19	642	19
NHG15.12rd3_02	5.6	1.3	681	21	652	18	643	19
NHG15.12rd6_91b	5.4	1.2	684	14	656	14	647	16
NHG15.12rd6_21b	5.3	1.2	688	18	659	14	651	15
NHG15.12rd3_17	-2.7	-0.6	635	23	648	19	652	21
NHG15.12rd6_90	5.7	1.3	694	17	663	15	654	17
NHG15.12rd3_16	-3.5	-0.8	634	24	650	19	656	20
NHG15.12rd3_04	5.2	1.2	693	20	665	17	657	19
NHG15.12rd6_22	-1.4	-0.4	649	22	656	16	658	17
NHG15.12rd6_46	6.2	1.5	703	16	669	13	659	14
NHG15.12rd6_88	4.9	1.1	694	16	667	15	659	17
NHG15.12rd6_91a	5.0	1.2	699	17	671	15	663	16
NHG15.12rd6_34	8.2	2.0	726	21	680	14	667	13
NHG15.12rd6_70	5.1	1.2	705	17	677	13	669	13
NHG15.12rd6_95	3.8	0.9	696	15	675	14	669	17
NHG15.12rd6_97	9.0	2.2	735	14	685	14	670	16
NHG15.12rd6_94a	2.0	0.4	686	17	675	15	672	17

Samples	Discordance %		Ages					
Analyses	6-38/7-6	6-38/7-35	$^{207}Pb/^{206}Pb$	2s abs	$^{207}Pb/^{235}U$	2s abs	$^{206}Pb/^{238}U$	2s abs
Sample NHG15:12. Outcrop belt 3. Penrhyn. NGR SH2845 8491. Volcaniclastic psammite								
NHG15.12rd6_48	5.1	1.2	709	22	681	16	673	16
NHG15.12rd6_36	3.6	0.8	699	19	679	13	673	13
NHG15.12rd6_73a	2.4	0.5	691	13	678	14	674	16
NHG15.12rd6_04	2.0	0.4	691	25	679	17	676	15
NHG15.12rd6_67	1.7	0.4	696	15	687	13	685	15
NHG15.12rd6_73b	2.6	0.6	705	16	690	15	686	17
NHG15.12rd6_94b	0.9	0.2	696	16	692	16	690	18
NHG15.12_10	0.4	0.1	694	20	692	18	692	20
NHG15.12rd6_37b	5.1	1.2	736	18	707	14	698	15
NHG15.12rd6_37a	5.3	1.3	749	19	718	15	709	16
NHG15.12rd3_22	-5.1	-1.2	693	19	719	17	728	18
NHG15.12rd3_08	4.9	1.3	812	18	782	18	772	22
NHG15.12rd6_38b	4.0	1.2	933	15	907	15	896	17
NHG15.12rd6_38a	3.8	1.1	961	21	936	19	925	20
NHG15.12rd3_23	0.7	0.2	1178	22	1172	27	1169	35
NHG15.12rd3_11	2.6	0.9	1200	16	1180	24	1169	32
NHG15.12rd6_74b	4.2	1.5	1221	14	1188	21	1170	28
NHG15.12rd6_74a	5.8	2.1	1236	15	1190	22	1165	29
NHG15.12rd6_61	9.3	3.5	1290	19	1213	25	1170	33
NHG15.12rd6_69	3.5	1.4	1473	11	1442	16	1422	23
NHG15.12rd6_16	0.2	0.1	1554	14	1551	22	1550	32
NHG15.12rd6_68	1.8	0.8	1703	17	1685	28	1672	43
NHG15.12rd6_95	-2.4	-1.2	1917	11	1940	26	1963	48
NHG15.12rd6_06	0.1	0.0	1946	13	1945	24	1945	41
NHG15.12rd6_27	0.3	0.1	1971	13	1967	24	1965	40
NHG15.12rd3_25	2.2	1.1	2081	14	2058	29	2035	52
NHG15.12rd6_17	6.3	3.6	2638	14	2563	29	2471	55
NHG15.12rd6_35	1.4	0.8	2736	11	2719	26	2697	54
Sample NHG15:2. Outcrop belt 4. Cemlyn Bay. NGR SH3368 9326. Volcaniclastic psammite								
NHG15.2rd3_10	2.8	0.5	543	22	531	15	528	16
NHG15.2rd3_03	3.9	0.7	551	18	534	13	530	14
NHG15.2rd3_22	2.9	0.5	559	31	546	18	543	17
NHG15.2.rd5_11	4.6	0.9	576	17	554	14	549	15
NHG15.2rd4a_17	-1.8	-0.4	542	16	549	13	551	15
NHG15.2rd4a_05a	0.1	0.0	554	16	553	12	553	13
NHG15.2rd4a_12b	3.5	0.7	576	17	560	13	556	14
NHG15.2.rd5_12	5.3	1.1	592	19	566	14	560	15
NHG15.2rd3_31	8.2	1.7	612	27	571	18	561	18
NHG15.2rd3_40	-1.3	-0.3	555	22	561	16	562	16
NHG15.2rd3_37	8.2	1.7	616	24	575	17	565	18
NHG15.2rd3_05	6.1	1.3	603	26	573	16	566	16
NHG15.2rd3_36	3.1	0.6	584	26	570	16	566	15
NHG15.2rd4a_19	1.3	0.2	579	12	573	11	572	13
NHG15.2rd4a_09a	-0.6	-0.1	570	13	572	12	573	14
NHG15.2rd3_23	-5.3	-1.1	544	20	567	15	573	16
NHG15.2rd4a_09b	0.8	0.1	583	15	579	13	578	14
NHG15.2rd3_24	5.7	1.2	614	22	586	15	579	15
NHG15.2.rd5_04	-0.1	0.0	581	21	581	15	581	16
NHG15.2rd3_26	4.9	1.0	611	24	587	16	581	16
NHG15.2rd4a_18	4.2	0.9	608	15	588	12	583	14
NHG15.2rd3_16	4.3	0.9	631	23	609	17	604	18
NHG15.2rd3_04	3.1	0.6	626	22	610	16	606	17
NHG15.2rd3_08	3.7	0.8	635	22	616	17	611	17
NHG15.2rd3_11	1.7	0.3	624	20	615	16	613	17
NHG15.2.rd5_01	3.4	0.7	636	16	618	14	614	16
NHG15.2rd3_12	-0.6	-0.2	612	22	615	16	616	16
NHG15.2rd3_38	6.1	1.4	658	21	627	16	618	17

Samples	Discordance %		Ages					
Analyses	6-38/7-6	6-38/7-35	$^{207}Pb/^{206}Pb$	2s abs	$^{207}Pb/^{235}U$	2s abs	$^{206}Pb/^{238}U$	2s abs
Sample NHG15:2. Outcrop belt 4. Cemlyn Bay. NGR SH3368 9326. Volcaniclastic psammite								
NHG15.2.rd5_03	1.0	0.2	627	17	622	16	621	19
NHG15.2rd3_20	-0.2	-0.1	622	20	622	16	623	17
NHG15.2rd3_15	3.4	0.7	646	18	628	15	624	17
NHG15.2rd4a_06a	6.2	1.4	669	19	637	15	628	16
NHG15.2rd4a_07b	-0.1	-0.1	628	15	628	14	629	16
NHG15.2rd3_17	-2.3	-0.5	616	27	627	18	631	18
NHG15.2rd3_42	6.1	1.4	672	23	640	17	631	18
NHG15.2rd4a_27a	3.5	0.8	654	16	636	14	631	16
NHG15.2rd3_30	3.4	0.7	654	20	636	17	631	19
NHG15.2rd4a_24a	4.8	1.1	664	13	639	14	632	16
NHG15.2rd4a_02	-5.0	-1.1	603	18	626	14	633	16
NHG15.2.rd5_02	2.6	0.5	650	19	636	16	633	17
NHG15.2rd3_44	-4.0	-0.9	610	19	629	16	634	18
NHG15.2rd4a_27b	1.0	0.2	643	14	637	13	636	15
NHG15.2rd3_19	5.7	1.3	675	18	645	16	637	17
NHG15.2rd3_27	-2.3	-0.5	623	21	634	18	638	19
NHG15.2rd4a_25	-1.1	-0.3	632	15	637	14	639	15
NHG15.2rd4a_29	5.7	1.3	679	17	648	14	640	16
NHG15.2rd4a_28	1.1	0.2	648	13	642	13	641	15
NHG15.2rd3_41	-2.0	-0.5	630	21	639	17	642	19
NHG15.2rd3_18	1.4	0.3	654	21	647	18	645	19
NHG15.2rd4a_24b	3.3	0.7	668	24	651	19	647	20
NHG15.2rd3_35	2.9	0.6	666	19	651	16	647	18
NHG15.2rd4a_20	0.7	0.1	652	16	648	14	647	16
NHG15.2rd4a_31	-2.8	-0.7	630	16	644	14	648	16
NHG15.2rd4a_14	-2.0	-0.5	638	17	647	14	650	16
NHG15.2rd4a_07a	-2.6	-0.6	635	16	648	15	652	17
NHG15.2.rd5_07	4.0	0.9	682	18	660	16	654	17
NHG15.2rd3_34	-0.6	-0.2	653	23	655	18	656	19
NHG15.2rd3_02	0.2	0.0	658	25	657	19	656	20
NHG15.2.rd5_06	-0.8	-0.2	657	21	661	18	663	20
NHG15.2rd4a_10a	-6.8	-1.5	623	14	656	14	665	16
NHG15.2rd4a_15	2.9	0.6	686	16	671	14	667	16
NHG15.2rd4a_06b	0.0	0.0	667	15	667	14	667	16
NHG15.2rd4a_11b	0.8	0.1	683	15	679	14	678	16
NHG15.2rd4a_06b	2.9	0.7	707	21	691	17	686	18
NHG15.2rd4a_30a	-0.5	-0.1	684	16	687	15	688	17
NHG15.2rd4a_11a	-1.0	-0.3	681	17	686	16	688	18
NHG15.2rd4a_30b	-4.4	-1.0	673	16	696	15	703	17
NHG15.2rd3_13	0.2	0.0	729	22	728	19	728	21
NHG15.2rd4a_13	-1.4	-0.4	737	14	745	15	748	18
NHG15.2rd3_28	-0.4	-0.1	784	17	786	17	788	20
NHG15.2rd3_43	0.2	0.0	808	18	806	18	806	21
NHG15.2rd4a_26	-4.3	-1.5	1164	13	1196	20	1215	28
NHG15.2rd4a_16a	-1.4	-0.5	1216	13	1227	21	1233	29
NHG15.2rd4a_16b	-1.4	-0.5	1218	13	1229	20	1235	28
NHG15.2rd3_07	0.3	0.1	1227	16	1225	24	1224	34
NHG15.2rd3_32	0.8	0.3	1231	16	1224	22	1221	30
NHG15.2.rd5_10	4.1	1.5	1251	14	1217	24	1199	34
NHG15.2rd3_01	2.1	0.8	1305	16	1287	24	1277	34
NHG15.2rd4a_23	-3.1	-1.2	1336	10	1361	20	1378	31
NHG15.2rd3_33	7.8	3.3	1530	14	1459	26	1411	39
NHG15.2rd4a_08a	-1.9	-0.9	1790	11	1808	24	1824	42
NHG15.2rd4a_08b	-0.6	-0.3	1815	12	1821	29	1827	50
NHG15.2rd3_06	2.6	1.2	1865	14	1840	29	1817	49
NHG15.2rd4a_22a	-2.4	-1.4	2704	9	2731	28	2768	63
NHG15.2rd4a_22b	0.1	0.1	2719	11	2717	34	2715	74
NHG15.2rd3_25	-0.4	-0.2	2855	13	2859	34	2865	74
NHG15.2rd4a_21	6.0	3.6	2912	9	2838	26	2736	56

Samples	Discordance %		Ages					
Analyses	6-38/7-6	6-38/7-35	$^{207}Pb/^{206}Pb$	2s abs	$^{207}Pb/^{235}U$	2s abs	$^{206}Pb/^{238}U$	2s abs
Sample PT15:1. Outcrop belt 2. Aberffraw. NGR SH3382 6833. Psammite								
PT15.1rd5_05b	-1.5	-0.3	576	23	582	15	584	14
PT15.1rd5_06	6.0	1.3	623	24	593	15	585	15
PT15.1_14	5.0	1.0	618	23	594	15	587	14
PT15.1_26	6.6	1.4	630	20	597	14	588	14
PT15.1_30	5.5	1.2	622	18	595	13	588	13
PT15.1_23	5.4	1.1	623	20	596	14	589	14
PT15.1_15	6.9	1.5	634	21	599	13	590	13
PT15.1rd5_07	4.9	1.0	620	23	596	14	590	13
PT15.1rd5_05a	4.6	1.0	619	24	596	15	590	15
PT15.1_09	8.9	2.0	649	23	603	15	591	14
PT15.1_12	7.3	1.6	640	26	603	16	594	15
PT15.1_13	5.5	1.2	629	20	601	14	594	14
PT15.1_20	3.7	0.8	619	22	601	14	596	13
PT15.1rd5_12	0.9	0.2	602	20	597	13	596	13
PT15.1rd5_14	5.8	1.2	633	28	604	16	596	14
PT15.1rd5_01	-0.1	-0.1	596	26	596	16	596	15
PT15.1_31	3.3	0.7	619	21	603	14	599	14
PT15.1_04	6.8	1.5	645	19	610	14	601	14
PT15.1_01	2.8	0.6	620	19	606	13	603	13
PT15.1_56	2.7	0.6	620	22	606	19	603	21
PT15.1_63	3.1	0.6	624	21	609	19	605	21
PT15.1_02	1.2	0.2	613	28	607	18	606	17
PT15.1_29	1.0	0.2	613	23	608	15	606	15
PT15.1_64	1.6	0.3	617	23	609	19	607	21
PT15.1_53	-2.3	-0.5	593	19	604	18	607	21
PT15.1_59	7.6	1.7	658	23	618	20	608	22
PT15.1_25	1.8	0.4	619	24	610	15	608	14
PT15.1_05	6.1	1.3	648	29	616	18	608	18
PT15.1_51	5.3	1.1	644	24	617	20	610	22
PT15.1_62	0.0	0.0	611	20	611	18	611	21
PT15.1_55	3.5	0.7	633	22	615	20	611	22
PT15.1_52	4.7	1.0	641	21	617	19	611	21
PT15.1_24	5.4	1.2	646	26	618	18	611	17
PT15.1_66	5.9	1.3	650	22	620	20	612	22
PT15.1_61	2.1	0.4	626	20	616	19	613	22
PT15.1_44	0.7	0.1	618	20	614	18	613	21
PT15.1_35	1.4	0.3	622	28	615	21	614	23
PT15.1_43	6.0	1.3	653	21	622	19	614	21
PT15.1_50	7.3	1.6	663	27	625	22	615	23
PT15.1_41	5.6	1.2	652	24	623	21	615	22
PT15.1_18	7.2	1.6	663	23	626	16	616	16
PT15.1_57	4.4	0.9	646	26	623	20	617	22
PT15.1_49	3.2	0.7	638	30	622	22	618	23
PT15.1_36	-2.7	-0.6	602	26	615	21	618	23
PT15.1_65	-1.1	-0.3	613	22	618	19	619	21
PT15.1_67	1.0	0.2	626	23	621	20	619	22
PT15.1_60	2.3	0.5	635	25	624	22	621	25
PT15.1_27	0.4	0.0	623	25	621	17	621	17
PT15.1_38	5.0	1.1	654	22	628	20	621	22
PT15.1_40	5.3	1.2	664	22	636	21	628	24
PT15.1_46	-3.1	-0.7	610	24	624	21	628	24
PT15.1_45	-3.1	-0.7	611	26	625	21	630	24
PT15.1_39	-2.6	-0.6	616	23	629	20	632	23
PT15.1_42	-5.0	-1.1	609	24	633	21	640	24
PT15.1_48	-1.7	-0.9	2424	15	2442	36	2465	73

Samples	Discordance %		Ages					
Analyses	6-38/7-6	6-38/7-35	$^{207}Pb/^{206}Pb$	2s abs	$^{207}Pb/^{235}U$	2s abs	$^{206}Pb/^{238}U$	2s abs
Sample VY473. Baron Hill, Beaumaris. NGR SH598 767. Fine grained ash tuff								
VY473_05	6.3	1.3	602	22	571	18	564	20
VY473rd4a_20a	6.1	1.3	608	19	578	15	570	15
VY473_16a	6.1	1.3	619	21	588	19	581	21
VY473rd5_06	6.8	1.4	627	24	593	15	585	15
VY473rd4a_04	1.8	0.3	597	22	588	16	586	16
VY473rd5_05b	-2.4	-0.5	573	24	584	15	587	14
VY473_14	5.7	1.2	623	28	595	21	587	22
VY473_19	5.8	1.2	625	22	596	20	588	22
VY473rd5_07a	4.8	1.0	620	23	596	14	590	13
VY473rd5_05a	4.5	0.9	619	24	597	15	591	15
VY473rd4a_02a	4.3	0.9	631	23	609	16	604	17
VY473rd4a_15a	9.7	2.2	670	20	619	15	605	15
VY473_02	6.4	1.4	650	25	616	22	608	24
VY473_12	1.4	0.3	616	21	610	19	608	21
VY473_06	1.2	0.2	616	22	610	19	608	22
VY473rd4a_18a	3.3	0.7	629	20	613	15	609	15
VY473rd4a_18b	4.8	1.0	640	17	616	14	609	15
VY473_18	8.3	1.9	666	26	623	21	611	22
VY473_11	9.4	2.1	677	21	627	20	614	22
VY473rd4a_02b	4.6	1.0	647	16	623	15	617	17
VY473rd4a_16	2.3	0.5	632	19	621	15	618	16
VY473rd4a_05	4.0	0.9	645	18	625	15	620	16
VY473rd4a_15b	-1.0	-0.3	615	19	620	15	621	17
VY473rd4a_12	2.2	0.5	663	18	651	16	648	18
VY473_07	6.6	1.6	722	21	685	21	674	24
VY473rd4a_03a	-3.1	-1.1	1204	19	1227	26	1241	36
VY473rd4a_03b	-1.5	-0.6	1217	16	1228	23	1236	32
VY473rd4a_22a	0.6	0.2	1500	12	1494	22	1491	34
VY473rd4a_22b	1.1	0.4	1513	14	1503	24	1497	37

Holy Island Group

This study presents no new data on the oldest Monian Supergroup strata, instead, a reconsideration of published geochronology is made. The Holy Island Group is associated with the Gwna Group in outcrop belt 3 and also in the Coeden Formation of outcrop belt 4 (Fig. 3.3). There are several occurrences of ichnofacies within the Holy Island Group – well-developed, abundant *Skolithos* burrows in both the South Stack and Rhoscolyn formations (Greenly, 1919a;

McIlroy and Horák, 2006; Treagus *et al.*, 2012) and these provide a cast-iron maximum depositional age of middle Terrenuevian, Age 2, currently 529 Ma (Ogg *et al.*, 2016), based on first appearance datum of "vertical dwelling structures, *Skolithos, Diplocraterion* and *Arenicolites*" (Buatois and Mángano, 2011). The *Skolithos* ichnofacies is characterised by a low diversity, high abundance trace fossil assemblage that inhabited high energy, mobile sand substrates in a typically shallow-marine environment above normal wave base and even ranging up into the tidal zone. Very rarely, *Skolithos* is found in association with other substrates such as the frequently perturbed top of storm beds and turbidites, but it tends to be less abundant and less densely packed in these cases. In these latter environments *Skolithos* is associated with post-event recolonisation of the substrate (Buatois and Mángano, 2011).

In the interpretation of Phillips (1991a), the mature continental sediment forming the Holy Island Group was supplied from the south-east in turbidity current flows and a continental margin fan system. Although the palaeontological age constraint is in accord with Collins and Buchan's (2004) maximum depositional age of 501 ±20 Ma, which has been cited freely, the single zircon analysis providing this age is a statistical outlier and does not fit within the applied criteria of the current study. This point is made, not necessarily to argue for an older Holy Island Group, but rather to underline the need for interpretive caution with respect to geochronology.

Figure 3.7 → Holy Island Group: Kernel density estimate plots and histograms showing the > 90% concordant zircon age populations analysed in studies by Collins and Buchan* and Asanuma *et al.*, 2017^. The Holy Island Group contains the oldest rocks of the Monian Supergroup, although recent studies suggested that it is the youngest, due to a regional interpretation of the supergroup as an accretionary complex (Kawai et al., 2007; Kusky *et al*., 2013; Asanuma *et al*., 2015; Asanuma *et al.*, 2017). The maximum depositional ages (MDA) shown are the weighted mean age of the youngest three grains of the youngest population analysed. The plots were made using IsoplotR (Vermeesch, 2018)

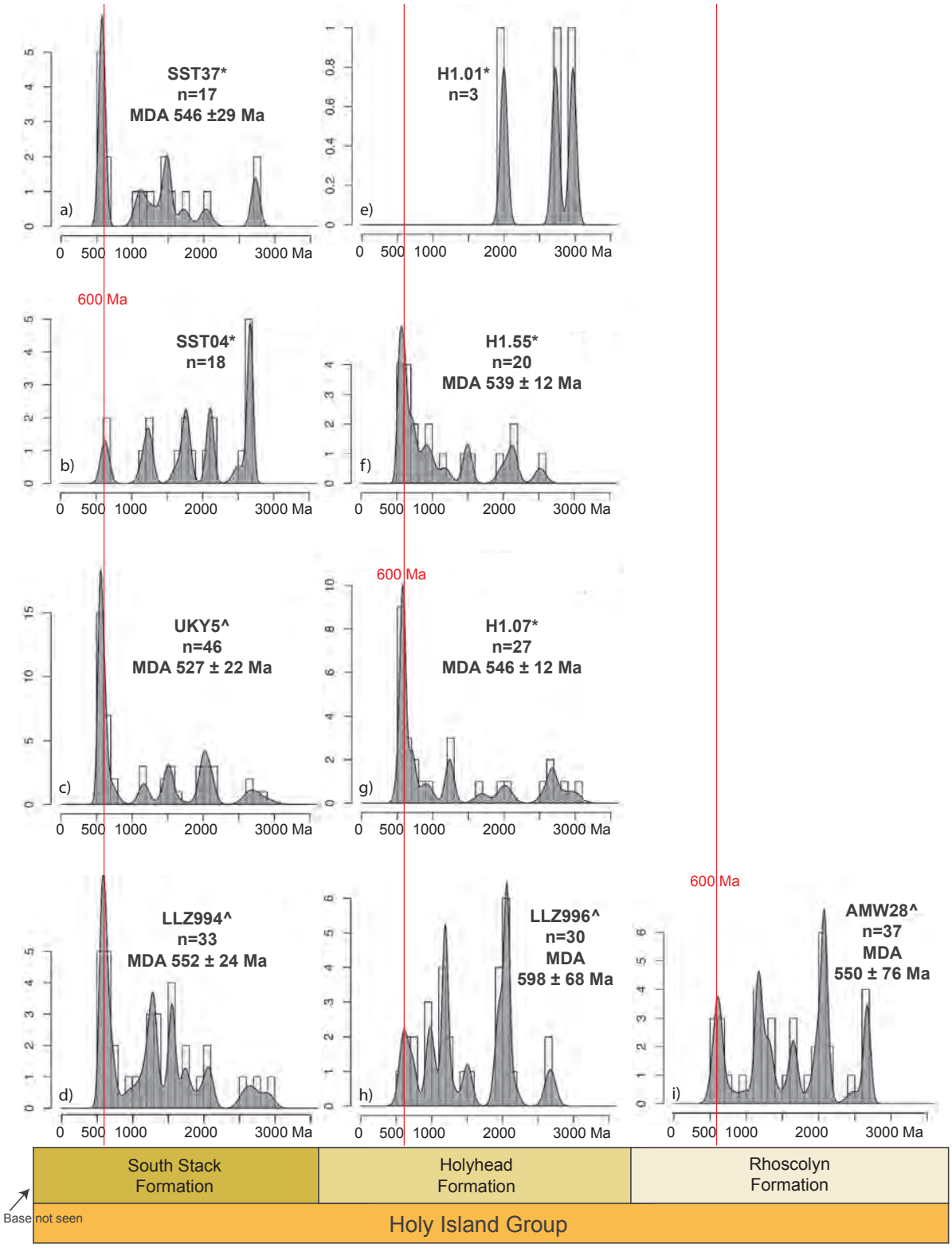
SST37*
n=17
MDA 546 ±29 Ma
a)
H1.01*
n=3
e)
600 Ma
SST04*
n=18
b)
H1.55*
n=20
MDA 539 ± 12 Ma
f)
UKY5^
n=46
MDA 527 ± 22 Ma
c)
600 Ma
H1.07*
n=27
MDA 546 ± 12 Ma
g)
LLZ994^
n=33
MDA 552 ± 24 Ma
d)
LLZ996^
n=30
MDA
598 ± 68 Ma
h)
600 Ma
AMW28^
n=37
MDA
550 ± 76 Ma
i)
0 500 1000 2000 3000 Ma
South Stack Formation
Holyhead Formation
Rhoscolyn Formation
Base not seen
Holy Island Group

Figure 3.7 compares histograms and KDE plots for the data-points considered here to be concordant. The following observations are noted:

- Despite the Holy Island Group lithofacies being dominantly coarse-grained to silt grade sand-rich metasediments, the number of concordant measurements is smaller than ideal.
- KDE age profiles in each formation contain dominant peaks between 550 and 650 Ma.
- Sample UKY5^ (Asanuma *et al.*, 2017) is based on the largest number of analyses and demonstrates a typical Gander Terrane KDE population spread (Waldron *et al.*, 2014; Pothier *et al.*, 2015).
- KDE population profiles imply Gander Terrane affinity within both the South Stack and Holyhead formations
- Affinity of the Rhoscolyn Formation with Gander Terrane cannot be established from these data, but the low quantity of data means this point is inconclusive.

New Harbour Group/Central Anglesey Shear Zone

The New Harbour Group consists of highly deformed laminated pelites and semi-pelites, interbedded with volcaniclastic sandstones sourced from the north to north-west. The lithological contrast with the underlying Holy Island Group accounts for the greater degree of deformation present (Phillips, 1991a; Phillips, 1991b).

Samples of volcaniclastic metasandstone were obtained from the uppermost New Harbour Group for this study, from outcrop belts 3 and 4. In addition, the psammitic metasediments of the CASZ near Aberffraw in outcrop belt 2 were sampled, beneath the Gwna basal unconformity. The concordant results are

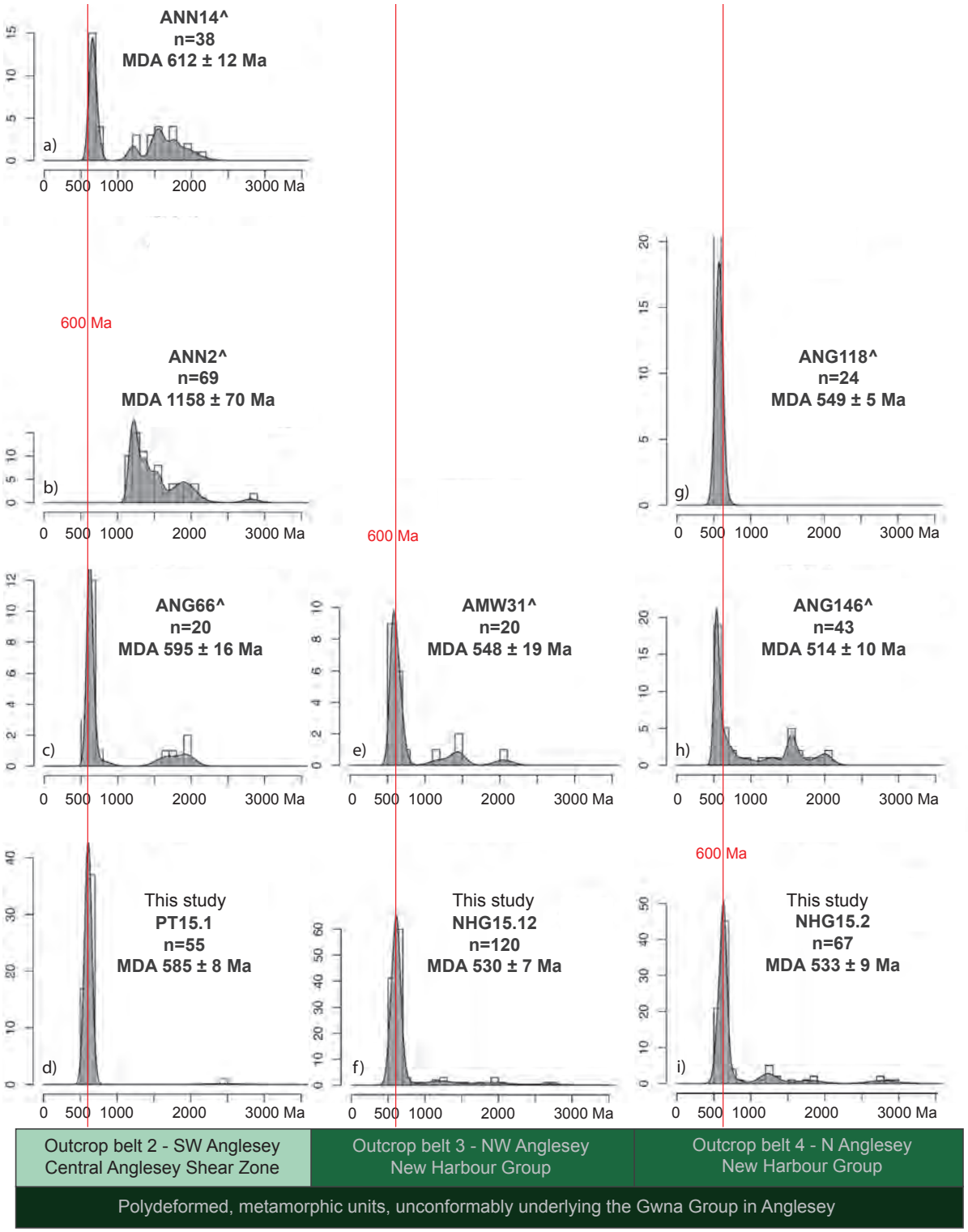
ANN14^
n=38
MDA 612 ± 12 Ma
a)
600 Ma
ANN2^
n=69
MDA 1158 ± 70 Ma
b)
600 Ma
ANG118^
n=24
MDA 549 ± 5 Ma
g)
ANG66^
n=20
MDA 595 ± 16 Ma
c)
AMW31^
n=20
MDA 548 ± 19 Ma
e)
ANG146^
n=43
MDA 514 ± 10 Ma
h)
This study
PT15.1
n=55
MDA 585 ± 8 Ma
d)
This study
NHG15.12
n=120
MDA 530 ± 7 Ma
f)
600 Ma
This study
NHG15.2
n=67
MDA 533 ± 9 Ma
i)
0 500 1000 2000 3000 Ma
Outcrop belt 2 - SW Anglesey
Central Anglesey Shear Zone
Outcrop belt 3 - NW Anglesey
New Harbour Group
Outcrop belt 4 - N Anglesey
New Harbour Group
Polydeformed, metamorphic units, unconformably underlying the Gwna Group in Anglesey

Figure 3.8 ← Ages of the New Harbour Group or the CASZ which directly underlie the Gwna Group unconformity surfaces in all three outcrop belts on Anglesey. Kernel density estimate plots and histograms showing the > 90% concordant zircon age populations analysed in this and other studies (Asanuma *et al*., 2017^) are compiled by stratigraphic unit and by outcrop belt. The maximum depositional ages (MDA) shown are the weighted mean age of the youngest three grains of the youngest population analysed. The plots were made using IsoplotR (Vermeesch, 2018).

---

plotted with other studies in Figure 3.8 using histograms and KDE diagrams, which lead to the following conclusions:

- In common with the Holy Island Group, but with the exception of sample ANN2^, all populations share a dominant age peak of 550 – 650 Ma.
- New Harbour Group ANG118^ has a single age peak of 550 – 650 Ma and an absence of older grains.
- CASZ PT15.1 has a dominant age peak of 550 – 650 Ma, an absence of Mesoproterozoic ages and a single concordant early Paleoproterozoic age of 2400 Ma, which is an age profile that correlates with Meguma Terrane populations, found to be present further south in Wales in the Harlech Dome (Pothier *et al.*, 2015).

Figure 3.9 → Gwna Group: Kernel density estimate plots and histograms showing the > 90% concordant zircon age populations analysed in **this study** and recent publications (Asanuma *et al*., 2015"; Asanuma *et al*., 2017^) are compiled by outcrop belt. The Gwna Group is the youngest constituent of the Monian Supergroup, although some recent studies suggested that it is the oldest, due to a regional interpretation of the supergroup as an accretionary complex (Kawai *et al*., 2007; Kusky *et al*., 2013; Asanuma *et al*., 2015; Asanuma *et al*., 2017). The maximum depositional ages (MDA) shown are the weighted mean age of the youngest three grains of the youngest population analysed. The plots were made using IsoplotR (Vermeesch, 2018).

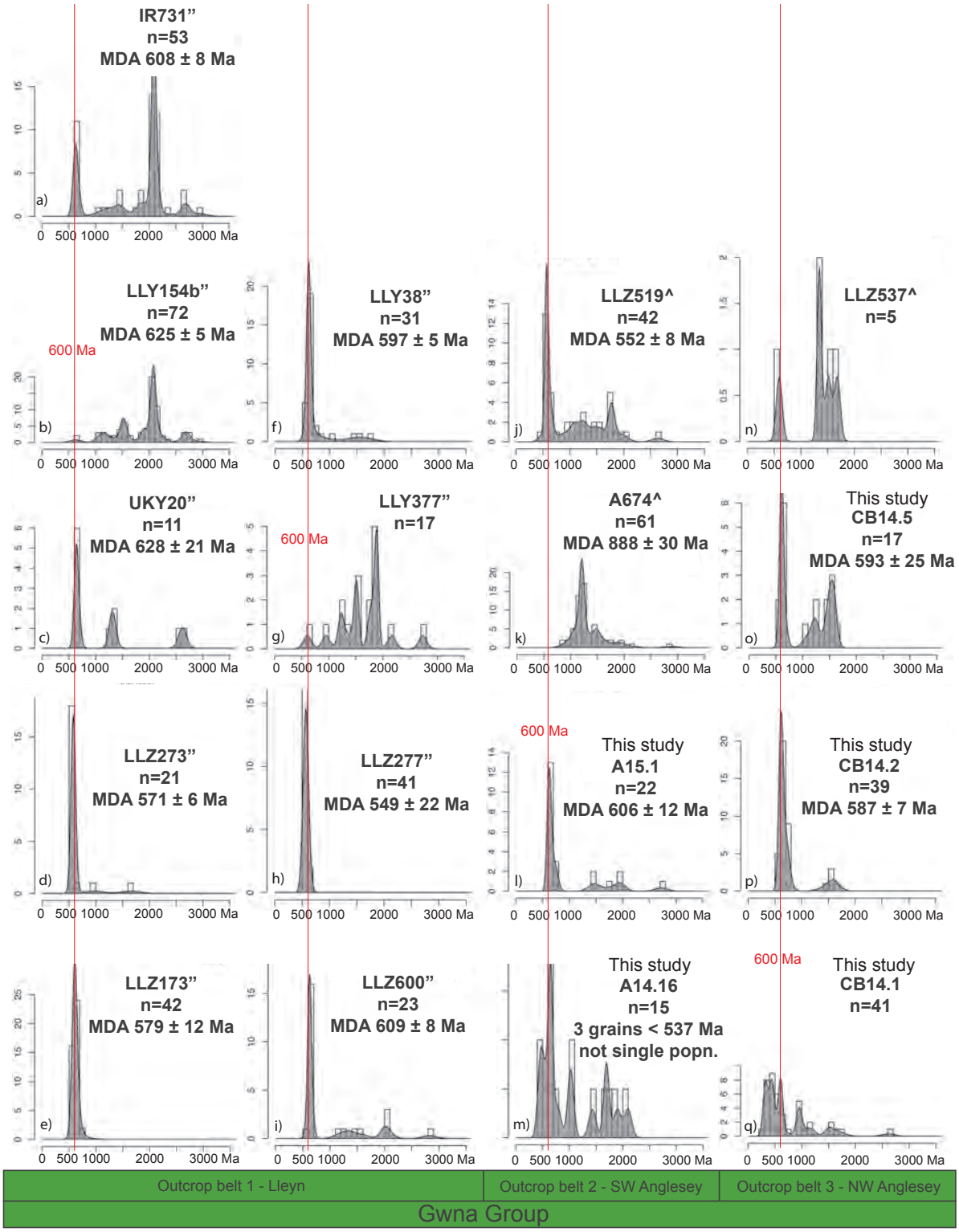
IR731"
n=53
MDA 608 ± 8 Ma
a)
LLY154b"
n=72
MDA 625 ± 5 Ma
600 Ma
b)
LLY38"
n=31
MDA 597 ± 5 Ma
f)
LLZ519^
n=42
MDA 552 ± 8 Ma
j)
LLZ537^
n=5
n)
UKY20"
n=11
MDA 628 ± 21 Ma
c)
LLY377"
n=17
600 Ma
g)
A674^
n=61
MDA 888 ± 30 Ma
k)
This study
CB14.5
n=17
MDA 593 ± 25 Ma
o)
LLZ273"
n=21
MDA 571 ± 6 Ma
d)
LLZ277"
n=41
MDA 549 ± 22 Ma
h)
600 Ma
This study
A15.1
n=22
MDA 606 ± 12 Ma
l)
This study
CB14.2
n=39
MDA 587 ± 7 Ma
p)
LLZ173"
n=42
MDA 579 ± 12 Ma
e)
LLZ600"
n=23
MDA 609 ± 8 Ma
i)
This study
A14.16
n=15
3 grains < 537 Ma
not single popn.
m)
600 Ma
This study
CB14.1
n=41
q)
0 500 1000 2000 3000 Ma
Outcrop belt 1 - Lleyn
Outcrop belt 2 - SW Anglesey
Outcrop belt 3 - NW Anglesey
Gwna Group

Gwna Group

The Gwna Group unconformably overlies the CASZ in outcrop belt 2 and the New Harbour Group in outcrop belts 3 and 4. Samples of interbedded Gwna Group volcaniclastic deposits (not debris flow clasts) from outcrop belts 2, 3 and 4 were analysed and the results are compared with data-points from other studies (Fig. 3.9), using histograms and KDE population profiles. The samples described in Asanuma *et al.* (2015) and Asanuma *et al.* (2017) are not precisely located using Grid References, and therefore it is unknown whether they were taken from clasts, the turbidite system or from debris flow matrix – an attempt has been made to estimate this based on lithological description and the maps provided (Figs. 3.10, 3.11 and 3.12).

Concordant plots are presented (Fig. 3.9) using histograms and KDE population profiles which suggest the following:

- Zircons were found to be in short supply in the Gwna Group samples collected in this study and this applies to other the other studies used for comparison. The populations, throughout 17 samples, are generally too low to be considered robust in terms of maximum depositional age, and capturing all age components (Vermeesch, 2004).
- Although varied zircon morphologies were present in the four Church Bay Tuff samples collected in this study, including acicular grains, the analytical ages do not fit with a contemporary volcanic origin and it is therefore concluded that primary zircons were not crystallised in the ignimbrite layers.
- Samples with very low to no zircon grains are excluded from the results.
- With the exception of samples LLY154b, LLY377, A674 (Asanuma *et al.*, 2015; Asanuma *et al.*, 2017) and CB14.1 (this study), the Gwna Group

lithologies have a dominant age peak of 550 – 650 Ma.

- Asanuma *et al.* (2017) considered sample A674 provides a Gwna Group maximum depositional age of 878 ± 43 Ma – the age of the single youngest zircon analysed. This study considers the sample to be from a clast within the Gwna Group polymictic debris flow lithofacies: the analysis may provide a maximum depositional age for the clast, but not for the deposition of the Gwna Group, in which the clast was later incorporated. Age peaks of 550 – 650 Ma in Gwna Group beds (particularly A14.16 and A15.1, in this study) from outcrop belt 2 clearly demonstrates that the deposit is far younger than 878 Ma.
- Sample CB14.1 (this study) has suffered substantial lead loss, clearly indicated by a population profile that fits with neither a) the field evidence, nor b) the populations in other samples. The ages are consistently too young and this sample must be ruled out from further discussion.

Monian Supergroup

In order to further interrogate the data, three aspects of all the data-points considered above (Figs. 3.10, 3.11 and 3.12) are discussed: the central age of each dominant age peak, the oldest single grain analysed and the maximum depositional age, based on the simple mean average of the three youngest grains within a common youngest population, per analysis (Spencer *et al.*, 2016). No youngest age is shown where a sample does not meet these criteria. For example, sample H1.01 (Collins and Buchan, 2004) contains a total of three concordant grains of unrelated age and sample LLZ537 (Asanuma *et al.*, 2017) consists 5 concordant analyses over 4 different age populations, where the maximum number of grains per population is 2. Neither of these samples contain

three grains from a single age population and a minimum age cannot therefore be offered. Conclusions drawn from this exercise include:

- Phillips (1991a) suggested a switch in sediment source direction from south-east to north/north-west at the contact between the Holy Island and New Harbour Groups. The oldest grains analysed in the Holy Island Group are consistently older than in the younger New Harbour and Gwna Groups, which supports a change in sediment supply direction.
- The maximum depositional age of 501 ± 20 Ma (Collins and Buchan, 2004) for the Holyhead Formation is not accepted under the proposed analytical standards, and this age should no longer be used (Spencer *et al.*, 2016).
- Dominant Ediacaran age peaks are demonstrated throughout the Monian Supergroup and the CASZ, which confirms a common peri-Gondwanan source, most likely to be of Gander Terrane provenance (Waldron *et al.*, 2014; Pothier *et al.*, 2015; Schofield *et al.*, 2016).
- Excluding sample CB14.1 with lead-loss, the youngest population measured is at 480 Ma, and is from the Gwna Group in outcrop belt 2, taken from a thin layer of mudstone deposited on the unconformity surface including few zircons (sample A14.16, this study). This maximum depositional age cannot be considered as robust however, as the total population within this sample comprises only 15 concordant zircons, and the youngest three ages do not overlap within uncertainty. This age does fit perfectly with the field evidence however, and suggests the depositional age is at least < 537 Ma. Certainly these data suggest there is no increasing depositional age up-stratigraphy, in contrast to the interpretation of several authors (Kawai *et al.*, 2007; Kusky *et al.*, 2013; Asanuma *et al.*, 2015; Asanuma *et al.*, 2017).

- The youngest reliable maximum depositional age of this study, i.e. based on three overlapping U-Pb dates, is 530 ±6.5 Ma (MSWD = 0.18). This sample (NHG15.12) is from the New Harbour Group in outcrop belt 3. A similar robust maximum depositional age of 533 ± 8.8 Ma (MSWD = 0.99) comes from sample NHG15.2, from the New Harbour Group in outcrop belt 4. These ages overlap and provide a maximum depositional age for the New Harbour Group in Anglesey.

Figure 3.10 → **(Page 160)** Using Monian Supergroup stratigraphy as a backdrop over four outcrop belts, the central age of the dominant peak of each analysis in **this study** and other publications (Collins and Buchan, 2004*; Asanuma *et al*., 2015"; Asanuma *et al*., 2017^) is listed in an attempt to reveal any pattern in the age populations of the detrital zircons. In broad terms, a shared typical Ganderian age distribution in sediment supply for the whole supergroup is demonstrated – not that this appears fully in every single sample, rather, the Ganderian pattern is present in each group or formation (see also Figs. 3.11 and 3.12).

Figure 3.11 → **(Page 161)** The oldest single grain analysed per sample, in **this study** and others (Collins and Buchan, 2004*; Asanuma *et al*., 2015"; Asanuma *et al*., 2017^) is overlaid onto Monian Supergroup stratigraphy. (see also Figs. 3.10 and 3.12).

Figure 3.12 → **(Page 162)** Maximum depositional age constraint. The unweighted mean age of the three youngest > 90% concordant grains per sample, of **this study** and other publications (Collins and Buchan, 2004*; Asanuma *et al*., 2015"; Asanuma *et al*., 2017^) are overlaid onto Monian Supergroup stratigraphy. The three youngest zircons must come from a common youngest population of < 3 zircons (Spencer, *et al*., 2015). Except sample A14.16 (outcrop belt 2, Gwna < 537 Ma), no date is included for those analyses where these criteria are not met. (See also Figs. 3.11 and 3.12).

Figure 3.10

Centre of dominant age peak	Lleyn Outcrop belt 1	South-west Anglesey Outcrop belt 2	North-west Anglesey Outcrop belt 3	North Anglesey Outcrop belt 4
unconformity	**Lleyn Shear Zone**			**Dapingian overstep**
Monian Supergroup **Gwna Group** unconformity	Clast/ fault Matrix block Unsure 600" 600" 600" 2100" 600" 2100" 600" 700" base 1900"	Matrix Clast Unsure **650** 120 600^ **650**	Matrix Clast Unsure **600** **600** **650** 1350^	Matrix Clast Unsure
New Harbour Group conformable (CC)	not seen	**600** 600^ 650^ 1200^ **Central Anglesey Shear Zone**	**600** 600^	550^ **600** 600^ conformable (CC)
Holy Island Group ***Skolithos*** **maximum possibile age is 521 Ma** base not seen	CC **Rhoscolyn Fm** **Holyhead Fm** CC **South Stack Fm**		2100^ 600* 600* 2050^ 600* 600^ 600^ 2700*	**Coeden Fm**

This study
^ Asanuma et al. 2017
" Asanuma et al. 2015
* Collins & Buchan 2004

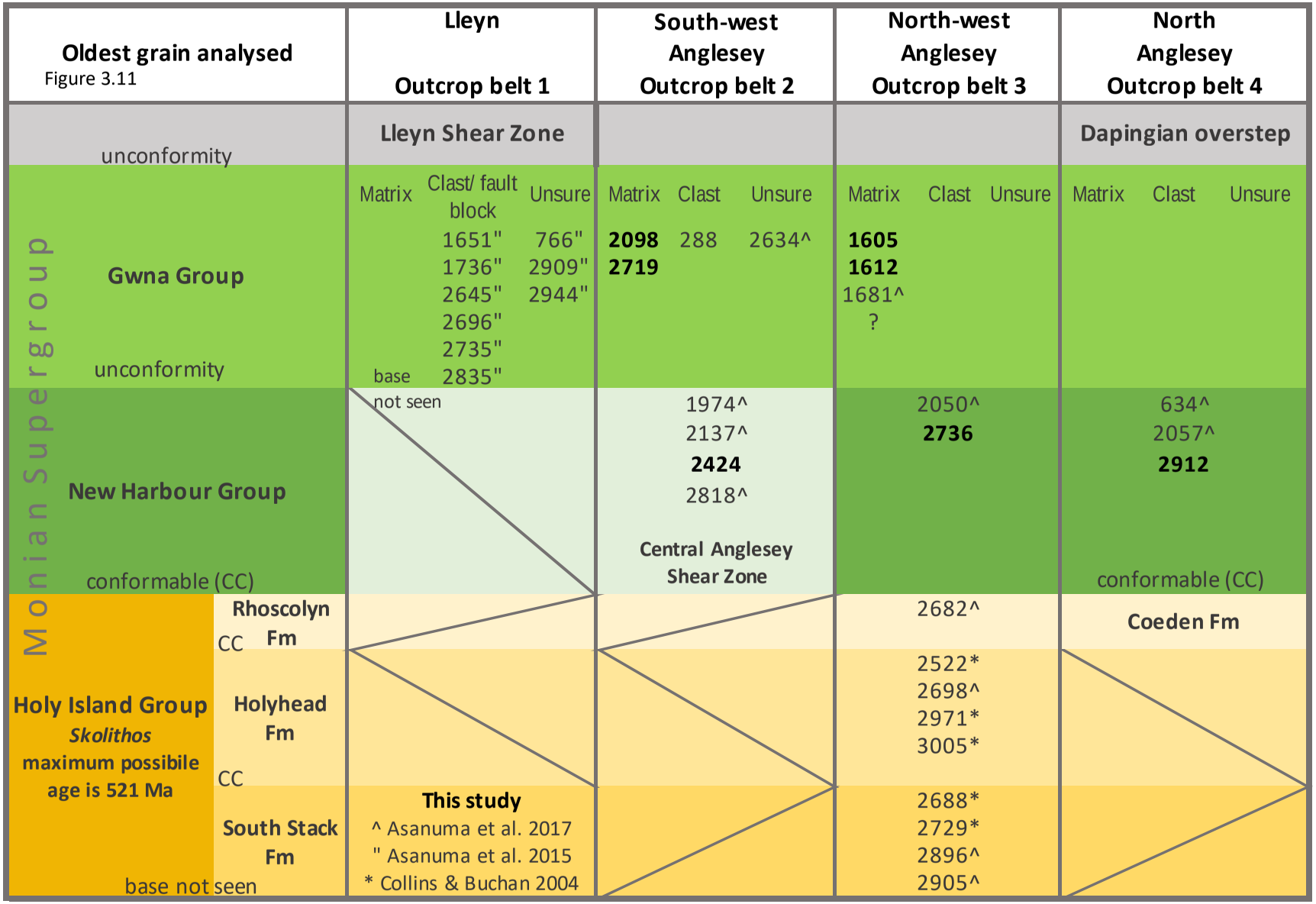
Oldest grain analysed
Figure 3.11
Lleyn
Outcrop belt 1
South-west Anglesey
Outcrop belt 2
North-west Anglesey
Outcrop belt 3
North Anglesey
Outcrop belt 4
Lleyn Shear Zone
Dapingian overstep
unconformity
Monian Supergroup
Gwna Group
unconformity
Matrix
Clast/ fault block
Unsure
1651"
1736"
2645"
2696"
2735"
base 2835"
766"
2909"
2944"
Matrix
Clast
Unsure
2098
2719
288
2634^
Matrix
Clast
Unsure
1605
1612
1681^
?
Matrix
Clast
Unsure
New Harbour Group
conformable (CC)
not seen
1974^
2137^
2424
2818^
Central Anglesey Shear Zone
2050^
2736
634^
2057^
2912
conformable (CC)
Rhoscolyn Fm
CC
2682^
Coeden Fm
Holy Island Group
Skolithos
maximum possibile age is 521 Ma
Holyhead Fm
CC
2522*
2698^
2971*
3005*
South Stack Fm
base not seen
This study
^ Asanuma et al. 2017
" Asanuma et al. 2015
* Collins & Buchan 2004
2688*
2729*
2896^
2905^

Youngest grains analysed** Figure 3.12	Lleyn Outcrop belt 1	South-west Anglesey Outcrop belt 2	North-west Anglesey Outcrop belt 3	North Anglesey Outcrop belt 4
unconformity	**Lleyn Shear Zone**			**Dapingian overstep**
Monian Supergroup — **Gwna Group** unconformity	Clast or fault block 609 ± 8" 579 ± 12" 571 ± 6.2" 625 ± 5" 608 ± 8" 549 ± 22" 628 ± 21" base 597 ± 5"	Matrix: **< 537**, **602 ±12** Clast or fault block: 579 ± 8^, 888 ± 30^, 552 ± 8^	Matrix: **586.8 ±7**, **593 ±25** Clast	
Monian Supergroup — **New Harbour Group** conformable (CC)	not seen	**585 ±8** 595 ±16^ 612 ±12^ 1158 ± 70^ **Central Anglesey Shear Zone**	**530 ±7** 548 ± 19^	**533 ± 9** 514 ± 10^ 549 ± 5^ conformable (CC)
Monian Supergroup — **Rhoscolyn Fm** CC			550 ± 76^	**Coeden Fm**
Monian Supergroup — **Holyhead Fm** CC			598 ± 68^ 546 ± 12* 539 ± 12*	
Holy Island Group ***Skolithos*** **maximum possibile age is 529 Ma** — **South Stack Fm** base not seen	**This study** ^ Asanuma et al. 2017 " Asanuma et al. 2015 * Collins & Buchan 2004		550 ± 76^ 552 ± 24 ^ 527 ± 22^ 546 ± 29*	** Youngest age is the weighted mean of 3 youngest grains from the youngest population analysed

3.7 Conclusions

- This study planned to establish a clear temporal framework for the formation of the Gwna Group, the youngest unit of the Monian Supergroup. The main intention was to ascertain absolute dates from primary volcanic zircons for the formation of the interbedded volcanic units within the basal and upper Gwna Group on Anglesey as a means of dating the deposition of the Gwna mélange. A secondary aim was to clarify whether there were two distinct periods of Gwna melange deposition (Fig. 3.2). To elucidate the basal contact relationships a detrital zircon analysis of the underlying metasedimentary units was undertaken: the CASZ in outcrop belt two and the New Harbour Group in outcrop belts three and four. It is important to understand whether the protoliths were sourced from a common source by analysing the zircon age distribution, as well as seeking a constraint on maximum sub-unconformity age constraint.

When combined with field evidence the results of the geochronological study indicate the following points:

- Ignimbrite and ash tuff horizons in the Church Bay Tuff Formation contain varied zircon morphologies, including acicular grains, but the ages obtained indicate that primary igneous zircons are absent. Consequently, the results have been combined to form a wider detrital zircon analysis, questioning the provenance of the sediments and/or protoliths with a view to placing this data within the setting of Iapetus Ocean opening and closure.

- Detrital analysis of the three Anglesey units situated unconformably beneath the Gwna Group confirms a peri-Gondwanan / Canadian Appalachian affinity. There is a clear correlation of the results from north-west Anglesey

(outcrop belt 3) and north Anglesey (outcrop belt 4) and the relative probability (KDE) plots show that the protolith sediments for the Gwna Group and Monian Supergroup were derived from the Gander Terrane.

- Data from sample PT15.1 (this study) of outcrop belt two (south-west Anglesey) shows U-Pb ages in a dominant Ediacaran peak around 600 Ma, a minor, secondary peak at 2,400 Ma, and a complete absence of any Mesoproterozoic grains, suggesting a different sediment supply than is present in the basement New Harbour Group rocks of outcrop belts 3 and 4 (above). The marked absence of inherited zircons between the two peaks, a well-populated interval in Ganderian distributions, could indicate that the CASZ protolith cannot be the product of the same Ganderian source. Instead, this U-Pb age distribution would imply correlation with the Amazonian margin Meguma Terrane (Waldron *et al.*, 2011) and would suggest that outcrop belt 2 shares terrane affinity with the Harlech Dome further to the south and, that at basement level, the south-west Anglesey block records the presence of a Meguma continental fragment caught up in the Silurian closure of the Iapetus Ocean in the eastern region. However, this hypothesis is brought into question by the comparison of this study with others, as Asanuma *et al.* (2015) have shown that CASZ samples from other localities include a spread of Mesoproterozoic ages and therefore this point requires further investigation.

- Detrital analysis of Church Bay Tuff samples in outcrop belt 4, and further samples from the upper section of the Church Bay Tuff in outcrop belt 3 did not yield zircons, despite being of crystalline, felsic volcanic character. This is disappointing, but since the north Anglesey outcrop of the New Harbour Group and Gwna Group is interpreted as a thrust block, one of several that repeat the

north-west Anglesey stratigraphy, and the correlation of the upper New Harbour Group metasediments in outcrop belts 3 and 4, overall the results of belt 3 are taken as evidence for both sections.

- Detrital analysis in this study of Gwna Group samples in outcrop belts 2 and 3 does not particularly help to constrain the depositional age of the Gwna Group other than to provide a maximum depositional age of latest Cambrian – earliest Ordovician, although for outcrop belts 3 and 4 this age was known prior to the U-Pb study: constrained by the presence of *Skolithos* in the lower Holy Island Group and the Dapingian age of the overstep. However, this study provides a clear correlation of the Gwna Group between outcrop belts 2 and 3 and by association, belt 4, showing that the deposition of the Gwna Group in Anglesey was from a continuous sediment source.

- Asanuma *et al.* (2015) and (2017) rely on maximum depositional ages from the single youngest zircon age obtained to support a model requiring the Gwna Group to be the oldest deposit of the Monian Supergroup. These ages are categorically not accepted by this study as representative of credible dates for deposition: first, the Gwna Group samples tested are from sections that lack potential to yield a depositional age. Instead, Lleyn fault blocks and Aberffraw and Bodorgan debris flow clasts appear to have been analysed. This problem is illustrated by a comment intended to lend support for an earliest Cambrian Gwna Group age in Lleyn: "*Horák and Evans (2011) reported from Sr isotopic stratigraphic data that limestone blocks in a pelitic mélange matrix in the Gwna Group formed in the early Neoproterozoic*." (Asanuma *et al.*, 2017. pp 191). The limestone is indeed Neoproterozoic (Horák and Evans, 2010), but it is a megaclast within a polymictic debris flow. Dating the clast does not provide

insight into the depositional age of the Gwna Group further than confirming that the mélange is younger than the clast. Second, the use of maximum depositional age based on the single youngest zircon analysed is not considered good practice among geochronology workers. This study included extensive field work aimed at understanding the complexities of the Gwna Group. A conditional model was developed based on field evidence (see Chapter 2) as a precursor to geochronology study and was highly influential in sample selection. Despite the results not yielding what was sought, this remains a reasonable approach. Third, should it be demonstrated that the Gwna Group contains older zircons than those contained in underlying sedimentary units there are alternative tectonic settings that could apply. For example, a turbidite system such as the Gwna Group, could form in a passive margin setting where, aside from local volcanism, the unroofing of a continental margin could provide progressively older inherited zircons into a marine basin. The resulting sedimentary unit would record an age profile that could imply the most recently deposited sediments were the oldest.

- Results from this study include robust maximum depositional ages of 530 ±6.5 Ma and 533 ±8.8 Ma for the New Harbour Group in outcrop belts 3 and 4 combined with numerically insufficient but concordant analyses for maximum deposition of the Gwna Group in outcrop belt 2 of < 537 Ma. There is no evidence to support the Gwna Group being the oldest Monian Supergroup lithostratigraphic unit.

- The substantial body of recent work that models a Pacific-style accretionary orogen setting for the region (Kawai *et al*., 2006; Kawai *et al*., 2007; Maruyama *et al*., 2010; Asanuma *et al*., 2015; Asanuma *et al*., 2017) relies in part on a series of U-Pb age determinations some of which are not concordant, and

thus are not robust. The data presented in Asanuma *et al*. (2015, 2017) is labelled simply as concordant or non-concordant without being quantified. These example data points are included as concordant in the published material, but were outside of the criteria required for discussion in this report:

Analysis	^{206}Pb-^{238}U age, 2σ abs	^{207}Pb-^{206}Pb age, 2σ abs	Discordance
UKY2-55	586 ± 29 Ma	659 ± 81 Ma	-25.5%
LLZ537-7	625 ± 13 Ma	715 ± 100 Ma	-14.4%
LLZ519-5	559 ±24 Ma	440 ± 169 Ma	21.3%

The fully concordant maximum depositional ages from U-Pb zircon analysis in this study and those reassessed (Collins and Buchan, 2004; Asanuma *et al.*, 2015; Asanuma *et al.*, 2017) are:

Gwna B (outcrop belts 3 and 4)	< 587 Ma (but, younger than 474 Ma?)
Gwna A (belt 2)	< 552 Ma (but, unlikely older than 537 Ma)
Gwna A (belt 1)	< 549 Ma (seafloor unit, underlying Gwna A)
New Harbour Group (belt 4)	< 514 Ma
New Harbour Group (belt 3)	< 530 Ma
Holy Island Group: Rhoscolyn Fm.	< 550 Ma (but, 529 Ma or younger)
Holy Island Group: Holyhead Fm.	< 539 Ma (cannot postdate Rhoscolyn Fm.)
Holy Island Group: South Stack Fm.	< 527 Ma (but, 529 Ma or younger)
Central Anglesey Shear Zone	< 585 Ma

Overall, comparing recent work with this study confirms that there is limited age constraint available through U-Pb zircon geochronology in respect of the Gwna Group. It also highlights the essential requirement for robustness in radiometric studies, particularly when considering contentious and complex geology, such as the Monian Supergroup and associated deposits. Robustness and best practice is as vital to interpretation as it is to all aspects of sample processing. Uncorroborated single lines of evidence can lead to incorrect models becoming accepted in the literature and once embedded, those models become difficult to overturn. An example of this is the maximum depositional age of 501 ±20 Ma for the Holyhead Formation (Collins and Buchan, 2004). The paper has so far been cited by 47 authors although it comes from a single analysis that was a statistical outlier, not acceptable as MDA by current standards. For some authors it appears, the maximum depositional age has become simply, age.

Chapter 4

CARBONATE FACIES IN GWNA GROUP POLYMICT DEBRIS FLOWS

The two major clast groups of the Gwna Group debris flows consist of carbonate and quartzite lithofacies. Jointly they dominate the Gwna mélange both volumetrically and numerically. Rounded carbonate and quartz arenite clasts occur together in a series of polymictic debris flows of varied thickness, set within a mud to coarse sand matrix.

Clast size is variable over several orders of magnitude: the maximum diameter varies from mm scale to several hundred metres, but most common clast dimensions are between a few decimetres to 8 m. Most sedimentary clasts have been fractured more-or-less along bedding planes and therefore contain a limited amount of sedimentary information individually.

Gwna Group carbonate clasts are compositionally pure with almost no primary siliciclastic content, which is in stark contrast to the exclusively siliciclastic lithofacies of the underlying Monian Supergroup. Individual carbonate clasts mostly contain a single lithofacies but there are some notable exceptions where coherent sedimentary sequences are incorporated within single clasts.

In this chapter field and petrographic study of the sedimentology of one such clast, a large carbonate clast at Llanbadrig (the 'megaclast), in outcrop belt 4, is compared to other clasts and considered alongside an analysis of isotopes, $\delta^{13}C$ and $\delta^{18}O$, and $^{87}Sr/^{86}Sr$, in Gwna Group carbonate clasts from this and other studies. Horák and Evans' (2010) isotope study of the megaclast resulted in an interpreted Neoproterozoic age of 860–800 Ma leading to a number of questions addressed in this study:

- Are typical characteristic Neoproterozoic sedimentary features, such as molar tooth microspar, present in the megaclast?
- Are other carbonate clasts in the mélange comparable to the megaclast?
- Is the estimated megaclast age of 860–800 Ma supported by isotope analyses in this and other studies?

In broad terms, this chapter is concerned with testing whether there is any affinity between the many carbonate clasts of the outcrop belts of the Gwna Group debris flows. If sufficient common attributes can be identified, it may then be possible to assert that the carbonate clasts were derived from a single sedimentary unit. Conversely, if no relationship can be demonstrated, they will be shown to be of differing extraction and thus add strength to Edward Greenly's (1919) chaotic characterisation of the Gwna Group mélange.

4.1 Precambrian shallow-marine carbonate characteristics

Proterozoic carbonates differ from their Palaeozoic counterparts in several major respects. Formed before the existence of anything but microbial life forms, pre-Ediacaran sequences lack fossil assemblages and bioturbation, both of which are important diagnostic features in rocks through Phanerozoic time. While successions of this age create analytical and interpretive difficulty due to the absence of biogenic input, which, in later Earth history are sensitive indicators of environmental change, many primary features may be preserved (Pratt, 2001). Neoproterozoic carbonates were formed by both microbial and abiotic means (Grotzinger and James, 2000) and are characterised by microbialites such as stromatolites or microbial laminites combined with high degrees of syndepositional and diagenetic dolomitisation (Fairchild *et al*., 1991). Rapid near sediment surface dolomitisation is considered to have occurred widely in the

Neoproterozoic, a difference attributed to ocean water composition and the kinetics of marine water moving through carbonate sediments (Fairchild *et al.*, 1991; James and Jones, 2016). Dolomite crusts formed in shore face to platform settings provided intraclastic material for later inclusion in relatively distal storm beds (Fairchild and Herrington, 1989). Analysis of carbonate isotopic signatures in many Precambrian marine carbonate sediments show that Neoproterozoic seawater compositions were very different to those of the Phanerozoic (Halverson *et al.*, 2007).

Stromatolites are commonly found in Neoproterozoic carbonates due to the absence of metazoan grazing and their dominance increases going back in time. Whereas in post-Ordovician sequences they are unusual sedimentary structures associated with mass extinctions or restricted environments, stromatolites are commonly found in Precambrian rocks where they provide a detrital sediment trap and represent the single biotic contributor of precipitated carbonate (Grotzinger and Knoll, 1999).

Molar tooth (MT) microspar - equant, polygonal calcite microspar crystals typically sized 5-15 μm (Fig. 4.1.1A), is a characteristic feature of shallow-marine limestone sequences of Meso- to Neoproterozoic age, but do not occur in post-Tonian strata. The prevalence and diagnostic nature of MT microspar in Neoproterozoic sediments is comparable to that of fossiliferous, shallow subtidal deposits in the Phanerozoic (James *et al.*, 1998). MT microspar, formed as a pore filling in surface cracks opened in recently deposited or semi-lithified carbonate mud or as an intergranular cement in grainstones, has been discussed in primary literature for many years (Bauerman, 1885; Smith, 1968; Fairchild and Spiro, 1987; Furniss *et al*., 1998; Pollock *et al*., 2006; Kuang, 2014). Despite many papers, more than 300 according to Kuang (2014), where attempts have been made to understand the genetic history of MT microspar, the characteristic

structures it formed (MT structure) and the reasons for the temporal constraint, MT microspar and MT structure formation is not fully understood.

MT microspar infilled synsedimentary veins, called molar tooth structure (MT structure) were first recognised and named by the Canadian geologist Bauerman, who likened the intensely folded, tapered forms to the folded dentine of elephant teeth (Bauerman, 1885). Both MT microspar and MT structure are found frequently in carbonate sediments of Mesoproterozoic to Tonian age, but some occurrences have been described in Palaeoproterozoic and Archaean rocks (Smith, 1968; Fairchild *et al.*, 1997; Furniss *et al.*, 1998; James *et al.*, 1998; Pratt, 1998; Liu *et al.*, 2005; Bishop and Sumner, 2006; Pollock *et al.*, 2006).

MT structure takes many forms including veins, conical, ribbon-like or spheroidal bodies filled with MT microspar. Veins can be normal to bedding, tapering downwards from the bed interface, obliquely angled or bedding parallel. MT structure is commonly several millimetres wide, up to 20 cm long and exhibit ptygmatic folding not found in the surrounding sediments, considered by Shields (2002) to indicate comparatively rapid precipitation and compaction of the vein material within unlithified sediment. Where the MT microspar infills a crack or other void in the host sediment, later compaction shows distortion in the sedimentary laminae as the relatively rigid MT structure is accommodated and often the vein is folded but where the MT microspar forms a cement, for example in a grainstone, a rigid structure is formed, binding the allochems in a layer resistant to later compaction. The sedimentary host beds tend to be argillaceous lime mudstones and compaction of <80% is related to crack formation (Pratt, 1998). MT microspar is found in a variety of carbonate lithofacies formed before the Sturtian “Snowball glaciation”, 720 Ma (Shields-Zhou, 2016) and there are two known examples of MT microspar in Archean siliciclastic mudstone (Shields, 2002; Bishop and Sumner, 2006).

The uniform MT microspar crystals formed in two stages – a sub-rounded core with secondary polygonal calcite overgrowth (Pollock *et al.*, 2006) (Fig. 4.1.1B) and the vein fill propagated inward from the sediment/cavity interface, often in more than one generation (Fairchild and Spiro, 1987) and precipitated from supersaturated marine water (Pratt, 1998).

MT microspar in MT structure veins is always pure and uncontaminated, with a marked lack of alteration at the crack margins and little to no incorporation of detritus within the microspar, implying that both the veins and microspar infill formed contemporaneously, before the cavities were closed. Many models have been suggested for the formation of the cracks that become MT structure, including osmotic dewatering, seismicity, synaeresis, sub-aerial desiccation, the mechanical effects of compaction, gypsum pseudomorphing and biogenic gas migration (Fairchild *et al.*, 1997; Furniss *et al.*, 1998; Pratt, 1998; Pollock *et al.*, 2006).

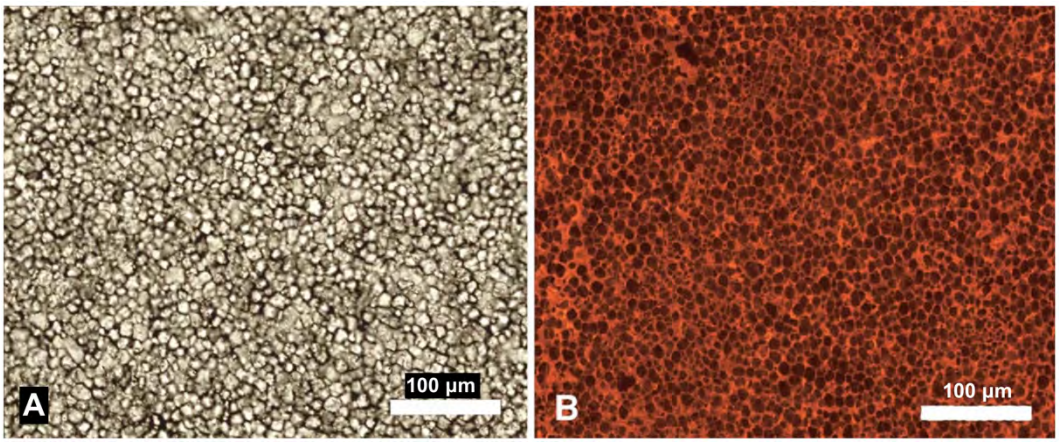

Figure 4.1 Molar tooth (MT) microspar images from the Helena Formation, Belt Supergroup, Montana, USA. (Pollock *et al.,* 2006) show typical characteristics of MT microspar. **A.** Plane polarised light image. Whether infilling a sedimentary void or forming a cement, MT microspar crystals are uniformly equant and polygonal, with a consistent diameter between 5 – 15 µm. **B.** Cathodoluminescence photomicrograph showing low luminescence, sub-rounded MT microspar cores, surrounded by luminescent calcite overgrowths which represent crystal growth in two stages (Pollock *et al*., 2006).

Earlier work often separates cavity formation and MT microspar precipitation in the voids, but an acceptable hypothesis must allow for both features to be formed penecontemporaneously while explaining the late Precambrian ubiquity of MT microspar followed by an abrupt disappearance from the rock record before the Cryogenian at 720 Ma (Shields, 2002). Metazoan sediment disruption was first considered to be implicated in the disappearance from the rock record of MT microspar as workers hypothesised that all trace of MT microspar/MT structure were obliterated by bioturbation. But the effects of bioturbation are not quantitatively significant in the rock record until ~550 Ma (Shields, 2002; Buatois and Mangano, 2011). A change in ocean water chemistry where saturation levels of $CaCO_3$ decreased, and/or a concurrent increase in the ratio of precipitation inhibitors was put forward as a model that also explains the broadly contemporaneous decline in stromatolite populations (Shields, 2002).

A model for crack formation linked to the upwards migration of biogenic gases through the substrate was proposed and supported by laboratory experiments first by Furniss *et al.* (1998) and then by Pollock *et al.* (2006), the latter relying on the empirical studies of Naka and Chujo (Naka and Chujo, 2001; Naka *et al.,* 2002). The gas bubble model, also favoured by Smith (Smith, 2016) grew from study of the abundant molar tooth structures of the Mesoproterozoic Helena Formation, Belt Supergroup, in Montana, USA and Pollock *et al.* (2006) found a correlation between differing vein morphology and substrate type: tightly folded tapered veins, or ribbons, occurred in a variety of lithofacies and the many spherical bodies of molar tooth fabric were restricted to fine grained, clay-rich carbonates. Conversely, molar tooth microspar was mainly absent in coarser grained facies, such as oolitic limestone in the Helena Formation and elsewhere (Smith, 1968; Fairchild *et al.*, 1997; Pratt, 1998) and in coarse silt or sandstone implying that the host sediment type exerted a control on vein morphology

(Pollock *et al.*, 2006). Cavity formation and infill have long been recognised as related: Unfilled voids would not have stayed open for a long time. The purity of the MT microspar itself, and the clean contacts seen between host rock cavities and MT structure indicates that void formation and infill must be penecontemporaneous (Furniss *et al.*, 1998; James *et al.*, 1998; Pollock *et al.*, 2006; Petrov, 2011) and attributed to the reaction of intra-sediment gas, formed during the decomposition of microbial mats or stromatolites, with seawater supersaturated at a critical level above the sediment surface and in pore fluids (Pollock *et al*., 2006). This model requires that marine water composition be finely balanced to jointly effect a delay on substrate lithification but, when in contact with biogenic gas in the host sediment, to allow rapid crystallisation of MT microspar (Pollock *et al*., 2006). Expansion of intrasedimentary biogenic gas bubbles would increase to a point where the gas could migrate upwards through the sediment, its progress controlled by the ratio between gas pressure and the cohesive strength of the surrounding host sediment. In clay-rich sediments a spherical body of gas constrained by sediment bond strength would react *in situ* with near surface pore fluids whereas gas in coarser grained material would migrate via a contorted route dictated by grain size difference, variable pore space size and pore space connectivity to form sinuous vein shapes that became ribbons of molar tooth fabric. At or close to the sediment surface gas reaction with seawater occurred and molar tooth microspar precipitated rapidly in the voids. Interstitial molar tooth fabric in oolitic limestone was interpreted as recording a less constrained rise of gas between grains reacting at the sediment/ocean interface (Pollock *et al.*, 2006).

4.2 Molar tooth microspar: A petrographic comparison

Molar tooth microspar petrographic thin sections from three groups of Precambrian carbonate sediments are considered here. The properties of the MT microspar and the MT structure formed are used for comparison with those present in the Gwna mélange carbonate clasts. The stratigraphic MT microspar sections are:

Xinmincun Formation. The uppermost unit of a > 4 km thick Neoproterozoic sedimentary sequence, formed at the eastern margin of the North China Block that retains primary sedimentary features despite having undergone metamorphism. The Xinmincun Formation records eustatic sea-level fall from the underlying shallow

marine sequence. It is characterised by laminated carbonate strata which, in the upper half, are interbedded with high energy storm deposits indicating a peritidal environment, locally expressed at the top of the formation (Fairchild *et al.*, 1997).

Andrée Land Group, North East Greenland. A shallowing-upwards carbonate ramp sequence, correlated between two localities in the NE Greenland fjord region, that are ~ 65 km apart; Ella Ø and Kap Weber. These sediments occupy a late Tonian stratigraphic position, overlain by glacial lithofacies of the Cryogenian Tillite Group (Herrington, 1988; Sønderholm *et al.*, 2008).

Keills Member, Lossit Limestone Formation, Appin Group, Islay, west Scotland. A >4 km thick Dalradian Supergroup marine shelf sequence of carbonate and siliciclastic deposits that crop out on Islay, and the Garvellach Islands, overstepped by the glacigenic Port Askaig Formation, a Sturtian panglaciation deposit of Cryogenian age.

The region was subjected to metamorphism at 470 Ma during the Grampian orogeny. MT structure is present on Islay, in the lower part of the Keills Member (Fairchild *et al.*, 2017).

A variety of MT microspar crystal sizes, recrystallised MT microspar and MT structure is demonstrated in figures 4.2 and 4.3. They include:

- *Tapering downwards veins, either bedding normal or oblique to bedding.* Figure 4.2A shows twin molar tooth tapered veins oblique to bedding orientation. The MT structure to the right is a simple structure whereas the vein on the left is a composite MT structure consisting of two separate parallel tapered structures of the same age. The veins are in sharp contact with the laminated micrite-microbial host sediment with no inclusion of the micrite fragments in the MT microspar vein fill, a common feature of MT structure. Figures 4.2C 4.2D and 4.3B illustrate bedding normal MT structure veins with varying degrees of tapering.

- *Contorted, or ptygmatically folded tapering veins*. Ptygmatically folded MT structures are distinctive convolute MT microspar filled veins (Fig. 4.2C) that underline the difference in lithification between the crystallised MT microspar vein and the semi- to unlithified host sediment – at the time of MT microspar precipitation. Burial compaction causes a dissimilar response in the crystallised vein to that of the sediment, controlled by the ductility differential. MT structure is frequently seen to exhibit corrugated folding, far more complex than the gentle folds in the surrounding sediments (Figs. 4.2C, D, E and 4.3B).

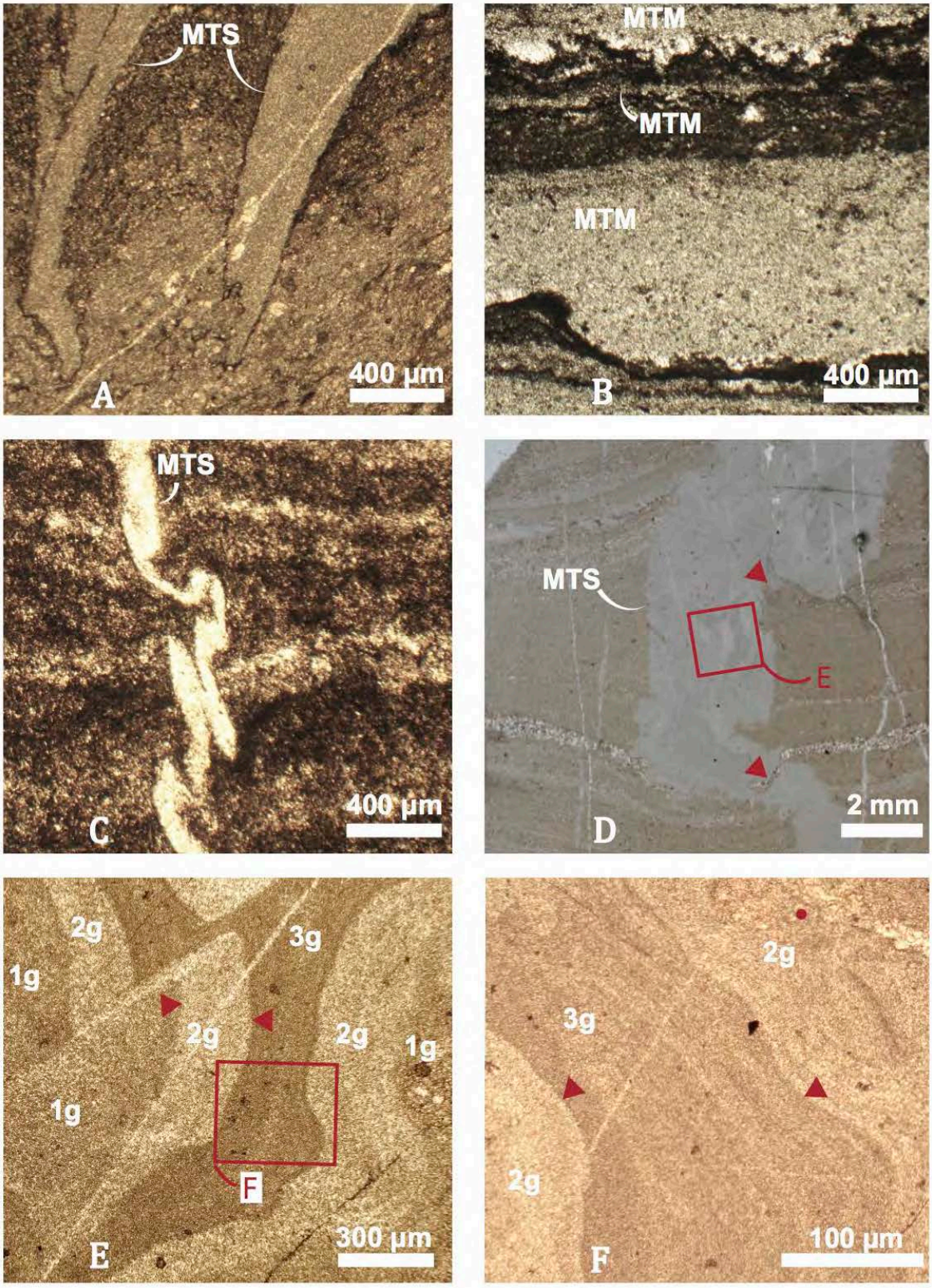
MTS
400 µm
A
MTM
MTM
MTM
400 µm
B
MTS
400 µm
C
MTS
E
2 mm
D
2g
3g
1g
2g
2g
1g
1g
F
300 µm
E
2g
3g
2g
100 µm
F

Figure 4.2 ← Plane polarised light photomicrographs of MT microspar and MT structure from Neoproterozoic carbonate platforms. **A. Xinmincun Formation, north China**. Twin tapered molar tooth veins (MTS), oblique to bedding, in sharp contact with carbonate sediment. The host sediment consists of micrite mudstone passing upwards into microbial anastomosing layers. **B**. **Xinmincun Formation, north China.** In the centre a 1 mm thick MT microspar layer (MTM), under- and overlain by microbial limestone with further sub mm MT microspar horizons. The uppermost MT microspar layer, at the top of the image, contains dolomitised MT microspar in clusters disrupting the top of the underlying microbial layer. **C. Xinmincun Formation, north China.** A ptygmatically folded, bedding-normal, slightly tapering molar tooth vein (MTS) sits in a pivotal position with regard to gentle folding in the laminated microbial carbonate host sediment. **D. Andrée Land Group, North-East Greenland.** Folded molar tooth bedding-normal, tapered vein in limestone micrite with minor silt horizons. The laminated host sediment/MT structure contact is sharp and ripped-up strips of silt bedding are incorporated within the MT structure (red triangles). The host sediment strata (left) are deflected both upwards and downwards around the vein. In the centre the MT structure is seen to consist of generations of vein fill – the near bisected structure (boxed) is magnified further in image E and the folding within is broadly mirrored in folding of the composite MT structure and the host beds. Further second and third generation bodies are evident at the top and bottom of the MT structure. **E. Andrée Land Group, North-East Greenland.** High magnitude image of the centre of the MT structure boxed in image D, demonstrating by differently coloured individual bodies, three progressive generations of MT microspar precipitation in a single vein; 1g, an elongate, pinched out MT structure, predates 2g. which in turn, is older than the crack widening/precipitation of 3g. Later folding of the composite MT structure almost bisects the vein and is repeated, albeit in a less contorted fold, in the host beds. Red triangles point to the sharp contacts between generations of MT precipitation. The boxed section is further magnified in F. **F. Andrée Land Group, North-East Greenland.** Sharp contacts between MT microspar generations are highlighted by red triangles in repeated vein development events.

Figure 4.3 → Plane polarised light photomicrographs of MT microspar and MT structure from Neoproterozoic carbonate platforms. **A. Xinmincun Formation, north China.** Interconnected MT structure - infilled fenestral voids (MTS) in microbialite micrite. **B. Xinmincun Formation, north China.** A bifurcating MT structure vein cross-cuts layers of dark microbial micrite with microscale beds preferentially dolomitised (pale beds). The dolostone layers include dark clots and anastomosing strips of microbial origin. The host sediments are folded in opposing directions on either side of the MT structure. **C. Keills Member, Islay, Scotland.** Pyritised micrite interbedded with parallel MT microspar layers 2-3 mm thick (MTM) are disrupted by transgressive zoned calcite veins, which are partly dolomitised. **D. Keills Member, Islay, Scotland.** A higher magnitude image of C, showing the contact between the MT microspar layer and the zoned calcite/dolomitised veins. There is evidence for partial recrystallisation (MTM rx) of the MT microspar where the individual microspar crystals are enlarged (MTM RX), resulting in a mixture of larger anhedral calcite crystals, often clustered, within the body of equant MT microspar crystals. **E. Keills Member, Islay, Scotland.** A high magnitude image of a recrystallised MT vein (MTM rx). Crystal uniformity is no longer evident apart from a few patches. Average crystal size is 30 – 50 μm. **F. Xinmincun Formation, north China.** Shapeless MT structure (MTS) in a host sediment of microbial micrite host with minor dolomite, contains a central filling of zoned calcite (ZC). The drusy zoned calcite/MT microspar inner margin, and the outer MT microspar/micrite contacts are unusually diffuse.

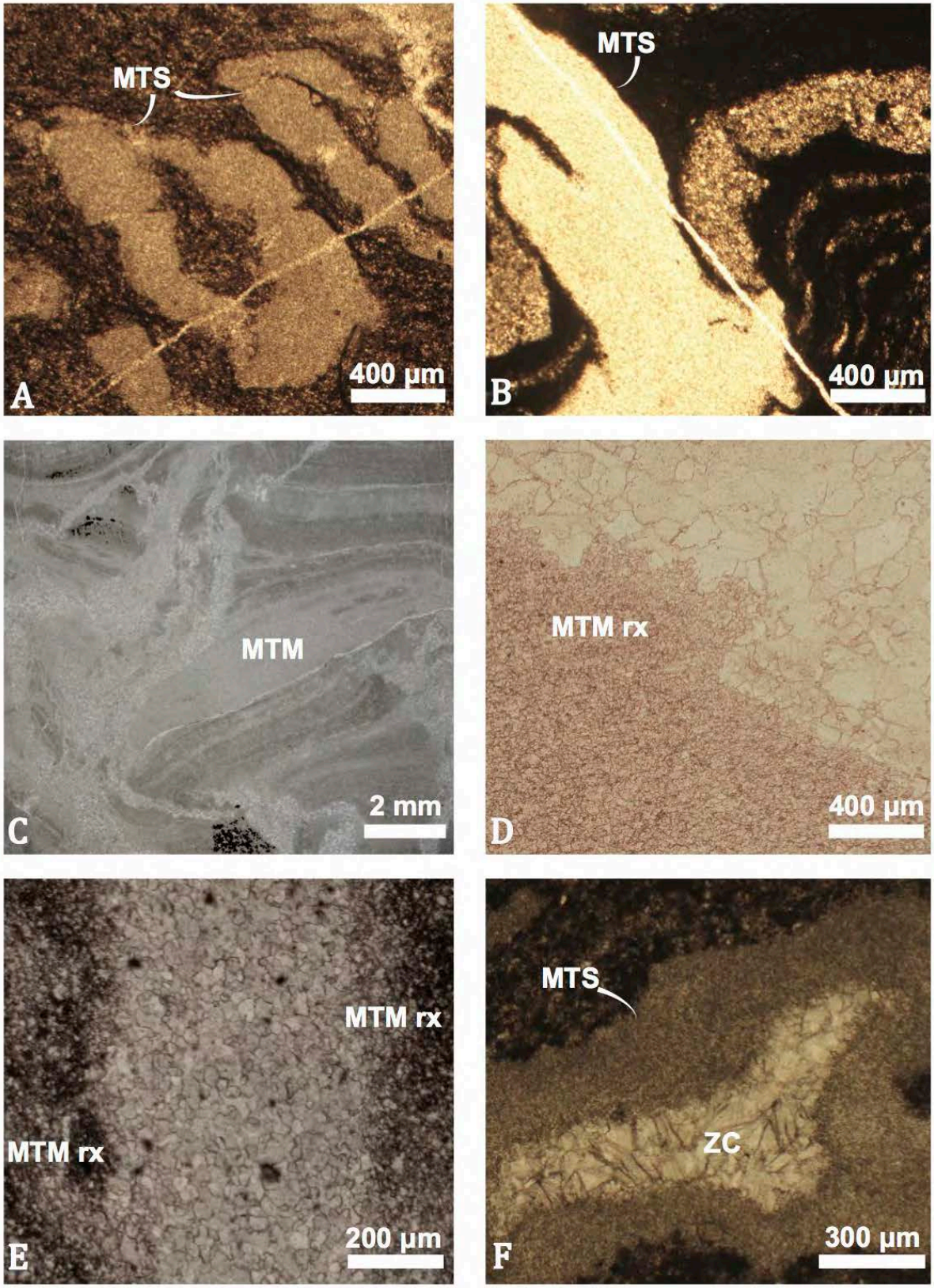
MTS
400 µm
A
MTS
400 µm
B
MTM
2 mm
C
MTM rx
400 µm
D
MTM rx
MTM rx
200 µm
E
MTS
ZC
300 µm
F

- *Composite veins formed in generations.* Figure 4.2D shows a grey molar tooth structure that tapers from 4 mm to 1 mm wide, sitting in buff coloured micrite with minor silt horizons. In the centre of the MT structure vein there is a darker off-set structure (boxed). At greater magnification in figures 4.2E and F three clean contacts between MT microspar of different colours are evident. The composite MT structure is repeated above and below the central off-set body clearly outlined by the MT microspar colour variation. This is interpreted as vein formation over three generations, which may represent either partial infilling of the cavity followed by two further episodes of fluid ingress and MT microspar precipitation, or a series of three events each consisting of cavity formation and near contemporaneous MT microspar infill. The latter is the most likely given the sharp contacts between the three MT microspar bodies. The folding of the MT structure and the host sediment has taken place after all three MT structure events were precipitated, as demonstrated by the broad similarity in fold morphology shared by the MT structure and the host sediment as well as the offsetting of the generations of MT microspar.

- *MT microspar strata.* Five MT microspar strata are interbedded with microbial layers in figure 4.2B. The upper layer, where only the base is shown, includes bunches of dolomitised MT microspar ~~in bunches~~ loading the microbial horizon beneath.

- *Shapeless MT structure.* Figure 4.3A illustrates looped bodies of MT microspar formed in interlinked fenestral cavities in microbial carbonate

sediment and in figure 4.3F an MT structure has a parallel sided internal zoned calcite centre, that represents two generations of infill. Recrystallised MT microspar. MT microspar increase in diameter from their primary size of between 5 – 15 µm under diagenetic or metamorphic conditions. Figures 4.3D and E show high magnification images of recrystallised MT microspar. The individual crystals are less uniform than pristine MT microspar; the polygonal shapes are evident only in unaltered patches of MT microspar and crystal diameter, where recrystallised, is between 30 and 50 µm.

In addition to the MT structures illustrated above, there are several shared characteristics in the Xinmincun Formation (north China), the Andrée Land Group, (North-East Greenland) and the Keills Member (Islay) MT lithofacies;

- Early Neoproterozoic age; Pre-Cryogenian, as MT microspar is present and, for Islay and North-East Greenland, this is reconfirmed by an upper contact with Sturtian glacigenic deposits.
- Continental shelf (Islay) to peritidal depositional environment (Xinmincun and North-East Greenland). All units contain stromatolitic horizons, which further confirming a marginal, shallow-marine setting.
- Cratonic margin tectonic setting.
- Shallow-marine depositional environment
- Metamorphism is present in the Xinmincun Formation and in the Keills Member and the resulting recrystallisation of MT microspar is demonstrated in the Keills Member, and can be seen at some horizons in the Xinmincun Formation, although the latter is not illustrated here.

4.3 Shallow-marine clast sedimentology

Geological setting

The megaclast at Trwyn y Parc, on the north Anglesey coast between Cemaes Bay and Llanbadrig Point (Fig. 4.4) is a notable feature of the Gwna Mélange (Greenly, 1919). Sub-vertical bedding in the carbonate block displays a continuous stratigraphic section of ~230 m thickness interrupted by several minor mélange matrix injection horizons. The megaclast, previously quarried, sits within exposed mélange stratigraphy to the north and south: It does not represent *in situ* deposition, instead it is demonstrably an individual clast within a debris flow (Fig. 4.4B and C), under- and overlain by siliciclastic mélange matrix with further transport evidence provided by repeated injections of matrix into the clast and around the margins. To the east, the megaclast is fault-bounded and the coastline limits available exposure westwards. Within these boundaries outcrop dimensions extend to a maximum of 650 m x 250 m. Although not fully exposed, this is the largest single clast of the Gwna mélange. Horák and Evans (2010) suggested that the clast may be mappable to the west of Wylfa Head, where limestone outcrop occurs along strike.

Figure 4.4 → Geological setting of the megaclast. **A.** Monian Supergroup map (after Greenly, 1920). **B**. Geological map (after BGS Anglesey map, in production) of the Wylfa Head to Llanbadrig area, locating the carbonate megaclast at Trwyn y Parc within the Gwna Group mélange. The polydeformed New Harbour Group lies unconformably beneath the Gwna Group: the contact demonstrates sedimentary unconformity as well as metamorphic and tectonic discontinuity. The upper Gwna Group is overstepped by Dapingian (middle Ordovician) transgressive deposits. A series of thrust slices repeat the contact. **C.** Generalised vertical diagram (not to scale) showing the stratigraphical relationships of the Monian Supergroup with the Dapingian overstep and the position of the megaclast within the Gwna Group.

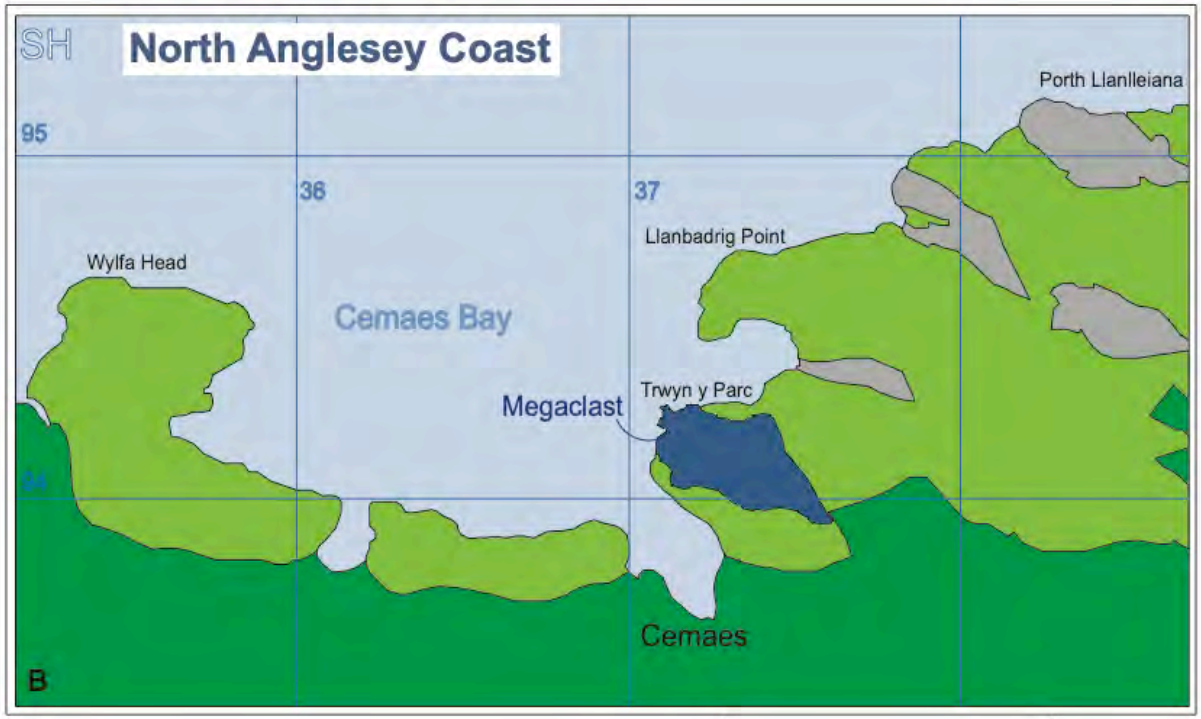
SH
North Anglesey Coast
95
36
37
Porth Llanlleiana
Llanbadrig Point
Wylfa Head
Cemaes Bay
Trwyn y Parc
Megaclast
94
Cemaes
B

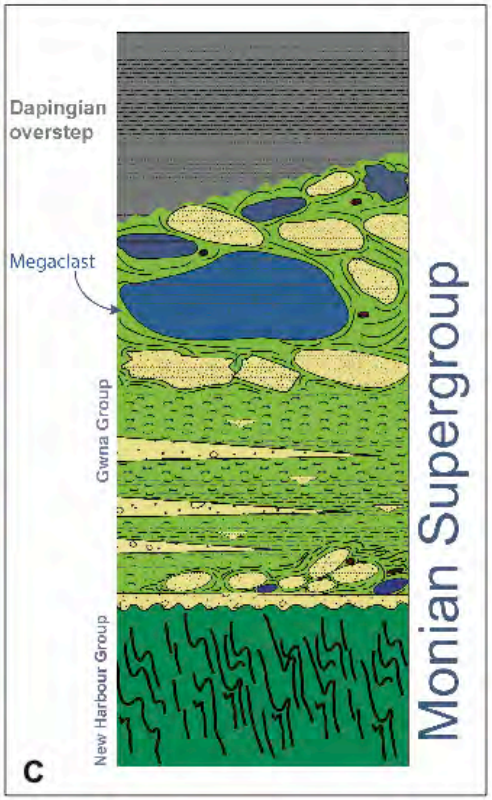
Dapingian
overstep
Megaclast
Gwna Group
New Harbour Group
Monian Supergroup
C


Key
Younger cover
sucessions
Monian Supergroup
Gwna Group
Church Bay Tuff
New Harbour Group

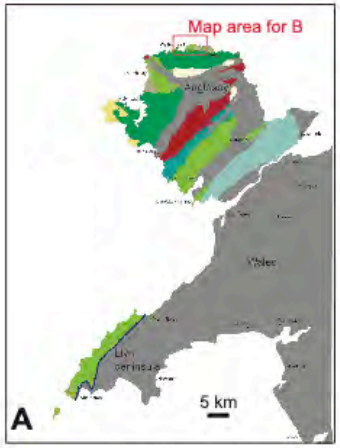
Map area for B
5 km
A

This mélange section unconformably overlies the New Harbour Group and crops out along the Anglesey north coast from Wylfa Head in the west to Bull Bay in the east as a series of polymict debris flows. The siliciclastic mud matrix displays a scaly fabric containing minor clasts of basalt, rare jasper and sandstones with chlorite matrix but is dominated by >5 m diameter clasts of white and orange weathered quartzite and grey carbonate rocks. Many of the carbonate clasts contain MT microspar, as a cement and in a variety of MT structure forms.

Chemostratigraphic analysis of the megaclast (Horák and Evans, 2010) compared $^{87}Sr/^{86}Sr$, $\delta^{18}O$ and $\delta^{13}C$ compositions in samples from a variety of stratigraphic levels to the synthesised seawater composition record of the entire Neoproterozoic of Halverson *et al*. (2007) and Archaean to Ordovician compilations (Shields, 1999; Walter *et al.*, 2000). Oceanic levels of $^{87}Sr/^{86}Sr$ increase steadily through the late Neoproterozoic, a systematic alteration related to the break-up of Rodinia where spikes and dips record major biogeochemical climatic events (Halverson *et al.*, 2007). Horák and Evans (2010) estimated the megaclast depositional age at *c*.860-800 Ma and, finding no suitable correlative units within Britain, suggested the Greenhead Group of the Brookville Terrane, New Brunswick as potentially correlative sedimentary units deposited on an outboard terrane of similar age.

The sedimentology of the megaclast

The coherent stratigraphy of the megaclast provides a framework against which to compare and contrast the numerous individual carbonate clasts within the Gwna mélange that by their nature offer only a fragmentary view of the parent sediment's character. Figure 4.5 illustrates in a ~12 m log section, the

typically Neoproterozoic sedimentary features and textures that comprise the megaclast. Internally undisturbed laminated micrite, microbialites, intraclastic grainstones and MT microspar are present and the sediment is dolomitised to varying degrees. This combination of features is diagnostic of Precambrian carbonate platform sequences formed before the Cryogenian. Globally MT microspar is most commonly found in MT structure (Kuang, 2014) and thus represents a volumetrically minor part of the whole rock, unlikely to exceed 5% in a given sedimentary layer. The Gwna mélange megaclast MT microspar includes such minor MT structure at many levels (Fig. 4.6A, C and F) but the MT Microspar, when forming an intergranular cement, represents a significant portion of rock volume frequently accounting for ~ 40% (Fig. 4.6B) and in some places representing greater than 50% of individual intraclastic grainstone beds, between 20 and 50 cm thick.

Lithofacies comprising the megaclast section (Figs. 4.5, 4.6 and 4.7) include the following:

- Laminated limestone lithofacies. This lithofacies consists of argillaceous carbonate mud– silt grade material deposited in laminae several mm thick. In some beds, single MT microspar layers up to 2 mm thick are interbedded with the mud- silt grade layers. The limestone beds are characterised by either

---

Figure 4.5 → Sedimentary log through a section of the megaclast at Trwyn y Parc, north Anglesey. NGR, SH3718 9419, bearing 221º. The carbonate sequence consists exclusively of typical Neoproterozoic sedimentary features and textures such as stromatolites and abundant molar tooth microspar. The MT microspar is present as an intergranular cement and within MT structure; bedding-parallel ribbons, fenestral shapeless MT structure and, rare, tapered veins normal to bedding. Relatively rapid near-surface dolomitisation occurred widely in the Neoproterozoic and this is recorded in these sediments. There is no evidence for metazoans; no body fossils and no bioturbation.

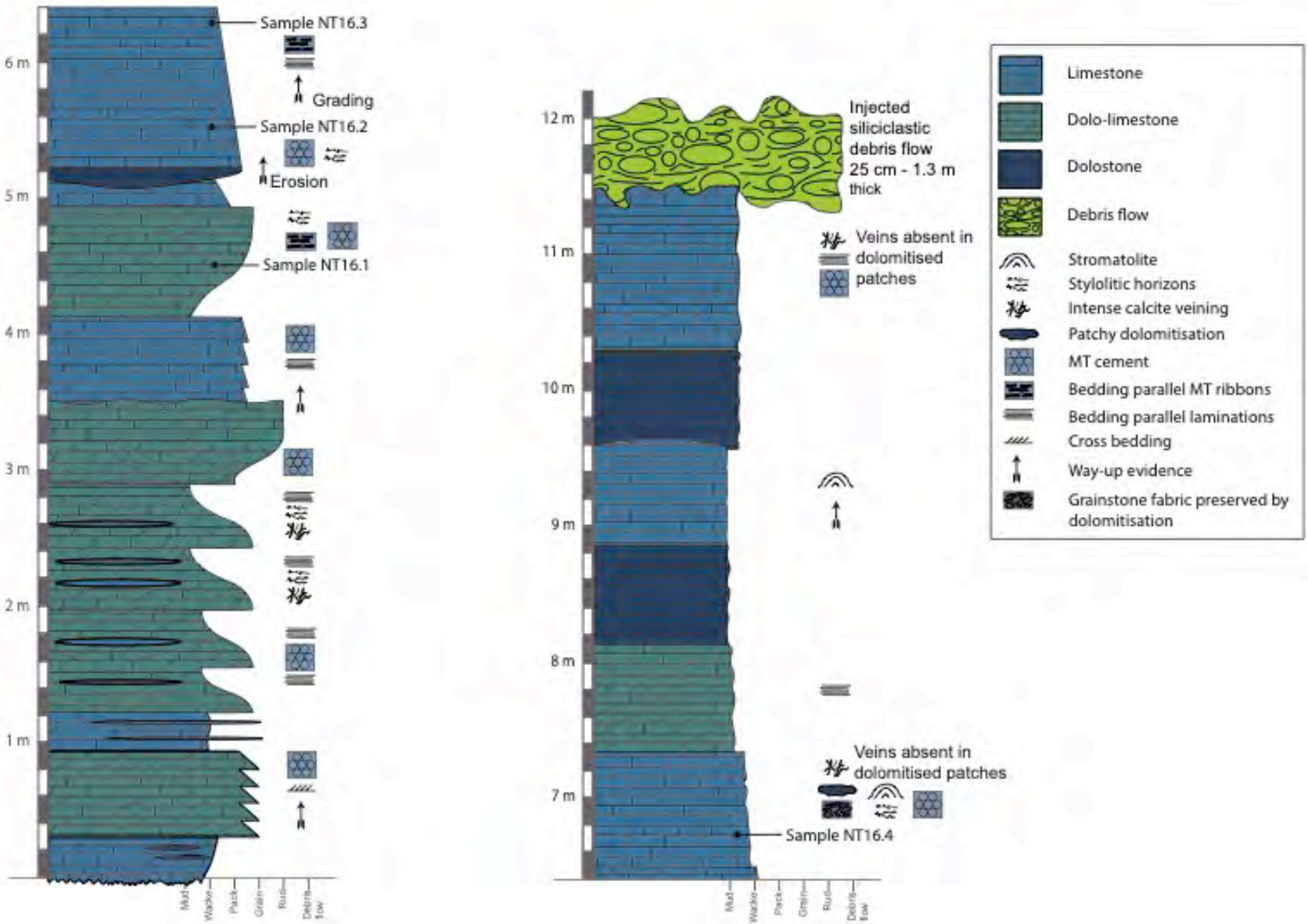
Sample NT16.3
Grading
Sample NT16.2
Erosion
Sample NT16.1
6 m
5 m
4 m
3 m
2 m
1 m
Mud
Wacke
Pack
Grain
Rud
Debris flow
12 m
11 m
10 m
9 m
8 m
7 m
Injected siliciclastic debris flow 25 cm - 1.3 m thick
Veins absent in dolomitised patches
Veins absent in dolomitised patches
Sample NT16.4
Limestone
Dolo-limestone
Dolostone
Debris flow
Stromatolite
Stylolitic horizons
Intense calcite veining
Patchy dolomitisation
MT cement
Bedding parallel MT ribbons
Bedding parallel laminations
Cross bedding
Way-up evidence
Grainstone fabric preserved by dolomitisation

planar parallel, or anastomosing laminae formed at the top of a normally graded bed, or a package of sediments in the lower half of the logged section. Both styles of lamination occur in two orientations: they are either bedding parallel or cross-laminated. In the characterised by either planar parallel, or anastomosing laminae formed In the upper half of the logged section, the laminated micrite lithofacies forms continuous sedimentary beds up to 60 cm thick. Post-depositional dolomitisation is variable: laminated micrite beds are partially or fully dolomitised but some beds have been completely resistant to dolomitisation.

- *Stromatolite lithofacies.* The stromatolite lithofacies can be difficult to identify in the field as crinkled laminations are not visible to the naked eye, and convex bedding planes are not always evident. At a microscopic scale, the stromatolite lithofacies takes the textural form of a simple network of dark laminae representing micritised mats orientated broadly parallel to bedding with interbedded fine grained limestone and some dolomite rhombic crystals. The laminae are convex upwards and sometimes exhibit a loosely crinkled form, which can be discerned where a fenestra (MT structure) gives visual emphasis to the stromatolite form. There are well-developed stylolites positioned mostly at lamination planes but others can cross-cut laminations and pre-existing stylolitic horizons: they are sometimes overlain by clusters of dolomite crystals that have exerted a localised compaction on the filaments beneath. Fenestral MT structure in this lithofacies is either shapeless or loosely elongate, where the latter are parallel to bedding. The fenestrae are commonly located towards the top of individual beds, often in contact with an overlying intraclastic grainstone layer. There is sometimes structural continuity between the MT microspar cement in the overlying grainstone bed and individual fenestrae in the uppermost

stromatolitic layer beneath.

- *Intraclastic grainstone lithofacies*. This lithofacies dominates the lower half of the logged section. Intraclasts of a fragmented, dolomitised crust are supported by an MT microspar cement. Most commonly the intraclasts consist of ripped up fragments of a cortoid lithofacies (that is composed of allochems, each with a micrite envelope). Generally, the cortoids are non-spherical individual grains composed of grainstone or carbonate mudstone surrounded by a well-developed micrite envelope. The appearance of the envelope varies: it can be dark and highly conspicuous, or a faded grey rim. Individual cortoids are rare, but

---

Figure 4.6 → Field photographs illustrating selected features from the megaclast log (Fig. 4.5). The measurements from the log base refer to the image base, unless indicated otherwise. **A**. 40 cm from base. Laminated limestone lithofacies including cross-laminae in oblique contact with the basal bedding plane. Small transgressive stylolites are more prevalent in the finest grain material with anastomosing laminations. **B.** 3.2 m from base. Dolostone intraclasts in the intraclastic grainstone lithofacies. **C.** 3.5 m from base. Bedding parallel laminae and slight normal grading in the laminated micrite mud lithofacies. **D.** 4.8 m from base. MT structure (MTS) in the form of bedding parallel and shapeless fenestrae in the stromatolite lithofacies. The MT microspar filled MT structures are glassy white and dolomite crystals in the microbial sediment are evident in the image centre. **E.** 4.95 m from base. A graded channel deposit forms the main body of the image and this is overlain by the intraclastic grainstone lithofacies (ig), which consists of sub-mm composite cortoid intraclasts and MT microspar cement (MTcem). **F.** Image taken facing north-east, looking over the injected debris flow horizon towards the top of the megaclast at 11.45 m from the base of the log. The injected contact of Gwna Group mélange (df) with the megaclast (mc) is shown with a white line. The contact is demonstrably injected as all minor megaclast cavities are filled with debris flow, or debris flow matrix. The debris flow fabric is indicated by thick blue lines, which converge steeply where the debris flow has been forced through a narrow gap. Several larger clasts in the debris flow are delineated in blue. The debris flow is packed with small black-weathered, yellow sandstone clasts from 1 – 4 cm diameter.

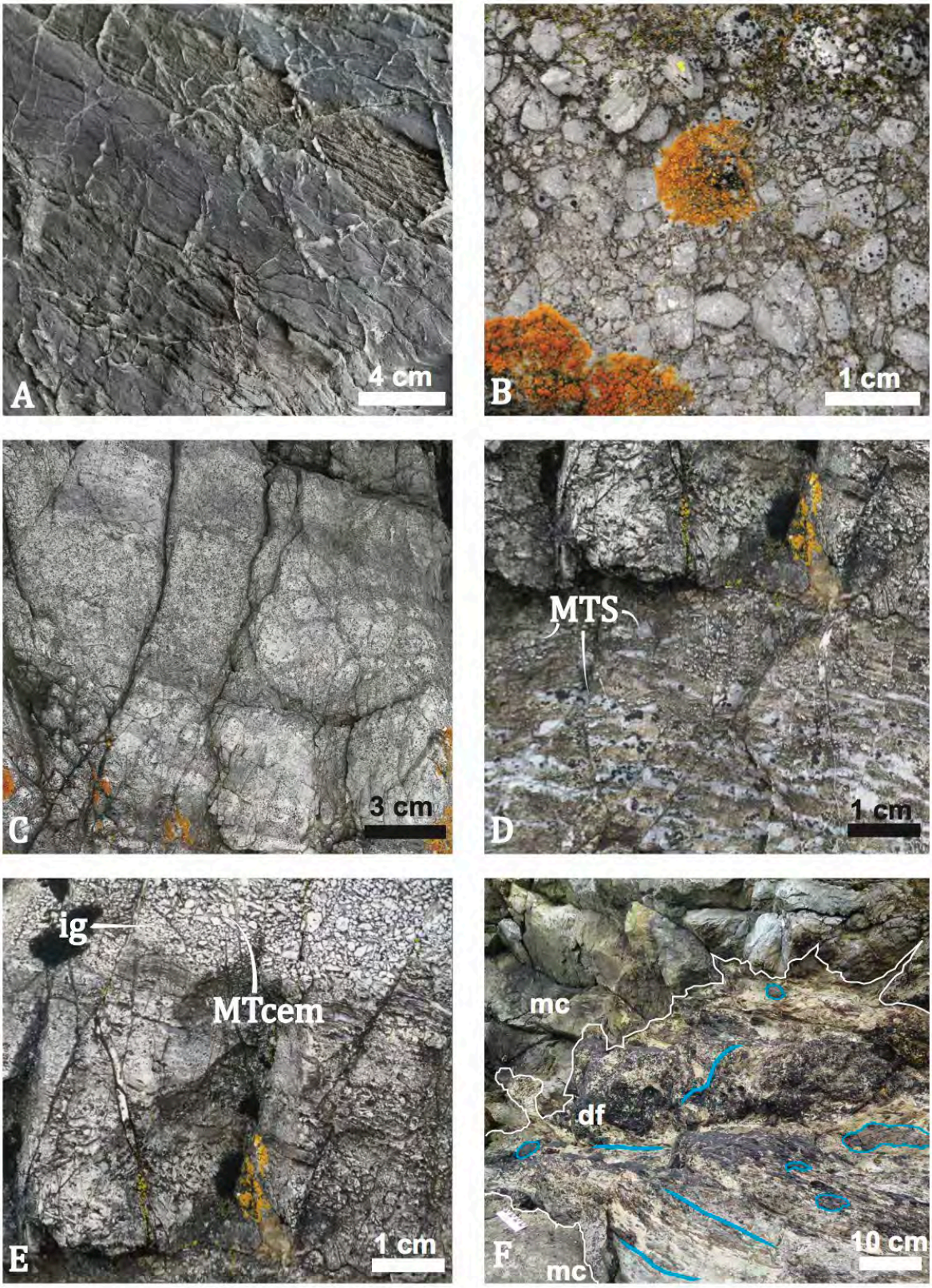
A
4 cm
B
1 cm
C
3 cm
D
MTS
1 cm
E
ig
MTcem
1 cm
F
mc
df
mc
10 cm

composite grains where several cortoids are combined to form an intraclast are pervasive. Some composite cortoid grains have an exterior micrite envelope and others do not. Some strata contain more regular spheroidal cortoids and these can be present within intraclasts or as individual allochems. Intraclasts of dolomite crust, and MT microspar are also present. Intraclastic grainstone dominates the lower half of the logged section in laterally extensive units, at the base of normally graded beds, containing finer grained layers in < 2 cm thick pinched-out pods, with an aspect ratio of 4:1 – 5:1.

Figure 4.7 → Photomicrographs from the megaclast. Sample numbers are stratigraphically located in figure 4.5. **A.** Sample NT16.1 shows a bedding-parallel MT structure (MTS) ribbon in contact with the partially dolomitised host sediment (Part dol). The equant molar tooth crystals measure ~ 10 μm. In common with MT structure globally the contact between the vein and the microspar is sharp (MTS), with minimal transfer of host sediment grains into the vein fill, providing evidence for penecontemporaneous void formation and sedimentary infill. **B.** Sample NT16.1. Dolomitised intraclasts of composite cortoids in a MT microspar intergranular cement (MTM ic). The MT microspar grains measure between 8 and 12 μm. The individual cortoid nuclei are usually dolomitised fragments wrapped in a micrite envelope, evident as a dark rim in the intraclasts (marked with a red circle). Rarely seen molar tooth microspar nuclei are present, as are others with, later, zoned calcite replacement (zc), but these are the exception. The individual cortoids, in a dolostone matrix, feature in the intraclastic grainstone lithofacies facies in composite, equant to elongate fragments, the latter with an aspect ratio between 2:1 and 3:1. The margins of the individual fragments are micritised (red triangle) and in direct contact with the MT microspar cement (MTM IC). **C.** Sample NT16.1. The contact between the stromatolite lithofacies, lower right, and the intraclastic grainstone lithofacies, upper left. The grainstone cement consists of dolomitised clasts and MT microspar intergranular cement (MTM IC). MT structure, in the form bedding parallel and normal to bedding veins, are situated in the upper region of microbialite (red triangles). The microbialite facies exhibits a dark, broadly bedding-parallel fabric which represents repeated microbial mat layers. **D.** Sample NT16.2. The sharp contact (red triangle) between MT microspar intergranular cement (MTM IC), and two closely packed cortoidal intraclasts (red circles). The top-right intraclast contains allochems with faded or no micrite envelope and the lower right clast has thick, dark micrite envelopes around each dolomitised cortoid. **E.** Sample NT16.4. The dark anastomosing horizons aligned laterally are mat fragments with sediment trapped between, now dolomitised. **F.** Sample NT16.3. Pale MT microspar ribbons (red squares) filling fenestrae within the stromatolitic lithofacies. MT structure (MTS) in microbial horizons are either shapeless (red triangle) with no preferred orientation, or, where elongate (red squares), they are broadly aligned parallel to bedding. The characteristically crinkled and convex upwards mat fragments of stromatolites are seen (cr). The crinkled top is emphasised by the contact of the host sediment with the fenestral MT structure (MTS).

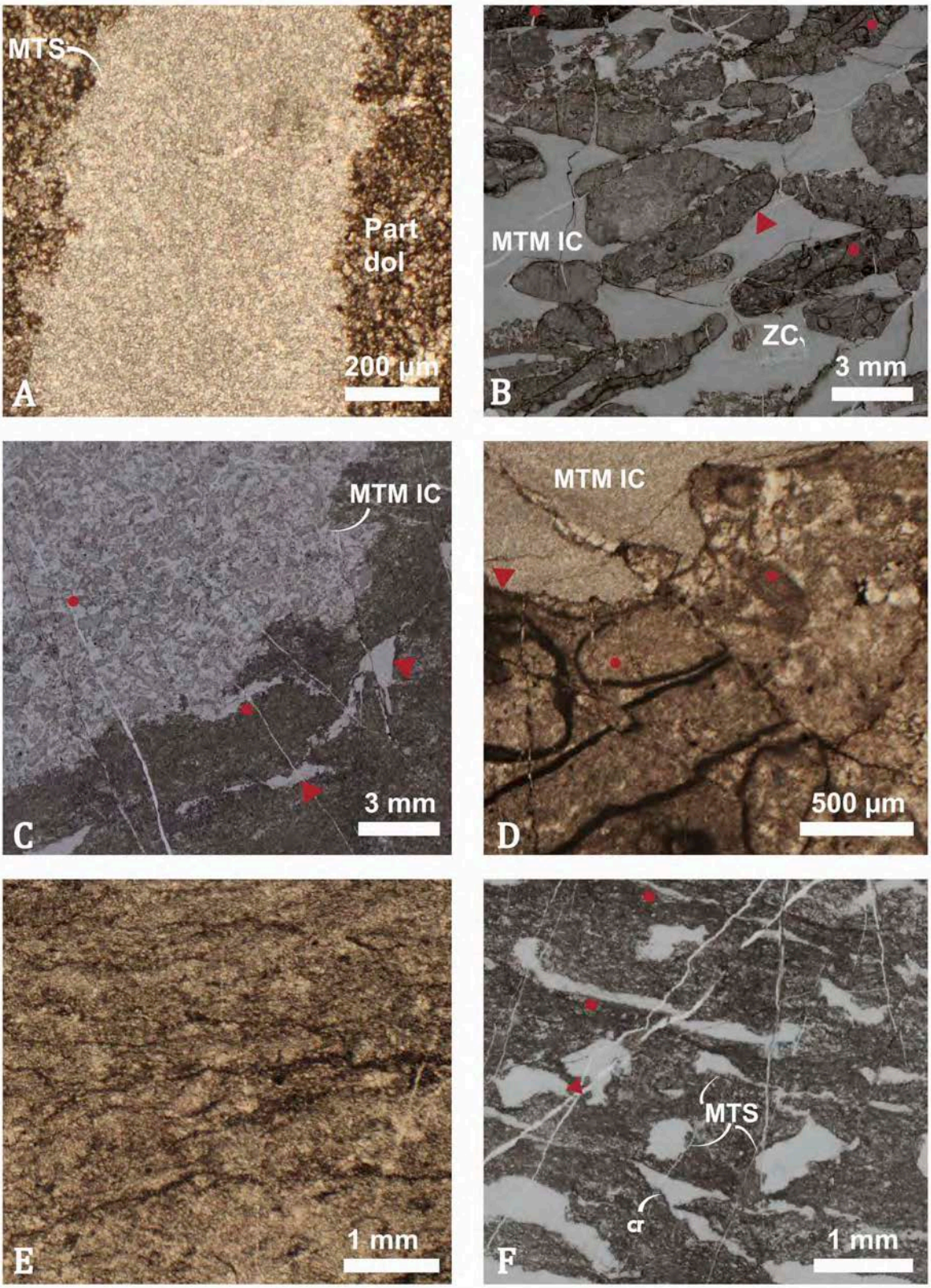
MTS
Part dol
200 µm
A
MTM IC
ZC
3 mm
B
MTM IC
3 mm
C
MTM IC
500 µm
D
1 mm
E
MTS
cr
1 mm
F

- Dolomitisation in the megaclast is widespread (Fig. 4.5), some horizons are fully recrystallised, others are partly altered (indicated as dolo-limestone in figure 4.5, where the content of dolostone is equivalent to ~50%) and in some limestone layers there are dolomitised pods of 10 – 20 cm diameter. Neoproterozoic sea water composition and the kinetics of ocean water moving through carbonate sediments are jointly associated with widespread, rapid near-surface dolomitisation (Fairchild *et al.*, 1991; James and Jones, 2016). The intraclastic grainstone lithofacies is interpreted as a progressively reworked deposit that contains evidence for early dolomitisation in the megaclast. Interpretation of the events leading up to deposition and lithification of the grainstone include:

- *Cortoid grain formation and development of a micrite envelope.* Micrite envelopes are formed by interaction between carbonate allochems and cyanobacteria, which happens within the photic zone in modern analogues (Flügel, 2010; James and Jones, 2016). The cortoids are rounded and exhibit low sphericity, and in most cases they are symmetrical, suggesting a depositional environment above normal wave base.

- *Dolomitisation of the cortoid facies – the uppermost sediment surface.* The crust has been completely dolomitised in all samples. This stage of diagenesis affected the cortoid nuclei and intergranular cement, which consist of rhombic dolomite crystals. There is no crystal continuity between the individual cortoids and the cement: the micrite envelopes remain broadly intact. Therefore, the primary composition of the cortoid nuclei and intergranular cement of the composite cortoid grains is unknown.

- *Disruption and fragmentation of the dolostone crust*. The creation of composite oncoidal clasts was achieved by tearing up the surface dolostone layer, most likely in a storm event, but potentially in a tectonic or transgressive or simply an erosional setting. Some clasts developed a micrite envelope and others did not. Some clasts are rounded, and some are angular to sub-angular. This suggests the temporary accommodation of the ripped-up clasts in separate environments: perhaps those with micrite envelopes and rounded shape remained in a proximal setting whereas the remainder may have been transported to a more distal position.

- *Deposition of the cortoidal intraclasts.* The final deposition of the intraclasts in the intraclastic grainstone facies includes rounded, sub-angular and angular clasts, both with and without clast micrite envelopes leading to the interpretation of a storm deposit accrued below the storm wave base, mixing intraclasts ripped-up and delivered to the site of deposition in a single event, with those involved in transport over 2, or more, stages.

- *Other intraclasts.* Allochems consisting of fragments of MT microspar and dolomite crust are included in the intraclastic grainstone, either mixed with the more ubiquitous cortoidal intraclasts, or, in the case of the dolostone fragments, occasionally dominating horizons of the grainstone. These intraclasts are interpreted as reworked grains created in events similar to those discussed above.

- *Burial and cementation.* Soon after, or during, burial an MT intergranular cement formed completely filling the pore space between intraclastic grains.

- *Later diagenesis.* All the lithofacies in the megaclast exhibit later zoned

calcite veins. Some intraclastic samples show later diagenetic replacement: either dedolomitisation, where MT microspar has aggressively replaced dolomitised cortoidal intraclasts, or conversely, where dolomitisation has almost entirely replaced MT microspar.

In the megaclast, MT structures present (Figs. 4.6, 4.7 and 4.8) include tapered veins, fenestral MT structure, bedding parallel ribbons as well as intergranular MT microspar cement and pure MT microspar layers. The intraclastic grainstone is a complex lithofacies, deposited in a varied number of generations. The intraclasts are commonly dolomitised fragments of a cortoid-rich sediment, but there is evidence for other clast types such as whole MT microspar clasts, MT microspar replaced cortoids or composite cortoids and dolomite flakes (Figs. 4.6, 4.7 and 4.8). Therefore repetitions of dolomitisation and MT microspar precipitation events are recorded in the progressive reworking of the sediments forming the lower half of the log section (Fig. 4.5) prior to the final deposition of this lithofacies. Overall the log section records an increase in water depth, reflected in a broad upwards reduction in grain size. This leads to an interpretation of depositional environment that is sub-tidal, but above storm wave base for the lower half of the logged section. The injected debris flow contact is a much later event that records the incorporation of this large carbonate raft within the Gwna mélange.

Other carbonate clasts in the Gwna Group polymict debris flow facies

MT microspar is present in many of the carbonate clasts in the outcrop sections

of the Gwna mélange from the central Lleyn area, around Porth Colman moving north to Nefyn (belt 1), north-western and north Anglesey (belts 3 and 4). There are limited numbers of carbonate clasts in outcrop belt 2, and although these have not been sampled for petrography field evidence shows they are composed of shallow-marine lime – dolostone of Neoproterozoic character — they lack bioturbation and consist of similar lithofacies: laminated mud - grainstone.

In the lower Lleyn (outcrop belt 1), south of Porth Colman, deep-marine carbonates are dominant. These are often fully dolomitised, composed of well-developed dolomite rhomboid crystals, and sometimes minor zones of dedolomitisation (Fig. 4.8F). In outcrop the deep marine carbonates are associated with basalt pillows, where the top one or two metres of the pillow mass contains interstitial carbonate in progressively increased proportion, which passes upwards to full carbonate. Clasts in the polymict debris flow facies generally consist of a single lithology, but the marine carbonates are often found as broken stratigraphic sections within fault blocks. The deep marine carbonates contain no evidence for metazoans, and, as would be expected, there is no trace of MT microspar as it is a sedimentary feature of the near shore.

4.4 Isotope analysis of carbonate clasts of the polymict debris flow facies

Twenty-five Gwna mélange carbonate clast samples from three of the four outcrop belts were analysed for $\delta^{13}C$ and $\delta^{18}O$ ratios to constrain their depositional age and to test whether the apparently similar lithofacies represented in clasts throughout the Gwna mélange may originate from the same parent unit. Horák and Evans (2010), in their strontium isotope study, included stable isotope values from the megaclast at Trwyn y Parc, near Cemaes

Bay, north Anglesey. Ying Shields-Zhou (PhD student at UCL) kindly carried out an additional $^{87}Sr/^{86}Sr$ analysis of two megaclast samples to test the strontium signal in both the host grainstone and the molar tooth microspar cement. These strontium data from the Gwna Group are compared with global Neoproterozoic $^{87}Sr/^{86}Sr$ analyses (Cox *et al*., 2016).

Figure 4.8 → Plane polarised light photomicrographs from the megaclast (A, B, D and F) and from other shallow marine carbonate clasts in the Gwna mélange (C, E, G and H). **A.** Alizarin red stained megaclast thin section. Dolomitised cortoidal intraclast, partially dedolomitised (red triangles), in a pink stained intergranular MT microspar cement (MTM). The MT microspar is patchily replaced by zoned calcite (zc) and there are remnants of allochems with micrite envelopes (red circle), interpreted as MT microspar replaced cortoids. **B.** Alizarin red stained megaclast thin section. Central pink stained pristine MT microspar (MTM), surrounded by dolomite and saddle dolomite (red triangles) crystals. The red circles show the remnants, after dolomitisation, of cortoidal micrite envelopes. **C.** Clearly demarked bodies of pure MT microspar (MTS) surrounded by rhombic dolomite crystals (dol) and diffuse patches of MT microspar uniform crystals within the dolomite. This is interpreted as partial dolomitisation of the MT microspar cement. **D.** Stylolitic horizons at megaclast bedding margins; Two MT microspar layers (MTM) between stromatolitic micrite layers above and below. To the left and right there are later sub-vertical veins of zoned calcite. **E.** The intraclastic grainstone lithofacies with zoned calcite intraclastic cement, which is potentially a late replacive feature. Intraclasts of dolostone, with no micrite envelope are situated at the top and base of the image. Two cortoids are centrally placed: the blue triangle points to a dolostone rim surrounding a composite cortoid, with micrite envelopes around the individual cortoids (red square) and at various stages of composite grain formation (e.g. red triangle). The red circle points out a rare spheroidal grain with concentric micrite envelopes, or cortices. This cortoid nucleus is dolomitised but contains a central panel of zoned calcite as well as patches of zoned calcite between the cortices. There is zoned calcite (zc) surrounding the grains, interpreted as late stage replacement of both MT microspar intergranular cement and of dolomitised intraclasts. **F.** Alizarin red stained megaclast thin section. A red circle points out a cortoid grain with a micrite envelope within a partially replaced dedolomitised composite cortoidal intraclast (dol) of the intraclastic grainstone lithofacies. The pink stained MT microspar here forms an intergranular cement but has also partially replaced the dolomite (red triangles) in dedolomitisation. **G.** A sub-millimetre MT microspar allochem in the intraclastic grainstone lithofacies, with red triangles pointing to the grain margin where it is in contact with the MT microspar intergranular cement (MTM ic). There are dolomite grains (red squares) and composite cortoidal intraclasts (red circles). **H.** Further variety in grainstone intraclasts and replacement is demonstrated here. Red circles identify dolomitised composite cortoid intraclasts with micrite envelopes and a red square shows a dolostone intraclast, with no evidence for cortoids. A small, dark MT microspar grain (red triangle) contains several isolated dolomite crystals. The intergranular cement is MT microspar (MTM ic) and, in the centre of the image, the MT microspar is partially replaced by euhedral rhombic dolomite crystals.

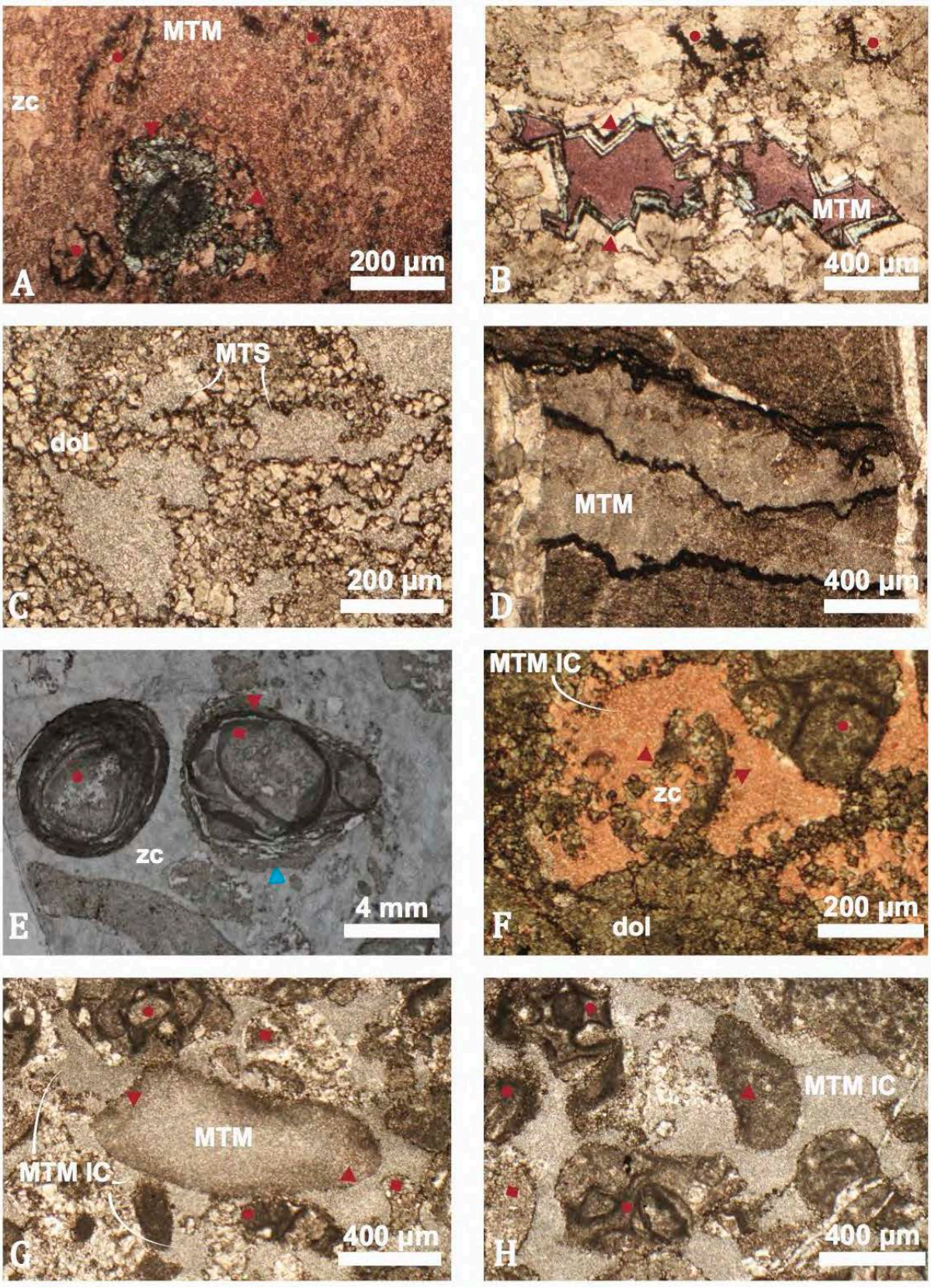
MTM
zc
200 µm
A
MTM
400 µm
B
MTS
dol
200 µm
C
MTM
400 µm
D
zc
4 mm
E
MTM IC
zc
dol
200 µm
F
MTM
MTM IC
400 µm
G
MTM IC
400 µm
H

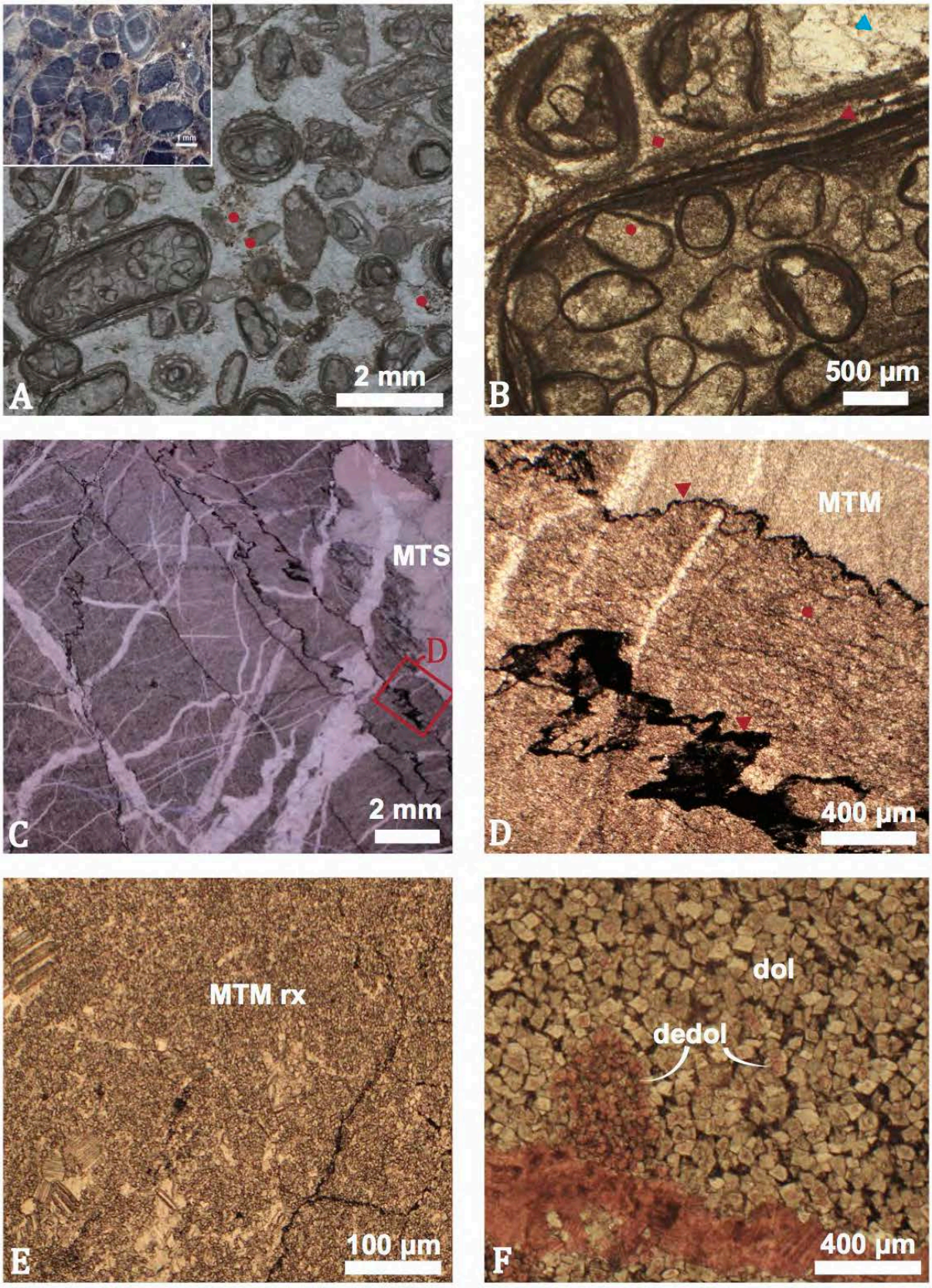
1 mm
2 mm
A
500 µm
B
MTS
D
2 mm
C
MTM
400 µm
D
MTM rx
100 µm
E
dol
dedol
400 µm
F

Figure 4.9 ← Plane polarised light photomicrographs of Gwna debris flow carbonate clast samples**. A.** Individual cortoid grains between 300-500 µm diameter within 1.5-4 mm diameter composite cortoids in a zoned calcite cement. Red circles point to partially replaced intraclasts, leading to the interpretation that the zoned calcite cement has replaced both dolomitised composite intraclasts and a pre-existing intergranular cement (probably MT microspar, but this is not evidenced directly here). The inset is an image of the polished hand specimen surface showing composite grains of 1.5 – 4 mm diameter. **B**. Large dolomitised composite cortoid intraclast with zoned calcite cement (blue triangle). A red circle shows a typical cortoid containing inequigranular dolomite crystals within a micrite envelope. The red square points to the dolomitised intergranular cement of the cortoid sediment – formed before inclusion of the inclusion of the intraclasts in the intraclastic grainstone lithofacies. **C.** Laminated stromatolitic micrite with MT microspar layers, stylolites and a later calcite vein network. The red box indicates the position of D. **D.** Higher magnification of the stromatolite lithofacies (red circle) overlain by MT microspar (MTM) with stylolites (red triangles) at the bedding contact and later zoned carbonate veins. **E.** Partial recrystallisation of MT microspar and replacement with zoned calcite (MTM rx). **F.** Alizarin red stained thin section. Euhedral dolomite rhomboid crystals (dol) in deep marine carbonate with evidence for some dedolomitisation (dedol) and later zoned calcite.

Neoproterozoic chemostratigraphy

Strontium isotope studies are not generally undertaken in such highly tectonised regions as Anglesey and north-west Wales because fluid interactions associated with deformation alter primary geochemistry. Where chemostratigraphy is the aim, samples as pristine as possible are used. Of course, it is not always possible to access unaltered ancient sediments but mostly intracratonic, laterally extensive units worldwide have been used to build a record of seawater evolution through time (Veizer *et al*., 1999; Halverson *et al*., 2007). In such studies, the $^{87}Sr/^{86}Sr$ ratios present in marine carbonate rock are taken to reflect directly the strontium signal present in seawater at the time of deposition. Modern dissolved strontium residence time in ocean water is $\approx 10^6$ years, of a much greater order than whole ocean mixing cycles, which operate at $\approx 10^3$ years. Whether these relative time scales have operated through Earth history is unknown, but strontium isotope stratigraphy relies on the assumption

of chemically homogeneous oceans at all times (McArthur *et al.,* 2012; Shields-Zhou, 2016). Ratios of $^{87}Sr/^{86}Sr$ can be skewed by rock/meteoric fluid interaction during diagenesis or deformation where a fraction of enhanced ^{87}Sr values present are the decay products of ^{87}Rb. Rubidium, leached from silicate rocks where Rb substitutes for potassium, can be introduced into carbonate rocks during diagenetic alteration. A correction for added rubidium is made where the acid soluble Rb level is relatively high, in an attempt to restore the strontium isotope ratio to a primary value.

Strontium isotopes in seawater have been analysed through the global marine carbonate rock record from the earliest Neoproterozoic and through the Phanerozoic. As a result we have a continuous record of the compositional evolution of ocean water through much of Earth history, within which the conspicuously low strontium ratios of the early Neoproterozoic (Fig. 4.10) and the steady rise and dip towards the first panglaciation at 720 Ma, provides a distinctive curve against which to compare isotopic analyses (Halverson *et al.*, 2007; McArthur *et al.*, 2012; Shields-Zhou, 2016).

Ocean composition fluctuates though time and is markedly influenced by global scale phenomena, such as the break-up of supercontinents and enhanced volcanic activity during the emplacement of large igneous provinces. The characteristic strontium record of seawater in the Tonian is associated with the onset of rifting and later dispersal of the Rodinian supercontinent (Halverson *et al*., 2010; Cox *et al*., 2016; Spence *et al*., 2016). Chemostratigraphy is used as a correlative and age constraint tool in many successions, but it is of primary significance in Precambrian studies as alternative parameters are not readily available. Cox *et al*. (2016) update previous compilations of the Neoproterozoic marine record of $^{87}Sr/^{86}Sr$ ratios. Data from this publication are used in discussion later in this section.

A secondary geochemical parameter for age constraint in Neoproterozoic marine carbonate stratigraphy is $\delta^{13}C$. As with strontium, many workers have contributed to the $\delta^{13}C$ seawater evolution curve (Halverson *et al*., 2010). The $\delta^{13}C$ values present in carbonate minerals are taken as a proxy for dissolved inorganic carbon present in the ocean water from which the sediment was formed because $\delta^{13}C$ is relatively resistant to post-depositional alteration. In comparison oxygen isotope signatures are more readily altered (Spence *et al*., 2016).

The Tonian $\delta^{13}C$ curve (Fig. 4.10A) is characterised by sustained positive inorganic carbon values ≥ +5 ‰, except for two high-amplitude, short-lived negative excursions: the Bitter Springs and Islay anomalies (Fig. 4.10A). The Bitter Springs Anomaly is a global signal constrained to a discrete period of 24 million years, from 812 to 788 Ma, recorded in chemostratigraphic studies in central Australia, north-west Canada, Svalbard and Ethiopia (Halverson *et al.*, 2007; Swanson-Hysell *et al.*, 2015). The Islay Anomaly is demonstrated immediately below the glacial deposits of the Port Askaig Tillite Formation of western Scotland in the Lossit Limestone Formation. A rapid negative excursion lasting <10 million years is tightly wedged between positive $\delta^{13}C$ values of 5 – 10 ‰ (Prave *et al.*, 2009; Swanson-Hysell *et al.*, 2010). Some workers have suggested the Islay Anomaly (720 – 710 Ma) is represented in negative carbon isotope excursions in north – west Canada; Yukon 739 Ma (Rooney *et al.*, 2014), and North West Territories 732 Ma (Strauss *et al.*, 2014) , but this is far from certain on the grounds of differing ages and is discussed in Fairchild *et al.* (2017), where the Islay Anomaly is renamed the Garvellach Anomaly.

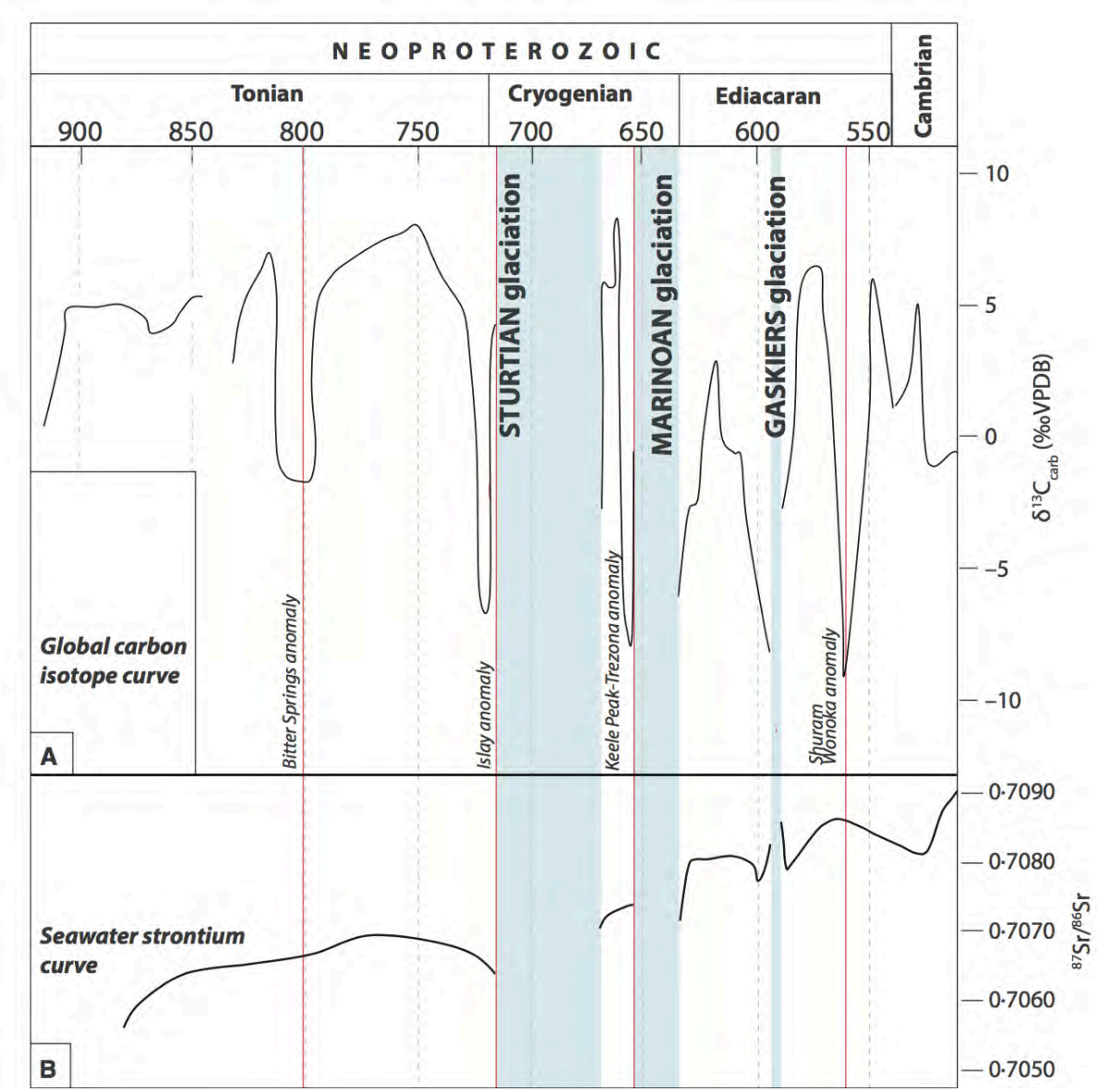

Figure 4.10. Neoproterozoic isotope curves showing global $\delta^{13}C$. **A.** and $^{87}Sr/^{86}Sr$ in seawater. **B.** from Spence *et al.* (2016). The Bitter Springs and Islay carbon isotope anomalies (A) are short-lived, high-amplitude negative excursions. The onset of the first panglaciation, the Sturtian, at 720 Ma represents the minimum age of the Gwna Group shallow marine carbonate mélange clasts, due to the presence of molar tooth microspar.

The application of oxygen isotopic analyses for Precambrian stratigraphic purposes is controversial. Studies of ancient marine carbonates almost exclusively report depleted oxygen compositions, in comparison to Cenozoic sediments (Veizer *et al.*, 1999; Jaffrés *et al.*, 2007; Halverson *et al.*, 2010). There are two opposing schools of thought regarding the significance of the difference: 1. Marine $\delta^{18}O$ has evolved through Earth history to current levels, evidenced by consistently low $\delta^{18}O$ signatures in well-preserved marine fossils considered compositionally analogous to sea water. 2. Marine $\delta^{18}O$ values have remained unchanged through Earth history, buffered by demonstrably constant oxygen isotope ratios in silicate minerals of oceanic crust and ocean/crust interactions, particularly at mid-ocean ridges (Jaffrés *et al.*, 2007; Halverson *et al.*, 2010). Nonetheless, multi-study compilations of $\delta^{18}O$ in calcitic or dolomitic rocks and pristine biogenic material record increasing $\delta^{18}O$ in sea water through geological time (Jaffrés *et al.*, 2007).

Gwna Group stable isotope study: Results and discussion

A late Neoproterozoic age of 860-800 Ma for the megaclast was hypothesised by Horák and Evans (2010) based on $^{87}Sr/^{86}Sr$ data and this broad age is reinforced by the typical nature of the sediment described above. In this section, chemostratigraphy is used to re-evaluate the ages of the megaclast and the carbonate clasts found throughout the Gwna mélange. Carbonate clasts are present in all outcrop belts of the mélange, and based on field and petrographic evidence, there are two categories: 1. Shallow marine facies, associated with quartz arenite clasts. 2. Deep water carbonates are associated with, and even interdigitated with basalt, pillow basalt and jasper.

Questions addressed by this study include;

- Do the carbonate clasts share common $\delta^{13}C$ and $\delta^{18}O$ ratios?
- If not, is there correlation by outcrop belt?
- Is there correlation by lithofacies?
- Can primary $\delta^{13}C$ and $\delta^{18}O$ values be estimated using alteration pathways?
- If so, does the $\delta^{13}C$ signal allow for a reasonable depositional age estimate?

Alteration plots modelled by Skelton *et al.* (2015) for the Dalradian Supergroup of western Scotland are employed to consider how the deformation expressed in the four Gwna Group outcrop belts may have altered the isotopic signature of carbonate clasts. Skelton *et al.* (2015) calibrated the curves based on modelled primary $\delta^{13}C$ and $\delta^{18}O$ in folded metasediments, characterised by a presumed open system protolith of interbedded shale and carbonate, to demonstrate the loss of the primary $\delta^{18}O$ signature in the early stages of deformation compared with the resilience of $\delta^{13}C$ (Fig. 4.11). As deformation progresses, or in areas of more intense deformation, the $^{87}Sr/^{86}Sr$ signal diminishes next, followed by a reduction in the $\delta^{13}C$ signal (Skelton *et al.*, 2015).

The Skelton *et al*. (2015) study analysed the effect of elevated metamorphic fluid:rock ratios on stable isotope composition in the Islay Anticline (> 30:1 compared to the regional mean of 7.6±1.5:1) by close-interval sampling of metasediments between the intensely veined axial region outward to the relatively less altered fold flanks in an attempt to compare systematic modification patterns in the stable isotope chemistry. They propose that the

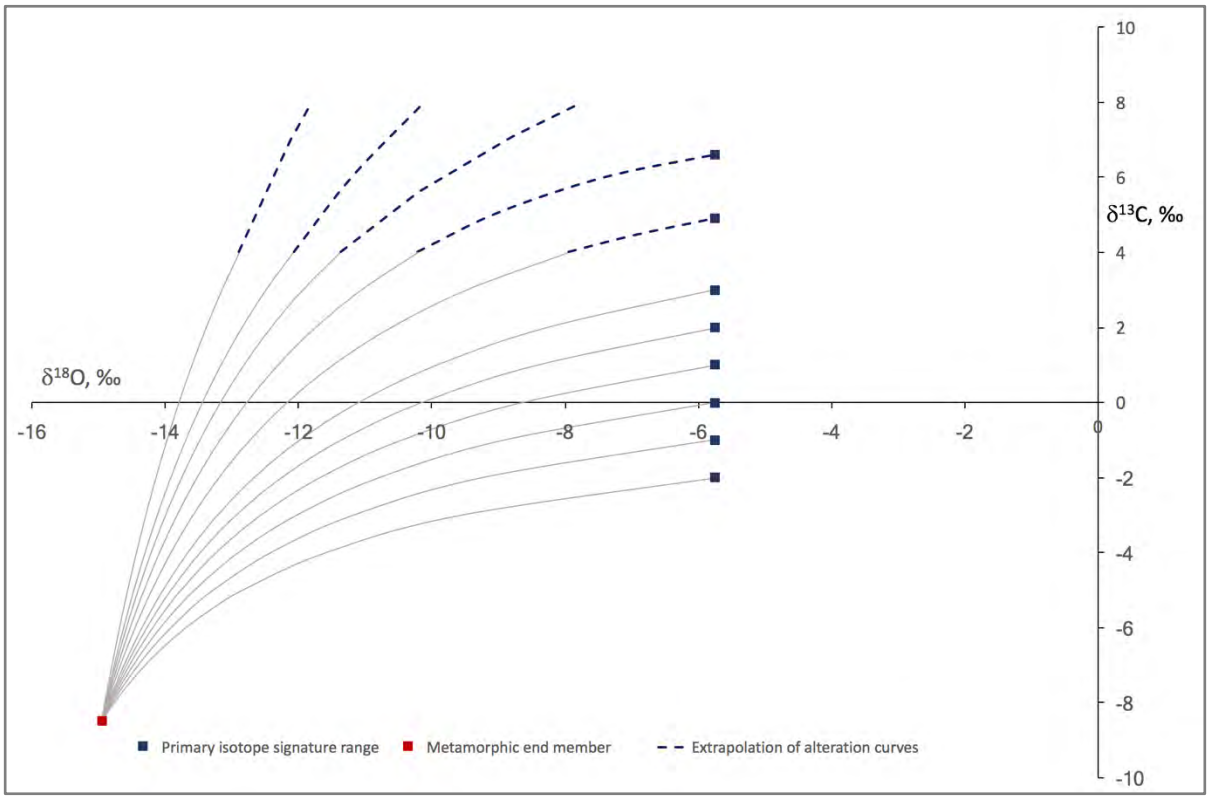

Figure 4.11. The systematic lowering of stable isotope values of $\delta^{13}C$ and $\delta^{18}O$, compared with the VPDB standard, during metamorphic alteration, after Skelton *et al.* (2015). The two end members in the system, represented by a series of primary protolith isotopic compositions and the maximum metamorphic end member value (peak Dalradian metamorphism < 470°C) are connected by a series of mixing pathways that demonstrate the progressive alteration of isotope signal as alteration intensifies. Metamorphosed sample analyses can be extrapolated upwards along the mixing paths to estimate primary isotopic composition. The curves indicate visually the vulnerability of oxygen to alteration during early metamorphism, compared with a more resistant carbon signal.

---

original carbon isotope values can be estimated by restoring data points along alteration pathways for chemostratigraphy. Figure 4.11 shows the Skelton *et al.* (2015) mixing pathways, combined into a group of curves between two end members; a single fluid alteration end member composition and a series of

potential protolith primary compositions based on commonly accepted Neoproterozoic $\delta^{13}C$ average values of 5‰ (VPDB) (Fig. 5.10) and an estimated protolith $\delta^{18}O$ mean level of 25‰ (VSMOW) (Jaffrés *et al.*, 2007). The single metamorphic end member represents peak Dalradian metamorphism reaching a temperature of ~470℃. The mixing lines record the progressive exchange of stable isotopes in a reaction between the host rock and the supercritical metamorphic fluid, likely to be dominated by H_2O or CO_2 and H_2O.

It must be noted that the alteration pathways are not calibrated for Anglesey, and that no such analysis has been carried out. Minimum $\delta^{18}O$ values from this

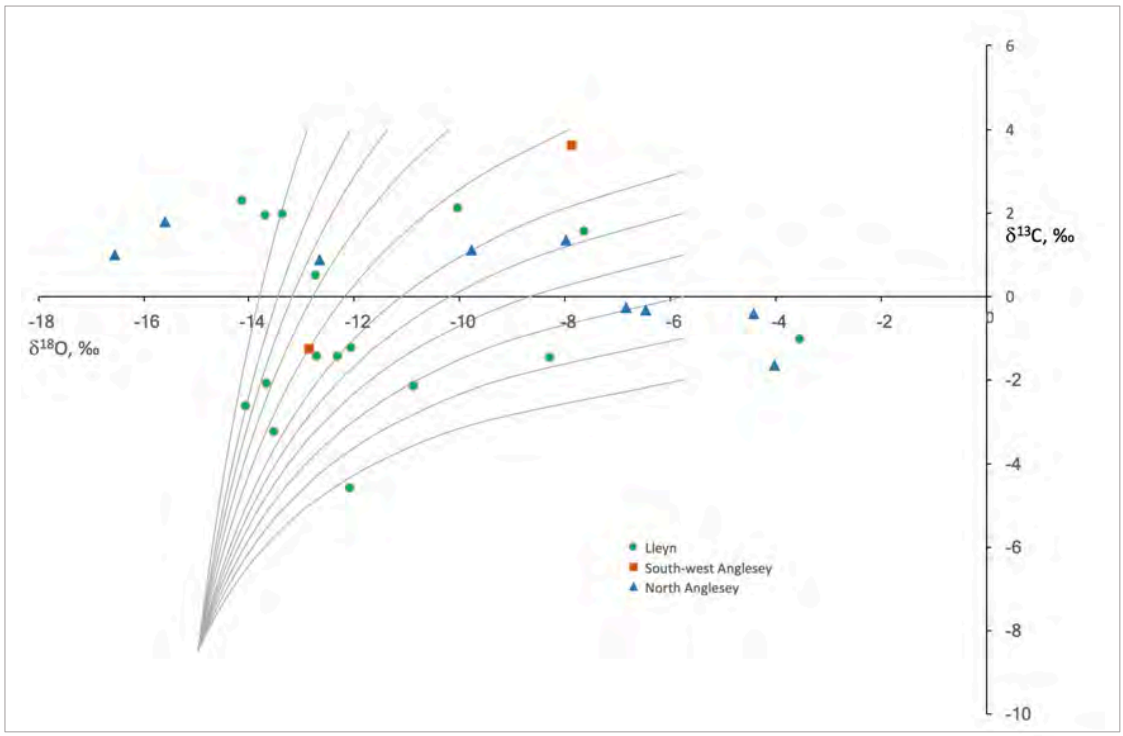

Figure 4.12. Isotope ratios of $\delta^{13}C/\delta^{18}O$ in Gwna Group marine carbonate samples from three of the four outcrop belts (1 = Lleyn, 2 = south-west Anglesey and 4 = north Anglesey). The overlaid grid of alteration curves is modified after Skelton *et al.* (2015).

analysis are more negative than those of the Dalradian (Horák and Evans, 2010; Skelton *et al*., 2015) but the alteration trends are used to consider the data from the Gwna Group. Figures 4.12 and 4.13 compare $\delta^{13}C$ and $\delta^{18}O$ values measured in Gwna Group carbonate clast samples.

Samples from outcrop belt 1, Lleyn, are clustered around the central and lower part of the alteration grid in figure 4.12 implying the greatest degree of sample alteration from metamorphism, which is entirely consistent with the field evidence. Some Lleyn data points plot on the alteration curves but no strong commonality in either carbon or oxygen is demonstrated. Oxygen values are generally very negative within a range of carbon. Several data points at or above -14 $\delta^{18}O$ extrapolate to primary values along the alteration curve resulting in a $\delta^{13}C$ range between +5 and – 2. However, other belt 1 points with positive $\delta^{13}C$ values would extrapolate to unfeasible primary values of +10 or even +12. Deformation in this field area is considerable, with evidence for folding and thrusting seen throughout the entire section, leading to increased burial rates and with it, more alteration. Outcrop belt 2, south-west Anglesey, has two points, which plot on an alteration curve and suggest primary 13C of ≤+5. Samples from outcrop belt 4, north Anglesey do not follow the alteration curve, but instead exhibit a tighter range of ^{13}C, between +2 and -2 with extremely varied ^{18}O signals. The least negative $\delta^{18}O$ values are to be expected here as north Anglesey contains the least altered outcrop section of the Gwna Group.

When considering the somewhat heterogeneous stable isotope data by lithofacies (Fig. 4.13), it is helpful to combine the facies into deep- and shallow-water groups and to consider the dolostones separately from the limestones, due to lithologically controlled chemical responses.

Shallow marine carbonates in the Gwna Group have been altered by

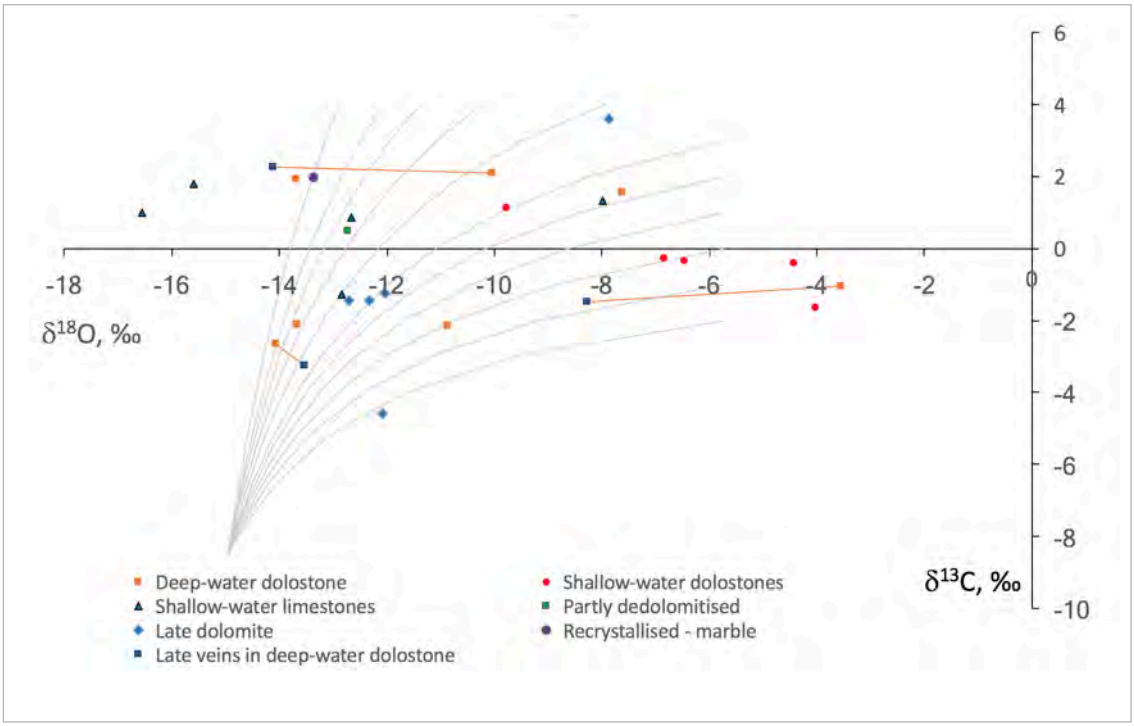

Figure 4.13. Isotope ratios of $\delta^{13}C/\delta^{18}O$ in Gwna Group debris flow marine carbonate samples plotted by lithofacies. The overlaid grid of alteration curves is modified after Skelton *et al*. (2015).

---

dolomitisation to varying degrees. Whereas dolomitisation is generally patchy in the shallow-water facies, the deep-water carbonates are thoroughly dolomitised, and in some cases, show a degree of dedolomitisation. Deep-water Neoproterozoic facies deposited in ferruginous oceans (Canfield *et al.*, 2008) might be expected to contain relatively low $\delta^{13}C$ values. Dolostones are more resistant to recrystallisation during deformation than are limestones and therefore tend to retain their isotopic signature (Spence *et al.*, 2016). Facies present in the less-deformed outcrop belts 3 and 4, and the more deformed belt 2, include shallow-water dolostones (Fig. 4.13) and shallow-water limestones, which are grouped in carbon values between +2 and -2 ‰ and vary in $\delta^{18}O$, showing a mild degree of alteration from primary signals. The shallow-water

limestones have a more consistent range of carbon, between +2 to 0 ‰. The variability of the oxygen isotope values is interpreted as a record of alteration.

The deep water dolostones and late dolomite facies (Fig. 4.13) are found exclusively in the deformed outcrop belts 1 and 2 and have therefore been subject to alteration, but there is a surprisingly heterogeneous set of both oxygen and carbon isotopes. The dolomitic facies demonstrate therefore a lack of correlation with the alteration pathways due to the presence of some samples with highly negative oxygen with positive carbon values.

The megaclast (Fig. 4.14) samples are organised by lithofacies. Carbon values are consistently ~ zero to + 2 and average oxygen in the dolomite samples is higher than that of the limestones, including two micrite samples with very light oxygen, suggesting that both have been subject to some alteration. Figure 4.15 compares the megaclast $\delta^{13}C$ and $\delta^{18}O$ of this study with those of Horák and Evans (2010). The first observation is that the 2010 samples broadly have lower $\delta^{18}O$ values than those of this study, likely to be attributable to sampling strategy; sampling in this study was led by sedimentology, primarily aiming to understand the depositional features present whereas Horák and Evans sampled at regular stratigraphic intervals looking for geochemical evolution. All samples at or greater than -10 ‰ $\delta^{18}O$ are dolostones, the remainder are limestones. The $\delta^{13}C$ signal, except for one low value outlier, is consistently between zero and +2 ‰.

Figure 4.14 → Isotope ratios of $\delta^{13}C/\delta^{18}O$ in Gwna Group debris flow shallow marine carbonates by lithofacies in outcrop belt 4, from the megaclast at Trwyn y Parc, near Cemaes Bay, north Anglesey.

Figure 4.15 → Isotope ratios of $\delta^{13}C/\delta^{18}O$ in Gwna Group debris flow shallow marine carbonates in outcrop belt 4, from the megaclast at Trwyn y Parc, near Cemaes Bay, north Anglesey. Samples from this study and from Horák and Evans (2010) are compared.

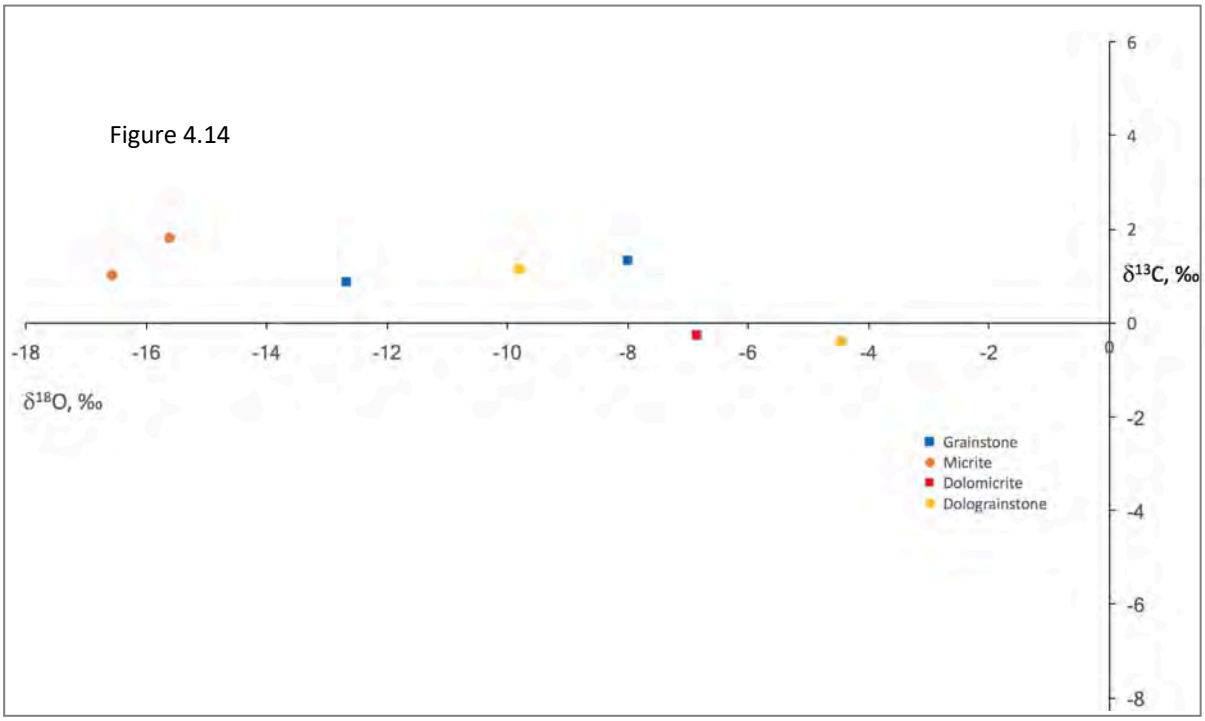

Figure 4.14

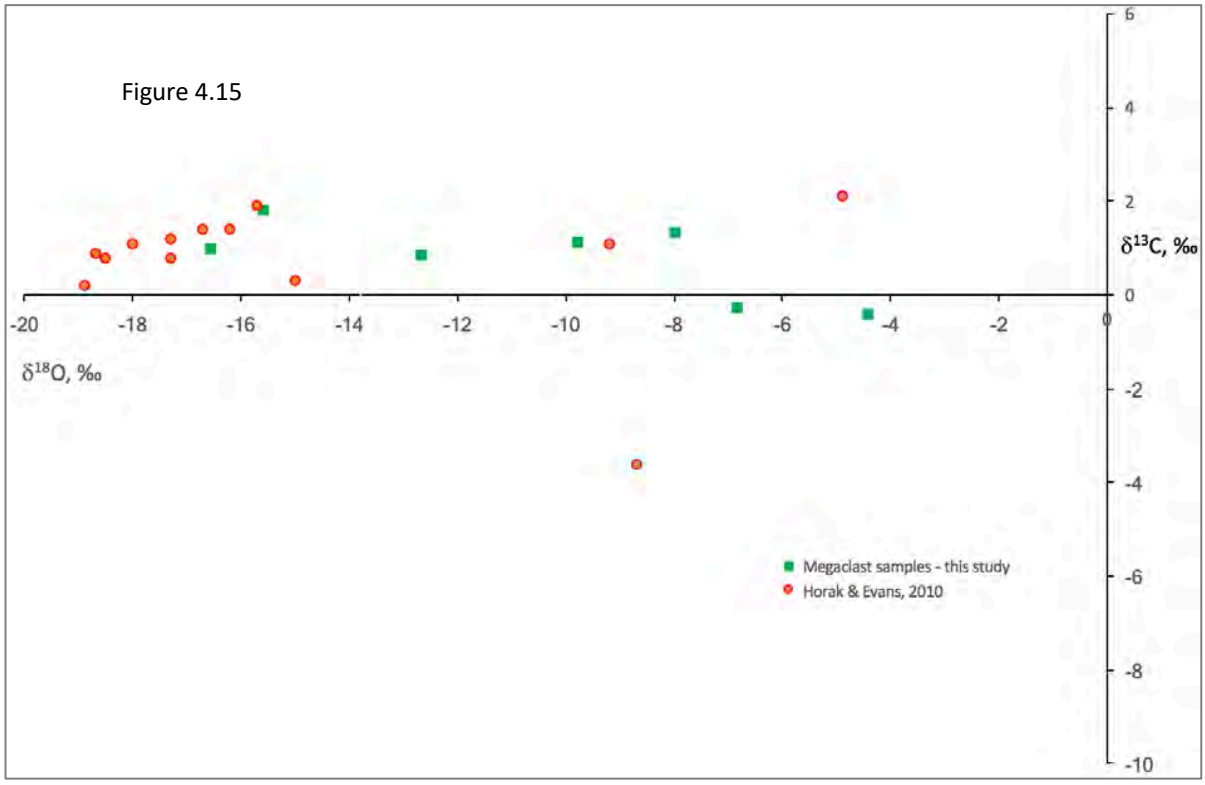

Figure 4.15

Strontium ratios and total strontium concentrations are considered in figure 4.16 using a selected summary of global $^{87}Sr/^{86}Sr$ isotope studies from Cox *et al.* (2015), with Gwna Group values from; 1. Samples collected in this study with 2. Values from Horák and Evans (2010). The Cox *et al.* (2015) values have been plotted by absolute age, instead of by geological formation.

Figure 4.10 shows that $^{87}Sr/^{86}Sr$ ratios in ocean water in the Neoproterozoic were at low levels which enables chemostratigraphic analysis to establish depositional age. High strontium concentrations in samples for analysis is generally considered to provide for the most accurate $^{87}Sr/^{86}Sr$ results. Therefore, the plot of samples from the Cox *et al.,* (2015) compilation by absolute age (Fig. 4.16) should yield a set of age clusters along parallel lines, but this is not the case. It is not the intention of this study to refute the many data points summarised, but instead to point out that the strontium signal, even where concentrations are high, may not reflect the primary composition and as such, will not give the correct depositional age. Gwna Group data points added to figure 4.10B suggest a depositional age for the megaclast of between 850 and 720 Ma, which conflicts with the $\delta^{13}C$ values indicating an older age of 950– 900 Ma. This study asserts that where alteration has taken place the most reliable isotopic analysis for establishing the age of a Neoproterozoic sample is $\delta^{13}C$, due to the relative resistance of stable carbon isotopes to alteration, in comparison to that of oxygen and strontium.

Figure 4.16 → A study of $^{87}Sr/^{86}Sr$ ratios and total Sr concentrations based on Meso-Neoproterozoic data compiled in Cox *et al.,* (2015). Gwna Group data points are added from Horák & Evans (2010) and from samples in this study, analysed by Ying Shields. Data points are plotted by absolute age, irrespective of the formation, or geography to which they belong. The objective is to test the idea that higher strontium concentrations produce the most accurate strontium isotope ratios, and therefore the most reliable ages. **A.** All data are included and this shows that several of the Gwna Group samples are outliers, with very low total strontium concentrations. **B.** The x-axis is expanded to cover only the highest strontium concentrations.

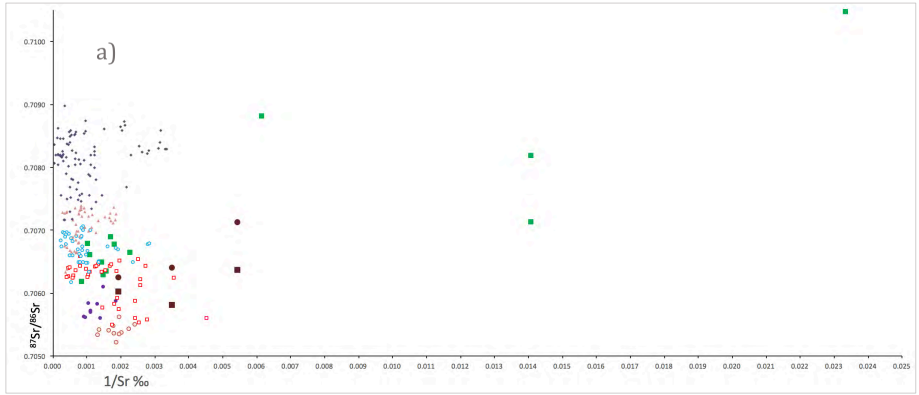
a)
87Sr/86Sr
1/Sr ‰

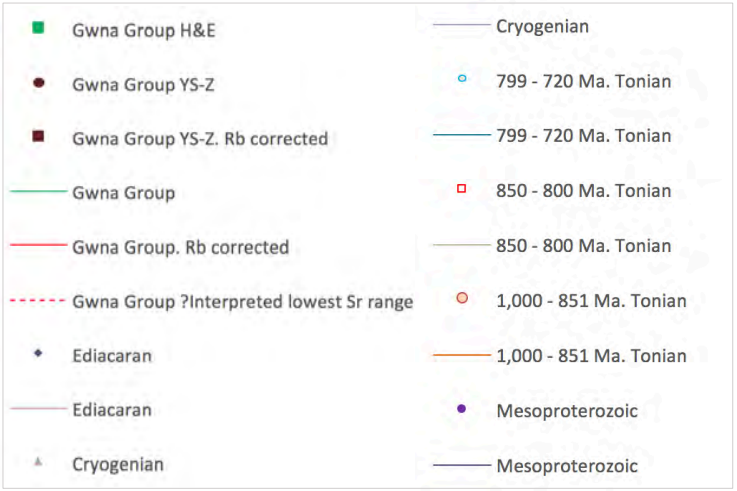
Gwna Group H&E
Gwna Group YS-Z
Gwna Group YS-Z. Rb corrected
Gwna Group
Gwna Group. Rb corrected
Gwna Group ?Interpreted lowest Sr range
Ediacaran
Ediacaran
Cryogenian
Cryogenian
799 - 720 Ma. Tonian
799 - 720 Ma. Tonian
850 - 800 Ma. Tonian
850 - 800 Ma. Tonian
1,000 - 851 Ma. Tonian
1,000 - 851 Ma. Tonian
Mesoproterozoic
Mesoproterozoic

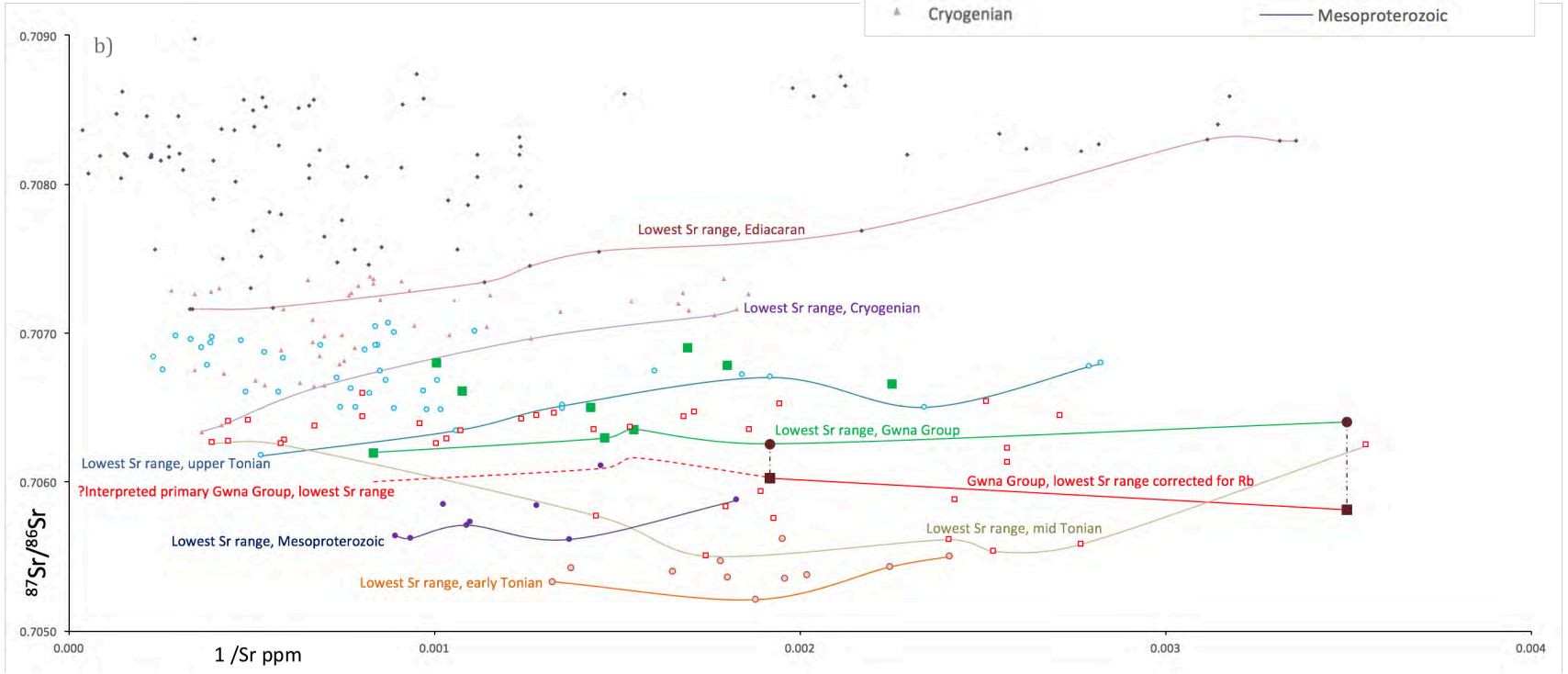
b)
Lowest Sr range, Ediacaran
Lowest Sr range, Cryogenian
Lowest Sr range, Gwna Group
Lowest Sr range, upper Tonian
?Interpreted primary Gwna Group, lowest Sr range
Gwna Group, lowest Sr range corrected for Rb
Lowest Sr range, mid Tonian
Lowest Sr range, Mesoproterozoic
Lowest Sr range, early Tonian
87Sr/86Sr
1 /Sr ppm

4.5 The significance of Neoproterozoic clasts in the polymict debris flow facies

This study concludes with the following lines of evidence;

- The carbonate megaclast and other shallow-marine carbonate clasts in the north and north-west and south-west of Anglesey as well as the northern section of the Lleyn, exhibit many typical Neoproterozoic sedimentary features.
- The formation of the intraclastic grainstone lithofacies, seen in all four outcrop belts, gives evidence for the rapid formation of dolomite crusts at the near sediment surface, which is a characteristic of Neoproterozoic carbonate facies.
- Evidence for microbial sedimentary mechanisms are present.
- There is no evidence for the presence of metazoans.
- The presence of abundant MT microspar in several lithofacies of the shallow-marine carbonate clasts within the Gwna Group debris flows confirms a pre-Cryogenian age of ≥720 Ma.

Furthermore, the stable isotope analysis, specifically of $\delta^{13}C$, indicates that an early Neoproterozoic age is most likely. Negative primary $\delta^{13}C$ does not occur commonly in the Neoproterozoic: it is a feature limited to the Bitter Springs and Islay/Garvellach anomalies in extremely time-restricted intervals. This data is therefore interpreted to infer a depositional age corresponding to either; the Bitter Springs or Islay/Garvellach anomalies, or an absolute age between 950-900 Ma (Fig. 4.10). The Bitter Springs anomaly is demonstrated in central Australia, north-west Canada, Svalbard and Ethiopia and the Islay/Garvellach

anomaly is recorded in west Scotland and no reports of negative $\delta^{13}C$ excursions exist in the north Wales region. Therefore, it is extremely unlikely that the Gwna Group carbonates contain a snapshot of such an anomaly and this study concludes that an early Neoproterozoic age of 950-900 Ma is most likely.

Elucidating the sedimentary character and age of one of the major clasts groups within the Gwna Group debris flows is a significant contribution to the study of the Gwna Group. Although determining the age of a clast group within a sequence of debris flows does nothing to constrain the age of the final deposit in this case, it does raise questions about the sediment supply delivered in this uppermost unit of the Monian Supergroup. It would be reasonable to expect that the major clast constituents would be of similar age, or composition to the underlying Monian Supergroup siliciclastic lithofacies, yet there is a demonstrable age difference of ~ four hundred million years. Given that there is no relationship in terms of either age, or composition, the sediment supply to the Gwna Group was quite distinct from that which was available when the Cambrian metasediments underlying the basal Gwna Group unconformity were deposited. A good deal of geology can happen in 400 million years and therefore many widely varied scenarios could be considered. Potential hypotheses that might explain the Gwna Group circumstances include

- *Change of tectonic setting.* A broad change in the regional tectonic setting, for example, replacing collision with rifting, alternatively, a change in the prevailing direction of relative plate movement.
- *Cratonic rifting*. A (peri-Gondwanan) cratonic fragment rifted into a proximal position to the Monian Supergroup metasediments providing a new sediment supply while cutting off another.
- *Tectonic base level change.* Passive margin wasting of a recently uplifted continental margin that exposed older sediments to erosion.

- *Unroofing of a sedimentary sequence.* The supply of sedimentary clasts older than those previously available could be the result of the sustained wasting over extended time, of a continental margin where progressively older sediments are revealed.

The provenance of the main clast groups is a compelling subject with potential to inform circum-Iapetus tectonic discussion. The shallow-marine carbonate clasts of the Gwna Group are demonstrably of typical early Neoproterozoic sedimentary character, including the presence of abundant MT microspar. The identification of similar lithofacies in other peri-Gondwanan terranes, probably located in eastern Canada or north-west America, could confirm the parent sediment's current position and add to our understanding of tectonic activity in the wider region in early Palaeozoic times.

Chapter 5

DEPOSITIONAL FRAMEWORK OF THE GWNA GROUP MÉLANGES - CONCLUSIONS

This final chapter summarises and synthesises the components of this study to consider how they might be combined to provide a depositional framework for the Gwna Group, taking into account previous studies, supplemented by the new data provided here, including:

- The significance of the ubiquitous sedimentary system identified (Chapter 2)
- New time constraints introduced by the U-Pb zircon study (Chapter 3)
- The confirmation of Neoproterozoic shallow-marine clasts in the polymict debris flow lithofacies (Chapter 4)
- Elucidation of the potential tectonic setting

5.1 The Gwna Group sedimentary system

The Gwna Group, whether considered as a whole or by lithofacies, contains many of the hallmarks of olistostromes throughout all exposure zones. It has been established that the Gwna Group formed through gravitational processes and not by tectonic subduction or accretionary systems. However, it also cannot be said that the Gwna Group is a single olistostrome, as it is evident that the sedimentary system bearing the slump bed and debris flow facies operated over at least four megacycles. Therefore, the next section briefly considers how and where olistostromes form.

Tectonic settings for olistostromes

Olistostromes, or sedimentary mélanges, are sedimentary mass transport deposits that extend over thousands of km^2 and form in a variety of tectonic settings:

- Collisional boundary – convergent margins bear olistostromes, either during the process of subduction or continental collision. Gravitational processes related to progressive uplift and related slope instability lead to a variety of olistostromes, or sedimentary mélanges during subduction or continental collision (Festa *et al*., 2016).

- Rifting or passive margin settings – olistostromes formed by gravitationally controlled wasting of, for example, detrital material moving downslope from topographical highs such as horsts or basin shoulders, created by crustal thinning in extensional tectonics, or continental slope processes at passive margins (Zagorevski *et al*., 2012; Festa *et al*., 2016).

Olistostromes have been defined as follows:

- "*Sedimentary deposits occurring within normal geological sequences that are sufficiently continuous to be mappable, and that are characterized by lithologically and (or) petrographically heterogeneous materials, more or less intimately admixed, that were accumulated as a semi-fluid body*." (Flores, 1955, p. 46-47 ; Flores, 1956, p. 46-47). Flores added further, that olistostrome "*matrix consists of heterogeneous, pelitic sediment void of true internal bedding and containing bodies of harder rocks, from pebbles to boulders up to several* km^3." (Flores, 1956, p. 46-47; Festa *et al*., 2016, p. 181)

- A sedimentary slide deposit characterised by bodies of harder rock mixed and dispersed in a matrix. (Abbate *et al*., 1970; Raymond, 1984)

Figure 5.1 shows how the three genetic types of olistostrome are formed in each tectonic setting. Considering the sedimentology described in Chapter 2, the

---

Figure 5.1 Schematic block diagrams illustrating tectonic settings in which olistostromes are formed, with a comparison of the preservation frequency of Precambrian and Palaeozoic Appalachian (east coast region of north America and Canada) olistostromes and mass transport deposits (MTD) in active and passive margin settings (Festa *et al*., 2016). **A. – D.** relate to convergent tectonic margins. **E. – H.** relate to passive margins and back-arc settings. Relative sea level curve in **J.** from Snedden and Liu, (2010) and Festa *et al*. (2016). **A.** Olistostromes and mass transport deposits form at the toe of an accretionary prism during subduction in an ocean – continent collision zone. The accretionary orogen develops as material is progressively translated onto the upper plate and the complexities of tectonic shortening and flexure creates numerous slope instability events. **B.** Slope instability in foreland basins during lithospheric translation creates olistostromes and mass transport deposits. **C.** Nappe development in intracontinental collision. **D.** Specific olistostrome locations within convergent margins for A – C. **E.** Mafic and ultramafic blocks form olistostromes at ocean spreading ridges during crustal thinning and rifting. **F.** A combination of olistostromes, blocky flows, olistoliths and slumps formed on slope and basin floor settings during rifting in ocean – continent transition zones.**G.** The progressive winnowing of a carbonate platform delivers olistoliths and megabreccias downslope during extensional faulting. **H.** Passive margin evolution within a back arc setting during active divergent tectonism showing the locations for the formation and deposition of olistostromes figured in E - G.. **I.** Comparison between preservation frequencies of olistostromes formed in active (collisional) tectonic and passive margin zones in Precambrian to Paleozoic olistostromes in the North American Appalachian region. Provenance of the Monian Supergroup sediments is shown in Chapter 3 to correlate with Gander Terrane, one of the peri-Gondwanan terranes of the region. **J.** Appalachian olistostrome events of thelate Precambrian - early Palaeozoic, summarised in Festa *et al*. 2016 and references therein with the Monian Orogen added (Waldron *et al*. 2018). Sea level curve shows first and second order cycles of sea level change (Snedden and Liu, 2010). Chapter 3 demonstrates Appalachian provenance affinity for the Monian Supergroup and it can be seen that from the Ediacaran to the upper Middle Ordovician varied types of tectonic events from passive margin evolution to subduction and continental collision occurred in which olistostromes could have been created.

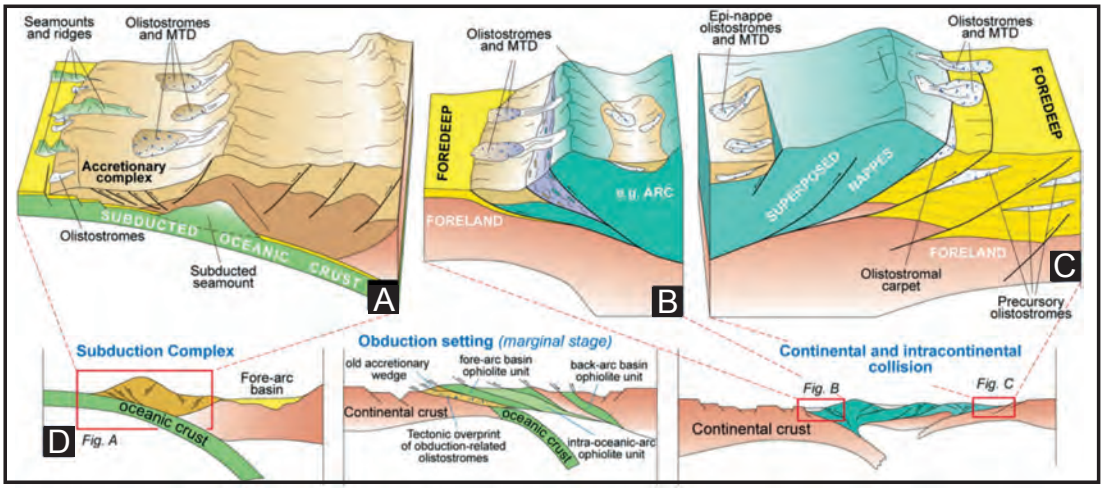

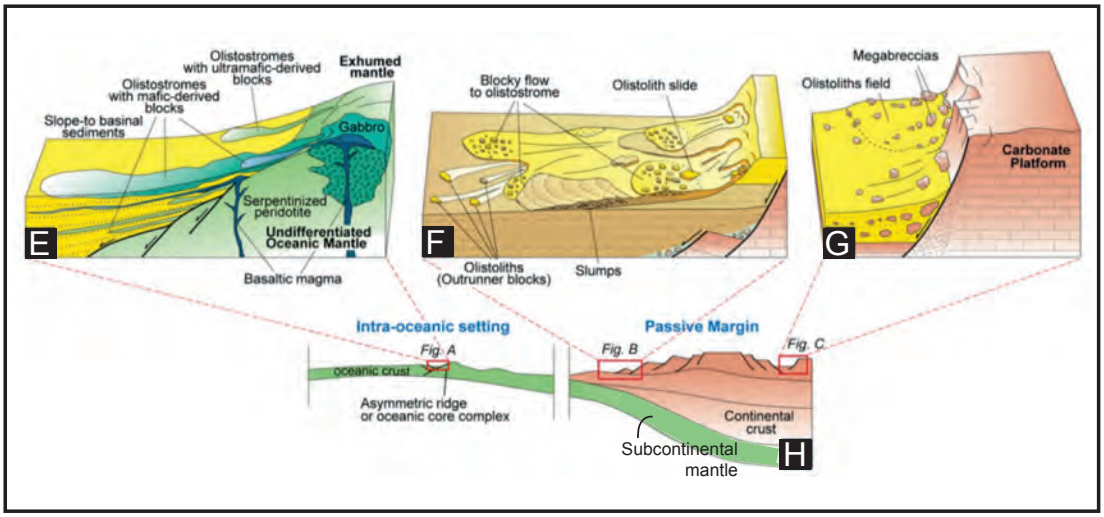

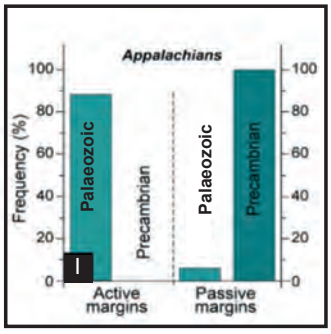

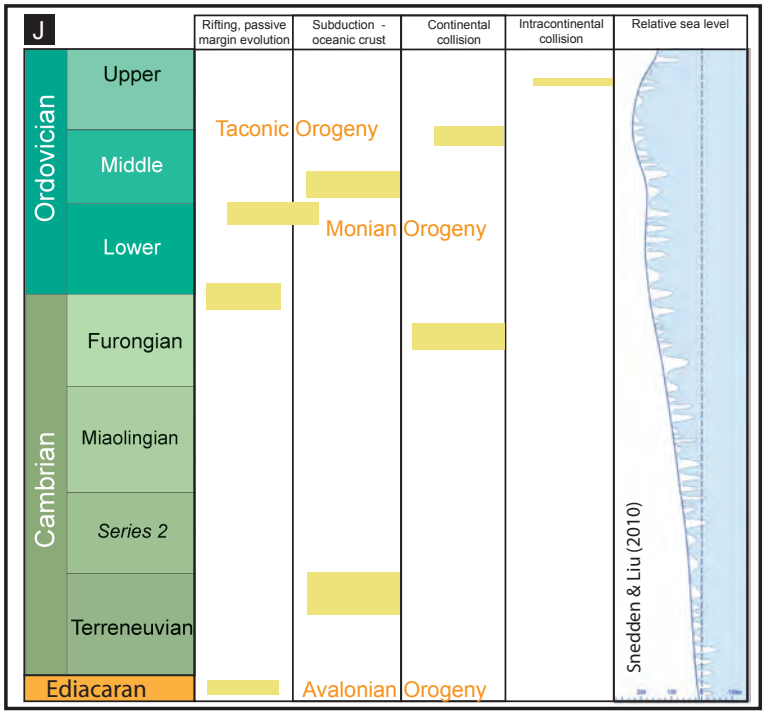

Figures, apart from the sea level curve are from, or after, Festa *et al.* (2016)

scenarios in Figures 5.1A, B and C are unlikely to apply to the Gwna Group as they feature olistostromes deposited in an accretionary prism during final closure (Fig. 5.1C), rather than in a setting capable of returning to a deep marine environment after individual olistostromal events. Synsedimentary faulting, truncated and overlain by further sedimentation, would be expected and this is not seen in the Gwna Group. Figure 5.1E is limited to mafic lithologies and therefore not relevant. Figures 5.1F and G of passive margin origin, demonstrate olistostrome types that in part fit with the evidence available: Figure 5.1F illustrates a variety of downslope slides, flows and slumps that dominate the basin and may explain both Gwna Group slump bed and debris flow lithofacies. Figure 5.1G shows the progressive wasting of a carbonate platform during extensional faulting which episodically drops blocks, or olistoliths, into unlithified basin sediments. There are carbonate platform blocks in the Gwna Group, which form the second most important clast group by lithology, but they are clasts within cohesive bimodal debris flows, rather than isolated rafts.

Woodcock (1979) raised questions about the relative size of ancient and modern olistostromes — modern olistostromes are several orders of magnitude larger in cross section than their ancient counterparts. This is related to preservation probability (Fig. 5.1I), for example, deposition during nappe formation in tectonic shortening reduces preservation potential (Codegone *et al*., 2012; Festa *et al*., 2016) and the random nature of available outcrop is of course a factor. Scale is a consideration relevant to the Gwna Group. The accretionary complex Makran olistostrome in Iran is the largest known ancient (Miocene) example (Festa *et al*. 2016). It has been interpreted both as a sedimentary and diapiric mélange and accounts for 42,000 km3 volume and area coverage of 10,000 km2 dispersed over 72,000 km2 regionally. The maximum

measured thickness is 600 m (Burg *et al*., 2008). The Dunnage Mélange of Newfoundland, of uncertain genetic history, although interpreted as formed tectonically in a fore arc trench (Zagorevski *et al*., 2012) crops out over an area of ~ 40 km displaying up to 10 km thickness (Hibbard, 1979).

Although it has not been possible to provide an exact thickness for the Gwna Group as a whole (Table 2.1), the scale of the subordinate polymict debris flow lithofacies within the broader Gwna Group does not compare to the deposits mentioned above. The thickest debris flow exposure is ~ 500 m, which is achieved by a series of layered flows. The polymict debris flow facies differs in significant ways when compared to the olistostrome definitions of Flores (1955, 1956) above — :

- Extent — some flows are mappable, but most are not
- Matrix —not heterogeneous

The slump bed lithofacies compares as follows:

- Extent — no flows are mappable
- Matrix —not heterogeneous
- Clasts —there is very little size variation within the clasts

— but they both conform to the less stringent version of Raymond (1984), following the modifications of Abbate (1970).

The coherent and repetitive sedimentary succession of the three main lithofacies that comprise the Gwna Group place it outside the single olistostrome or sedimentary mélange category when considered as a whole. The optimal

interpretation is that a series of olistostromes/large-scale debris flows formed in a passive margin setting within a coherent sedimentary density flow succession.

Defining the Gwna Group

The Gwna mélange, the term mélange and the debate about how it should be used and what Edward Greenly (1919) intended when he brought it to the geological lexicon almost 100 years ago, have all been controversial subjects at times that have served as a fulcrum for heated debate (Hsü, 1968; Silver and Beutner, 1980; Raymond, 1984). It is appropriate that the sedimentary succession of the Gwna Group described in this study contains an internal dichotomy in that two of the main lithofacies are somewhat opposed to each other. For example, the predominantly fine-grained turbidite facies is an end member of the sort of deposits accrued in fluidised density current domains characterised by distal depocentres, run-out and attenuating energy (Mutti and Ricci Lucchi, 1973; Bouma, 2000). The polymict debris flow facies, with exotic clasts up to 650 m diameter, conversely represents deposition by cohesive flow of sediment that is relatively diverse in terms of composition and grain size (Stow and Mayall, 2000).

Bouma (2000) tabulated the relative differences in aspects of turbidite systems dominated by (1) coarse-grained sediments and (2) fine-grained sediments. He treated them as end member facies of the extremely diverse successions designated as turbidites (Mutti and Normak, 1987; Stow, 2000; Mutti *et al*., 2009), and warned that exceptions exist. Coarse grained systems are characterised by high sand: shale ratios throughout containing little to no clay minerals, fed by small deltaic sources on narrow coastal plains with short source to coast distances, inefficiently feeding small—medium sized basins. They are

common in active tectonic margins. Fine-grained turbidites are often formed by efficient gravity flows that bypass the turbidite system and prograde from the slope base, with leveed channels that alternate sand and mud deposits. The sand: shale ratio is low overall, but high in restricted horizons. Sediment supply is from large deltaic systems, on wide coastal plains, subject to the influence of sea level change. They are common in passive margin settings where they supply medium to large sized basins (Bouma, 2000).

The field evidence points decisively to a fine-grained turbidite system (Mutti and Normark, 1987) that developed in an ocean-continent transition zone (Bouma, 2000), during the evolution of a passive margin with numerous slope instability events controlled by low order sea level change accompanied by extensional faulting. Figure 5.1J illustrates early Palaeozoic Appalachian olistostrome forming tectonic events but do any of these correspond with the conclusions of this study?

5.2 Sedimentology within a tectonic and temporal framework

Figure 5.2 combines what is currently known of the historic evolution of the Gwna Group and the Monian Supergroup within the broader North American — Canadian Appalachian and British — Irish Caledonide region (Waldron *et al*., 2014; Waldron *et al*., 2018). Tectonic episodes, deposition and deformation through the Cambrian to Middle Ordovician are ordered to show developing relationships in a temporal framework. Significant and far older regional events, such as the Avalonian Orogen, the exhumation of the Anglesey blueschist unit,

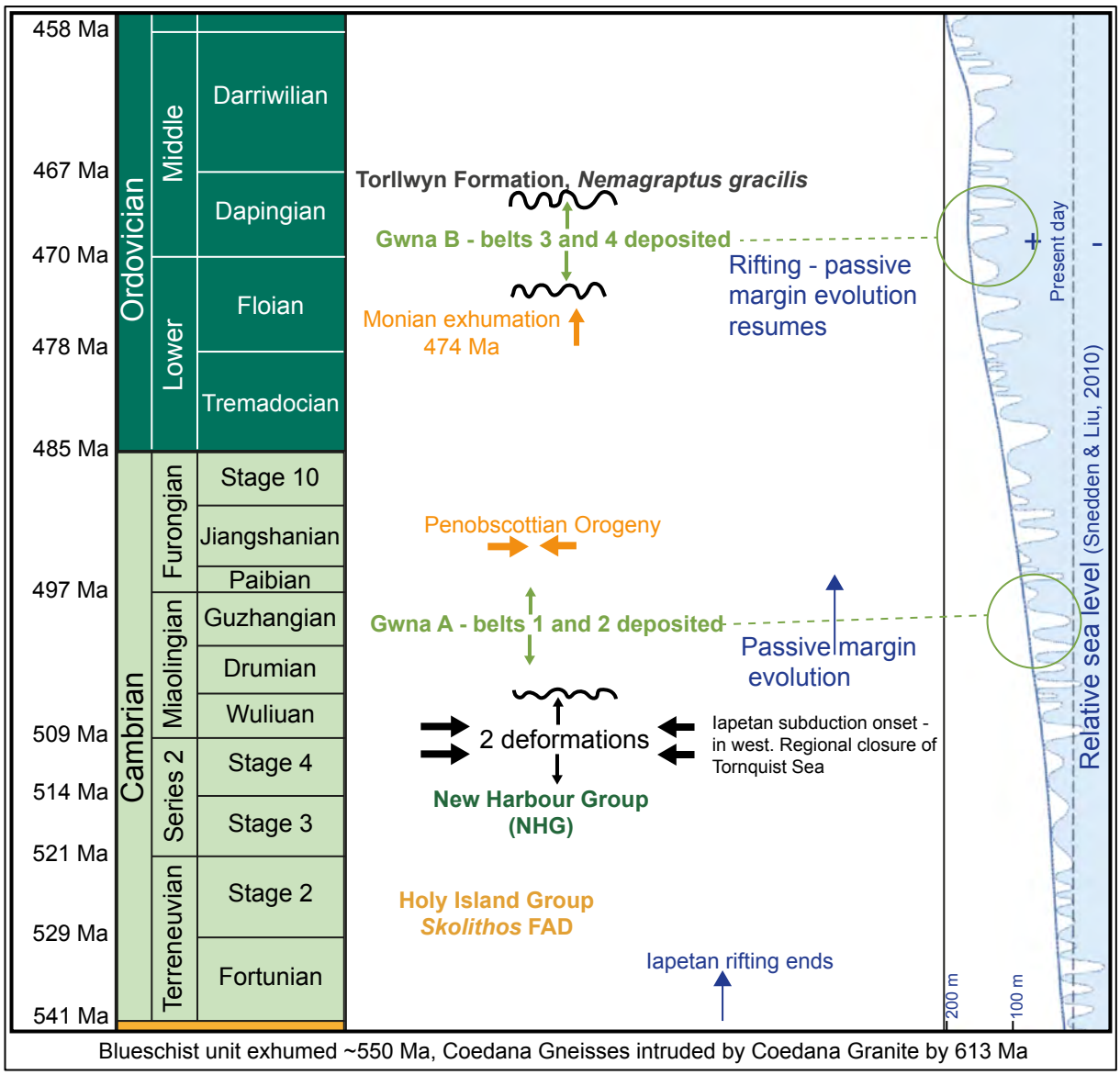

Figure 5.2 Model for the deposition of Gwna Group successions Gwna A and Gwna B framed within known Appalachian – British Caledonide tectonic events (Waldron *et al.*, 2014) related to the geological history of the Monian Supergroup, all of which occurred after exhumation of the Anglesey blueschist unit ~560 – 550 Ma, (Dallmeyer and Gibbons, 1987), post intrusion by the Coedana Granite ~613 Ma (Tucker and Pharaoh, 1991) into the Coedana Gneisses, metamorphic age ~666 Ma (Strachan *et al.*, 2007). Prior to 474 Ma (Asanuma *et al.*, 2017) and constrained by U-Pb zircon dates in Chapter 3, deposition of Gwna A in outcrop belts 1 and 2 overly the CASZ. Subsequent deformation in the Monian – Penobscottian Orogen interrupted Gwna Group deposition. Exhumation of the Monian Orogen at 474 Ma (Asanuma *et al.*, 2017) is expressed in the relic subaerial unconformity that crops out in outcrop belt 3, south of Porth Trefadog (Chapter 2). Deposition of Gwna Group lithofacies resumed (Gwna B), in the same style and with the same lithological composition of Gwna A (excepting minor local felsic volcanics) in outcrop

belts 3 and 4. Outcrop belt 4 Gwna Group overlies the New Harbour Group unconformably, but the New Harbour Group here, although polydeformed, lacks evidence for Monian Orogen deformation. Second order fluctuations in relative sea level are present during deposition of the Gwna Group (Snedden and Liu, 2010). Cambrian timescale (Ogg *et al*., 2016). *Skolithos* — first appearance datum (FAD) (Buatois and Mangano, 2011). *Nemagraptus gracilis* Graptolite Biozone in latest Dapingian Torllwyn Formation (Bates, 1972; Rushton and Fortey, 2000; Ogg *et al*., 2008).

---

the metamorphism and intrusion of the Coedana Complex predate the formation of the Monian Supergroup and are therefore not featured. Equally, later events are not represented, such as final Iapetan Ocean closure, which began in the west (West Avalonia) in maritime Canada and ended in the east (Britain and Ireland) with Ordovician western closure along a suture called the Red Indian Line (Williams *et al*., 1988). Closure was diachronous. Accretion was completed in Silurian East Avalonia along the Iapetus suture, which most authors agree is the Solway Line, situated considerably to the north of Anglesey, connecting the north of Britain (Avalonia) with the Southern Uplands (Laurentia) as well as, conjoining the north and south of Ireland (McKerrow and Soper, 1989).

Neoproterozoic to early Cambrian rifting opened the Iapetus Ocean, followed by passive margin evolution allows for deposition of the Holy Island and New Harbour Groups, their deformation and subsequent Gwna Group sedimentary succession – the first episode (in outcrop belts 1 and 2) prior to tectonic shortening in the Monian Orogen which onset ~ 490 Ma, according to Waldron *et al*. (2018). Early Ordovician exhumation of the New Harbour Group subaerial relic surface south of Porth Trefadog at the base of the Gwna Group in outcrop belt 3 took place < 474 Ma (Asanuma *et al*. 2017) and must have been followed by a return to passive margin conditions, at least locally, to allow for repeated deposition of the pre-orogenic Gwna Group lithofacies. It is difficult to reconcile such a setting within the broader backdrop of ongoing Iapetan closure at that time, but the Gwna Group provides evidence for the existence of tectonic

extension. Waldron *et al*., (2014) postulated a sinuous subduction suture for diachronous closure, and other lines of evidence point towards a geometry in the regional tectonics that allowed for separation of the strain effects. For example, the New Harbour Group in outcrop belt 4 is polydeformed in an equivalent manner to the pre-Monian Orogen state of the New Harbour Group in belt 3 and the CASZ in belt 2, however, it lacks evidence for the Monian event. This remains an open question.

Accretionary orogen hypothesis

The regional geological maps show, at a glance, that Anglesey and Lleyn are composed of multiple elongate, fault-bound and stacked geological units of varying genetic type, age and geological history. Barber and Max (1979) were first to publish an accretionary complex hypothesis that set the Gwna Group as a tectonic mélange within an encompassing tectonstratigraphy, formed in two separate collisional events. The accretionary orogen model depends entirely on the Gwna Group having formed tectonically, which is not supported by the field evidence demonstrated in this study. The current fragmented condition of the Anglesey and Lleyn Monian rocks has understandably led to many similar interpretations.

The Neoproterozoic Pacific-type, accretionary orogen hypothesis was suggested for the Anglesey and Lleyn Peninsula region by Kawai *et al*. (2007) and subsequently supported by Kusky *et al*. (2013), Saito *et al*. (2015), Asanuma *et al*. (2015) and Asanuma *et al*. (2017). However, this study has found strong evidence for the Gwna Group sedimentary succession that fundamentally contradicts the Pacific-style accretionary orogenic model. Examples of the irreconcilable facts include the following:

1. The Gwna Group would have to be a tectonic mélange – yet it has been shown here to be a coherent sedimentary succession, deposited in a passive margin setting. In addition, diagnostic features within the Gwna Group have been tested using criteria from many published mélange studies worldwide in tables 1.2 and 2.2 resulting in a clear indication that the Gwna Group is not a tectonic mélange.
2. Asanuma *et al*., (2015) specifically assert that the Gwna Group is older than the Holy Island and New Harbour Groups in an accretionary orogen. Yet, it is demonstrably younger: unconformable sedimentary relationships have been described in four locations on Anglesey where the simply deformed, low grade metamorphic Gwna Group overlies polydeformed metasediments of consistently higher metamorphic grade.
3. "*The Gwna Group, best exposed on Porth Dinllaen Peninsula, mostly consists of a 1 km-thick pile of pillow lavas, massive basaltic flows and minor pillow breccias, the pillows being largely undeformed*." Kawai *et al*. (2007. p. 15). This statement is incorrect, and misleading. This study has approached the Gwna Group from the standpoint of investigating the outcrop of the region, which is a sedimentary succession. The pillow basalts and associated seafloor sections of outcrop belts 1 and 2 are minor components of the Gwna Group that lie beneath the sedimentary succession, yet in the accretionary orogen hypothesis they are considered representative of the entire Gwna Group.
4. Exhumation of the blueschist unit took place 560 – 550 Ma (Dallmeyer and Gibbons, 1987). It has been demonstrated, in Chapter 3, that Gwna A is unlikely to be older than 537 Ma, which means the Gwna Group formed after the exhumation of the blueschist unit. The seafloor fault blocks occur in association with a series of lens-shaped mafic intrusions in restricted

sections of Gwna A in outcrop belts 1 and belt 2. An alternative hypothesis for the presence of these units, which accords with the ocean island pillow basalt geochemistry of Thorpe (1993), involves rifting and crustal thinning during the separation of Avalonia from Gondwana, followed by passive margin evolution, during which the Gwna Group was deposited.

5.3 Depositional, temporal and tectonic framework

- The Gwna Group is an unconformity bound, internally conformable, sedimentary sequence of many hundreds of discrete polymict debris flows and monomict slump beds interbedded within a background turbidite system that unconformably overlies polydeformed metasediments of the New Harbour Group and is unconformably overlain by the Torllwyn Formation.
- The Gwna Group records a passive margin sedimentary sequence that was deposited after the late Precambrian Avalonian orogeny and exhumation of the blueschist rocks of the Anglesey Penmynydd Zone. The Gwna Group was deposited, potentially in two marine sedimentary basins between the earliest Cambrian (< 537 Ma) to early Middle Ordovician (468 Ma) under tectonic conditions controlling the dispersal of the peri-Gondwanan terranes that gave rise to an extended period of passive margin evolution.
- There is no evidence in the Gwna Group sedimentary succession that indicates it was located in, or associated with, a subduction zone.
- There is tectonic discontinuity within the Gwna Group and, based on the K-Ar in phengite exhumation date of < 474 Ma for the New Harbour Group (Asanuma *et al*., 2017), this thesis suggests Gwna A, in outcrop

belts 1 and 2, was deposited before ~ 490 Ma. Gwna B, in outcrop belts 3 and 4 was deposited between 474 and 468 Ma. Deposition, throughout both time periods, occurred during passive margin evolution.

- The Gwna Group is fragmented and limited in outcrop and it is comprised of a repeated sequence that includes minor slump beds and large polymict debris flows therefore it is complex and hard to deconstruct. However, there is primary evidence throughout all outcrop regions in Anglesey and the Lleyn Peninsula for the sedimentary succession described in this thesis that demonstrates a shared genetic history between all outcrop belts of the Gwna Group, both compositionally and systematically.

The diachronous depositional framework proposed for the Gwna Group relies on a pivotal age constraint for the Monian Orogeny (Waldron *et al*., 2018) of < 474 ± 9 Ma (Asanuma *et al*., 2017). The Floian exhumation age was derived from a single sample, yet seven of the eight samples analysed (the ninth was unsuccessful) provided consistently Ediacaran to early Cambrian ages between 578 ± 11 and 530 ± 10 Ma (Asanuma *et al*., 2017). It has not been possible, within the confines of the current study, to interrogate work that underpins these ages. However, if for the purpose of discussion, the Floian age is withheld as subject to confirmation, the Gwna Group depositional framework takes on a relatively parsimonious character. It would be as follows;

1. Early Palaeozoic Rheic Ocean rifting followed post-collisional transform tectonics, the latter potentially associated with the exhumation of the Penmynyd Zone blueschist at 550 Ma (Dallmeyer and Gibbons, 1987) on the

northern margin of Gondwana (Nance *et al*., 2010).

2. The peri-Gondwanan terranes: the "ribbon continents" Avalonia, Ganderia, Meguma, Carolinia and Suwanee, accreted to Gondwana in the Neoproterozoic, began to rift from the supercontinent exploiting pre-existing sutures in the growth of the Iapetus Ocean and the incipient formation of the Rheic Ocean, between the terranes and Gondwana (Murphy *et al*., 2006; Nance *et al*., 2010; Murphy *et al*, 2010; Waldron *et al*., 2011; Nance *et al*., 2012).

3. Seafloor blocks in outcrop belt 1 are interpreted as the fragmented Monian basin floor underlying the Gwna Group sedimentary succession with a maximum depositional age of < 549 Ma (Asanuma *et al*., 2015).

4. Passive margin evolution was accompanied by ongoing crustal thinning as the Rheic Ocean widened, due to subduction driven slab-pull from the convergence of the Iapetus Ocean with Laurentia (Murphy *et al*., 2010).

5. The linear ensialic margin of the Gander continent, facing Avalonia and Meguma across a relatively narrow but broadening oceanic tract was the location of several sedimentary basins in at least one of which the earliest Monian Supergroup was deposited (Fig. 1.3). U-Pb zircon analysis of CASZ sample PT15.1 (Chapter 3) suggests a basin nearby with Meguma terrane affinity and a maximum depositional age of 585 Ma.

6. Terreneuvian deposition of the broadly proximal sand-dominated lithofacies of the Holy Island Group (Phillips, 1991a) ~ 529 Ma: the frequently cited 501 Ma maximum depositional age was excluded by the application of current

interpretative standards, in Chapter 3.

7. Rifting and continental drift continued between Gondwana and the peri-Gondwanan terranes.

8. Conformable deposition of the Terreneuvian New Harbour Group over the Holy Island Group.

9. Two collisional events impacted upon the CASZ, Holy Island and New Harbour Groups, subsequent exhumation, partly sub-aerial, revealed erosional surfaces.

10. Gwna Group deposition began to form on the margin between Ganderia, Avalonia and Meguma onto the marine basin floor, directly overlying fault blocks of deep-marine basalt, basalt pillows and sedimentary cover in outcrop belt 1 – most likely forming an asymmetrical basin above the footwall of an extensional fault. The hanging wall furnishing latest Precambrian to early Cambrian quartz arenite and Tonian carbonate clasts, the two main clast groups, into repeated occurrences of the polymict debris flow lithofacies.

11. Subsequent Gwna Group megacycle deposition of lithofacies A, B and C continued to be accumulate on the lower slopes and abyssal plains of the extensive Gander coastline in outcrop belts 1 and over the CASZ unconformity in outcrop belt 2. The megacycles were driven by normal sea level fluctuation accentuated by tectonic base level change: repeated crustal thinning and extensional faults related to rifting and continental drift – an environment in which the varied magnitude slope instability events the Gwna

Group records are commonplace.

12. The Gwna Group sedimentary megacycle system continued, progressively overstepping the New Harbour Group unconformity surfaces of both outcrop belts 3 (sub-aerial) and 4, with continued sampling of quartz arenite and Tonian carbonate clasts for lithofacies C.

13. A hypothesised episode – evidenced by the intense deformation limited to outcrop belt 2, that deforms the CASZ and overlying Gwna Group and is broadly contemporaneous with the wider Gwna Group system, involves a tectonic collision of a crustal fragment, now outboard of Anglesey and north Wales, the result of localised concomitant transform tectonics within the overall rifting/passive margin setting. In outcrop belt 3 there is evidence for this deformation in the New Harbour Group but the overlying Gwna Group, although gently folded, does not contain a well-developed cleavage.

14. The closure of both the Iapetus and Rheic Oceans was diachronous (Nance *et al*., 2010; Waldron *et al*., 2011). The change from regional rifting to convergence led finally to the formation of the supercontinent Pangea. Iapetan subduction concluded with Ordovician continental closure in the west (USA and Canada) and, in the east (Ireland and Britain), accretion was achieved in the Silurian (McKerrow and Soper, 1989). The Rheic Ocean continued to open at the expense of Iapetan subduction and closed between the Devonian and Carboniferous (Nance *et al*., 2010). The change from a continental drift setting brought passive margin evolution to an end and with it came the end of the Gwna Group sedimentary system.

15. The upper Gwna Group unconformity is overstepped by Middle Ordovician

marine sediments in outcrop belts 3 and 4 and outcrop belt 2 is overlain unconformably by Carboniferous Limestone.

The difference between the geological history directly above that excludes the Monian Orogeny exhumation date and the main hypothesis evidenced throughout this thesis relates to the further implications of the K-Ar phengite date offered by Asanuma *et al*. (2017). The New Harbour Group in outcrop belt 4 has experienced two episodes of tectonic deformation – the third event, the Monian Orogeny (Waldron *et al*., 2018), is evidenced by cleavage in the CASZ of outcrop belt 2 and the New Harbour Group of outcrop belt 3. If the exhumation date is correct, it must be concluded that the New Harbour Group of outcrop belt 4 was positioned sufficiently outboard to avoid the impacts of the convergence event and that passive margin Gwna Group deposition (Gwna B) resumed post exhumation, in the exact manner and system, sampling the same clast types as the Gwna Group prior to the collisional event (Gwna A).

Lithostratigraphy of the Monian Supergroup and Gwna Group

The British Geological Survey is currently reviewing the formal lithostratigraphy of Anglesey following a remapping project, to which this study was affiliated. A logical conclusion of this research is to offer comment on the Gwna Group, and its parent, the Monian Supergroup considering the current stratigraphy in the light of the new findings.

The Gwna Group must young from outcrop belt 1 – Lleyn to outcrop belt 4 – north Anglesey. There are two lines of evidence supporting this assertion: the presence of basin floor material that outcrops on Lleyn only and the Monian

Orogeny deformation that occurred within the time period(s) of Gwna Group deposition. It is possible that the four outcrop belts record sequential deposition, in other words, outcrop belt 2 overlies 1, and both are overlain progressively by 3 and then outcrop belt 4 represents the youngest Gwna Group sediments. However, it is also credible that outcrop belts 1 and 2 are broadly contemporaneous and laterally equivalent and that the same applies to outcrop belts 3 and 4. It is also entirely plausible that a combination of either scenario is true – that Lleyn is the base, and belt 2 is interleaved and partly laterally continuous.

In short, because there are no marker beds within the Gwna Group and because the main clast populations consist of the same lithologies throughout, it is not currently possible to attain greater clarity. Therefore, it is recommended that group status remains in force for the Gwna Group in both Anglesey and Lleyn, but that four subordinate formations are added - one for each of the four outcrop belts defined in this study. Minor faulted Gwna Group outcrop sections, such as the fragment that crops out at Carmel Head, on the north-west corner of Anglesey, should be allied to the most likely host formation – outcrop belt 3 in this case.

It is essential that the turbidite succession of the Church Bay Tuff Formation of outcrop belt 3 and 4 is incorporated clearly into the Gwna Group, without the current distinction, as, with the exception of the minor felsic ignimbrite horizons, the rocks record the turbidite system of the Gwna Group tripartite model. There are no grounds for separation: the formal stratigraphy should be updated to reflect the sedimentary system that operated in megacycles throughout the region, rather than isolating the turbidite lithofacies in two of the four outcrop belts.

It may become possible to correlate the formations following future research. In which case, the individual megacycles should be numbered or named, giving them each member status, which would recognise the accumulation of the repeated cycles over time within a sedimentary system that reflects the process sedimentology.

It would be reasonable to remove the Gwna Group from the Monian Supergroup, based on the wider significance of the basal unconformity and the homogenous nature of the Gwna sediments;

- The polydeformed metasedimentary rocks that underlie the Gwna Group record a shared history, demonstrated by the two deformation episodes

- The relic surface of the New Harbour Group exposed in outcrop belt 3 is likely to represent a substantial time period, and, the physical properties shared by three basal unconformities suggest similar duration

- The underlying metasediments may represent separate sedimentary basins, even in the case of CASZ, different provenance. In gross terms, the Gwna Group is ubiquitous and laterally homogeneous and as such, is unique in the region in recording an extended period of passive margin evolution along a drifting tectonic margin.

The Monian Supergroup would then comprise the remaining Holy Island and New Harbour Groups, but questions remain about stratigraphic units outside the supergroup that may be lateral equivalents. For example, the CASZ, shares with the New Harbour Group sedimentary protolith characteristics and the

unconformity/Gwna Group relationship. Although the CASZ is more deformed and this research raised questions about different provenance, there may be a lateral connection. The Monian Supergroup should be discarded.

References

ABBATE, E., BORTOLOTTI, V. & PASSERINI, P. 1970. Olistostromes and olistoliths. *Sedimentary Geology,* 4**,** 521-557.

ÁRKAI, P., SASSI, F. & DESMONS, J. 2007. Very low- to low-grade metamorphic rocks. *In:* FETTES, D. J. & DESMONS, J. (eds.) *Metamorphic rocks: a classification and glossary of terms: recommendations of the International Union of Geological Sciences Subcommission on the systematics of metamorphic rocks.* Cambridge, U.K.: Cambridge University Press.

ASANUMA, H., FUJISAKI, W., SATO, T., SAKATA, S., SAWAKI, Y., AOKI, K., OKADA, Y., MARUYAMA, S., HIRATA, T., ITAYA, T. & WINDLEY, B. F. 2017. New isotopic age data constrain the depositional age and accretionary history of the Neoproterozoic-Ordovician Mona Complex (Anglesey-Lleyn, Wales). *Tectonophysics,* 706-707**,** 164-195.

ASANUMA, H., OKADA, Y., FUJISAKI, W., SUZUKI, K., SATO, T., SAWAKI, Y., SAKATA, S., YAMAMOTO, S., HIRATA, T., MARUYAMA, S. & WINDLEY, B. F. 2015. Reconstruction of ocean plate stratigraphy in the Gwna Group, NW Wales: Implications for the subduction–accretion process of a latest Proterozoic trench-forearc. *Tectonophysics,* 662**,** 195-207.

BAILEY, R. H., SKEHAN, J. W., DREIER, R. B. & WEBSTER, M. J. 1989. Olistostromes of the Avalonian terrane of southeastern New England. . *In:* HORTON JR., J. W. & RAST, N. (eds.) *Mélanges and Olistostromes of the Appalachians.* Boulder, Colorado, USA: Geological Society of America.

BAKER, J. W. 1969. Correlation problems of metamorphosed Pre-Cambrian rocks in Wales and S.E. Ireland. *Geological Magazine,* 106**,** 249.

BARBER, A. J. 2013. The origin of mélanges: Cautionary tales from Indonesia. *Journal of Asian Earth Sciences,* 76**,** 428-438.

BARBER, A. J. & MAX, M. D. 1979. A new look at the Mona Complex (Anglesey, North Wales). *Journal of the Geological Society,* 136**,** 407-432.

BATES, D. E. B. 1972. The Stratigraphy of the Ordovician rocks of Anglesey. *Geological Journal,* 8**,** 29-58.

BAUERMAN, H. 1885. Report on the geology of country near the forty-ninth parallel of the north latitude west of the Rocky Mountains. . *Geological Survey of Canada, Report of Progress 1882–84,* Report of Progress 1882–84**,** 1-42.

BISHOP, J. W. & SUMNER, D. Y. 2006. Molar tooth structures of the Neoarchean Monteville Formation, Transvaal Supergroup, South Africa. I: Constraints on microcrystalline CaCO3 precipitation. *Sedimentology,* 53**,** 1049-1068.

BLAKE, J. F. 1888. On the Monian system of rocks. *Quarterly Journal of the Geological Society,* 44**,** 463-546.

BOTTING, J. P., CÁRDENAS, P. & PEEL, J. S. 2015. A crown-group demosponge from the early Cambrian Sirius Passet Biota, North Greenland. *Palaeontology,* 58**,** 35-43.

BOUMA, A. H. 2000. Coarse-grained and fine-grained turbidite systems as end member models: applicability and dangers. *Marine and Petroleum Geology,* 17**,** 137-143.

BRENCHLEY, P. J. & RAWSON, P. F. 2006. England and Wales through geological time. *In:* BRENCHLEY, P. J. & RAWSON, P. F. (eds.) *The Geology of England and Wales.* 2 ed. Bath, U.K.: Geological Society Publishing House.

BUATOIS, L. & MANGANO, M. G. 2011. *Ichnology,* Cambridge, UK, Cambridge University Press.

BURG, J.-P., BERNOULLI, D., SMIT, J., DOLATI, A. & BAHROUDI, A. 2008. A giant catastrophic mud-and-debris flow in the Miocene Makran. *Terra Nova,* 20**,** 188-193.

CAMERLENGHI, A. & PINI, G. A. 2009. Mud volcanoes, olistostromes and Argille scagliose in the Mediterranean region. *Sedimentology,* 56**,** 319-365.

CANFIELD, D. E., POULTON, S. W., KNOLL, A. H., NARBONNE, G. M., ROSS, G., GOLDBERG, T. & STRAUSS, H. 2008. Ferruginous Conditions Dominated Later Neoproterozoic Deep-Water Chemistry. *Science,* 321**,** 949-952.

CAVAZZA, W. & BARONE, M. 2010. Large-scale sedimentary recycling of tectonic mélange in a forearc setting: The Ionian basin (Oligocene–Quaternary, southern Italy).

CAWOOD, P. A., MCCAUSLAND, P. J. A. & DUNNING, G. R. 2001. Opening Iapetus: Constraints from the Laurentian margin in Newfoundland. *Geological Society of America Bulletin,* 113**,** 443-453.

CHERNIAK, D. J. & WATSON, E. B. 2003. Diffusion in Zircon. *Reviews in Mineralogy and Geochemistry,* 53 (1)**,** 113-143.

CLOOS, M. & SHREVE, R. L. 1988. Subduction-channel model of prism accretion, melange formation, sediment subduction, and subduction erosion at convergent plate margins: 2. Implications and discussion. *Pure and Applied Geophysics PAGEOPH,* 128**,** 501-545.

COCKS, L. R. M., McKERROW, W. S., VAN STAAL, C. R. 1997. The margins of Avalonia. Geology Magazine, 134 (5), 627-636.

CODEGONE, G., FESTA, A., DILEK, Y. & PINI, G. A. 2012. Small-scale polygenetic mélanges in the Ligurian accretionary complex, Northern Apennines, Italy, and the role of shale diapirism in superposed mélange evolution in orogenic belts. *Tectonophysics,* 568-569**,** 170-184.

COLLINS, A. S. & BUCHAN, C. 2004. Provenance and age constraints of the South Stack Group, Anglesey, UK: U-Pb SIMS detrital zircon data. *Journal of the Geological Society,* 161**,** 743-746.

CONDON, D. J. & BOWRING, S. A. 2011. Chapter 9. A user's guide to Neoproterozoic geochronology. *Geological Society, London, Memoirs,* 36**,** 135-149.

CORFU, F., HANCHAR, J. M., HOSKIN, P. W. O. & KINNI, P. 2003. Atlas of zircon textures. *Reviews in Mineralogy and Geochemistry,* 53 (1)**,** 469-500.

COUSINEAU, P. A. & ST-JULIEN, P. 1992. The Saint-Daniel Melange: Evolution of an accretionary complex in the Dunnage Terrane of the Quebec Appalachians. *Tectonics,* 11**,** 898-909.

COWAN, D. S. 1985. Structural styles in Mesozoic and Cenozoic mélanges in the western Cordillera of North America. *Geological Society of America Bulletin,* 96**,** 451.

COX, G. M., HALVERSON, G. P., STEVENSON, R. K., VOKATY, M., POIRIER, A., KUNZMANN, M., LI, Z. X., DENYSZYN, S. W., STRAUSS, J. V. & MACDONALD, F. A. 2016. Continental flood basalt weathering as a trigger for Neoproterozoic Snowball Earth. *Earth and Planetary Science Letters,* 446**,** 89-99.

DALLMEYER, R. D. & GIBBONS, W. 1987. The age of blueschist metamorphism in Anglesey, North Wales: evidence from 40Ar/39Ar mineral dates of the Penmynydd schists. *Journal of the Geological Society,* 144**,** 843-852.

DAVIS, D. W., WILLIAMS, I. S. & KROGH, T. E. 2003. Historical Development of Zircon Geochronology. *Reviews in Mineralogy and Geochemistry,* 53 (1)**,** 145-181.

DELA PIERRE, F., FESTA, A. & IRACE, A. 2007. Interaction of tectonic, sedimentary, and diapiric processes in the origin of chaotic sediments: An example from the Messinian of Torino Hill (Tertiary Piedmont Basin, northwestern Italy). *Geological Society of America Bulletin,* 119**,** 1107-1119.

DEWEY, J. F. 1969. Evolution of Appalachian/Caledonian Orogen. *Nature,* 222**,** 124-129.

DILEK, Y., FESTA, A., OGAWA, Y. & PINI, G. A. 2012. Chaos and geodynamics: Mélanges, mélange-forming processes and their significance in the geological record. *Tectonophysics,* 568-569**,** 1-6.

FAGGETTER, L. E., WIGNALL, P. B., PRUSS, S. B., SUN, Y., RAINE, R. J., NEWTON, R. J., WIDDOWSON, M., JOACHIMSKI, M. M. & SMITH, P. M. 2016. Sequence stratigraphy, chemostratigraphy and facies analysis of Cambrian Series 2 – Series 3 boundary strata in northwestern Scotland. *Geological Magazine,* 155**,** 865-877.

FAIRCHILD, I. J. 1991. Origins of Carbonate in Neoproterozoic Stromatolites and the Identification of Modern Analogs. *Precambrian Research,* 53**,** 281-299.

FAIRCHILD, I. J., EINSELE, G. & SONG, T. R. 1997. Possible seismic origin of molar tooth structures in Neoproterozoic carbonate ramp deposits, north China. *Sedimentology,* 44**,** 611-636.

FAIRCHILD, I. J. & HERRINGTON, P. M. 1989. A tempestite-stromatolite-evaporite association (Late Vendian, East Greenland): a shoreface-lagoon model. *Precambrian Research,* 43**,** 101-127.

FAIRCHILD, I. J., SPENCER, A. M., ALI, D. O., ANDERSON, R. P., ANDERTON, R., BOOMER, I., DOVE, D., EVANS, J. D., HAMBREY, M. J., HOWE, J., SAWAKI, Y., SHIELDS, G. A., SKELTON, A., TUCKER, M. E., WANG, Z. & ZHOU, Y. 2017. Tonian-Cryogenian boundary sections of Argyll, Scotland. *Precambrian Research*.

FAIRCHILD, I. J. & SPIRO, B. 1987. Petrological and isotopic implications of some contrasting Late Precambrian carbonates, NE Spitsbergen. *Sedimentology,* 34**,** 973-989.

FEDO, C. M., SIRCOMBE, K. N. & RAINBIRD, R. H. 2003. Detrital Zircon Analysis of the Sedimentary Record. *Reviews in Mineralogy and Geochemistry,* 53 (1)**,** 277-303.

FESTA, A., OGATA, K., PINI, G. A., DILEK, Y. & ALONSO, J. L. 2016. Origin and significance of olistostromes in the evolution of orogenic belts: A global synthesis. *Gondwana Research,* 39**,** 180-203.

FESTA, A., PINI, G. A., DILEK, Y. & CODEGONE, G. 2010. Mélanges and mélange-forming processes: a historical overview and new concepts. *International Geology Review,* 52**,** 1040-1105.

FINCH, R. J. & HANCHAR, J. M. 2003. Structure and Chemistry of Zircon and Zircon-Group Minerals. *Reviews in Mineralogy and Geochemistry,* 53 (1), 1-25.

FLORES, G. 1955. Les résultats des études pour les recherches pétroliféres en Sicile: Discussion. . *In:* COLOMBO, C. (ed.) *Proceedings of the 4th World Petroleum Congress.* Rome.

FLORES, G. 1956. The results of the studies on petroleum exploration in Sicily: discussion. . *In:* COLOMBO, C. (ed.). Rome.

FLÜGEL, E. 2010. *Microfacies of carbonate rocks,* Berlin-Heidelberg, Springer-Verlag.

FURNISS, G., RITTEL, J. F. & WINSTON, D. 1998. Gas buble and expansion crack origin of "molar-tooth" calcite structures in the middle Proterozoic, Western Montana. *Journal of Sedimentary Research,* 68, 104-114.

GEHRELS, G. 2012. Detrital zircon U-Pb geochronology: current methods and new opportunities. *In:* BUSBY, C. & AZOR, A. (eds.) *Tectonics of Sedimentary Basins - Recent Advances.* Blackwell Publishing Ltd.

GIBBONS, W. 1983a. Stratigraphy, subduction and strike-slip faulting in the Mona Complex of North Wales—a review. *Proceedings of the Geologists' Association,* 94, 147-163.

GIBBONS, W. 1983b. The Monian “Penmynydd Zone of Metamorphism” in Llyn, North Wales. *Geological Journal,* 18 (1), 21-41.

GIBBONS, W. 1987. Menai Strait fault system: An early Caledonian terrane boundary in north Wales. *Geology,* 15, 744.

GIBBONS, W. 1990. Transcurrent ductile shear zones and the dispersal of the Avalon superterrane. *Geological Society, London, Special Publications,* 51, 407-423.

GIBBONS, W. & BALL, M. J. 1991. A discussion of Monian Supergroup stratigraphy in northwest Wales. *Journal of the Geological Society,* 148, 5-8.

GIBBONS, W. & GYOPARI, M. 1986. A greenschist protolith for blueschist on Anglesey UK. *In:* EVANS, B. W. & BROWN, E. H. (eds.) *Blueschist and eclogites.*

GIBBONS, W. & HORÁK, J. M. 1990. Contrasting metamorphic terranes in northwest Wales. *Geological Society, London, Special Publications,* 51, 315-327.

GIBBONS, W. & HORÁK, J. M. 1996. The evolution of the Neoproterozoic Avalonian subduction system: Evidence from the British Isles. *In:* NANCE, D. R. & THOMPSON, M. D. (eds.) *Special Paper 304: Avalonian and related peri-Gondwanan terranes of the Circum-North Atlantic.* Boulder, Colorado, USA: Geological Society of America.

GIBBONS, W. & McCARROLL, D. 1993. *Geology of the country around Aberdaron, including Bardsey Island*. Memoir for 1:50 000 Geological Sheet 133.

GREENLY, E. 1896. The geology of the eastern corner of Anglesey. *Quarterly Journal of the Geological Society***,** 618-632.

GREENLY, E. 1919a. *The Geology of Anglesey. Volume 1.,* London, H. M. Stationery Office.

GREENLY, E. 1919b. *The Geology of Anglesey. Volume 2.,* London, H.M. Stationery Office.

GREENLY, E. 1920. *One inch geological map of Anglesey*. Geological Survey of Great Britain.

GROTZINGER, J. P. & JAMES, N. P. 2000. Precambrian carbonates: Evolution of understanding. *SEPM Special Publication,* 67.

GROTZINGER, J. P. & KNOLL, A. H. 1999. Stromatolites in Precambrian carbonates: evolutionary mileposts or environmental dipsticks? *Annual Review Earth and Planetary Sciences,* 27**,** 313-58.

GUTSCHER, M.-A., KUKOWSKI, N., MALAVIEILLE, J. & LALLEMAND, S. 1998. Material transfer in accretionary wedges from analysis of a systematic series of analog experiments. *Journal of Structural Geology,* 20**,** 407-416.

HALVERSON, G. P., DUDÁS, F. Ö., MALOOF, A. C. & BOWRING, S. A. 2007. Evolution of the 87Sr/86Sr composition of Neoproterozoic seawater. *Palaeogeography, Palaeoclimatology, Palaeoecology,* 256**,** 103-129.

HALVERSON, G. P., WADE, B. P., HURTGEN, M. T. & BAROVICH, K. M. 2010. Neoproterozoic chemostratigraphy. *Precambrian Research,* 182**,** 337-350.

HANCHAR, J. M. & WATSON, E. B. 2003. Zircon Saturation Thermometry. *Reviews in Mineralogy and Geochemistry,* 53 (1)**,** 89-112.

HAUGHTON, P., DAVIS, C., MCCAFFREY, W. & BARKER, S. 2009. Hybrid sediment gravity flow deposits – Classification, origin and significance. *Marine and Petroleum Geology,* 26**,** 1900-1918.

HAUGHTON, P. D. W. 2000. Evolving turbidite systems on a deforming basin floor, Tabernas, SE Spain. *Sedimentology,* 47**,** 497-518.

HERNÁNDEZ-MOLINA, F. J., CAMPBELL, S., BADALINI, G., THOMPSON, P., WALKER, R., SOTO, M., CONTI, B., PREU, B., THIEBLEMONT, A., HYSLOP, L., MIRAMONTES, E. & MORALES, E. 2017. Large bedforms on contourite terraces: Sedimentary and conceptual implications. *Geology,* 46**,** 27-30.

HERRINGTON, P. M. 1988. *Stratigraphy, sedimentology and diagenesis of Late Precambrian carbonates from the Upper Limestone Dolomite "series", Central East Greenland.* PhD thesis, University of Birmingham.

HIBBARD, J. P., VAN STAAL, C. R. & MILLER, B. V. 2007. Links among Carolinia, Avalonia, and Ganderia in the Appalachian peri-Gondwanan realm. 433**,** 291-311.

HIBBARD, J. P., VAN STAAL, C. R., RANKIN, D. W., WILLIAMS, H. 2006. Lithotectonic map of the Appalachian Orogen, Canada – United States of America. Geological Survey of Canada, Map 2096A, scale 1:1 500 000.

HIBBARD, J. W., H. 1979. Regional setting of the Dunnage Melange in the Newfoundland Appalachians. *American Journal of Science,* 279**,** 993-1021.

HORÁK, J. M., DOIG, R., EVANS, J. A. & GIBBONS, W. 1996. Avalonian magmatism and terrane linkage: New isotopic data from the Precambrian of North Wales. *Journal of the Geological Society,* 153**,** 91-99.

HORÁK, J. M. & EVANS, J. A. 2010. Early Neoproterozoic limestones from the Gwna Group, Anglesey. *Geological Magazine,* 148**,** 78-88.

HOSKIN, P. W. O. & SCHALTEGGER, U. 2003. The Composition of Zircon and Igneous and Metamorphic Petrogenesis. *Reviews in Mineralogy and Geochemistry,* 53 (1)**,** 27-62.

HOWELLS, M. F. 2007. *British Regional Guide: Wales,* Keyworth, Nottingham, UK, British Geological Society.

HSÜ, K. J. 1968. Principles of mélanges and their bearing on the Franciscan-Knoxville Paradox. *Geological Society of America Bulletin,* 79**,** 1063.

HUANG, C.-Y., CHIEN, C.-W., YAO, B. & CHANG, C.-P. 2008. The Lichi Mélange: A collision mélange formation along early arcward backthrusts during forearc basin closure, Taiwan arc-continent collision. *Geological Society of America Special Paper,* 436.

JAFFRÉS, J. B. D., SHIELDS, G. A. & WALLMANN, K. 2007. The oxygen isotope evolution of seawater: A critical review of a long-standing controversy and an improved geological water cycle model for the past 3.4 billion years. *Earth-Science Reviews,* 83**,** 83-122.

JAMES, N. P. & JONES, B. 2016. *Origin of Carbonate Sedimentary Rocks,* Chichester, West Sussex, UK, John Wiley & Sons.

JAMES, N. P., NARBONNE, G. M. & SHERMAN, A. G. 1998. Molar-tooth carbonates: Shallow subtidal facies of the mid- to late Proterozoic. *Journal of Sedimentary Research,* 68**,** 716-722.

KAWAI, T., WINDLEY, B. F., TERABAYASHI, M., YAMAMOTO, H., MARUYAMA, S. & ISOZAKI, Y. 2006. Mineral isograds and metamorphic zones of the Anglesey blueschist belt, UK: implications for the metamorphic development of a Neoproterozoic subduction-accretion complex. *Journal of Metamorphic Geology,* 24**,** 591-602.

KAWAI, T., WINDLEY, B. F., TERABAYASHI, M., YAMAMOTO, H., MARUYAMA, S., OMORI, S., SHIBUYA, T., SAWAKI, Y. & ISOZAKI, Y. 2007. Geotectonic framework of the Blueschist Unit on Anglesey–Lleyn, UK, and its role in the development of a Neoproterozoic accretionary orogen. *Precambrian Research,* 153**,** 11-28.

KENNEDY, M. J. 1979. The continuation of the Canadian Appalachians into the Caledonides of Britain and Ireland. *Geological Society, London, Special Publications,* 8**,** 33-64.

KLEMPERER, S. L., HOBBS, R. W. & FREEMAN, B. 1990. Dating the source of lower crystal reflectivity using BIRPS deep Seismic profiles across the lapetus suture. *Tectonophysics,* 173**,** 445-454.

KOHNSTAMM, M. A. & MANN, A. 1981. Transcurrent faulting and pre-Carboniferous Anglesey. *Nature,* 293**,** 762-762.

KOPF, A. J. 2002. Significance of mud diapirism.

KROGH, T. E. 1982. Improved accuracy of U-Pb ages by the creation of more concordant systems using an air abrasion technique. *Geochim Cosmochim Acta,* 46**,** 637-649.

KUANG, H. W. 2014. Review of molar tooth structure research. *Journal of Palaeogeography,* 3.

KUSKY, T. M., WINDLEY, B. F., SAFONOVA, I., WAKITA, K., WAKABAYASHI, J., POLAT, A. & SANTOSH, M. 2013. Recognition of ocean plate stratigraphy in accretionary orogens through Earth history: A record of 3.8billion years of sea floor spreading, subduction, and accretion. *Gondwana Research,* 24**,** 501-547.

LI, Z. X., BOGDANOVA, S. V., COLLINS, A. S., DAVIDSON, A., DE WAELE, B., ERNST, R. E., FITZSIMONS, I. C. W., FUCK, R. A., GLADKOCHUB, D. P., JACOBS, J.,

KARLSTROM, K. E., LU, S., NATAPOV, L. M., PEASE, V., PISAREVSKY, S. A., THRANE, K. & VERNIKOVSKY, V. 2008. Assembly, configuration, and break-up history of Rodinia: A synthesis. *Precambrian Research,* 160**,** 179-210.

LIU, Y. Q., GAO, L. Z. & LIU, Y. X. 2005. Neoproterozoic molar-tooth structure and constraint of depositional facies and environment in the North China platform in Jiangsu, Anhui and Liaoning, Eastern China. *Acta Geologica Sinica-English Edition,* 79**,** 533-539.

MANN, P. & GORDON, M. B. 2013. Tectonic Uplift and Exhumation of Blueschist Belts Along Transpressional Strike-Slip Fault Zones. *Subduction Top to Bottom.*

MARUYAMA, S., KAWAI, T. & WINDLEY, B. F. 2010. Ocean plate stratigraphy and its imbrication in an accretionary orogen: the Mona Complex, Anglesey-Lleyn, Wales, UK. *Geological Society, London, Special Publications,* 338**,** 55-75.

MASSON, D. G., MILSOM, J., BARBER, A. J., SIKUMBANG, N. & DWIYANTO, B. 1991. Recent Tectonics around the Island of Timor, Eastern Indonesia. *Marine and Petroleum Geology,* 8**,** 35-49.

MATLEY, C. A. 1899. On the geology of Northern Anglesey. *Quarterly Journal of the Geological Society,* 55**,** 635-675.

MATLEY, C. A. 1900. On the geology of Northern Anglesey : Part II. *Quarterly Journal of the Geological Society,* 56**,** 233-NP.

MATLEY, C. A. 1901. The Geology of Mynydd-y-garn (Anglesey). *Quarterly Journal of the Geological Society,* 57**,** 20-30.

MATLEY, C. A. 1928. The Pre-Cambrian complex and associated rocks of south-western Lleyn (Carnarvonshire). *Quarterly Journal of the Geological Society,* lxxxiv**,** 440-446.

MATTINSON, J. M. 2005. Zircon U–Pb chemical abrasion ("CA-TIMS") method: Combined annealing and multi-step partial dissolution analysis for improved precision and accuracy of zircon ages. *Chemical Geology,* 220**,** 47-66.

MAX, D. M. 1975. Precambrian rocks of south-east Ireland. *In:* HARRIS, A. L. (ed.) *A correlation of the Precambrian rocks in the British Isles.* Edinburgh: Geological Society of London Special Report.

MCARTHUR, J. M., HOWARTH, R. J. & SHIELDS, G. A. 2012. Strontium Isotope Stratigraphy. *Geologic Time Scale 2012, Vols 1 & 2***,** 127-144.

MCILROY, D. & HORÁK, J. M. 2006. The Neoproterozoic: the late Precambrian terranes that formed Estern Avalonia. *In:* BRENCHLEY, P. J. & RAWSON, P. F. (eds.) *The Geology of England and Wales.* 2 ed. Bath, U.K.: Geological Society Publishing House.

MCKERROW, W. S. & COCKS, L. R. M. 1986. Oceans, island arcs and olistostromes: the use of fossils in distinguishing sutures, terranes and environments around the Iapetus Ocean. *Journal of the Geological Society,* 143**,** 185-191.

MCKERROW, W. S. & SOPER, N. J. 1989. The Iapetus suture in the British Isles. *Geological Magazine,* 126.

MOORBATH, S. & SHACKLETON, R. M. 1966. Isotopic ages from the Precambrian Mona Complex of Anglesey, North Wales (Great Britain). *Earth and Planetary Science Letters,* 1**,** 113-117.

MOSHER, D. C., CAMPBELL, D. C., GARDNER, J. V., PIPER, D. J. W., CHAYTOR, J. D. & REBESCO, M. 2017. The role of deep-water sedimentary processes in shaping a continental margin: The Northwest Atlantic. *Marine Geology,* 393**,** 245-259.

MURPHY, J. B., GUTIÉRREZ-ALONSO, G., NANCE, R. D., FERNANDEZ-SUAREZ, J., KEPPIE, J. D., QUESADA, C., STRACHAN, R. A., DOSTAL, J. 2006. Origin of the Rheic Ocean: Rifting along a Neoproterozoic suture? *Geology,* 34 (5)**,** 325-328.

MURPHY, J. B., KEPPIE, J. D., NANCE, D. R. & DOSTAL, J. 2010. Comparative evolution of the Iapetus and Rheic Oceans: A North America perspective. *Gondwana Research,* 17**,** 482-499.

MUTTI, E., BERNOULLI, D., LUCCHI, F. R. & TINTERRI, R. 2009. Turbidites and turbidity currents from Alpine 'flysch' to the exploration of continental margins. *Sedimentology,* 56**,** 267-318.

MUTTI, E. & NORMARK, W. R. 1987. Comparing examples of modern and ancient turbidite systems: problems and concepts. *In:* LEGGET, J. K. & ZUFFA, G. G. (eds.) *Marine Clastic Sedimentology.* London: Graham and Trotman.

MUTTI, E. & RICCI LUCCHI, F. 1973. Turbidites of the northern Apennines, introduction to facies analysis (English translation by T.H. Nilsen, 1978). *International Geology Review,* 20**,** 125-166.

NAKA, K. & CHUJO, Y. 2001. Control of crystal nucleation and growth of calcium carbonate by synthetic substrates. *Chemistry of Materials,* 13**,** 3245-3259.

NAKA, K., TANAKA, Y. & CHUJO, Y. 2002. Effect of Anionic Starburst Dendrimers on the Crystallization of CaCO3in Aqueous Solution: Size Control of Spherical Vaterite Particles. *Langmuir,* 18**,** 3655-3658.

NANCE, D. R. & THOMPSON, M. D. 1996. Avalonian and related peri-Gondwanan terranes of the circum-North Atlantic: An introduciton. *In:* NANCE, D. R. & THOMPSON, M. D. (eds.) *Avalonian and related peri-Gondwanan terranes of the circum-North Altlantic.* Boulder, Colorado, USA: Geological Society of America.

NANCE, R. D., MURPHY, J. B. & KEPPIE, J. D. 2004. Nick Rast and the recognition of the Avalonian Arc. *Journal of Geodynamics,* 37**,** 437-455.

NANCE, R. D., GUTIÉRREZ-ALONSO, G., KEPPIE, J. D., LINNEMANN, U., MURPHY, J. B., QUESADA, C., STRACHAN, R. A., WOODCOCK, N. H. 2010 Evolution of the Rheic Ocean. Gondwana Research, 17, 194-222.

NANCE, R. D., GUTIÉRREZ-ALONSO, G., KEPPIE, J. D., LINNEMANN, U., MURPHY, J. B., QUESADA, C., STRACHAN, R. A., WOODCOCK, N. H. 2012 A brief history of the Rheic Ocean. Geoscience Frontiers, 3 (2), 125-135.

NUTT, M. J. C. & SMITH, E. G. 1981. Transcurrent faulting and the anomalous position of pre-Carboniferous Anglesey. *Nature,* 290**,** 492-495.

OGG, J. G., OGG, G. M. & GRADSTEIN, F. M. 2008. *The Concise Geologic Time Scale*.

OGG, J. G., OGG, G. M. & GRADSTEIN, F. M. 2016. *A concise geologic time scale 2016,* Amsterdam, Elsevier BV.

ORANGE, D. L. 1990. Criteria helpful in recognizing shear-zone and diapiric mélanges: Examples from the Hoh accretionary complex, Olympic Peninsula, Washington. *Geological Society of America Bulletin,* 102**,** 935-951.

PARRISH, R. R. & NOBLE, S. R. 2003. Zircon U-Th-Pb Geochronology by Isotope Dilution -- Thermal Ionization Mass Spectrometry (ID-TIMS). *Reviews in Mineralogy and Geochemistry,* 53 (1)**,** 183-213.

PETROV, P. Y. 2011. Molar tooth structures: Formation and specificity of carbonate diagenesis in the Late Precambrian, Middle Riphean Sukhaya Tunguska Formation of the Turukhansk Uplift, Siberia. *Stratigraphy and Geological Correlation,* 19**,** 247-267.

PHILLIPS, E. 1991a. The lithostratigraphy, sedimentology and tectonic setting of the Monian Supergroup, western Anglesey, North Wales. *Journal of the Geological Society,* 148**,** 1079-1090.

PHILLIPS, E. 1991b. Progressive deformation of the South Stack and New Harbour Groups, Holy Island, western Anglesey, North Wales. *Journal of the Geological Society,* 148**,** 1091-1100.

PHILLIPS, E. 2010. The Geology of Anglesey, North Wales: project scoping study. British Geological Survey.

PIPER, D. J. W. & DEPTUCK, M. 1997. FINE-GRAINED TURBIDITES OF THE AMAZON FAN: FACIES CHARACTERIZATION AND INTERPRETATION.

POLLOCK, J. C., HIBBARD, J. P. & VAN STAAL, C. R. 2012. A paleogeographical review of the peri- Gondwanan realm of the Appalachian orogen.

POLLOCK, M. D., KAH, L. C. & BARTLEY, J. K. 2006. Morphology of molar-tooth structures in precambrian carbonates: Influence of substrate rheology and implications for genesis. *Journal of Sedimentary Research,* 76**,** 310-323.

POTHIER, H. D., WALDRON, J. W. F., SCHOFIELD, D. I. & DUFRANE, S. A. 2015. Peri-Gondwanan terrane interactions recorded in the Cambrian–Ordovician detrital zircon geochronology of North Wales. *Gondwana Research,* 28**,** 987-1001.

PRATT, B. R. 1998. Molar-tooth structure in Proterozoic carbonate rocks: Origin from synsedimentary earthquakes, and implications for the nature and evolution of basins and marine sediment. *Geological Society of America Bulletin,* 110**,** 1028-1045.

PRATT, B. R. 2001. Oceanography, bathymetry and syndepositional tectonics of a Precambrian intracratonic basin: integrating sediments, storms, earthquakes and tsunamis in the Belt Supergroup (Helena Formation, ca. 1.45Ga), western North America. *Sedimentary Geology,* 141-142**,** 371-394.

PRAVE, A. R., FALLICK, A. E., THOMAS, C. W. & GRAHAM, C. M. 2009. A composite C-isotope profile for the Neoproterozoic Dalradian Supergroup of Scotland and Ireland. *Journal of the Geological Society,* 166**,** 845-857.

RAST, N., O'BRIEN, B. H. & WARDLE, R. J. 1976. Relationships between Precambrian and Lower Palaeozoic rocks of the 'Avalon Platform' in New Brunswick, the northeast Appalachians and the British Isles. *Tectonophysics,* 30**,** 315-338.

RAYMOND, L. A. (ed.) 1984. *Classification of melanges,* U.S.A.: Geological Society of America.

RAYMOND, L. A. & TERRANOVA, T. (eds.) 1984. *The melange problem - a review,* U.S.A.: Geological Society of America.

ROBERTS, N. M. W. & SPENCER, C. J. 2015. The zircon archive of continent formation through time. *Geological Society, London, Special Publications,* 389**,** 197-225.

ROBERTSON, A. H. F. 2000. Formation of melanges in the Indus Suture Zone, Ladakh Himalaya by successive subduction-related, collisional and post-collisional processes during Late Mesozoic-Late Tertiary time. *Tectonics of the Nanga Parbat Syntaxis and the Western Himalaya,* 170**,** 333-374.

ROONEY, A. D., MACDONALD, F. A., STRAUSS, J. V., DUDAS, F. O., HALLMANN, C. & SELBY, D. 2014. Re-Os geochronology and coupled Os-Sr isotope constraints on the Sturtian snowball Earth. *Proc Natl Acad Sci U S A,* 111**,** 51-6.

ROYDEN, L. H. 1993. THE TECTONIC EXPRESSION SLAB PULL AT CONTINENTAL CONVERGENT BOUNDARIES. *Tectonics,* 12**,** 303-325.

ROYDEN, L. H. & HUSSON, L. 2006. Trench motion, slab geometry and viscous stresses in subduction systems. *Geophysical Journal International,* 167**,** 881-905.

RUSHTON, A. W. A. & FORTEY, R. A. 2000. North Wales. *In:* FORTEY, R. A., HARPER, D. A. T., INGHAM, J. K., OWEN, A. W., PARKES, M. A., RUSHTON, A. W. A. & WOODCOCK, N. H. (eds.) *A Revised Correlation of Ordovician Rocks in the British Isles.* London, Bath: Geological Society of London.

SAITO, T., UNO, M., SATO, T., FUJISAKI, W., HARAGUCHI, S., LI, Y.-B., SAWAKI, Y., YAMAMOTO, S. & MARUYAMA, S. 2015. Geochemistry of accreted metavolcanic rocks from the Neoproterozoic Gwna Group of Anglesey–Lleyn, NW Wales, U.K.: MORB and OIB in the Iapetus Ocean. *Tectonophysics,* 662**,** 243-255.

SCHOFIELD, D. I., DAVIES, J. R., WATERS, R. A., WILLIAMS, M. & WILSON, D. 2008. A new Early Silurian turbidite system in Central Wales: insights into eustatic and tectonic controls on deposition in the southern Welsh Basin. *Geological Magazine,* 146**,** 121-132.

SCHOFIELD, D. I., POTTER, J., BARR, S. M., HORÁK, J. M., MILLAR, I. L. & LONGSTAFFE, F. J. 2016. Reappraising the Neoproterozoic 'East Avalonian' terranes of southern Great Britain. *Gondwana Research,* 35**,** 257-271.

SCHUSTER, D. C. 1979. Gwna Melange, Upper Precambrian Olistostromal Sequence, North Wales, United Kingdom: ABSTRACT. *AAPG Bulletin,* 63.

SCHUSTER, D. C. 1980. *The nature and origin of the Late Precambrian Gwna Melange, North Wales, United Kingdom. .* Unpublished thesis. Doctor of Philosophy in Geology. , University of Illinois at Urbana-Champaign.

ŞENGÖR, A. M. C. 2003. The repeated rediscovery of melanges and its implications for the possibility and the role of objective evidence in the scientific enterprise. *In:* DILEK, Y. & NEWCOMB, S. (eds.) *Special Paper 373: Ophiolite concept and the evolution of geological thought.* Boulder. Colorado: Geological Society of America.

SHACKLETON, R. M. 1951. The structural evolution of north wales. *Geological Journal,* 1**,** 261-297.

SHACKLETON, R. M. 1954a. Notes on the structure and relations of the Pre-Cambrian and Ordovician rocks of the south-western Lleyn (Caernarvonshire). *Geological Journal,* 1**,** 400 - 409.

SHACKLETON, R. M. 1954b. The structure and succession of Anglesey and the Lleyn peninsula. *Advancement of Science,* 11**,** 106 - 108.

SHACKLETON, R. M. 1969. The Precambrian of North Wales. *In:* WOOD, A. (ed.) *The Precambrian and Lower Palaeozoic rocks of Wales.* Cardiff: University of Wales Press.

SHACKLETON, R. M. 1975. Precambrian rocks of Wales. *In:* HARRIS, A. L., SHACKLETON, R. M., WATSON, J., DOWNIE, C., HARLAND, W. B. & MOORBATH, S. (eds.) *A correlation of the Precambrian rocks in the British Isles.* Edinburgh: Geological Society of London Special Report.

SHANMUGAM, G. 2016. Submarine fans: A critical retrospective (1950–2015). *Journal of Palaeogeography,* 5**,** 110-184.

SHANMUGAM, G., MOIOLA, R. J., MCPHERSON, J. G. & O'CONNELL, S. 1988. Comparison of turbidite facies associations in modern passive-margin Mississippi fan with ancient active-margin fans. *Sedimentary Geology,* 58**,** 63-77.

SHIELDS, G. A. 1999. Working towards a new stratigraphic calibration scheme for the Neoproterozoic–Cambrian. *Eclogae Geologicae Helvetiae,* 92**,** 221-233.

SHIELDS, G. A. 2002. 'Molar-tooth microspar': a chemical explanation for its disappearance ~ 750 Ma. *Terra Nova,* 14**,** 108-113.

SHIELDS-ZHOU, G. A. 2016. A new rock-based definition for the Cryogenian Period (circa 720 – 635 Ma). *Episodes,* 39.

SHREVE, R. L. & CLOOS, M. 1986. Dynamics of sediment subduction, melange formation, and prism accretion. *Journal of Geophysical Research,* 91**,** 10229.

SILVER, E. A. & BEUTNER, E. C. 1980. Melanges. *Geology,* 8**,** 32.

SILVER, E. A., BREEN, N. A., PRASETYO, H. & HUSSONG, D. M. 1986. Multibeam Study of the Flores Backarc Thrust Belt, Indonesia. *Journal of Geophysical Research,* 91**,** 3489-3500.

SKELTON, A., LEWERENTZ, A., KLEINE, B., WEBSTER, D. & PITCAIRN, I. 2015. Structural Channelling of Metamorphic Fluids on Islay, Scotland: Implications for Paleoclimatic Reconstruction. *Journal of Petrology,* 56**,** 2145-2172.

SMITH, A. G. 1968. The Origin and Deformation of Some "Molar-Tooth" Structures in the Precambrian Belt-Purcell Supergroup. . *The Journal of Geology,* 76**,** 426-443.

SNEDDEN, J. W. & LIU, C. 2010. A compilation of Phanerozoic sea-level change, coastal onlaps and recommended sequence designations. *Search and Discovery Article.* AAPG.

SØNDERHOLM, M., FREDERIKSEN, K. S., SMITH, M. P. & TIRSGAARD, H. 2008. Neoproterozoic sedimentary basins with glacigenic deposits of the East Greenland Caledonides. 202**,** 99-136.

SPENCE, G. H., LE HERON, D. P. & FAIRCHILD, I. J. 2016. Sedimentological perspectives on climatic, atmospheric and environmental change in the Neoproterozoic Era. *Sedimentology,* 63**,** 253-306.

SPENCER, C. J., KIRKLAND, C. L. & TAYLOR, R. J. M. 2016. Strategies towards statistically robust interpretations of in situ U–Pb zircon geochronology. *Geoscience Frontiers,* 7**,** 581-589.

STOW, D. 2009. Bedform-velocity matrix: The estimation of bottom current velocity from bedform observations. *Geology,* 37**,** 327-330.

STOW, D. & LOVELL, J. P. B. 1979. Contourites - Their Recognition in Modern and Ancient Sediments. *Earth-Science Reviews,* 14**,** 251-291.

STOW, D. & MAYALL, M. 2000. Deep-water sedimentary systems: New models for the 21st century. *Marine and Petroleum Geology,* 17**,** 125-135.

STRACHAN, R. A., COLLINS, A. S., BUCHAN, C., NANCE, R. D., MURPHY, J. B. & D'LEMOS, R. S. 2007. Terrane analysis along a Neoproterozoic active margin of Gondwana: insights from U-Pb zircon geochronology. *Journal of the Geological Society,* 164**,** 57-60.

STRAUSS, J. V., ROONEY, A. D., MACDONALD, F. A., BRANDON, A. D. & KNOLL, A. H. 2014. 740 Ma vase-shaped microfossils from Yukon, Canada: Implications for Neoproterozoic chronology and biostratigraphy. *Geology,* 42**,** 659-662.

SWANSON-HYSELL, N. L., MALOOF, A. C., CONDON, D. J., JENKIN, G. R. T., ALENE, M., TREMBLAY, M. M., TESEMA, T., ROONEY, A. D. & HAILEAB, B. 2015. Stratigraphy and geochronology of the Tambien Group, Ethiopia: Evidence for globally synchronous carbon isotope change in the Neoproterozoic. *Geology,* 43.

SWANSON-HYSELL, N. L., ROSE, C. V., CALMET, C. C., HALVERSON, G. P., HURTGEN, M. T. & MALOOF, A. C. 2010. Cryogenian glaciation and the onset of carbon-isotope decoupling. *Science,* 328**,** 608-11.

THORPE, R. S. 1972. Possible Subduction Zone Origin for Two Precambrian Calc-Alkaline Plutonic Complexes from Southern Britain. *Geological Society of America Bulletin,* 83**,** 3663.

THORPE, R. S. 1993. Geochemistry and eruptive environment of metavolcanic rocks from the Mona complex of Anglesey, North Wales, U.K. *Geological Magazine,* 130**,** 85-91.

TIETZSCH-TYLER, D. & PHILLIPS, E. 1989. Extended Abstract; Correlation of the Monian Supergroup in NW Anglesey with the Cahore Group in SE Ireland. *Journal of the Geological Society,* 146**,** 417-418.

TIETZSCH-TYLER, D. & PHILLIPS, E. 1996. Precambrian and Early Caledonian Orogeny in South-East Ireland. *Irish Journal of Earth Sciences,* 15**,** 19-39.

TREAGUS, J. E., TREAGUS, S. H. & WOODCOCK, N. H. 2012. The significance of the boundary between the Rhoscolyn and New Harbour formations on Holy Island, North Wales, to the deformation history of Anglesey. *Geological Magazine,* 150**,** 519-535.

TUCKER, R. D. & PHARAOH, T. C. 1991. U-Pb zircon ages for Late Precambrian igneous rocks in southern Britain. *Journal of the Geological Society,* 148**,** 435-443.

VAN STAAL, C. R., SULLIVAN, R. W. & WHALEN, J. B. 1996. Provenanace and tectonic history of the Gander Zone in the Caledonian/Appalachian

orogen: Implications for the origin and assembly of Avalon. *In:* NANCE, D. R. & THOMPSON, M. D. (eds.) *Special Paper 304: Avalonian and related peri-Gondwanan terranes of the Circum-North Atlantic.* Boulder, Colorado, USA: Geological Society of America.

VAN STAAL, C. R., DEWEY, J. F., MAC NIOCAILL, C. & MCKERROW, W. S. 1998. The Cambrian-Silurian tectonic evolution of the northern Appalachians and British Caledonides: history of a complex, west and southwest Pacific-type segment of Iapetus. *Geological Society, London. Special Publication,* 143**,** 199-242.

VAN STAAL, C. R., BARR, S. M. & MURPHY, J. B. 2012. Provenance and tectonic evolution of Ganderia: Constraints on the evolution of the Iapetus and Rheic oceans. *Geology,* 40**,** 987-990.

VEIZER, J., ALA, D., AZMY, K., BRUCKSCHEN, P., BUHL, D., BRUHN, F., CARDEN, G. A. F., DIENER, A., EBNETH, S., GODDERIS, Y., JASPER, T., KORTE, C., PAWELLEK, F., PODLAHA, O. G. & STRAUSS, H. 1999. $^{87}Sr/^{86}Sr$, δ^{13} and δ^{18} evolution of Phanerozoic seawater. *Chemical Geology,* 161**,** 59-88.

VERMEESCH, P. 2004. How many grains are needed for a provenance study? *Earth and Planetary Science Letters,* 224**,** 441-451.

VERMEESCH, P. 2012. On the visualisation of detrital age distributions. *Chemical Geology,* 312-313**,** 190-194.

VERMEESCH, P. 2018. IsoplotR : A free and open toolbox for geochronology. *Geoscience Frontiers*.

WAKABAYASHI, J. 2011. Mélanges of the Franciscan Complex, California: Diverse structural settings, evidence for sedimentary mixing, and their connection to subduction processes. 480**,** 117-141.

WAKITA, K. & METCALFE, I. 2005. Ocean Plate Stratigraphy in East and Southeast Asia. *Journal of Asian Earth Sciences,* 24**,** 679-702.

WALDRON, J. W. F., SCHOFIELD, D. I., MURPHY, J. B. & THOMAS, C. W. 2014. How was the Iapetus Ocean infected with subduction? *Geology,* 42**,** 1095-1098.

WALDRON, J. W. F., SCHOFIELD, D. I., PEARSON, G., SARKAR, C., LUO, Y. A. N. & DOKKEN, R. 2018. Detrital zircon characterization of early Cambrian sandstones from East Avalonia and SE Ireland: implications for terrane affinities in the peri-Gondwanan Caledonides. *Geological Magazine***,** 1-16.

WALDRON, J. W. F., SCHOFIELD, D. I., WHITE, C. E. & BARR, S. M. 2011. Cambrian successions of the Meguma Terrane, Nova Scotia, and Harlech Dome,

North Wales: dispersed fragments of a peri-Gondwanan basin? *Journal of the Geological Society,* 168**,** 83-98.

WALDRON, J. W. F., WHITE, C. E., BARR, S. M., SIMONETTI, A. & HEAMAN, L. M. 2009. Provenance of the Meguma terrane, Nova Scotia: rifted margin of early Paleozoic Gondwana. *Canadian Journal of Earth Sciences,* 46**,** 1-8.

WALTER, M. R., VEEVERS, J. J., CALVER, C. R., GORJAN, P. & HILL, A. C. 2000. Dating the 840–544 Ma Neoproterozoic interval by isotopes of strontium, carbon, and sulfur in seawater, and some interpretative models. . *Precambrian Research,* 100**,** 371-433.

WESTBROOK, G. K. & SMITH, M. J. 1983. Long decollements and mud volcanoes: Evidence from the Barbados Ridge Complex for the role of high pore-fluid pressure in the development of an accretionary complex. *Geology,* 11.

WILLIAMS, H., COLMAN-SADD, S. P. & SWINDEN, H. S. 1988. Tectonic-stratigraphic subdivisions of central Newfoundland. In , pp. 91–98. Geological Survey of Canada Paper 88–1B. *Geological Survey of Canada* Paper 88-1B**,** 91-98.

WOOD, D. S. 1974. Ophiolites Melanges Blueschists and Ignimbrites Early Caledonian Subduction in Wales? *In:* DOTT, R. H. & SHAVER, R. H. (eds.) *Modern and ancient geosynclinal sedimentation.* SEPM.

WOODCOCK, N. H. 1979. The use of slump structures as palaeoslope orientation estimators. *Sedimentology,* 26**,** 83-99.

WOODCOCK, N. H. & MORRIS, J. H. 1999. Debris flows on the Ordovician margin of Avalonia: Lady Port Formation, Manx Group, Isle of Man.

ZAGOREVSKI, A., VAN STAAL, C. R., MCNICOLL, V. J., HARTREE, L. & ROGERS, N. 2012. Tectonic evolution of the Dunnage Mélange tract and its significance to the closure of Iapetus. *Tectonophysics,* 568-569**,** 371-387.

Appendix 1. Zircon geochronology mass spectrometry. Primary data - Part A

			Concentrations											Ratios			
#Sample + #analysis		#Sample + comments	^{204}Pb	f206c	^{206}Pb	^{207}Pb	^{208}Pb	^{232}Th	^{235}U	Th/U	Pbppm	Thppm	Uppm	$^{238}U/^{206}Pb$	1s %	$^{207}Pb/^{206}Pb$	1s %
A14.16_12	12	A14.16 - detrital	-4	0.0	382974	23244	73684	1347103	31001	0.6	90	450	795	9.60	1.9	0.060	1.01
A14.16_07	7		23	0.1	307945	22737	18687	202385	14832	0.2	66	68	381	5.70	1.9	0.073	1.01
A14.16_10	10		83	3.1	47552	2801	4829	101888	4643	0.3	10	34	119	11.52	2.0	0.058	1.18
A14.16rd5_02	24		80	5.5	26195	1500	2641	89187	2953	0.3	6	23	79	12.98	1.3	0.056	1.46
A14.16rd5_04	26		13	2.0	10196	1091	4986	58851	279	2.0	3	15	8	3.21	2.6	0.105	1.67
A14.16.RD4a_4	17		49	1.8	48104	2898	17643	335619	4177	1.0	13	112	107	10.15	1.9	0.060	1.18
A14.16.RD4a_3	16		3	0.1	82448	6139	10445	120707	4053	0.4	19	40	104	5.90	1.9	0.074	1.17
A14.16_11	11		128	1.1	167177	21959	40709	242036	3905	0.8	43	81	100	2.77	1.9	0.130	0.95
A14.16.RD4a_2	15		37	0.9	68654	4649	20206	305586	4444	0.9	18	102	114	7.75	2.0	0.067	1.34
A14.16.RD4a_8	21		57	0.2	443913	52150	72154	509478	11836	0.6	107	170	304	3.16	1.9	0.116	1.01
A14.16_01	1		186	2.2	150551	9727	45240	774143	11899	0.8	39	259	305	9.30	1.8	0.063	1.11
A14.16_09	9		104	1.1	153529	16078	72334	498209	4697	1.4	45	166	121	3.63	2.1	0.103	1.00
A14.16.RD4a_1	13		115	0.8	244137	15701	31142	566484	18698	0.4	55	189	480	9.07	1.9	0.064	1.08
A14.16rd5_01	23		114	0.6	311396	28092	49397	537412	12441	0.4	77	138	335	4.49	2.0	0.090	1.08
A14.16_04	4		103	2.1	87990	5042	21227	531893	10651	0.7	21	178	273	14.13	1.9	0.057	1.06
A14.16_05	5		110	4.3	44988	3100	28189	496891	3794	1.7	14	166	97	9.97	2.0	0.065	2.44
A14.16.RD4a_6	19		-49	-3.0	29011	1766	8637	232018	3601	0.8	7	78	92	14.53	2.1	0.058	2.16
A14.16_03	3		36	0.7	87587	5836	18718	586834	7484	1.0	21	196	192	9.87	2.7	0.065	2.21
A14.16_02	2		133	2.3	102711	6808	32099	684458	8601	1.0	27	229	221	9.96	1.9	0.066	1.03
A14.16rd5_03	25		-14	-0.9	27644	1707	9396	323329	3294	0.9	8	83	89	13.83	1.4	0.060	1.14
A14.16_08	8		33	6.8	8521	527	146	1959	991	0.0	2	1	25	13.77	2.4	0.061	2.19
A14.16.RD4a_9	22		91	2.7	57299	3909	12981	252670	5166	0.6	14	84	133	10.70	1.9	0.067	1.49
~~A14.16_06~~	~~6~~	~~high common Pb~~	~~1286~~	~~1.1~~	~~1559383~~	~~303100~~	~~139878~~	~~1129376~~	~~49333~~	~~0.3~~	~~376~~	~~377~~	~~1266~~	~~3.05~~	~~5.3~~	~~0.192~~	~~1.05~~
~~A14.16.RD4a_10~~	~~14~~	~~not zircon~~	~~106~~	~~3260.6~~	~~37~~	~~33~~	~~74~~	~~14~~	~~4~~	~~0.0~~	~~0~~	~~0~~	~~0~~	~~-54.16~~	~~48.9~~	~~0.337~~	~~51.80~~
~~A14.16.RD4a_7~~	~~20~~	~~not zircon~~	~~34~~	~~806.4~~	~~39~~	~~28~~	~~62~~	~~7~~	~~1~~	~~0.1~~	~~0~~	~~0~~	~~0~~	~~135.56~~	~~68.6~~	~~0.527~~	~~38.90~~
~~A14.16.RD4a_5~~	~~18~~	~~not zircon~~	~~-28~~	~~-737.5~~	~~39~~	~~25~~	~~81~~	~~0~~	~~-5~~	~~0.0~~	~~0~~	~~0~~	~~0~~	~~-42.63~~	~~32.5~~	~~0.457~~	~~39.49~~
A15.1.rd5_04	27	A15.1 - volcanic	70	1.1	112472	7014	18305	397301	8463	0.5	23	95	201	8.85	1.5	0.062	0.93
A15.1_08	8		71	1.5	82049	4979	13469	317351	6929	0.5	20	85	186	10.17	1.9	0.060	1.17
A15.1.rd5_02	25		-5	-0.1	86274	7874	7124	77972	2881	0.3	17	19	68	3.93	1.6	0.090	0.94
A15.1.rd5_05	28		-25	-0.4	112116	7279	29415	576816	7571	0.8	25	138	179	8.06	1.5	0.064	0.87
A15.1_20	20		100	0.9	171684	16542	26322	250763	5436	0.5	42	67	146	3.79	2.0	0.093	1.05
A15.1.rd5_06	29		85	1.5	88346	10632	40560	326278	2151	1.5	24	78	51	2.84	1.8	0.118	0.96
A15.1_12	12		51	2.5	35373	2214	8538	204507	2955	0.7	9	55	79	9.98	2.1	0.060	1.43
A15.1_21	21		-3	-0.1	93316	5725	21982	554037	7860	0.7	24	148	211	10.11	1.8	0.060	1.13
A15.1_17	17		149	5.7	46207	2899	20306	481306	3600	1.3	14	128	97	9.47	1.9	0.061	1.21
A15.1_10	10		-16	-0.5	51550	3183	12523	309058	4431	0.7	13	82	119	10.17	1.9	0.060	1.11
A15.1_14	14		-1	0.0	82305	5085	17495	428782	6835	0.6	21	114	184	10.11	2.0	0.060	1.12
A15.1_23	23		75	2.4	43053	8292	19418	105240	682	1.5	14	28	18	1.92	2.6	0.187	1.05
A15.1rd6_01	30		176	1.1	273629	17621	82291	1320960	18759	0.8	50	289	355	8.23	1.4	0.064	0.73
A15.1_19	19		87	1.9	82900	5264	22012	481619	6605	0.7	22	129	178	9.50	1.9	0.062	1.15
A15.1_11	11		103	2.1	88384	5441	29424	710026	7322	1.0	24	189	197	10.09	1.9	0.060	1.05
A15.1.rd5_03	26		37	0.6	103337	6730	10955	229043	7178	0.3	21	55	170	8.24	1.3	0.064	0.86
A15.1_15	15		103	1.7	94991	11810	29436	226900	2267	1.0	27	61	61	2.85	2.0	0.122	1.02
A15.1_07	7		-124	-0.9	205965	22256	52935	446587	5683	0.8	55	119	153	3.33	2.0	0.106	1.02
A15.1_09	9		-73	-1.9	67857	4251	15410	350486	5353	0.6	17	94	144	9.44	1.9	0.062	1.15
A15.1_16	16		73	1.1	113074	7243	39669	896383	8821	1.0	31	239	237	9.38	1.9	0.062	1.23
A15.1_03	3		62	1.1	100430	6327	15183	354351	8084	0.4	24	95	217	9.76	1.9	0.062	1.07
A15.1_01	1		62	1.3	85994	5424	21387	533916	7076	0.7	22	142	190	10.08	1.9	0.061	1.03
A15.1_05	5		178	0.7	382247	40811	38102	338670	12151	0.3	90	90	327	3.80	1.8	0.104	0.96
A15.1_02	2		122	0.6	327043	29224	44399	1044516	13339	0.8	79	279	359	4.91	1.9	0.087	1.08
A15.1_18	18		61	0.9	116045	7589	29184	777411	9053	0.9	30	207	244	9.51	1.9	0.064	1.09
A15.1_13	13		47	0.5	170817	11180	89369	2259219	13759	1.6	53	603	370	9.64	1.9	0.064	1.20
A15.1_22	22		25	0.4	112778	7237	37142	1080806	9515	1.1	31	288	256	10.26	1.9	0.063	1.16
A15.1.rd5_01	24		28	0.8	62145	4080	14365	339584	5012	0.7	14	81	119	9.57	1.5	0.065	1.10
A15.1_06	6		63	0.5	210172	14371	67634	2021245	16849	1.2	57	539	453	9.68	1.9	0.066	1.00
A15.1_04	4		83	1.3	108132	7525	14528	288276	8135	0.4	26	77	219	8.90	2.0	0.069	1.11
B15.1rd4a_01	1	B15.1 - volcanic	197	1.1	272865	37666	33856	196014	5502	0.4	46	43	104	2.46	1.3	0.136	0.57
B15.1rd4a_04a	4		150	0.5	485758	29568	68978	1602411	42748	0.4	78	350	809	10.68	1.2	0.060	0.60
B15.1rd4a_04b	5		55	0.2	445793	27260	68810	1585007	39373	0.5	72	346	745	10.61	1.3	0.061	0.71
B15.1rd4a_03	3		510	3.6	225059	22464	30144	174610	11180	0.2	37	38	212	6.07	1.5	0.101	1.94
B15.1rd4a_02	2		442	5.7	118835	14291	36803	527228	13832	0.4	23	115	262	14.29	1.3	0.119	2.83
CB14.1.rd4_10	46	CB14.1 - volcanic	-56	-0.9	109557	6432	22647	448513	9935	0.6	22	141	219	11.03	1.1	0.058	0.80
CB14.1.rd1_11	12		2	0.0	88551	4909	10776	291826	10017	0.4	16	92	221	13.82	1.2	0.055	1.06
CB14.1.rd1_06a	6		80	2.3	63738	3623	5357	152467	6510	0.3	11	48	143	12.65	1.3	0.057	1.23
CB14.1.rd1_12	13		-25	-0.1	469995	47563	5121	37721	13131	0.0	82	12	289	3.40	1.2	0.099	0.87
CB14.1.rd1_05	5		-46	-0.2	339338	36717	42023	292953	8780	0.5	65	92	193	3.14	1.1	0.106	0.74
CB14.1.rd1_18	19		101	0.3	575325	59887	71255	481048	15659	0.4	111	151	345	3.28	1.1	0.102	0.83
CB14.1.rd1_07	8		111	2.3	82934	6648	8797	92529	3334	0.4	15	29	73	4.93	1.3	0.079	0.94
CB14.1.rd5_02	48		135	3.2	73834	4499	7281	169256	6047	0.3	15	40	143	9.84	1.5	0.060	1.00
CB14.1.rd1_13	14		76	0.6	185634	35345	64275	248172	2841	1.2	45	78	63	1.86	1.4	0.187	0.82
CB14.1.rd1_04	4		46	1.1	74032	4018	14345	563086	11653	0.7	14	177	257	19.18	1.1	0.053	0.95
CB14.1.rd1_17	18		106	0.3	488140	94648	49665	199262	7413	0.4	99	63	163	1.85	1.2	0.192	0.77
CB14.1.rd1_03	3		25	0.2	228236	13943	62577	1262458	19197	0.9	48	396	423	10.26	1.1	0.060	0.80
CB14.1.rd4_09	45		9	0.3	58476	3230	7372	196642	7327	0.4	11	62	161	15.15	1.1	0.055	0.96
CB14.1.rd4_07a	41		34	0.3	216344	15546	75711	866917	11306	1.1	48	272	249	6.24	1.1	0.071	0.79
CB14.15rd5_04	55		24	0.6	65772	3971	36336	809016	5887	1.3	21	208	158	10.30	1.1	0.060	0.97
CB14.1.rd4_06b	40		72	2.2	60084	3198	20857	695333	9892	1.0	13	218	218	19.84	1.2	0.053	1.02
CB14.1.rd4_02b	35		-90	-0.9	171624	13709	17087	152470	7277	0.3	32	48	160	5.05	1.3	0.079	0.90
CB14.1.rd4_08a	43		-99	-0.3	429653	55383	40334	220468	9626	0.3	82	69	212	2.69	1.1	0.126	0.75
CB14.1.rd1_09	10		133	7.3	30369	2422	4409	46300	1258	0.5	6	15	28	5.04	1.5	0.079	1.16
CB14.1.rd4_07b	42		141	3.3	73089	5250	28691	316717	3756	1.2	17	99	83	6.29	1.3	0.071	1.01
CB14.1.rd1_26a	31		82	0.5	280427	29594	27439	185979	7820	0.3	53	58	172	3.39	1.2	0.103	0.73
CB14.1.rd5_01	47		39	0.3	186685	18751	4068	32078	5513	0.1	36	8	131	3.54	1.5	0.100	0.83
CB14.1.rd1_22a	24		119	0.9	239416	15499	7776	117620	16366	0.1	41	37	361	8.32	1.2	0.064	0.83
CB14.1.rd4_04	37		64	0.4	262068	19552	41963	406739	12405	0.5	51	128	273	5.73	1.2	0.074	0.88
CB14.1.rd4_03	36		-24	-0.3	155098	14803	24261	157297	4955	0.5	30	49	109	3.84	1.3	0.094	0.86
CB14.1.rd1_14	15		-22	-0.7	53183	3294	26431	489235	4294	1.6	13	154	95	9.88	1.2	0.061	0.88
CB14.1.rd1_10	11		-45	-0.3	302540	18921	42222	823515	24693	0.5	57	259	544	9.83	1.1	0.061	0.82
CB14.1.rd5_04	50		12	0.9	23047	1315	3898	130420	2631	0.5	5	31	62	13.67	1.7	0.056	1.28
CB14.1.rd4_02a	34		43	0.6	129390	10289	13364	117410	5654	0.3	24	37	125	5.27	1.3	0.078	0.92
CB14.1.rd1_19	20		79	2.1	66706	3680	6441	205298	9549	0.3	12	64	210	17.22	1.2	0.054	1.06
CB14.1.rd1_01	1		63	1.0	108142	6169	22952	728296	12572	0.8	21	229	277	14.23	1.1	0.056	0.92
CB14.1.rd4_05	38		98	1.8	98920	6105	21053	354617	8391	0.6	20	111	185	10.25	1.2	0.061	0.93

Appendix 1. Zircon geochronology mass spectrometry. Primary data - Part B

		Ratios					Ages and errors						Discordance	
#Sample - analysis	#Sample + comments	$^{207}Pb/^{235}U$	1s %	$^{206}Pb/^{238}U$	1s %	Rho	$^{207}Pb/^{206}Pb$	2s abs	$^{206}Pb/^{238}U$	2s abs	$^{207}Pb/^{235}U$	2s abs	6-38/7-6	6-38/7-35
A14.16_12	A14.16 - detrital	0.86	2.14	0.10	1.89	0.88	595	22	639	23	629	20	-7.3	-1.6
A14.16_07		1.76	2.11	0.18	1.85	0.88	1007	21	1043	36	1031	27	-3.6	-1.1
A14.16_10		0.69	2.28	0.09	1.95	0.86	520	26	537	20	533	19	-3.3	-0.6
A14.16rd5_02		0.60	1.96	0.08	1.31	0.67	465	32	478	12	476	15	-2.9	-0.5
A14.16rd5_04		4.49	3.05	0.31	2.55	0.84	1708	31	1746	78	1728	49	-2.3	-1.0
A14.16.RD4a_4		0.82	2.28	0.10	1.95	0.86	610	26	606	23	607	21	0.7	0.1
A14.16.RD4a_3		1.73	2.25	0.17	1.92	0.85	1047	24	1010	36	1021	29	3.6	1.1
A14.16_11		6.47	2.14	0.36	1.92	0.90	2098	17	1988	65	2042	37	5.3	2.7
A14.16.RD4a_2		1.18	2.37	0.13	1.96	0.83	827	28	782	29	794	26	5.5	1.5
A14.16.RD4a_8		5.08	2.12	0.32	1.86	0.88	1899	18	1775	58	1832	35	6.6	3.1
A14.16_01		0.93	2.15	0.11	1.84	0.86	705	24	658	23	668	21	6.6	1.6
A14.16_09		3.91	2.30	0.28	2.07	0.90	1682	19	1567	57	1616	37	6.8	3.0
A14.16.RD4a_1		0.97	2.18	0.11	1.90	0.87	727	23	674	24	686	22	7.3	1.8
A14.16rd5_01		2.78	2.26	0.22	1.99	0.88	1433	21	1297	47	1349	33	9.5	3.8
A14.16_04		0.56	2.21	0.07	1.95	0.88	489	23	441	17	449	16	9.8	1.7
A14.16_05		0.90	3.15	0.10	2.00	0.63	772	51	616	23	651	30	20.2	5.3
A14.16.RD4a_6		0.55	2.98	0.07	2.06	0.69	541	47	429	17	447	21	20.7	4.0
A14.16_03		0.91	3.48	0.10	2.68	0.77	788	46	622	32	659	33	21.0	5.6
A14.16_02		0.91	2.12	0.10	1.85	0.87	799	22	617	22	657	20	22.8	6.1
A14.16rd5_03		0.60	1.77	0.07	1.35	0.76	610	25	450	12	477	13	26.2	5.7
A14.16_08		0.61	3.23	0.07	2.37	0.73	648	47	452	21	485	25	30.2	6.9
A14.16.RD4a_9		0.87	2.41	0.09	1.90	0.79	852	31	576	21	635	23	32.4	9.3
~~A14.16_06~~	~~high common Pb~~	~~8.66~~	~~5.37~~	~~0.33~~	~~5.27~~	~~0.98~~	~~2759~~	~~17~~	~~1826~~	~~165~~	~~2303~~	~~93~~	~~33.8~~	~~20.7~~
~~A14.16.RD4a_10~~	~~not zircon~~	~~-0.86~~	~~71.22~~	~~-0.02~~	~~48.88~~	~~0.69~~	~~3649~~	~~792~~	~~-120~~	~~-120~~	~~-1979~~	#VALUE!	~~103.3~~	~~93.9~~
~~A14.16.RD4a_7~~	~~not zircon~~	~~0.54~~	~~78.90~~	~~0.01~~	~~68.64~~	~~0.87~~	~~4318~~	~~571~~	~~47~~	~~64~~	~~436~~	~~445~~	~~98.9~~	~~89.1~~
~~A14.16.RD4a_5~~	~~not zircon~~	~~-1.48~~	~~51.11~~	~~-0.02~~	~~32.46~~	~~0.64~~	~~4108~~	~~587~~	~~-153~~	~~-101~~	#VALUE!	#VALUE!	~~103.7~~	#VALUE!
A15.1.rd5_04	A15.1 - volcanic	0.96	1.81	0.11	1.55	0.86	668	20	690	20	685	18	-3.4	-0.8
A15.1_08		0.81	2.25	0.10	1.92	0.85	590	25	604	22	601	20	-2.5	-0.6
A15.1.rd5_02		3.16	1.85	0.25	1.60	0.86	1427	18	1461	42	1447	28	-2.4	-1.0
A15.1.rd5_05		1.09	1.75	0.12	1.52	0.87	742	18	754	22	751	18	-1.7	-0.5
A15.1_20		3.40	2.26	0.26	1.99	0.88	1497	20	1510	53	1504	35	-0.8	-0.4
A15.1.rd5_06		5.72	2.05	0.35	1.81	0.88	1926	17	1942	60	1934	35	-0.8	-0.4
A15.1_12		0.83	2.52	0.10	2.07	0.82	614	31	616	24	615	23	-0.3	-0.1
A15.1_21		0.82	2.16	0.10	1.85	0.85	606	24	608	21	608	20	-0.3	-0.1
A15.1_17		0.89	2.27	0.11	1.92	0.85	650	26	647	24	648	21	0.4	0.1
A15.1_10		0.81	2.18	0.10	1.87	0.86	607	24	604	22	605	20	0.5	0.1
A15.1_14		0.82	2.29	0.10	1.99	0.87	611	24	608	23	609	21	0.5	0.1
A15.1_23		13.42	2.77	0.52	2.57	0.93	2719	17	2698	112	2709	51	0.8	0.4
A15.1rd6_01		1.07	1.61	0.12	1.43	0.89	748	15	739	20	741	17	1.2	0.3
A15.1_19		0.89	2.20	0.11	1.88	0.85	657	25	645	23	648	21	1.8	0.4
A15.1_11		0.83	2.17	0.10	1.89	0.87	621	23	609	22	612	20	1.9	0.4
A15.1.rd5_03		1.08	1.59	0.12	1.34	0.84	755	18	738	19	742	17	2.2	0.5
A15.1_15		5.88	2.28	0.35	2.03	0.89	1982	18	1937	68	1959	39	2.3	1.1
A15.1_07		4.40	2.23	0.30	1.98	0.89	1736	19	1693	59	1712	36	2.4	1.1
A15.1_09		0.90	2.22	0.11	1.89	0.85	667	25	649	23	653	21	2.8	0.6
A15.1_16		0.91	2.25	0.11	1.88	0.84	680	26	653	23	659	22	4.0	0.9
A15.1_03		0.87	2.21	0.10	1.93	0.87	658	23	629	23	635	21	4.5	1.0
A15.1_01		0.84	2.15	0.10	1.89	0.88	641	22	610	22	616	20	4.9	1.1
A15.1_05		3.78	2.08	0.26	1.85	0.89	1698	18	1507	49	1588	33	11.2	5.1
A15.1_02		2.45	2.18	0.20	1.89	0.87	1365	21	1196	41	1257	31	12.4	4.9
A15.1_18		0.93	2.16	0.11	1.87	0.86	737	23	645	23	666	21	12.6	3.1
A15.1_13		0.92	2.24	0.10	1.89	0.85	743	25	636	23	660	21	14.4	3.6
A15.1_22		0.85	2.26	0.10	1.93	0.86	707	25	600	22	623	21	15.2	3.7
A15.1.rd5_01		0.93	1.90	0.10	1.55	0.81	767	23	641	19	669	18	16.5	4.3
A15.1_06		0.94	2.13	0.10	1.88	0.88	813	21	634	23	674	21	22.0	6.0
A15.1_04		1.06	2.33	0.11	2.05	0.88	888	23	687	27	735	24	22.7	6.6
B15.1rd4a_01	B15.1 - volcanic	7.60	1.41	0.41	1.28	0.91	2175	10	2197	48	2185	25	-1.0	-0.5
B15.1rd4a_04a		0.78	1.33	0.09	1.19	0.89	620	13	577	13	586	12	7.0	1.5
B15.1rd4a_04b		0.79	1.50	0.09	1.32	0.88	640	15	581	15	593	13	9.3	2.0
B15.1rd4a_03		2.28	2.48	0.16	1.54	0.62	1635	36	983	28	1207	34	39.9	18.6
B15.1rd4a_02		1.14	3.12	0.07	1.30	0.42	1934	51	436	11	774	33	77.5	43.7
CB14.1.rd4_10	CB14.1 - volcanic	0.72	1.40	0.09	1.15	0.82	516	18	559	12	551	12	-8.5	-1.6
CB14.1.rd1_11		0.55	1.58	0.07	1.18	0.75	426	24	450	10	446	11	-5.8	-0.9
CB14.1.rd1_06a		0.62	1.78	0.08	1.29	0.72	474	27	490	12	487	14	-3.5	-0.6
CB14.1.rd1_12		4.01	1.47	0.29	1.18	0.81	1606	16	1662	35	1637	24	-3.5	-1.5
CB14.1.rd1_05		4.65	1.36	0.32	1.14	0.84	1732	14	1783	35	1759	22	-2.9	-1.3
CB14.1.rd1_18		4.30	1.38	0.30	1.11	0.80	1668	15	1716	33	1694	23	-2.9	-1.3
CB14.1.rd1_07		2.20	1.63	0.20	1.33	0.82	1161	19	1191	29	1180	23	-2.6	-0.9
CB14.1.rd5_02		0.84	1.78	0.10	1.48	0.83	609	22	624	18	620	16	-2.5	-0.6
CB14.1.rd1_13		13.82	1.59	0.54	1.36	0.86	2712	14	2772	61	2737	30	-2.2	-1.3
CB14.1.rd1_04		0.38	1.47	0.05	1.11	0.76	323	22	328	7	327	8	-1.3	-0.2
CB14.1.rd1_17		14.32	1.42	0.54	1.19	0.84	2758	13	2789	54	2771	27	-1.1	-0.7
CB14.1.rd1_03		0.80	1.38	0.10	1.12	0.81	596	17	600	13	599	12	-0.6	-0.2
CB14.1.rd4_09		0.50	1.50	0.07	1.15	0.77	411	22	412	9	412	10	-0.2	-0.1
CB14.1.rd4_07a		1.57	1.38	0.16	1.13	0.82	956	16	958	20	957	17	-0.2	-0.1
CB14.15rd5_04		0.80	1.50	0.10	1.14	0.76	597	21	597	13	597	13	-0.1	0.0
CB14.1.rd4_06b		0.37	1.56	0.05	1.18	0.75	318	23	317	7	317	8	0.3	0.0
CB14.1.rd4_02b		2.15	1.56	0.20	1.27	0.81	1169	18	1164	27	1165	21	0.4	0.1
CB14.1.rd4_08a		6.47	1.30	0.37	1.05	0.81	2048	13	2036	37	2041	23	0.6	0.3
CB14.1.rd1_09		2.16	1.87	0.20	1.46	0.78	1175	23	1166	31	1169	26	0.7	0.2
CB14.1.rd4_07b		1.56	1.66	0.16	1.31	0.79	959	21	951	23	953	20	0.8	0.2
CB14.1.rd1_26a		4.21	1.38	0.30	1.17	0.85	1685	13	1668	34	1675	22	1.0	0.4
CB14.1.rd5_01		3.89	1.70	0.28	1.48	0.87	1622	15	1605	42	1612	27	1.0	0.4
CB14.1.rd1_22a		1.06	1.48	0.12	1.23	0.83	740	18	731	17	733	15	1.1	0.2
CB14.1.rd4_04		1.79	1.51	0.17	1.23	0.81	1049	18	1038	23	1041	20	1.1	0.3
CB14.1.rd4_03		3.38	1.54	0.26	1.28	0.83	1515	16	1491	34	1501	24	1.6	0.7
CB14.1.rd1_14		0.85	1.50	0.10	1.22	0.81	635	19	621	14	624	14	2.1	0.4
CB14.1.rd1_10		0.86	1.40	0.10	1.14	0.81	640	18	625	14	628	13	2.4	0.5
CB14.1.rd5_04		0.57	2.11	0.07	1.67	0.79	470	28	455	15	457	15	3.1	0.5
CB14.1.rd4_02a		2.05	1.57	0.19	1.27	0.81	1156	18	1120	26	1132	21	3.1	1.1
CB14.1.rd1_19		0.43	1.58	0.06	1.17	0.74	379	24	364	8	366	10	4.1	0.5
CB14.1.rd1_01		0.54	1.45	0.07	1.13	0.78	458	20	438	10	441	10	4.4	0.7
CB14.1.rd4_05		0.82	1.53	0.10	1.21	0.79	630	20	600	14	606	14	4.8	1.0

Appendix 1. Zircon geochronology mass spectrometry. Primary data - Part A

			Concentrations											Ratios			
#Sample + #analysis		#Sample + comments	^{204}Pb	f206c	^{206}Pb	^{207}Pb	^{208}Pb	^{232}Th	^{235}U	Th/U	Pbppm	Thppm	Uppm	^{238}U/^{206}Pb	1s %	^{207}Pb/^{206}Pb	1s %
CB14.1.rd1_23	27		212	0.1	2642861	471417	31359	141817	47280	0.0	493	45	1042	2.14	1.1	0.176	0.70
CB14.1.rd4_06a	39		-3	-0.1	50164	2712	25457	839263	8272	1.4	12	264	182	19.77	1.2	0.053	0.98
CB14.1.rd5_05	51		64	1.6	67156	4930	9638	162600	3573	0.5	14	39	85	6.36	1.5	0.073	0.94
CB14.1.rd1_21	23		5	0.1	131538	7049	9827	383115	22975	0.2	23	120	506	21.20	1.1	0.053	0.86
CB14.1.rd1_20a	21		-43	-1.2	66300	3595	13557	475706	10616	0.6	13	149	234	19.49	1.3	0.053	0.98
CB14.15rd5_06	57		16	0.9	31616	1977	8922	198209	2854	0.7	8	51	77	10.33	1.2	0.061	1.28
CB14.1.rd1_27a	32		66	0.5	206107	19679	41693	347426	7039	0.7	42	109	155	4.18	1.5	0.094	0.80
CB14.1.rd4_01	33		-22	-0.9	47132	2542	19606	627982	7848	1.1	11	197	173	20.39	1.2	0.053	1.13
CB14.1.rd1_15	16		164	8.4	34990	2038	4239	108670	4111	0.4	6	34	91	14.20	1.2	0.057	1.21
CB14.1.rd1_08	9		-126	-7.7	29192	1703	5798	161902	3255	0.7	6	51	72	13.74	1.4	0.057	1.15
CB14.15rd5_01	52		36	1.7	38255	2409	26837	606003	3383	1.7	13	156	91	10.23	1.3	0.062	1.18
CB14.1.rd1_06b	7		28	0.7	68645	4091	10248	299374	7341	0.6	13	94	162	12.78	1.3	0.058	1.02
CB14.1.rd1_24	28		214	2.6	147934	8361	16245	430703	18796	0.3	27	135	414	15.31	1.4	0.056	0.84
CB14.15rd5_02	53		175	9.9	31159	1995	23476	555099	2666	2.0	11	143	72	9.92	1.2	0.063	1.38
CB14.1.rd1_22b	25		-94	-0.5	298355	28712	43832	383112	10780	0.5	58	120	238	4.42	1.1	0.095	0.77
CB14.1.rd1_16	17		44	0.8	91954	5832	28855	551120	7905	1.0	20	173	174	10.41	1.2	0.062	0.84
CB14.1.rd1_25b	30		-8	0.0	275531	35014	36089	208480	7856	0.4	54	65	173	3.45	1.1	0.125	0.74
CB14.1.rd1_22c	26		130	0.8	283051	21185	18555	202384	16592	0.2	51	64	366	6.97	1.5	0.075	0.86
CB14.1.rd1_25a	29		107	0.5	335770	41597	43779	264175	11013	0.3	66	83	243	4.03	1.1	0.123	0.76
CB14.1.rd5_03	49		22	0.3	104984	13087	9056	96876	3596	0.3	22	23	85	4.13	1.6	0.124	0.85
CB14.15rd5_05	56		50	1.8	49287	3329	19106	465248	4758	0.9	14	120	128	11.05	1.3	0.066	1.14
CB14.1.rd1_20b	22		83	1.6	91228	5326	37981	1307112	14861	1.3	21	410	327	19.83	1.1	0.058	1.56
CB14.1.rd1_02	2		254	1.8	236793	17801	45948	1407424	32146	0.6	47	442	708	16.45	1.2	0.075	1.00
CB14.15rd5_03	54		262	25.8	14988	2049	7855	111499	1148	0.9	5	29	31	8.64	2.3	0.138	4.17
~~CB14.1.rd4_08b~~	~~44~~	~~high common Pb~~	~~683~~	~~0.7~~	~~1557557~~	~~205821~~	~~44514~~	~~138450~~	~~40533~~	~~0.0~~	~~283~~	~~43~~	~~893~~	~~3.15~~	~~1.2~~	~~0.131~~	~~0.70~~
CB14.2.rd4_09	39	CB14.2 - volcanic	132	5.8	40215	2438	11037	206809	3382	0.9	8	65	75	9.71	1.3	0.060	1.08
CB14.2.rd4_01	27		42	0.6	124370	7575	42760	738044	10235	1.0	27	232	225	9.94	1.2	0.060	0.86
CB14.2.RD1_01	1		43	0.1	655225	65409	98049	832987	17975	0.5	112	184	359	3.39	0.9	0.098	0.64
CB14.2.rd4_02a	28		14	0.4	68215	4172	15971	273527	5710	0.7	14	86	126	10.04	1.3	0.060	0.92
CB14.2.rd4_03a	30		89	1.2	126474	8034	14645	229676	9128	0.4	23	72	201	8.69	1.2	0.062	0.80
CB14.2.rd4_04	32		-7	-0.1	148944	9774	22012	333859	9682	0.5	28	105	213	7.82	1.3	0.065	0.91
CB14.2.rd4_05a	33		-93	-1.3	124291	7621	29665	532403	10273	0.7	25	167	226	9.88	1.2	0.060	0.82
CB14.2.RD1_04	4		9	0.0	417283	41864	106894	946596	11622	0.9	78	209	232	3.51	0.9	0.099	0.64
CB14.2.rd4_10a	40		141	3.9	64606	3920	15651	293230	5393	0.8	13	92	119	10.02	1.2	0.060	1.03
CB14.2.rd4_03b	31		113	0.7	270193	17413	62491	920049	18667	0.7	55	289	411	8.25	1.1	0.064	0.80
CB14.2.RD1_21b	23		-101	-1.9	90995	5901	18003	384399	5922	0.7	16	85	118	8.24	1.2	0.064	0.83
CB14.2.rd4_08a	37		-12	-0.3	71560	4387	25834	470953	5971	1.1	16	148	132	10.04	1.2	0.060	0.87
CB14.2.RD1_02	2		138	4.0	61793	3799	18134	424379	4957	0.9	12	94	99	10.03	1.2	0.060	0.88
CB14.2.RD1_09	10		116	0.3	604311	38928	133123	2791549	40519	0.8	107	617	809	8.41	0.8	0.064	0.61
CB14.2.RD1_24	26		114	0.8	223025	20345	20897	223675	7408	0.3	36	49	148	4.08	1.0	0.090	0.63
CB14.2.RD1_08b	9		96	0.3	484582	30997	86130	1688329	32743	0.6	83	373	654	8.51	0.9	0.064	0.71
CB14.2.RD1_14	15		116	2.5	82902	5038	37901	980939	7014	1.5	17	217	140	10.55	1.1	0.060	0.79
CB14.2.RD1_06	6		4	0.0	155326	9564	27837	649159	12153	0.6	26	143	243	9.79	1.1	0.061	0.72
CB14.2.rd4_12	43		-16	-0.4	73909	4585	24828	456623	6122	1.1	16	143	135	9.89	1.3	0.061	0.95
CB14.2.rd4_06	35		146	12.6	20506	1262	6129	104149	1667	0.9	4	33	37	9.85	1.6	0.061	1.20
CB14.2.rd4_14a	45		-14	-0.2	126464	7718	57888	1054211	10837	1.4	30	331	239	10.22	1.1	0.060	0.83
CB14.2.RD1_20	21		29	0.4	111970	7267	25057	505668	7423	0.8	20	112	148	8.38	1.0	0.064	0.84
CB14.2.rd4_13	44		-70	-0.7	174819	11198	37966	594657	12550	0.7	35	187	277	8.64	1.1	0.064	0.78
CB14.2.rd4_10b	41		218	5.7	68049	4201	21299	403175	5713	1.0	15	127	126	10.03	1.1	0.061	1.04
CB14.2.RD1_22	24		74	1.6	79163	4827	51733	1332392	6388	2.3	19	294	128	10.09	1.0	0.061	0.86
CB14.2.rd4_11	42		107	1.5	115643	11042	12794	105164	3809	0.4	22	33	84	3.98	1.2	0.094	0.79
CB14.2.RD1_23	25		-26	-0.3	162703	9896	26342	651252	13585	0.5	27	144	271	10.30	0.9	0.061	0.67
CB14.2.RD1_10	11		70	2.5	50065	3107	24964	567387	3954	1.6	11	125	79	10.00	1.2	0.061	0.97
CB14.2.rd4_05b	34		29	0.8	66258	4138	27930	501198	5703	1.3	15	157	126	10.18	1.3	0.061	1.04
CB14.2.RD1_13	14		106	0.5	336717	33886	90272	876238	10171	1.0	63	194	203	3.77	0.9	0.099	0.68
CB14.2.RD1_12	13		262	2.8	168344	10285	45945	1168383	13971	0.9	31	258	279	10.33	1.1	0.061	0.74
CB14.2.RD1_18	19		-53	-1.6	57062	3632	9474	217400	4245	0.6	10	48	85	9.28	1.1	0.063	0.92
CB14.2.RD1_05	5		-1	0.0	89455	5531	39418	955159	7096	1.5	18	211	142	10.03	0.9	0.061	0.75
CB14.2.RD1_11	12		50	1.1	83155	5131	39913	963784	6729	1.6	18	213	134	10.22	1.0	0.061	0.82
CB14.2.RD1_21a	22		122	2.2	98660	6209	14992	358651	7395	0.5	16	79	148	9.48	1.0	0.063	0.79
CB14.2.rd4_08b	38		5	0.2	51451	3191	18894	355170	4465	1.1	12	112	98	10.49	1.2	0.061	1.14
CB14.2.rd4_02b	29		166	4.8	61849	3821	14262	248431	5324	0.7	13	78	117	10.42	1.3	0.061	1.10
CB14.2.RD1_08a	8		108	0.8	234860	15117	18033	409934	17067	0.3	37	91	341	9.25	0.8	0.064	0.63
CB14.2.RD1_16	17		25	0.3	141880	9317	47113	1031811	9820	1.2	27	228	196	8.63	0.9	0.065	0.72
CB14.2.rd4_07	36		168	24.4	12130	757	4885	84630	1031	1.2	3	27	23	10.11	1.9	0.062	1.60
CB14.2.RD1_19	20		91	1.6	103263	6522	47573	1187826	8362	1.6	22	262	167	10.13	1.0	0.063	0.95
CB14.2.RD1_17	18		-14	-0.3	94969	5989	44554	1146710	7893	1.6	20	253	158	10.36	1.0	0.062	0.78
CB14.2.rd4_14b	46		165	2.0	140470	9475	60630	1083419	11753	1.3	33	340	259	9.95	1.2	0.066	0.87
CB14.2.RD1_03	3		223	1.3	287601	19834	113315	2664217	23150	1.3	58	589	462	10.17	1.1	0.068	1.26
CB14.2.RD1_07	7		232	6.0	66126	4548	32739	734878	5309	1.5	14	162	106	9.95	1.2	0.069	1.48
CB14.2.RD1_15	16		289	1.1	401312	42472	34243	317946	17378	0.2	66	70	347	5.45	1.0	0.103	0.75
CB14.5.RD1_17a	17	CB14.5 - volcanic	94	1.1	134081	12484	19348	127001	4034	0.3	23	28	81	3.68	1.1	0.092	0.74
CB14.5.RD1_09	9		40	0.4	159443	10017	35795	555332	11557	0.5	28	123	231	8.96	1.0	0.062	0.86
CB14.5.RD1_05	5		-60	-0.3	321620	26277	35496	276113	12193	0.3	53	61	243	4.70	1.0	0.081	0.76
CB14.5.RD1_17b	18		149	1.5	157709	14885	25923	168743	4883	0.4	27	37	97	3.74	1.1	0.094	0.73
CB14.5.RD1_04	4		65	1.8	64996	3897	25216	447304	5281	0.9	13	99	105	10.02	1.1	0.060	1.02
CB14.5.RD1_19	20		154	2.0	128579	9837	42367	363008	5774	0.7	25	80	115	5.43	1.0	0.076	0.92
CB14.5.RD1_08	8		122	0.7	303839	27649	33548	245163	9749	0.3	50	54	195	3.99	1.0	0.091	0.80
CB14.5.RD1_20	21		128	0.9	215204	21583	33310	190492	6282	0.3	37	42	125	3.54	1.2	0.099	0.74
CB14.5.RD1_21a	22		44	0.5	142889	13833	14607	82766	4244	0.2	24	18	85	3.65	1.0	0.097	0.83
CB14.5.RD1_21b	23		5	0.0	399279	39161	78535	449893	12149	0.4	71	99	243	3.67	1.1	0.097	0.82
CB14.5.RD1_15	15		62	0.8	145169	8866	33707	568934	12534	0.5	26	126	250	10.56	1.1	0.060	0.82
CB14.5.RD1_16	16		43	0.7	110077	9178	23556	180837	4365	0.5	20	40	87	4.79	1.2	0.082	0.90
CB14.5.RD1_03	3		94	4.1	40485	2559	13752	216309	3181	0.8	8	48	64	9.67	1.1	0.062	1.17
CB14.5.RD1_18	19		-64	-1.4	81689	5005	43348	688486	6876	1.1	18	152	137	10.22	1.2	0.061	0.96
CB14.5.RD1_14	14		38	0.9	71802	4482	40073	688500	5933	1.3	16	152	118	10.02	1.1	0.062	0.83
CB14.5.RD1_22	24		248	3.9	112331	6931	53657	900274	9658	1.0	24	199	193	10.28	1.2	0.061	0.82
CB14.5.RD1_02	2		-89	-2.4	66006	4113	21621	344466	5335	0.7	13	76	107	10.09	1.2	0.062	0.99
CB14.5.RD1_12	12		-29	-0.9	57897	3609	16803	258078	4848	0.6	11	57	97	10.09	1.1	0.062	0.94
CB14.5.RD1_10	10		63	2.8	39186	2502	9736	166649	3167	0.6	7	37	63	9.96	1.2	0.063	1.10
CB14.5.RD1_07	7		-31	-0.7	81456	5198	40198	581796	6684	1.0	17	129	133	9.98	1.1	0.063	1.00
CB14.5.RD1_11	11		-59	-1.5	67641	4249	42434	630559	5630	1.2	16	139	112	10.21	1.2	0.063	0.89
CB14.5.RD1_06	6		1	0.0	63026	4024	22929	337917	5371	0.7	12	75	107	10.41	1.1	0.063	1.04
CB14.5.RD1_13	13		282	1.7	283856	18195	60997	976971	23217	0.5	50	216	464	10.21	1.0	0.064	0.86
CB14.5.RD1_01	1		114	2.4	82592	5732	32999	615684	7219	0.9	17	136	144	10.60	1.2	0.066	1.23

Appendix 1. Zircon geochronology mass spectrometry. Primary data - Part B

		Ratios					Ages and errors						Discordance	
#Sample - analysis	#Sample + comments	$^{207}Pb/^{235}U$	1s %	$^{206}Pb/^{238}U$	1s %	Rho	$^{207}Pb/^{206}Pb$	2s abs	$^{206}Pb/^{238}U$	2s abs	$^{207}Pb/^{235}U$	2s abs	6-38/7-6	6-38/7-35
CB14.1.rd1_23		11.35	1.33	0.47	1.13	0.85	2617	12	2472	46	2552	25	5.6	3.1
CB14.1.rd4_06a		0.37	1.57	0.05	1.23	0.78	337	22	318	8	320	9	5.7	0.7
CB14.1.rd5_05		1.57	1.73	0.16	1.45	0.84	1001	19	941	25	959	21	5.9	1.8
CB14.1.rd1_21		0.34	1.42	0.05	1.12	0.79	316	20	297	7	299	7	6.0	0.7
CB14.1.rd1_20a		0.38	1.60	0.05	1.26	0.79	346	22	323	8	325	9	6.9	0.9
CB14.15rd5_06		0.82	1.79	0.10	1.25	0.70	643	27	596	14	606	16	7.4	1.6
CB14.1.rd1_27a		3.09	1.69	0.24	1.49	0.88	1503	15	1384	37	1431	26	7.9	3.3
CB14.1.rd4_01		0.36	1.63	0.05	1.18	0.72	340	26	309	7	312	9	9.2	1.1
CB14.1.rd1_15		0.55	1.74	0.07	1.25	0.72	487	27	439	11	446	12	9.9	1.7
CB14.1.rd1_08		0.57	1.85	0.07	1.45	0.78	503	25	453	13	461	14	10.0	1.8
CB14.15rd5_01		0.84	1.73	0.10	1.27	0.73	675	25	601	15	617	16	10.9	2.5
CB14.1.rd1_06b		0.63	1.63	0.08	1.27	0.78	548	22	486	12	497	13	11.4	2.2
CB14.1.rd1_24		0.51	1.65	0.07	1.42	0.86	468	19	408	11	417	11	12.8	2.1
CB14.15rd5_02		0.88	1.83	0.10	1.20	0.65	710	29	619	14	639	17	12.8	3.1
CB14.1.rd1_22b		2.95	1.35	0.23	1.11	0.82	1520	14	1316	26	1395	20	13.5	5.7
CB14.1.rd1_16		0.83	1.50	0.10	1.24	0.83	688	18	591	14	611	14	14.1	3.3
CB14.1.rd1_25b		4.98	1.36	0.29	1.14	0.84	2025	13	1641	33	1817	23	19.0	9.7
CB14.1.rd1_22c		1.49	1.76	0.14	1.53	0.87	1076	17	864	25	926	21	19.7	6.6
CB14.1.rd1_25a		4.20	1.38	0.25	1.15	0.83	1997	14	1428	29	1673	22	28.5	14.7
CB14.1.rd5_03		4.12	1.77	0.24	1.55	0.88	2009	15	1397	39	1659	29	30.5	15.8
CB14.15rd5_05		0.83	1.74	0.09	1.31	0.76	818	24	558	14	612	16	31.8	8.8
CB14.1.rd1_20b		0.40	1.88	0.05	1.06	0.56	526	34	317	7	343	11	39.7	7.6
CB14.1.rd1_02		0.63	1.56	0.06	1.19	0.77	1077	20	380	9	497	12	64.7	23.4
CB14.15rd5_03		2.21	4.74	0.12	2.25	0.48	2206	72	706	30	1183	64	68.0	40.3
~~CB14.1.rd4_08b~~	~~high common Pb~~	~~5.73~~	~~1.38~~	~~0.32~~	~~1.19~~	~~0.86~~	~~2107~~	~~12~~	~~1780~~	~~37~~	~~1935~~	~~24~~	~~15.5~~	~~8.0~~
CB14.2.rd4_09	CB14.2 - volcanic	0.85	1.69	0.10	1.30	0.77	596	23	632	16	624	16	-6.1	-1.3
CB14.2.rd4_01		0.83	1.45	0.10	1.17	0.81	588	19	618	14	611	13	-5.1	-1.1
CB14.2.RD1_01		3.99	1.12	0.29	0.92	0.82	1593	12	1664	27	1633	18	-4.5	-2.0
CB14.2.rd4_02a		0.82	1.55	0.10	1.25	0.81	591	20	612	15	607	14	-3.6	-0.8
CB14.2.rd4_03a		0.99	1.48	0.12	1.24	0.84	690	17	702	17	699	15	-1.8	-0.4
CB14.2.rd4_04		1.14	1.58	0.13	1.28	0.81	766	19	776	19	773	17	-1.3	-0.4
CB14.2.rd4_05a		0.84	1.45	0.10	1.20	0.83	614	18	622	14	620	13	-1.3	-0.3
CB14.2.RD1_04		3.88	1.10	0.29	0.90	0.82	1598	12	1618	26	1609	18	-1.2	-0.6
CB14.2.rd4_10a		0.83	1.61	0.10	1.24	0.77	609	22	613	15	612	15	-0.7	-0.2
CB14.2.rd4_03b		1.07	1.37	0.12	1.10	0.81	738	17	738	15	737	14	0.0	0.0
CB14.2.RD1_21b		1.07	1.45	0.12	1.19	0.82	742	18	738	17	739	15	0.5	0.1
CB14.2.rd4_08a		0.83	1.47	0.10	1.19	0.81	617	19	612	14	613	13	0.7	0.1
CB14.2.RD1_02		0.83	1.51	0.10	1.23	0.81	620	19	613	14	614	14	1.2	0.2
CB14.2.RD1_09		1.05	1.04	0.12	0.84	0.81	733	13	725	11	726	11	1.2	0.3
CB14.2.RD1_24		3.05	1.16	0.25	0.97	0.84	1432	12	1414	25	1421	18	1.3	0.5
CB14.2.RD1_08b		1.03	1.18	0.12	0.94	0.80	726	15	716	13	718	12	1.4	0.3
CB14.2.RD1_14		0.78	1.32	0.09	1.06	0.80	593	17	584	12	586	12	1.6	0.3
CB14.2.RD1_06		0.86	1.28	0.10	1.06	0.82	640	16	627	13	630	12	2.0	0.4
CB14.2.rd4_12		0.85	1.63	0.10	1.32	0.81	634	20	621	16	623	15	2.1	0.4
CB14.2.rd4_06		0.85	2.02	0.10	1.63	0.81	639	26	623	19	627	19	2.4	0.5
CB14.2.rd4_14a		0.81	1.40	0.10	1.13	0.81	618	18	602	13	605	13	2.5	0.5
CB14.2.RD1_20		1.05	1.31	0.12	1.01	0.77	746	18	726	14	731	14	2.6	0.6
CB14.2.rd4_13		1.01	1.34	0.12	1.09	0.81	727	17	706	15	711	14	2.9	0.7
CB14.2.rd4_10b		0.84	1.52	0.10	1.12	0.73	632	22	613	13	617	14	3.0	0.6
CB14.2.RD1_22		0.83	1.35	0.10	1.04	0.77	633	19	609	12	614	12	3.8	0.8
CB14.2.rd4_11		3.26	1.43	0.25	1.19	0.83	1507	15	1446	31	1471	22	4.0	1.7
CB14.2.RD1_23		0.81	1.14	0.10	0.93	0.81	622	14	597	11	602	10	4.0	0.8
CB14.2.RD1_10		0.84	1.51	0.10	1.16	0.77	643	21	614	14	620	14	4.5	1.0
CB14.2.rd4_05b		0.82	1.67	0.10	1.30	0.78	634	22	604	15	610	15	4.7	1.0
CB14.2.RD1_13		3.62	1.17	0.27	0.95	0.81	1605	13	1516	26	1553	18	5.6	2.4
CB14.2.RD1_12		0.81	1.29	0.10	1.06	0.82	633	16	596	12	603	12	5.9	1.3
CB14.2.RD1_18		0.93	1.44	0.11	1.10	0.77	702	20	660	14	669	14	6.0	1.4
CB14.2.RD1_05		0.84	1.19	0.10	0.92	0.77	654	16	613	11	621	11	6.2	1.4
CB14.2.RD1_11		0.83	1.28	0.10	0.98	0.77	647	18	602	11	611	12	6.9	1.5
CB14.2.RD1_21a		0.91	1.26	0.11	0.99	0.78	702	17	647	12	659	12	7.8	1.8
CB14.2.rd4_08b		0.80	1.64	0.10	1.18	0.72	641	24	587	13	598	15	8.3	1.8
CB14.2.rd4_02b		0.81	1.69	0.10	1.29	0.76	646	24	590	14	602	15	8.5	1.9
CB14.2.RD1_08a		0.95	1.03	0.11	0.81	0.79	728	13	661	10	677	10	9.1	2.2
CB14.2.RD1_16		1.04	1.16	0.12	0.91	0.79	782	15	707	12	725	12	9.6	2.5
CB14.2.rd4_07		0.85	2.52	0.10	1.94	0.77	686	34	608	22	625	23	11.4	2.7
CB14.2.RD1_19		0.85	1.35	0.10	0.96	0.71	693	20	607	11	625	13	12.4	2.9
CB14.2.RD1_17		0.83	1.30	0.10	1.04	0.80	686	17	594	12	613	12	13.5	3.2
CB14.2.rd4_14b		0.91	1.47	0.10	1.19	0.81	805	18	618	14	659	14	23.3	6.3
CB14.2.RD1_03		0.92	1.64	0.10	1.05	0.64	854	26	605	12	660	16	29.2	8.4
CB14.2.RD1_07		0.96	1.93	0.10	1.24	0.64	898	30	618	15	681	19	31.2	9.3
CB14.2.RD1_15		2.61	1.28	0.18	1.04	0.81	1681	14	1086	21	1303	19	35.4	16.6
CB14.5.RD1_17a	CB14.5 - volcanic	3.46	1.29	0.27	1.06	0.82	1476	14	1550	29	1519	20	-5.0	-2.1
CB14.5.RD1_09		0.95	1.34	0.11	1.03	0.77	660	18	682	13	677	13	-3.3	-0.8
CB14.5.RD1_05		2.38	1.29	0.21	1.04	0.81	1222	15	1244	24	1236	18	-1.8	-0.7
CB14.5.RD1_17b		3.47	1.34	0.27	1.12	0.84	1513	14	1528	30	1521	21	-1.0	-0.4
CB14.5.RD1_04		0.83	1.50	0.10	1.09	0.73	608	22	613	13	612	14	-0.9	-0.2
CB14.5.RD1_19		1.92	1.39	0.18	1.04	0.75	1086	18	1090	21	1088	18	-0.4	-0.1
CB14.5.RD1_08		3.13	1.31	0.25	1.04	0.79	1439	15	1440	27	1439	20	-0.1	-0.1
CB14.5.RD1_20		3.87	1.39	0.28	1.17	0.84	1612	14	1606	33	1608	22	0.4	0.2
CB14.5.RD1_21a		3.67	1.31	0.27	1.02	0.77	1572	16	1559	28	1564	21	0.8	0.3
CB14.5.RD1_21b		3.65	1.38	0.27	1.10	0.80	1571	15	1554	30	1561	22	1.1	0.5
CB14.5.RD1_15		0.78	1.36	0.09	1.08	0.79	594	18	583	12	585	12	1.7	0.3
CB14.5.RD1_16		2.37	1.48	0.21	1.17	0.79	1255	18	1222	26	1233	21	2.7	1.0
CB14.5.RD1_03		0.88	1.60	0.10	1.09	0.68	664	25	634	13	641	15	4.5	1.0
CB14.5.RD1_18		0.82	1.55	0.10	1.22	0.78	642	21	602	14	610	14	6.2	1.4
CB14.5.RD1_14		0.85	1.36	0.10	1.08	0.79	660	18	613	13	623	13	7.1	1.6
CB14.5.RD1_22		0.82	1.47	0.10	1.22	0.83	645	18	598	14	608	13	7.3	1.6
CB14.5.RD1_02		0.84	1.52	0.10	1.16	0.76	658	21	609	13	619	14	7.5	1.7
CB14.5.RD1_12		0.85	1.42	0.10	1.06	0.75	681	20	609	12	624	13	10.6	2.4
CB14.5.RD1_10		0.87	1.64	0.10	1.21	0.74	695	24	617	14	634	15	11.2	2.6
CB14.5.RD1_07		0.87	1.48	0.10	1.09	0.73	697	21	616	13	633	14	11.6	2.7
CB14.5.RD1_11		0.85	1.47	0.10	1.17	0.80	702	19	602	13	623	14	14.2	3.4
CB14.5.RD1_06		0.83	1.48	0.10	1.06	0.71	696	22	591	12	613	14	15.0	3.6
CB14.5.RD1_13		0.87	1.32	0.10	1.00	0.76	748	18	602	12	634	12	19.5	4.9
CB14.5.RD1_01		0.86	1.70	0.09	1.18	0.69	806	26	581	13	629	16	28.0	7.6

Appendix 1. Zircon geochronology mass spectrometry. Primary data - Part A

			Concentrations											Ratios			
#Sample + #analysis		#Sample + comments	^{204}Pb	f206c	^{206}Pb	^{207}Pb	^{208}Pb	^{232}Th	^{235}U	Th/U	Pbppm	Thppm	Uppm	^{238}U/^{206}Pb	1s %	^{207}Pb/^{206}Pb	1s %
NHG15.12rd6_49a	82	NHG15.12 - detrital	-8	-0.1	113143	6861	29697	853947	9607	0.8	30	220	258	9.62	1.0	0.060	0.77
NHG15.12_22	22	RD3	15	0.1	179559	11402	8515	174318	12377	0.1	34	42	293	8.36	1.3	0.063	0.91
NHG15.12rd6_53	88		-6	-0.1	142677	8648	33384	964009	11840	0.8	37	248	318	9.63	1.0	0.060	0.80
NHG15.12rd6_26	55		4	0.2	47247	2754	12413	364559	4525	0.8	12	94	122	11.13	1.1	0.058	1.02
NHG15.12_16	16	RD3	41	2.1	35308	2194	7952	158491	2704	0.6	8	38	64	9.34	1.6	0.061	1.13
NHG15.12_17	17	RD3	-3	-0.1	57181	3521	11487	264889	4352	0.6	12	63	103	9.39	1.7	0.061	1.05
NHG15.12rd6_29	58		-55	-0.9	107246	6348	42773	1338466	10374	1.2	31	344	279	11.07	1.1	0.058	0.87
NHG15.12rd6_100	36		-110	-1.9	102227	6015	21933	575237	9218	0.7	17	126	174	11.09	1.3	0.058	0.78
NHG15.12rd6_99	144		122	1.2	175465	10797	48244	1001391	14483	0.8	31	219	274	9.91	1.4	0.060	0.70
NHG15.12rd6_95	141		-17	-0.2	149940	17800	21340	149095	3442	0.5	25	33	65	2.81	1.4	0.117	0.61
NHG15.12rd6_01	26		24	2.2	19182	1178	5522	146341	1641	0.9	5	38	44	9.79	1.6	0.060	1.26
NHG15.12rd6_47	80		40	1.1	65696	3862	29254	1022805	6462	1.5	20	263	174	11.31	1.1	0.058	0.84
NHG15.12rd6_82a	122		4	0.1	140443	8421	26781	590920	12210	0.6	23	129	231	10.79	1.4	0.059	0.72
NHG15.12_06	6	RD3	38	0.9	77157	4727	24684	507298	6228	0.8	18	121	148	9.76	1.5	0.060	1.01
NHG15.12rd6_22	50		78	2.4	58187	3617	14834	362851	4748	0.7	15	93	128	9.31	1.4	0.061	1.02
NHG15.12_07	7	RD3	162	3.7	78236	4712	35580	774069	6580	1.2	20	185	156	10.24	1.4	0.060	0.91
NHG15.12rd6_10	35		1	0.0	254713	15511	53508	1444308	21807	0.6	64	371	587	9.87	1.1	0.060	0.83
NHG15.12rd6_06	31		73	0.7	167631	20465	36068	301164	4148	0.7	45	77	112	2.84	1.2	0.119	0.75
NHG15.12rd6_83	124		24	0.3	135082	8214	33344	675202	10918	0.7	23	148	207	9.93	1.4	0.060	0.73
NHG15.12rd6_16	43		64	0.4	239564	23410	54621	597607	7677	0.7	63	154	207	3.68	1.2	0.096	0.74
NHG15.12rd6_27	56		74	0.5	206392	25657	39079	340346	5084	0.6	54	88	137	2.81	1.2	0.121	0.70
NHG15.12_10	10	RD3	-18	-0.3	103097	6475	22488	406640	7484	0.5	22	97	177	8.83	1.5	0.063	0.92
NHG15.12rd6_25	54		-55	-1.1	91653	5356	28221	889100	9298	0.9	25	229	250	11.52	1.1	0.058	0.85
NHG15.12rd6_101	37		219	4.7	83737	5081	34064	848785	7407	1.3	16	185	140	10.69	1.4	0.059	0.79
NHG15.12_23	23	RD3	-91	-3.5	43697	3500	9583	117597	1768	0.7	10	28	42	5.03	1.6	0.079	1.13
NHG15.12rd6_94b	139		-125	-2.7	82517	5187	27905	565122	5939	1.1	15	123	112	8.85	1.4	0.063	0.76
NHG15.12rd6_58	93		-27	-0.7	66920	4066	21090	690864	6027	1.1	18	178	162	10.42	0.9	0.060	0.85
NHG15.12rd6_77a	115		81	1.3	110280	6534	36969	870793	10089	1.0	20	190	191	11.50	1.3	0.058	0.68
NHG15.12rd6_35	66		-30	-0.2	177746	33839	26509	170845	2925	0.6	47	44	79	1.92	1.2	0.189	0.65
NHG15.12rd6_67	103		25	0.3	142876	9062	28236	801557	11286	0.7	36	206	304	8.93	1.2	0.063	0.69
NHG15.12rd6_68	104		-30	-1.2	39511	4167	13848	153865	1166	1.3	11	40	31	3.38	1.5	0.104	0.91
NHG15.12rd6_94a	138		63	1.0	106872	6748	35818	743335	7852	1.1	20	162	149	9.10	1.3	0.062	0.79
NHG15.12rd6_04	29		44	0.8	95323	6094	16416	378447	7510	0.5	23	97	202	9.04	1.2	0.062	1.19
NHG15.12_21	21	RD3	-13	-0.3	70940	4198	26607	664821	6697	1.0	17	159	159	11.62	1.5	0.058	0.93
NHG15.12rd6_11	38		175	8.9	34911	2150	8961	227624	2970	0.7	9	59	80	9.95	1.4	0.061	1.38
NHG15.12_25	25	RD3	16	0.1	177938	23040	33247	222826	3881	0.6	40	53	92	2.69	1.5	0.129	0.77
NHG15.12rd6_40	73		129	5.0	45900	2804	10402	298688	3990	0.7	12	77	107	9.95	1.0	0.061	1.09
NHG15.12rd6_73a	109		-42	-0.6	123067	7649	32885	693169	8868	0.9	22	151	168	9.07	1.2	0.062	0.63
NHG15.12rd6_64a	99		-48	-0.6	137598	8130	49948	1757833	13684	1.2	39	452	368	11.51	0.9	0.059	0.75
NHG15.12_11	11	RD3	0	0.0	288528	23544	34237	343071	11943	0.3	59	82	283	5.03	1.5	0.080	0.83
NHG15.12rd6_60	95		-4	-0.1	92753	5624	29461	953381	8095	1.1	25	245	218	10.18	1.0	0.060	0.79
NHG15.12_19	19	RD3	-69	-2.4	51623	3158	26713	589912	4338	1.4	14	141	103	10.12	1.6	0.061	1.00
NHG15.12rd6_73b	110		78	1.2	118098	7471	30999	638783	8436	0.9	21	140	160	8.91	1.3	0.063	0.76
NHG15.12rd6_66	102		145	3.5	73171	4530	22586	674806	6016	1.1	20	174	162	9.80	0.9	0.061	0.79
NHG15.12rd6_64b	100		53	1.2	80556	4796	21782	759267	8011	0.9	21	195	215	11.48	1.0	0.059	0.84
NHG15.12_14	14	RD3	-14	-0.2	119502	7269	15551	321385	9707	0.3	24	77	230	9.87	1.5	0.061	0.99
NHG15.12rd6_72	108		-69	-0.5	227188	14022	75007	1720194	18824	1.1	42	376	356	10.20	1.2	0.060	0.58
NHG15.12rd6_23	51		82	2.1	70563	4158	31365	1031937	7055	1.4	21	265	190	11.58	1.2	0.059	0.98
NHG15.12rd6_28	57		87	1.6	99345	5839	29537	989831	9905	1.0	27	255	266	11.55	1.0	0.059	0.88
NHG15.12rd6_57	92		152	1.9	140409	8454	35434	1170049	13361	0.8	37	301	359	10.94	1.0	0.059	0.70
NHG15.12rd6_50b	85		97	2.9	60230	3757	13204	390697	5177	0.7	15	100	139	9.81	1.1	0.061	0.91
NHG15.12rd6_31	60		79	1.7	83192	4943	49691	1642777	8522	1.8	27	422	229	11.64	1.1	0.058	0.91
NHG15.12rd6_55	90		64	1.0	109267	6731	33921	1088504	9427	1.1	30	280	254	9.84	1.1	0.061	0.72
NHG15.12rd6_85	127		11	0.2	124404	7733	21136	417362	10059	0.5	20	91	190	10.04	1.3	0.061	0.79
NHG15.12rd6_76	114		147	2.4	107661	6441	33324	756004	10078	0.9	20	165	191	11.55	1.5	0.059	0.78
NHG15.12rd6_69	105		130	0.3	717629	67055	18376	361884	25554	0.1	159	93	687	4.05	0.9	0.092	0.58
NHG15.12rd6_39	72		52	1.3	72539	4499	18727	526580	6325	0.8	19	135	170	9.93	1.1	0.061	0.87
NHG15.12rd6_20	47		-67	-2.5	46943	2929	9502	238961	4083	0.6	12	61	110	9.55	1.6	0.062	1.27
NHG15.12rd6_36	67		123	3.3	65356	4150	18379	489013	5162	0.9	17	126	139	9.08	1.0	0.063	0.88
NHG15.12rd6_24b	53		57	1.2	82746	5077	12323	337962	7766	0.4	20	87	209	10.59	1.1	0.060	0.89
NHG15.12rd6_38a	70		76	3.2	40261	2906	6540	120865	2263	0.5	10	31	61	6.48	1.1	0.071	1.02
NHG15.12rd6_95	140		162	2.2	130623	8267	36216	864978	9729	1.0	23	189	184	9.14	1.3	0.063	0.69
NHG15.12_13	13	RD3	146	1.2	222719	13687	88921	2048742	18759	1.1	55	489	445	10.23	1.4	0.061	0.82
NHG15.12rd6_38b	71		19	0.3	121502	8648	8804	175913	7120	0.2	28	45	192	6.71	1.0	0.070	0.74
NHG15.12rd6_93	137		93	1.2	132014	8069	34756	781085	10859	0.8	23	171	205	10.14	1.2	0.061	0.71
NHG15.12rd6_50a	84		122	6.5	33291	2029	8036	242095	2840	0.8	9	62	76	9.96	1.2	0.061	1.19
NHG15.12rd6_08	33		-22	-0.7	52143	3234	20302	539881	4409	1.2	15	139	119	9.65	1.3	0.062	1.05
NHG15.12rd6_92a	135		41	0.8	93396	5580	20833	497493	8798	0.7	16	109	166	11.41	1.4	0.059	0.81
NHG15.12_03	3	RD3	-10	-0.2	102136	6110	21137	456392	9114	0.5	22	109	216	10.91	1.5	0.060	1.03
NHG15.12rd6_74b	112		183	2.0	154927	12597	23063	257141	6223	0.5	25	56	118	5.03	1.3	0.081	0.72
NHG15.12rd6_71	107		115	2.5	80218	4935	24174	584901	6733	1.0	15	128	127	10.53	1.3	0.060	0.76
NHG15.12rd6_09	34		-40	-1.0	73773	4497	22648	594175	6457	0.9	20	153	174	10.12	1.3	0.061	1.01
NHG15.12_05	5	RD3	140	2.8	88869	5215	28789	671325	8423	0.8	21	160	200	11.58	1.4	0.059	0.94
NHG15.12rd6_75	113		166	1.5	199122	11971	38652	869890	17980	0.6	33	190	340	11.17	1.3	0.059	0.67
NHG15.12_12	12	RD3	88	2.8	55758	3340	16777	412646	5093	0.8	13	99	121	11.06	1.5	0.060	1.10
NHG15.12rd6_62	97		74	2.5	53470	3217	14566	484977	5017	0.9	14	125	135	10.81	1.1	0.060	0.91
NHG15.12_08	8	RD3	-4	-0.1	89056	5946	16903	291138	5789	0.5	19	70	137	7.86	1.5	0.066	0.84
NHG15.12rd6_88	130		-4	-0.1	127516	8115	29200	513201	9725	0.6	22	112	184	9.28	1.4	0.063	0.77
NHG15.12rd6_15	42		-17	-0.3	88118	5516	26048	700972	7539	0.9	24	180	203	9.95	1.0	0.061	0.87
NHG15.12rd6_91a	133		37	1.0	68321	4297	19960	370959	5087	0.8	12	81	96	9.22	1.3	0.063	0.78
NHG15.12rd6_70	106		35	0.8	80070	5086	14972	422440	6421	0.6	20	109	173	9.14	1.0	0.063	0.81
NHG15.12rd6_48	81		131	3.5	65381	4208	8810	234189	5092	0.4	16	60	137	9.08	1.3	0.063	1.02
NHG15.12rd6_37b	69		34	0.9	63645	4082	10508	272674	4873	0.5	16	70	131	8.74	1.1	0.064	0.83
NHG15.12_04	4	RD3	106	2.3	80840	5140	13335	254929	6167	0.4	17	61	146	9.32	1.5	0.063	0.92
NHG15.12rd6_21b	49		10	0.1	126317	8008	51264	1302034	10423	1.2	37	335	280	9.40	1.2	0.062	0.83
NHG15.12rd6_37a	68		109	3.2	59495	3860	7394	191118	4473	0.4	14	49	120	8.60	1.2	0.064	0.89
NHG15.12rd6_91b	134		245	2.9	148841	9387	66876	1277766	11458	1.3	30	279	217	9.46	1.3	0.062	0.66
NHG15.12rd6_51	86		-79	-2.5	55038	3436	16337	474757	4644	1.0	15	122	125	9.78	1.1	0.062	0.87
NHG15.12rd6_59	94		50	1.4	61294	3795	22575	728237	5392	1.3	17	187	145	10.17	1.0	0.061	0.92
NHG15.12_02	2	RD3	39	1.0	65656	4078	18594	355160	5135	0.7	15	85	122	9.53	1.6	0.062	0.99
NHG15.12rd6_78b	118		-62	-0.6	191742	11841	69468	1297006	15713	1.0	36	283	297	10.22	1.4	0.061	0.84
NHG15.12rd6_90	132		12	0.2	88276	5507	33345	654512	6631	1.1	17	143	125	9.36	1.3	0.063	0.79
NHG15.12rd6_45	78		78	2.2	64083	3831	15756	501391	6346	0.8	17	129	171	11.49	1.1	0.059	0.85
NHG15.12rd6_74a	111		244	2.6	158172	13004	19515	212847	6413	0.4	25	47	121	5.05	1.4	0.082	0.78
NHG15.12rd6_21a	48		-16	-0.4	72215	4615	14420	329802	6105	0.5	18	85	164	9.65	1.3	0.062	1.02
NHG15.12rd6_78a	117		15	0.4	60571	3726	39879	887334	5039	2.0	14	194	95	10.34	1.3	0.061	0.74
NHG15.12rd6_46	79		67	1.2	101479	6449	39688	1114696	8254	1.3	29	287	222	9.29	1.1	0.063	0.74

Appendix 1. Zircon geochronology mass spectrometry. Primary data - Part B

		Ratios					Ages and errors						Discordance	
#Sample - analysis	#Sample + comments	$^{207}Pb/^{235}U$	1s %	$^{206}Pb/^{238}U$	1s %	Rho	$^{207}Pb/^{206}Pb$	2s abs	$^{206}Pb/^{238}U$	2s abs	$^{207}Pb/^{235}U$	2s abs	6-38/7-6	6-38/7-35
NHG15.12rd6_49a	NHG15.12 - detrital	0.86	1.26	0.10	1.00	0.79	606	17	637	12	630	12	-5.2	-1.1
NHG15.12_22	RD3	1.03	1.62	0.12	1.34	0.83	693	19	728	18	719	17	-5.1	-1.2
NHG15.12rd6_53		0.86	1.28	0.10	0.99	0.78	608	17	637	12	630	12	-4.7	-1.0
NHG15.12rd6_26		0.72	1.50	0.09	1.09	0.73	532	22	555	12	550	13	-4.3	-0.8
NHG15.12_16	RD3	0.90	1.97	0.11	1.61	0.82	634	24	656	20	650	19	-3.5	-0.8
NHG15.12_17	RD3	0.89	1.98	0.11	1.68	0.85	635	23	652	21	648	19	-2.7	-0.6
NHG15.12rd6_29		0.73	1.39	0.09	1.09	0.78	543	19	557	12	554	12	-2.7	-0.5
NHG15.12rd6_100		0.72	1.51	0.09	1.29	0.86	543	17	556	14	553	13	-2.6	-0.5
NHG15.12rd6_99		0.84	1.54	0.10	1.37	0.89	605	15	620	16	616	14	-2.5	-0.6
NHG15.12rd6_95		5.76	1.53	0.36	1.41	0.92	1917	11	1963	48	1940	26	-2.4	-1.2
NHG15.12rd6_01		0.85	2.06	0.10	1.63	0.79	614	27	627	19	624	19	-2.1	-0.5
NHG15.12rd6_47		0.71	1.39	0.09	1.11	0.80	537	18	546	12	544	12	-1.7	-0.4
NHG15.12rd6_82a		0.75	1.55	0.09	1.37	0.88	562	16	571	15	569	13	-1.7	-0.4
NHG15.12_06	RD3	0.85	1.79	0.10	1.48	0.83	618	22	629	18	626	17	-1.7	-0.4
NHG15.12rd6_22		0.91	1.70	0.11	1.36	0.80	649	22	658	17	656	16	-1.4	-0.4
NHG15.12_07	RD3	0.80	1.66	0.10	1.38	0.83	594	20	600	16	599	15	-1.0	-0.2
NHG15.12rd6_10		0.84	1.39	0.10	1.12	0.80	617	18	622	13	621	13	-0.9	-0.2
NHG15.12rd6_06		5.79	1.43	0.35	1.21	0.85	1946	13	1945	41	1945	24	0.1	0.0
NHG15.12rd6_83		0.84	1.55	0.10	1.36	0.88	619	16	619	16	619	14	0.1	0.0
NHG15.12rd6_16		3.61	1.38	0.27	1.17	0.84	1554	14	1550	32	1551	22	0.2	0.1
NHG15.12rd6_27		5.94	1.37	0.36	1.18	0.86	1971	13	1965	40	1967	24	0.3	0.1
NHG15.12_10	RD3	0.98	1.79	0.11	1.54	0.86	694	20	692	20	692	18	0.4	0.1
NHG15.12rd6_25		0.70	1.35	0.09	1.05	0.78	541	19	537	11	537	11	0.7	0.1
NHG15.12rd6_101		0.77	1.59	0.09	1.38	0.87	581	17	577	15	577	14	0.7	0.1
NHG15.12_23	RD3	2.17	2.00	0.20	1.64	0.82	1178	22	1169	35	1172	27	0.7	0.2
NHG15.12rd6_94b		0.98	1.56	0.11	1.36	0.87	696	16	690	18	692	16	0.9	0.2
NHG15.12rd6_58		0.79	1.27	0.10	0.94	0.74	599	18	591	11	592	11	1.3	0.2
NHG15.12rd6_77a		0.70	1.45	0.09	1.29	0.89	545	15	538	13	539	12	1.4	0.2
NHG15.12rd6_35		13.55	1.40	0.52	1.24	0.89	2736	11	2697	54	2719	26	1.4	0.8
NHG15.12rd6_67		0.97	1.34	0.11	1.15	0.86	696	15	685	15	687	13	1.7	0.4
NHG15.12rd6_68		4.26	1.72	0.30	1.45	0.85	1703	17	1672	43	1685	28	1.8	0.8
NHG15.12rd6_94a		0.94	1.54	0.11	1.33	0.86	686	17	672	17	675	15	2.0	0.4
NHG15.12rd6_04		0.95	1.69	0.11	1.20	0.71	691	25	676	15	679	17	2.0	0.4
NHG15.12_21	RD3	0.69	1.77	0.09	1.51	0.85	544	20	532	15	534	15	2.1	0.4
NHG15.12rd6_11		0.84	1.97	0.10	1.40	0.71	631	30	617	16	620	18	2.2	0.5
NHG15.12_25	RD3	6.59	1.68	0.37	1.49	0.89	2081	14	2035	52	2058	29	2.2	1.1
NHG15.12rd6_40		0.84	1.50	0.10	1.02	0.68	633	24	617	12	620	14	2.4	0.5
NHG15.12rd6_73a		0.95	1.38	0.11	1.22	0.89	691	13	674	16	678	14	2.4	0.5
NHG15.12rd6_64a		0.70	1.16	0.09	0.88	0.76	551	16	537	9	540	10	2.6	0.5
NHG15.12_11	RD3	2.20	1.73	0.20	1.51	0.88	1200	16	1169	32	1180	24	2.6	0.9
NHG15.12rd6_60		0.82	1.29	0.10	1.01	0.79	620	17	604	12	607	12	2.6	0.5
NHG15.12_19	RD3	0.83	1.87	0.10	1.57	0.84	624	22	608	18	611	17	2.6	0.5
NHG15.12rd6_73b		0.97	1.48	0.11	1.27	0.86	705	16	686	17	690	15	2.6	0.6
NHG15.12rd6_66		0.86	1.22	0.10	0.93	0.76	644	17	626	11	630	11	2.7	0.6
NHG15.12rd6_64b		0.70	1.29	0.09	0.98	0.76	554	18	538	10	541	11	2.8	0.5
NHG15.12_14	RD3	0.85	1.82	0.10	1.53	0.84	640	21	622	18	626	17	2.8	0.6
NHG15.12rd6_72		0.82	1.36	0.10	1.23	0.91	620	12	603	14	606	12	2.8	0.6
NHG15.12rd6_23		0.70	1.54	0.09	1.18	0.77	550	21	534	12	537	13	2.9	0.5
NHG15.12rd6_28		0.70	1.35	0.09	1.02	0.76	552	19	535	10	538	11	3.0	0.6
NHG15.12rd6_57		0.75	1.25	0.09	1.04	0.83	582	15	564	11	567	11	3.0	0.6
NHG15.12rd6_50b		0.86	1.46	0.10	1.15	0.78	645	20	626	14	630	14	3.1	0.6
NHG15.12rd6_31		0.69	1.42	0.09	1.10	0.77	548	20	531	11	534	12	3.1	0.6
NHG15.12rd6_55		0.86	1.28	0.10	1.06	0.83	645	16	624	13	628	12	3.2	0.7
NHG15.12rd6_85		0.84	1.51	0.10	1.28	0.85	633	17	612	15	617	14	3.3	0.7
NHG15.12rd6_76		0.70	1.71	0.09	1.52	0.89	554	17	535	16	539	14	3.4	0.6
NHG15.12rd6_69		3.14	1.08	0.25	0.91	0.85	1473	11	1422	23	1442	16	3.5	1.4
NHG15.12rd6_39		0.85	1.44	0.10	1.14	0.80	641	19	619	13	623	13	3.5	0.7
NHG15.12rd6_20		0.89	2.04	0.10	1.59	0.78	666	27	642	19	647	19	3.5	0.8
NHG15.12rd6_36		0.95	1.34	0.11	1.01	0.75	699	19	673	13	679	13	3.6	0.8
NHG15.12rd6_24b		0.78	1.42	0.09	1.11	0.78	604	19	582	12	586	13	3.6	0.7
NHG15.12rd6_38a		1.51	1.53	0.15	1.14	0.74	961	21	925	20	936	19	3.8	1.1
NHG15.12rd6_95		0.94	1.47	0.11	1.30	0.88	696	15	669	17	675	14	3.8	0.9
NHG15.12_13	RD3	0.82	1.63	0.10	1.41	0.86	626	18	601	16	606	15	3.9	0.8
NHG15.12rd6_38b		1.44	1.28	0.15	1.04	0.81	933	15	896	17	907	15	4.0	1.2
NHG15.12rd6_93		0.83	1.43	0.10	1.25	0.87	632	15	606	14	611	13	4.0	0.9
NHG15.12rd6_50a		0.85	1.70	0.10	1.22	0.72	643	26	617	14	622	16	4.1	0.9
NHG15.12rd6_08		0.88	1.68	0.10	1.31	0.78	663	22	635	16	641	16	4.2	0.9
NHG15.12rd6_92a		0.71	1.63	0.09	1.41	0.87	565	18	542	15	546	14	4.2	0.8
NHG15.12_03	RD3	0.75	1.83	0.09	1.51	0.82	590	22	565	16	570	16	4.2	0.8
NHG15.12rd6_74b		2.22	1.50	0.20	1.31	0.88	1221	14	1170	28	1188	21	4.2	1.5
NHG15.12rd6_71		0.79	1.46	0.09	1.25	0.85	611	16	585	14	590	13	4.3	0.9
NHG15.12rd6_09		0.83	1.67	0.10	1.33	0.80	635	22	607	15	613	15	4.4	0.9
NHG15.12_05	RD3	0.70	1.68	0.09	1.39	0.83	559	21	534	14	538	14	4.4	0.8
NHG15.12rd6_75		0.73	1.42	0.09	1.25	0.88	580	15	553	13	558	12	4.7	0.9
NHG15.12_12	RD3	0.74	1.85	0.09	1.49	0.81	586	24	558	16	563	16	4.7	0.9
NHG15.12rd6_62		0.76	1.43	0.09	1.10	0.77	599	20	570	12	576	12	4.8	1.0
NHG15.12_08	RD3	1.16	1.71	0.13	1.49	0.87	812	18	772	22	782	18	4.9	1.3
NHG15.12rd6_88		0.93	1.59	0.11	1.39	0.88	694	16	659	17	667	15	4.9	1.1
NHG15.12rd6_15		0.85	1.36	0.10	1.05	0.77	649	19	617	12	624	13	4.9	1.1
NHG15.12rd6_91a		0.94	1.52	0.11	1.30	0.86	699	17	663	16	671	15	5.0	1.2
NHG15.12rd6_70		0.95	1.31	0.11	1.03	0.79	705	17	669	13	677	13	5.1	1.2
NHG15.12rd6_48		0.96	1.64	0.11	1.29	0.78	709	22	673	16	681	16	5.1	1.2
NHG15.12rd6_37b		1.01	1.39	0.11	1.11	0.80	736	18	698	15	707	14	5.1	1.2
NHG15.12_04	RD3	0.92	1.76	0.11	1.50	0.85	693	20	657	19	665	17	5.2	1.2
NHG15.12rd6_21b		0.91	1.45	0.11	1.19	0.82	688	18	651	15	659	14	5.3	1.2
NHG15.12rd6_37a		1.03	1.51	0.12	1.22	0.81	749	19	709	16	718	15	5.3	1.3
NHG15.12rd6_91b		0.91	1.46	0.11	1.30	0.89	684	14	647	16	656	14	5.4	1.2
NHG15.12rd6_51		0.87	1.41	0.10	1.11	0.79	663	19	628	13	635	13	5.4	1.2
NHG15.12rd6_59		0.83	1.35	0.10	0.99	0.73	640	20	604	11	612	12	5.5	1.2
NHG15.12_02	RD3	0.90	1.87	0.10	1.58	0.85	681	21	643	19	652	18	5.6	1.3
NHG15.12rd6_78b		0.82	1.61	0.10	1.37	0.85	638	18	602	16	609	15	5.6	1.2
NHG15.12rd6_90		0.92	1.55	0.11	1.33	0.86	694	17	654	17	663	15	5.7	1.3
NHG15.12rd6_45		0.71	1.43	0.09	1.15	0.80	571	18	538	12	544	12	5.7	1.1
NHG15.12rd6_74a		2.23	1.57	0.20	1.35	0.87	1236	15	1165	29	1190	22	5.8	2.1
NHG15.12rd6_21a		0.89	1.67	0.10	1.32	0.79	676	22	635	16	644	16	6.0	1.4
NHG15.12rd6_78a		0.81	1.49	0.10	1.30	0.87	633	16	595	15	603	13	6.0	1.3
NHG15.12rd6_46		0.93	1.31	0.11	1.08	0.83	703	16	659	14	669	13	6.2	1.5

Appendix 1. Zircon geochronology mass spectrometry. Primary data - Part A

			Concentrations											Ratios			
#Sample + #analysis		#Sample + comments	^{204}Pb	f206c	^{206}Pb	^{207}Pb	^{208}Pb	^{232}Th	^{235}U	Th/U	Pbppm	Thppm	Uppm	$^{238}U/^{206}Pb$	1s %	$^{207}Pb/^{206}Pb$	1s %
NHG15.12rd6_17	44		46	0.5	130056	23770	55527	354720	2412	1.4	42	91	65	2.14	1.3	0.178	0.83
NHG15.12_20	20	RD3	-6	-0.1	143301	8822	41778	927335	11649	0.8	33	221	276	9.99	1.4	0.061	0.90
NHG15.12rd6_33b	64		141	9.1	27294	1700	6087	186465	2403	0.7	7	48	65	10.02	1.1	0.061	1.10
NHG15.12rd6_89	131		200	3.7	94909	5828	11376	232950	7850	0.3	15	51	149	10.21	1.2	0.061	0.90
NHG15.12rd6_77b	116		19	0.4	80873	4905	24287	569246	7279	0.9	15	124	138	11.31	1.3	0.059	0.81
NHG15.12rd6_02	27		85	1.7	89547	5560	17026	444324	7725	0.5	22	114	208	9.93	1.2	0.062	1.00
NHG15.12rd6_84a	125		-23	-0.2	199209	11863	89153	2113750	18666	1.3	40	462	353	11.48	1.4	0.059	0.74
NHG15.12rd6_03	28		77	2.0	67909	4041	20546	599484	6733	0.9	18	154	181	11.38	1.0	0.060	1.11
NHG15.12rd6_33a	63		-15	-1.5	17404	1078	5291	152508	1543	0.9	5	39	42	10.24	1.5	0.061	1.31
NHG15.12rd6_79	119		-3	0.0	216577	13336	94741	1923754	17986	1.2	43	420	340	10.47	1.3	0.061	0.74
NHG15.12rd6_84b	126		119	0.8	253047	15191	65115	1497671	23790	0.7	44	327	450	11.55	1.3	0.059	0.65
NHG15.12rd6_42	75		77	1.8	76547	4596	12422	350109	7330	0.5	19	90	197	11.11	1.2	0.060	0.91
NHG15.12rd6_41	74		155	2.1	133450	8414	36837	1250974	11432	1.0	35	322	308	9.86	1.1	0.062	0.91
NHG15.12rd6_34	65		34	1.0	59248	3853	39266	1118900	4732	2.3	20	288	127	9.18	1.0	0.064	0.99
NHG15.12rd6_32a	61		13	0.9	25698	1562	6292	197617	2442	0.8	7	51	66	11.08	1.3	0.060	1.32
NHG15.12rd6_24a	52		101	2.5	71234	4390	13315	384736	6854	0.5	18	99	184	10.93	1.2	0.060	1.00
NHG15.12rd6_82b	123		2	0.0	56438	3445	11388	260422	5068	0.6	9	57	96	10.88	1.5	0.060	0.89
NHG15.12rd6_63	98		-9	-0.2	69120	4155	21940	771449	7024	1.0	19	198	189	11.64	1.0	0.059	0.84
NHG15.12rd6_49b	83		73	0.9	143012	8901	44000	1837237	12842	1.4	39	472	345	10.35	0.9	0.061	0.72
NHG15.12rd6_97	142		106	1.3	142381	9132	43871	886527	10628	1.0	26	194	201	9.14	1.3	0.064	0.66
NHG15.12rd6_61	96		95	3.3	47449	4011	6991	118490	2067	0.5	12	30	56	5.02	1.5	0.084	0.98
NHG15.12rd6_19	46		-5	-0.1	61110	3808	17084	453764	5399	0.8	16	117	145	10.32	1.3	0.062	0.98
NHG15.12rd6_81	121		137	1.6	150304	8999	50050	1163393	14212	0.9	28	254	269	11.77	1.5	0.059	0.78
NHG15.12rd6_05	30		59	1.6	63263	3937	14477	354229	5669	0.6	16	91	152	10.45	1.3	0.061	0.97
NHG15.12rd6_14	41		20	0.9	38184	2327	9190	279779	3783	0.7	10	72	102	11.41	1.1	0.060	0.99
NHG15.12rd6_56	91		47	4.0	20857	1272	5473	192321	2072	0.9	5	49	56	11.40	1.2	0.060	1.34
NHG15.12_01	1	RD3	42	1.0	76750	4594	22279	497520	7031	0.7	18	119	167	11.43	1.4	0.060	0.88
NHG15.12rd6_65	101		26	0.8	54258	3425	10687	316064	4709	0.6	14	81	127	10.05	1.1	0.062	0.86
NHG15.12rd6_86	128		183	3.9	83513	5301	30801	590564	6857	1.0	16	129	130	10.05	1.5	0.062	0.71
NHG15.12rd6_12	39		137	15.7	15311	1014	3150	81542	1233	0.6	4	21	33	9.17	1.5	0.064	1.44
NHG15.12rd6_44	77		-55	-4.0	24525	1477	9020	290831	2505	1.1	7	75	67	11.68	1.3	0.060	1.37
NHG15.12rd6_43	76		60	0.7	143615	9266	10678	267722	11837	0.2	32	69	318	9.40	1.3	0.064	0.86
NHG15.12_09	9	RD3	20	2.9	12242	744	1801	40936	1188	0.3	3	10	28	11.84	1.7	0.060	1.32
NHG15.12rd6_92b	136		62	0.9	123616	7794	36009	643143	10911	0.7	22	141	206	10.93	1.4	0.062	0.95
NHG15.12rd6_30	59		115	2.9	71211	4315	40073	1426712	7237	1.9	23	367	195	11.67	1.2	0.061	1.08
NHG15.12rd6_32b	62		161	11.4	25041	1527	6312	202604	2427	0.8	7	52	65	11.50	1.3	0.061	1.11
NHG15.12rd6_07	32		131	0.8	286895	18295	62455	2062872	25853	0.8	73	530	695	10.39	1.0	0.063	0.85
NHG15.12rd6_18	45		-68	-2.5	48090	2975	13980	426796	4710	0.9	13	110	127	11.36	1.2	0.061	1.04
NHG15.12_18	18	RD3	197	10.0	34271	2262	8179	158710	2473	0.6	8	38	59	8.90	1.6	0.066	1.33
NHG15.12rd6_80	120		102	0.9	198730	13676	79805	1599766	15284	1.2	39	350	289	9.57	1.2	0.066	1.05
NHG15.12_24	24	RD3	106	2.3	80631	5432	30481	685516	6327	1.1	20	164	150	9.48	1.6	0.067	1.20
NHG15.12rd6_87	129		260	2.4	170616	19475	26081	153677	5778	0.3	29	34	109	4.14	1.6	0.112	0.76
NHG15.12rd6_54	89		-47	-3.4	24360	1663	11467	411190	2434	1.6	7	106	65	11.42	1.3	0.064	1.26
NHG15.12rd6_52	87		129	1.9	114011	7989	27360	803646	9303	0.8	30	207	250	9.46	0.9	0.069	0.85
NHG15.12rd6_13	40		65	4.4	25280	1823	9837	282564	2361	1.1	7	73	64	10.91	1.5	0.071	1.41
NHG15.12_15	15	RD3	54	1.9	47821	3497	12622	931857	5887	1.6	11	223	140	14.38	3.4	0.072	2.00
~~NHG15.12rd6_98~~	~~143~~	~~high common Pb~~	~~472~~	~~8.6~~	~~82842~~	~~10391~~	~~28129~~	~~251600~~	~~5394~~	~~0.5~~	~~16~~	~~55~~	~~102~~	~~8.15~~	~~1.6~~	~~0.128~~	~~3.94~~
NHG15.2rd4a_10a	71	NHG15.2 - detrital	53	0.5	173805	10712	52338	1043815	13593	0.9	31	228	257	9.20	1.2	0.061	0.66
NHG15.2_23	35	RD3	-28	-0.6	82710	4956	31785	931151	7470	1.3	20	222	177	10.76	1.5	0.058	0.92
NHG15.2rd4a_02	58		-47	-0.8	105903	6492	39722	888670	8557	1.2	20	194	162	9.69	1.3	0.060	0.82
NHG15.2rd4a_30b	99		-106	-3.0	62993	3930	17044	340415	4614	0.9	11	74	87	8.68	1.3	0.062	0.75
NHG15.2rd4a_26	93		-142	-1.6	144811	11465	39959	455878	5962	0.9	26	100	113	4.82	1.3	0.079	0.66
NHG15.2_44	56	RD3	57	1.3	80501	4866	37598	927185	6560	1.4	21	221	156	9.67	1.5	0.060	0.88
NHG15.2rd4a_23	89		61	0.1	720107	62892	85658	852552	25644	0.4	115	186	485	4.20	1.2	0.086	0.51
NHG15.2rd4a_31	100		7	0.1	104607	6420	30551	672680	8289	0.9	19	147	157	9.46	1.3	0.061	0.76
NHG15.2rd4a_07a	65		186	4.7	70716	4348	14891	327047	5556	0.7	12	71	105	9.40	1.4	0.061	0.75
NHG15.2rd4a_22a	87		79	0.7	156381	29238	45065	212600	2466	1.0	31	46	47	1.86	1.4	0.186	0.54
NHG15.2_17	29	RD3	55	3.2	30589	1872	7457	163078	2475	0.7	7	39	59	9.73	1.5	0.060	1.25
NHG15.2_27	39	RD3	40	1.2	57912	3598	10382	254619	4741	0.5	12	61	112	9.62	1.6	0.061	1.00
NHG15.2_41	53	RD3	134	4.3	55553	3420	11226	259565	4402	0.6	12	62	104	9.54	1.5	0.061	1.00
NHG15.2rd4a_14	78		-13	-0.3	72667	4480	17473	388613	5862	0.8	13	85	111	9.42	1.3	0.061	0.77
NHG15.2rd4a_08a	67		33	0.2	222964	24683	58860	449270	5581	0.9	41	98	106	3.06	1.3	0.109	0.62
NHG15.2rd4a_17	82		176	3.2	97638	5811	27283	679922	9236	0.9	17	149	175	11.20	1.4	0.058	0.72
NHG15.2rd4a_16a	80		106	1.8	99064	8179	10471	115188	3928	0.3	16	25	74	4.74	1.3	0.081	0.68
NHG15.2rd4a_13	77		-18	-0.2	186482	12017	38876	726419	12603	0.7	32	159	238	8.13	1.3	0.064	0.68
NHG15.2rd4a_16b	81		-68	-0.7	161325	13343	17780	200647	6500	0.4	26	44	123	4.74	1.2	0.081	0.65
NHG15.2_40	52	RD3	20	0.4	90779	5372	25564	723704	8316	0.9	21	173	197	10.97	1.5	0.059	1.02
NHG15.2rd4a_25	92		49	0.5	181996	11242	44696	997199	14906	0.8	32	218	282	9.60	1.3	0.061	0.70
NHG15.2rd4a_11a	73		98	2.3	75459	4736	18544	385073	5629	0.8	13	84	107	8.88	1.4	0.062	0.79
NHG15.2.rd5_06	6		7	0.3	40226	2509	8199	203263	3080	0.7	9	49	73	9.24	1.6	0.062	1.00
NHG15.2rd4a_08b	68		39	0.6	103832	11654	20605	152248	2661	0.7	18	33	50	3.05	1.6	0.111	0.68
NHG15.2_12	24	RD3	-118	-1.7	122911	7498	38931	807739	10296	0.8	29	193	244	9.98	1.4	0.060	1.03
NHG15.2_34	46	RD3	-36	-1.3	48985	3052	17612	433146	3863	1.1	12	103	92	9.33	1.5	0.061	1.05
NHG15.2rd4a_09a	69		-50	-0.4	231481	13689	72068	1722437	21063	0.9	42	376	399	10.76	1.2	0.059	0.61
NHG15.2rd4a_30a	98		95	2.1	77861	4899	28281	586417	5778	1.2	15	128	109	8.88	1.3	0.062	0.77
NHG15.2_28	40	RD3	150	1.4	192024	12625	8304	162953	12281	0.1	36	39	291	7.70	1.4	0.065	0.83
NHG15.2_25	37	RD3	-25	-0.3	132453	27034	43132	235313	1977	1.2	34	56	47	1.79	1.6	0.204	0.77
NHG15.2_20	32	RD3	67	0.7	176941	10814	48474	1254023	14600	0.9	40	299	346	9.86	1.4	0.061	0.94
NHG15.2rd4a_07b	66		55	1.1	87985	5401	19027	418328	7217	0.7	15	91	137	9.76	1.3	0.061	0.71
NHG15.2.rd5_04	4		120	3.7	57460	3382	8093	230445	4971	0.5	12	55	118	10.60	1.5	0.059	0.95
NHG15.2rd4a_06b	63		-20	-0.2	170967	10398	48281	1045514	12874	0.9	30	228	244	9.17	1.2	0.062	0.70
NHG15.2rd4a_05a	60		43	0.6	117462	6964	23735	589220	10707	0.6	20	129	203	11.16	1.2	0.059	0.75
NHG15.2rd4a_22b	88		32	0.5	81657	15452	25209	124363	1324	1.1	16	27	25	1.91	1.7	0.187	0.69
NHG15.2_13	25	RD3	-68	-1.1	104275	6660	18075	322212	7317	0.4	22	77	173	8.37	1.5	0.064	1.03
NHG15.2_02	14	RD3	-64	-3.3	34871	2157	12728	237010	2728	0.9	8	57	65	9.33	1.6	0.062	1.16
NHG15.2_43	55	RD3	57	0.8	127367	8520	5372	155194	8059	0.2	24	37	191	7.51	1.4	0.066	0.87
NHG15.2_07	19	RD3	-30	-0.2	238014	19406	15217	154334	9524	0.2	46	37	226	4.78	1.5	0.081	0.84
NHG15.2rd4a_20	85		15	0.2	119499	7424	27190	581844	9685	0.7	20	127	183	9.47	1.3	0.061	0.75
NHG15.2rd4a_11b	74		189	2.8	118540	7475	29008	589066	8949	0.8	21	129	169	9.02	1.2	0.062	0.72
NHG15.2_32	44	RD3	1	0.0	251712	21273	25502	343978	10188	0.3	51	82	242	4.80	1.4	0.081	0.83
NHG15.2rd4a_09b	70		45	0.3	239112	14379	60241	1462591	21503	0.8	42	320	407	10.66	1.3	0.059	0.67
NHG15.2.rd5_03	3		-8	-0.1	109101	6683	17372	465750	8992	0.5	23	111	213	9.89	1.6	0.061	0.77
NHG15.2rd4a_27b	95		106	0.9	217335	13605	73431	1647111	17891	1.1	40	360	339	9.64	1.3	0.061	0.64
NHG15.2rd4a_28	96		133	1.8	134303	8351	29265	636410	10864	0.7	23	139	206	9.57	1.3	0.061	0.59
NHG15.2rd4a_19	84		-17	-0.1	302333	18139	99455	2499477	27636	1.0	56	546	523	10.79	1.2	0.059	0.56

Appendix 1. Zircon geochronology mass spectrometry. Primary data - Part B

		Ratios					Ages and errors						Discordance	
#Sample - analysis	#Sample + comments	$^{207}Pb/^{235}U$	1s %	$^{206}Pb/^{238}U$	1s %	Rho	$^{207}Pb/^{206}Pb$	2s abs	$^{206}Pb/^{238}U$	2s abs	$^{207}Pb/^{235}U$	2s abs	6-38/7-6	6-38/7-35
NHG15.12rd6_17		11.48	1.57	0.47	1.34	0.85	2638	14	2471	55	2563	29	6.3	3.6
NHG15.12_20	RD3	0.85	1.69	0.10	1.43	0.85	657	19	615	17	624	16	6.3	1.4
NHG15.12rd6_33b		0.84	1.55	0.10	1.09	0.70	655	24	613	13	622	14	6.3	1.4
NHG15.12rd6_89		0.82	1.53	0.10	1.24	0.81	643	19	602	14	611	14	6.3	1.4
NHG15.12rd6_77b		0.72	1.52	0.09	1.29	0.85	584	17	546	13	553	13	6.4	1.3
NHG15.12rd6_02		0.86	1.55	0.10	1.19	0.76	662	21	619	14	628	14	6.5	1.5
NHG15.12rd6_84a		0.71	1.61	0.09	1.43	0.89	578	16	538	15	546	14	6.8	1.4
NHG15.12rd6_03		0.72	1.53	0.09	1.05	0.69	586	24	543	11	551	13	7.4	1.5
NHG15.12rd6_33a		0.83	2.02	0.10	1.54	0.76	652	28	601	18	611	18	7.8	1.7
NHG15.12rd6_79		0.80	1.49	0.10	1.29	0.87	639	16	588	15	599	13	8.0	1.7
NHG15.12rd6_84b		0.71	1.48	0.09	1.33	0.90	582	14	535	14	544	12	8.0	1.6
NHG15.12rd6_42		0.74	1.50	0.09	1.20	0.80	604	20	556	13	565	13	8.0	1.7
NHG15.12rd6_41		0.87	1.45	0.10	1.13	0.78	678	19	623	13	635	14	8.1	1.9
NHG15.12rd6_34		0.95	1.44	0.11	1.05	0.73	726	21	667	13	680	14	8.2	2.0
NHG15.12rd6_32a		0.75	1.88	0.09	1.34	0.71	607	29	557	14	567	16	8.2	1.7
NHG15.12rd6_24a		0.76	1.54	0.09	1.18	0.76	616	22	564	13	574	13	8.3	1.8
NHG15.12rd6_82b		0.77	1.70	0.09	1.45	0.85	619	19	567	16	577	15	8.3	1.8
NHG15.12rd6_63		0.70	1.31	0.09	1.01	0.77	580	18	531	10	540	11	8.4	1.7
NHG15.12rd6_49b		0.82	1.13	0.10	0.87	0.77	651	16	595	10	606	10	8.7	1.9
NHG15.12rd6_97		0.96	1.45	0.11	1.29	0.89	735	14	670	16	685	14	9.0	2.2
NHG15.12rd6_61		2.30	1.82	0.20	1.53	0.84	1290	19	1170	33	1213	25	9.3	3.5
NHG15.12rd6_19		0.82	1.60	0.10	1.27	0.79	658	21	596	14	609	15	9.4	2.1
NHG15.12rd6_81		0.70	1.65	0.08	1.45	0.88	581	17	526	15	536	14	9.5	1.9
NHG15.12rd6_05		0.81	1.62	0.10	1.31	0.80	656	21	589	15	603	15	10.2	2.3
NHG15.12rd6_14		0.72	1.51	0.09	1.14	0.75	605	21	541	12	554	13	10.5	2.2
NHG15.12rd6_56		0.73	1.79	0.09	1.19	0.67	608	29	542	12	555	15	10.9	2.3
NHG15.12_01	RD3	0.73	1.69	0.09	1.45	0.85	610	19	540	15	554	14	11.4	2.4
NHG15.12rd6_65		0.86	1.36	0.10	1.05	0.77	691	18	612	12	629	13	11.4	2.7
NHG15.12rd6_86		0.86	1.62	0.10	1.46	0.90	691	15	611	17	628	15	11.5	2.7
NHG15.12rd6_12		0.97	2.11	0.11	1.53	0.73	757	30	667	19	688	21	11.8	3.0
NHG15.12rd6_44		0.71	1.89	0.09	1.31	0.69	606	30	530	13	544	16	12.6	2.7
NHG15.12rd6_43		0.94	1.52	0.11	1.26	0.82	746	18	652	16	673	15	12.7	3.2
NHG15.12_09	RD3	0.70	2.16	0.08	1.71	0.79	609	28	523	17	539	18	14.2	3.0
NHG15.12rd6_92b		0.78	1.69	0.09	1.39	0.83	659	20	564	15	583	15	14.4	3.3
NHG15.12rd6_30		0.72	1.60	0.09	1.19	0.74	624	23	530	12	548	13	15.0	3.3
NHG15.12rd6_32b		0.73	1.70	0.09	1.29	0.76	635	24	538	13	556	14	15.4	3.4
NHG15.12rd6_07		0.83	1.33	0.10	1.02	0.77	703	18	593	12	616	12	15.7	3.8
NHG15.12rd6_18		0.74	1.59	0.09	1.20	0.76	649	22	544	13	565	14	16.2	3.7
NHG15.12_18	RD3	1.03	2.08	0.11	1.60	0.77	821	28	687	21	719	21	16.3	4.4
NHG15.12rd6_80		0.95	1.61	0.10	1.22	0.76	796	22	641	15	676	16	19.5	5.2
NHG15.12_24	RD3	0.98	1.96	0.11	1.56	0.79	842	25	646	19	691	20	23.3	6.5
NHG15.12rd6_87		3.72	1.80	0.24	1.63	0.91	1827	14	1395	41	1575	28	23.6	11.4
NHG15.12rd6_54		0.77	1.77	0.09	1.25	0.71	741	27	541	13	581	16	27.0	6.9
NHG15.12rd6_52		1.00	1.26	0.11	0.93	0.74	891	18	647	11	704	13	27.4	8.1
NHG15.12rd6_13		0.89	2.04	0.09	1.48	0.72	947	29	566	16	648	19	40.3	12.7
NHG15.12_15	RD3	0.69	3.96	0.07	3.42	0.86	976	41	433	29	531	32	55.6	18.4
~~NHG15.12rd6_98~~	~~high common Pb~~	~~2.16~~	~~4.25~~	~~0.12~~	~~1.58~~	~~0.37~~	~~2067~~	~~69~~	~~746~~	~~22~~	~~1169~~	~~57~~	~~63.9~~	~~36.1~~
NHG15.2rd4a_10a	NHG15.2 - detrital	0.91	1.41	0.11	1.24	0.88	623	14	665	16	656	14	-6.8	-1.5
NHG15.2_23	RD3	0.75	1.74	0.09	1.48	0.85	544	20	573	16	567	15	-5.3	-1.1
NHG15.2rd4a_02		0.85	1.53	0.10	1.29	0.85	603	18	633	16	626	14	-5.0	-1.1
NHG15.2rd4a_30b		0.98	1.51	0.12	1.31	0.87	673	16	703	17	696	15	-4.4	-1.0
NHG15.2rd4a_26		2.25	1.45	0.21	1.29	0.89	1164	13	1215	28	1196	20	-4.3	-1.5
NHG15.2_44	RD3	0.86	1.73	0.10	1.48	0.86	610	19	634	18	629	16	-4.0	-0.9
NHG15.2rd4a_23		2.82	1.34	0.24	1.24	0.93	1336	10	1378	31	1361	20	-3.1	-1.2
NHG15.2rd4a_31		0.89	1.52	0.11	1.32	0.87	630	16	648	16	644	14	-2.8	-0.7
NHG15.2rd4a_07a		0.89	1.57	0.11	1.37	0.88	635	16	652	17	648	15	-2.6	-0.6
NHG15.2rd4a_22a		13.72	1.51	0.54	1.42	0.93	2704	9	2768	63	2731	28	-2.4	-1.4
NHG15.2_17	RD3	0.86	1.97	0.10	1.52	0.77	616	27	631	18	627	18	-2.3	-0.5
NHG15.2_27	RD3	0.87	1.87	0.10	1.58	0.85	623	21	638	19	634	18	-2.3	-0.5
NHG15.2_41	RD3	0.88	1.84	0.10	1.55	0.84	630	21	642	19	639	17	-2.0	-0.5
NHG15.2rd4a_14		0.89	1.50	0.11	1.28	0.86	638	17	650	16	647	14	-2.0	-0.5
NHG15.2rd4a_08a		4.93	1.45	0.33	1.31	0.91	1790	11	1824	42	1808	24	-1.9	-0.9
NHG15.2rd4a_17		0.72	1.58	0.09	1.41	0.89	542	16	551	15	549	13	-1.8	-0.4
NHG15.2rd4a_16a		2.35	1.46	0.21	1.30	0.89	1216	13	1233	29	1227	21	-1.4	-0.5
NHG15.2rd4a_13		1.08	1.44	0.12	1.27	0.88	737	14	748	18	745	15	-1.4	-0.4
NHG15.2rd4a_16b		2.35	1.39	0.21	1.23	0.89	1218	13	1235	28	1229	20	-1.4	-0.5
NHG15.2_40	RD3	0.74	1.83	0.09	1.52	0.83	555	22	562	16	561	16	-1.3	-0.3
NHG15.2rd4a_25		0.87	1.44	0.10	1.25	0.87	632	15	639	15	637	14	-1.1	-0.3
NHG15.2rd4a_11a		0.97	1.57	0.11	1.35	0.86	681	17	688	18	686	16	-1.0	-0.3
NHG15.2.rd5_06		0.92	1.86	0.11	1.57	0.84	657	21	663	20	661	18	-0.8	-0.2
NHG15.2rd4a_08b		5.01	1.72	0.33	1.57	0.92	1815	12	1827	50	1821	29	-0.6	-0.3
NHG15.2_12	RD3	0.83	1.73	0.10	1.39	0.80	612	22	616	16	615	16	-0.6	-0.2
NHG15.2_34	RD3	0.91	1.84	0.11	1.50	0.82	653	23	656	19	655	18	-0.6	-0.2
NHG15.2rd4a_09a		0.76	1.38	0.09	1.23	0.90	570	13	573	14	572	12	-0.6	-0.1
NHG15.2rd4a_30a		0.97	1.53	0.11	1.32	0.86	684	16	688	17	687	15	-0.5	-0.1
NHG15.2_28	RD3	1.17	1.61	0.13	1.38	0.86	784	17	788	20	786	17	-0.4	-0.1
NHG15.2_25	RD3	15.70	1.79	0.56	1.61	0.90	2855	13	2865	74	2859	34	-0.4	-0.2
NHG15.2_20	RD3	0.85	1.68	0.10	1.40	0.83	622	20	623	17	622	16	-0.2	-0.1
NHG15.2rd4a_07b		0.86	1.49	0.10	1.31	0.88	628	15	629	16	628	14	-0.1	-0.1
NHG15.2.rd5_04		0.77	1.75	0.09	1.47	0.84	581	21	581	16	581	15	-0.1	0.0
NHG15.2rd4a_06b		0.93	1.43	0.11	1.24	0.87	667	15	667	16	667	14	0.0	0.0
NHG15.2rd4a_05a		0.72	1.44	0.09	1.23	0.85	554	16	553	13	553	12	0.1	0.0
NHG15.2rd4a_22b		13.52	1.81	0.52	1.67	0.92	2719	11	2715	74	2717	34	0.1	0.1
NHG15.2_13	RD3	1.05	1.86	0.12	1.55	0.83	729	22	728	21	728	19	0.2	0.0
NHG15.2_02	RD3	0.91	1.96	0.11	1.58	0.81	658	25	656	20	657	19	0.2	0.0
NHG15.2_43	RD3	1.21	1.65	0.13	1.41	0.85	808	18	806	21	806	18	0.2	0.0
NHG15.2_07	RD3	2.34	1.74	0.21	1.53	0.88	1227	16	1224	34	1225	24	0.3	0.1
NHG15.2rd4a_20		0.89	1.51	0.11	1.31	0.87	652	16	647	16	648	14	0.7	0.1
NHG15.2rd4a_11b		0.95	1.43	0.11	1.23	0.86	683	15	678	16	679	14	0.8	0.1
NHG15.2_32	RD3	2.34	1.59	0.21	1.36	0.85	1231	16	1221	30	1224	22	0.8	0.3
NHG15.2rd4a_09b		0.77	1.44	0.09	1.28	0.89	583	15	578	14	579	13	0.8	0.1
NHG15.2.rd5_03		0.84	1.78	0.10	1.60	0.90	627	17	621	19	622	16	1.0	0.2
NHG15.2rd4a_27b		0.87	1.43	0.10	1.28	0.90	643	14	636	15	637	13	1.0	0.2
NHG15.2rd4a_28		0.88	1.39	0.10	1.26	0.91	648	13	641	15	642	13	1.1	0.2
NHG15.2rd4a_19		0.76	1.30	0.09	1.17	0.90	579	12	572	13	573	11	1.3	0.2

Appendix 1. Zircon geochronology mass spectrometry. Primary data - Part A

			Concentrations											Ratios			
#Sample + #analysis		#Sample + comments	^{204}Pb	f206c	^{206}Pb	^{207}Pb	^{208}Pb	^{232}Th	^{235}U	Th/U	Pbppm	Thppm	Uppm	^{238}U/^{206}Pb	1s %	^{207}Pb/^{206}Pb	1s %
NHG15.2_18	30	RD3	-45	-1.3	58903	3609	10567	235442	4661	0.5	12	56	110	9.51	1.6	0.061	0.98
NHG15.2_11	23	RD3	28	0.3	175024	10687	24873	519343	14476	0.4	36	124	343	10.02	1.5	0.061	0.93
NHG15.2_01	13	RD3	54	0.4	207861	17519	5894	56982	7942	0.1	39	14	188	4.56	1.5	0.085	0.82
NHG15.2.rd5_02	2		129	2.1	110721	6856	5048	127932	8896	0.1	21	31	211	9.69	1.4	0.061	0.87
NHG15.2_06	18	RD3	-2	0.0	231510	27093	62387	420448	5928	0.7	54	100	141	3.07	1.6	0.114	0.79
NHG15.2_10	22	RD3	-22	-0.4	92227	5488	22500	528203	8894	0.6	20	126	211	11.71	1.5	0.058	0.99
NHG15.2_35	47	RD3	100	1.2	150727	9165	68215	1653359	11662	1.4	39	395	276	9.47	1.5	0.062	0.90
NHG15.2rd4a_15	79		104	2.5	73718	4662	19754	402594	5635	0.8	13	88	107	9.18	1.3	0.062	0.74
NHG15.2_22	34	RD3	62	4.3	25570	1516	7257	198885	2413	0.8	6	47	57	11.38	1.6	0.059	1.40
NHG15.2rd4a_06b	64		136	5.4	43909	2803	5943	118191	3195	0.4	7	26	60	8.90	1.4	0.063	1.01
NHG15.2_36	48	RD3	-93	-3.0	55635	3338	15922	417591	5059	0.8	13	100	120	10.89	1.4	0.059	1.18
NHG15.2_04	16	RD3	158	2.6	106034	6492	31712	640586	9071	0.7	24	153	215	10.14	1.4	0.061	1.03
NHG15.2rd4a_24b	91		147	8.4	30782	1925	6110	130038	2472	0.6	5	28	47	9.48	1.6	0.062	1.12
NHG15.2.rd5_01	1		60	0.5	221761	13681	24330	656883	18354	0.4	44	157	435	10.01	1.4	0.061	0.74
NHG15.2_30	42	RD3	91	2.3	69771	4325	15471	395909	5566	0.7	15	95	132	9.72	1.6	0.061	0.91
NHG15.2_15	27	RD3	84	0.8	184388	11285	46320	1007412	15175	0.7	41	241	360	9.85	1.4	0.061	0.83
NHG15.2rd4a_27a	94		97	1.3	128655	7958	44072	985113	10624	1.1	24	215	201	9.72	1.3	0.061	0.75
NHG15.2rd4a_12b	76		66	1.2	94468	5566	30674	779696	8689	1.0	17	170	164	11.10	1.3	0.059	0.78
NHG15.2_08	20	RD3	70	1.8	68395	4269	19851	428851	5698	0.8	16	102	135	10.05	1.5	0.061	1.01
NHG15.2_03	15	RD3	-93	-1.0	159713	9453	67407	1614263	15468	1.1	40	386	367	11.67	1.4	0.059	0.84
NHG15.2.rd5_07	7		22	0.3	115734	7250	23621	600562	8834	0.7	25	143	209	9.36	1.4	0.062	0.85
NHG15.2.rd5_10	10		156	3.0	88040	7373	9470	124527	3609	0.3	18	30	86	4.89	1.6	0.082	0.73
NHG15.2rd4a_18	83		35	0.4	171840	10307	36585	896705	15298	0.7	29	196	289	10.57	1.2	0.060	0.69
NHG15.2_16	28	RD3	73	2.4	53982	3346	9537	213019	4647	0.5	11	51	110	10.19	1.6	0.061	1.06
NHG15.2.rd5_11	11		39	0.4	164542	9766	24945	749594	15321	0.5	34	179	363	11.24	1.4	0.059	0.78
NHG15.2rd4a_24a	90		40	0.4	200841	12529	88774	2027599	16356	1.4	40	443	310	9.71	1.3	0.062	0.60
NHG15.2_26	38	RD3	34	1.0	59302	3618	8558	242976	5283	0.5	12	58	125	10.60	1.5	0.060	1.09
NHG15.2.rd5_12	12		-72	-1.7	75869	4606	17755	527753	6928	0.8	17	126	164	11.01	1.4	0.060	0.86
NHG15.2_19	31	RD3	2	0.1	81393	5083	22665	521268	6614	0.8	19	124	157	9.63	1.4	0.062	0.85
NHG15.2rd4a_29	97		114	2.8	73179	4658	16825	373857	5909	0.7	13	82	112	9.58	1.3	0.062	0.81
NHG15.2_24	36	RD3	10	0.3	60958	3728	20048	558187	5475	1.0	14	133	130	10.64	1.4	0.060	1.01
NHG15.2rd4a_21	86		4	0.0	402282	86319	145245	661618	6377	1.2	84	145	121	1.89	1.3	0.211	0.54
NHG15.2_42	54	RD3	201	8.8	40256	2503	15607	406964	3292	1.2	10	97	78	9.73	1.5	0.062	1.10
NHG15.2_38	50	RD3	74	1.6	83696	5196	28127	726299	6843	1.1	20	173	162	9.93	1.4	0.062	0.96
NHG15.2_05	17	RD3	-86	-5.1	29888	1804	6372	133454	2715	0.5	6	32	64	10.90	1.5	0.060	1.18
NHG15.2rd4a_06a	62		24	0.6	76529	4760	15412	335953	6188	0.6	13	73	117	9.78	1.3	0.062	0.89
NHG15.2_33	45	RD3	20	0.1	518196	49684	63035	772422	17799	0.4	107	184	422	4.09	1.5	0.095	0.75
NHG15.2_31	43	RD3	166	10.8	27354	1642	10188	295347	2517	1.2	7	71	60	10.99	1.6	0.060	1.25
NHG15.2_37	49	RD3	40	1.7	41172	2521	6866	174858	3771	0.5	9	42	89	10.91	1.6	0.060	1.10
NHG15.2.rd5_09	9		76	3.2	41978	2571	9653	290592	3971	0.7	9	69	94	11.22	1.5	0.061	0.93
NHG15.2rd4a_12a	75		40	1.7	40903	2513	10773	252962	3780	0.8	7	55	72	10.96	1.4	0.061	1.30
NHG15.2rd4a_32	101		135	0.5	441832	36881	57946	1014924	19417	0.6	71	222	367	5.20	1.3	0.084	0.69
NHG15.2_09	21	RD3	60	0.7	153101	11691	9918	175353	8985	0.2	30	42	213	6.35	3.6	0.075	1.15
NHG15.2_21	33	RD3	71	3.4	36431	2359	11525	266962	2958	0.9	9	64	70	9.73	1.7	0.063	1.26
NHG15.2.rd5_08	8		-64	-2.0	54960	3521	23115	588324	4431	1.3	14	141	105	9.54	1.5	0.064	0.88
NHG15.2rd4a_10b	72		47	0.8	99184	6550	35729	708302	7600	1.1	19	155	144	9.26	1.7	0.065	0.84
NHG15.2rd4a_03	59		-13	-0.1	354027	29310	30070	325927	16257	0.2	55	71	308	5.55	1.4	0.082	0.61
NHG15.2rd4a_01	57		-28	-0.5	103114	7254	31335	587549	7531	0.9	19	128	143	8.83	1.4	0.066	1.08
NHG15.2_29	41	RD3	32	4.0	14221	880	3411	93220	1332	0.7	3	22	32	11.20	2.0	0.061	1.62
NHG15.2_14	26	RD3	37	4.1	15996	1000	3407	81572	1544	0.5	3	19	37	11.63	1.7	0.061	1.51
NHG15.2rd4a_05b	61		49	0.2	359312	23815	94349	2746269	30593	1.0	63	600	579	10.12	1.6	0.065	0.89
NHG15.2.rd5_05	5		103	14.6	12335	815	2653	78481	1187	0.7	3	19	28	11.63	1.8	0.064	1.61
NHG15.2_39	51	RD3	48	1.6	52484	3620	19454	421557	4265	1.0	13	101	101	9.67	1.6	0.070	1.49
PT15.1_42	42	PT15.1 - detrital	73	2.7	48385	2935	16578	399000	3864	1.2	11	101	86	9.59	2.0	0.060	1.09
PT15.1_45	45		73	2.3	55993	3453	12742	305851	4536	0.8	11	77	101	9.75	2.0	0.060	1.22
PT15.1_46	46		134	6.5	36473	2216	14728	345707	2953	1.3	8	88	66	9.77	2.0	0.060	1.11
PT15.1_36	36		93	5.9	28105	1694	19469	480579	2325	2.3	8	122	52	9.93	1.9	0.060	1.21
PT15.1_39	39		104	2.6	71724	4415	24857	589433	5816	1.1	16	149	130	9.70	1.9	0.060	1.08
PT15.1_53	53		13	0.1	217112	13087	64798	1544469	18290	1.0	47	391	408	10.13	1.8	0.060	0.87
PT15.1_48	48		86	0.2	691270	109957	60176	329037	12302	0.3	137	83	275	2.15	1.8	0.157	0.87
PT15.1rd5_05b	75		-20	-0.5	64860	3923	26037	612061	5945	1.0	19	157	160	10.55	1.3	0.059	1.08
PT15.1_65	65		59	0.9	113691	6933	66982	1626474	9305	2.0	30	412	208	9.91	1.8	0.060	1.03
PT15.1rd5_01	68		93	4.4	37747	2274	20006	461427	3374	1.3	12	119	91	10.32	1.3	0.060	1.20
PT15.1_62	62		191	2.0	169999	10338	45687	1076318	14220	0.9	36	273	317	10.06	1.8	0.060	0.92
PT15.1_27	27		36	1.6	39591	2444	14166	401134	3399	1.2	10	99	84	9.89	1.4	0.061	1.17
PT15.1_44	44		-70	-0.4	332631	20172	95943	2329729	27491	1.0	71	590	614	10.02	1.8	0.060	0.92
PT15.1rd5_12	82		-4	-0.1	66192	3987	36515	814135	5930	1.3	21	209	160	10.32	1.1	0.060	0.91
PT15.1_29	29		16	0.4	75700	4618	43876	1263295	6632	1.9	23	313	164	10.14	1.3	0.060	1.05
PT15.1_67	67		33	0.4	147829	9101	47784	1116169	12247	1.0	32	283	273	9.91	1.9	0.061	1.05
PT15.1_02	2		49	3.0	29035	1741	16896	485772	2528	1.9	9	120	63	10.14	1.5	0.060	1.29
PT15.1_35	35		234	11.2	37158	2270	18529	435094	3041	1.6	9	110	68	10.01	1.9	0.061	1.28
PT15.1_64	64		8	0.2	90060	5464	25340	586551	7623	0.9	19	149	170	10.13	1.8	0.060	1.06
PT15.1_25	25		105	4.2	44357	2708	18957	542992	3912	1.4	12	135	97	10.11	1.2	0.060	1.09
PT15.1_61	61		114	1.2	162963	9887	56737	1354177	13623	1.1	36	343	304	10.02	1.9	0.061	0.92
PT15.1_60	60		114	5.9	34177	2097	25449	588510	2836	2.4	10	149	63	9.90	2.1	0.061	1.15
PT15.1_56	56		-82	-1.7	87921	5379	37101	860492	7505	1.3	21	218	167	10.20	1.8	0.060	1.01
PT15.1_01	1		69	0.7	163502	10059	52942	1590144	14523	1.1	42	394	360	10.21	1.2	0.060	0.88
PT15.1_63	63		-24	-0.4	100766	6163	39673	937404	8539	1.2	23	237	191	10.16	1.9	0.061	0.99
PT15.1_49	49		-35	-1.8	33612	2050	20298	486119	2759	2.0	9	123	62	9.95	2.0	0.061	1.38
PT15.1_31	31		-7	-0.2	86213	5266	33020	949610	7675	1.2	23	235	190	10.27	1.2	0.060	0.98
PT15.1_55	55		13	0.5	42913	2656	16502	396507	3505	1.3	10	100	78	10.06	1.9	0.061	1.01
PT15.1_20	20		44	1.7	44936	2764	14287	417480	4022	1.0	11	103	100	10.32	1.2	0.060	1.03
PT15.1_57	57		141	4.1	61529	3798	38052	883960	5148	1.9	16	224	115	9.95	1.9	0.061	1.22
PT15.1rd5_05a	74		61	1.0	110737	6719	53467	1212515	10009	1.2	34	312	269	10.43	1.3	0.060	1.13
PT15.1_52	52		83	1.4	107888	6620	43091	1033300	8965	1.3	25	262	200	10.06	1.8	0.061	0.99
PT15.1rd5_07	77		170	5.0	59724	3690	13337	302768	5401	0.5	15	78	145	10.44	1.2	0.060	1.09
PT15.1_14	14		-2	-0.1	48301	2899	21730	623755	4328	1.4	13	155	107	10.48	1.3	0.060	1.07
PT15.1_38	38		-68	-1.9	64680	4030	11152	263033	5287	0.6	13	67	118	9.88	1.9	0.061	1.03
PT15.1_51	51		-12	-0.4	53431	3283	22987	535791	4449	1.4	13	136	99	10.08	1.9	0.061	1.10
PT15.1_40	40		-119	-2.8	74351	4663	40340	973083	6109	1.8	19	246	136	9.77	2.0	0.062	1.05
PT15.1_24	24		-4	-0.3	25288	1594	15123	433661	2234	1.9	8	107	55	10.06	1.5	0.061	1.19
PT15.1_23	23		-28	-0.8	64086	3945	25176	724928	5849	1.2	17	180	145	10.45	1.2	0.061	0.94
PT15.1_30	30		28	0.4	129586	7918	43707	1226232	11843	1.0	33	304	293	10.47	1.2	0.061	0.86
PT15.1_13	13		-1	0.0	135692	8401	35652	1009161	12149	0.8	33	250	301	10.36	1.2	0.061	0.91
PT15.1_41	41		-32	-1.2	45730	2796	22439	547291	3750	1.7	11	139	84	9.99	1.9	0.061	1.12
PT15.1rd5_14	84		-3	-0.2	31651	1976	8946	199755	2852	0.7	8	51	77	10.32	1.2	0.061	1.31

Appendix 1. Zircon geochronology mass spectrometry. Primary data - Part B

		Ratios					Ages and errors						Discordance	
#Sample - analysis	#Sample + comments	$^{207}Pb/^{235}U$	1s %	$^{206}Pb/^{238}U$	1s %	Rho	$^{207}Pb/^{206}Pb$	2s abs	$^{206}Pb/^{238}U$	2s abs	$^{207}Pb/^{235}U$	2s abs	6-38/7-6	6-38/7-35
NHG15.2_18	RD3	0.89	1.85	0.11	1.57	0.85	654	21	645	19	647	18	1.4	0.3
NHG15.2_11	RD3	0.83	1.72	0.10	1.45	0.84	624	20	613	17	615	16	1.7	0.3
NHG15.2_01	RD3	2.55	1.69	0.22	1.48	0.87	1305	16	1277	34	1287	24	2.1	0.8
NHG15.2.rd5_02		0.87	1.68	0.10	1.44	0.85	650	19	633	17	636	16	2.6	0.5
NHG15.2_06	RD3	5.12	1.75	0.33	1.56	0.89	1865	14	1817	49	1840	29	2.6	1.2
NHG15.2_10	RD3	0.69	1.83	0.09	1.55	0.84	543	22	528	16	531	15	2.8	0.5
NHG15.2_35	RD3	0.90	1.73	0.11	1.47	0.85	666	19	647	18	651	16	2.9	0.6
NHG15.2rd4a_15		0.94	1.48	0.11	1.28	0.87	686	16	667	16	671	14	2.9	0.6
NHG15.2_22	RD3	0.71	2.12	0.09	1.59	0.75	559	31	543	17	546	18	2.9	0.5
NHG15.2rd4a_06b		0.97	1.69	0.11	1.36	0.80	707	21	686	18	691	17	2.9	0.7
NHG15.2_36	RD3	0.75	1.85	0.09	1.43	0.77	584	26	566	15	570	16	3.1	0.6
NHG15.2_04	RD3	0.82	1.77	0.10	1.45	0.81	626	22	606	17	610	16	3.1	0.6
NHG15.2rd4a_24b		0.90	1.95	0.11	1.60	0.82	668	24	647	20	651	19	3.3	0.7
NHG15.2.rd5_01		0.84	1.56	0.10	1.38	0.88	636	16	614	16	618	14	3.4	0.7
NHG15.2_30	RD3	0.87	1.82	0.10	1.57	0.86	654	20	631	19	636	17	3.4	0.7
NHG15.2_15	RD3	0.86	1.63	0.10	1.40	0.86	646	18	624	17	628	15	3.4	0.7
NHG15.2rd4a_27a		0.87	1.50	0.10	1.30	0.87	654	16	631	16	636	14	3.5	0.8
NHG15.2rd4a_12b		0.74	1.50	0.09	1.28	0.85	576	17	556	14	560	13	3.5	0.7
NHG15.2_08	RD3	0.83	1.80	0.10	1.50	0.83	635	22	611	17	616	17	3.7	0.8
NHG15.2_03	RD3	0.69	1.63	0.09	1.39	0.86	551	18	530	14	534	13	3.9	0.7
NHG15.2.rd5_07		0.92	1.61	0.11	1.37	0.85	682	18	654	17	660	16	4.0	0.9
NHG15.2.rd5_10		2.32	1.73	0.20	1.57	0.91	1251	14	1199	34	1217	24	4.1	1.5
NHG15.2rd4a_18		0.78	1.40	0.09	1.22	0.87	608	15	583	14	588	12	4.2	0.9
NHG15.2_16	RD3	0.82	1.91	0.10	1.59	0.83	631	23	604	18	609	17	4.3	0.9
NHG15.2.rd5_11		0.73	1.64	0.09	1.44	0.88	576	17	549	15	554	14	4.6	0.9
NHG15.2rd4a_24a		0.88	1.46	0.10	1.33	0.91	664	13	632	16	639	14	4.8	1.1
NHG15.2_26	RD3	0.78	1.82	0.09	1.45	0.80	611	24	581	16	587	16	4.9	1.0
NHG15.2.rd5_12		0.75	1.67	0.09	1.43	0.86	592	19	560	15	566	14	5.3	1.1
NHG15.2_19	RD3	0.89	1.67	0.10	1.44	0.86	675	18	637	17	645	16	5.7	1.3
NHG15.2rd4a_29		0.89	1.52	0.10	1.28	0.84	679	17	640	16	648	14	5.7	1.3
NHG15.2_24	RD3	0.78	1.72	0.09	1.40	0.81	614	22	579	15	586	15	5.7	1.2
NHG15.2rd4a_21		15.36	1.37	0.53	1.26	0.92	2912	9	2736	56	2838	26	6.0	3.6
NHG15.2_42	RD3	0.88	1.85	0.10	1.49	0.81	672	23	631	18	640	17	6.1	1.4
NHG15.2_38	RD3	0.85	1.74	0.10	1.45	0.83	658	21	618	17	627	16	6.1	1.4
NHG15.2_05	RD3	0.76	1.87	0.09	1.45	0.77	603	26	566	16	573	16	6.1	1.3
NHG15.2rd4a_06a		0.87	1.58	0.10	1.31	0.83	669	19	628	16	637	15	6.2	1.4
NHG15.2_33	RD3	3.21	1.70	0.24	1.53	0.90	1530	14	1411	39	1459	26	7.8	3.3
NHG15.2_31	RD3	0.76	2.06	0.09	1.64	0.80	612	27	561	18	571	18	8.2	1.7
NHG15.2_37	RD3	0.76	1.97	0.09	1.63	0.83	616	24	565	18	575	17	8.2	1.7
NHG15.2.rd5_09		0.74	1.78	0.09	1.52	0.85	623	20	550	16	564	15	11.6	2.5
NHG15.2rd4a_12a		0.77	1.90	0.09	1.38	0.73	641	28	563	15	579	17	12.1	2.7
NHG15.2rd4a_32		2.23	1.47	0.19	1.30	0.88	1292	13	1134	27	1189	20	12.3	4.7
NHG15.2_09	RD3	1.63	3.77	0.16	3.59	0.95	1075	23	942	63	983	46	12.3	4.1
NHG15.2_21	RD3	0.90	2.16	0.10	1.75	0.81	720	27	631	21	650	21	12.4	3.0
NHG15.2.rd5_08		0.92	1.76	0.10	1.53	0.87	737	19	643	19	664	17	12.7	3.2
NHG15.2rd4a_10b		0.96	1.87	0.11	1.67	0.89	766	18	661	21	685	18	13.7	3.5
NHG15.2rd4a_03		2.03	1.49	0.18	1.36	0.91	1238	12	1067	27	1125	20	13.8	5.1
NHG15.2rd4a_01		1.03	1.80	0.11	1.44	0.80	804	23	692	19	718	18	14.0	3.7
NHG15.2_29	RD3	0.76	2.58	0.09	2.01	0.78	655	35	551	21	572	22	15.9	3.6
NHG15.2_14	RD3	0.73	2.31	0.09	1.74	0.75	646	33	532	18	554	19	17.6	3.9
NHG15.2rd4a_05b		0.89	1.86	0.10	1.63	0.88	775	19	607	19	644	18	21.7	5.7
NHG15.2.rd5_05		0.76	2.41	0.09	1.80	0.75	739	34	532	18	573	21	28.0	7.1
NHG15.2_39	RD3	0.99	2.17	0.10	1.58	0.73	918	31	634	19	700	22	30.9	9.4
PT15.1_42	PT15.1 - detrital	0.86	2.24	0.10	1.95	0.87	609	24	640	24	633	21	-5.0	-1.1
PT15.1_45		0.85	2.31	0.10	1.97	0.85	611	26	630	24	625	21	-3.1	-0.7
PT15.1_46		0.85	2.28	0.10	1.99	0.87	610	24	628	24	624	21	-3.1	-0.7
PT15.1_36		0.83	2.29	0.10	1.94	0.85	602	26	618	23	615	21	-2.7	-0.6
PT15.1_39		0.86	2.20	0.10	1.91	0.87	616	23	632	23	629	20	-2.6	-0.6
PT15.1_53		0.81	1.99	0.10	1.79	0.90	593	19	607	21	604	18	-2.3	-0.5
PT15.1_48		10.08	2.00	0.47	1.80	0.90	2424	15	2465	73	2442	36	-1.7	-0.9
PT15.1rd5_05b		0.77	1.67	0.09	1.28	0.76	576	23	584	14	582	15	-1.5	-0.3
PT15.1_65		0.84	2.07	0.10	1.79	0.87	613	22	619	21	618	19	-1.1	-0.3
PT15.1rd5_01		0.80	1.77	0.10	1.29	0.73	596	26	596	15	596	16	-0.1	-0.1
PT15.1_62		0.82	2.01	0.10	1.79	0.89	611	20	611	21	611	18	0.0	0.0
PT15.1_27		0.84	1.83	0.10	1.41	0.77	623	25	621	17	621	17	0.4	0.0
PT15.1_44		0.83	2.02	0.10	1.80	0.89	618	20	613	21	614	18	0.7	0.1
PT15.1rd5_12		0.80	1.46	0.10	1.14	0.78	602	20	596	13	597	13	0.9	0.2
PT15.1_29		0.82	1.67	0.10	1.30	0.78	613	23	606	15	608	15	1.0	0.2
PT15.1_67		0.84	2.18	0.10	1.91	0.88	626	23	619	22	621	20	1.0	0.2
PT15.1_02		0.82	1.96	0.10	1.48	0.76	613	28	606	17	607	18	1.2	0.2
PT15.1_35		0.83	2.32	0.10	1.94	0.83	622	28	614	23	615	21	1.4	0.3
PT15.1_64		0.82	2.13	0.10	1.84	0.87	617	23	607	21	609	19	1.6	0.3
PT15.1_25		0.82	1.64	0.10	1.23	0.75	619	24	608	14	610	15	1.8	0.4
PT15.1_61		0.83	2.08	0.10	1.86	0.90	626	20	613	22	616	19	2.1	0.4
PT15.1_60		0.85	2.41	0.10	2.12	0.88	635	25	621	25	624	22	2.3	0.5
PT15.1_56		0.82	2.08	0.10	1.82	0.88	620	22	603	21	606	19	2.7	0.6
PT15.1_01		0.82	1.46	0.10	1.16	0.80	620	19	603	13	606	13	2.8	0.6
PT15.1_63		0.82	2.10	0.10	1.85	0.88	624	21	605	21	609	19	3.1	0.6
PT15.1_49		0.84	2.41	0.10	1.97	0.82	638	30	618	23	622	22	3.2	0.7
PT15.1_31		0.81	1.56	0.10	1.21	0.77	619	21	599	14	603	14	3.3	0.7
PT15.1_55		0.83	2.15	0.10	1.90	0.88	633	22	611	22	615	20	3.5	0.7
PT15.1_20		0.81	1.55	0.10	1.16	0.75	619	22	596	13	601	14	3.7	0.8
PT15.1_57		0.85	2.22	0.10	1.86	0.84	646	26	617	22	623	20	4.4	0.9
PT15.1rd5_05a		0.80	1.73	0.10	1.30	0.76	619	24	590	15	596	15	4.6	1.0
PT15.1_52		0.84	2.07	0.10	1.82	0.88	641	21	611	21	617	19	4.7	1.0
PT15.1rd5_07		0.80	1.61	0.10	1.19	0.74	620	23	590	13	596	14	4.9	1.0
PT15.1_14		0.79	1.66	0.10	1.26	0.76	618	23	587	14	594	15	5.0	1.0
PT15.1_38		0.86	2.12	0.10	1.85	0.87	654	22	621	22	628	20	5.0	1.1
PT15.1_51		0.84	2.17	0.10	1.88	0.86	644	24	610	22	617	20	5.3	1.1
PT15.1_40		0.87	2.24	0.10	1.98	0.88	664	22	628	24	636	21	5.3	1.2
PT15.1_24		0.84	1.91	0.10	1.49	0.78	646	26	611	17	618	18	5.4	1.2
PT15.1_23		0.80	1.53	0.10	1.21	0.79	623	20	589	14	596	14	5.4	1.1
PT15.1_30		0.80	1.46	0.10	1.18	0.81	622	18	588	13	595	13	5.5	1.2
PT15.1_13		0.81	1.52	0.10	1.21	0.80	629	20	594	14	601	14	5.5	1.2
PT15.1_41		0.85	2.22	0.10	1.92	0.86	652	24	615	22	623	21	5.6	1.2
PT15.1rd5_14		0.81	1.80	0.10	1.24	0.69	633	28	596	14	604	16	5.8	1.2

Appendix 1. Zircon geochronology mass spectrometry. Primary data - Part A

			Concentrations											Ratios			
#Sample + #analysis		#Sample + comments	^{204}Pb	f206c	^{206}Pb	^{207}Pb	^{208}Pb	^{232}Th	^{235}U	Th/U	Pbppm	Thppm	Uppm	^{238}U/^{206}Pb	1s %	^{207}Pb/^{206}Pb	1s %
PT15.1_66	66		34	0.7	85199	5281	29950	731236	7138	1.2	19	185	159	10.04	1.9	0.061	1.04
PT15.1_43	43		68	1.1	108641	6751	53387	1262699	9030	1.6	27	320	202	10.01	1.8	0.061	0.99
PT15.1rd5_06	76		-17	-0.4	73629	4504	32708	737643	6744	1.0	22	190	181	10.52	1.3	0.061	1.11
PT15.1_05	5		117	8.7	23835	1455	7301	224622	2084	1.1	6	56	52	10.11	1.5	0.061	1.33
PT15.1_26	26		54	1.6	61287	3765	23451	634464	5592	1.1	16	157	138	10.47	1.3	0.061	0.95
PT15.1_04	4		54	0.8	123903	7682	86758	2649153	10918	2.4	40	657	270	10.24	1.2	0.061	0.88
PT15.1_15	15		-75	-1.7	78497	4785	29343	867673	7044	1.2	21	215	174	10.44	1.1	0.061	0.99
PT15.1_18	18		95	5.2	32219	2005	11127	297017	2826	1.1	8	74	70	9.98	1.4	0.062	1.08
PT15.1_12	12		7	0.4	37296	2302	17867	516304	3328	1.6	11	128	82	10.37	1.3	0.061	1.22
PT15.1_50	50		47	2.0	41403	2574	28604	675247	3372	2.3	12	171	75	9.99	2.0	0.062	1.27
PT15.1_59	59		-19	-0.7	44119	2718	24330	552269	3729	1.7	11	140	83	10.12	1.9	0.062	1.09
PT15.1_09	9		67	1.9	62759	3836	54597	1609762	5591	2.9	22	399	138	10.41	1.2	0.061	1.07
PT15.1rd5_03a	70		-101	-10.0	17810	1107	8923	201778	1619	1.2	6	52	44	10.45	1.6	0.061	1.35
PT15.1_54	54		118	1.7	124246	7822	50953	1195181	10308	1.3	29	303	230	10.02	1.8	0.062	0.93
PT15.1_10	10		-34	-1.0	58614	3625	27020	804773	5296	1.5	16	199	131	10.55	1.3	0.061	1.15
PT15.1rd5_09	79		36	1.7	38256	2409	26837	606004	3383	1.7	13	156	91	10.24	1.3	0.062	1.18
PT15.1_22	22		55	3.6	27330	1686	18817	537709	2442	2.2	9	133	60	10.37	1.3	0.062	1.32
PT15.1_28	28		42	3.7	19755	1246	5172	151784	1773	0.9	5	38	44	10.33	1.7	0.062	1.54
PT15.1rd5_02	69		-108	-5.3	35742	2256	19221	423941	3206	1.3	11	109	86	10.35	1.5	0.062	1.27
PT15.1_17	17		18	0.4	79641	5054	32868	891924	7166	1.2	22	221	177	10.25	1.2	0.063	0.94
PT15.1rd5_04a	72		83	0.6	226877	18818	33320	413164	11239	0.4	55	106	302	5.65	1.2	0.081	0.84
PT15.1_58	58		121	10.2	20808	1385	13670	305953	1654	2.1	6	77	37	9.52	2.1	0.064	1.42
PT15.1_19	19		-85	-15.5	9601	611	4401	125563	852	1.5	3	31	21	10.19	1.8	0.063	1.81
PT15.1rd5_10	80		147	8.4	30540	1967	22982	542317	2628	2.0	11	139	71	9.97	1.3	0.064	1.38
PT15.1_47	47		-37	-1.0	65082	4160	30670	761475	5453	1.6	16	193	122	10.15	1.9	0.063	1.06
PT15.1rd5_03b	71		116	15.5	13085	832	5478	122764	1177	1.0	4	32	32	10.34	1.6	0.064	1.62
PT15.1rd5_04b	73		14	0.1	210517	15553	14214	183128	13833	0.1	48	47	372	7.59	1.2	0.072	0.91
PT15.1rd5_08	78		-17	-0.5	55497	3938	25857	498261	4441	1.1	17	128	119	9.83	1.9	0.065	1.97
PT15.1_03	3		-5	-0.6	13574	924	7031	198109	1222	1.6	4	49	30	10.36	1.6	0.065	1.72
PT15.1_32	32		69	12.8	9422	624	4833	137413	815	1.7	3	34	20	10.14	1.8	0.066	1.95
PT15.1_34	34		71	1.6	74550	4963	31407	738672	6178	1.4	18	187	138	9.95	1.9	0.066	1.07
PT15.1_16	16		111	12.7	15225	1010	9311	250356	1361	1.8	5	62	34	10.33	1.5	0.065	1.63
PT15.1_11	11		40	1.9	36774	2440	23365	712828	3371	2.1	12	177	83	10.57	1.3	0.065	1.13
PT15.1_33	33		118	2.5	81595	5628	36398	849495	6564	1.5	20	215	146	9.67	1.9	0.069	1.62
PT15.1rd5_13	83		59	2.1	49255	3328	18960	465872	4730	0.9	14	120	127	11.05	1.3	0.066	1.14
PT15.1_07	7		-39	-1.5	42424	3218	12621	341457	3083	1.1	11	85	76	8.31	2.5	0.076	1.98
PT15.1_06	6		33	1.2	45680	3362	13847	386063	3926	1.0	12	96	97	9.98	1.3	0.073	1.22
PT15.1_37	37		72	4.0	29905	2284	17759	412536	2489	1.9	8	104	56	10.13	2.0	0.078	2.15
PT15.1_08	8	iit two common lead spike	6	0.3	35027	3339	29876	765979	2941	2.6	13	190	73	9.83	1.5	0.094	5.28
PT15.1rd5_11	81		262	25.5	15261	2052	7819	112758	1194	0.9	5	29	32	8.91	2.3	0.135	3.62
PT15.1_21	21	high common Pb?	23	1.2	26331	4321	14597	262031	1998	1.3	8	65	49	8.73	1.6	0.167	4.57
VY473_03a	3	VY473 - volcanic	115	1.0	206572	10398	6150	413947	52366	0.1	35	105	1169	30.40	1.8	0.050	0.99
VY473rd4a_03a	26		79	1.9	69942	5622	8390	83056	2742	0.3	11	18	52	4.71	1.6	0.080	0.95
VY473rd5_05b	60		-7	-0.2	64727	3912	25969	611169	5903	1.0	19	157	159	10.48	1.3	0.059	1.09
VY473rd4a_03b	27		55	0.4	230930	18721	25982	265032	9196	0.3	37	58	174	4.73	1.4	0.081	0.81
VY473rd4a_15b	43		-12	-0.2	89552	5487	18728	375136	7284	0.6	15	82	138	9.89	1.4	0.060	0.86
VY473rd4a_22a	52		-52	-0.3	296536	27984	112204	987157	9316	1.2	58	216	176	3.84	1.3	0.094	0.64
VY473rd4a_22b	53		158	0.4	599802	56389	94214	784795	18604	0.5	100	172	352	3.83	1.4	0.094	0.76
VY473_06	7		189	3.5	96086	5843	34993	820860	8123	1.1	22	208	181	10.11	1.9	0.060	1.00
VY473_12	13		47	0.6	136632	8359	32601	777442	11562	0.8	28	197	258	10.11	1.8	0.060	0.96
VY473rd4a_04	28		153	6.4	42553	2568	12113	257258	3764	0.8	8	56	71	10.50	1.5	0.060	1.03
VY473rd4a_12	38		202	3.5	100477	6304	29394	561388	8010	0.8	18	123	152	9.45	1.5	0.062	0.84
VY473rd4a_16	44		26	0.5	92716	5704	34009	725166	7562	1.1	18	158	143	9.94	1.3	0.061	0.88
VY473rd4a_18a	46		84	2.1	69609	4276	24955	539828	5842	1.1	13	118	111	10.09	1.3	0.061	0.92
VY473rd4a_05	29		69	0.9	140669	8705	29777	602930	11885	0.6	24	132	225	9.91	1.3	0.061	0.83
VY473rd4a_02a	24		137	5.9	41196	2532	11434	221840	3520	0.7	7	48	67	10.19	1.5	0.061	1.04
VY473rd5_05a	59		61	1.0	110736	6719	53467	1212514	10009	1.2	34	312	269	10.42	1.3	0.060	1.13
VY473rd4a_02b	25		114	1.2	170769	10659	61047	1253364	14423	1.0	32	274	273	9.95	1.4	0.061	0.73
VY473rd4a_18b	47		98	1.6	105466	6521	38468	835134	8843	1.1	20	183	167	10.09	1.3	0.061	0.78
VY473rd5_07a	62		170	5.0	59724	3690	13337	302767	5402	0.5	15	78	145	10.43	1.2	0.060	1.09
VY473_14	15		186	3.6	92342	5636	15118	362191	8100	0.5	18	92	181	10.48	1.9	0.061	1.31
VY473_19	21		-125	-2.1	106978	6525	26024	650143	9258	0.8	22	165	207	10.46	1.9	0.061	1.00
VY473_16a	17		30	0.4	128646	7853	30245	746465	11480	0.7	26	189	256	10.61	1.9	0.060	0.96
VY473rd4a_20a	49		115	3.1	65373	3962	33557	755088	5855	1.5	14	165	111	10.81	1.4	0.060	0.90
VY473_05	6		3	0.0	134353	8079	44276	1170837	12134	1.1	30	296	271	10.94	1.8	0.060	1.03
VY473_02	2		40	1.4	51745	3215	16603	383940	4346	1.0	11	97	97	10.12	2.1	0.061	1.17
VY473_07	8		211	2.6	144937	9260	8558	171186	10830	0.2	26	43	242	9.07	1.9	0.063	0.99
VY473rd5_06	61		-21	-0.5	73835	4525	33021	743976	6775	1.0	22	191	182	10.54	1.3	0.061	1.09
VY473_18	20		24	0.8	55005	3424	13456	307774	4595	0.8	11	78	103	10.06	1.9	0.062	1.23
VY473_11	12		-160	-2.5	112824	7059	16505	395180	9410	0.5	22	100	210	10.01	1.9	0.062	1.00
VY473rd4a_15a	42		70	1.6	78052	4920	22538	465522	6542	0.8	14	102	124	10.16	1.3	0.062	0.91
VY473rd5_02a	55		-92	-9.1	17832	1114	8960	202357	1637	1.2	6	52	44	10.45	1.6	0.062	1.34
VY473_13	14		24	1.3	33875	2124	8112	193122	2857	0.8	7	49	64	10.25	2.0	0.062	1.15
VY473_16b	18		-17	-0.3	97091	5979	25102	583321	8498	0.8	20	148	190	10.54	1.9	0.061	1.07
VY473rd4a_14a	40		62	0.9	118596	7312	46916	1073452	10649	1.2	23	235	202	10.84	1.3	0.061	0.91
VY473rd4a_09b	34		-1	-0.1	42364	2615	8650	177135	3705	0.6	7	39	70	10.55	1.4	0.062	1.14
VY473_03b	4		39	0.2	371688	19120	90487	5216094	100206	0.6	76	1321	2236	32.22	2.1	0.051	0.93
VY473rd5_01	54		-94	-4.7	35534	2227	18752	420533	3142	1.3	11	108	85	10.26	1.4	0.062	1.25
VY473_10	11		71	1.9	65541	4035	16459	414393	5957	0.8	14	105	133	10.97	1.9	0.061	1.03
VY473rd4a_21	51		68	0.3	386655	29785	46796	654513	20602	0.4	61	143	390	6.91	3.1	0.073	1.49
VY473rd5_03	57		109	0.8	231253	19026	34045	420673	11528	0.3	56	108	310	5.66	1.1	0.081	0.83
VY473rd4a_08	32		134	1.1	198546	20735	67004	570117	6777	1.0	38	125	128	4.05	1.8	0.103	0.70
VY473rd4a_20b	50		-55	-1.0	97981	6173	57404	1311522	8632	1.8	21	287	163	10.77	1.4	0.062	0.78
VY473_01	1		-20	-0.2	178375	16094	58890	636282	7280	1.0	40	161	162	5.54	4.9	0.083	2.28
VY473_15	16		20	0.1	268818	17358	78760	1822081	22797	0.9	58	461	509	10.16	1.8	0.063	1.26
VY473rd4a_10a	35		-76	-3.3	40059	2457	7781	185835	3562	0.6	7	41	67	10.71	1.6	0.063	1.27
VY473_17	19		42	3.4	21380	1349	4199	103093	1966	0.6	4	26	44	11.06	2.0	0.062	1.34
VY473rd5_02b	56		116	15.5	13084	832	5478	122764	1177	1.0	4	32	32	10.33	1.6	0.064	1.62
VY473rd5_04	58		25	0.2	211872	15657	14307	184263	13906	0.1	48	47	374	7.57	1.2	0.072	0.91
VY473rd5_07b	63		-14	-0.4	54304	3842	25237	482766	4350	1.1	17	124	117	9.85	1.9	0.065	1.98
VY473rd4a_09a	33		-89	-3.1	51007	3320	15426	310840	4454	0.8	9	68	84	10.47	1.6	0.064	1.14
VY473rd4a_14b	41		123	3.5	61428	3977	14552	306142	5526	0.6	11	67	105	10.88	1.4	0.064	0.93
VY473rd4a_06a	30		50	0.9	95295	7659	13012	228521	5401	0.5	15	50	102	6.80	2.7	0.079	1.22
VY473_20	22		-69	-1.6	73502	4904	18330	472012	6645	0.8	15	120	148	10.85	1.9	0.066	1.64
VY473rd4a_17	45		133	2.6	89549	6169	23708	486799	7799	0.7	16	106	148	10.58	1.3	0.068	1.04
VY473rd4a_11	37		-81	-1.4	100018	7118	31404	650837	8958	0.8	18	142	170	10.70	1.4	0.068	1.31
VY473rd4a_01	23		246	2.0	210309	15494	80500	1618341	18442	1.0	41	354	349	10.31	1.5	0.071	1.87
VY473_09	10		81	1.5	93159	7025	28646	564021	7626	0.8	20	143	170	9.76	1.9	0.075	1.37
VY473_04	5		11	0.3	61313	4797	22087	467404	5307	1.0	14	118	118	10.32	1.9	0.077	1.37
VY473rd4a_19	48		229	6.0	59607	6374	16696	224798	4991	0.5	11	49	94	10.28	1.4	0.105	1.09
VY473rd4a_10b	36		49	1.5	51899	5613	16670	245288	4428	0.6	10	54	84	10.06	1.8	0.109	5.12
~~VY473_08~~	~~9~~	~~high common Pb~~	~~3471~~	~~4.4~~	~~1255227~~	~~126367~~	~~780353~~	~~16693290~~	~~112169~~	~~1.7~~	~~343~~	~~4227~~	~~2503~~	~~10.56~~	~~2.2~~	~~0.099~~	~~1.44~~
~~VY473rd4a_06b~~	~~31~~	~~high common Pb~~	~~337~~	~~6.1~~	~~84588~~	~~10304~~	~~26519~~	~~261985~~	~~4747~~	~~0.6~~	~~16~~	~~57~~	~~90~~	~~6.68~~	~~1.8~~	~~0.119~~	~~2.25~~
~~VY473rd4a_13~~	~~39~~	~~high common Pb~~	~~322~~	~~7.5~~	~~68288~~	~~6872~~	~~20054~~	~~307111~~	~~5580~~	~~0.6~~	~~13~~	~~67~~	~~106~~	~~9.90~~	~~1.7~~	~~0.101~~	~~2.14~~

Appendix 1. Zircon geochronology mass spectrometry. Primary data - Part B

		Ratios					Ages and errors						Discordance	
#Sample - analysis	#Sample + comments	$^{207}Pb/^{235}U$	1s %	$^{206}Pb/^{238}U$	1s %	Rho	$^{207}Pb/^{206}Pb$	2s abs	$^{206}Pb/^{238}U$	2s abs	$^{207}Pb/^{235}U$	2s abs	6-38/7-6	6-38/7-35
PT15.1_66		0.84	2.13	0.10	1.86	0.87	650	22	612	22	620	20	5.9	1.3
PT15.1_43		0.85	2.06	0.10	1.80	0.88	653	21	614	21	622	19	6.0	1.3
PT15.1rd5_06		0.79	1.72	0.10	1.32	0.76	623	24	585	15	593	15	6.0	1.3
PT15.1_05		0.84	2.02	0.10	1.51	0.75	648	29	608	18	616	18	6.1	1.3
PT15.1_26		0.80	1.60	0.10	1.29	0.81	630	20	588	14	597	14	6.6	1.4
PT15.1_04		0.82	1.49	0.10	1.20	0.81	645	19	601	14	610	14	6.8	1.5
PT15.1_15		0.80	1.50	0.10	1.12	0.75	634	21	590	13	599	13	6.9	1.5
PT15.1_18		0.85	1.74	0.10	1.37	0.79	663	23	616	16	626	16	7.2	1.6
PT15.1_12		0.81	1.80	0.10	1.33	0.74	640	26	594	15	603	16	7.3	1.6
PT15.1_50		0.85	2.35	0.10	1.98	0.84	663	27	615	23	625	22	7.3	1.6
PT15.1_59		0.84	2.18	0.10	1.88	0.87	658	23	608	22	618	20	7.6	1.7
PT15.1_09		0.81	1.63	0.10	1.24	0.76	649	23	591	14	603	15	8.9	2.0
PT15.1rd5_03a		0.81	2.08	0.10	1.59	0.76	655	29	589	18	603	19	10.1	2.3
PT15.1_54		0.86	2.06	0.10	1.84	0.89	684	20	613	21	628	19	10.4	2.4
PT15.1_10		0.80	1.74	0.09	1.31	0.75	654	25	584	15	598	16	10.7	2.4
PT15.1rd5_09		0.83	1.73	0.10	1.27	0.73	675	25	601	15	616	16	11.0	2.5
PT15.1_22		0.82	1.87	0.10	1.33	0.71	673	28	593	15	610	17	11.8	2.7
PT15.1_28		0.83	2.29	0.10	1.69	0.74	685	33	596	19	614	21	13.0	3.0
PT15.1rd5_02		0.83	1.94	0.10	1.46	0.75	690	27	594	17	615	18	13.9	3.3
PT15.1_17		0.84	1.54	0.10	1.22	0.79	697	20	600	14	620	14	13.9	3.3
PT15.1rd5_04a		1.98	1.43	0.18	1.15	0.81	1230	16	1051	22	1110	19	14.6	5.4
PT15.1_58		0.93	2.57	0.11	2.14	0.83	756	30	644	26	669	25	14.8	3.8
PT15.1_19		0.85	2.55	0.10	1.80	0.70	709	39	603	21	626	24	14.9	3.6
PT15.1rd5_10		0.88	1.89	0.10	1.29	0.68	726	29	616	15	640	18	15.1	3.7
PT15.1_47		0.86	2.17	0.10	1.89	0.87	713	23	606	22	629	20	15.1	3.7
PT15.1rd5_03b		0.85	2.28	0.10	1.61	0.71	731	34	595	18	624	21	18.6	4.6
PT15.1rd5_04b		1.30	1.47	0.13	1.16	0.79	981	19	798	17	848	17	18.6	5.8
PT15.1rd5_08		0.92	2.73	0.10	1.89	0.69	789	41	624	22	661	26	20.9	5.6
PT15.1_03		0.86	2.32	0.10	1.56	0.67	767	36	594	18	631	22	22.6	5.9
PT15.1_32		0.89	2.67	0.10	1.82	0.68	791	41	607	21	647	25	23.4	6.2
PT15.1_34		0.92	2.19	0.10	1.91	0.87	811	22	617	22	660	21	24.0	6.5
PT15.1_16		0.87	2.23	0.10	1.52	0.68	788	34	596	17	637	21	24.4	6.5
PT15.1_11		0.85	1.72	0.09	1.30	0.75	777	24	583	14	624	16	25.0	6.6
PT15.1_33		0.98	2.47	0.10	1.86	0.75	890	34	634	22	693	25	28.8	8.5
PT15.1rd5_13		0.83	1.69	0.09	1.26	0.74	819	24	558	13	613	15	31.8	8.8
PT15.1_07		1.26	3.17	0.12	2.48	0.78	1088	40	733	34	826	35	32.7	11.3
PT15.1_06		1.00	1.81	0.10	1.33	0.74	1004	25	616	16	705	18	38.7	12.7
PT15.1_37		1.06	2.96	0.10	2.03	0.69	1143	43	607	24	734	30	46.9	17.3
PT15.1_08	ıit two common lead spike	1.31	5.50	0.10	1.53	0.28	1504	100	625	18	852	61	58.5	26.7
PT15.1rd5_11		2.08	4.28	0.11	2.29	0.54	2158	63	686	30	1143	57	68.2	40.0
PT15.1_21	high common Pb?	2.64	4.86	0.11	1.64	0.34	2530	77	699	22	1312	69	72.4	46.7
VY473_03a	VY473 - volcanic	0.23	2.07	0.03	1.82	0.88	182	23	209	7	206	8	-14.6	-1.1
VY473rd4a_03a		2.35	1.86	0.21	1.61	0.86	1204	19	1241	36	1227	26	-3.1	-1.1
VY473rd5_05b		0.78	1.67	0.10	1.27	0.76	573	24	587	14	584	15	-2.4	-0.5
VY473rd4a_03b		2.35	1.65	0.21	1.44	0.87	1217	16	1236	32	1228	23	-1.5	-0.6
VY473rd4a_15b		0.84	1.65	0.10	1.41	0.85	615	19	621	17	620	15	-1.0	-0.3
VY473rd4a_22a		3.36	1.42	0.26	1.27	0.89	1500	12	1491	34	1494	22	0.6	0.2
VY473rd4a_22b		3.40	1.58	0.26	1.38	0.88	1513	14	1497	37	1503	24	1.1	0.4
VY473_06		0.82	2.12	0.10	1.87	0.88	616	22	608	22	610	19	1.2	0.2
VY473_12		0.82	2.06	0.10	1.82	0.88	616	21	608	21	610	19	1.4	0.3
VY473rd4a_04		0.78	1.79	0.10	1.47	0.82	597	22	586	16	588	16	1.8	0.3
VY473rd4a_12		0.90	1.70	0.11	1.48	0.87	663	18	648	18	651	16	2.2	0.5
VY473rd4a_16		0.84	1.60	0.10	1.34	0.84	632	19	618	16	621	15	2.3	0.5
VY473rd4a_18a		0.83	1.60	0.10	1.30	0.82	629	20	609	15	613	15	3.3	0.7
VY473rd4a_05		0.85	1.58	0.10	1.35	0.85	645	18	620	16	625	15	4.0	0.9
VY473rd4a_02a		0.82	1.80	0.10	1.47	0.81	631	23	604	17	609	16	4.3	0.9
VY473rd5_05a		0.80	1.73	0.10	1.30	0.76	619	24	591	15	597	15	4.5	0.9
VY473rd4a_02b		0.85	1.60	0.10	1.43	0.89	647	16	617	17	623	15	4.6	1.0
VY473rd4a_18b		0.83	1.54	0.10	1.33	0.86	640	17	609	15	616	14	4.8	1.0
VY473rd5_07a		0.80	1.61	0.10	1.19	0.74	620	23	590	13	596	14	4.8	1.0
VY473_14		0.80	2.33	0.10	1.93	0.83	623	28	587	22	595	21	5.7	1.2
VY473_19		0.80	2.19	0.10	1.94	0.89	625	22	588	22	596	20	5.8	1.2
VY473_16a		0.78	2.10	0.09	1.86	0.89	619	21	581	21	588	19	6.1	1.3
VY473rd4a_20a		0.77	1.66	0.09	1.40	0.84	608	19	570	15	578	15	6.1	1.3
VY473_05		0.75	2.11	0.09	1.84	0.87	602	22	564	20	571	18	6.3	1.3
VY473_02		0.84	2.37	0.10	2.06	0.87	650	25	608	24	616	22	6.4	1.4
VY473_07		0.96	2.11	0.11	1.86	0.88	722	21	674	24	685	21	6.6	1.6
VY473rd5_06		0.79	1.70	0.09	1.31	0.77	627	24	585	15	593	15	6.8	1.4
VY473_18		0.85	2.27	0.10	1.91	0.84	666	26	611	22	623	21	8.3	1.9
VY473_11		0.85	2.11	0.10	1.86	0.88	677	21	614	22	627	20	9.4	2.1
VY473rd4a_15a		0.84	1.61	0.10	1.33	0.82	670	20	605	15	619	15	9.7	2.2
VY473rd5_02a		0.81	2.08	0.10	1.59	0.76	658	29	589	18	603	19	10.5	2.4
VY473_13		0.83	2.29	0.10	1.98	0.86	673	25	600	23	615	21	10.8	2.5
VY473_16b		0.80	2.19	0.09	1.91	0.87	655	23	584	21	599	20	10.9	2.4
VY473rd4a_14a		0.78	1.57	0.09	1.28	0.82	640	19	569	14	583	14	11.2	2.5
VY473rd4a_09b		0.80	1.85	0.09	1.45	0.79	658	24	584	16	599	17	11.2	2.5
VY473_03b		0.22	2.29	0.03	2.10	0.91	225	21	197	8	199	8	12.5	1.1
VY473rd5_01		0.84	1.87	0.10	1.39	0.74	686	27	600	16	618	17	12.6	2.9
VY473_10		0.77	2.13	0.09	1.86	0.87	655	22	562	20	581	19	14.2	3.2
VY473rd4a_21		1.46	3.46	0.14	3.13	0.90	1016	30	871	51	913	41	14.3	4.6
VY473rd5_03		1.98	1.42	0.18	1.15	0.81	1227	16	1049	22	1108	19	14.5	5.3
VY473rd4a_08		3.50	1.96	0.25	1.83	0.93	1677	13	1422	46	1527	30	15.2	6.9
VY473rd4a_20b		0.80	1.59	0.09	1.38	0.87	679	17	573	15	594	14	15.7	3.7
VY473_01		2.07	5.39	0.18	4.89	0.91	1270	45	1070	96	1137	71	15.8	5.9
VY473_15		0.86	2.22	0.10	1.82	0.82	721	27	605	21	630	21	16.1	3.9
VY473rd4a_10a		0.81	2.04	0.09	1.60	0.78	697	27	576	18	601	18	17.5	4.2
VY473_17		0.78	2.42	0.09	2.01	0.83	683	29	558	21	583	21	18.3	4.3
VY473rd5_02b		0.85	2.28	0.10	1.61	0.71	731	34	596	18	624	21	18.5	4.6
VY473rd5_04		1.31	1.47	0.13	1.16	0.79	982	18	800	17	849	17	18.6	5.8
VY473rd5_07b		0.91	2.75	0.10	1.90	0.69	786	42	623	22	659	26	20.7	5.5
VY473rd4a_09a		0.84	2.00	0.10	1.64	0.82	746	24	588	18	621	18	21.2	5.4
VY473rd4a_14b		0.81	1.66	0.09	1.38	0.83	732	20	567	15	601	15	22.5	5.6
VY473rd4a_06a		1.60	2.95	0.15	2.69	0.91	1171	24	884	44	970	36	24.5	8.9
VY473_20		0.84	2.52	0.09	1.91	0.76	815	34	568	21	620	23	30.3	8.4
VY473rd4a_17		0.88	1.64	0.09	1.27	0.77	858	22	582	14	642	15	32.2	9.3
VY473rd4a_11		0.88	1.91	0.09	1.38	0.72	868	27	576	15	639	18	33.7	9.8
VY473rd4a_01		0.95	2.41	0.10	1.53	0.63	954	38	597	17	677	24	37.4	11.8
VY473_09		1.05	2.37	0.10	1.93	0.82	1055	28	629	23	730	24	40.4	13.9
VY473_04		1.03	2.36	0.10	1.92	0.81	1125	27	596	22	719	24	47.0	17.1
VY473rd4a_19		1.41	1.81	0.10	1.44	0.80	1721	20	598	16	894	21	65.2	33.1
VY473rd4a_10b		1.49	5.43	0.10	1.80	0.33	1777	93	611	21	925	64	65.6	34.0
~~VY473_08~~	~~high common Pb~~	~~1.30~~	~~2.60~~	~~0.09~~	~~2.16~~	~~0.83~~	~~1610~~	~~27~~	~~583~~	~~24~~	~~844~~	~~29~~	~~63.8~~	~~30.9~~
~~VY473rd4a_06b~~	~~high common Pb~~	~~2.45~~	~~2.89~~	~~0.15~~	~~1.81~~	~~0.63~~	~~1938~~	~~40~~	~~899~~	~~30~~	~~1258~~	~~41~~	~~53.6~~	~~28.5~~
~~VY473rd4a_13~~	~~high common Pb~~	~~1.41~~	~~2.73~~	~~0.10~~	~~1.69~~	~~0.62~~	~~1644~~	~~40~~	~~621~~	~~20~~	~~892~~	~~32~~	~~62.3~~	~~30.4~~

Appendix 2. Summary concordant data only. U-Pb zircon analyses. R.Dartnall.

Plotted ages are highlighted green and boxed

Samples	Concentrations					Isotope ratios								Discordance %		Ratios to Dates					
Analyses	Uppm	Pbppm	Thppm	Th/U	^{204}Pb	^{207}Pb/^{206}Pb	1s%	^{207}Pb/^{235}U	1s%	^{206}Pb/^{238}U	1s%	^{238}U/^{206}Pb	1s%	6-38/7-6	6-38/7-35	^{207}Pb/^{206}Pb	2s abs	^{207}Pb/^{235}U	2s abs	^{206}Pb/^{238}U	2s abs
Sample A14:16. Outcrop belt 2. Aberffraw. NGR SH3380 6754. Mudstone layer, directly overlying the basal Gwna Group unconformity																					
A14.16_04	273	21	178	0.7	103	0.057	1.06	0.556	2.21	0.071	1.95	14.126	1.95	9.8	1.7	489	23	449	16	441	17
A14.16rd5_02	79	6	23	0.3	80	0.056	1.46	0.598	1.96	0.077	1.31	12.981	1.31	-2.9	-0.5	465	32	476	15	478	12
A14.16_10	119	10	34	0.3	83	0.058	1.18	0.691	2.28	0.087	1.95	11.517	1.95	-3.3	-0.6	520	26	533	19	537	20
A14.16.RD4a_4	107	13	112	1.0	49	0.060	1.18	0.818	2.28	0.099	1.95	10.146	1.95	0.7	0.1	610	26	607	21	606	23
A14.16_12	795	90	450	0.6	-4	0.060	1.01	0.860	2.14	0.104	0.89	9.595	1.89	-7.3	-1.6	595	22	629	20	639	23
A14.16_01	305	39	259	0.8	186	0.063	1.11	0.932	2.15	0.107	1.84	9.304	1.84	6.6	1.6	705	24	668	21	658	23
A14.16.RD4a_1	480	55	189	0.4	115	0.064	1.08	0.965	2.18	0.110	1.90	9.073	1.90	7.3	1.8	727	23	686	22	674	24
A14.16.RD4a_2	114	18	102	0.9	37	0.067	1.34	1.185	2.37	0.129	1.96	7.755	1.96	5.5	1.5	827	28	794	26	782	29
A14.16_07	381	66	68	0.2	23	0.073	1.01	1.761	2.11	0.176	1.85	5.695	1.85	-3.6	-1.1	1007	21	1031	27	1043	36
A14.16.RD4a_3	104	19	40	0.4	3	0.074	1.17	1.734	2.25	0.170	1.92	5.897	1.92	3.6	1.1	1047	24	1021	29	1010	36
A14.16rd5_01	335	77	138	0.4	114	0.090	1.08	2.776	2.26	0.223	1.99	4.486	1.99	9.5	3.8	1433	21	1349	33	1297	47
A14.16_09	121	45	166	1.4	104	0.103	1.00	3.914	2.30	0.275	2.07	3.633	2.07	6.8	3.0	1682	19	1616	37	1567	57
A14.16rd5_04	8	3	15	2.0	13	0.105	1.67	4.485	3.05	0.311	2.55	3.214	2.55	-2.3	-1.0	1708	31	1728	49	1746	78
A14.16.RD4a_8	304	107	170	0.6	57	0.116	1.01	5.078	2.12	0.317	1.86	3.155	1.86	6.6	3.1	1899	18	1832	35	1775	58
A14.16_11	100	43	81	0.8	128	0.130	0.95	6.472	2.14	0.361	1.92	2.769	1.92	5.3	2.7	2098	17	2042	37	1988	65
Sample A15:1. Outcrop belt 2. Aberffraw. NGR SH3417 6764. Ignimbrite interbedded with laminated tuff																					
A15.1_08	186	20	85	0.5	71	0.060	1.17	0.807	2.25	0.098	1.92	10.174	1.92	-2.5	-0.6	590	25	601	20	604	22
A15.1_10	119	13	82	0.7	-16	0.060	1.11	0.814	2.18	0.098	1.87	10.174	1.87	0.5	0.1	607	24	605	20	604	22
A15.1_21	211	24	148	0.7	-3	0.060	1.13	0.819	2.16	0.099	1.85	10.108	1.85	-0.3	-0.1	606	24	608	20	608	21
A15.1_14	184	21	114	0.6	-1	0.060	1.12	0.821	2.29	0.099	1.99	10.107	1.99	0.5	0.1	611	24	609	21	608	23
A15.1_11	197	24	189	1.0	103	0.060	1.05	0.827	2.17	0.099	1.89	10.086	1.89	1.9	0.4	621	23	612	20	609	22
A15.1_01	190	22	142	0.7	62	0.061	1.03	0.835	2.15	0.099	1.89	10.076	1.89	4.9	1.1	641	22	616	20	610	22
A15.1_12	79	9	55	0.7	51	0.060	1.43	0.833	2.52	0.100	2.07	9.977	2.07	-0.3	-0.1	614	31	615	23	616	24
A15.1_03	217	24	95	0.4	62	0.062	1.07	0.870	2.21	0.103	1.93	9.755	1.93	4.5	1.0	658	23	635	21	629	23
A15.1_19	178	22	129	0.7	87	0.062	1.15	0.893	2.20	0.105	1.88	9.498	1.88	1.8	0.4	657	25	648	21	645	23
A15.1_17	97	14	128	1.3	149	0.061	1.21	0.892	2.27	0.106	1.92	9.467	1.92	0.4	0.1	650	26	648	21	647	24
A15.1_09	144	17	94	0.6	-73	0.062	1.15	0.902	2.22	0.106	1.89	9.443	1.89	2.8	0.6	667	25	653	21	649	23
A15.1_16	237	31	239	1.0	73	0.062	1.23	0.914	2.25	0.107	1.88	9.376	1.88	4.0	0.9	680	26	659	22	653	23
A15.1.rd5_04	201	23	95	0.5	70	0.062	0.93	0.963	1.81	0.113	1.55	8.846	1.55	-3.4	-0.8	668	20	685	18	690	20
A15.1.rd5_03	170	21	55	0.3	37	0.064	0.86	1.077	1.59	0.121	1.34	8.239	1.34	2.2	0.5	755	18	742	17	738	19
A15.1rd6_01	355	50	289	0.8	176	0.064	0.73	1.075	1.61	0.121	1.43	8.231	1.43	1.2	0.3	748	15	741	17	739	20
A15.1.rd5_05	179	25	138	0.8	-25	0.064	0.87	1.095	1.75	0.124	1.52	8.056	1.52	-1.7	-0.5	742	18	751	18	754	22
A15.1.rd5_02	68	17	19	0.3	-5	0.090	0.94	3.156	1.85	0.254	1.60	3.932	1.60	-2.4	-1.0	1427	18	1447	28	1461	42
A15.1_20	146	42	67	0.5	100	0.093	1.05	3.399	2.26	0.264	1.99	3.790	1.99	-0.8	-0.4	1497	20	1504	35	1510	53
A15.1_07	153	55	119	0.8	-124	0.106	1.02	4.397	2.23	0.300	1.98	3.329	1.98	2.4	1.1	1736	19	1712	36	1693	59
A15.1_15	61	27	61	1.0	103	0.122	1.02	5.883	2.28	0.351	2.03	2.853	2.03	2.3	1.1	1982	18	1959	39	1937	68
A15.1.rd5_06	51	24	78	1.5	85	0.118	0.96	5.718	2.05	0.352	1.81	2.845	1.81	-0.8	-0.4	1926	17	1934	35	1942	60
A15.1_23	18	14	28	1.5	75	0.187	1.05	13.418	2.77	0.520	2.57	1.924	2.57	0.8	0.4	2719	17	2709	51	2698	112
Sample CB14:1. Outcrop belt 3. Porth Trefadog. NGR SH2899 8587. Laminated tuff																					
CB14.1.rd1_21	506	23	120	0.2	5	0.053	0.86	0.343	1.42	0.047	1.12	21.198	1.12	6.0	0.7	316	20	299	7	297	7
CB14.1.rd4_01	173	11	197	1.1	-22	0.053	1.13	0.360	1.63	0.049	1.18	20.391	1.18	9.2	1.1	340	26	312	9	309	7
CB14.1.rd4_06b	218	13	218	1.0	72	0.053	1.02	0.366	1.56	0.050	1.18	19.844	1.18	0.3	0.0	318	23	317	8	317	7
CB14.1.rd4_06a	182	12	264	1.4	-3	0.053	0.98	0.371	1.57	0.051	1.23	19.770	1.23	5.7	0.7	337	22	320	9	318	8
CB14.1.rd1_20a	234	13	149	0.6	-43	0.053	0.98	0.378	1.60	0.051	1.26	19.491	1.26	6.9	0.9	346	22	325	9	323	8
CB14.1.rd1_04	257	14	177	0.7	46	0.053	0.95	0.380	1.47	0.052	1.11	19.177	1.11	-1.3	-0.2	323	22	327	8	328	7
CB14.1.rd1_19	210	12	64	0.3	79	0.054	1.06	0.434	1.58	0.058	1.17	17.222	1.17	4.1	0.5	379	24	366	10	364	8
CB14.1.rd4_09	161	11	62	0.4	9	0.055	0.96	0.500	1.50	0.066	1.15	15.151	1.15	-0.2	-0.1	411	22	412	10	412	9
CB14.1.rd1_01	277	21	229	0.8	63	0.056	0.92	0.544	1.45	0.070	1.13	14.225	1.13	4.4	0.7	458	20	441	10	438	10
CB14.1.rd1_15	91	6	34	0.4	164	0.057	1.21	0.552	1.74	0.070	1.25	14.199	1.25	9.9	1.7	487	27	446	12	439	11
CB14.1.rd1_11	221	16	92	0.4	2	0.055	1.06	0.552	1.58	0.072	1.18	13.822	1.18	-5.8	-0.9	426	24	446	11	450	10
CB14.1.rd5_04	62	5	31	0.5	12	0.056	1.28	0.569	2.11	0.073	1.67	13.670	1.67	3.1	0.5	470	28	457	15	455	15
CB14.1.rd1_06a	143	11	48	0.3	80	0.057	1.23	0.616	1.78	0.079	1.29	12.652	1.29	-3.5	-0.6	474	27	487	14	490	12
CB14.1.rd4_10	219	22	141	0.6	-56	0.058	0.80	0.720	1.40	0.091	1.15	11.033	1.15	-8.5	-1.6	516	18	551	12	559	12
CB14.15rd5_06	77	8	51	0.7	16	0.061	1.28	0.816	1.79	0.097	1.25	10.326	1.25	7.4	1.6	643	27	606	16	596	14
CB14.15rd5_04	158	21	208	1.3	24	0.060	0.97	0.800	1.50	0.097	1.14	10.299	1.14	-0.1	0.0	597	21	597	13	597	13
CB14.1.rd1_03	423	48	396	0.9	25	0.060	0.80	0.803	1.38	0.097	1.12	10.257	1.12	-0.6	-0.2	596	17	599	12	600	13
CB14.1.rd4_05	185	20	111	0.6	98	0.061	0.93	0.817	1.53	0.098	1.21	10.251	1.21	4.8	1.0	630	20	606	14	600	14
CB14.1.rd1_14	95	13	154	1.6	-22	0.061	0.88	0.849	1.50	0.101	1.22	9.885	1.22	2.1	0.4	635	19	624	14	621	14
CB14.1.rd5_02	143	15	40	0.3	135	0.060	1.00	0.842	1.78	0.102	1.48	9.844	1.48	-2.5	-0.6	609	22	620	16	624	18
CB14.1.rd1_10	544	57	259	0.5	-45	0.061	0.82	0.856	1.40	0.102	1.14	9.828	1.14	2.4	0.5	640	18	628	13	625	14
CB14.1.rd1_22a	361	41	37	0.1	119	0.064	0.83	1.059	1.48	0.120	1.23	8.323	1.23	1.1	0.2	740	18	733	15	731	17
CB14.1.rd5_05	85	14	39	0.5	64	0.073	0.94	1.571	1.73	0.157	1.45	6.361	1.45	5.9	1.8	1001	19	959	21	941	25
CB14.1.rd4_07b	83	17	99	1.2	141	0.071	1.01	1.556	1.66	0.159	1.31	6.293	1.31	0.8	0.2	959	21	953	20	951	23
CB14.1.rd4_07a	249	48	272	1.1	34	0.071	0.79	1.566	1.38	0.160	1.13	6.243	1.13	-0.2	-0.1	956	16	957	17	958	20
CB14.1.rd4_04	273	51	128	0.5	64	0.074	0.88	1.788	1.51	0.175	1.23	5.726	1.23	1.1	0.3	1049	18	1041	20	1038	23
CB14.1.rd4_02a	125	24	37	0.3	43	0.078	0.92	2.050	1.57	0.190	1.27	5.269	1.27	3.1	1.1	1156	18	1132	21	1120	26
CB14.1.rd1_07	73	15	29	0.4	111	0.079	0.94	2.198	1.63	0.203	1.33	4.926	1.33	-2.6	-0.9	1161	19	1180	23	1191	29
CB14.1.rd4_02b	160	32	48	0.3	-90	0.079	0.90	2.151	1.56	0.198	1.27	5.053	1.27	0.4	0.1	1169	18	1165	21	1164	27
CB14.1.rd1_09	28	6	15	0.5	133	0.079	1.16	2.162	1.87	0.198	1.46	5.043	1.46	0.7	0.2	1175	23	1169	26	1166	31
CB14.1.rd1_27a	155	42	109	0.7	66	0.094	0.80	3.092	1.69	0.239	1.49	4.177	1.49	7.9	3.3	1503	15	1431	26	1384	37
CB14.1.rd4_03	109	30	49	0.5	-24	0.094	0.86	3.383	1.54	0.260	1.28	3.844	1.28	1.6	0.7	1515	16	1501	24	1491	34
CB14.1.rd1_12	289	82	12	0.0	-25	0.099	0.87	4.013	1.47	0.294	1.18	3.401	1.18	-3.5	-1.5	1606	16	1637	24	1662	35
CB14.1.rd5_01	131	36	8	0.1	39	0.100	0.83	3.894	1.70	0.283	1.48	3.536	1.48	1.0	0.4	1622	15	1612	27	1605	42
CB14.1.rd1_18	345	111	151	0.4	101	0.102	0.83	4.304	1.38	0.305	1.11	3.279	1.11	-2.9	-1.3	1668	15	1694	23	1716	33
CB14.1.rd1_26a	172	53	58	0.3	82	0.103	0.73	4.205	1.38	0.295	1.17	3.386	1.17	1.0	0.4	1685	13	1675	22	1668	34
CB14.1.rd1_05	193	65	92	0.5	-46	0.106	0.74	4.655	1.36	0.319	1.14	3.139	1.14	-2.9	-1.3	1732	14	1759	22	1783	35
CB14.1.rd4_08a	212	82	69	0.3	-99	0.126	0.75	6.467	1.30	0.371	1.05	2.692	1.05	0.6	0.3	2048	13	2041	23	2036	37
CB14.1.rd1_23	1042	493	45	0.0	212	0.176	0.70	11.346	1.33	0.467	1.13	2.140	1.13	5.6	3.1	2617	12	2552	25	2472	46
CB14.1.rd1_13	63	45	78	1.2	76	0.187	0.82	13.817	1.59	0.537	1.36	1.861	1.36	-2.2	-1.3	2712	14	2737	30	2772	61
CB14.1.rd1_17	163	99	63	0.4	106	0.192	0.77	14.317	1.42	0.541	1.19	1.847	1.19	-1.1	-0.7	2758	13	2771	27	2789	54

Appendix 2. Summary concordant data only. U-Pb zircon analyses. R.Dartnall.

Plotted ages are highlighted green and boxed

Samples	Concentrations					Isotope ratios								Discordance %		Ratios to Dates					
Analyses	Uppm	Pbppm	Thppm	Th/U	^{204}Pb	^{207}Pb/^{206}Pb	1s%	^{207}Pb/^{235}U	1s%	^{206}Pb/^{238}U	1s%	^{238}U/^{206}Pb	1s%	6-38/7-6	6-38/7-35	^{207}Pb/^{206}Pb	2s abs	^{207}Pb/^{235}U	2s abs	^{206}Pb/^{238}U	2s abs
Sample A14:16. Outcrop belt 2. Aberffraw. NGR SH3380 6754. Mudstone layer, directly overlying the basal Gwna Group unconformity																					
A14.16_04	273	21	178	0.7	103	0.057	1.06	0.556	2.21	0.071	1.95	14.126	1.95	9.8	1.7	489	23	449	16	441	17
A14.16rd5_02	79	6	23	0.3	80	0.056	1.46	0.598	1.96	0.077	1.31	12.981	1.31	-2.9	-0.5	465	32	476	15	478	12
A14.16_10	119	10	34	0.3	83	0.058	1.18	0.691	2.28	0.087	1.95	11.517	1.95	-3.3	-0.6	520	26	533	19	537	20
A14.16.RD4a_4	107	13	112	1.0	49	0.060	1.18	0.818	2.28	0.099	1.95	10.146	1.95	0.7	0.1	610	26	607	21	606	23
A14.16_12	795	90	450	0.6	-4	0.060	1.01	0.860	2.14	0.104	0.89	9.595	1.89	-7.3	-1.6	595	22	629	20	639	23
A14.16_01	305	39	259	0.8	186	0.063	1.11	0.932	2.15	0.107	1.84	9.304	1.84	6.6	1.6	705	24	668	21	658	23
A14.16.RD4a_1	480	55	189	0.4	115	0.064	1.08	0.965	2.18	0.110	1.90	9.073	1.90	7.3	1.8	727	23	686	22	674	24
A14.16.RD4a_2	114	18	102	0.9	37	0.067	1.34	1.185	2.37	0.129	1.96	7.755	1.96	5.5	1.5	827	28	794	26	782	29
A14.16_07	381	66	68	0.2	23	0.073	1.01	1.761	2.11	0.176	1.85	5.695	1.85	-3.6	-1.1	1007	21	1031	27	1043	36
A14.16.RD4a_3	104	19	40	0.4	3	0.074	1.17	1.734	2.25	0.170	1.92	5.897	1.92	3.6	1.1	1047	24	1021	29	1010	36
A14.16rd5_01	335	77	138	0.4	114	0.090	1.08	2.776	2.26	0.223	1.99	4.486	1.99	9.5	3.8	1433	21	1349	33	1297	47
A14.16_09	121	45	166	1.4	104	0.103	1.00	3.914	2.30	0.275	2.07	3.633	2.07	6.8	3.0	1682	19	1616	37	1567	57
A14.16rd5_04	8	3	15	2.0	13	0.105	1.67	4.485	3.05	0.311	2.55	3.214	2.55	-2.3	-1.0	1708	31	1728	49	1746	78
A14.16.RD4a_8	304	107	170	0.6	57	0.116	1.01	5.078	2.12	0.317	1.86	3.155	1.86	6.6	3.1	1899	18	1832	35	1775	58
A14.16_11	100	43	81	0.8	128	0.130	0.95	6.472	2.14	0.361	1.92	2.769	1.92	5.3	2.7	2098	17	2042	37	1988	65
Sample A15:1. Outcrop belt 2. Aberffraw. NGR SH3417 6764. Ignimbrite interbedded with laminated tuff																					
A15.1_08	186	20	85	0.5	71	0.060	1.17	0.807	2.25	0.098	1.92	10.174	1.92	-2.5	-0.6	590	25	601	20	604	22
A15.1_10	119	13	82	0.7	-16	0.060	1.11	0.814	2.18	0.098	1.87	10.174	1.87	0.5	0.1	607	24	605	20	604	22
A15.1_21	211	24	148	0.7	-3	0.060	1.13	0.819	2.16	0.099	1.85	10.108	1.85	-0.3	-0.1	606	24	608	20	608	21
A15.1_14	184	21	114	0.6	-1	0.060	1.12	0.821	2.29	0.099	1.99	10.107	1.99	0.5	0.1	611	24	609	21	608	23
A15.1_11	197	24	189	1.0	103	0.060	1.05	0.827	2.17	0.099	1.89	10.086	1.89	1.9	0.4	621	23	612	20	609	22
A15.1_01	190	22	142	0.7	62	0.061	1.03	0.835	2.15	0.099	1.89	10.076	1.89	4.9	1.1	641	22	616	20	610	22
A15.1_12	79	9	55	0.7	51	0.060	1.43	0.833	2.52	0.100	2.07	9.977	2.07	-0.3	-0.1	614	31	615	23	616	24
A15.1_03	217	24	95	0.4	62	0.062	1.07	0.870	2.21	0.103	1.93	9.755	1.93	4.5	1.0	658	23	635	21	629	23
A15.1_19	178	22	129	0.7	87	0.062	1.15	0.893	2.20	0.105	1.88	9.498	1.88	1.8	0.4	657	25	648	21	645	23
A15.1_17	97	14	128	1.3	149	0.061	1.21	0.892	2.27	0.106	1.92	9.467	1.92	0.4	0.1	650	26	648	21	647	24
A15.1_09	144	17	94	0.6	-73	0.062	1.15	0.902	2.22	0.106	1.89	9.443	1.89	2.8	0.6	667	25	653	21	649	23
A15.1_16	237	31	239	1.0	73	0.062	1.23	0.914	2.25	0.107	1.88	9.376	1.88	4.0	0.9	680	26	659	22	653	23
A15.1.rd5_04	201	23	95	0.5	70	0.062	0.93	0.963	1.81	0.113	1.55	8.846	1.55	-3.4	-0.8	668	20	685	18	690	20
Sample CB14:2. Outcrop belt 3. Porth Trefadog. NGR SH2902 8587. Ignimbrite																					
CB14.2.RD1_14	140	17	217	1.5	116	0.060	0.79	0.781	1.32	0.095	1.06	10.545	1.06	1.6	0.3	593	17	586	12	584	12
CB14.2.rd4_08b	98	12	112	1.1	5	0.061	1.14	0.802	1.64	0.095	1.18	10.485	1.18	8.3	1.8	641	24	598	15	587	13
CB14.2.rd4_02b	117	13	78	0.7	166	0.061	1.10	0.809	1.69	0.096	1.29	10.425	1.29	8.5	1.9	646	24	602	15	590	14
CB14.2.RD1_12	279	31	258	0.9	262	0.061	0.74	0.812	1.29	0.097	1.06	10.328	1.06	5.9	1.3	633	16	603	12	596	12
CB14.2.RD1_23	271	27	144	0.5	-26	0.061	0.67	0.809	1.14	0.097	0.93	10.304	0.93	4.0	0.8	622	14	602	10	597	11
CB14.2.rd4_14a	239	30	331	1.4	-14	0.060	0.83	0.815	1.40	0.098	1.13	10.217	1.13	2.5	0.5	618	18	605	13	602	13
CB14.2.RD1_11	134	18	213	1.6	50	0.061	0.82	0.826	1.28	0.098	0.98	10.216	0.98	6.9	1.5	647	18	611	12	602	11
CB14.2.rd4_05b	126	15	157	1.3	29	0.061	1.04	0.824	1.67	0.098	1.30	10.180	1.30	4.7	1.0	634	22	610	15	604	15
CB14.2.RD1_22	128	19	294	2.3	74	0.061	0.86	0.831	1.35	0.099	1.04	10.090	1.04	3.8	0.8	633	19	614	12	609	12
CB14.2.rd4_02a	126	14	86	0.7	14	0.060	0.92	0.819	1.55	0.100	1.25	10.041	1.25	-3.6	-0.8	591	20	607	14	612	15
CB14.2.rd4_08a	132	16	148	1.1	-12	0.060	0.87	0.829	1.47	0.100	1.19	10.038	1.19	0.7	0.1	617	19	613	13	612	14
CB14.2.RD1_02	99	12	94	0.9	138	0.060	0.88	0.830	1.51	0.100	1.23	10.032	1.23	1.2	0.2	620	19	614	14	613	14
CB14.2.RD1_05	142	18	211	1.5	-1	0.061	0.75	0.844	1.19	0.100	0.92	10.028	0.92	6.2	1.4	654	16	621	11	613	11
CB14.2.rd4_10b	126	15	127	1.0	218	0.061	1.04	0.836	1.52	0.100	1.12	10.027	1.12	3.0	0.6	632	22	617	14	613	13
CB14.2.rd4_10a	119	13	92	0.8	141	0.060	1.03	0.827	1.61	0.100	1.24	10.018	1.24	-0.7	-0.2	609	22	612	15	613	15
CB14.2.RD1_10	79	11	125	1.6	70	0.061	0.97	0.842	1.51	0.100	1.16	10.004	1.16	4.5	1.0	643	21	620	14	614	14
CB14.2.rd4_01	225	27	232	1.0	42	0.060	0.86	0.826	1.45	0.101	1.17	9.938	1.17	-5.1	-1.1	588	19	611	13	618	14
CB14.2.rd4_12	135	16	143	1.1	-16	0.061	0.95	0.848	1.63	0.101	1.32	9.893	1.32	2.1	0.4	634	20	623	15	621	16
CB14.2.rd4_05a	226	25	167	0.7	-93	0.060	0.82	0.841	1.45	0.101	1.20	9.877	1.20	-1.3	-0.3	614	18	620	13	622	14
CB14.2.rd4_06	37	4	33	0.9	146	0.061	1.20	0.854	2.02	0.102	1.63	9.848	1.63	2.4	0.5	639	26	627	19	623	19
CB14.2.RD1_06	243	26	143	0.6	4	0.061	0.72	0.859	1.28	0.102	1.06	9.790	1.06	2.0	0.4	640	16	630	12	627	13
CB14.2.rd4_09	75	8	65	0.9	132	0.060	1.08	0.848	1.69	0.103	1.30	9.711	1.30	-6.1	-1.3	596	23	624	16	632	16
CB14.2.RD1_21a	148	16	79	0.5	122	0.063	0.79	0.913	1.26	0.106	0.99	9.476	0.99	7.8	1.8	702	17	659	12	647	12
CB14.2.RD1_18	85	10	48	0.6	-53	0.063	0.92	0.933	1.44	0.108	1.10	9.280	1.10	6.0	1.4	702	20	669	14	660	14
CB14.2.RD1_08a	341	37	91	0.3	108	0.064	0.63	0.947	1.03	0.108	0.81	9.255	0.81	9.1	2.2	728	13	677	10	661	10
CB14.2.rd4_03a	201	23	72	0.4	89	0.062	0.80	0.991	1.48	0.115	1.24	8.687	1.24	-1.8	-0.4	690	17	699	15	702	17
CB14.2.rd4_13	277	35	187	0.7	-70	0.064	0.78	1.013	1.34	0.116	1.09	8.642	1.09	2.9	0.7	727	17	711	14	706	15
CB14.2.RD1_16	196	27	228	1.2	25	0.065	0.72	1.041	1.16	0.116	0.91	8.633	0.91	9.6	2.5	782	15	725	12	707	12
CB14.2.RD1_08b	654	83	373	0.6	96	0.064	0.71	1.029	1.18	0.117	0.94	8.512	0.94	1.4	0.3	726	15	718	12	716	13
CB14.2.RD1_09	809	107	617	0.8	116	0.064	0.61	1.045	1.04	0.119	0.84	8.406	0.84	1.2	0.3	733	13	726	11	725	11
CB14.2.RD1_20	148	20	112	0.8	29	0.064	0.84	1.054	1.31	0.119	1.01	8.383	1.01	2.6	0.6	746	18	731	14	726	14
CB14.2.rd4_03b	411	55	289	0.7	113	0.064	0.80	1.067	1.37	0.121	1.10	8.250	1.10	0.0	0.0	738	17	737	14	738	15
CB14.2.RD1_21b	118	16	85	0.7	-101	0.064	0.83	1.071	1.45	0.121	1.19	8.239	1.19	0.5	0.1	742	18	739	15	738	17
CB14.2.rd4_04	213	28	105	0.5	-7	0.065	0.91	1.141	1.58	0.128	1.28	7.817	1.28	-1.3	-0.4	766	19	773	17	776	19
CB14.2.RD1_24	148	36	49	0.3	114	0.090	0.63	3.054	1.16	0.245	0.97	4.076	0.97	1.3	0.5	1432	12	1421	18	1414	25
CB14.2.rd4_11	84	22	33	0.4	107	0.094	0.79	3.257	1.43	0.252	1.19	3.975	1.19	4.0	1.7	1507	15	1471	22	1446	31
CB14.2.RD1_01	359	112	184	0.5	43	0.098	0.64	3.992	1.12	0.295	0.92	3.395	0.92	-4.5	-2.0	1593	12	1633	18	1664	27
CB14.2.RD1_04	232	78	209	0.9	9	0.099	0.64	3.876	1.10	0.285	0.90	3.506	0.90	-1.2	-0.6	1598	12	1609	18	1618	26
CB14.2.RD1_13	203	63	194	1.0	106	0.099	0.68	3.617	1.17	0.265	0.95	3.773	0.95	5.6	2.4	1605	13	1553	18	1516	26
Sample CB14:5. Outcrop belt 3. Port Trefadog. NGR SH2903 8589. Coarse crystalline ignimbrite																					
CB14.5.RD1_15	250	26	126	0.5	62	0.060	0.82	0.780	1.36	0.095	1.08	10.556	1.08	1.7	0.3	594	18	585	12	583	12
CB14.5.RD1_22	193	24	199	1.0	248	0.061	0.82	0.061	0.82	0.097	1.22	10.285	1.22	7.3	1.6	645	18	608	13	598	14
CB14.5.RD1_18	137	18	152	1.1	-64	0.061	0.96	0.061	0.96	0.098	1.22	10.217	1.22	6.2	1.4	642	21	610	14	602	14
CB14.5.RD1_02	107	13	76	0.7	-89	0.062	0.99	0.062	0.99	0.099	1.16	10.093	1.16	7.5	1.7	658	21	619	14	609	13
CB14.5.RD1_04	105	13	99	0.9	65	0.060	1.02	0.827	1.50	0.100	1.09	10.020	1.09	-0.9	-0.2	608	22	612	14	613	13
CB14.5.RD1_14	118	16	152	1.3	38	0.062	0.83	0.062	0.83	0.100	1.08	10.018	1.08	7.1	1.6	660	18	623	13	613	13
CB14.5.RD1_03	64	8	48	0.8	94	0.062	1.17	0.879	1.60	0.103	1.09	9.672	1.09	4.5	1.0	664	25	641	15	634	13
CB14.5.RD1_09	231	28	123	0.5	40	0.062	0.86	0.947	1.34	0.112	1.03	8.963	1.03	-3.3	-0.8	660	18	677	13	682	13
CB14.5.RD1_19	115	25	80	0.7	154	0.076	0.92	1.920	1.39	0.184	1.04	5.430	1.04	-0.4	-0.1	1086	18	1088	18	1090	21
CB14.5.RD1_05	243	53	61	0.3	-60	0.081	0.76	2.377	1.29	0.213	1.04	4.697	1.04	-1.8	-0.7	1222	15	1236	18	1244	24
CB14.5.RD1_16	87	20	40	0.5	43	0.082	0.90	2.370	1.48	0.209	1.17	4.793	1.17	2.7	1.0	1255	18	1233	21	1222	26
CB14.5.RD1_08	195	50	54	0.3	122	0.091	0.80	3.128	1.31	0.250	1.04	3.994	1.04	-0.1	-0.1	1439	15	1439	20	1440	27
CB14.5.RD1_17a	81	23	28	0.3	94	0.092	0.74	3.463	1.29	0.272	1.06	3.678	1.06	-5.0	-2.1	1476	14	1519	20	1550	29
CB14.5.RD1_17b	97	27	37	0.4	149	0.094	0.73	3.474	1.34	0.267	1.12	3.738	1.12	-1.0	-0.4	1513	14	1521	21	1528	30
CB14.5.RD1_21b	243	71	99	0.4	5	0.097	0.82	3.651	1.38	0.273	1.10	3.669	1.10	1.1	0.5	1571	15	1561	22	1554	30
CB14.5.RD1_21a	85	24	18	0.2	44	0.097	0.83	3.667	1.31	0.274	1.02	3.655	1.02	0.8	0.3	1572	16	1564	21	1559	28
CB14.5.RD1_20	125	37	42	0.3	128	0.099	0.74	3.874	1.39	0.283	1.17	3.535	1.17	0.4	0.2	1612	14	1608	22	1606	33

Appendix 2. Summary concordant data only. U-Pb zircon analyses. R.Dartnall. | Plotted ages are highlighted green and boxed

Samples	Concentrations					Isotope ratios								Discordance %		Ratios to Dates					
Analyses	Uppm	Pbppm	Thppm	Th/U	^{204}Pb	^{207}Pb/^{206}Pb	1s%	^{207}Pb/^{235}U	1s%	^{206}Pb/^{238}U	1s%	^{238}U/^{206}Pb	1s%	6-38/7-6	6-38/7-35	^{207}Pb/^{206}Pb	2s abs	^{207}Pb/^{235}U	2s abs	^{206}Pb/^{238}U	2s abs
Sample NHG15:12. Outcrop belt 3. Penrhyn. NGR SH2845 8491. Psammite																					
NHG15.12rd6_81	269	28	254	0.9	137	0.059	0.78	0.695	1.65	0.085	1.45	11.769	1.45	9.5	1.9	581	17	536	14	526	15
NHG15.12rd6_31	229	27	422	1.8	79	0.058	0.91	0.692	1.42	0.086	1.10	11.641	1.10	3.1	0.6	548	20	534	12	531	11
NHG15.12rd6_63	189	19	198	1.0	-9	0.059	0.84	0.703	1.31	0.086	1.01	11.641	1.01	8.4	1.7	580	18	540	11	531	10
NHG15.12rd3_21	159	17	159	1.0	-13	0.058	0.93	0.692	1.77	0.086	1.51	11.619	1.51	2.1	0.4	544	20	534	15	532	15
NHG15.12rd3_05	200	21	160	0.8	140	0.059	0.94	0.700	1.68	0.086	1.39	11.580	1.39	4.4	0.8	559	21	538	14	534	14
NHG15.12rd6_23	190	21	265	1.4	82	0.059	0.98	0.697	1.54	0.086	1.18	11.577	1.18	2.9	0.5	550	21	537	13	534	12
NHG15.12rd6_76	191	20	165	0.9	147	0.059	0.78	0.700	1.71	0.087	1.52	11.553	1.52	3.4	0.6	554	17	539	14	535	16
NHG15.12rd6_84b	450	44	327	0.7	119	0.059	0.65	0.709	1.48	0.087	1.33	11.550	1.33	8.0	1.6	582	14	544	12	535	14
NHG15.12rd6_28	266	27	255	1.0	87	0.059	0.88	0.699	1.35	0.087	1.02	11.548	1.02	3.0	0.6	552	19	538	11	535	10
NHG15.12rd6_25	250	25	229	0.9	-55	0.058	0.85	0.697	1.35	0.087	1.05	11.518	1.05	0.7	0.1	541	19	537	11	537	11
NHG15.12rd6_64a	368	39	452	1.2	-48	0.059	0.75	0.701	1.16	0.087	0.88	11.509	0.88	2.6	0.5	551	16	540	10	537	9
NHG15.12rd6_77a	191	20	190	1.0	81	0.058	0.68	0.700	1.45	0.087	1.29	11.497	1.29	1.4	0.2	545	15	539	12	538	13
NHG15.12rd6_45	171	17	129	0.8	78	0.059	0.85	0.709	1.43	0.087	1.15	11.494	1.15	5.7	1.1	571	18	544	12	538	12
NHG15.12rd6_84a	353	40	462	1.3	-23	0.059	0.74	0.712	1.61	0.087	1.43	11.483	1.43	6.8	1.4	578	16	546	14	538	15
NHG15.12rd6_64b	215	21	195	0.9	53	0.059	0.84	0.704	1.29	0.087	0.98	11.480	0.98	2.8	0.5	554	18	541	11	538	10
NHG15.12rd6_92a	166	16	109	0.7	41	0.059	0.81	0.712	1.63	0.088	1.41	11.409	1.41	4.2	0.8	565	18	546	14	542	15
NHG15.12rd6_03	181	18	154	0.9	77	0.060	1.11	0.721	1.53	0.088	1.05	11.376	1.05	7.4	1.5	586	24	551	13	543	11
NHG15.12rd6_47	174	20	263	1.5	40	0.058	0.84	0.709	1.39	0.088	1.11	11.312	1.11	-1.7	-0.4	537	18	544	12	546	12
NHG15.12rd6_77b	138	15	124	0.9	19	0.059	0.81	0.725	1.52	0.088	1.29	11.306	1.29	6.4	1.3	584	17	553	13	546	13
NHG15.12rd6_75	340	33	190	0.6	166	0.059	0.67	0.732	1.42	0.090	1.25	11.171	1.25	4.7	0.9	580	15	558	12	553	13
NHG15.12rd6_26	122	12	94	0.8	4	0.058	1.02	0.719	1.50	0.090	1.09	11.128	1.09	-4.3	-0.8	532	22	550	13	555	12
NHG15.12rd6_42	197	19	90	0.5	77	0.060	0.91	0.745	1.50	0.090	1.20	11.110	1.20	8.0	1.7	604	20	565	13	556	13
NHG15.12rd6_100	174	17	126	0.7	-110	0.058	0.78	0.725	1.51	0.090	1.29	11.093	1.29	-2.6	-0.5	543	17	553	13	556	14
NHG15.12rd6_32a	66	7	51	0.8	13	0.060	1.32	0.748	1.88	0.090	1.34	11.077	1.34	8.2	1.7	607	29	567	16	557	14
NHG15.12rd6_29	279	31	344	1.2	-55	0.058	0.87	0.726	1.39	0.090	1.09	11.074	1.09	-2.7	-0.5	543	19	554	12	557	12
NHG15.12rd3_12	121	13	99	0.8	88	0.060	1.10	0.742	1.85	0.090	1.49	11.057	1.49	4.7	0.9	586	24	563	16	558	16
NHG15.12rd6_57	359	37	301	0.8	152	0.059	0.70	0.748	1.25	0.091	1.04	10.938	1.04	3.0	0.6	582	15	567	11	564	11
NHG15.12rd6_24a	184	18	99	0.5	101	0.060	1.00	0.761	1.54	0.091	1.18	10.930	1.18	8.3	1.8	616	22	574	13	564	13
NHG15.12rd3_03	216	22	109	0.5	-10	0.060	1.03	0.753	1.83	0.092	1.51	10.913	1.51	4.2	0.8	590	22	570	16	565	16
NHG15.12rd6_82b	96	9	57	0.6	2	0.060	0.89	0.766	1.70	0.092	1.45	10.876	1.45	8.3	1.8	619	19	577	15	567	16
NHG15.12rd6_62	135	14	125	0.9	74	0.060	0.91	0.764	1.43	0.093	1.10	10.808	1.10	4.8	1.0	599	20	576	12	570	12
NHG15.12rd6_82a	231	23	129	0.6	4	0.059	0.72	0.751	1.55	0.093	1.37	10.793	1.37	-1.7	-0.4	562	16	569	13	571	15
NHG15.12rd6_101	140	16	185	1.3	219	0.059	0.79	0.766	1.59	0.094	1.38	10.686	1.38	0.7	0.1	581	17	577	14	577	15
NHG15.12rd6_24b	209	20	87	0.4	57	0.060	0.89	0.781	1.42	0.094	1.11	10.589	1.11	3.6	0.7	604	19	586	13	582	12
NHG15.12rd6_71	127	15	128	1.0	115	0.060	0.76	0.788	1.46	0.095	1.25	10.532	1.25	4.3	0.9	611	16	590	13	585	14
NHG15.12rd6_79	340	43	420	1.2	-3	0.061	0.74	0.803	1.49	0.096	1.29	10.468	1.29	8.0	1.7	639	16	599	13	588	15
NHG15.12rd6_58	162	18	178	1.1	-27	0.060	0.85	0.792	1.27	0.096	0.94	10.416	0.94	1.3	0.2	599	18	592	11	591	11
NHG15.12rd6_49b	345	39	472	1.4	73	0.061	0.72	0.817	1.13	0.097	0.87	10.347	0.87	8.7	1.9	651	16	606	10	595	10
NHG15.12rd6_78a	95	14	194	2.0	15	0.061	0.74	0.810	1.49	0.097	1.30	10.343	1.30	6.0	1.3	633	16	603	13	595	15
NHG15.12rd6_19	145	16	117	0.8	-5	0.062	0.98	0.822	1.60	0.097	1.27	10.318	1.27	9.4	2.1	658	21	609	15	596	14
NHG15.12rd3_07	156	20	185	1.2	162	0.060	0.91	0.804	1.66	0.098	1.38	10.244	1.38	-1.0	-0.2	594	20	599	15	600	16
NHG15.12rd6_33a	42	5	39	0.9	-15	0.061	1.31	0.826	2.02	0.098	1.54	10.239	1.54	7.8	1.7	652	28	611	18	601	18
NHG15.12rd3_13	445	55	489	1.1	146	0.061	0.82	0.817	1.63	0.098	1.41	10.230	1.41	3.9	0.8	626	18	606	15	601	16
NHG15.12rd6_78b	297	36	283	1.0	-62	0.061	0.84	0.822	1.61	0.098	1.37	10.224	1.37	5.6	1.2	638	18	609	15	602	16
NHG15.12rd6_89	149	15	51	0.3	200	0.061	0.90	0.824	1.53	0.098	1.24	10.214	1.24	6.3	1.4	643	19	611	14	602	14
NHG15.12rd6_72	356	42	376	1.1	-69	0.060	0.58	0.817	1.36	0.098	1.23	10.199	1.23	2.8	0.6	620	12	606	12	603	14
NHG15.12rd6_60	218	25	245	1.1	-4	0.060	0.79	0.819	1.29	0.098	1.01	10.179	1.01	2.6	0.5	620	17	607	12	604	12
NHG15.12rd6_59	145	17	187	1.3	50	0.061	0.92	0.826	1.35	0.098	0.99	10.174	0.99	5.5	1.2	640	20	612	12	604	11
NHG15.12rd6_93	205	23	171	0.8	93	0.061	0.71	0.826	1.43	0.099	1.25	10.143	1.25	4.0	0.9	632	15	611	13	606	14
NHG15.12rd6_09	174	20	153	0.9	-40	0.061	1.01	0.829	1.67	0.099	1.33	10.122	1.33	4.4	0.9	635	22	613	15	607	15
NHG15.12rd3_19	103	14	141	1.4	-69	0.061	1.00	0.825	1.87	0.099	1.57	10.116	1.57	2.6	0.5	624	22	611	17	608	18
NHG15.12rd6_85	190	20	91	0.5	11	0.061	0.79	0.835	1.51	0.100	1.28	10.037	1.28	3.3	0.7	633	17	617	14	612	15
NHG15.12rd6_33b	65	7	48	0.7	141	0.061	1.10	0.845	1.55	0.100	1.09	10.023	1.09	6.3	1.4	655	24	622	14	613	13
NHG15.12rd3_20	276	33	221	0.8	-6	0.061	0.90	0.848	1.69	0.100	1.43	9.990	1.43	6.3	1.4	657	19	624	16	615	17
NHG15.12rd6_50a	76	9	62	0.8	122	0.061	1.19	0.845	1.70	0.100	1.22	9.962	1.22	4.1	0.9	643	26	622	16	617	14
NHG15.12rd6_11	80	9	59	0.7	175	0.061	1.38	0.841	1.97	0.100	1.40	9.953	1.40	2.2	0.5	631	30	620	18	617	16
NHG15.12rd6_40	107	12	77	0.7	129	0.061	1.09	0.842	1.50	0.100	1.02	9.952	1.02	2.4	0.5	633	24	620	14	617	12
NHG15.12rd6_15	203	24	180	0.9	-17	0.061	0.87	0.849	1.36	0.100	1.05	9.951	1.05	4.9	1.1	649	19	624	13	617	12
NHG15.12rd6_39	170	19	135	0.8	52	0.061	0.87	0.847	1.44	0.101	1.14	9.930	1.14	3.5	0.7	641	19	623	13	619	13
NHG15.12rd6_83	207	23	148	0.7	24	0.060	0.73	0.839	1.55	0.101	1.36	9.929	1.36	0.1	0.0	619	16	619	14	619	16
NHG15.12rd6_02	208	22	114	0.5	85	0.062	1.00	0.856	1.55	0.101	1.19	9.928	1.19	6.5	1.5	662	21	628	14	619	14
NHG15.12rd6_99	274	31	219	0.8	122	0.060	0.70	0.835	1.54	0.101	1.37	9.906	1.37	-2.5	-0.6	605	15	616	14	620	16
NHG15.12rd3_14	230	24	77	0.3	-14	0.061	0.99	0.852	1.82	0.101	1.53	9.872	1.53	2.8	0.6	640	21	626	17	622	18
NHG15.12rd6_10	587	64	371	0.6	1	0.060	0.83	0.843	1.39	0.101	1.12	9.871	1.12	-0.9	-0.2	617	18	621	13	622	13
NHG15.12rd6_41	308	35	322	1.0	155	0.062	0.91	0.869	1.45	0.101	1.13	9.855	1.13	8.1	1.9	678	19	635	14	623	13
NHG15.12rd6_55	254	30	280	1.1	64	0.061	0.72	0.857	1.28	0.102	1.06	9.839	1.06	3.2	0.7	645	16	628	12	624	13
NHG15.12rd6_50b	139	15	100	0.7	97	0.061	0.91	0.859	1.46	0.102	1.15	9.811	1.15	3.1	0.6	645	20	630	14	626	14
NHG15.12rd6_66	162	20	174	1.1	145	0.061	0.79	0.860	1.22	0.102	0.93	9.799	0.93	2.7	0.6	644	17	630	11	626	11
NHG15.12rd6_01	44	5	38	0.9	24	0.060	1.26	0.849	2.06	0.102	1.63	9.792	1.63	-2.1	-0.5	614	27	624	19	627	19
NHG15.12rd6_51	125	15	122	1.0	-79	0.062	0.87	0.869	1.41	0.102	1.11	9.780	1.11	5.4	1.2	663	19	635	13	628	13
NHG15.12rd3_06	148	18	121	0.8	38	0.060	1.01	0.853	1.79	0.102	1.48	9.764	1.48	-1.7	-0.4	618	22	626	17	629	18
NHG15.12rd6_08	119	15	139	1.2	-22	0.062	1.05	0.880	1.68	0.104	1.31	9.654	1.31	4.2	0.9	663	22	641	16	635	16
NHG15.12rd6_21a	164	18	85	0.5	-16	0.062	1.02	0.886	1.67	0.104	1.32	9.653	1.32	6.0	1.4	676	22	644	16	635	16
NHG15.12rd6_53	318	37	248	0.8	-6	0.060	0.80	0.860	1.28	0.104	0.99	9.634	0.99	-4.7	-1.0	608	17	630	12	637	12
NHG15.12rd6_49a	258	30	220	0.8	-8	0.060	0.77	0.860	1.26	0.104	1.00	9.622	1.00	-5.2	-1.1	606	17	630	12	637	12
NHG15.12rd6_20	110	12	61	0.6	-67	0.062	1.27	0.891	2.04	0.105	1.59	9.547	1.59	3.5	0.8	666	27	647	19	642	19
NHG15.12rd3_02	122	15	85	0.7	39	0.062	0.99	0.900	1.87	0.105	1.58	9.527	1.58	5.6	1.3	681	21	652	18	643	19
NHG15.12rd6_91b	217	30	279	1.3	245	0.062	0.66	0.907	1.46	0.106	1.30	9.465	1.30	5.4	1.2	684	14	656	14	647	16
NHG15.12rd6_21b	280	37	335	1.2	10	0.062	0.83	0.914	1.45	0.106	1.19	9.403	1.19	5.3	1.2	688	18	659	14	651	15
NHG15.12rd3_17	103	12	63	0.6	-3	0.061	1.05	0.894	1.98	0.107	1.68	9.389	1.68	-2.7	-0.6	635	23	648	19	652	21
NHG15.12rd6_90	125	17	143	1.1	12	0.063	0.79	0.921	1.55	0.107	1.33	9.360	1.33	5.7	1.3	694	17	663	15	654	17
NHG15.12rd3_16	64	8	38	0.6	41	0.061	1.13	0.898	1.97	0.107	1.61	9.341	1.61	-3.5	-0.8	634	24	650	19	656	20
NHG15.12rd3_04	146	17	61	0.4	106	0.063	0.92	0.925	1.76	0.107	1.50	9.322	1.50	5.2	1.2	693	20	665	17	657	19
NHG15.12rd6_22	128	15	93	0.7	78	0.061	1.02	0.907	1.70	0.107	1.36	9.307	1.36	-1.4	-0.4	649	22	656	16	658	17
NHG15.12rd6_46	222	29	287	1.3	67	0.063	0.74	0.932	1.31	0.108	1.08	9.292	1.08	6.2	1.5	703	16	669	13	659	14
NHG15.12rd6_88	184	22	112	0.6	-4	0.063	0.77	0.929	1.59	0.108	1.39	9.283	1.39	4.9	1.1	694	16	667	15	659	17
NHG15.12rd6_91a	96	12	81	0.8	37	0.063	0.78	0.937	1.52	0.108	1.30	9.225	1.30	5.0	1.2	699	17	671	15	663	16
NHG15.12rd6_34	127	20	288	2.3	34	0.064	0.99	0.954	1.44	0.109	1.05	9.179	1.05	8.2	2.0	726	21	680	14	667	13
NHG15.12rd6_70	173	20	109	0.6	35	0.063	0.81	0.948	1.31	0.109	1.03	9.142	1.03	5.1	1.2	705	17	677	13	669	13
NHG15.12rd6_95	184	23	189	1.0	162	0.063	0.69	0.945	1.47	0.109	1.30	9.139	1.30	3.8	0.9	696	15	675	14	669	17
NHG15.12rd6_97	201	26	194	1.0	106	0.064	0.66	0.963	1.45	0.109	1.29	9.136	1.29	9.0	2.2	735	14	685	14	670	16
NHG15.12rd6_94a	149	20	162	1.1	63	0.062	0.79	0.945	1.54	0.110	1.33	9.097	1.33	2.0	0.4	686	17	675	15	672	17
NHG15.12rd6_48	137	16	60	0.4	131	0.063	1.02	0.957	1.64	0.110	1.29	9.082	1.29	5.1	1.2	709	22	681	16	673	16
NHG15.12rd6_36	139	17	126	0.9	123	0.063	0.88	0.952	1.34	0.110	1.01	9.081	1.01	3.6	0.8	699	19	679	13	673	13
NHG15.12rd6_73a	168	22	151	0.9	-42	0.062	0.63	0.950	1.38	0.110	1.22	9.069	1.22	2.4	0.5	691	13	678	14	674	16
NHG15.12rd6_04	202	23	97	0.5	44	0.062	1.19	0.953	1.69	0.111	1.20	9.039	1.20	2.0	0.4	691	25	679	17	676	15
NHG15.12rd6_67	304	36	206	0.7	25	0.063	0.69	0.967	1.34	0.112	1.15	8.926	1.15	1.7	0.4	696	15	687	13	685	15

Appendix 2. Summary concordant data only. U-Pb zircon analyses. R.Dartnall. | Plotted ages are highlighted green and boxed

Samples	Concentrations					Isotope ratios								Discordance %		Ratios to Dates					
Analyses	Uppm	Pbppm	Thppm	Th/U	^{204}Pb	^{207}Pb/^{206}Pb	1s%	^{207}Pb/^{235}U	1s%	^{206}Pb/^{238}U	1s%	^{238}U/^{206}Pb	1s%	6-38/7-6	6-38/7-35	^{207}Pb/^{206}Pb	2s abs	^{207}Pb/^{235}U	2s abs	^{206}Pb/^{238}U	2s abs
Sample NHG15:12. Outcrop belt 3. Penrhyn. NGR SH2845 8491. Psammite																					
NHG15.12rd6_73b	160	21	140	0.9	78	0.063	0.76	0.973	1.48	0.112	1.27	8.906	1.27	2.6	0.6	705	16	690	15	686	17
NHG15.12rd6_94b	112	15	123	1.1	-125	0.063	0.76	0.976	1.56	0.113	1.36	8.846	1.36	0.9	0.2	696	16	692	16	690	18
NHG15.12_10	177	22	97	0.5	-18	0.063	0.92	0.977	1.79	0.113	1.54	8.826	1.54	0.4	0.1	694	20	692	18	692	20
NHG15.12rd6_37b	131	16	70	0.5	34	0.064	0.83	1.006	1.39	0.114	1.11	8.744	1.11	5.1	1.2	736	18	707	14	698	15
NHG15.12rd6_37a	120	14	49	0.4	109	0.064	0.89	1.029	1.51	0.116	1.22	8.601	1.22	5.3	1.3	749	19	718	15	709	16
NHG15.12rd3_22	293	34	42	0.1	15	0.063	0.91	1.031	1.62	0.120	1.34	8.362	1.34	-5.1	-1.2	693	19	719	17	728	18
NHG15.12rd3_08	137	19	70	0.5	-4	0.066	0.84	1.161	1.71	0.127	1.49	7.858	1.49	4.9	1.3	812	18	782	18	772	22
NHG15.12rd6_38b	192	28	45	0.2	19	0.070	0.74	1.442	1.28	0.149	1.04	6.705	1.04	4.0	1.2	933	15	907	15	896	17
NHG15.12rd6_38a	61	10	31	0.5	76	0.071	1.02	1.513	1.53	0.154	1.14	6.481	1.14	3.8	1.1	961	21	936	19	925	20
NHG15.12rd3_23	42	10	28	0.7	-91	0.079	1.13	2.171	2.00	0.199	1.64	5.030	1.64	0.7	0.2	1178	22	1172	27	1169	35
NHG15.12rd3_11	283	59	82	0.3	0	0.080	0.83	2.196	1.73	0.199	1.51	5.029	1.51	2.6	0.9	1200	16	1180	24	1169	32
NHG15.12rd6_74b	118	25	56	0.5	183	0.081	0.72	2.221	1.50	0.199	1.31	5.026	1.31	4.2	1.5	1221	14	1188	21	1170	28
NHG15.12rd6_74a	121	25	47	0.4	244	0.082	0.78	2.227	1.57	0.198	1.35	5.050	1.35	5.8	2.1	1236	15	1190	22	1165	29
NHG15.12rd6_61	56	12	30	0.5	95	0.084	0.98	2.302	1.82	0.199	1.53	5.023	1.53	9.3	3.5	1290	19	1213	25	1170	33
NHG15.12rd6_69	687	159	93	0.1	130	0.092	0.58	3.140	1.08	0.247	0.91	4.051	0.91	3.5	1.4	1473	11	1442	16	1422	23
NHG15.12rd6_16	207	63	154	0.7	64	0.096	0.74	3.608	1.38	0.272	1.17	3.679	1.17	0.2	0.1	1554	14	1551	22	1550	32
NHG15.12rd6_68	31	11	40	1.3	-30	0.104	0.91	4.257	1.72	0.296	1.45	3.378	1.45	1.8	0.8	1703	17	1685	28	1672	43
NHG15.12rd6_95	65	25	33	0.5	-17	0.117	0.61	5.757	1.53	0.356	1.41	2.810	1.41	-2.4	-1.2	1917	11	1940	26	1963	48
NHG15.12rd6_06	112	45	77	0.7	73	0.119	0.75	5.793	1.43	0.352	1.21	2.839	1.21	0.1	0.0	1946	13	1945	24	1945	41
NHG15.12rd6_27	137	54	88	0.6	74	0.121	0.70	5.943	1.37	0.356	1.18	2.807	1.18	0.3	0.1	1971	13	1967	24	1965	40
NHG15.12rd3_25	92	40	53	0.6	16	0.129	0.77	6.587	1.68	0.371	1.49	2.694	1.49	2.2	1.1	2081	14	2058	29	2035	52
NHG15.12rd6_17	65	42	91	1.4	46	0.178	0.83	11.484	1.57	0.467	1.34	2.140	1.34	6.3	3.6	2638	14	2563	29	2471	55
NHG15.12rd6_35	79	47	44	0.6	-30	0.189	0.65	13.549	1.40	0.520	1.24	1.925	1.24	1.4	0.8	2736	11	2719	26	2697	54
Sample NHG15:2. Outcrop belt 4. Cemlyn Bay. NGR SH3368 9326. Psammite																					
NHG15.2rd3_10	-22	20	126	0.6	-22	0.058	0.99	0.687	1.83	0.085	1.55	11.714	1.55	2.8	0.5	543	22	531	15	528	16
NHG15.2rd3_03	-93	40	386	1.1	-93	0.059	0.84	0.692	1.63	0.086	1.39	11.668	1.39	3.9	0.7	551	18	534	13	530	14
NHG15.2rd3_22	62	6	47	0.8	62	0.059	1.40	0.712	2.12	0.088	1.59	11.379	1.59	2.9	0.5	559	31	546	18	543	17
NHG15.2.rd5_11	39	34	179	0.5	39	0.059	0.78	0.726	1.64	0.089	1.44	11.241	1.44	4.6	0.9	576	17	554	14	549	15
NHG15.2rd4a_17	176	17	149	0.9	176	0.058	0.72	0.717	1.58	0.089	1.41	11.204	1.41	-1.8	-0.4	542	16	549	13	551	15
NHG15.2rd4a_05a	43	20	129	0.6	43	0.059	0.75	0.724	1.44	0.090	1.23	11.164	1.23	0.1	0.0	554	16	553	12	553	13
NHG15.2rd4a_12b	66	17	170	1.0	66	0.059	0.78	0.736	1.50	0.090	1.28	11.101	1.28	3.5	0.7	576	17	560	13	556	14
NHG15.2.rd5_12	164	17	126	0.8	-72	0.060	0.86	0.747	1.67	0.091	1.43	11.013	1.43	5.3	1.1	592	19	566	14	560	15
NHG15.2rd3_31	60	7	71	1.2	166	0.060	1.25	0.755	2.06	0.091	1.64	10.989	1.64	8.2	1.7	612	27	571	18	561	18
NHG15.2rd3_40	20	21	173	0.9	20	0.059	1.02	0.737	1.83	0.091	1.52	10.969	1.52	-1.3	-0.3	555	22	561	16	562	16
NHG15.2rd3_37	89	9	42	0.5	40	0.060	1.10	0.762	1.97	0.092	1.63	10.912	1.63	8.2	1.7	616	24	575	17	565	18
NHG15.2rd3_05	64	6	32	0.5	-86	0.060	1.18	0.759	1.87	0.092	1.45	10.897	1.45	6.1	1.3	603	26	573	16	566	16
NHG15.2rd3_36	-93	13	100	0.8	-93	0.059	1.18	0.752	1.85	0.092	1.43	10.892	1.43	3.1	0.6	584	26	570	16	566	15
NHG15.2rd4a_19	-17	56	546	1.0	-17	0.059	0.56	0.758	1.30	0.093	1.17	10.786	1.17	1.3	0.2	579	12	573	11	572	13
NHG15.2rd4a_09a	-50	42	376	0.9	-50	0.059	0.61	0.756	1.38	0.093	1.23	10.761	1.23	-0.6	-0.1	570	13	572	12	573	14
NHG15.2rd3_23	177	20	222	1.3	-28	0.058	0.92	0.748	1.74	0.093	1.48	10.758	1.48	-5.3	-1.1	544	20	567	15	573	16
NHG15.2rd4a_09b	45	42	320	0.8	45	0.059	0.67	0.769	1.44	0.094	1.28	10.657	1.28	0.8	0.1	583	15	579	13	578	14
NHG15.2rd3_24	130	14	133	1.0	10	0.060	1.01	0.781	1.72	0.094	1.40	10.643	1.40	5.7	1.2	614	22	586	15	579	15
NHG15.2.rd5_04	120	12	55	0.5	120	0.059	0.95	0.772	1.75	0.094	1.47	10.599	1.47	-0.1	0.0	581	21	581	15	581	16
NHG15.2rd3_26	34	12	58	0.5	34	0.060	1.09	0.783	1.82	0.094	1.45	10.595	1.45	4.9	1.0	611	24	587	16	581	16
NHG15.2rd4a_18	35	29	196	0.7	35	0.060	0.69	0.784	1.40	0.095	1.22	10.573	1.22	4.2	0.9	608	15	588	12	583	14
NHG15.2rd3_16	73	11	51	0.5	73	0.061	1.06	0.822	1.91	0.098	1.59	10.188	1.59	4.3	0.9	631	23	609	17	604	18
NHG15.2rd3_04	158	24	153	0.7	158	0.061	1.03	0.824	1.77	0.099	1.45	10.141	1.45	3.1	0.6	626	22	610	16	606	17
NHG15.2rd3_08	70	16	102	0.8	70	0.061	1.01	0.834	1.80	0.099	1.50	10.055	1.50	3.7	0.8	635	22	616	17	611	17
NHG15.2rd3_11	28	36	124	0.4	28	0.061	0.93	0.833	1.72	0.100	1.45	10.018	1.45	1.7	0.3	624	20	615	16	613	17
NHG15.2.rd5_01	60	44	157	0.4	60	0.061	0.74	0.839	1.56	0.100	1.38	10.008	1.38	3.4	0.7	636	16	618	14	614	16
NHG15.2rd3_12	-118	29	193	0.8	-118	0.060	1.03	0.832	1.73	0.100	1.39	9.979	1.39	-0.6	-0.2	612	22	615	16	616	16
NHG15.2rd3_38	162	20	173	1.1	74	0.062	0.96	0.854	1.74	0.101	1.45	9.934	1.45	6.1	1.4	658	21	627	16	618	17
NHG15.2.rd5_03	-8	23	111	0.5	-8	0.061	0.77	0.845	1.78	0.101	1.60	9.895	1.60	1.0	0.2	627	17	622	16	621	19
NHG15.2rd3_20	67	40	299	0.9	67	0.061	0.94	0.846	1.68	0.101	1.40	9.857	1.40	-0.2	-0.1	622	20	622	16	623	17
NHG15.2rd3_15	84	41	241	0.7	84	0.061	0.83	0.856	1.63	0.102	1.40	9.847	1.40	3.4	0.7	646	18	628	15	624	17
NHG15.2rd4a_06a	117	13	73	0.6	24	0.062	0.89	0.872	1.58	0.102	1.31	9.777	1.31	6.2	1.4	669	19	637	15	628	16
NHG15.2rd4a_07b	55	15	91	0.7	55	0.061	0.71	0.857	1.49	0.102	1.31	9.761	1.31	-0.1	-0.1	628	15	628	14	629	16
NHG15.2rd3_17	55	7	39	0.7	55	0.060	1.25	0.855	1.97	0.103	1.52	9.729	1.52	-2.3	-0.5	616	27	627	18	631	18
NHG15.2rd3_42	78	10	97	1.2	201	0.062	1.10	0.877	1.85	0.103	1.49	9.726	1.49	6.1	1.4	672	23	640	17	631	18
NHG15.2rd4a_27a	97	24	215	1.1	97	0.061	0.75	0.871	1.50	0.103	1.30	9.719	1.30	3.5	0.8	654	16	636	14	631	16
NHG15.2rd3_30	91	15	95	0.7	91	0.061	0.91	0.871	1.82	0.103	1.57	9.718	1.57	3.4	0.7	654	20	636	17	631	19
NHG15.2rd4a_24a	40	40	443	1.4	40	0.062	0.60	0.876	1.46	0.103	1.33	9.709	1.33	4.8	1.1	664	13	639	14	632	16
NHG15.2rd4a_02	-47	20	194	1.2	-47	0.060	0.82	0.853	1.53	0.103	1.29	9.695	1.29	-5.0	-1.1	603	18	626	14	633	16
NHG15.2.rd5_02	129	21	31	0.1	129	0.061	0.87	0.872	1.68	0.103	1.44	9.691	1.44	2.6	0.5	650	19	636	16	633	17
NHG15.2rd3_44	57	21	221	1.4	57	0.060	0.88	0.857	1.73	0.103	1.48	9.673	1.48	-4.0	-0.9	610	19	629	16	634	18
NHG15.2rd4a_27b	106	40	360	1.1	106	0.061	0.64	0.873	1.43	0.104	1.28	9.644	1.28	1.0	0.2	643	14	637	13	636	15
NHG15.2rd3_19	157	19	124	0.8	2	0.062	0.85	0.887	1.67	0.104	1.44	9.632	1.44	5.7	1.3	675	18	645	16	637	17
NHG15.2rd3_27	40	12	61	0.5	40	0.061	1.00	0.868	1.87	0.104	1.58	9.619	1.58	-2.3	-0.5	623	21	634	18	638	19
NHG15.2rd4a_25	49	32	218	0.8	49	0.061	0.70	0.873	1.44	0.104	1.25	9.598	1.25	-1.1	-0.3	632	15	637	14	639	15
NHG15.2rd4a_29	112	13	82	0.7	114	0.062	0.81	0.894	1.52	0.104	1.28	9.579	1.28	5.7	1.3	679	17	648	14	640	16
NHG15.2rd4a_28	133	23	139	0.7	133	0.061	0.59	0.882	1.39	0.104	1.26	9.570	1.26	1.1	0.2	648	13	642	13	641	15
NHG15.2rd3_41	134	12	62	0.6	134	0.061	1.00	0.877	1.84	0.105	1.55	9.545	1.55	-2.0	-0.5	630	21	639	17	642	19
NHG15.2rd3_18	-45	12	56	0.5	-45	0.061	0.98	0.890	1.85	0.105	1.57	9.506	1.57	1.4	0.3	654	21	647	18	645	19
NHG15.2rd4a_24b	147	5	28	0.6	147	0.062	1.12	0.899	1.95	0.106	1.60	9.478	1.60	3.3	0.7	668	24	651	19	647	20
NHG15.2rd3_35	100	39	395	1.4	100	0.062	0.90	0.898	1.73	0.106	1.47	9.474	1.47	2.9	0.6	666	19	651	16	647	18
NHG15.2rd4a_20	15	20	127	0.7	15	0.061	0.75	0.893	1.51	0.106	1.31	9.468	1.31	0.7	0.1	652	16	648	14	647	16
NHG15.2rd4a_31	7	19	147	0.9	7	0.061	0.76	0.885	1.52	0.106	1.32	9.458	1.32	-2.8	-0.7	630	16	644	14	648	16
NHG15.2rd4a_14	-13	13	85	0.8	-13	0.061	0.77	0.892	1.50	0.106	1.28	9.420	1.28	-2.0	-0.5	638	17	647	14	650	16
NHG15.2rd4a_07a	186	12	71	0.7	186	0.061	0.75	0.892	1.57	0.106	1.37	9.403	1.37	-2.6	-0.6	635	16	648	15	652	17
NHG15.2.rd5_07	22	25	143	0.7	22	0.062	0.85	0.916	1.61	0.107	1.37	9.358	1.37	4.0	0.9	682	18	660	16	654	17
NHG15.2rd3_34	-36	12	103	1.1	-36	0.061	1.05	0.907	1.84	0.107	1.50	9.330	1.50	-0.6	-0.2	653	23	655	18	656	19
NHG15.2rd3_02	-64	8	57	0.9	-64	0.062	1.16	0.909	1.96	0.107	1.58	9.329	1.58	0.2	0.0	658	25	657	19	656	20
NHG15.2.rd5_06	7	9	49	0.7	7	0.062	1.00	0.918	1.86	0.108	1.57	9.239	1.57	-0.8	-0.2	657	21	661	18	663	20
NHG15.2rd4a_10a	257	31	228	0.9	53	0.061	0.66	0.907	1.41	0.109	1.24	9.195	1.24	-6.8	-1.5	623	14	656	14	665	16
NHG15.2rd4a_15	104	13	88	0.8	104	0.062	0.74	0.936	1.48	0.109	1.28	9.181	1.28	2.9	0.6	686	16	671	14	667	16
NHG15.2rd4a_06b	-20	30	228	0.9	-20	0.062	0.70	0.929	1.43	0.109	1.24	9.173	1.24	0.0	0.0	667	15	667	14	667	16
NHG15.2rd4a_11b	189	21	129	0.8	189	0.062	0.72	0.952	1.43	0.111	1.23	9.015	1.23	0.8	0.1	683	15	679	14	678	16
NHG15.2rd4a_06b	136	7	26	0.4	136	0.063	1.01	0.975	1.69	0.112	1.36	8.901	1.36	2.9	0.7	707	21	691	17	686	18
NHG15.2rd4a_30a	95	15	128	1.2	95	0.062	0.77	0.966	1.53	0.113	1.32	8.883	1.32	-0.5	-0.1	684	16	687	15	688	17
NHG15.2rd4a_11a	98	13	84	0.8	98	0.062	0.79	0.965	1.57	0.113	1.35	8.882	1.35	-1.0	-0.3	681	17	686	16	688	18
NHG15.2rd4a_30b	-106	11	74	0.9	-106	0.062	0.75	0.984	1.51	0.115	1.31	8.681	1.31	-4.4	-1.0	673	16	696	15	703	17
NHG15.2rd3_13	-68	22	77	0.4	-68	0.064	1.03	1.048	1.86	0.120	1.55	8.366	1.55	0.2	0.0	729	22	728	19	728	21
NHG15.2rd4a_13	-18	32	159	0.7	-18	0.064	0.68	1.082	1.44	0.123	1.27	8.134	1.27	-1.4	-0.4	737	14	745	15	748	18
NHG15.2rd3_28	150	36	39	0.1	150	0.065	0.83	1.170	1.61	0.130	1.38	7.695	1.38	-0.4	-0.1	784	17	786	17	788	20
NHG15.2rd3_43	57	24	37	0.2	57	0.066	0.87	1.213	1.65	0.133	1.41	7.508	1.41	0.2	0.0	808	18	806	18	806	21

Appendix 2. Summary concordant data only. U-Pb zircon analyses. R.Dartnall.

Plotted ages are highlighted green and boxed

Samples	Concentrations					Isotope ratios								Discordance %		Ratios to Dates					
Analyses	Uppm	Pbppm	Thppm	Th/U	^{204}Pb	^{207}Pb/^{206}Pb	1s%	^{207}Pb/^{235}U	1s%	^{206}Pb/^{238}U	1s%	^{238}U/^{206}Pb	1s%	6-38/7-6	6-38/7-35	^{207}Pb/^{206}Pb	2s abs	^{207}Pb/^{235}U	2s abs	^{206}Pb/^{238}U	2s abs
Sample NHG15:2. Outcrop belt 4. Cemlyn Bay. NGR SH3368 9326. Psammite																					
NHG15.2rd4a_26	-142	26	100	0.9	-142	0.079	0.66	2.248	1.45	0.207	1.29	4.823	1.29	-4.3	-1.5	1164	13	1196	20	1215	28
NHG15.2rd4a_16a	106	16	25	0.3	106	0.081	0.68	2.347	1.46	0.211	1.30	4.744	1.30	-1.4	-0.5	1216	13	1227	21	1233	29
NHG15.2rd4a_16b	-68	26	44	0.4	-68	0.081	0.65	2.353	1.39	0.211	1.23	4.736	1.23	-1.4	-0.5	1218	13	1229	20	1235	28
NHG15.2rd3_07	-30	46	37	0.2	-30	0.081	0.84	2.341	1.74	0.209	1.53	4.783	1.53	0.3	0.1	1227	16	1225	24	1224	34
NHG15.2rd3_32	1	51	82	0.3	1	0.081	0.83	2.338	1.59	0.208	1.36	4.797	1.36	0.8	0.3	1231	16	1224	22	1221	30
NHG15.2.rd5_10	156	18	30	0.3	156	0.082	0.73	2.317	1.73	0.204	1.57	4.891	1.57	4.1	1.5	1251	14	1217	24	1199	34
NHG15.2rd3_01	54	39	14	0.1	54	0.085	0.82	2.553	1.69	0.219	1.48	4.563	1.48	2.1	0.8	1305	16	1287	24	1277	34
NHG15.2rd4a_23	61	115	186	0.4	61	0.086	0.51	2.820	1.34	0.238	1.24	4.198	1.24	-3.1	-1.2	1336	10	1361	20	1378	31
NHG15.2rd3_33	422	107	184	0.4	20	0.095	0.75	3.207	1.70	0.245	1.53	4.086	1.53	7.8	3.3	1530	14	1459	26	1411	39
NHG15.2rd4a_08a	33	41	98	0.9	33	0.109	0.62	4.932	1.45	0.327	1.31	3.058	1.31	-1.9	-0.9	1790	11	1808	24	1824	42
NHG15.2rd4a_08b	39	18	33	0.7	39	0.111	0.68	5.011	1.72	0.328	1.57	3.052	1.57	-0.6	-0.3	1815	12	1821	29	1827	50
NHG15.2rd3_06	-2	54	100	0.7	-2	0.114	0.79	5.121	1.75	0.326	1.56	3.070	1.56	2.6	1.2	1865	14	1840	29	1817	49
NHG15.2rd4a_22a	79	31	46	1.0	79	0.186	0.54	13.720	1.51	0.536	1.42	1.865	1.42	-2.4	-1.4	2704	9	2731	28	2768	63
NHG15.2rd4a_22b	32	16	27	1.1	32	0.187	0.69	13.525	1.81	0.524	1.67	1.909	1.67	0.1	0.1	2719	11	2717	34	2715	74
NHG15.2rd3_25	-25	34	56	1.2	-25	0.204	0.77	15.703	1.79	0.560	1.61	1.787	1.61	-0.4	-0.2	2855	13	2859	34	2865	74
NHG15.2rd4a_21	121	84	145	1.2	4	0.211	0.54	15.355	1.37	0.529	1.26	1.892	1.26	6.0	3.6	0	9	2838	26	2736	56
Sample PT15:1. Outcrop belt 2. Aberffraw. NGR SH3382 6833. Psammite																					
PT15.1rd5_05b	160	19	157	1.0	-20	0.059	1.08	0.774	1.67	0.095	1.28	10.548	1.28	-1.5	-0.3	576	23	582	15	584	14
PT15.1rd5_06	181	22	190	1.0	-17	0.061	1.11	0.793	1.72	0.095	1.32	10.523	1.32	6.0	1.3	623	24	593	15	585	15
PT15.1_14	107	13	155	1.4	-2	0.060	1.07	0.794	1.66	0.095	1.26	10.481	1.26	5.0	1.0	618	23	594	15	587	14
PT15.1_26	138	16	157	1.1	54	0.061	0.95	0.800	1.60	0.096	1.29	10.467	1.29	6.6	1.4	630	20	597	14	588	14
PT15.1_30	293	33	304	1.0	28	0.061	0.86	0.797	1.46	0.096	1.18	10.466	1.18	5.5	1.2	622	18	595	13	588	13
PT15.1_23	145	17	180	1.2	-28	0.061	0.94	0.798	1.53	0.096	1.21	10.453	1.21	5.4	1.1	623	20	596	14	589	14
PT15.1_15	174	21	215	1.2	-75	0.061	0.99	0.803	1.50	0.096	1.12	10.438	1.12	6.9	1.5	634	21	599	13	590	13
PT15.1rd5_07	145	15	78	0.5	170	0.060	1.09	0.798	1.61	0.096	1.19	10.436	1.19	4.9	1.0	620	23	596	14	590	13
PT15.1rd5_05a	269	34	312	1.2	61	0.060	1.13	0.799	1.73	0.096	1.30	10.427	1.30	4.6	1.0	619	24	596	15	590	15
PT15.1_09	138	22	399	2.9	67	0.061	1.07	0.811	1.63	0.096	1.24	10.408	1.24	8.9	2.0	649	23	603	15	591	14
PT15.1_12	82	11	128	1.6	7	0.061	1.22	0.811	1.80	0.096	1.33	10.368	1.33	7.3	1.6	640	26	603	16	594	15
PT15.1_13	301	33	250	0.8	-1	0.061	0.91	0.808	1.52	0.097	1.21	10.359	1.21	5.5	1.2	629	20	601	14	594	14
PT15.1_20	100	11	103	1.0	44	0.060	1.03	0.807	1.55	0.097	1.16	10.322	1.16	3.7	0.8	619	22	601	14	596	13
PT15.1rd5_12	160	21	209	1.3	-4	0.060	0.91	0.800	1.46	0.097	1.14	10.321	1.14	0.9	0.2	602	20	597	13	596	13
PT15.1rd5_14	77	8	51	0.7	-3	0.061	1.31	0.812	1.80	0.097	1.24	10.320	1.24	5.8	1.2	633	28	604	16	596	14
PT15.1rd5_01	91	12	119	1.3	93	0.060	1.20	0.799	1.77	0.097	1.29	10.317	1.29	-0.1	-0.1	596	26	596	16	596	15
PT15.1_31	190	23	235	1.2	-7	0.060	0.98	0.811	1.56	0.097	1.21	10.270	1.21	3.3	0.7	619	21	603	14	599	14
PT15.1_04	270	40	657	2.4	54	0.061	0.88	0.823	1.49	0.098	1.20	10.235	1.20	6.8	1.5	645	19	610	14	601	14
PT15.1_01	360	42	394	1.1	69	0.060	0.88	0.816	1.46	0.098	1.16	10.205	1.16	2.8	0.6	620	19	606	13	603	13
PT15.1_56	167	21	218	1.3	-82	0.060	1.01	0.817	2.08	0.098	1.82	10.200	1.82	2.7	0.6	620	22	606	19	603	21
PT15.1_63	191	23	237	1.2	-24	0.061	0.99	0.822	2.10	0.098	1.85	10.162	1.85	3.1	0.6	624	21	609	19	605	21
PT15.1_02	63	9	120	1.9	49	0.060	1.29	0.819	1.96	0.099	1.48	10.143	1.48	1.2	0.2	613	28	607	18	606	17
PT15.1_29	164	23	313	1.9	16	0.060	1.05	0.819	1.67	0.099	1.30	10.138	1.30	1.0	0.2	613	23	608	15	606	15
PT15.1_64	170	19	149	0.9	8	0.060	1.06	0.821	2.13	0.099	1.84	10.130	1.84	1.6	0.3	617	23	609	19	607	21
PT15.1_53	408	47	391	1.0	13	0.060	0.87	0.813	1.99	0.099	1.79	10.128	1.79	-2.3	-0.5	593	19	604	18	607	21
PT15.1_59	83	11	140	1.7	-19	0.062	1.09	0.838	2.18	0.099	1.88	10.115	1.88	7.6	1.7	658	23	618	20	608	22
PT15.1_25	97	12	135	1.4	105	0.060	1.09	0.824	1.64	0.099	1.23	10.110	1.23	1.8	0.4	619	24	610	15	608	14
PT15.1_05	52	6	56	1.1	117	0.061	1.33	0.835	2.02	0.099	1.51	10.107	1.51	6.1	1.3	648	29	616	18	608	18
PT15.1_51	99	13	136	1.4	-12	0.061	1.10	0.836	2.17	0.099	1.88	10.078	1.88	5.3	1.1	644	24	617	20	610	22
PT15.1_62	317	36	273	0.9	191	0.060	0.92	0.825	2.01	0.099	1.79	10.061	1.79	0.0	0.0	611	20	611	18	611	21
PT15.1_55	78	10	100	1.3	13	0.061	1.01	0.833	2.15	0.099	1.90	10.060	1.90	3.5	0.7	633	22	615	20	611	22
PT15.1_52	200	25	262	1.3	83	0.061	0.99	0.837	2.07	0.099	1.82	10.058	1.82	4.7	1.0	641	21	617	19	611	21
PT15.1_24	55	8	107	1.9	-4	0.061	1.19	0.839	1.91	0.099	1.49	10.056	1.49	5.4	1.2	646	26	618	18	611	17
PT15.1_66	159	19	185	1.2	34	0.061	1.04	0.841	2.13	0.100	1.86	10.044	1.86	5.9	1.3	650	22	620	20	612	22
PT15.1_61	304	36	343	1.1	114	0.061	0.92	0.834	2.08	0.100	1.86	10.022	1.86	2.1	0.4	626	20	616	19	613	22
PT15.1_44	614	71	590	1.0	-70	0.060	0.92	0.831	2.02	0.100	1.80	10.016	1.80	0.7	0.1	618	20	614	18	613	21
PT15.1_35	68	9	110	1.6	234	0.061	1.28	0.833	2.32	0.100	1.94	10.010	1.94	1.4	0.3	622	28	615	21	614	23
PT15.1_43	202	27	320	1.6	68	0.061	0.99	0.845	2.06	0.100	1.80	10.010	1.80	6.0	1.3	653	21	622	19	614	21
PT15.1_50	75	12	171	2.3	47	0.062	1.27	0.851	2.35	0.100	1.98	9.990	1.98	7.3	1.6	663	27	625	22	615	23
PT15.1_41	84	11	139	1.7	-32	0.061	1.12	0.847	2.22	0.100	1.92	9.989	1.92	5.6	1.2	652	24	623	21	615	22
PT15.1_18	70	8	74	1.1	95	0.062	1.08	0.852	1.74	0.100	1.37	9.976	1.37	7.2	1.6	663	23	626	16	616	16
PT15.1_57	115	16	224	1.9	141	0.061	1.22	0.847	2.22	0.100	1.86	9.952	1.86	4.4	0.9	646	26	623	20	617	22
PT15.1_49	62	9	123	2.0	-35	0.061	1.38	0.845	2.41	0.101	1.97	9.947	1.97	3.2	0.7	638	30	622	22	618	23
PT15.1_36	52	8	122	2.3	93	0.060	1.21	0.832	2.29	0.101	1.94	9.932	1.94	-2.7	-0.6	602	26	615	21	618	23
PT15.1_65	208	30	412	2.0	59	0.060	1.03	0.838	2.07	0.101	1.79	9.914	1.79	-1.1	-0.3	613	22	618	19	619	21
PT15.1_67	273	32	283	1.0	33	0.061	1.05	0.843	2.18	0.101	1.91	9.914	1.91	1.0	0.2	626	23	621	20	619	22
PT15.1_60	63	10	149	2.4	114	0.061	1.15	0.848	2.41	0.101	2.12	9.895	2.12	2.3	0.5	635	25	624	22	621	25
PT15.1_27	84	10	99	1.2	36	0.061	1.17	0.844	1.83	0.101	1.41	9.888	1.41	0.4	0.0	623	25	621	17	621	17
PT15.1_38	118	13	67	0.6	-68	0.061	1.03	0.857	2.12	0.101	1.85	9.882	1.85	5.0	1.1	654	22	628	20	621	22
PT15.1_40	136	19	246	1.8	-119	0.062	1.05	0.870	2.24	0.102	1.98	9.771	1.98	5.3	1.2	664	22	636	21	628	24
PT15.1_46	66	8	88	1.3	134	0.060	1.11	0.849	2.28	0.102	1.99	9.766	1.99	-3.1	-0.7	610	24	624	21	628	24
PT15.1_45	101	11	77	0.8	73	0.060	1.22	0.851	2.31	0.103	1.97	9.747	1.97	-3.1	-0.7	611	26	625	21	630	24
PT15.1_39	130	16	149	1.1	104	0.060	1.08	0.857	2.20	0.103	1.91	9.703	1.91	-2.6	-0.6	616	23	629	20	632	23
PT15.1_42	86	11	101	1.2	73	0.060	1.09	0.865	2.24	0.104	1.95	9.588	1.95	-5.0	-1.1	609	24	633	21	640	24
PT15.1_48	275	137	83	0.3	86	0.157	0.87	10.081	2.00	0.466	1.80	2.147	1.80	-1.7	-0.9	2424	15	2442	36	2465	73
Sample VY473. Barons Hill, Beaumaris. NGR SH598 767. Tuff																					
VY473_05	271	30	296	1.1	3	0.060	1.03	0.755	2.11	0.091	1.84	10.943	1.84	6.3	1.3	602	22	571	18	564	20
VY473rd4a_20a	111	14	165	1.5	115	0.060	0.90	0.766	1.66	0.092	1.40	10.812	1.40	6.1	1.3	608	19	578	15	570	15
VY473_16a	256	26	189	0.7	30	0.060	0.96	0.785	2.10	0.094	1.86	10.610	1.86	6.1	1.3	619	21	588	19	581	21
VY473rd5_06	182	22	191	1.0	-21	0.061	1.09	0.794	1.70	0.095	1.31	10.535	1.31	6.8	1.4	627	24	593	15	585	15
VY473rd4a_04	71	8	56	0.8	153	0.060	1.03	0.785	1.79	0.095	1.47	10.503	1.47	1.8	0.3	597	22	588	16	586	16
VY473rd5_05b	159	19	157	1.0	-7	0.059	1.09	0.778	1.67	0.095	1.27	10.484	1.27	-2.4	-0.5	573	24	584	15	587	14
VY473_14	181	18	92	0.5	186	0.061	1.31	0.796	2.33	0.095	1.93	10.483	1.93	5.7	1.2	623	28	595	21	587	22
VY473_19	207	22	165	0.8	-125	0.061	1.00	0.798	2.19	0.096	1.94	10.465	1.94	5.8	1.2	625	22	596	20	588	22
VY473rd5_07a	145	15	78	0.5	170	0.060	1.09	0.799	1.61	0.096	1.19	10.426	1.19	4.8	1.0	620	23	596	14	590	13
VY473rd5_05a	269	34	312	1.2	61	0.060	1.13	0.799	1.73	0.096	1.30	10.416	1.30	4.5	0.9	619	24	597	15	591	15
VY473rd4a_02a	67	7	48	0.7	137	0.061	1.04	0.822	1.80	0.098	1.47	10.187	1.47	4.3	0.9	631	23	609	16	604	17
VY473rd4a_15a	124	14	102	0.8	70	0.062	0.91	0.840	1.61	0.098	1.33	10.158	1.33	9.7	2.2	670	20	619	15	605	15
VY473_02	97	11	97	1.0	40	0.061	1.17	0.835	2.37	0.099	2.06	10.115	2.06	6.4	1.4	650	25	616	22	608	24
VY473_12	258	28	197	0.8	47	0.060	0.96	0.823	2.06	0.099	1.82	10.110	1.82	1.4	0.3	616	21	610	19	608	21
VY473_06	181	22	208	1.1	189	0.060	1.00	0.823	2.12	0.099	1.87	10.106	1.87	1.2	0.2	616	22	610	19	608	22
VY473rd4a_18a	111	13	118	1.1	84	0.061	0.92	0.829	1.60	0.099	1.30	10.095	1.30	3.3	0.7	629	20	613	15	609	15
VY473rd4a_18b	167	20	183	1.1	98	0.061	0.78	0.834	1.54	0.099	1.33	10.087	1.33	4.8	1.0	640	17	616	14	609	15
VY473_18	103	11	78	0.8	24	0.062	1.23	0.846	2.27	0.099	1.91	10.058	1.91	8.3	1.9	666	26	623	21	611	22
VY473_11	210	22	100	0.5	-160	0.062	1.00	0.855	2.11	0.100	1.86	10.012	1.86	9.4	2.1	677	21	627	20	614	22
VY473rd4a_02b	273	32	274	1.0	114	0.061	0.73	0.848	1.60	0.101	1.43	9.950	1.43	4.6	1.0	647	16	623	15	617	17
VY473rd4a_16	143	18	158	1.1	26	0.061	0.88	0.843	1.60	0.101	1.34	9.945	1.34	2.3	0.5	632	19	621	15	618	16
VY473rd4a_05	225	24	132	0.6	69	0.061	0.83	0.850	1.58	0.101	1.35	9.914	1.35	4.0	0.9	645	18	625	15	620	16
VY473rd4a_15b	138	15	82	0.6	-12	0.060	0.86	0.841	1.65	0.101	1.41	9.886	1.41	-1.0	-0.3	615	19	620	15	621	17
VY473rd4a_12	152	18	123	0.8	202	0.062	0.84	0.899	1.70	0.106	1.48	9.451	1.48	2.2	0.5	663	18	651	16	648	18
VY473_07	242	26	43	0.2	211	0.063	0.99	0.964	2.11	0.110	1.86	9.067	1.86	6.6	1.6	722	21	685	21	674	24
VY473rd4a_03a	52	11	18	0.3	79	0.080	0.95	2.350	1.86	0.212	1.61	4.709	1.61	-3.1	-1.1	1204	19	1227	26	1241	36
VY473rd4a_03b	174	37	58	0.3	55	0.081	0.81	2.353	1.65	0.211	1.44	4.734	1.44	-1.5	-0.6	1217	16	1228	23	1236	32
VY473rd4a_22a	176	58	216	1.2	-52	0.094	0.64	3.356	1.42	0.260	1.27	3.844	1.27	0.6	0.2	1500	12	1494	22	1491	34
VY473rd4a_22b	352	100	172	0.5	158	0.094	0.76	3.396	1.58	0.261	1.38	3.826	1.38	1.1	0.4	1513	14	1503	24	1497	37

Appendix 3. Stable isotope mass spectrometry.

Run IJF06	Sample	Grid ref.	mass, µg	$\delta^{18}O$	$\delta^{13}C$	*peak ht, mA*	%IR		Outcrop belt	$\delta^{18}O$ Belt 1	$\delta^{13}C$ Blt 1	$\delta^{18}O$ Blt 2	$\delta^{13}C$ Blt 2	$\delta^{18}O$ Blt 3	$\delta^{13}C$ Blt 3	$\delta^{18}O$ Blt 4	$\delta^{13}C$ Blt 4
IJF229	13W10	SH36493 93846	156	-15.57	-7.11	0.67	91	pale dolomite with dol veins cut by cc veins during fracturing episode	4								
IJF231	13W21	SH36606 93816	203	-6.47	-0.35	9.05	6	all NF dolomite; some dol veins	4							-6.47	-0.35
IJF230	13W22	SH36606 93816	150	-4.02	-1.65	5.39	24	slightly F dol cut by F dol veins; isotope value is in a dark (fgr) area	4							-4.02	-1.65
IJF217	A14.5	SH33795 67695	190	-12.84	-1.29	5.54	39	Grainstone, with oncoids and jig-saw fit intraclasts, zoned calcite veins - intense veining.	2			-12.84	-1.29				
IJF218	AF1	SH3584 6748	201	-7.86	3.60	7.97	17	Fully dolomitised, bands of coarse grained dolomite. Finer grains ~ 30 microns, coarse grains ~ 200 - 250 microns	2			-7.86	3.60				
IJF222	L1-13	SH37357 94542	162	-6.85	-0.29	6.74	13	NF dolomicrite with F dol veins, Llanbadrog	4							-6.85	-0.29
IJF223	L5-13	SH37506 94676	138	-12.67	0.86	6.01	8	grainstone (limestone) ; local dol replacement of allochems; later than cc veins; Llanbadrog area	4							-12.67	0.86
IJF213	MN23	SH27279 41026	161	-12.08	-4.59	0.53	93	Siliceous rock. Unstained. High IR	1	-12.08	-4.59						
IJF214	MN28	SH2726 4104	234			0.04	100	peak too small; dolomicrite									
IJF215	MN69	SH2447 3947	153	-12.04	-1.25	0.30	96	Pink dolomite (deep-sea). F dol patches on polished surface. V high IR and powder was drilled not in area staining for F dol	1	-12.04	-1.25						
IJF216	MN72	SH2447 3947	158	-12.73	0.48	6.74	10	NF dolomite with cc veins and region of dedolomitization; isotope powder in largely dedolomitized area. Fresh rock is very pale pink. Possibly deep-sea assocation?	1	-12.73	0.48						
IJF224	NL22	SH3738 9466	145	-4.43	-0.42	5.90	14	oncolitic dolomite in extremely veined sample but vein content minor in drilled area, Llanbadrog area	4							-4.43	-0.42
IJF225	NL39	SH37548 94682	177	-9.78	1.11	8.10	4	dolomite oncoids with white rim and cc cement, Llanbadrog area. Isotope sample will be mixed dol-cc	4							-9.78	1.11
IJF220	**NT19**	SH37169 94084	197	-15.60	1.79	8.01	15	Intensely veined micrite, some MT - MT is recrystalised.Some stylolites.	4							-15.60	1.79
IJF221	NT3	SH37166 94073	241	-16.56	0.99	10.00	13	limestone; locally has MT cement; partly stromatolitic; from megaclast	4							-16.56	0.99
IJF227	PN12	SH15653 28841	250	-7.63	1.56	9.79	18	99% dolomitised. Dolo cx ~ 100 microns. Minor micrite remains, some stylolites evident. Coarser grained dolo in veins.	1	-7.63	1.56						
IJF228	PN20	SH15646 28872	250	-13.36	1.95	8.36	30	Marble with veins	1	-13.36	1.95						
IJF226	PN7	SH15652 28860	191	-12.32	-1.47	0.71	92	F dol veins cut siliceous rock	1	-12.32	-1.47						
IJF219	T1-2	SH37190 94180	204	-7.99	1.33	9.70	0	Classic peritidal grainstones, micrite enveolpes. MT veins in intraclastic grainstone, minor patches of dolomitisation	4							-7.99	1.33
IJF209	U1.6c	SH14590 24705	134	-3.54	-1.03	6.16	3	deep-sea dol	1	-3.54	-1.03						
IJF203	U1.6S	SH14590 24705	208	-8.28	-1.50	8.31	16	Dolospar with 50-80 um crystals (coarser in veins). This is vein sample.	1	-8.28	-1.50						
IJF205	U12.11	SH13848 25176	230	-13.66	-2.11	3.68	66	deep sea dol	1	-13.66	-2.11						
IJF206	U2-5C	SH14503 24824	201	-14.06	-2.64	7.45	22	deep sea dol	1	-14.06	-2.64						
IJF208	U2.5S	SH14503 24824	214	-13.53	-3.24	8.23	19	F dol vein in deep sea dol	1	-13.53	-3.24						
IJF212	U98	SH14550 24731	191	-10.86	-2.15	7.88	13	Unstained rock is pink - deep-water assocation. F dol, ?grainstone or are the allochems actually crystals. Drilled in area of fgr matrix. Rosemary thinks may be dyke.	1	-10.86	-2.15						
IJF207	U71c	SH13845 25177	203	-10.04	2.09	8.24	15	deep sea dol	1	-10.04	2.09						
IJF210	U71s	SH13845 25177	200	-14.13	2.27	8.37	12	deep-sea dol Vein- subsample	1	-14.13	2.27						
IJF204	U73	SH13847 25156	194	-13.70	1.93	6.30	32	Coarse dolomicrospar, partly dedolmitised, generations of veins. Grains ~100 micro. Fully dolomitised. In patchy areas cores of cx leaching out - dedolomitisation.	1	-13.70	1.93						
IJF211	U88	SH14539 24763	199	-12.71	-1.44	0.59	94	Pale siliceous area "breccia fragment" sampled and carboante is only 6% of sample - might be same as F dol matrix	1	-12.71	-1.44						

NB %IR calculated from peak height compared with peak height of samples with no insoluble residue

Methodology for stable isotope analysis – Chapter 4

Each of the 25 Gwna Group carbonate samples were drilled to obtain 100 -140 µg of powdered carbonate which was placed into individual 4 ml glass vials and then sealed with a lid and pierceable septum. The vials were placed in a heated sample rack (90°C) where the vial head space was replaced by pure helium via an automated needle system, as part of an Isoprime Multiflow preparation system. The samples were then manually injected with approximately 200µl of phosphoric acid and left to react for at least 1 hour before the headspace gas was sampled by automated needle and introduced into a continuous-flow Isoprime mass-spectrometer. Duplicate samples were extracted from each vial and a mean value obtained for both $\delta^{13}C$ and $\delta^{18}O$. The samples were then calibrated using IAEA standards NBS-18 and NBS-19 and reported as ‰ on the VPDB scale. An external precision of better than 0.1 ‰ is typically achieved for both $\delta^{13}C$ and $\delta^{18}O$.

Lithological codes

1 Deep water dolostone, U2.5c, U1.6c, U12.11, U71, U73, U98
2 Mixed - dolo/limestone. MN72
3 Shallow water dolostone. NL22, 13W10, 13W21, 13W22, L1-13
4 Shallow water limestone. NT3, L5-13
5 Late dolomite. U88, PN7, MN69, MN23
6 Recrystalised limestone, marble. PN20
7 Veins. U1.6s, U71s, U2.5s